INTERNATIONAL AEGEAN CONFERENCES ON INNOVATION TECHNOLOGIES & ENGINEERING-XIII

October 26-27, 2026 / Izmir, Türkiye

PROCEEDINGS BOOK

EDITOR

Assoc. Prof. Dr. Mehmet Emin KALGI



Liberty
Publishing House

INTERNATIONAL AEGEAN CONFERENCES

ON INNOVATION TECHNOLOGIES & ENGINEERING-XIII

October 26-27, 2026 / Izmir, Türkiye

PROCEEDINGS BOOK

EDITOR

Assoc. Prof. Dr. Mehmet Emin KALGI

Liberty Publishing House
Water Street Corridor New York, NY 10038
www.libertyacademicbooks.com
+1 (314) 597-0372

ALL RIGHTS RESERVED NO PART OF THIS BOOK MAY BE REPRODUCED IN ANY FORM, BY PHOTOCOPYING OR BY ANY ELECTRONIC OR MECHANICAL MEANS, INCLUDING INFORMATION STORAGE OR RETRIEVAL SYSTEMS, WITHOUT PERMISSION IN WRITING FROM BOTH THE COPYRIGHT OWNER AND THE PUBLISHER OF THIS BOOK.
© Liberty Academic Publishers 2026
The digital PDF version of this title is available Open Access and distributed under the terms of the Creative Commons Attribution-Non-Commercial 4.0 license (http://creativecommons. org/licenses/by-nc/4.0/) which permits adaptation, alteration, reproduction and distribution for noncommercial use, without further permission provided the original work is attributed. The derivative works do not need to be licensed on the same terms.

adopted by Mariam Rasulan
Issued: 02.11.2026

ISBN: 979-8-89695-620-4

CONFERENCE ID

CONFERENCE TITLE

INTERNATIONAL AEGEAN CONFERENCES
on Innovation Technologies & Engineering

DATE and PLACE

October 26-27, 2026 / Izmir, Türkiye

ORGANIZATION

IKSAD- INSTITUTE OF ECONOMIC DEVLOPMENT AND SOCIAL RESEARCHES
ATLAS INTERNATIONAL JOURNAL ON SOCIAL SCIENCES ISSN - 2616 - 936X

ORGANIZING COMMITTEE

Assoc. Prof. Dr. Mehmet Emin KALGI
Head of Conference
Prof. Dr. Salih ÖZTÜRK
Head of Scientific Committee
Prof. Dr. Natalia LATIGINA
Member of Organizing Committee
Prof. Dr. Akbar VALADBIGI
Member of Organizing Committee
Prof. Dr. Gülzar IBRAGIMOVA
Member of Organizing Committee
Prof. Dr. Ökkeş KESİCİ
Member of Organizing Committee
Prof. Dr. Osman BAYRAKTUTAN
Member of Organizing Committee
Prof. Dr. Mustafa YILDIZ
Member of Organizing Committee
Prof. Dr. Abdullah MOHAMMADİ
Member of Organizing Committee
Assist. Prof. Dr. Sinan ÖZYURT
Member of Organizing Committee
Dr. Muhammad Shoaib KHAN PATHAN
Member of Organizing Committee
Dr. Elvan CAFEROV
Member of Organizing Committee
Lect. Ahmet ALINCA
Member of Organizing Committee
Samiksha JAIN
Member of Organizing Committee
Sandeep APPIKATLA
Member of Organizing Committee

NUMBER of ACCEPTED PAPERS- 105

NUMBER of REJECTED PAPERS- 42

PARTICIPANTS' COUNTRIES

Türkiye: 48, India: 6, Kazakhstan: 3, Nigeria: 13, Slovenia: 2, Pakistan: 3, Botswana: 6, Morocco: 11, Algeria: 1, Lithuania: 1, Azerbaijan: 1, Kosovo: 1, China: 1, QATAR: 1, Romania: 7

**Double blinded evaluation process*

SCIENTIFIC COMMITTEE BOARD

Dr. Maha Hamdan ALANAZI - *Riyad King Abdullah University*
Dr. Tamalika SULTANA - *Dakka University of Bangladesh*
Dr. Kenes JUSIPOV - *Kazak Transportation Academy*
Dr. Nilgün ULUTASDEMİR - *Gumushane University*
Dr. Murat EYVAZ - *Gebze Technical University*
Dr. Menekşe ŞAKİR - *Erciyes University*
Dr. Mehmet GÖKTÜRK - *Gebze Yüksek Teknoloji institute*
Dr. Sezen TEKİN - *Çankırı Karatekin University*
Dr. Hakan EYGÜ - *Atatürk University*
Dr. G. C. Rana - *NSCBM Govt. College Hamirpur*
Dr. Mohamed El Malki - *Department of Physics*
Dr. H. Burçin HENDEN ŞOLT - *Zonguldak Bülent Ecevit University*
Dr. Fatih YILDIRIM - *Atatürk University*
Dr. F. Gül KOÇSOY - *Fırat University*
Dr. Praveen KUMAR - *HR & OB Division*
Dr. Norma-Aurea Rangel-Vázquez - *TECNM/Instituto Tecnológico de Aguascalientes*
Dr. Yeşim TARHAN- *Ardahan University*
Sandeep APPIKATLA – Andhra University

INTERNATIONAL AEGEAN CONFERENCES
Innovation Technologies & Engineering-XIII

October 26-27, 2026 | Izmir, Türkiye

CONFERENCES PROGRAM

Online (with ZOOM Conference)
Meeting ID: 833 1287 1999
Passcode: 123456
https://us02web.zoom.us/j/83312871999?pwd=VTgLScOvATDun9WkCmTiPsTMarWVzb.1

IMPORTANT, PLEASE READ CAREFULLY

- To be able to attend a meeting online, login via **https://zoom.us/join** site, enter ID "Meeting ID or Personal Link Name" and solidify the session.
- The Zoom application is free and no need to create an account.
- The Zoom application can be used without registration.
- The application works on tablets, phones and PCs.
- The participant must be connected to the session 5 minutes before the presentation time.
- All congress participants can connect live and listen to all sessions.
- Moderator is responsible for the presentation and scientific discussion (question-answer) section of the session.

Points to Take into Consideration - TECHNICAL INFORMATION

- Make sure your computer has a microphone and is working.
- You should be able to use screen sharing feature in Zoom.
- Attendance certificates will be sent to you as pdf at the end of the congress.
- Requests such as change of place and time will not be taken into consideration in the congress program.

Önemli, Dikkatle Okuyunuz Lütfen

- Kongremizde Yazım Kurallarına uygun gönderilmiş ve bilim kurulundan geçen bildiriler için online (video konferans sistemi üzerinden) sunum imkanı sağlanmıştır.
- Online sunum yapabilmek için **https://zoom.us/join** sitesi üzerinden giriş yaparak "Meeting ID or Personal Link Name" yerine ID numarasını girerek oturuma katılabilirsiniz.
- Zoom uygulaması ücretsizdir ve hesap oluşturmaya gerek yoktur.
- Zoom uygulaması kaydolmadan kullanılabilir.
- Uygulama tablet, telefon ve PC'lerde çalışıyor.
- Her oturumdaki sunucular, sunum saatinden 5 dk öncesinde oturuma bağlanmış olmaları gerekmektedir.
- Tüm kongre katılımcıları canlı bağlanarak tüm oturumları dinleyebilir.
- Moderatör – oturumdaki sunum ve bilimsel tartışma (soru-cevap) kısmından sorumludur.

Dikkat Edilmesi Gerekenler- TEKNİK BİLGİLER

- Bilgisayarınızda mikrofon olduğuna ve çalıştığına emin olun.
- Zoom'da ekran paylaşma özelliğine kullanabilmelisiniz.
- Kabul edilen bildiri sahiplerinin mail adreslerine Zoom uygulamasında oluşturduğumuz oturuma ait ID numarası gönderilecektir.
- Katılım belgeleri kongre sonunda tarafınıza pdf olarak gönderilecektir
- Kongre programında yer ve saat değişikliği gibi talepler dikkate alınmayacaktır

---

Before you login to Zoom please indicate your name_surname and HALL number:

exp. Hall-1, Name SURNAME

DATE
- 26.10.2026

TIME
- 09^{00}–11^{00}

SESSION
- HALL-3
- SESSION-1

HEAD OF SESSION: Assist. Prof. Dr. Muhammed ONAY		
Dr. Yasemin HEKİMOĞLU Assoc. Prof. Dr. Mine TUNÇOK SARIBERBEROĞLU	Bolu Abant Izzet Baysal University (Türkiye) Bolu Abant Izzet Baysal University (Türkiye)	READING CLASS DIFFERENCE THROUGH SPACES IN LITERARY TEXTS
Ali FEYZI Prof. Dr. T.Didem AKYOL ALTUN	Dokuz Eylül University (TÜRKİYE) Dokuz Eylül University (TÜRKİYE)	AN EVALUATION OF BIOLOGICAL STABILIZATION APPROACHES FOR COMPRESSED EARTH BUILDING SYSTEMS IN TERMS OF SUSTAINABILITY
Dr. Emin SARLI Gülşen YILDIZ	Istinye University (TÜRKİYE) Achitex Minerva Chemical Industry Limited Company (TÜRKİYE)	DEVELOPMENT OF AN INNOVATIVE SIZING FORMULATION TO REDUCE CHEMICAL CONSUMPTION AND WASTEWATER LOAD FOR SUSTAINABLE TEXTILE PRODUCTION
Dr. Emin SARLI Gülşen YILDIZ	Istinye University (TÜRKİYE) Achitex Minerva Chemical Industry Limited Company (TÜRKİYE)	INTEGRATION OF BIO-STARCH OBTAINED FROM FOOD WASTE INTO TEXTILE SIZING
Dr. Abdullah Kürşat DEMİR	Tokat Gaziosmanpaşa University (Türkiye)	ANALYTICAL INVESTIGATION OF THE P–Δ EFFECT ON THE NATURAL FREQUENCY BEHAVIOR OF HYBRID OFFSHORE WIND–HYDROKINETIC SYSTEMS
Assist. Prof. Dr. Muhammed ONAY	Malatya Turgut Özal University (Türkiye)	FIXED-BED COLUMN DYNAMICS FOR CONTINUOUS PB(II) SEQUESTRATION ONTO PEANUT SHELL BIOCHAR: INFLUENCE OF INFLUENT CONCENTRATION AND KINETIC BREAKTHROUGH MODELING
Assoc. Prof. Dr. Ali DOGAN MSc. Mohammad Bilal JALALI	Iskenderun Technical University (Türkiye) Sakarya University (Türkiye)	FINITE ELEMENT INVESTIGATION OF CFRP TEXTILE WRAPPING GEOMETRY AND STRIP WIDTH EFFECTS ON THE FLEXURAL BEHAVIOR OF REINFORCED CONCRETE BEAMS
Yiğithan YILMAZ	Oyak Renault Automobile Factories (Türkiye)	CONTRIBUTION OF CRITICAL SUCCESS FACTORS TO AGILITY IN PRODUCTION, R&D AND AFTER-SALES PROJECTS AND SECTORAL ANALYSIS WITH MULTI CRITERIA DECISION TECHNIQUES

DATE
- 26.10.2026

TIME
- 11^{30}–13^{30}

SESSION
- HALL-3
- SESSION-2

HEAD OF SESSION: Dr. Jerneja Bogovič		
S. Suresh Krishna F. Joshwa Santhosh Dr. S. Selvam	Nadar Mahajana Sangam S. Vellaichamy Nadar College (INDIA)	BEYOND ARTIFICIAL INTELLIGENCE: EXPLORING THE RISE OF SYNTHETIC INTELLIGENCE
B.DHARSHINI Dr. S. Selvam	Nadar Mahajana Sangam S. Vellaichamy Nadar College (INDIA)	KOREA'S CULTURAL RENAISSANCE: THE EVOLUTION OF CINEMA AND K-POP
M. Dhinesh Kumar Dr. S. SELVAM	Nadar Mahajana Sangam S. Vellaichamy Nadar College (INDIA)	WAYS TO REDUCE AND RESOLVE MISUNDERSTANDINGS BETWEEN PEOPLE
Prof. Kamalbek BERKİMBAYEV Assist. Prof. Dr. Dinara BERDİ Assist. Prof. Dr. Sherzod RAMANKULOV Shakhrizada KHIKMATULLA Kazhymukan KELESBAYEV	Khoja Akhmet Yassawi International Kazakh-Turkish University (KAZAKHISTAN)	DEVELOPING LEARNERS' SOFT SKILLS IN A STEM-BASED VIRTUAL LEARNING ENVIRONMENT
Senior Lect. Yelmurat DOSYMOV Senior Lect. Serik POLATULY Assist. Prof. Dr. Sherzod RAMANKULOV Shakhrizada KHIKMATULLA Munisa RAKHMATULLAEVA	Khoja Akhmet Yassawi International Kazakh-Turkish University (KAZAKHISTAN)	STEM-BASED METHODOLOGICAL RECOMMENDATIONS FOR TEACHERS: DEVELOPING SOFT SKILLS IN NATURAL SCIENCE SUBJECTS
Ebole Alpha Friday Aremu Idris Abiodun Ayinde Yusuf Olatunji	Lagos State University of Science and Technology (NIGERIA)	AN INTEGRATED CYBERSECURITY FRAMEWORK FOR SECURING CONNECTED DIGITAL ECOSYSTEMS (DE)
Arypzhan ABEN Dinmukhammed GABDULLAULY	Khoja Akhmet Yassawi International Kazakh-Turkish University (KAZAKHISTAN)	CLASSIFICATION OF CLOTHING TYPES USING A CONVOLUTIONAL NEURAL NETWORK: EXPERIMENTAL EVALUATION AND ERROR ANALYSIS ON THE MYNTRA FASHION PRODUCT IMAGES DATASET
Dr. Jerneja Bogovič	University of Ljubljana (SLOVENIA)	ASSESSMENT OF THE EXPLICIT FLEXIBILITY POTENTIAL OF SLOVENIAN BUSINESS CONSUMERS
Dr. Jerneja Bogovič	University of Ljubljana (SLOVENIA)	IMPACT OF HYDROLOGY AND THERMAL POWER PLANT AVAILABILITY ON RESOURCE ADEQUACY IN SLOVENIA
Olajide O. Ogunbodede	Federal University of Technology (NIGERIA)	A GAME-THEORETIC INSIDER THREAT MITIGATION FRAMEWORK: LSTM-AUTOENCODER BASED USER BEHAVIOUR ANALYTICS APPROACH
Prof. Afaq AHMAD Assoc. Prof. Dr. M Mohammed Sabir HUSSAIN	Modern College of Business and Science (INDIA) Muffakham Jah College of Engineering and Technology (INDIA)	DESIGN AND SIMULATION-BASED EVALUATION OF AN LFSR-DRIVEN BUILT-IN SELF-TEST ARCHITECTURE FOR FAULT DETECTION USING VERILOG HDL

DATE
- 26.10.2026

TIME
- 14^{00}–16^{00}

SESSION
- HALL-3
- SESSION-3

HEAD OF SESSION: Dr. Burcu Nilgün ÇETİNER		
Tuğba Özcan	ZF Lemförder (TÜRKİYE)	IMPROVEMENT OF ROLLED EDGE CORROSION RESISTANCE OF OUTER TIE-ROD
Ebru GÜDÜL Şükrü SARI Ayça ÖZEN Samet DURMUŞ Onur ADIGÜZEL Ekrem ALTAN	Borsan R&D Center (Türkiye)	OPTIMIZATION OF FLAME-RETARDANT GRANULE PROCESSING PARAMETERS AND INVESTIGATION OF CPR FIRE REACTION PERFORMANCE IN H07Z-K CABLES
Dr. Burcu Nilgün ÇETİNER Dr. Gökçen BAYRAM	Marmara University (Türkiye) Istanbul Beykent University (Türkiye)	VALORIZATION OF SHELL-BASED AGRICULTURAL RESIDUES INTO VALUE-ADDED ENGINEERING MATERIALS THROUGH INDUSTRIAL SYMBIOSIS IN TÜRKİYE: A CRITICAL ASSESSMENT OF TECHNICAL POTENTIAL, REGIONAL RESOURCE DISTRIBUTION, AND IMPLEMENTATION FEASIBILITY
İlayda DEMİR	Yildiz Technical University (Türkiye)	HIGH TEMPERATURE BEHAVIOR OF CARBON FIBER REINFORCED EPOXYCOMPOSITES CONTAINING GRAPHENE AND H-BN HYBRID NANOFILLERS
Yaren DEVİREN	Çukurova Machinery Manufacturing and Trading Inc. (Türkiye)	EVALUATION OF CAB MOUNT SELECTION FOR A BACKHOE LOADER BASED ON VIBRATION ISOLATION AND DESIGN CRITERIA
Oğuzhan CAN Baran BULUT Safa Melik TÜZÜNER Dr. Süreyya Ergün BOZDAĞ Prof. Dr. Emin SÜNBÜLOĞLU	Istanbul Technical University (Türkiye)	AN EVALUATION OF IMPEDANCE MATCHING TECHNIQUES FOR SHPB TESTING OF LOW-IMPEDANCE SOFT MATERIALS
Baran BULUT Safa Melik TÜZÜNER Oğuzhan CAN Dr. Süreyya Ergün BOZDAĞ Prof. Dr. Emin SÜNBÜLOĞLU	Istanbul Technical University (Türkiye)	DESIGN AND ANALYSIS OF VARIOUS CROSS-SECTION TRANSFORMING HORN DESIGNS FOR TESTING LOW-IMPEDANCE MATERIALS IN SPLIT HOPKINSON PRESSURE BAR SYSTEMS

DATE
- 26.10.2026

TIME
- 16^{30}–18^{30}

SESSION
- HALL-1
- SESSION-4

HEAD OF SESSION: AKPAN CHRISTOPHER ANIEKAN

Ar. Shayan Zulfiqar Ar. Dr. Omer Shujat Bhatti Ar. Syed Usman Raza Kazmi Engr. Nouman Zulfiqar Engr. Hamza Rashid	IEB Nexus Hub (DUBAI) School of Architecture & Planning (PAKISTAN) School of Architecture & Planning (PAKISTAN) Practicing Engineer (PAKISTAN) Infrastructure Development Authority (PAKISTAN)	GRAVITY-LESS IN ARCHITECTURE AS A DESIGN PROBLEM: CASE STUDIES OF SINGAPORE NATIONAL STADIUM AND MERCEDES-BENZ STADIUM, ATLANTA
AKPAN CHRISTOPHER ANIEKAN	Federal College of Education (Technical) Ekiadolor Benin City (NIGERIA)	LEVERAGING DIGITAL TRANSFORMATION TO DRIVE SUSTAINABLE FOOD SYSTEMS IN AFRICA: A CASE STUDY OF MKPAT ENIN LOCAL GOVERNMENT AREA OF AKWA IBOM STATE, NIGERIA
Kater Titus A.J. Simon D.O. Alonge	Federal University of Technology (NIGERIA)	ENHANCING SAFETY AND ACCESSIBILITY IN THE DESIGN OF A PUBLIC TRANSPORTATION HUB IN MINNA, NIGER STATE
Ali Akbar Firoozi Ali Asghar Firoozi	University of Botswana (BOSTWANA) National University of Malaysia (UKM) (MALAYSIA)	A DIMENSIONLESS HYDRO-MECHANICAL FRAMEWORK FOR SCREENINGRAINFALL-INDUCED SHALLOW SLOPE INSTABILITY: ANALYTICAL THRESHOLDS AND PARAMETRIC SENSITIVITY
Ali Akbar Firoozi Ali Asghar Firoozi	University of Botswana (BOSTWANA) National University of Malaysia (UKM) (MALAYSIA)	TRANSIENT WETTING AND REPEATED MOISTURE PULSES IN EXPANSIVE SUBGRADES: A DIMENSIONLESS SCREENING FRAMEWORK FOR VERTICAL HEAVE
Ali Akbar Firoozi Ali Asghar Firoozi	University of Botswana (BOSTWANA) National University of Malaysia (UKM) (MALAYSIA)	DESIGN-TIME SCREENING OF RESIDUAL PRIMARY CONSOLIDATION IN SOFT CLAY UNDER STAGED EMBANKMENT LOADING: ANALYTICAL SUPERPOSITION AND SENSITIVITY MAPS
Ali Akbar Firoozi Ali Asghar Firoozi	University of Botswana (BOSTWANA) National University of Malaysia (UKM) (MALAYSIA)	DIMENSIONLESS SCREENING OF SOLUTE BREAKTHROUGH IN COMPACTED CLAY BARRIERS: HYDRAULIC–DIFFUSIVE COMPETITION AND EQUILIBRIUM SORPTION
Ali Akbar Firoozi Ali Asghar Firoozi	University of Botswana (BOSTWANA) National University of Malaysia (UKM) (MALAYSIA)	GROUNDWATER-SENSITIVE RELIABILITY SCREENING OF STRIP FOOTINGS ON SAND: A REPRODUCIBLE BEARING-CAPACITY DESIGN MAP
Ali Akbar Firoozi Ali Asghar Firoozi	University of Botswana (BOSTWANA) National University of Malaysia (UKM) (MALAYSIA)	GRAIN-SIZE COMPATIBILITY AND PRODUCTION TOLERANCE OF GRANULAR FILTERS FOR EMBANKMENT DAMS: A PARAMETRIC SCREENING FRAMEWORK

DATE
- 26.10.2026

TIME
- 16^{30}–18^{30}

SESSION
- HALL-2
- SESSION-4

HEAD OF SESSION: Khadija Zair		
Khadija Zair M'hamed El Omari	Sultan Moulay Slimane University (MOROCCO)	SPECTRAL AND NUMERICAL ANALYSIS OF BIFURCATIONS AND COMPLEX DYNAMICS IN FRACTIONAL BURGERS EQUATIONS
Ouassila Riouchi Khalid Elkalay	Cadi Ayyad University (MOROCCO)	MICROALGAE: TINY ORGANISMS WITH GREAT ENVIRONMENTAL POTENTIAL
Hajar Sadrati Youssef Arif Younes Abbas Sanaa Sabour-Alaoui Mohammed El idrissi	Sultan Moulay Slimane University (MOROCCO)	IN SILICO ANALYSIS OF MAJOR CONSTITUENTS OF THYMUS VULGARIS ESSENTIAL OIL AGAINST PENICILLIUM DIGITATUM: MOLECULAR DOCKING, MOLECULAR DYNAMICS, AND TOXICITY PROFILING
El Hassania El Hamzaoui Hind ElHamzaoui	Sultan Moulay Slimane University (MOROCCO)	UNDERSTANDING THE LOW APPEAL OF GEOSCIENCES IN THE MOROCCAN EDUCATION SYSTEM: A SURVEY OF PROSPECTIVE TEACHERS
Ms. Minahil Fatima Dr Irfan Bashir Dr Yasira Waqar	University of management and Technology (PAKISTAN)	EXPLORING UNDERGRADUATE STUDENTS' EXPERIENCES OF PEER TUTORING AT HIGHER EDUCATION INSTITUTES: A QUALITATIVE PHENOMENOLOGICAL STUDY
Maryem Arraji Khaoula EL BARBI Fatima Zahra BOUCHACHI Mohamed Khalis Mohamed Chahboune	Hassan First University of Settat (MOROCCO) Mohammed VI Center of Research and Innovation (MOROCCO) Mohammed VI University of Health Sciences (MOROCCO) Higher Institute of Nursing Professions and Technical Health (MOROCCO) Laboratory of BiostatisticsMohamed V University in Rabat (MOROCCO)	USE OF ARTIFICIAL INTELLIGENCE FOR MEDICATION ADHERENCE ASSESSMENT IN PATIENTS WITH TYPE 2 DIABETES: AN EXPLORATORY STUDY IN MOROCCO USING CHATGPT AND THE VALIDATED GENERAL MEDICATION ADHERENCE SCALE

DATE
- 26.10.2026

TIME
- 16^{30}–18^{30}

SESSION
- HALL-3
- SESSION-4

HEAD OF SESSION: DR ASABE EDWARD BASH		
Salihu SULEIMAN Aisha N. SULEIMAN	Federal University Birnin Kebbi (NIGERIA) University of Calabar (NIGERIA)	THE ENERGY PERFORMANCE GAP IN AFRICAN BUILDINGS: A COMPARATIVE ASSESSMENT OF BUILDING REGULATIONS, CLIMATE ZONES AND ENERGY-EFFICIENCY STRATEGIES IN NIGERIA AND SELECTED AFRICAN COUNTRIES
Salihu SULEIMAN Gambo B. WURMA	Federal University Birnin Kebbi (NIGERIA)	NIGERIA'S ARCHITECTURAL TRANSITION TOWARDS NET-ZERO BUILDINGS: A BIBLIOMETRIC, POLICY AND GLOBAL BENCHMARKING ANALYSIS OF BUILDING ENERGY EFFICIENCY AND SUSTAINABLE DESIGN
OUNIS HADJ MOHAMED OUNIS ABDELHAFID	Engineering/University of Mostefa Ben Boulaid Batna (ALGERIA) Company University Mohamed Khider (ALGERIA)	CONTEMPORARY SEISMIC ISOLATION TECHNIQUES: IMPLEMENTATION UNDER ALGERIAN REGULATION AND COMPARISON WITH INTERNATIONAL CODES
EWETOLA, E. A. AFOLORUNSO, G.T. JAYEOBA, A. D. OKE, S. A. AYENI, B. O.	Ladoke Akintola University of Technology (NIGERIA)	ASSESSMENT OF SOIL LOSS FROM CARROT (DAUCUS CAROTA) AS INFLUENCED BY NPK 15:15:15 AND POULTRY MANURE
Olugbemi Victor EKUNDARE Oluwadamilare Emmanuel OBAYEMI	University of Ilesa (NIGERIA)	AQUACULTURE POTENTIALS of PARENTAL CLARIAS GARIEPINUS and BACKCROSS PROGENY DERIVED from FEMALE CLARIAS HETEROBRANCHUS HYBRID and MALE CLARIAS GARIEPINUS
DR ASABE EDWARD BASH CHRISTIANA DAVID DALOK	University of Jos (NIGERIA)	EFFECTS OF INTERACTIVE WHITE BOARD TEACHING METHOD ON STUDENTS' ACHIEVEMENT IN BASIC SCIENCE AND TECHNOLOGY IN JUNIOR SECONDARY SCHOOL, JOS NORTH, PLATEAU STATE, NIGERIA

DATE
- 27.10.2026

TIME
- 09^{00}–11^{00}

SESSION
- HALL-2
- SESSION-1

HEAD OF SESSION: Assist. Prof. Dr. Esra Tayat		
Assist. Prof. Dr. Talip AKBIYIK Prof. Dr. Nafiz KAHRAMAN	Aksaray University (TÜRKİYE) Erciyes University (TÜRKİYE)	EFFECTS OF BORON-BASED ADDITIVE CONCENTRATION ON THE PERFORMANCE OF A LOMBARDINI LGW 523 ENGINE FUELED WITH E0 AND E20: DETERMINATION OF OPTIMUM OPERATING CONDITIONS
Assist. Prof. Dr. Talip AKBIYIK Prof. Dr. Nafiz KAHRAMAN	Aksaray University (TÜRKİYE) Erciyes University (TÜRKİYE)	EXPERIMENTAL INVESTIGATION OF THE EFFECTS OF TWO DIFFERENT BORON-BASED ADDITIVES ON THE PERFORMANCE OF A GASOLINE ENGINE AND DETERMINATION OF THE OPTIMUM ADDITIVE CONCENTRATION
Meriçsu KARAHAN Dr. Şölen ZENGİN	Tarsus University (Türkiye) Tarsus University (Türkiye)	MACHINE LEARNING-BASED DEMAND FORECASTING FOR FOOD WASTE REDUCTION: A CASE STUDY
Yağmur ÇİÇEK Dr. Şölen ZENGİN	Tarsus University (Türkiye) Tarsus University (Türkiye)	SUSTAINABLE RISK MANAGEMENT IN TEXTILE SECTOR: A MULTI-DIMENSIONAL FMEA APPROACH
Dr. Şükran YALPIR	Konya Technical University (Türkiye)	AN EMPIRICAL EXAMINATION OF THE RELATIONSHIP BETWEEN ECONOMIC INDICATORS AND THE REAL ESTATE MARKET
Handan SOYDABİRCAN Dr. Şükran YALPIR Dr. Vildan ÖNEN	Konya Technical University (Türkiye) Konya Technical University (Türkiye) Konya Technical University (Türkiye)	AN ANALYSIS OF THE ECONOMIC, SOCIAL, AND ENVIRONMENTAL IMPACTS OF THE REGIONAL TRANSFORMATION CAUSED BY CHANGES IN THE ROLE OF MINING ACTIVITIES IN ERMENEK'S REGIONAL ECONOMY AND THE CONSTRUCTION OF A DAM IN ERMENEK
Prof. Dr. Nihal Özder Assist. Prof. Dr. Esra Tayat	Tekirdağ Namık Kemal University (Türkiye) Tekirdağ Namık Kemal University (Türkiye)	DEFENSIVE BEHAVIOURS IN INSECTS
Assist. Prof. Dr. Esra Tayat Prof. Dr. Nihal Özder	Tekirdağ Namık Kemal University (Türkiye) Tekirdağ Namık Kemal University (Türkiye)	CHEMICAL HOST-PLANT RECOGNITION AND FEEDING BEHAVIOR IN PHYTOPHAGOUS INSECTS

DATE
- 27.10.2026

TIME
- 09^{00}–11^{00}

SESSION
- HALL-3
- SESSION-1

HEAD OF SESSION: Dr. Iram Liaqat		
K.R.Padma K. Sri Vidya K.R.Don	Sri Padmavati Mahila Visvavidyalayam (Women's) University (INDIA)	GREENS FOR A HEALTHIER BRAIN: DIETARY FIBRE, THE GUT–BRAIN AXIS, AND NEUROPROTECTION FROM SPINACH AND AMARANTHUS
Imadojemu, P.E. Imadojemu, O.I.	Federal University Wukari (NIGERIA)	MINERALOGICAL CHARACTERISTICS OF FLOODPLAIN SOILS IN SOUTHERN TARABA STATE NORTHEAST, NIGERIA
Ibrahim Sani Dikko	Umaru Musa Yar'adua University Katsina (NIGERIA)	ARTIFICIAL INTELLIGENCE AND MULTI-OMICS INTEGRATION IN PRECISION MEDICINE: DECIPHERING MOLECULAR MECHANISMS OF DISEASE AND ADVANCING BIOMARKER-GUIDED THERAPEUTIC DEVELOPMENT
Dr. Iram Liaqat	Government College University (PAKISTAN)	INHIBITORY EFFICACY OF HONEY AGAINST MULTISPECIES BACTERIAL BIOFILM
Vilma Šalkauskienė Daiva Gudritienė	Lietuvos Inžinerijos Kolegija (LITHUANIA)	ASSESSMENT OF URBANIZATION DYNAMICS IN SUBURBAN AREAS IN LITHUANIA USING GIS-BASED MONITORING
Mustapha Oukbab	Beni Mellal Faculty of Science and Technology (MOROCCO)	MACHINE LEARNING-ENHANCED CLASSIFICATION AND ANALYSISOF MODIFIED CARBON PASTE ELECTRODES FOR METHANOL FUELCELL APPLICATIONS
DJEBBARA BENZERGA FAYCAL SOTEHI NOUREDDINE BOUALEM	University of Sciences and Technology of Oran Mohamed Boudiaf (USTO-MB) (MOROCCO)	NUMERICAL ASSESSMENT OF HYDROGEN EMBRITTLEMENT SUSCEPTIBILITY IN API 5L PIPELINE STEELS FOR HYDROGEN TRANSPORT
Ilyasse Joubbi Fatima Aqel Nour Eddine Alaa	Hassan First University (MOROCCO) Cadi Ayyad University (MOROCCO)	PHYSICS-INFORMED NEURAL APPROXIMATION OF DISCRETE ANISOTROPIC VARIABLE-EXPONENT PROBLEMS

DATE
- 27.10.2026

TIME
- 11^{30}–13^{30}

SESSION
- HALL-2
- SESSION-2

HEAD OF SESSION: Dr. Mediha Gürel		
Dr. Mediha Gürel Dr. Fatih Özoğul	Çukurova University (TÜRKİYE) Çukurova University (TÜRKİYE)	METHODOLOGICAL ADVANCES IN PATIENT-DERIVED GLIOBLASTOMA ORGANOIDS, EXTRACELLULAR VESICLES, AND CAR-T CELL THERAPY
Dr. Mediha Gürel Dr. Fatih Özoğul	Çukurova University (TÜRKİYE) Çukurova University (TÜRKİYE)	METHODOLOGICAL ADVANCES IN THE PRODUCTION OF CULTURED SEAFOOD AND ITS POTENTIAL IN THE FOOD INDUSTRY
ScD. Prof. Azad Bayramov Michail Awtushko	Republican Seismic Survey Center of the Azerbaijan National Academy of Sciences (AZERBAIJAN)	ATMOSPHERIC FACTORS AND THE DYNAMICS OF RADON EMISSION
Recep GÜNENÇ Hasan KASIM	PEGA Automotive Suspension Systems Inc. (TÜRKİYE) PEGA Automotive Suspension Systems Inc. (TÜRKİYE)	EXPERIMENTAL INVESTIGATION OF THE GEOMETRIC BEHAVIOR OF AN AXLE LIFT AIR SPRING UNDER STATIC PRESSURE VARIATION USING 3D LASER SCANNING AND CROSS-SECTIONAL SYMMETRY CENTER DISPLACEMENT METHOD
Keziban ÇAKMAKTAŞI HULUD BAYRAM	Ilsan Textile Industry and Trade Inc. (Türkiye) Ilsan Textile Industry and Trade Inc. (Türkiye)	REUSE OF SUGAR BEET WASTE IN THE TEXTILE INDUSTRY: EVALUATION AS A DYEING AGENT
Berkay ARSLAN Nilüfer DUYGULU	Yıldız Technical University (TÜRKİYE) Yıldız Technical University (TÜRKİYE)	THE EFFECTS OF ZnO AND MnO ADDITIONS ON THE MORPHOLOGY AND FIBER DIAMETER DISTRIBUTION OF PVA-BASED ELECTROSPUN NANOFIBERS

DATE
- 27.10.2026

TIME
- 11^{30}–13^{30}

SESSION
- HALL-3
- SESSION-2

HEAD OF SESSION: Assoc. Prof. Dr. Faruk AHMETI		
Oduntan. A.S. Adewale. V.O.	Federal University of Technology (NIGERIA)	GREEN SYNTHESIS OF BIMETALLIC ZIRCRONIUM-COPPER NANOPARTICLES USING BAUHINIA MONANDRA LEAF EXTRACT: INVESTIGATION OF ITS ANTIBACTERIAL PROPERTIES
Kamal BOUCHIT Dr. Jilali ABOUIR Dr. Abderrahim CHARKAOUI Dr. Anouar BEN-LOGHFYRY	Hassan First University (MOROCCO)	CONTRIBUTION TO THE MATHEMATICAL ANALYSIS OF SOME NONLINEAR PDES ARISING FROM ELECTRORHEOLOGICAL FLUIDS MODELING
Assoc. Prof. Dr. Faruk AHMETI Assoc. Prof. Dr. Kushtrim GASHI	University "Isa Boletini" Mitrovica (KOSOVO) University "Ukshin Hoti" Prizren (KOSOVO)	THE INFLUENCE OF DIGITAL MARKETING CAPABILITIES ON CUSTOMER LOYALTY: THE MEDIATING EFFECTS OF CUSTOMER ENGAGEMENT AND BRAND TRUST
Tabussam Tufail Huma Bader Ul Ain Farhan Saeed Muhammad Afzaal Tanazzam Tufail Muhammad Umair Arshad	Government College University Faisalabad (PAKISTAN) Zhejiang University of Technology (CHINA)	GLOBAL HEALTH CHALLENGES AND OUR RESPONSE: SPECIAL FOCUS TO PAKISTAN
Ahmed Osmane Khadija Zidan Hasnae Sabri Moustapha Belmouden	University Cadi Ayyad (MOROCCO) University Cadi Ayyad (MOROCCO) University Cadi Ayyad (MOROCCO) Agadir University Ibn Zohr (MOROCCO)	SUSTAINABLE WATER MANAGEMENT UNDER CLIMATE STRESS: EVIDENCE FROM MARRAKECH ON TREATED WASTEWATER IRRIGATION, SOIL FERTILITY, AND MAIZE AGRO-PHYSIOLOGY
Ahmed Osmane Khadija Zidan Hasnae Sabri Moustapha Belmouden	University Cadi Ayyad (MOROCCO) University Cadi Ayyad (MOROCCO) University Cadi Ayyad (MOROCCO) Agadir University Ibn Zohr (MOROCCO)	SYNTHESIS AND ADSORPTION PERFORMANCE OF POZZOLAN–ALGINATE COMPOSITE BEADS TOWARD OLIVE OIL POLYPHENOLS

DATE
- 27.10.2026

TIME
- 14^{00}–16^{00}

SESSION
- HALL-2
- SESSION-3

HEAD OF SESSION: Lect. Dr. Ömer SEVİNÇ		
Lect. Seyit AKPANCAR Lect. Eyüp ÇAKI	Isparta University of Applied Sciences (TÜRKİYE) Gaziantep University (TÜRKİYE)	COMPARATIVE EVALUATION OF OBSTACLE AVOIDANCE AND PATH PLANNING ALGORITHMS FOR AUTONOMOUS UAVS IN A ROS-GAZEBO SIMULATION ENVIRONMENT
Lect. Dr. Burcu DURMUŞ	Tekirdağ Namık Kemal University (TÜRKİYE)	EFFECTS OF RESAMPLING METHODS ON MACHINE LEARNING PERFORMANCE IN HEALTH DATA: A DERMATOLOGICAL APPLICATION
Lect. Dr. Ömer SEVİNÇ	Ondokuz Mayıs University (TÜRKİYE)	A LAYERED CYBERSECURITY MODEL FOR ZERO TRUST AND AI-BASED ANOMALY DETECTION IN HYBRID WORK ENVIRONMENTS
Lect. Dr. Ömer SEVİNÇ	Ondokuz Mayıs University (TÜRKİYE)	A HUMAN–MACHINE COLLABORATION MODEL FOR ORGANIZATIONAL DEFENSE AGAINST GENERATIVE AI-ENABLED PHISHING
Cem ALİŞEN Prof. Dr. Fikri GÖKPINAR	Gazi University (Türkiye) Gazi University (Türkiye)	PERFORMANCE ANALYSIS OF MISSING DATA IMPUTATION METHODS
Meral ERGÜN Prof. Dr. Mustafa KURBAN Prof. Dr. Erchin SERPEDIN Assoc. Prof. Dr. Buket DOĞAN	Marmara University (Türkiye) Ankara University (Türkiye) & Texas A&M University (QATAR) Texas A&M University (QATAR) Marmara University (Türkiye)	TRANSFERABILITY OF SQL SERVER MEMORY SETTINGS ACROSS WORKLOADS
İbrahim Akdeniz Assoc. Prof. Dr. Halil Erdi Gülcan Assoc. Prof. Dr. Samet Çelebi Assist. Prof. Dr. Emrah Arda	Selçuk University (Türkiye) Selçuk University (Türkiye) Sakarya University of Applied Sciences (Türkiye) Sakarya University of Applied Sciences (Türkiye)	THE EFFECT OF USING DIFFERENT TYPES OF BORON FUEL ADDITIVES ON ENGINE PERFORMANCE AND EXHAUST EMISSIONS IN A GASOLINE ENGINE
Dr. Deniz ÇOBAN ÖZKAN Dr. Fikret SÖNMEZ	Manisa Celal Bayar University (Türkiye) Manisa Celal Bayar University (Türkiye)	SURFACE ROUGHNESS AND TOOL WEAR IN HELICAL RAMPING POCKET MILLING OF TI-6AL-4V ELI (GRADE 23)

DATE
- 27.10.2026

TIME
- 14^{00}–16^{00}

SESSION
- HALL-3
- SESSION-3

HEAD OF SESSION: Bogdan-Catalin SERBAN

Bogdan-Catalin SERBAN Maria Ruxandra SALAGEAN Matei-Gabriel URSACHESCU Vlad DİACONESCU Caterina ZETU Diana DUMITRAȘCU Maria Ruxandra DİMA Marius BUMBAC	IMT Bucharest (ROMANIA) National College “Saint Sava” (ROMANIA) National College “B. P. Hasdeu” (ROMANIA) University of Medicine and Pharmacy “Carol Davila” (ROMANIA) International Theoretical High School of Computer Science (ROMANIA) Valahia University of Targoviste (ROMANIA)	BILIRUBIN IN THE HUMAN BODY: FROM A WASTE PRODUCT TO AN ENDOGENOUS ANTIOXIDANT
		D-AMINO ACIDS IN THE HUMAN BODY: EXCEPTIONS TO THE RULE OF BIOLOGICAL HOMOCHIRALITY
		CYANIDE IN THE FOODS WE EAT: NATURAL PLANT DEFENSE, HUMAN TOXICITY, AND DETOXIFICATION
		WHY DOES THE HUMAN BODY PRODUCE FORMALDEHYDE? FROM A TOXIC CHEMICAL TO AN ENDOGENOUS METABOLITE
		WHY CAN GRAPEFRUIT TURN A SAFE MEDICINE INTO A DANGEROUS ONE? CHEMISTRY AND BIOCHEMISTRY OF A CLASSIC FOOD–DRUG INTERACTION
		THE CHEMISTRY OF HUMAN BODY ODOR: WHY DO WE SMELL AND WHY DOES OUR SMELL CHANGE WITH AGE?
		HYDROGEN SULFIDE IN THE HUMAN BODY: FROM A TOXIC GAS TO AN ESSENTIAL BIOLOGICAL MESSENGER
Jatinkumar Bhimjibhai Kotadiya	Atmiya University (INDIA)	ZERO-/FEW-SHOT MULTILINGUAL STUDENT FEEDBACK ANALYSIS IN LOW-RESOURCE LANGUAGES USING LIGHTWEIGHT TRANSFORMER VARIANTS FOR MOBILE EDUCATIONAL PLATFORMS

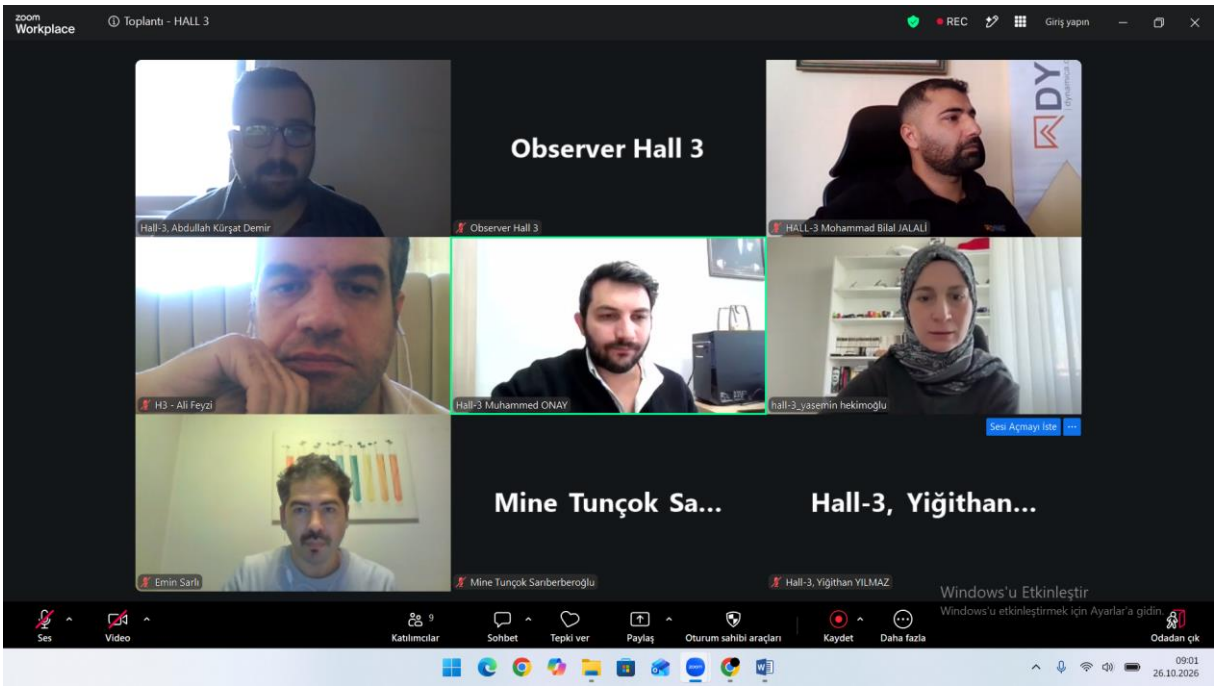
DATE
- 27.10.2026

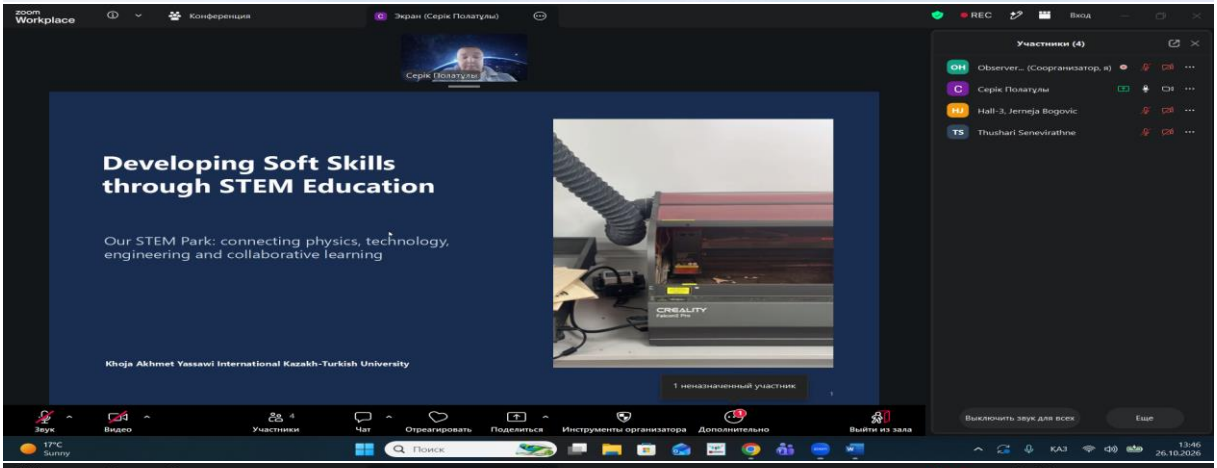
TIME
- 16^{30}–18^{30}

SESSION
- HALL-2
- SESSION-4

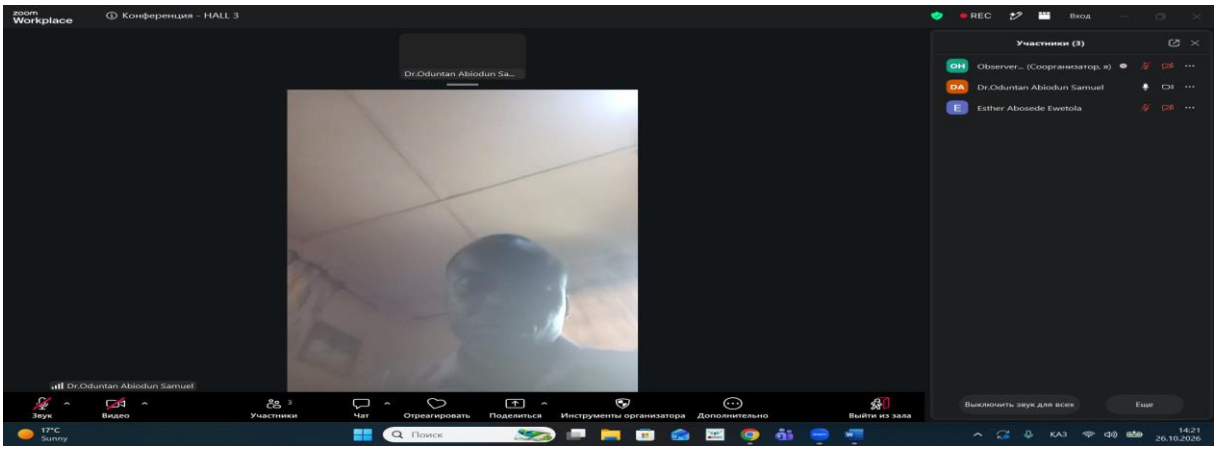
HEAD OF SESSION: Assoc. Prof. Dr. Özgür TAMER

Efra KALKAN Dr. Ayşe Nuray CANAT	Istanbul Sabahattin Zaim University (Türkiye) Istanbul Sabahattin Zaim University (Türkiye)	PIEZOELECTRIC ENERGY HARVESTING SYSTEMS IN HIGH-DENSITY PEDESTRIAN AREAS: LITERATURE REVIEW AND MECHANISM CLASSIFICATION
Ahmet TURGUT Muhammet Rıza KARADAVUT	Ondokuz Mayıs University (TÜRKİYE) Ondokuz Mayıs University (TÜRKİYE)	EFFECTS OF PHASE QUANTIZATION ON POINTING ERROR AND POWER LOSS IN THE TARGET DIRECTION OF AN IDEAL UNIFORM LINEAR ANTENNA ARRAY
Ahmet TURGUT Muhammet Rıza KARADAVUT	Ondokuz Mayıs University (TÜRKİYE) Ondokuz Mayıs University (TÜRKİYE)	POLARIZATION SELECTION IN PASSIVE UHF RFID SYSTEMS BASED ON TAG ORIENTATION DISTRIBUTION AND POWER MARGIN
Assoc. Prof. Dr. Özgür TAMER Dr. Ömür ÖCAL Mehmet ÖZTEMEL	Dokuz Eylül University (TÜRKİYE) Core Building Automation Technologies Industry and Trade Co., Ltd. (TÜRKİYE) Core Building Automation Technologies Industry and Trade Co., Ltd. (TÜRKİYE)	DESIGN OF A PORTABLE DEVICE BASED ON DOUBLE-BLIND PAIRING FOR THE CHARACTERIZATION OF PIEZO HAPTIC SIGNALS
Beliz HÜNKAR Assoc. Prof. Dr. Ahsen RAYMAN ERGÜN Assist. Prof. Dr. Neslihan ÇOLAK	Ege University (Türkiye) Ege University (Türkiye) Ege University (Türkiye)	EVALUATION OF THE PHYSICAL, TEXTURAL AND SENSORY PROPERTIES OF SNACK PROTEIN BARS ENRICHED WITH APPLE AND GRAPE POMACE
Res. Assist. Ekin Emek DİLBAZ Assoc. Prof. Dr. Ersin SAYAR	Istanbul Technical University (Türkiye) Istanbul Technical University (Türkiye)	NUMERICAL INVESTIGATION OF NUCLEATE FLOW BOILING OF R744 UNDER CONSTANT HEAT FLUX
Melike YAPAR Prof. Dr. İkbal ESKİ	Erciyes University (Türkiye) Erciyes University (Türkiye)	COMPARISON OF THE PERFORMANCE OF METAHEURISTIC OPTIMIZATION-BASED PID CONTROLLERS FOR A QUADROTOR UAV UNDER DIFFERENT FLIGHT SCENARIOS
Ali CELEN	Gümüşhane University (Türkiye)	A BRIEF REVIEW OF NUSSELT NUMBER CORRELATIONS DEVELOPED FOR TRIPLY PERIODIC MINIMAL SURFACES


Toplantı - HALL 3
Observer Hall 3
Hall-3, Abdullah Kürşat Demir
HALL-3 Mohammad Bilal JALALİ
H3 - Ali Feyzi
Hall-3 Muhammed ONAY
hall-3_yasemin hekimoğlu
Sesi Açmayı İste
Emin Sarlı
Mine Tunçok Sa...
Hall-3, Yiğithan...
Mine Tunçok Sarıberberoğlu
Hall-3, Yiğithan YILMAZ
Windows'u Etkinleştir
Windows'u etkinleştirmek için Ayarlar'a gidin.
Ses
Video
Katılımcılar
Sohbet
Tepki ver
Paylaş
Oturum sahibi araçları
Kaydet
Daha fazla
Odadan çık


Developing Soft Skills through STEM Education
Our STEM Park: connecting physics, technology, engineering and collaborative learning
Khoja Akhmet Yassawi International Kazakh-Turkish University
Участники (4)
Observer... (Соорганизатор, я)
Serik Polatuly
Hall-3, Jerneja Bogovic
Thushari Senevirathne
1 неназначенный участник
Звук
Видео
Участники
Чат
Отреагировать
Поделиться
Инструменты организатора
Дополнительно
Выйти из зала


The Relationship Between Education And Economic Development In Rural Area (Monaragala District)
Presented by: R.M.T.N. Senevirathne
M.A.Fathima Jeha
Участники (4)
Observer... (Соорганизатор, я)
Thushari Senevirathne
Hall-3, Jerneja Bogovic
Serik Polatuly
3 неназначенных участников
Звук
Видео
Участники
Чат
Отреагировать
Поделиться
Инструменты организатора
Дополнительно
Выйти из зала



Numerical Bifurcation Results for $N = 15$

The finite-dimensional system exhibits several candidate bifurcation points.

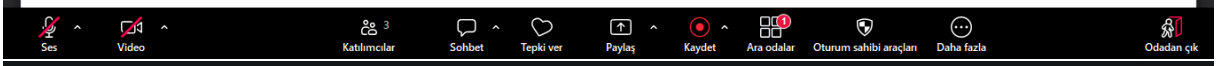
Quantity	Symbol	Reported value
Branch point	δ_{BP}	0.0024392115
Fold point	δ_{FP}	0.0071248606
Hopf-compatible threshold	δ_{H}	0.0084172404
Hopf frequency	ω_{H}	4.3588
Critical fractional order at $\delta = 0.005$	α_c	0.946628

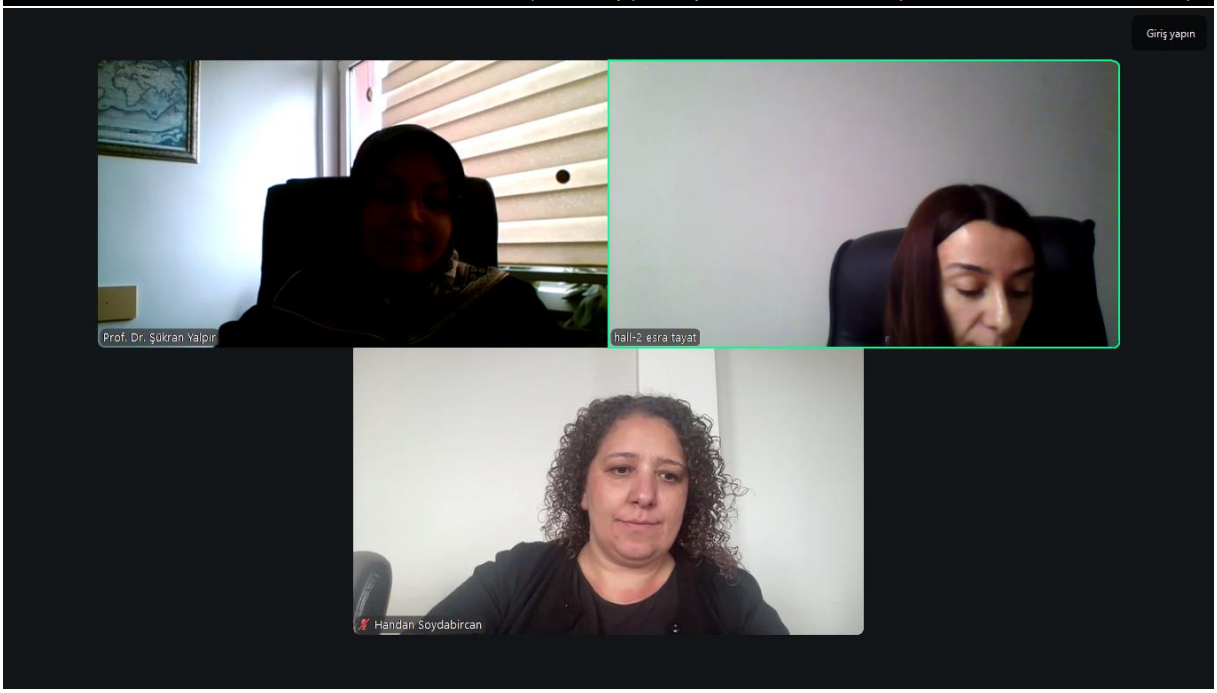
Observer Hall-2

Observer Hall-2

Important qualification

These values are numerical results for the discretized system with $N = 15$. They do not, by themselves, establish bifurcations of the continuous PDE.





CONTENT

CONFERENCES ID	**I**
PROGRAM	**II**
PHOTO GALLERY	**III**
CONTENT	**IV**

Author	Title	No
Yasemin HEKİMOĞLU Mine TUNÇOK SARIBERBEROĞLU	READING CLASS DIFFERENCE THROUGH SPACES IN LITERARY TEXTS	1
Ali FEYZI T.Didem AKYOL ALTUN	AN EVALUATION OF BIOLOGICAL STABILIZATION APPROACHES FOR COMPRESSED EARTH BUILDING SYSTEMS IN TERMS OF SUSTAINABILITY	11
Emin SARLI Gülşen YILDIZ	DEVELOPMENT OF AN INNOVATIVE SIZING FORMULATION TO REDUCE CHEMICAL CONSUMPTION AND WASTEWATER LOAD FOR SUSTAINABLE TEXTILE PRODUCTION	16
Emin SARLI Gülşen YILDIZ	INTEGRATION OF BIO-STARCH OBTAINED FROM FOOD WASTE INTO TEXTILE SIZING	14
Abdullah Kürşat DEMİR	ANALYTICAL INVESTIGATION OF THE P–Δ EFFECT ON THE NATURAL FREQUENCY BEHAVIOR OF HYBRID OFFSHORE WIND–HYDROKINETIC SYSTEMS	19
Muhammed ONAY	FIXED-BED COLUMN DYNAMICS FOR CONTINUOUS PB(II) SEQUESTRATION ONTO PEANUT SHELL BIOCHAR: INFLUENCE OF INFLUENT CONCENTRATION AND KINETIC BREAKTHROUGH MODELING	46
Ali DOGAN Mohammad Bilal JALALI	FINITE ELEMENT INVESTIGATION OF CFRP TEXTILE WRAPPING GEOMETRY AND STRIP WIDTH EFFECTS ON THE FLEXURAL BEHAVIOR OF REINFORCED CONCRETE BEAMS	57
Yiğithan YILMAZ	CONTRIBUTION OF CRITICAL SUCCESS FACTORS TO AGILITY IN PRODUCTION,	77

	R&D AND AFTER-SALES PROJECTS AND SECTORAL ANALYSIS WITH MULTI CRITERIA DECISION TECHNIQUES	
S. Suresh Krishna F. Joshwa Santhosh S. Selvam	BEYOND ARTIFICIAL INTELLIGENCE: EXPLORING THE RISE OF SYNTHETIC INTELLIGENCE	79
B.DHARSHINI S. Selvam	KOREA'S CULTURAL RENAISSANCE: THE EVOLUTION OF CINEMA AND K-POP	80
M. Dhinesh Kumar S. SELVAM	WAYS TO REDUCE AND RESOLVE MISUNDERSTANDINGS BETWEEN PEOPLE	85
Kamalbek BERKİMBAYEV Dinara BERDİ Sherzod RAMANKULOV Shakhrizada KHIKMATULLA Kazhymukan KELESBAYEV	DEVELOPING LEARNERS' SOFT SKILLS IN A STEM-BASED VIRTUAL LEARNING ENVIRONMENT	86
Yelmurat DOSYMOV Serik POLATULY Sherzod RAMANKULOV Shakhrizada KHIKMATULLA Munisa RAKHMATULLAEVA	STEM-BASED METHODOLOGICAL RECOMMENDATIONS FOR TEACHERS: DEVELOPING SOFT SKILLS IN NATURAL SCIENCE SUBJECTS	97
Ebole Alpha Friday Aremu Idris Abiodun Ayinde Yusuf Olatunji	AN INTEGRATED CYBERSECURITY FRAMEWORK FOR SECURING CONNECTED DIGITAL ECOSYSTEMS (DE)	112
Arypzhan ABEN Dinmukhammed GABDULLAULY	CLASSIFICATION OF CLOTHING TYPES USING A CONVOLUTIONAL NEURAL NETWORK: EXPERIMENTAL EVALUATION AND ERROR ANALYSIS ON THE MYNTRA FASHION PRODUCT IMAGES DATASET	113
Jerneja Bogovič	ASSESSMENT OF THE EXPLICIT FLEXIBILITY POTENTIAL OF SLOVENIAN BUSINESS CONSUMERS	114
Jerneja Bogovič	IMPACT OF HYDROLOGY AND THERMAL POWER PLANT AVAILABILITY ON RESOURCE ADEQUACY IN SLOVENIA	121
Olajide O. Ogunbodede	A GAME-THEORETIC INSIDER THREAT MITIGATION FRAMEWORK: LSTM-AUTOENCODER BASED USER BEHAVIOUR ANALYTICS APPROACH	127
Afaq AHMAD M Mohammed Sabir HUSSAIN	DESIGN AND SIMULATION-BASED EVALUATION OF AN LFSR-DRIVEN BUILT-IN SELF-TEST ARCHITECTURE FOR FAULT DETECTION USING VERILOG HDL	128
Tuğba Özcan	IMPROVEMENT OF ROLLED EDGE CORROSION RESISTANCE OF OUTER TIE-ROD	129
Ebru GÜDÜL Şükrü SARI Ayça ÖZEN	OPTIMIZATION OF FLAME-RETARDANT GRANULE PROCESSING PARAMETERS AND INVESTIGATION OF CPR FIRE	131

Samet DURMUŞ Onur ADIGÜZEL Ekrem ALTAN	REACTION PERFORMANCE IN H07Z-K CABLES	
Burcu Nilgün ÇETİNER Gökçen BAYRAM	VALORIZATION OF SHELL-BASED AGRICULTURAL RESIDUES INTO VALUE-ADDED ENGINEERING MATERIALS THROUGH INDUSTRIAL SYMBIOSIS IN TÜRKİYE: A CRITICAL ASSESSMENT OF TECHNICAL POTENTIAL, REGIONAL RESOURCE DISTRIBUTION, AND IMPLEMENTATION FEASIBILITY	133
İlayda DEMİR	HIGH TEMPERATURE BEHAVIOR OF CARBON FIBER REINFORCED EPOXYCOMPOSITES CONTAINING GRAPHENE AND H-BN HYBRID NANOFILLERS	135
Yaren DEVİREN	EVALUATION OF CAB MOUNT SELECTION FOR A BACKHOE LOADER BASED ON VIBRATION ISOLATION AND DESIGN CRITERIA	137
Oğuzhan CAN Baran BULUT Safa Melik TÜZÜNER Süreyya Ergün BOZDAĞ Emin SÜNBÜLOĞLU	AN EVALUATION OF IMPEDANCE MATCHING TECHNIQUES FOR SHPB TESTING OF LOW-IMPEDANCE SOFT MATERIALS	139
Baran BULUT Safa Melik TÜZÜNER Oğuzhan CAN Süreyya Ergün BOZDAĞ Emin SÜNBÜLOĞLU	DESIGN AND ANALYSIS OF VARIOUS CROSS-SECTION TRANSFORMING HORN DESIGNS FOR TESTING LOW-IMPEDANCE MATERIALS IN SPLIT HOPKINSON PRESSURE BAR SYSTEMS	141
Shayan Zulfiqar Omer Shujat Bhatti Syed Usman Raza Kazmi Nouman Zulfiqar Hamza Rashid	GRAVITY-LESS IN ARCHITECTURE AS A DESIGN PROBLEM: CASE STUDIES OF SINGAPORE NATIONAL STADIUM AND MERCEDES-BENZ STADIUM, ATLANTA	143
AKPAN CHRISTOPHER ANIEKAN	LEVERAGING DIGITAL TRANSFORMATION TO DRIVE SUSTAINABLE FOOD SYSTEMS IN AFRICA: A CASE STUDY OF MKPAT ENIN LOCAL GOVERNMENT AREA OF AKWA IBOM STATE, NIGERIA	144
Kater Titus A.J. Simon D.O. Alonge	ENHANCING SAFETY AND ACCESSIBILITY IN THE DESIGN OF A PUBLIC TRANSPORTATION HUB IN MINNA, NIGER STATE	145
Ali Akbar Firoozi Ali Asghar Firoozi	A DIMENSIONLESS HYDRO-MECHANICAL FRAMEWORK FOR SCREENINGRAINFALL-INDUCED SHALLOW SLOPE INSTABILITY: ANALYTICAL THRESHOLDS AND PARAMETRIC SENSITIVITY	147
Ali Akbar Firoozi Ali Asghar Firoozi	TRANSIENT WETTING AND REPEATED MOISTURE PULSES IN EXPANSIVE	161

	SUBGRADES: A DIMENSIONLESS SCREENING FRAMEWORK FOR VERTICAL HEAVE	
Ali Akbar Firoozi Ali Asghar Firoozi	DESIGN-TIME SCREENING OF RESIDUAL PRIMARY CONSOLIDATION IN SOFT CLAY UNDER STAGED EMBANKMENT LOADING: ANALYTICAL SUPERPOSITION AND SENSITIVITY MAPS	176
Ali Akbar Firoozi Ali Asghar Firoozi	DIMENSIONLESS SCREENING OF SOLUTE BREAKTHROUGH IN COMPACTED CLAY BARRIERS: HYDRAULIC–DIFFUSIVE COMPETITION AND EQUILIBRIUM SORPTION	190
Ali Akbar Firoozi Ali Asghar Firoozi	GROUNDWATER-SENSITIVE RELIABILITY SCREENING OF STRIP FOOTINGS ON SAND: A REPRODUCIBLE BEARING-CAPACITY DESIGN MAP	206
Ali Akbar Firoozi Ali Asghar Firoozi	GRAIN-SIZE COMPATIBILITY AND PRODUCTION TOLERANCE OF GRANULAR FILTERS FOR EMBANKMENT DAMS: A PARAMETRIC SCREENING FRAMEWORK	221
Khadija Zair M'hamed El Omari	SPECTRAL AND NUMERICAL ANALYSIS OF BIFURCATIONS AND COMPLEX DYNAMICS IN FRACTIONAL BURGERS EQUATIONS	237
Ouassila Riouchi Khalid Elkalay	MICROALGAE: TINY ORGANISMS WITH GREAT ENVIRONMENTAL POTENTIAL	238
Hajar Sadrati Youssef Arif Younes Abbas Sanaa Sabour-Alaoui Mohammed El idrissi	IN SILICO ANALYSIS OF MAJOR CONSTITUENTS OF THYMUS VULGARIS ESSENTIAL OIL AGAINST PENICILLIUM DIGITATUM: MOLECULAR DOCKING, MOLECULAR DYNAMICS, AND TOXICITY PROFILING	239
El Hassania El Hamzaoui Hind ElHamzaoui	UNDERSTANDING THE LOW APPEAL OF GEOSCIENCES IN THE MOROCCAN EDUCATION SYSTEM: A SURVEY OF PROSPECTIVE TEACHERS	241
Minahil Fatima Irfan Bashir Yasira Waqar	EXPLORING UNDERGRADUATE STUDENTS' EXPERIENCES OF PEER TUTORING AT HIGHER EDUCATION INSTITUTES: A QUALITATIVE PHENOMENOLOGICAL STUDY	242
Maryem Arraji Khaoula EL BARBI Fatima Zahra BOUCHACHI Mohamed Khalis Mohamed Chahboune	USE OF ARTIFICIAL INTELLIGENCE FOR MEDICATION ADHERENCE ASSESSMENT IN PATIENTS WITH TYPE 2 DIABETES: AN EXPLORATORY STUDY IN MOROCCO USING CHATGPT AND THE VALIDATED GENERAL MEDICATION ADHERENCE SCALE	243
Salihu SULEIMAN Aisha N. SULEIMAN	THE ENERGY PERFORMANCE GAP IN AFRICAN BUILDINGS: A COMPARATIVE ASSESSMENT OF BUILDING	245

	REGULATIONS, CLIMATE ZONES AND ENERGY-EFFICIENCY STRATEGIES IN NIGERIA AND SELECTED AFRICAN COUNTRIES	
Salihu SULEIMAN Gambo B. WURMA	NIGERIA'S ARCHITECTURAL TRANSITION TOWARDS NET-ZERO BUILDINGS: A BIBLIOMETRIC, POLICY AND GLOBAL BENCHMARKING ANALYSIS OF BUILDING ENERGY EFFICIENCY AND SUSTAINABLE DESIGN	246
OUNIS HADJ MOHAMED OUNIS ABDELHAFID	CONTEMPORARY SEISMIC ISOLATION TECHNIQUES: IMPLEMENTATION UNDER ALGERIAN REGULATION AND COMPARISON WITH INTERNATIONAL CODES	247
EWETOLA, E. A. AFOLORUNSO, G.T. JAYEOBA, A. D. OKE, S. A. AYENI, B. O.	ASSESSMENT OF SOIL LOSS FROM CARROT (DAUCUS CAROTA) AS INFLUENCED BY NPK 15:15:15 AND POULTRY MANURE	248
Olugbemi Victor EKUNDARE Oluwadamilare Emmanuel OBAYEMI	AQUACULTURE POTENTIALS of PARENTAL CLARIAS GARIEPINUS and BACKCROSS PROGENY DERIVED from FEMALE CLARIAS HETEROBRANCHUS HYBRID and MALE CLARIAS GARIEPINUS	249
Talip AKBIYIK Nafiz KAHRAMAN	EFFECTS OF BORON-BASED ADDITIVE CONCENTRATION ON THE PERFORMANCE OF A LOMBARDINI LGW 523 ENGINE FUELED WITH E0 AND E20: DETERMINATION OF OPTIMUM OPERATING CONDITIONS	251
Talip AKBIYIK Nafiz KAHRAMAN	EXPERIMENTAL INVESTIGATION OF THE EFFECTS OF TWO DIFFERENT BORON-BASED ADDITIVES ON THE PERFORMANCE OF A GASOLINE ENGINE AND DETERMINATION OF THE OPTIMUM ADDITIVE CONCENTRATION	270
Meriçsu KARAHAN Şölen ZENGİN	MACHINE LEARNING-BASED DEMAND FORECASTING FOR FOOD WASTE REDUCTION: A CASE STUDY	290
Yağmur ÇİÇEK Şölen ZENGİN	SUSTAINABLE RISK MANAGEMENT IN TEXTILE SECTOR: A MULTI-DIMENSIONAL FMEA APPROACH	291
Şükran YALPIR	AN EMPIRICAL EXAMINATION OF THE RELATIONSHIP BETWEEN ECONOMIC INDICATORS AND THE REAL ESTATE MARKET	292
Handan SOYDABİRCAN Şükran YALPIR Vildan ÖNEN	AN ANALYSIS OF THE ECONOMIC, SOCIAL, AND ENVIRONMENTAL IMPACTS OF THE REGIONAL TRANSFORMATION CAUSED BY CHANGES IN THE ROLE OF MINING ACTIVITIES IN ERMENEK'S REGIONAL	300

	ECONOMY AND THE CONSTRUCTION OF A DAM IN ERMENEK	
Nihal Özder Esra Tayat	DEFENSIVE BEHAVIOURS IN INSECTS	308
Esra Tayat Nihal Özder	CHEMICAL HOST-PLANT RECOGNITION AND FEEDING BEHAVIOR IN PHYTOPHAGOUS INSECTS	318
K.R.Padma K. Sri Vidya K.R.Don	GREENS FOR A HEALTHIER BRAIN: DIETARY FIBRE, THE GUT–BRAIN AXIS, AND NEUROPROTECTION FROM SPINACH AND AMARANTHUS	331
Imadojemu, P.E. Imadojemu, O.I.	MINERALOGICAL CHARACTERISTICS OF FLOODPLAIN SOILS IN SOUTHERN TARABA STATE NORTHEAST, NIGERIA	343
Ibrahim Sani Dikko	ARTIFICIAL INTELLIGENCE AND MULTI-OMICS INTEGRATION IN PRECISION MEDICINE: DECIPHERING MOLECULAR MECHANISMS OF DISEASE AND ADVANCING BIOMARKER-GUIDED THERAPEUTIC DEVELOPMENT	344
Iram Liaqat	INHIBITORY EFFICACY OF HONEY AGAINST MULTISPECIES BACTERIAL BIOFILM	346
Vilma Šalkauskienė Daiva Gudritienė	ASSESSMENT OF URBANIZATION DYNAMICS IN SUBURBAN AREAS IN LITHUANIA USING GIS-BASED MONITORING	347
ASABE EDWARD BASH CHRISTIANA DAVID DALOK	EFFECTS OF PERSONALISED LEARNING METHOD ON THE ACHIEVEMENT OF STUDENTS IN JOS NORTH LOCAL GOVERNMENT AREA, PLATEAU STATE, NIGERIA	250
Mustapha Oukbab	MACHINE LEARNING-ENHANCED CLASSIFICATION AND ANALYSISOF MODIFIED CARBON PASTE ELECTRODES FOR METHANOL FUELCELL APPLICATIONS	348
DJEBBARA BENZERGA FAYCAL SOTEHI NOUREDDINE BOUALEM	NUMERICAL ASSESSMENT OF HYDROGEN EMBRITTLEMENT SUSCEPTIBILITY IN API 5L PIPELINE STEELS FOR HYDROGEN TRANSPORT	349
Ilyasse Joubbi Fatima Aqel Nour Eddine Alaa	PHYSICS-INFORMED NEURAL APPROXIMATION OF DISCRETE ANISOTROPIC VARIABLE-EXPONENT PROBLEMS	351
Mediha Gürel Fatih Özoğul	METHODOLOGICAL ADVANCES IN PATIENT-DERIVED GLIOBLASTOMA ORGANOIDS, EXTRACELLULAR VESICLES, AND CAR-T CELL THERAPY	353
Mediha Gürel Fatih Özoğul	METHODOLOGICAL ADVANCES IN THE PRODUCTION OF CULTURED SEAFOOD AND ITS POTENTIAL IN THE FOOD	355

	INDUSTRY	
Azad Bayramov Michail Awtushko	ATMOSPHERIC FACTORS AND THE DYNAMICS OF RADON EMISSION IN SOIL	357
Recep GÜNENÇ Hasan KASIM	EXPERIMENTAL INVESTIGATION OF THE GEOMETRIC BEHAVIOR OF AN AXLE LIFT AIR SPRING UNDER STATIC PRESSURE VARIATION USING 3D LASER SCANNING AND CROSS-SECTIONAL SYMMETRY CENTER DISPLACEMENT METHOD	369
Keziban ÇAKMAKTAŞI HULUD BAYRAM	REUSE OF SUGAR BEET WASTE IN THE TEXTILE INDUSTRY: EVALUATION AS A DYEING AGENT	371
Berkay ARSLAN Nilüfer DUYGULU	THE EFFECTS OF ZnO AND MnO ADDITIONS ON THE MORPHOLOGY AND FIBER DIAMETER DISTRIBUTION OF PVA-BASED ELECTROSPUN NANOFIBERS	378
Oduntan. A.S. Adewale. V.O.	GREEN SYNTHESIS OF BIMETALLIC ZIRCRONIUM-COPPER NANOPARTICLES USING BAUHINIA MONANDRA LEAF EXTRACT: INVESTIGATION OF ITS ANTIBACTERIAL PROPERTIES	380
Kamal BOUCHIT Jilali ABOUIR Abderrahim CHARKAOUI Anouar BEN-LOGHFYRY	CONTRIBUTION TO THE MATHEMATICAL ANALYSIS OF SOME NONLINEAR PDES ARISING FROM ELECTRORHEOLOGICAL FLUIDS MODELING	381
Faruk AHMETI Kushtrim GASHI	THE INFLUENCE OF DIGITAL MARKETING CAPABILITIES ON CUSTOMER LOYALTY: THE MEDIATING EFFECTS OF CUSTOMER ENGAGEMENT AND BRAND TRUST	382
Tabussam Tufail Huma Bader Ul Ain Farhan Saeed Muhammad Afzaal Tanazzam Tufail Muhammad Umair Arshad	GLOBAL HEALTH CHALLENGES AND OUR RESPONSE: SPECIAL FOCUS TO PAKISTAN	383
Ahmed Osmane Khadija Zidan Hasnae Sabri Moustapha Belmouden	SUSTAINABLE WATER MANAGEMENT UNDER CLIMATE STRESS: EVIDENCE FROM MARRAKECH ON TREATED WASTEWATER IRRIGATION, SOIL FERTILITY, AND MAIZE AGRO-PHYSIOLOGY	384
Ahmed Osmane Khadija Zidan Hasnae Sabri Moustapha Belmouden	SYNTHESIS AND ADSORPTION PERFORMANCE OF POZZOLAN–ALGINATE COMPOSITE BEADS TOWARD OLIVE OIL POLYPHENOLS	386
Seyit AKPANCAR Eyüp ÇAKI	COMPARATIVE EVALUATION OF OBSTACLE AVOIDANCE AND PATH PLANNING ALGORITHMS FOR AUTONOMOUS UAVS IN A ROS-GAZEBO SIMULATION ENVIRONMENT	387

Burcu DURMUŞ	EFFECTS OF RESAMPLING METHODS ON MACHINE LEARNING PERFORMANCE IN HEALTH DATA: A DERMATOLOGICAL APPLICATION	400
Ömer SEVİNÇ	A LAYERED CYBERSECURITY MODEL FOR ZERO TRUST AND AI-BASED ANOMALY DETECTION IN HYBRID WORK ENVIRONMENTS	410
Ömer SEVİNÇ	A HUMAN–MACHINE COLLABORATION MODEL FOR ORGANIZATIONAL DEFENSE AGAINST GENERATIVE AI-ENABLED PHISHING	417
Cem ALİŞEN Fikri GÖKPINAR	PERFORMANCE ANALYSIS OF MISSING DATA IMPUTATION METHODS	424
Meral ERGÜN Mustafa KURBAN Erchin SERPEDIN Buket DOĞAN	TRANSFERABILITY OF SQL SERVER MEMORY SETTINGS ACROSS WORKLOADS	426
İbrahim Akdeniz Halil Erdi Gülcan Samet Çelebi Emrah Arda	THE EFFECT OF USING DIFFERENT TYPES OF BORON FUEL ADDITIVES ON ENGINE PERFORMANCE AND EXHAUST EMISSIONS IN A GASOLINE ENGINE	435
Deniz ÇOBAN ÖZKAN Fikret SÖNMEZ	SURFACE ROUGHNESS AND TOOL WEAR IN HELICAL RAMPING POCKET MILLING OF TI-6AL-4V ELI (GRADE 23)	448
Bogdan-Catalin SERBAN Maria Ruxandra SALAGEAN Matei-Gabriel URSACHESCU Vlad DİACONESCU Caterina ZETU Diana DUMITRAŞCU Maria Ruxandra DİMA Marius BUMBAC	BILIRUBIN IN THE HUMAN BODY: FROM A WASTE PRODUCT TO AN ENDOGENOUS ANTIOXIDANT	457
Bogdan-Catalin SERBAN Maria Ruxandra SALAGEAN Matei-Gabriel URSACHESCU Vlad DİACONESCU Caterina ZETU Diana DUMITRAŞCU Maria Ruxandra DİMA Marius BUMBAC	D-AMINO ACIDS IN THE HUMAN BODY: EXCEPTIONS TO THE RULE OF BIOLOGICAL HOMOCHIRALITY	459
Bogdan-Catalin SERBAN Maria Ruxandra SALAGEAN Matei-Gabriel URSACHESCU Vlad DİACONESCU Caterina ZETU Diana DUMITRAŞCU Maria Ruxandra DİMA Marius BUMBAC	CYANIDE IN THE FOODS WE EAT: NATURAL PLANT DEFENSE, HUMAN TOXICITY, AND DETOXIFICATION	461
Bogdan-Catalin SERBAN Maria Ruxandra SALAGEAN Matei-Gabriel URSACHESCU Vlad DİACONESCU	WHY DOES THE HUMAN BODY PRODUCE FORMALDEHYDE? FROM A TOXIC CHEMICAL TO AN ENDOGENOUS METABOLITE	463

Caterina ZETU Diana DUMITRAȘCU Maria Ruxandra DİMA Marius BUMBAC		
Bogdan-Catalin SERBAN Maria Ruxandra SALAGEAN Matei-Gabriel URSACHESCU Vlad DİACONESCU Caterina ZETU Diana DUMITRAȘCU Maria Ruxandra DİMA Marius BUMBAC	WHY CAN GRAPEFRUIT TURN A SAFE MEDICINE INTO A DANGEROUS ONE? CHEMISTRY AND BIOCHEMISTRY OF A CLASSIC FOOD–DRUG INTERACTION	465
Bogdan-Catalin SERBAN Maria Ruxandra SALAGEAN Matei-Gabriel URSACHESCU Vlad DİACONESCU Caterina ZETU Diana DUMITRAȘCU Maria Ruxandra DİMA Marius BUMBAC	THE CHEMISTRY OF HUMAN BODY ODOR: WHY DO WE SMELL AND WHY DOES OUR SMELL CHANGE WITH AGE?	467
Bogdan-Catalin SERBAN Maria Ruxandra SALAGEAN Matei-Gabriel URSACHESCU Vlad DİACONESCU Caterina ZETU Diana DUMITRAȘCU Maria Ruxandra DİMA Marius BUMBAC	HYDROGEN SULFIDE IN THE HUMAN BODY: FROM A TOXIC GAS TO AN ESSENTIAL BIOLOGICAL MESSENGER	469
Jatinkumar Bhimjibhai Kotadiya	ZERO-/FEW-SHOT MULTILINGUAL STUDENT FEEDBACK ANALYSIS IN LOW-RESOURCE LANGUAGES USING LIGHTWEIGHT TRANSFORMER VARIANTS FOR MOBILE EDUCATIONAL PLATFORMS	471
Efra KALKAN Ayşe Nuray CANAT	PIEZOELECTRIC ENERGY HARVESTING SYSTEMS IN HIGH-DENSITY PEDESTRIAN AREAS: LITERATURE REVIEW AND MECHANISM CLASSIFICATION	472
Ahmet TURGUT Muhammet Rıza KARADAVUT	EFFECTS OF PHASE QUANTIZATION ON POINTING ERROR AND POWER LOSS IN THE TARGET DIRECTION OF AN IDEAL UNIFORM LINEAR ANTENNA ARRAY	474
Ahmet TURGUT Muhammet Rıza KARADAVUT	POLARIZATION SELECTION IN PASSIVE UHF RFID SYSTEMS BASED ON TAG ORIENTATION DISTRIBUTION AND POWER MARGIN	486
Özgür TAMER Ömür ÖCAL Mehmet ÖZTEMEL	DESIGN OF A PORTABLE DEVICE BASED ON DOUBLE-BLIND PAIRING FOR THE CHARACTERIZATION OF PIEZO HAPTIC SIGNALS	499
Beliz HÜNKAR Ahsen RAYMAN ERGÜN Neslihan ÇOLAK	EVALUATION OF THE PHYSICAL, TEXTURAL AND SENSORY PROPERTIES OF SNACK PROTEIN BARS ENRICHED	508

	WITH APPLE AND GRAPE POMACE	
Ekin Emek DİLBAZ Ersin SAYAR	NUMERICAL INVESTIGATION OF NUCLEATE FLOW BOILING OF R744 UNDER CONSTANT HEAT FLUX	519
Melike YAPAR İkbal ESKİ	COMPARISON OF THE PERFORMANCE OF METAHEURISTIC OPTIMIZATION-BASED PID CONTROLLERS FOR A QUADROTOR UAV UNDER DIFFERENT FLIGHT SCENARIOS	520
Ali CELEN	A BRIEF REVIEW OF NUSSELT NUMBER CORRELATIONS DEVELOPED FOR TRIPLY PERIODIC MINIMAL SURFACES	522

EDEBİ METİNLERDE MEKANLAR ÜZERİNDEN SINIF FARKININ OKUNMASI

READING CLASS DIFFERENCE THROUGH SPACES IN LITERARY TEXTS

Yasemin HEKİMOĞLU
Dr., Bolu Abant İzzet Baysal Üniversitesi, Mimarlık Fakültesi, Mimarlık Fakültesi.
Ph.D., Bolu Abant Izzet Baysal University, Faculty of Architecture, Department of Architecture.
ORCID ID: 0000-0001-8830-3724

Mine TUNÇOK SARIBERBEROĞLU
Doç. Dr., Bolu Abant İzzet Baysal Üniversitesi, Mimarlık Fakültesi, Mimarlık Fakültesi.
Assoc. Prof. Dr., Bolu Abant Izzet Baysal University, Faculty of Architecture, Department of Architecture.
ORCID ID: 0000-0002-6931-0539

ÖZET

Toplumsal üretimin bir parçası olan mekan, edebi metinlerde yalnızca olayların geçtiği bir arka plan olarak değil; toplumsal yapı, kültürel değerler, sınıfsal ayrımlar ve gündelik yaşam pratikleri hakkında anlam üreten etkin bir anlatı unsuru olarak nitelenmektedir. Mimarlık ve edebiyatın kesişiminde konumlanan bu çalışma, mekanın fiziksel nitelikleri aracılığıyla sosyal gerçekliğin nasıl görünür hale geldiğine odaklanmakta ve edebiyatın mekan tasvirinin ötesine geçen bir veri kaynağı olma özelliklerini tartışmaktadır. Edebi metinlerde ev, mahalle, sokak, oda, eşya ve yapı malzemesi gibi unsurlar; kullanıcılarının ekonomik imkanlarını, yaşam biçimlerini, toplumsal konumlarını ve kültürel dünyalarını aktaran göstergeler olarak okunabilmektedir. Bu yönüyle mekan, sınıfsal hiyerarşileri, güç ilişkilerini, dışlanma biçimlerini ve toplumsal mesafeleri anlatının içinde taşıyan bir bilgi alanına dönüşmekte; mimari mekan da sosyal ilişkileri düzenleyen, kültürel anlamları görünür kılan ve toplumsal ayrımları kodlayan bir temsil düzlemi olarak konumlanmaktadır. Yapılan çalışmada bu ilişki, Suat Derviş'in Sınır romanı üzerinden bir durum çalışması olarak ele alınmakta; mekansal konum, yapı niteliği, iç düzenleme, malzeme, bakım durumu ve çevresel doku gibi mimari unsurların, karakterlerin toplumsal statüsü ve yaşam koşulları hakkında ne tür veriler sunduğu değerlendirilmektedir. Böylece edebiyatın, mimarlık disiplininin tek başına erişmekte zorlanabileceği gündelik yaşam deneyimlerini, mekansal eşitsizlikleri ve dönemin sosyal-kültürel atmosferini aktaran özgün bir kaynak olduğu tartışmaya açılacaktır.

Anahtar Kelimeler: Mekan temsili, toplumsal mekan, edebi mekan, sosyal statü, sınıf farkı.

ABSTRACT

As an integral component of social production, space in literary texts is not merely a passive backdrop against which events unfold; rather, it is an active narrative element that generates meaning about social structure, cultural values, class distinctions, and everyday practices. Situated at the intersection of architecture and literature, this study examines how social reality becomes discernible through the physical qualities of space and how literature can function as a data source that extends beyond mere spatial depiction. In literary texts,

elements such as the house, the neighborhood, the street, the room, furnishings, and building materials can be read as signifiers that convey their inhabitants' economic means, ways of living, social positions, and cultural worlds. In this respect, space becomes a domain of knowledge that embeds class hierarchies, power relations, forms of exclusion, and social distance within the narrative; architectural space, in turn, functions as a representational plane that regulates social relations, renders cultural meanings visible, and encodes social distinctions. In this study, this relationship is examined through Suat Derviş's novel Sınır, evaluating what data architectural elements such as spatial location, structural quality, interior arrangement, material, state of maintenance, and surrounding texture provide about the characters' social status and living conditions. In doing so, the study argues that literature offers a distinctive source for capturing everyday life experiences, spatial inequalities, and the period's socio-cultural atmosphere—dimensions that architecture may struggle to access on its own.

Keywords: Spatial representation, social space, literary space, social status, class distinction.

GİRİŞ

Mimarlık ve edebiyat, toplumsal gerçekliği anlamlandırma ve aktarma bakımından ortak bir zeminde buluşmaktadır. Mimarlık; malzeme, form ve mekansal düzenlemeler aracılığıyla fiziksel bir çevre inşa ederken, aynı zamanda içinde bulunduğu toplumun değerlerini, hiyerarşilerini ve gündelik yaşam pratiklerini de görünür kılan bir söylem üretmektedir. Spurr (2012) bu ilişkiyi, mimarlık ve edebiyatın yalnızca ortak temalar paylaşan sanat biçimleri olmadığını, modernitenin yol açtığı anlam krizine karşı geliştirilmiş birbirine bağlı iki anlatı pratiği olduğunu öne sürerek temellendirmektedir. Benzer biçimde Szpakowska-Loranc (2019), alıntı, metafor ve bakış açısı gibi anlatısal araçların hem mimari hem edebi üretimde ortak bir işlev gördüğünü, bir yapının da tıpkı bir metin gibi kendi sözdizimine ve anlambilimine sahip olabileceğini vurgulamaktadır. Topolovská (2022) ise mimarlık kuramındaki metinsel dönüş ile edebiyat kuramındaki mekansal dönüşün birbirini besleyen paralel süreçler olduğunu belirterek, çizim ve maket gibi geleneksel temsil araçlarının mekanın duygusal ve deneyimsel katmanlarını aktarmakta yetersiz kalabildiğini, iki disiplinin güçlü bir bağ kurduğunu ve birbirlerini önemli anlamlarda tamamladığını iddia etmektedir. Bu birbirini tamamlama sürecinde, mimarlığın metin kullanarak çok katmanlı hale gelmesi dışında edebiyatın da mimarlığı yeniden dönüştürdüğü görülmektedir. Edebiyatla birlikte mekansal bilgi sadece aktarılmaz aynı zamanda yeniden üretilip, dolaşıma girer (Pocock, 1981). Bu sebeple, iki disiplin çerçevesinde yapılan araştırmaların içeriğinin zengin bir potansiyele sahip olduğu, bu kapsamda ele alınan tartışmaların çok katmanlı nitelik kazandığı değerlendirilmektedir.

Toplumu ve sınıf farkını ele alan bu çalışma, öncelikle kullanıcıya yani bireye odaklanmaktadır. Mekan hem toplumun bir parçası olma hem de bulunduğu coğrafyanın toplumunu yansıtma özellikleriyle toplumsal bir ürün olarak tanımlanırken (Lefebvre, 2014; Harvey, 2019); toplumda yaşayan bireyler de mekanı şekillendiren ve mekanla şekillenen

kullanıcılar olarak nitelenmektedir. Kullanıcı mekan içerisinde yalnızca eylemleriyle değil, duyuları, duyguları, hafızası, kimliği, cinsiyeti, statüsü gibi birden fazla parametrelerin etkisiyle varolmaktadır (Massey, 1994; Pallasmaa, 2006; Foucault, 2011; Merleau-Ponty, 2017). Bu sebeple, mekan analizi çalışmaları bu çok katmanlı ve çok yönlü durumu göz önünde bulundurmalı ve süreci buna göre yönetmelidir.

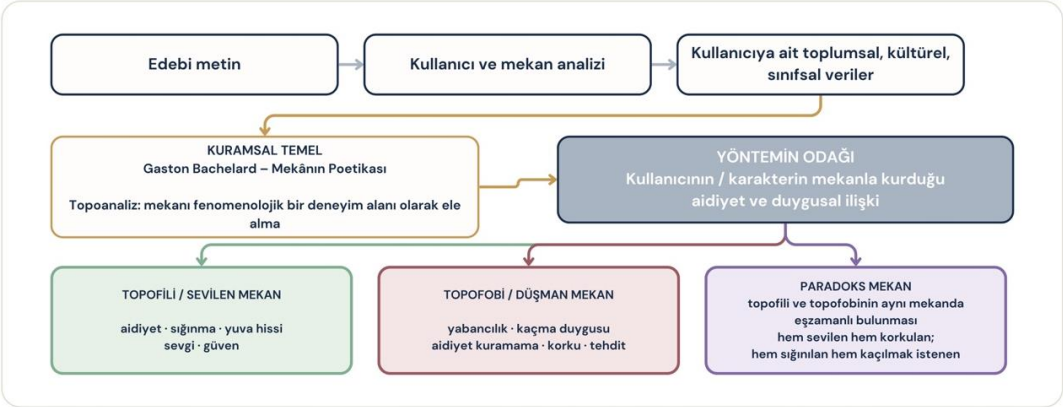
Bu çalışma, söz konusu çok katmanlı ilişkiden hareketle edebi metinlerdeki mekan tasvirlerini yalnızca anlatının arka planı olarak değil, kullanıcının toplumsal konumunu ve yaşam koşullarını okunabilir kılan mimari bir veri kaynağı olarak ele almayı amaçlamaktadır. Bu doğrultuda çalışmanın kapsamı, Suat Derviş'in (2021) *Sınır* (1943) romanı üzerinden ele alınmakta; romanda yer alan mekanlar, mekansal konum, yapı niteliği, iç düzenleme, malzeme, bakım durumu ve çevresel doku gibi niteliklerin yanı sıra başkarakterin konumu, statüsü ve kullandığı mekanların mekan analizi gerçekleştirilmektedir.

Çalışmanın temel hipotezi, edebi metinlerde mekanın fiziksel niteliklerinin rastlantısal biçimde aktarılmadığı; aksine karakterlerin ekonomik imkanlarını, toplumsal statülerini ve kültürel dünyalarını görünür kılan, sınıfsal ayrımları ve toplumsal mesafeleri kodlayan bir anlatı stratejisi olarak kurgulandığıdır. Bu hipotez doğrultusunda çalışma, mimari unsurların karakterler hakkında hangi tür bilgileri ilettiğini, bu bilgilerin sınıfsal farkı nasıl temsil ettiğini ve edebi metnin bu yönüyle mimarlık araştırmalarına nasıl bir veri sunabileceğini sorgulamaktadır. Mimarlık disiplininin tek başına erişmekte zorlandığı gündelik yaşam deneyimlerine, mekansal eşitsizliklere ve dönemin sosyal-kültürel atmosferine edebiyat aracılığıyla ulaşılabileceğini göstermek, bu çalışmanın literatür için önemini tanımlamaktadır. Plan, kesit ve fotoğraf gibi geleneksel belgeler mekanın biçimsel ve teknik özelliklerini aktarabilirken, mekanın kullanıcısı için ne ifade ettiğini, kimler için erişilebilir ya da kapalı olduğunu ve gündelik hayatta nasıl deneyimlendiğini çoğunlukla ortaya koyamamaktadır. Üstelik günümüze ulaşmamış ya da dönüşmüş mekanlar söz konusu olduğunda edebi metinler, bu eksikliği giderebilecek nitelikte bir kaynak olarak öne çıkmaktadır. Literatürde mimarlık ve edebiyat ilişkisi ağırlıklı olarak ortak anlatı araçları, kuramsal paralellikler ve temsil biçimleri üzerinden tartışılırken; bu çalışma ilişkiyi kullanıcı ve sınıf ekseninde ele almakta, edebi mekanı toplumsal ayrımların okunabileceği bir analiz alanı olarak konumlandırmaktadır. Böylece çalışmanın literatüre katkısı üç noktada toplanmaktadır: edebi metni mimari analizde tamamlayıcı bir veri kaynağı olarak tartışmaya açması, mekansal ögeleri sınıfsal ve toplumsal statü göstergeleri olarak okumaya olanak tanıyan bir çerçeve önermesi ve Türk edebiyatından bir örnek üzerinden bu çerçevenin işleyişini göstermesi. Bu yönüyle çalışma, mekanı yalnızca fiziksel bir çevre olarak değil, kullanıcısının toplumsal konumunu, yaşam koşullarını ve kültürel dünyasını taşıyan bir temsil alanı olarak ele almakta; mimarlık ve edebiyat arasındaki ilişkiye kullanıcı ve sınıf ekseninde yeni bir okuma olanağı sunmaktadır.

YÖNTEM

Edebi metinler üzerinden mekan analizine odaklanan bu çalışma, edebi mekanların içinde barındırdığı veri potansiyelleriyle ilgilenmekte, söz konusu potansiyelleri etkin bir biçimde

kullanmak için yöntem sunmayı amaçlamakta ve nitel araştırma kapsamında değerlendirilmektedir. Önerilen okuma yöntemi tasarlanırken, Gaston Bachelard'ın 1957'de Mekanın Poetikası (2013; 2014) adlı eserinde ele aldığı topoanaliz (mekan çözümleme) yöntemi referans alınmaktadır. Topoanaliz, kullanıcının mekanla duyduğu aidiyet hissi üzerinden mekanı çözümler. Bachelard (2013; 2014) topoanaliz yönteminde mekanı fenomenolojik bir deneyim alanı olarak kurgularken, aynı zamanda mekanı *sevilen mekan* ve *düşman mekan* (sevilmeyen mekan) olarak tanımlar ve sevilen mekanları topofili mekanlar (*topophilia*) olarak adlandırır. Yi-Fu Tuan (1990; 2013), topoanaliz yönteminin mekan çözümlemede çok kritik değerler taşıdığını vurgular fakat, bu analizleri topofili üzerinden değil zıttı olan düşman mekanlar üzerinden ele alır ve bu mekanları topofobi (*topophobia*) olarak adlandırır. Tuan'ın (1990) çalışmalarının ardından topoanaliz kapsamında topofili ve topofobi analizlerinin gerçekleştiği çalışmalara rastlanmaktadır (Brisudová, Chataway ve Moir, 2024; Çakmaker ve Ergelen, 2025; Paquet, 2024). Genel olarak bakıldığında, sevilen, aidiyet duyulan, sığınılan ve yuva hissi veren mekanlar topofili; yabancılık hissi veren, kaçma duygusu uyandıran, aidiyet hissettirmeyen, korkulan mekanlar ise topofobi olarak değerlendirilmektedir. Her iki duyguyu aynı anda barındıran, hem topofili hem de topofobi olarak tanımlanan mekan analizlerine de rastlanmakta; bu mekanlar yapılan çalışmalarda *paradoks mekan* olarak ele alınmaktadır (Şekil 1) (Brisudová ve diğerleri, 2024; Çakmaker ve Ergelen, 2025; González, 2005).



Şekil 1. Çalışmanın yöntem şeması.

Yapılan çalışma, topoanalizdeki söz konusu topofili, topofobi ve paradoks mekan kavramlarını ele alarak Sınır romanındaki Ayla karakterinin kullandığı mekanlar analiz edilmektedir. Karakter ve romanın tek bir örnek üzerinden seçilme sebebi ise yöntemin okunurluğu ve etkisi üzerinde yoğunlaşma amacına dayanmaktadır.

EDEBİ MEKAN ANALİZLERİ

Mimarlıkta ele alınan mekan kuramlarına bakıldığında bireyin çoğu zaman genel ve nötr olarak değerlendirildiği görülmektedir. Bu çalışmalarda mekan kullanıcısı; özne, beden, kişi gibi tanımlarla ele alınırken (Foucault, 2011; Merleau-Ponty, 2017), sunulan teori de bu tanımlar kadar genellenen ifadeler olmaktadır. Bu durumun aksine kullanıcıyı flanör (Benjamin, 1993), işçi sınıfı (Lefebvre, 2014), kadın özne (Braidotti, 2017) gibi farklı

kategorilerde ele alıp, bu sınıflandırmaya uygun biçimde teori üreten çalışmalara rastlamak da mümkündür. Bunlar arasında Lefebvre (2014), işçi sınıfının kamusal mekan kullanımına odaklanırken, aynı zamanda bu mekanların erişilebilirliğini de tartışmaktadır. Benzer durum edebi metinlerin mekan analizlerinde de kendini göstermektedir. Söz konusu mekan analizleri yapılırken, mekanın fiziksel ve duyusal özellikleri detaylı incelenmekte fakat kullanıcı daha yüzeysel ele alınmaktadır. Bu tür analizlerde kullanıcının da çok katmanlı biçimde tartışılması, mekan analizinin doğru veriler üretmesi bakımından önem arz etmektedir.

Edebi metinler üzerinden mekan okumaları, coğrafya disiplininde 19. yüzyıl romanlarına kadar uzanmaktadır (Brosseau, 2017). Coğrafyacılar romanları mekansal bilgiyi ve bir yerin kültürel ve duyusal özelliklerini kavramak için bir araç olarak kullanmıştır (Alexander, 2015; Porteous, 1985). Pocock (1981) ise romanla coğrafya arasındaki ilişkiyi, romanın atmosferi yansıtması, coğrafi gerçekliği sorgulaması ve veri kaynağı olarak kullanılması şeklinde üç yaklaşım altında ele almıştır. Edebi metinlerin mekan çalışmalarında veri kaynağı olarak kullanımı Türkiye'de de giderek artmaktadır. Serin Güner ve Gökmen (2020), YÖK Ulusal Tez Merkezi'nde 1987-2020 yılları arasında mimarlık ve edebiyat ilişkisini ele alan 125 tezi sınıflandırarak bu kesişim alanının disiplinlerarası verimliliğini göstermiştir. Genel olarak bakıldığında hem ulusal hem de uluslararası çalışmalar, mimarlık ve edebiyat bağlamında ele alınan araştırmaları verimli bulmaktadır.

Türkiye bağlamında ise edebi metni birincil veri kaynağı olarak kullanan, mimarlık disiplini içinden ve toplumsal cinsiyet ile statü değişkenlerini birlikte analiz eden çalışmaların sınırlı kaldığı görülmektedir. Bu çalışma, söz konusu boşluktan hareketle kadın özneyi ve statü değişkenini edebi mekan analizinin merkezine almaktadır. Kadınların kamusal mekan deneyimi sınıfsal konuma göre farklılaşmakta, aynı kadın karakter bile bulunduğu mekana göre aidiyet ya da yabancılık hissedebilmektedir. Bu nedenle statü, analizde sabit bir arka plan olarak değil, mekanın nasıl deneyimlendiğini belirleyen bir değişken olarak ele alınmaktadır. Kullanıcıyı işçi sınıfı olarak ele alan kuramlar (Lefebvre, 2014) mekana erişimin eşitsiz dağılımını görünür kılmışken, bu çalışma yüksek statülü bir kadın karakterin kamusal mekan kullanımına odaklanarak ayrıcalıklı konumun da mekansal özgürlüğü kendiliğinden güvence altına almadığı olasılığını sınamaktadır. Böylece *Sınır* romanındaki Ayla karakteri, topoanalizin topofili, topofobi ve paradoks mekan kavramları üzerinden okunmakta; kamusal açık alan olan mahalleler, eğlence, eğitim ve ulaşım mekanları gibi kamusal alanlarda hangi koşullarda aidiyet, hangi koşullarda dışlanma ve korku deneyimlendiği çözümlenmektedir. Bu yönüyle analiz, edebi mekanı yalnızca tematik ya da sembolik düzeyde yorumlamanın ötesine geçerek, kadın öznenin toplumsal cinsiyet rolleri ve statüsüyle şekillenen mekansal deneyimini okunabilir kılmayı amaçlamaktadır.

SINIR ROMANININ SINIF FARKI ODAĞINDA MEKAN ÇÖZÜMLEMESİ

Suat Derviş (Hatice Saadet Baraner), Cumhuriyet'in kuruluş sürecine tanıklık etmiş, 1972'de hayatını kaybetmiş bir yazar ve gazetecidir. Gazetecilik kariyeri, yazarlığının biçimlenmesinde belirleyici rol oynamıştır. 1926'da İkdam gazetesinde kadın sayfası hazırlayarak Türk basınında öncü olmuş, Lozan ve Montrö konferanslarını izleyen ilk Türk

kadın muhabiri olmuştur (Çekin Işık, 2021). 1930'lardaki röportajları ve 1937'deki Sovyetler Birliği gezisinin ardından toplumcu gerçekçi bir çizgi benimsemiş, eşi Reşat Fuat Baraner'le birlikte Yeni Edebiyat Dergisi'ni (1940-1941) yayımlamıştır. Elliden fazla eseri bulunan Derviş'e göre edebiyat, sosyal hayatı olduğu gibi aktardığında doğruya ulaşır (Kaya, 2018). Karakterlerini ideolojik semboller olarak değil, açlık, yalnızlık ve dışlanmışlıkla boğuşan gerçek bireyler olarak kurgular (Lordoğlu, 2024). Gazetecilikten gelen gözlem gücü, İstanbul'un yoksul semtlerini ve kenar mahalle hayatını bir sosyal belge titizliğiyle eserlerine taşımasını sağlamıştır.

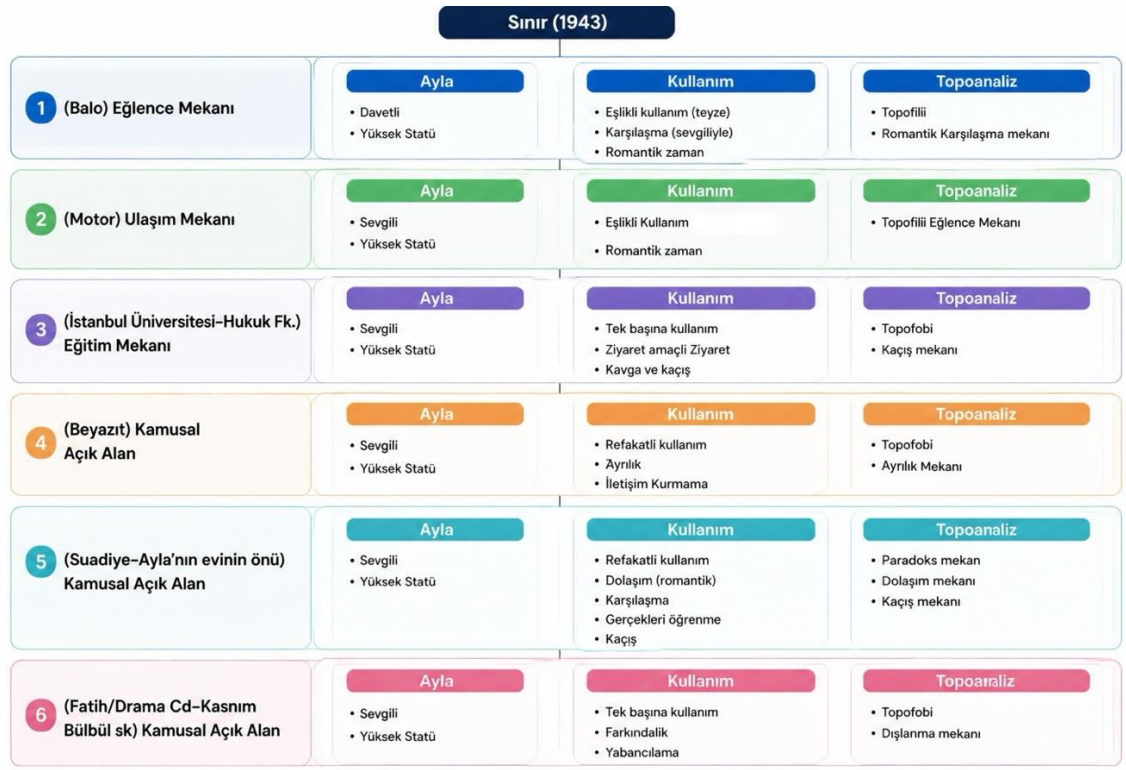
Derviş'in 1943-1944 yıllarında tefrika edilen Sınır romanı, İkinci Dünya Savaşı yıllarında geçmektedir. Romanın merkezinde varlıklı bir ailenin kızı olan Ayla ile son derece yoksul bir genç olan Osman arasındaki aşk yer alır. Ayla ve Osman, sınıfsal farka rağmen bir arada olabileceklerine inanır. Ayla'nın hikayesi, aşkın peşinden kendi çevresinin dışına çıktıkça Suadiye'deki evinin sokaklarından Beyazıt'a, Hukuk Fakültesi'ne ve Fatih'teki Draman Caddesi'ne uzanır. Ayla, başta Osman'ın yoksul olduğunu bilmez ve öğrenince yine de ilişkisine devam etmek ister. Tüm şartlara ve ihtimallere rağmen Osman'dan vazgeçmek istemez ve beraberlik için ısrarcı olup, herkesi karşısına alır. Fakat Ayla, Osman'ın yoksulluk seviyesini yanlış tahmin etmektedir. Çünkü kendisi daha önce yoksul biriyle tanışmamış, düşük statü olarak konumlanabilecek bir mekanda bulunmamıştır. Her şeyi bırakıp, Osman'ın mahallesine gidince aradaki farkı anlamaya başlar. Hikayenin sonunda Osman'ın evini gören Ayla, bu mekanda yaşayamayacağını ve ilişkiyi yürütemeyeceğini idrak ederek, ilişkisini sonlandırır.

Sınır romanı odağında aşk hikayesi gibi görünse de baskın bir sınıf farkını aktarmaktadır. Bu sınıf farkı da sadece karakterler üzerinden değil; ev içi mekanlardan mahallelere, ulaşım mekanlarından eğlence mekanlarına kadar kendini göstermektedir. Bu sayede sınıfsal ayrım, yalnızca kişiler arasındaki ilişkilerde değil, semtlerin, sokakların ve yapıların niteliğinde de okunabilir hale gelmektedir. Roman, mekanın sınıfsal konumu nasıl kodladığını ve aynı kentin farklı sınıflar için nasıl farklı deneyimlendiğini izlemeye imkan tanıyan bir örnek sunmaktadır.

Ayla'nın romandaki mekan kullanımı altı mekan üzerinden okunmaktadır. Bunlar "balo, motor, İstanbul Üniversitesi Hukuk Fakültesi, Beyazıt, Suadiye (Ayla'nın evinin önü) ve Fatih'teki Draman Caddesi'nin Kasım Bülbül Sokağı" olarak tespit edilmektedir. Her mekanda Ayla'nın konumu, mekanı kullanma biçimi ve mekanla kurduğu duygusal ilişki topoanaliz yöntemi referans alınarak tasarlanan teknikle okunmaktadır.

Romanın ilk mekanı olan balo, Ayla'nın davetli olarak katıldığı bir eğlence mekanıdır. Ayla burada teyzesiyle birlikte bulunur ve Osman'la karşılaşır. Mekan romantik bir zamana denk geldiği için topofili ve romantik karşılaşma mekanı olarak okunmaktadır. Motor da benzer biçimde, Ayla'nın sevgilisiyle eşlikli kullandığı romantik bir ulaşım mekanıdır ve topofili bir eğlence mekanı niteliği taşır. Bu iki mekanda Ayla, yüksek statüsüyle uyumlu, güvenli ve aidiyet hissiyle bulunmaktadır.

Hukuk Fakültesi'nde ise söz konusu durumun değiştiği görülmektedir. Ayla bu eğitim mekanına tek başına, ziyaret amacıyla gider ve yaşadığı tartışma sonucu mekandan kaçarak uzaklaşır. Mekan topofobi ve kaçış mekanı olarak değerlendirilmektedir. Beyazıt'taki kamusal açık alanda ise Ayla refakatli bir kullanım sergilerken, bu mekanda bir ayrılık yaşar; bu nedenle mekan ayrılık mekanı olarak topofobi kapsamına girer. Suadiye'de Ayla'nın evinin önü hem romantik dolaşımın hem de gerçeklerin öğrenildiği ve kaçışın yaşandığı mekan olarak nitelenmektedir. Bu mekan, aynı anda hem aidiyet hem korku barındırdığı için paradoks mekan olarak tanımlanır. Fatih'teki Kasım Bülbül Sokağı'nda ise Ayla yine dışlayıcı bir deneyim yaşamaktadır. Ayla'nın deneyimlediği bu mekanların mekan çözümlemeleri Şekil 2'de şematize edilmiştir. Burada hangi mekanları hangi biçimlerde kullandığı kısaca gösterilmektedir.



Şekil 2. Sınır romanının mekan çözümleme analizi.

Sınır romanı genel olarak değerlendirildiğinde Ayla karakterinin mekan kullanımlarının sınıfsal olduğu açık olarak görülmektedir. Bunun yanı sıra, karakterin en son deneyimlediği Fatih/Draman caddesi ve Osman'ın evi, söz konusu sınıfsal kullanımı daha belirgin hale getirmektedir. Ayla mahalleye ilk girdiğinde yaşadığı yerlere hiç benzememesi sebebiyle bir şaşkınlık yaşamaktadır. Öncelikle bulunduğu ortamı ve mekanları tanımlamaya çalışır. Etrafını, mahalleyi, evleri, sokaktaki insanları, evlerinin önünü kullanma biçimlerini inceler ve yaşadığı şaşkınlık devamlı olarak artar. Kendi hayatından çok uzak olan bu yaşama biçimi onu tedirgin etmektedir. Sonrasında Osman'ın evini bularak, tedirginlikle içeri girer. Yaşadığı dehşet artmaya devam eder ve tamamen bambaşka bir hayatın içinde olduğunu anlar. Osman'la arasındaki farkı, yaşamlarının çok ayrı olduğunu ve birlikte yaşamalarının ne kadar imkansız olduğunu, Osman'ın evini gördüğünde tüm gerçekliğiyle farketmektedir. Yaşadığı

ve düşündüğü hiçbir olay ya da durum onu Osman'dan ayıramazken, mekanı birebir deneyimlemek ve idrak etmek birlikte yaşayamayacaklarını anlamaya yeterli gelmektedir.

Sınır romanının söz konusu mekan çözümlemesi, hem kullanıcının toplumsal verilerini ve duygu dünyasını hem de mekan ve kullanıcının sınıfsal verilerini aktarmaktadır. Bu analizlere göre altı mekanın ikisi topofili, üçü topofobi, biri paradoks mekandır. Topofili yaşanan mekanlar, Ayla'nın kendi statüsüne uygun eğlence ve ulaşım mekanlarıdır. Bu mekanlarda aidiyet; yüksek statü ve eşlikli kullanımla birlikte ortaya çıkmaktadır. Ayla'nın kendi sınıfının dışına çıktıkça mekanla ilişkisi aidiyetten kaçışa, ardından yabancılaşma ve dışlanmaya dönüşmektedir. Böylece roman, sınıf farkının mekan deneyimini belirleyen temel etken olduğunu göstermektedir.

SONUÇ

Mimarlık ve edebiyat kapsamında ele alınan bu çalışma, edebi mekanların mimarlık araştırmaları için sistematik biçimde okunabilir bir veri alanı sunabileceğini göstermektedir. Topoanaliz temelli mekan çözümleme tekniği, mekanın fiziksel tarifinden çok kullanıcının mekanla kurduğu ilişkiye dair analiz sunmaktadır. Bu yöntemle her mekan için kullanıcının konumu, mekanı kullanma biçimi (tek başına ya da eşlikli, amaçlı ya da rastlantısal) ve mekanla kurduğu duygusal ilişki ayrı ayrı belirlenirken aynı zamanda bu kişinin sınıfsal durumu da göz önünde bulundurulmaktadır. Bu veriler, mekanın hangi kullanıcı için erişilebilir, güvenli ya da dışlayıcı olup olmadığını ortaya koymaktadır.

Sınıf farkının okunması bakımından bakıldığında, mekan çözümlemesi sınıfsal ayrımı yalnızca karakterlerin ilişkileri üzerinden değil, mekanların kullanım koşulları üzerinden de görünür kılmaktadır. Sınır romanında Ayla karakterinin kullandığı altı mekan topofili, topofobi ve paradoks mekan kategorileriyle sınıflandırılmış; ikisi topofili, üçü topofobi, biri paradoks mekan olarak belirlenmiştir. Topofili mekanlar, karakterin kendi statüsüyle uyumlu eğlence ve ulaşım mekanlarında yoğunlaşmıştır. Topofobi mekanlar ise eğitim, kamusal açık alan ve mahalle ölçeğinde ortaya çıkmıştır. Bu dağılım, aidiyet duygusunun sadece mekanın türüne bağlı olmadığını, mekanın kullanıcının sınıfsal konumuyla da ilişkili olduğunu göstermektedir.

Bulgular birlikte değerlendirildiğinde, kullanıcının sınıfsal konumunun dışına çıktıkça mekanla kurduğu ilişkinin aidiyetten kaçışa, ardından yabancılaşmaya ve dışlanmaya doğru değiştiği izlenmiştir. Ayrıca mekanın dolaylı tasvirlerinin yetersiz kaldığı, mekanın doğrudan deneyimlenmesinin sınıf farkının kavranmasında belirleyici olduğu görülmüştür. Bu sonuçlar, mekansal analiz yoluyla sınıf farkının okunmasının mümkün olduğunu ortaya koymaktadır. Mimarlık ve edebiyat ilişkisini ortak anlatı araçları üzerinden değil, kullanıcı ve sınıf ekseninde ele alan bu çalışma, uygulanabilir bir okuma çerçevesi önermesiyle literatüre katkı sunmaktadır. Bununla birlikte analiz tek bir roman ve tek bir karakterle sınırlıdır. Bu nedenle bulgular, diğer metinler ve kullanıcı grupları için genellenebilir sonuçlar olarak değil, yöntemin işleyişini gösteren bir örnek olarak değerlendirilmelidir.

Yöntemin kullanılabilirliğine ilişkin olarak birkaç öneri getirilebilir. İlk olarak, aynı metin içinde farklı sınıflardan karakterlerin mekan kullanımları karşılaştırılarak sınıfsal farkın

mekan deneyimine etkisi daha doğrudan test edilebilir. İkinci olarak, farklı dönemlerden ve yazarlardan metinler ile erkek karakterler ya da farklı statü gruplarından kullanıcılar analize dahil edilerek yöntemin sınırları sınanabilir. Üçüncü olarak, mekansal konum, yapı niteliği, iç düzenleme, malzeme, bakım durumu ve çevresel doku gibi mimari ögeler için ayrı kodlama kategorileri tanımlanırsa, duygusal okuma ile fiziksel nitelikler arasındaki ilişki daha ayrıntılı incelenebilir. Son olarak, okumaların birden fazla araştırmacı tarafından bağımsız olarak kodlanması, yorumun tutarlılığını artırabilir. Bu öneriler kapsamında, edebi metinlerin mimarlık ve mekansal okumalar adına nitelikli veri kaynaklarına dönüşmesi beklenmektedir.

KAYNAKLAR

Alexander, N. (2015). On literary geography. Literary Geographies, 1, 3-6.

Bachelard, G. (2013). Mekânın Poetikası. (A. Tümertekin, Çev.). İthaki Yayınları.

Bachelard, G. (2014). The Poetics of Space. (M. Jolas, Çev.). Boston: Beacon Press.

Benjamin, W. (1993). Son Bakışta Aşk. (Gürbilek N., Çev.). İstanbul: Metis Yayınları.

Braidotti, R. (2017). Göçebe Özneler. Kolektif Kitap.

Brisudová, L., Chataway, M. ve Moir, E. (2024). Mapping perceptions of topophilia and topophobia using a mobile app: A tale of two cities. Moravian Geographical Reports, 32(2), 90-100. doi: 10.2478/mgr-2024-0008

Brosseau, M. (2017). In, of, out, with, and through: New perspectives in literary geography. R. Tally Jr. (Ed.), The Routledge Handbook of Literature and Space içinde (ss. 9-27). London: Routledge.

Çakmaker, S. ve Ergelen, B. N. (2025). Gerçekle Kurgu Arasında: Rıfat Ilgaz'ın Karadeniz'in Kıyıcığında Romanı Üzerine Mekânsal Bir İnceleme, *Söylem Filoloji Dergisi*, 10(3), 1483-1508.

Çekin Işık, E. S. (2021). Suat Derviş'in Gazete Yazılarında Siyaset, Toplum ve Kadın. (Yüksek lisans tezi). İstanbul Üniversitesi.

Derviş, S. (2021). Sınır. İthaki Yayınları.

Foucault, M. (2011). Özne ve İktidar: Seçme Yazılar 2. (I. Ergüden ve O. Akınhay, Ed.). İstanbul: Ayrıntı Yayınları.

González, B. M. (2005). Topophilia and Topophobia:The Home as an Evocative Place of Contradictory Emotions. Space and Culture, 8(2), 193-213.

Harvey, D. (2019). Sosyal Adalet ve Şehir. (M. Moralı, Çev.). İstanbul: Metis Yayınları.

Kaya, Ş. (2018). Suat Derviş'in Romanlarında Kadın Karakterler. Folklor/Edebiyat, 24(96), 97- 110. doi:10.22559/folklor.354

Lefebvre, H. (2014). Mekanın Üretimi. (I. Ergüden, Çev.). İstanbul: Sel Yayıncılık.

Lordoğlu, C. (2024). Suat Derviş'in Metinlerinde "Ev ve Kentsel Mekan" Üzerine Bir Değerlendirme. S. Şahin (Ed.), "Ben Yazar Suat Derviş" Suat Derviş Kitabı içinde (ss. 71-99). İstanbul: İthaki Yayınları.

Massey, D. (1994). Space, Place and Gender. Polity.

Merleau-Ponty, M. (2017). Algının Fenomenolojisi. (E. Sarıkartal ve E. Hacımuratoğlu, Çev.). İstanbul: İthaki Yayınları.

Pallasmaa, J. (2006). An Architecture of the Seven Senses: Questions of Perception. William Stout Publishers.

Paquet, T. N. K. (2024). Entrenching systems of dominance in urban form: Exploring the origins of inequality in Secunda, South Africa. Geoforum, 157. doi:10.1016/j.geoforum.2024.104125

Pocock, D. (1981). Introduction: Imaginative literature and the geographer. D. Pocock (Ed.), Humanistic Geography and Literature: Essays on the Experience of Place içinde (ss. 9-19). London: Croom Helm.

Porteous, J. Douglas. (1985). Literature and Humanist Geography. The Royal Geographical Society, 17(2), 117-122.

Serin Güner, A. P. ve Gökmen, H. (2020). Mimarlık ve Edebiyat İlişkisine Dair Yapılmış Akademik Çalışmaların Bir Sınıflandırması. İdealkent, 11(31), 1722-1763. doi:10.31198/idealkent.829055

Szpakowska-Loranc, E. (2019). On the Relationship between Architectural and Literary Narrative. IOP Conference Series: Materials Science and Engineering içinde (C. 471). Institute of Physics Publishing. doi: 10.1088/1757-899X/471/7/072014

Spurr, D. (2012). Architecture and Modern Literature. Ann Arbor: University of Michigan Press.

Topolovská, T. (2022). Reading buildings: The textual turn of architecture as a parallel to the spatial turn in literary studies. Ars Aeterna, 14(1), 58-70. doi:10.2478/aa-2022-0006

Tuan, Y.-F. (1990). Topophilia: A Study of Environmental Perception, Attitudes, and. Values, Columbia University Press.

Tuan, Y.-F. (2013). Landscapes of Fear. Pantheon Books.

SIKIŞTIRILMIŞ TOPRAK YAPI SISTEMLERINDE BIYOLOJIK STABILIZASYON YAKLAŞIMLARININ SÜRDÜRÜLEBILIRLIK AÇISINDAN DEĞERLENDIRILMESI

AN EVALUATION OF BIOLOGICAL STABILIZATION APPROACHES FOR COMPRESSED EARTH BUILDING SYSTEMS IN TERMS OF SUSTAINABILITY

Ali FEYZI
Dokuz Eylül Üniversitesi Mimarlık Fakültesi, Bina bilgisi Anabilim dalı Doktora Öğrencisi, İzmir, Türkiye.
ORCID ID: 0000-0001-6208-4789

T. Didem AKYOL ALTUN
Prof. Dr. Dokuz Eylül Üniversitesi Mimarlık Fakültesi, Bina bilgisi Anabilim dalı Öğretim Üyesi, İzmir, Türkiye.
ORCID ID: 0000-0001-7938-3961

ÖZET

Günümüzde inşaat sektörünün yüksek enerji tüketimi, karbon salımı ve çevresel etkileri, sürdürülebilir yapı üretimine yönelik alternatif malzeme ve yapım sistemlerinin geliştirilmesini gerekli kılmaktadır. Bu kapsamda Sıkıştırılmış Toprak Yapım Sistemleri (STYS), doğal ve yerel malzeme kullanımı, düşük gömülü karbon potansiyeli ve yüksek ısıl kütle kapasitesi gibi özellikleriyle sürdürülebilir mimari açısından dikkat çeken bir yaklaşım sunmaktadır. Bununla birlikte, toprak yapıların sınırlı mekanik dayanımı, suya karşı hassasiyeti, erozyon riski ve uzun vadeli stabilite sorunları, sistemin çağdaş yapı sektöründeki uygulama alanını sınırlandırmaktadır.

Bu çalışma, sıkıştırılmış toprak yapı sistemlerinin performansını geliştirmeye yönelik biyolojik stabilizasyon yaklaşımlarını literatür temelinde değerlendirmeyi amaçlamaktadır. Bu doğrultuda, öncelikle çağdaş STYS uygulamalarının teknik ve mimari özellikleri incelenmiş; Tucson Dağı Rehabilite Merkezi, Sanbao Sanat Müzesi ve Ricola Kräuterzentrum gibi örnekler üzerinden toprak yapıların güncel mimari uygulamalardaki kullanım potansiyeli ele alınmıştır. Bununla birlikte, toprak esaslı yapı malzemelerinin dayanım ve dayanıklılık özelliklerinin geliştirilmesine yönelik farklı stabilizasyon yaklaşımları da değerlendirilmiştir. Çalışmanın biyolojik stabilizasyon boyutunda, özellikle üreolitik bakterilerin biyomineralizasyon kapasitesi ve Mikrobiyal Kalsiyum Karbonat Çökelmesi (MICP) yöntemi üzerinde durulmaktadır. *Sporosarcina pasteurii* gibi üreolitik bakterilerin metabolik faaliyetleri sonucunda meydana gelen kalsiyum karbonat çökelmesinin, toprak tanecikleri arasındaki boşlukların doldurulması ve tanecikler arası bağların güçlendirilmesi yoluyla malzemenin mekanik ve fiziksel özelliklerinin geliştirilmesine katkı sağlayabileceği literatürde ortaya konmaktadır.

İncelenen çalışmalar, sıkıştırılmış toprak yapı sistemleri ile biyolojik stabilizasyonun sürdürülebilir yapı üretimi açısından önemli potansiyeller taşıdığını göstermektedir. Bununla

birlikte, bu iki yaklaşımın birlikte ele alındığı çalışmaların sınırlı olması, konuya yönelik yeni araştırmalar için önemli bir potansiyel ortaya koymaktadır. Bu bağlamda biyokalsifikasyon temelli stabilizasyonun, çimento ve kireç gibi geleneksel bağlayıcılara alternatif bir yaklaşım olarak değerlendirilmesi; yapı malzemelerinin performansının geliştirilmesi ve yapı sektörünün çevresel etkilerinin azaltılması açısından önem taşımaktadır. Çalışmanın, biyolojik stabilizasyonun sıkıştırılmış toprak yapı sistemlerine entegrasyonuna yönelik gelecekteki araştırmalar için kuramsal bir temel oluşturması hedeflenmektedir.

Anahtar Kelimeler: Sıkıştırılmış Toprak Yapı Sistemleri; Biyolojik Stabilizasyon; Mikrobiyal Kalsiyum Karbonat Çökelmesi (MICP); Üreolitik Bakteriler; Sürdürülebilir Yapı; Biyomineralizasyon.

ABSTRACT

The high energy consumption, carbon emissions, and environmental impacts of the construction sector necessitate the development of alternative materials and building systems for sustainable construction. In this context, Compressed Earth Building Systems (CEBS) have emerged as a promising approach in sustainable architecture due to their use of natural and locally available materials, low embodied carbon potential, and high thermal mass capacity. However, the limited mechanical strength, water sensitivity, erosion susceptibility, and long-term stability issues of earth-based structures restrict their wider application in contemporary construction.

This study aims to evaluate biological stabilization approaches for improving the performance of compressed earth building systems based on the existing literature. Accordingly, contemporary CEBS applications are first examined in terms of their technical and architectural characteristics. Examples such as the Tucson Mountain Rehabilitation Center, Sanbao Art Museum, and Ricola Kräuterzentrum are reviewed to assess the potential of earth-based construction in contemporary architectural practice. In addition, different stabilization approaches developed to improve the strength and durability of earth-based building materials are considered. Within the scope of biological stabilization, particular attention is given to the biomineralization capacity of ureolytic bacteria and the Microbially Induced Calcium Carbonate Precipitation (MICP) technique. The literature indicates that calcium carbonate precipitation resulting from the metabolic activity of ureolytic bacteria, particularly *Sporosarcina pasteurii*, may contribute to the improvement of the mechanical and physical properties of soil-based materials by filling voids between soil particles and enhancing interparticle bonding.

The reviewed studies indicate that both compressed earth building systems and biological stabilization approaches have significant potential for sustainable construction. However, studies addressing the integration of these two approaches remain limited, indicating considerable potential for further research. In this context, the application of biomineralization-based stabilization as an alternative to conventional binders such as cement and lime may offer opportunities for improving material performance while reducing the

environmental impacts of the construction sector. This study aims to provide a theoretical basis for future research on the integration of biological stabilization into compressed earth building systems.

Keywords: Rammed Earth, Compressed Earth Building Systems; Biological Stabilization; Microbially Induced Calcium Carbonate Precipitation (MICP); Ureolytic Bacteria; Sustainable Construction; Biomineralization.

GIDA ATIKLARINDAN ELDE EDİLEN BİYO-NİŞASTANIN TEKSTİL HAŞILINA ENTEGRASYONU

INTEGRATION OF BIO-STARCH OBTAINED FROM FOOD WASTE INTO TEXTILE SIZING

Emin SARLI
Dr., İstinye Üniversitesi, Mühendislik ve Doğa Bilimleri Fakültesi, İstanbul, Türkiye
Dr., Istinye University, Faculty of Engineering and Natural Sciences, Istanbul, Türkiye
ORCID ID: 0000-0002-1013-414

Gülşen YILDIZ
Achitex Minerva Kimya Ltd. Şti., Ar-Ge Departmanı, İstanbul, Türkiye
Achitex Minerva Kimya Ltd. Şti., R&D Department, Istanbul, Türkiye
ORCID ID: 0000-0000-0000-0000

ÖZET

Tekstil sektöründe dokuma işlemi sırasında ipliklerin mukavemetini artırmak, sürtünme ve aşınma etkilerine karşı dayanımını geliştirmek amacıyla yaygın olarak haşıl maddeleri kullanılmaktadır. Bu amaçla kullanılan polivinil alkol (PVA) ve sentetik polimer esaslı haşıl maddeleri, sağladıkları teknik performansa rağmen fosil bazlı hammaddelere bağımlılıkları ve çevresel yükleri nedeniyle sürdürülebilir tekstil üretimi açısından önemli bir ihtiyaç alanı oluşturmaktadır. Diğer taraftan, gıda endüstrisinde oluşan ve yüksek oranda nişasta içeren organik atıkların önemli bir bölümü düşük katma değerli alanlarda değerlendirilmekte veya bertaraf edilmektedir. Bu çalışma, gıda atıklarından elde edilen nişastanın tekstil haşıl uygulamalarında kullanılabilecek biyobazlı bir hammaddeye dönüştürülmesini amaçlamaktadır.

Çalışma kapsamında öncelikle patates, mısır ve benzeri gıda endüstrisi atıklarının nişasta içerikleri, nem oranları, partikül boyutları ve safsızlık özellikleri açısından karakterize edilmiştir. Ardından ultrasonik destekli ekstraksiyon ve enzimatik işlemler kullanılarak nişastanın verimli şekilde elde edilmiştir. Elde edilen nişastanın tekstil haşıl uygulamalarına uygunluğunun artırılması amacıyla prejelatinizasyon ve kontrollü beyazlatma gibi fiziksel ve kimyasal modifikasyon işlemleri uygulanmıştır. Modifiye biyo-nişastanın viskozite, çözünürlük, film oluşturma kapasitesi, yapışma gücü ve reolojik özellikleri incelenmiştir. Ayrıca FTIR, SEM, XRD ve DSC/TGA analizleri ile ürünün yapısal ve termal özellikleri karakterize edilmiştir.

Geliştirilen biyo-nişasta formülasyonlarının pamuk ve pamuk karışımlı iplikler üzerinde uygulanmasıyla iplik mukavemeti, kopma direnci, sürtünme dayanımı ve dokuma performansı açısından değerlendirilmiştir. Elde edilen performans verilerinin PVA bazlı haşıl reçetesiyle karşılaştırılmıştır. Çalışma ile gıda atıklarının tekstil sektöründe yüksek katma değerli bir hammadde olarak değerlendirilmiş, biyobazlı ve sürdürülebilir bir haşıl reçetesi geliştirilmiştir.

Anahtar Kelimeler: Biyo-nişasta, Gıda Atıkları, Haşıl, PVA.

ABSTRACT

Sizing agents are widely used in the textile industry to increase the strength of yarns during weaving and to improve their resistance to friction and abrasion. Although polyvinyl alcohol (PVA) and synthetic polymer-based sizing agents provide high technical performance, their dependence on fossil-based raw materials and associated environmental impacts represent an important challenge for sustainable textile production. On the other hand, a significant proportion of organic waste generated by the food industry, which contains high levels of starch, is currently utilized in low-value applications or disposed of. This study aims to convert starch obtained from food waste into a bio-based raw material suitable for textile sizing applications.

Within the scope of the study, food industry wastes such as potato and corn residues were initially characterized in terms of starch content, moisture content, particle size, and impurity characteristics. Subsequently, starch was efficiently extracted using ultrasound-assisted extraction and enzymatic treatments. To improve the suitability of the extracted starch for textile sizing applications, physical and chemical modification processes, including pregelatinization and controlled bleaching, were applied. The viscosity, solubility, film-forming capacity, adhesion strength, and rheological properties of the modified bio-starch were investigated. In addition, FTIR, SEM, XRD, and DSC/TGA analyses were performed to characterize the structural and thermal properties of the developed material.

The developed bio-starch formulations were applied to cotton and cotton-blended yarns and evaluated in terms of yarn strength, breaking resistance, abrasion resistance, and weaving performance. The obtained performance data were compared with those of a PVA-based sizing formulation. The study demonstrated the potential for valorizing food waste as a high-value-added raw material for the textile industry and resulted in the development of a bio-based and sustainable sizing formulation.

Keywords: Bio-starch, Food Waste, Sizing Agent, PVA.

SÜRDÜRÜLEBİLİR TEKSTİL ÜRETİMİ İÇİN KİMYASAL TÜKETİMİNİ VE ATIK SU YÜKÜNÜ AZALTAN YENİLİKÇİ HAŞIL FORMÜLASYONU GELİŞTİRİLMESİ

DEVELOPMENT OF AN INNOVATIVE SIZING FORMULATION TO REDUCE CHEMICAL CONSUMPTION AND WASTEWATER LOAD FOR SUSTAINABLE TEXTILE PRODUCTION

Emin SARLI
Dr., İstinye Üniversitesi, Mühendislik ve Doğa Bilimleri Fakültesi, İstanbul, Türkiye
Dr., Istinye University, Faculty of Engineering and Natural Sciences, Istanbul, Türkiye
ORCID ID: 0000-0002-1013-414

Gülşen YILDIZ
Achitex Minerva Kimya Ltd. Şti., Ar-Ge Departmanı, İstanbul, Türkiye
Achitex Minerva Kimya Ltd. Şti., R&D Department, Istanbul, Türkiye
ORCID ID: 0000-0000-0000-0000

ÖZET

Tekstil endüstrisinde çözgü ipliklerine dokuma öncesinde uygulanan haşıl, ipliklerin dokuma sırasında karşılaşabileceği mekanik etkilere karşı korunması, mukavemet ve sürtünme direncinin artırılması açısından önemli bir aşamadır. Bununla birlikte, özellikle nişasta, polivinil alkol (PVA), karboksimetil selüloz (CMC) ve çeşitli sentetik polimerlerin kullanıldığı geleneksel haşıl maddeleri, haşıllama sonrasında gerçekleştirilen haşıl söküm işlemi nedeniyle önemli miktarda kimyasal yük ve atık su oluşumuna neden olabilmektedir. Bu durum, özellikle kimyasal oksijen ihtiyacı (KOİ) ve biyolojik oksijen ihtiyacı (BOİ) gibi atık su parametrelerinin yükselmesine ve arıtma proseslerinde ilave enerji ve kimyasal tüketimine yol açabilmektedir.

Bu çalışmanın amacı, haşıllamada kullanılan konvansiyonel nişasta bazlı, polivinil alkol (PVA) ve karboksimetil selüloz (CMC) içeren formülasyonların çevresel etkilerini azaltmak ve teknik performansı koruyarak daha sürdürülebilir bir haşıl reçetesi geliştirmektir. Bu kapsamda, mevcut formülasyonlardaki nişasta, PVA ve CMC oranlarının azaltılması ve bunların yerine biyobazlı, biyobozunur veya çevresel etkisi daha düşük alternatif polimerlerin reçeteye dahil edilmesi hedeflenmiştir. Çalışma kapsamında farklı hammadde ve bileşenlerin seçimi, reolojik ve fizikokimyasal özelliklerinin belirlenmesi, farklı formülasyon kombinasyonlarının hazırlanması ve laboratuvar ölçekli performans testlerinin gerçekleştirilmesi planlanmıştır.

Geliştirilen formülasyonların iplik mukavemeti, sürtünme direnci, haşıl tutunma performansı ve çözgü kopma oranı gibi teknik özellikleri mevcut haşıl reçeteleri ile karşılaştırılmıştır. Bunun yanında, haşıl söküm işlemi sonrasında oluşan atık sular KOİ, BOİ, pH, iletkenlik ve benzeri çevresel parametreler açısından değerlendirilmiştir. Çalışma kapsamında, mevcut haşıl formülasyonundaki nişasta oranı en az %30 azaltılmış ve atık suyun KOİ ve BOİ değerlerinde %25'in üzerinde iyileşme sağlanmıştır. Bununla birlikte, geliştirilen

formülasyonun mevcut sistemle eşdeğer veya daha yüksek teknik performans gösterdiği ve pilot/endüstriyel üretim koşullarına uyarlanabilir olduğu belirlenmiştir.
Çalışma sonucunda, kimyasal tüketimini ve atık su yükünü azaltırken tekstil üretimindeki teknik gereklilikleri karşılayabilen yenilikçi bir haşıl formülasyonu geliştirilmiştir. Çalışmanın laboratuvar ölçeğinden pilot ve endüstriyel uygulamaya kadar ilerleyen deneysel yapısı sayesinde, geliştirilen formülasyonun proses uyumluluğu, çevresel performansı ve ekonomik uygulanabilirliği birlikte değerlendirilmiştir. Böylece tekstil sektöründe daha düşük kimyasal ve su tüketimine dayalı sürdürülebilir üretim uygulamalarına katkı sağlanmıştır.
Anahtar Kelimeler: Haşıl, Sürdürülebilir Tekstil, PVA, Nişasta, Atık Su, KOİ, BOİ

ABSTRACT

Sizing applied to warp yarns before weaving is an important stage in the textile industry, as it protects yarns against the mechanical stresses encountered during weaving and improves their strength and abrasion resistance. However, conventional sizing agents, particularly those containing starch, polyvinyl alcohol (PVA), carboxymethyl cellulose (CMC), and various synthetic polymers, may generate significant chemical loads and wastewater due to the desizing process carried out after sizing. This may result in increased wastewater parameters such as chemical oxygen demand (COD) and biological oxygen demand (BOD), leading to additional energy and chemical consumption during wastewater treatment processes.
The aim of this study was to reduce the environmental impacts of conventional starch-based sizing formulations containing polyvinyl alcohol (PVA) and carboxymethyl cellulose (CMC) and to develop a more sustainable sizing formulation while maintaining technical performance. Within this scope, the proportions of starch, PVA, and CMC in the existing formulations were reduced, and bio-based, biodegradable, or lower-environmental-impact alternative polymers were incorporated into the formulations. Different raw materials and components were selected, their rheological and physicochemical properties were determined, different formulation combinations were prepared, and laboratory-scale performance tests were conducted.
The developed formulations were compared with the existing sizing formulations in terms of technical properties such as yarn strength, abrasion resistance, sizing adhesion performance, and warp breakage rate. In addition, wastewater generated after the desizing process was evaluated in terms of COD, BOD, pH, conductivity, and other relevant environmental parameters. As a result of the study, the starch content of the existing sizing formulation was reduced by at least 30%, and an improvement of more than 25% was achieved in the COD and BOD values of the wastewater. Furthermore, the developed formulation was determined to provide equivalent or higher technical performance compared with the existing system and to be adaptable to pilot- and industrial-scale production conditions.
As a result, an innovative sizing formulation capable of meeting the technical requirements of textile production while reducing chemical consumption and wastewater load was developed. Through the experimental approach progressing from laboratory-scale studies to pilot and

industrial applications, the process compatibility, environmental performance, and economic feasibility of the developed formulation were evaluated together. Thus, the study contributed to sustainable production practices in the textile industry based on reduced chemical and water consumption.

Keywords: Sizing Agent, Sustainable Textile, PVA, Starch, Wastewater, COD, BOD.

ANALYTICAL INVESTIGATION OF THE P–Δ EFFECT ON THE NATURAL FREQUENCY BEHAVIOR OF HYBRID OFFSHORE WIND–HYDROKINETIC SYSTEMS

Abdullah Kürşat DEMİR
Tokat Gaziosmanpaşa University, Engineering and Architecture Faculty, Department of Civil Engineering

ABSTRACT

This study presents an analytical investigation of the P–Δ (second-order) effect on the natural frequency of hybrid offshore wind–hydrokinetic systems. A deterministic model is developed to include soil–structure interaction and geometric nonlinearity, addressing the influence of axial loads and tower slenderness on overall stiffness and dynamic response. The system is idealized as a two-degree-of-freedom structure, and the displacements and rotations are derived using Castigliano's theorem. The pseudo-horizontal force method is applied to account for the moment amplification caused by axial loading. The model is verified against reference numerical results, showing close agreement. A case study is then performed for a 10 MW + 2 MW hybrid system proposed for the Western Black Sea. Results indicate that the P–Δ effect reduces the fundamental natural frequency by approximately 3–4%, highlighting its importance in large-capacity turbine design. The findings emphasize that including geometric nonlinearity is essential for accurate frequency prediction and for maintaining resonance-free operation within the soft–stiff design band.

Keywords: Hybrid Offshore System, Natural Frequency, P–Δ Effect, Soil–Structure İnteraction, Geometric Nonlinearity, Moment Amplification

INTRODUCTION

The growing global population and industrialization have led to a continuous increase in energy demand worldwide. As the adverse environmental impacts of fossil fuel–based energy systems have become more apparent, the transition toward renewable energy sources has accelerated. Among various renewable energy types, wind energy has shown one of the fastest technological advancements in recent years. Offshore wind turbines, in particular, have gained significant attention due to their higher and more stable wind speeds compared to onshore systems, resulting in substantially improved energy conversion efficiency. The smooth surface of the sea, the absence of topographical obstacles, and reduced turbulence ensure both directional and temporal stability of wind flow. Consequently, the annual energy output of turbines increases, thereby enhancing overall system efficiency. Moreover, the ability to employ taller towers and larger rotor diameters in offshore environments has markedly boosted the total energy production capacity compared to land-based systems. When the first offshore wind turbines were installed in Denmark in 1991, their rated power was only 0.45 MW. Today, capacities have reached up to 20 MW (Şahin, 2020). The rotor diameters have expanded from 35 m to 292 m, enabling a single rotation to sweep an area

equivalent to approximately nine football fields (Offshorewind, 2025). This rapid scaling has fundamentally altered the structural requirements of turbines, complicating the interrelationships among tower height, mass, stiffness, and dynamic behavior. As of 2024, 8 GW of new offshore wind capacity was commissioned globally, raising the total installed capacity to 83.2 GW—about 7.3% of the world's total wind power. Over the past decade, the sector has exhibited an average annual growth rate of 10%. Although new installations declined by 26% compared with the previous year, 2024 still marked the fourth-highest annual capacity increase in the history of offshore wind. China maintained its leadership for the seventh consecutive year, followed by the United Kingdom, Germany, the Netherlands, and Taiwan, which together account for a substantial portion of global capacity (GWEC, 2025). The industry is projected to sustain a compound annual growth rate of 21% over the next decade, reaching 441 GW of total installed capacity by 2034 (WFO, 2024). This global expansion has heightened interest in offshore wind investments, particularly in energy-importing countries seeking to enhance their energy security. In line with this trend, Türkiye has taken strategic steps to utilize its maritime jurisdiction zones for energy production and to support its manufacturing-based economy (Demir, 2025). Although no operational offshore wind farm currently exists, the Ministry of Energy and Natural Resources designated Kıyıköy, Gelibolu, and Saros as priority candidate sites in 2018. According to subsequent Renewable Energy Resource Area (YEKA) announcements, Karabiga, Bozcaada, and Bandırma were added to the list in 2023. The ESMAP report estimates Türkiye's total offshore wind potential at 75 GW, consisting of 63 GW floating and 12 GW fixed-bottom systems (ESMAP, 2020). By the end of 2025, the country's total installed capacity had reached 121,418 MW (Republic of Türkiye Ministry of Energy and Natural Sources, 2025). These data suggest that exploiting even a small portion of Türkiye's offshore area could supply a significant share of its current installed power capacity. Significant progress has also been achieved in developing domestic turbine technologies. ASELSAN has been leading the development of a 7–8 MW national offshore wind turbine. In addition, multi-criteria decision-making (MCDM) analyses identified Bozcaada and Kıyıköy in northwestern Türkiye as the most suitable locations for offshore development (Caceoğlu, 2023). In this context, Kıyıköy has become the focus of several conceptual and hydrodynamic design studies for both floating (Yıldırım, 2022) and fixed-bottom (Demir and Balas, 2024) systems. The marine environment holds considerable potential not only for wind energy but also for wave, tidal, and current energy. Theoretically, the energy extractable from these marine resources far exceeds global energy demand (Samso, 2023). However, due to current technological limitations, this potential cannot yet be fully harnessed. Therefore, improving the efficiency of ocean-based energy conversion remains a critical component of sustainable energy policies. In recent years, hybrid concepts have been developed that integrate wind and hydrokinetic turbines into a single structural system (HoWAT, 2019; Ma et al., 2025; Lande-Sudall, 2018; Demir and Balas, 2025a). The key advantage of such hybrid systems lies in their ability to simultaneously harvest wind and current energy through a single monopile foundation. Typically constructed in waters up to 50

m deep, these systems aim to maximize total energy extraction from the marine environment (Demir and Balas, 2025b). Among the most critical engineering stages in the design of offshore wind—and particularly hybrid—systems is natural frequency analysis. These structures operate throughout their lifetime under repeated environmental loads such as wind, waves, and currents. Since each loading type acts within a specific frequency range, resonance may occur if the system's natural frequency coincides with that of the excitation forces. Resonance can lead to structural damage or instability; thus, accurately determining the natural frequency is essential for ensuring structural safety (Arany et al., 2016). Although numerous researchers have investigated the natural frequency behavior of offshore wind turbines (Arany et al., 2016; Loken, 2017; Alkhoury et al., 2020; Amel et al., 2022), most studies have focused solely on wind turbine systems modeled using a single degree of freedom (SDOF) approach (Jiang et al., 2023). However, when a hydrokinetic turbine is integrated into the structure, the dynamic behavior must be modeled at least as a two-degree-of-freedom (2DOF) system. This distinction has been demonstrated numerically in previous studies (Demir and Balas, 2025b). Nevertheless, existing analyses have largely been restricted to lateral loading, while the role of axial loads—specifically the P–Δ effect—on natural frequency has often been neglected. With the continuing increase in turbine size and mass, the geometric nonlinearities induced by these axial loads have become non-negligible. In particular, bending moments occurring at the foundation level give rise to the P–Δ effect, also known as the Moment Amplification Factor (MAF), a topic extensively discussed in prior research (Sahu and Dutta, 2025; Kühn, 2001; Burgos and Silva, 2023; Lui, 1988). The magnitude of MAF depends primarily on two parameters: the vertical load carried by the structure (mainly proportional to the turbine and component masses) and the slenderness of the tower. As turbine dimensions increase, these effects become more pronounced, making it imperative to incorporate geometric nonlinearities into natural frequency analyses. To date, the influence of the P–Δ effect on the natural frequency behavior of hybrid offshore systems has not been investigated in the literature. This study analytically examines the influence of the P–Δ (second-order) effect on the natural frequency of a hybrid offshore wind–hydrokinetic turbine system proposed for deployment off the coast of Kıyıköy in the western Black Sea. A deterministic analytical approach is developed to quantify the impact of axial loading—caused by increased turbine mass and tower slenderness—on overall system stiffness. The proposed model is first validated using a representative system and subsequently applied under site-specific environmental conditions for Kıyıköy. The results reveal that increasing axial loads cause a measurable reduction in natural frequencies, highlighting that this effect becomes structurally critical for high-capacity turbines.

MATERIALS AND METHOD

As discussed in the Introduction, natural frequency analysis is among the most critical design parameters for offshore wind turbines. For systems consisting solely of wind turbines, the characteristic frequency content of external loads is summarized in Figure 1 (Bchattacharya, 2014).

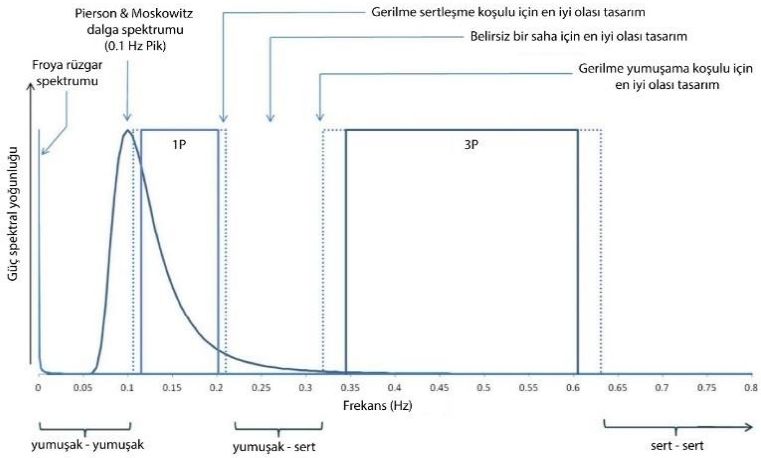


Figure 1. Characteristic frequency ranges for offshore wind turbines (Bchattacharya, 2014)

In Figure 1, the wind spectrum is represented by the Frøya wind spectrum (Andersen and Lovseth, 1992), while the wave spectrum follows the Pierson–Moskowitz formulation (Pierson and Moskowitz, 1964). The bands marked 1P and 3P correspond to excitation originating from rotor-level vibrations during turbine rotation. The 1P loading reflects once-per-revolution effects; thus, its frequency equals the rotor speed. Because turbines operate over a range between cut-in and cut-out, 1P excitation is shown as a band. The 3P loading arises from tower-shadow effects as the blades pass in front of the tower. For three-bladed rotors, the aerodynamic loading on the tower varies three times per revolution, producing a frequency band that also broadens with operating speed. The 3P band can be approximated as three times the 1P band. Adding safety margins of ±10% to both 1P and 3P defines the characteristic frequency ranges used in design.

Considering all bands in Figure 1, three generic design regions are identified: soft–soft, soft–stiff, and stiff–stiff (Bchattacharya 2014):

- Soft–soft region: The structural natural frequency is likely to overlap the wind and wave energy ranges. Structures are more slender, lighter, and more flexible, which can reduce construction cost but increases resonance risk. This region is generally not recommended.
- Soft–stiff region: The natural frequency is well above the wind-induced bands yet may still interact with wave energy. The structure is neither very stiff nor overly flexible. This region usually offers the most cost-effective and robust design space.
- Stiff–stiff region: The natural frequency exceeds all characteristic bands. Dynamic interactions are minimized, but the resulting structure is very stiff and typically uneconomic.

For hybrid offshore systems, two additional frequency bands associated with the hydrokinetic turbine appear, as shown in Figure 2 (Demir, 2025).

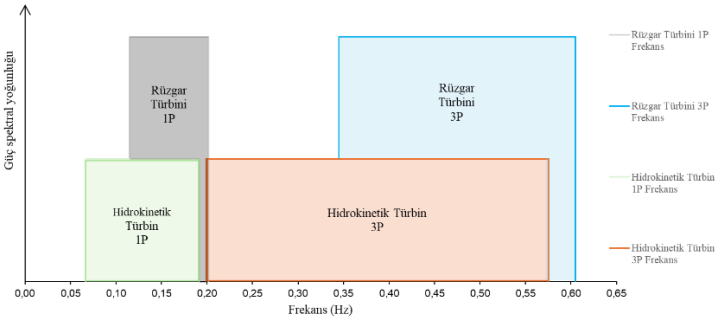


Figure 2. Characteristic frequency ranges for offshore hybrid (wind–hydrokinetic) turbines

Similar to wind turbines, the hydrokinetic turbine introduces 1P and 3P excitation bands. As seen in Figure 3, adding the hydrokinetic unit can eliminate the available soft–stiff window. To restore and widen this desirable region, the operating range of the hydrokinetic turbine can be modified, as illustrated in Figure 3 (HoWAT, 2019).

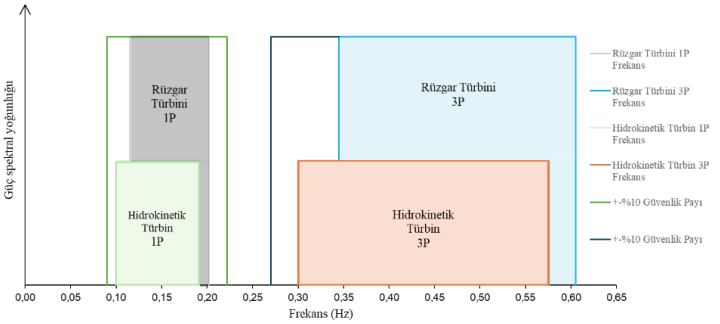


Figure 3. Modified characteristic frequency ranges for offshore hybrid turbine systems

Through such operating-range modification, the soft–stiff region—typically the optimal design window—can be re-established and enlarged.

For conventional offshore wind turbines with a single turbine, rotor loads are transmitted near the monopile head; the dynamic system is therefore commonly reduced to an SDOF model (Arany et al., 2016; Jiang et al., 2023). Early studies analyzing hybrid wind–hydrokinetic systems also relied on SDOF simplifications (Ma et al., 2025). Subsequent research derived and validated 2DOF analytical solutions against the literature (Demir and Balas, 2025a; Demir and Balas, 2025b). In this study, we adopt the 2DOF formulation and then investigate how the P–Δ (second-order) effect alters the natural frequency. The schematic of the 2DOF system is shown in Figure 4.

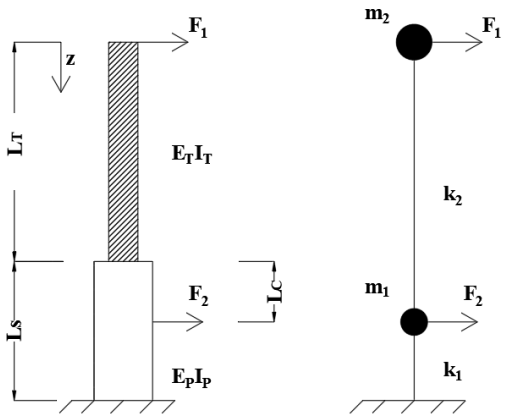


Figure 4. Schematic representation of a two-degree-of-freedom system (Demir, 2025)

On the left is the simplified tower–single-pile structure; the right shows the idealized model. Here, L_T is the tower length, L_S the pile length, L_C the vertical offset between tower base and hydrokinetic turbine center; F_1 and F_2 are the wind- and hydrokinetic-turbine forces; E_TI_T and E_PI_P are the bending stiffnesses of tower and pile; m_1,m_2 are the generalized masses of the lower and upper DOFs; and k_1,k_2 are the corresponding stiffness terms. Considering that the two-degree-of-freedom (2DOF) system undergoes free harmonic motion, the equations of motion can be expressed as in Eqaution (1) and Equation (2).

$$m_2\ddot{x}_2 = k_2(x_1 - x_2) \tag{1}$$

$$m_2\ddot{x}_2 + k_2x_2 - k_2x_1 = 0 \tag{2}$$

By considering Equations. (1) and (2), the general solution for free harmonic motion can be expressed as shown in Equation (3).

$$[M]\{\ddot{x}\} + [k]\{x\} = 0 \tag{3}$$

In this study, damping is neglected in the free vibration analysis, since typical total structural damping ratios range between 1% and 8%, which do not significantly alter the natural frequency values in the first order (Arany et al., 2016). Therefore, for free harmonic motion, the displacement can be expressed as given in Equation (4).

$$\{x\} = \{X\}e^{iwt} \tag{4}$$

Substituting the expression for free harmonic motion into Equation (3) yields the relation given in Equation (5).

$$([K] - w^2[M])\{X\} = 0 \tag{5}$$

Equation (5) represents an eigenvalue problem. The stiffness and mass matrices in Equation (5) are defined as shown in Equations. (6) and (7).

$$[K] = \begin{bmatrix} k_1 + k_2 & -k_2 \\ -k_2 & k_2 \end{bmatrix} \tag{6}$$

$$[m] = \begin{bmatrix} m_1 & 0 \\ 0 & m_2 \end{bmatrix} \tag{7}$$

Taking the determinant of Equation (5) with the matrices specified above leads to Equation (8), and the system's natural frequency is then obtained from Equation (9).

$$\omega_{1,2}^2 = \frac{k_1m_2 + k_2m_2 + k_2m_1 \pm \sqrt{(k_1m_2 + k_2m_2 + k_2m_1)^2 - 4m_1m_2k_1k_2}}{2m_1m_2} \quad (8)$$

$$f_1 = \frac{\omega_1}{2\pi} \quad (9)$$

In Equation (9), "ω" denotes the angular frequency. The unknowns in Equations. (8) and (9) are the stiffness values k_1 and k_2 of the idealized system. These are obtained from Equations. (10) and (11), respectively.

$$k_1 = \frac{F_1 + F_2}{x_1} \quad (10)$$

$$k_2 = \frac{F_2}{x_2 - x_1} \quad (11)$$

In Equations. (10) and (11), x_1 and x_2 represent the displacements at the hydrokinetic turbine level and the wind turbine level, respectively. These displacement values are determined using Castigliano's second theorem, and x_2 and x_1 are obtained as expressed in Equations. (12) and (13).

$$q_1 = x_2 = \frac{\partial U}{\partial F_1} \quad (12)$$

$$q_2 = x_1 = \frac{\partial U}{\partial F_2} \quad (13)$$

In Equations. (12) and (13), Udenotes the strain energy due to displacement, and qrepresents the deformation at the point of force application. The strain energy resulting from deformation can be expressed as given in Equation (14).

$$U = \int_0^{L_T+L_S} \frac{[M(z)]^2}{2EI(z)} dz \quad (14)$$

Since both the applied forces and the flexural rigidity vary along the structure, the bending moment M(z) in Equation (14) is expressed separately for three distinct regions, as shown in Equations (15), (16), and (17).

$$M(z) = F_1 z \qquad (0 \le z \le L_T) \qquad \text{1st region} \quad (15)$$

$$M(z) = F_1 z \qquad (L_T \le z \le L_T + L_C) \qquad \text{2nd region} \quad (16)$$

$$M(z) = F_1 z + F_2[z - (L_T + L_C)] \qquad (L_T + L_C \le z \le L_T + L_S) \qquad \text{3rd region} \quad (17)$$

Since there are three different moment expressions, the strain energy for each segment is formulated separately, as shown in Equations (18), (19), and (20).

$$U_1 = \int_0^{L_T} \frac{[M(z)]^2}{2EI(z)}dz = \int_0^{L_T} \frac{[F_1 z]^2}{2E_T I_T}dz = \frac{F_1^2 L_T^3}{6E_T I_T} \tag{18}$$

$$U_2 = \int_{L_T}^{L_T+L_C} \frac{[M(z)]^2}{2EI(z)}dz = \int_{L_T}^{L_T+L_C} \frac{[F_1 z]^2}{2E_P I_P}dz = \frac{F_1^2}{2E_P I_P}\left[\frac{(L_T+L_C)^3}{3} - \frac{L_T^3}{3}\right] \tag{19}$$

$$U_3 = \int_{L_T+L_C}^{L_T+L_S} \frac{[M(z)]^2}{2EI(z)}dz = \int_{L_T+L_C}^{L_T+L_S} \frac{[F_1 z + F_2[z-(L_T+L_C)]]^2}{2E_P I_P}dz$$

$$U_3 = \frac{1}{2E_P I_P}\left\{(F_1+F_2)^2\left[\frac{(L_T+L_S)^3}{3} - \frac{(L_T+L_C)^3}{3}\right] - \left[\frac{(L_T+L_S)^2}{2} - \frac{(L_T+L_C)^2}{2}\right] + 2(F_1+F_2)F_2(L_T+L_C)\right.$$
$$\left. F_2^2\,(L_T+L_C)^2\,[(L_T+L_S)-(L_T+L_C)]\right\} \tag{20}$$

By summing Equations (18), (19), and (20), the total strain energy due to deformation is obtained. Accordingly, by taking the derivative of the total energy with respect to the applied forces, the displacement values at both the wind turbine and hydrokinetic turbine levels are determined, as expressed in Equations (21) and (22).

$$q_1 = x_2 = \frac{\partial U}{\partial F_1} = \frac{F_1 L_T^3}{3E_T I_T} + \frac{F_1}{E_P I_P}\left[\frac{(L_T+L_C)^3}{3} - \frac{L_T^3}{3}\right] +$$
$$\frac{1}{2E_P I_P}\left\{2(F_1+F_2)\left[\frac{(L_T+L_S)^3}{3} - \frac{(L_T+L_C)^3}{3}\right] - 2F_2(L_T+L_C)\left[\frac{(L_T+L_S)^2}{2} - \frac{(L_T+L_C)^2}{2}\right]\right\} \tag{21}$$

$$q_2 = x_1 = \frac{\partial U}{\partial F_2} = \frac{1}{2E_P I_P}\left\{2(F_1+F_2)\left[\frac{(L_T+L_S)^3}{3} - \frac{(L_T+L_C)^3}{3}\right] -\right.$$
$$2(F_1+2F_2)(L_T+L_C)\left[\frac{(L_T+L_S)^2}{2} - \frac{(L_T+L_C)^2}{2}\right] +$$
$$\left. 2F_2(L_T+L_C)^2[(L_T+L_S)-(L_T+L_C)]\right\} \tag{22}$$

When soil–structure interaction (SSI) is taken into account, the structural response can be evaluated by considering the geometric configuration of the system (Jiang et al. 2023). The deformation arising from the geometry of the two-degree-of-freedom system is illustrated in Figure 5 (Demir, 2025).

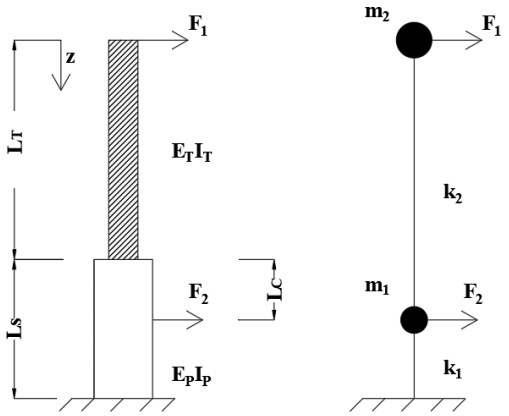


Figure 5. Schematic representation of the deformation-induced geometry of the hybrid system (Demir, 2025)

In Figure 5, y_0 denotes the deformation at the soil surface, ψ_0 represents the rotation at the soil level, y_1 is the deformation at the hydrokinetic turbine elevation, ψ_1 is the corresponding rotation, and y_2 denotes the displacement at the wind turbine level. Based on the geometric relationships illustrated in Figure 5, Equations (23) and (24) can be formulated.

$$y_1 = y_0 + (L_S - L_C)\sin\psi_0 + \frac{\partial U}{\partial F_2} \tag{23}$$

$$y_2 = y_1 + (L_T + L_C)\sin\psi_1 + \frac{\partial U}{\partial F_1} \tag{24}$$

Here, the value of y_0 is determined based on the soil–structure interaction, as expressed in Equations (25) and (26).

$$y_0 = \delta_L(F_1+F_2) + \delta_{LR}[F_1(L_T+L_S)+F_2(L_S-L_C)] \tag{25}$$

$$\psi_0 = \delta_{LR}(F_1+F_2) + \delta_R[F_1(L_T+L_S)+F_2(L_S-L_C)] \tag{26}$$

In Equations (25) and (26), δ_L represents the horizontal spring stiffness coefficient of the soil, δ_R denotes the rotational spring stiffness coefficient, and δ_{LR} is the coupling stiffness coefficient between translation and rotation. These coefficients vary depending on the soil type, pile rigidity, and embedded pile length. For slender piles in non-cohesive soils, the coefficients are given in matrix form as shown in Equation (27) (Poulos and Davis, 1980).

$$\begin{Bmatrix} y_0 \\ \psi_0 \end{Bmatrix} = \begin{bmatrix} \dfrac{2{,}40}{n_h^{3/5}(E_PI_P)^{2/5}} & \dfrac{1{,}60}{n_h^{2/5}(E_PI_P)^{3/5}} \\ \dfrac{1{,}60}{n_h^{2/5}(E_PI_P)^{3/5}} & \dfrac{1{,}74}{n_h^{1/5}(E_PI_P)^{4/5}} \end{bmatrix} \begin{Bmatrix} F_1+F_2 \\ F_1(L_T+L_S)+F_2(L_S-L_C) \end{Bmatrix} \tag{27}$$

In Equation (27), n_h denotes the subgrade reaction modulus, representing the soil's elasticity, and its values are provided in Table 1 (Terzaghi, 1955).

Table 1. Variation of subgrade reaction modulus values (n_h) with relative density and groundwater condition

Relative Density	n_h (kN/m^3)		
	Loose	Medium	Dense
Above the groundwater level	2424	7272	19393
Below the groundwater level	1385	4848	11774

For rigid piles in non-cohesive soils, the stiffness coefficients are given in matrix form as shown in Equation (28) (Poulos and Davis, 1980).

$$\begin{Bmatrix} y_0 \\ \psi_0 \end{Bmatrix} = \begin{bmatrix} \frac{18}{L_P^2 n_h} & \frac{24}{L_P^3 n_h} \\ \frac{24}{L_P^3 n_h} & \frac{36}{L_P^4 n_h} \end{bmatrix} \begin{Bmatrix} F_1+F_2 \\ F_1(L_T+L_S)+F_2(L_S-L_C) \end{Bmatrix} \quad (28)$$

In Equation (28), L_P represents the embedded length of the pile within the soil. One of the key considerations here is distinguishing whether the pile behaves as rigid or slender, since the stiffness matrices differ accordingly. In non-cohesive soils, the classification of pile behavior as rigid or slender depends on the limits defined in Equations (29) and (30) (Poulos and Davis, 1980).

$$L_P > 4.0\left(\frac{E_P I_P}{n_h}\right)^{\frac{1}{5}} \quad \text{Slender pile condition} \quad (29)$$

$$L_P < 2.0\left(\frac{E_P I_P}{n_h}\right)^{\frac{1}{5}} \quad \text{Rigid pile condition} \quad (30)$$

Piles with parameters falling between these two limits are referred to as transitional piles, and within this range, the behavior cannot be clearly classified as either slender or rigid. In cohesive soils, variations in the stiffness matrices are expected. For slender piles embedded in cohesive soils, the corresponding stiffness coefficients are provided in Equation (31) (Poulos and Davis, 1980).

$$\begin{Bmatrix} y_0 \\ \psi_0 \end{Bmatrix} = \begin{bmatrix} \frac{2\beta}{k_h D_P} & \frac{2\beta^2}{k_h D_P} \\ \frac{2\beta^2}{k_h D_P} & \frac{4\beta^3}{k_h D_P} \end{bmatrix} \begin{Bmatrix} F_1+F_2 \\ F_1(L_T+L_S)+F_2(L_S-L_C) \end{Bmatrix} \quad (31)$$

In Equation (31), k_h denotes the subgrade reaction modulus for cohesive soils, and βrepresents the slenderness ratio. The value of k_h for cohesive soils is given by Equation (32) (Vesic, 1964).

$$k_h = \frac{0.65}{D_P}\sqrt[12]{\frac{E D_P^4}{E_P I_P}}\left(\frac{E}{1-v_s^2}\right) \quad (32)$$

In Equation (32), E denotes the elastic modulus of the soil, and v_s represents the Poisson's ratio. The slenderness ratio (β) is given by Equation (33).

$$\beta=\sqrt[4]{\frac{k_h D_P}{4E_P I_P}} \tag{33}$$

For rigid piles in cohesive soils, the stiffness coefficient matrix is provided in Equation (34) (Poulos and Davis, 1980).

$$\begin{Bmatrix} y_0 \\ \psi_0 \end{Bmatrix} = \begin{bmatrix} \frac{4}{k_h D_P L_P} & \frac{6}{k_h D_P L_P^2} \\ \frac{6}{k_h D_P L_P^2} & \frac{12}{k_h D_P L_P^3} \end{bmatrix} \begin{Bmatrix} F_1+F_2 \\ F_1(L_T+L_S)+F_2(L_S-L_C) \end{Bmatrix} \tag{34}$$

The boundary conditions distinguishing rigid and slender behavior in cohesive soils are defined by Equations (35) and (36).

$$L_P > 2{,}5\left(\frac{4E_P I_P}{k_h D_P}\right)^{\frac{1}{4}} \quad \text{Slender pile condition} \tag{35}$$

$$L_P < 1{,}5\left(\frac{4E_P I_P}{k_h D_P}\right)^{\frac{1}{4}} \quad \text{Rigid pile condition} \tag{36}$$

Once y_0 is determined, the only remaining unknowns in Equations (23) and (24) are the rotation components ψ_1. To obtain this value, the rotation profile of the system must be established. For this purpose, the system is transformed into an equivalent two-segment model, as illustrated in Figure 6 (Demir, 2025).

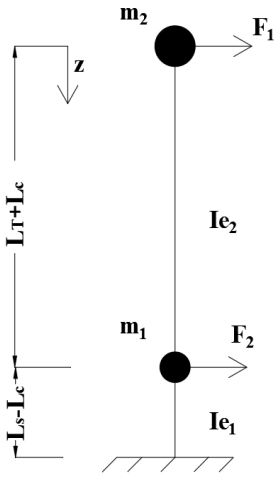


Figure 6. Schematic representation of the equivalent model of the hybrid system (Demir, 2025)

In Figure 6, I_{e1} denotes the equivalent moment of inertia for the first segment, and I_{e2} represents that of the second segment. The moments of inertia are proportional to the flexural rigidity, which in turn is related to the deformation values. The bending moments corresponding to the system deformation are calculated as given in Equations (37) and (38).

$$M(z) = F_1 z \qquad (0 \le z \le L_T) \qquad \text{1st region} \tag{37}$$

$$M(z)=F_1 z + F_2[z - (L_T + L_C)] \qquad (L_T + L_C \le z \le L_T + L_S) \quad \text{2nd region} \tag{38}$$

Similar to the previous section, the strain energy due to deformation is reformulated—this time expressed in two separate parts—as shown in Eqs. (39) and (40).

$$V_1=\int_0^{L_T+L_C}\frac{(F_1 z)^2}{2EI_{e2}}dz=\frac{F_1^2}{2EI_{e2}}\left[\frac{z^3}{3}\right]_0^{L_T+L_C}=\frac{F_1^2(L_T+L_C)^3}{6EI_{e2}} \tag{39}$$

$$V_2=\int_{L_T+L_C}^{L_T+L_S}\frac{(F_1 z + F_2[z - (L_T + L_C)])^2}{2EI_{e1}}dz$$

$$V_2=\frac{1}{2EI_{e1}}\left\{(F_1+F_2)^2\left[\frac{(L_T+L_S)^3}{3}-\frac{(L_T+L_C)^3}{3}\right]-\left[\frac{(L_T+L_S)^2}{2}-\frac{(L_T+L_C)^2}{2}\right]+F_2^2[(L_T+L_S)-(L_T+L_C)]\right\} \tag{40}$$
$$2(F_1+F_2)F_2(L_T+L_C)$$

Similarly, the deformation at the hydrokinetic turbine level is obtained by differentiating the strain energy with respect to the applied force at the hydrokinetic turbine position, as expressed in Equation (41).

$$\frac{\partial V}{\partial F_2}=\frac{1}{2EI_{e1}}\left\{2(F_1+F_2)\left[\frac{(L_T+L_S)^3}{3}-\frac{(L_T+L_C)^3}{3}\right]-\right.$$
$$2(F_1+2F_2)(L_T+L_C)\left[\frac{(L_T+L_S)^2}{2}-\frac{(L_T+L_C)^2}{2}\right]+ \tag{41}$$
$$\left.2F_2(L_T+L_C)^2[(L_T+L_S)-(L_T+L_C)]\right\}$$

By equating Equation (41) with Equation (25), the bending rigidity of the first segment of the equivalent system—corresponding to the displacement at the hydrokinetic turbine level—is obtained as given in Equation (42).

$$EI_{e1}=\frac{1}{2\left(y_0+(L_S-L_C)\sin\psi_0+\frac{\partial U}{\partial F_2}\right)}\left\{2(F_1+F_2)\left[\frac{(L_T+L_S)^3}{3}-\right.\right.$$
$$\left.\frac{(L_T+L_C)^3}{3}\right]-2(F_1+2F_2)(L_T+L_C)\left[\frac{(L_T+L_S)^2}{2}-\frac{(L_T+L_C)^2}{2}\right]+ \tag{42}$$
$$\left.2F_2(L_T+L_C)^2[(L_T+L_S)-(L_T+L_C)]\right\}$$

Therefore, the rotation profile of the first segment—and consequently the value of ψ_1—can now be determined. To obtain this value, the relationship between the bending moment and the second derivative of the deformation is expressed as shown in Equation (43).

$$EI_{e1}\frac{d^2w_1}{dz^2}=M=F_1 z + F_2[z - (L_T + L_C)] \tag{43}$$

By integrating Equation (43) and applying the necessary boundary conditions, the rotation profile is obtained as given in Equations (44) and (45).

$$z=L_T+L_S\,;\ \frac{dw_1}{dz}=-\psi_0 \tag{44}$$

$$\frac{dw_1}{dz}=\frac{1}{EI_{e1}}\left\{F_1\frac{z^2}{2}+F_2\left[\frac{z^2}{2}-(L_T+L_C)z\right]\right\}-\psi_0-\frac{1}{EI_{e1}}\left\{F_1\frac{(L_T+L_S)^2}{2}+F_2\left[\frac{(L_T+L_S)^2}{2}-(L_T+L_C)(L_T+L_S)\right]\right\} \tag{45}$$

By substituting the position of the hydrokinetic turbine into Equation (45), the rotation value at the hydrokinetic turbine level is obtained as expressed in Equation (46).

$$\frac{dw_1}{dz}=\frac{1}{EI_{e1}}\left\{F_1\frac{(L_T+L_C)^2}{2}+F_2\left[\frac{(L_T+L_C)^2}{2}-(L_T+L_C)(L_T+L_C)\right]\right\}-\psi_0-\frac{1}{EI_{e1}}\left\{F_1\frac{(L_T+L_S)^2}{2}+F_2\left[\frac{(L_T+L_S)^2}{2}-(L_T+L_C)(L_T+L_S)\right]\right\} \tag{46}$$

Another important aspect to address in natural frequency analysis is the definition of the effective mass to be considered. In addition to the top mass, a certain portion of the tower mass must also be included in the analysis (Passon, 2006). For single-degree-of-freedom (SDOF) systems—i.e., those consisting solely of a wind turbine—the tower mass is typically accounted for by multiplying it with specific coefficients proposed by various researchers (Arany et al., 2016; Jiang et al., 2023; Vught, 2000). These coefficients depend on the deformation (mode) shape of the structure (Timoshenko, 1937). To determine the deformation profile, the schematic representation of the idealized system can be drawn as shown in Figure 7.

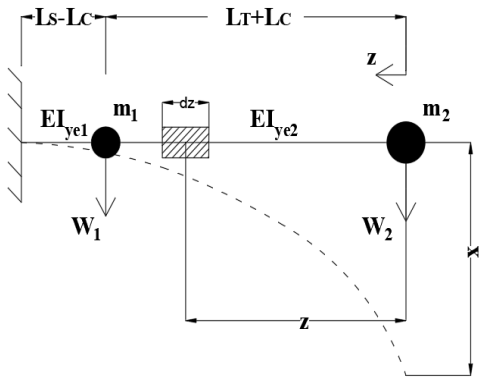


Figure 7. Schematic representation of the idealized system (Demir, 2025)

In Figure 7, EI_{ye1} and EI_{ye2} represent the modified flexural rigidity values of the first and second segments of the idealized system, respectively. Accordingly, the first step is to determine the deformation profile. For the deformation in the first segment, the relationship can be expressed as given in Equation (47).

$$EI_{ye1}\frac{d^2w_1}{dz^2}=M=F_1z+F_2[z-(L_T+L_C)] \tag{47}$$

In Equation (47), w_1 represents the displacement function in the first segment, which varies along the structure and is therefore expressed as a function of the position z. By integrating Equation (47), the rotation equation for the first segment is obtained as shown in Equation (48).

$$\frac{dw_1}{dz}=\frac{1}{EI_{ye1}}\left\{F_1\frac{z^2}{2}+F_2\left[\frac{z^2}{2}-(L_T+L_C)z\right]\right\}+C_1 \tag{48}$$

In Equation (48), C_1 is the integration constant, which naturally depends on the boundary conditions. Since soil–structure interaction is neglected, the soil is assumed to act as a fixed support. Accordingly, rotation at the soil level is taken as zero, leading to the boundary condition expressed in Equation (49), and the integration constant is obtained as given in Equation (50).

$$z=L_T+L_S\,;\,\frac{dw_1}{dz}=0 \tag{49}$$

$$C_1=-\frac{1}{EI_{ye1}}\left\{F_1\frac{(L_T+L_S)^2}{2}+F_2\left[\frac{(L_T+L_S)^2}{2}-(L_T+L_C)(L_T+L_S)\right]\right\} \tag{50}$$

Therefore, the rotation profile in the first segment is obtained as expressed in Equation (51).

$$\frac{dw_1}{dz}=\frac{z-(L_T+L_S)}{2EI_{ye1}}[(F_1+F_2)(z+L_T+L_S)-F_2(L_T+L_C)] \tag{51}$$

By integrating the rotation profile given in Equation (51), the deformation profile for the first segment is obtained as expressed in Equation (52).

$$w_1=\frac{1}{EI_{ye1}}\left\{F_1\frac{z^3}{6}+F_2\left[\frac{z^3}{6}-(L_T+L_C)\frac{z^2}{2}\right]\right\}-\frac{1}{EI_{ye1}}\left\{F_1\frac{(L_T+L_S)^2}{2}+F_2\left[\frac{(L_T+L_S)^2}{2}-(L_T+L_C)(L_T+L_S)\right]\right\}z+C_2 \tag{52}$$

By applying the boundary condition given in Equation (53), the deformation profile for the first segment is obtained as expressed in Equation (54).

$$z=L_T+L_S\,;\,w_1=0 \tag{53}$$

$$w_1=\frac{[z-(L_T+L_S)]^2}{6EI_{ye1}}[(F_1+F_2)z+2F_1(L_T+L_S)+F_2(2L_S-L_T-3L_C)] \tag{54}$$

In this case, the only unknown is the modified flexural rigidity of the first segment, denoted as EI_{ye1}. Since the displacement at the hydrokinetic turbine level, x_1, is known, this value can be determined using the boundary condition given in Equations (55) and (56).

$$z=L_T+L_C\,;\,w_1=x_1 \tag{55}$$

$$EI_{ye1}=\frac{(L_C-L_S)^2}{6EI_{ye1}}[(F_1(L_C+2L_S+3L_T)+2F_2(L_S-L_C)] \tag{56}$$

Since the deformation profile of the first segment is known, the coefficient corresponding to the tower mass can be determined. It can be stated that the maximum velocity occurs at the

location where the maximum deformation is observed. Accordingly, the velocity profile for the first segment can be expressed as given in Equation (57).

$$v_1 = \frac{w_1}{x_1} v_{max} \tag{57}$$

Therefore, for a differential element considered as shown in Figure 8, the kinetic energy equation can be expressed as given in Equation (58).

$$dT = \frac{1}{2} m v^2 = \frac{1}{2} \rho A dz \left(\frac{w_1}{x_1} v_{max} \right)^2 \tag{58}$$

In Equation (58), dz represents the length of the differential element, A is the cross-sectional area of the element, and m denotes its mass. By integrating Equation (58) along the first segment, the kinetic energy of the first region can be calculated as expressed in Equation (59).

$$T_1 = \frac{1}{2} \rho A {v_{max}}^2 \frac{1}{{x_1}^2} \int_{L_T + L_C}^{L_T + L_S} (w_1)^2 \, dz \tag{59}$$

By modifying the lower and upper limits of the integral in Equation (59), Equation (60) is obtained.

$$T_1 = \frac{1}{2} \rho A [(L_T + L_S) - (L_T + L_C)] \frac{{v_{max}}^2}{[(L_T + L_S) - (L_T + L_C)]} \frac{1}{{x_1}^2} \int_{L_T + L_C}^{L_T + L_S} (w_1)^2 \, dz \tag{60}$$

In this equation, the left-hand side represents the mass of the first segment, which is expressed in Equation (61).

$$m_{k1} = \frac{1}{2} \rho A [(L_T + L_S) - (L_T + L_C)] \tag{61}$$

In Equation (61), m_{k1} denotes the mass of the first segment. Therefore, the remaining part of the equation represents the coefficient that accounts for the tower mass, hereafter referred to as the effective mass coefficient. For the first segment, the effective mass coefficient is expressed as shown in Equation (62).

$$m_{eff1} = \frac{1}{[(L_T + L_S) - (L_T + L_C)]} \frac{1}{{x_1}^2} \int_{L_T + L_C}^{L_T + L_S} (w_1)^2 \, dz \tag{62}$$

For the second segment, the same procedure used in the first segment to obtain the deformation profile is followed. In the following section, the detailed steps are omitted, and only the boundary conditions are provided to explain the derivation of the corresponding equations. The relationship between the bending moment and the second derivative of the deformation is expressed in Equation (63).

$$EI_{ye2} \frac{d^2 w_2}{dz^2} = M = F_1 z \tag{63}$$

In Equation (63), EI_{ye2} represents the flexural rigidity of the idealized second segment, and w_2 denotes the deformation profile of this segment. The first integration of Equation (63) yields the rotation profile for the second segment, as expressed in Equation (64), while the second integration provides the deformation profile, as given in Equation (65).

$$\frac{dw_2}{dz}=\frac{1}{EI_{ye2}}\left\{F_1\frac{z^2}{2}\right\}+\psi_0-\psi_1-\frac{1}{EI_{ye2}}\left\{F_1\frac{(L_T+L_c)^2}{2}\right\} \quad (64)$$

$$w_2=\frac{1}{EI_{ye2}}\left\{F_1\frac{z^2}{2}\right\}+\psi_0-\psi_1-\frac{1}{EI_{ye2}}\left\{F_1\frac{(L_T+L_c)^2}{2}\right\} \quad (65)$$

$$z=0\ ;\ w_2=x_2 \quad (66)$$

$$EI_{ye2}=-\frac{1}{y_2-y_1+(\psi_0-\psi_1)(L_T+L_c)}\left\{F_1\frac{(L_T+L_c)^3}{6}\right\}+\frac{1}{y_2-y_1+(\psi_0-\psi_1)(L_T+L_c)}\left\{F_1\frac{(L_T+L_c)^2}{2}\right\}(L_T+L_c) \quad (67)$$

Here, the only unknown is EI_{ye2}, which represents the flexural rigidity of the modified second segment of the system. Since the displacement value at the wind turbine level (x_2) is known, this parameter can be determined using the boundary conditions given in Equations (66) and (67).

$$v_2=\frac{w_2}{x_2}v_{max} \quad (68)$$

Therefore, for a differential element considered as shown in Figure 7, the kinetic energy equation can be expressed as given in Equation (69).

$$dT=\frac{1}{2}mv^2=\frac{1}{2}\rho A dz\left(\frac{w_2}{x_2}v_{maks}\right)^2 \quad (69)$$

By integrating Equation (69) along the second segment, the kinetic energy of the second region can be calculated as expressed in Equation (70).

$$T_2=\frac{1}{2}\rho A{v_{max}}^2\frac{1}{{x_2}^2}\int_0^{L_T+L_C}(w_2)^2\,dz \quad (70)$$

By modifying the upper limit of the integral in Equation (70), Equation (71) is obtained.

$$T_2=\frac{1}{2}\rho A(L_T+L_C)\frac{{v_{max}}^2}{(L_T+L_C)}\frac{1}{{x_2}^2}\int_0^{L_T+L_C}(w_2)^2\,dz \quad (71)$$

In this equation, the left-hand side represents the mass of the second segment, which is expressed in Equation (72).

$$m_{k2}=\frac{1}{2}\rho A(L_T+L_C) \quad (72)$$

In Equation (72), m_{k2} denotes the mass of the second segment. Accordingly, the effective mass coefficient for the second segment is expressed as shown in Equation (73).

$$m_{eff2}=\frac{1}{(L_T+L_C)}\frac{1}{{x_2}^2}\int_0^{L_T+L_C}(w_2)^2\,dz \quad (73)$$

The generation of additional moments and deformations due to axial loads arising from geometric nonlinearity is referred to as the P–Δ effect. As previously mentioned, with the advancement of wind turbine technology, both tower dimensions and turbine weights have been continuously increasing. This increase has also attracted the attention of researchers, and

for piles subjected to horizontal loading with a single top mass—meaning those loaded axially and laterally from the top—the schematic representation of the moment amplification at the foundation level is illustrated in Figure 8 (Burgos and Silva, 2023).

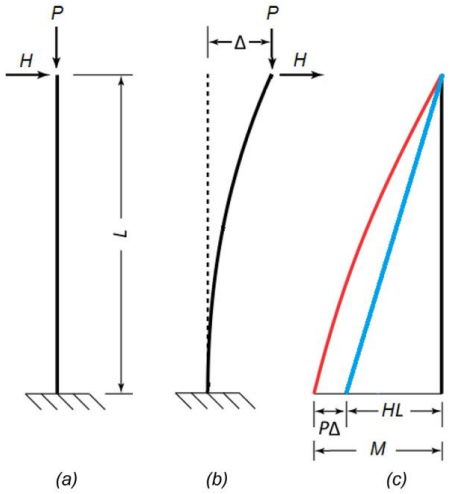


Figure 8. Schematic representation of the P–Δ effect: (a)Undeformed shape of a laterally loaded pile, (b)Additional moment generated by the axial load acting on the laterally deformed pile, (c)Initial moment distribution (shown in blue) and its modification due to the P–Δ effect (Burgos and Silva, 2023)

In Figure 8, H represents the horizontal force at the top of the tower, corresponding to the load acting on the rotor; P denotes the axial load, which represents the combined weight of the rotor–nacelle–assembly; and Δ is the lateral displacement at the tower top caused by the horizontal load. The increase in moment resulting from these effects is referred to as the moment amplification factor (MAF), and the total moment can be expressed as given in Equation (74) (Burgos and Silva, 2023).

$$M = MAF \times HL \tag{74}$$

The method used to account for the moment amplification factor (MAF) is known as the pseudo-horizontal force method (Burgos and Silva, 2023; Liu, 1988). In this approach, the axial forces are converted into equivalent horizontal forces that produce the same moment within the structure. The displacements resulting from these horizontal forces are computed iteratively, and the process continues until a specified convergence criterion is satisfied. For systems that are both laterally and axially loaded from the top, as illustrated in Fig. 8, the MAF value is defined by Equation (75).

$$MAF_{P\text{-}\Delta} = \frac{1}{1 - \frac{PL^2}{3EI}} \tag{75}$$

As can be observed from Equaton (75), the increase in axial load—representing the combined weight of the rotor–nacelle assembly—and the increase in tower height significantly influence the MAF value. Consequently, the effect of axial load on both the bending moment and the natural frequency becomes evident through this relationship. In the context of this study, since the system incorporates two different turbines, the corresponding turbine weights are

considered as axial loads. Additionally, the masses of the tower and turbines are also taken into account as axial loads, as schematically illustrated in Figure 9.

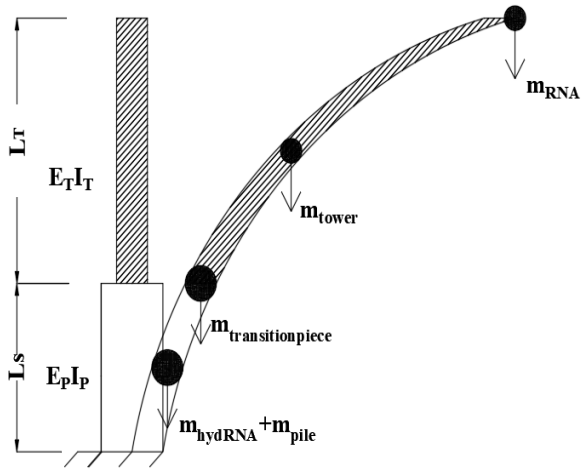


Figure 9. Schematic representation of the vertical forces considered in the analysis of the P–Δ effect

In Figure 9, mRNA represents the rotor–nacelle–assembly weight of the wind turbine, mtower is the mass of the tower, mtransition piece denotes the weight of the transition piece, mhydRNA corresponds to the rotor–nacelle–assembly weight of the hydrokinetic turbine, and mpile is the mass of the monopile. The reason for combining the hydrokinetic turbine and pile weights is that the hydrokinetic turbine is mounted approximately at the mid-depth of the pile (HoWAT, 2019; Ma et al., 2025; Demir and Balas, 2025b). These axial loads are then converted into equivalent forces that generate the same bending moments in the structure, as illustrated in Figure 10.

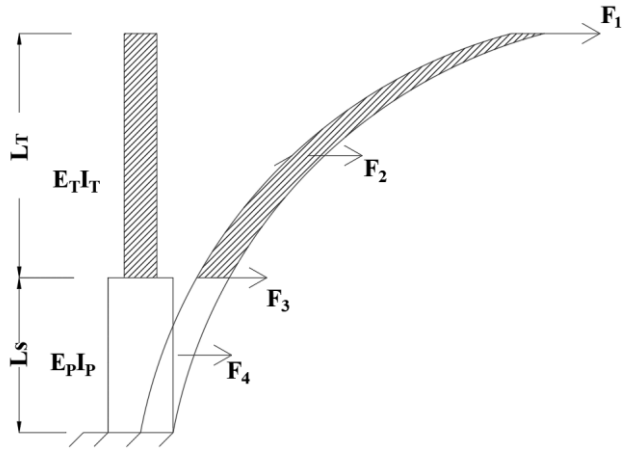


Figure 10. Schematic representation of the conversion of axial forces into equivalent pseudo-horizontal forces

The converted forces are obtained using the equations given between Equations (76) and (79).

$$F_1 = \frac{G_{RNA} \times w_1(0)}{L_T + L_S} \tag{76}$$

$$F_2=\frac{G_{tower}\times w_1(z_{gt})}{L_T+L_S-z_{gt}} \tag{77}$$

$$F_3=\frac{G_{transition\ piece}\times w_1(L_T)}{L_S} \tag{78}$$

$$F_4=\frac{G_{hydRNA+pile}\times w_2\left(L_T+\frac{L_S}{2}\right)}{\frac{L_S}{2}} \tag{79}$$

In these equations, z_{gt} denotes the position of the center of gravity of the tower mass; G_{RNA} represents the force-equivalent of the rotor–nacelle–assembly mass of the wind turbine; G_{tower} is the force-equivalent of the tower mass; $G_{transition\ piece}$ corresponds to the force-equivalent of the transition piece located at the tower–pile interface; and $G_{hydRNA+pile}$ represents the combined force-equivalent of the hydrokinetic turbine's rotor–nacelle–assembly and the pile mass. To determine the additional displacements caused by these forces, Castigliano's second theorem is employed. The strain energy due to deformation is expressed by Equation (80).

$$\begin{aligned}U&=\int_0^{L_T+L_S}\frac{[M(z)]^2}{2EI(z)}dz\\ U&=\int_0^{z_{tg}}\frac{[F_1z]^2}{2E_TI_T}dz+\int_{z_{tg}}^{L_T}\frac{\left[F_1z+F_2(z-z_{tg})\right]^2}{2E_TI_T}dz+\\ &\int_{L_T}^{L_T+\frac{L_S}{2}}\frac{\left[F_1z+F_2(z-z_{tg})+F_3(z-L_T)\right]^2}{2E_TI_T}dz+\\ &\int_{L_T+\frac{L_S}{2}}^{L_T+L_S}\frac{\left[F_1z+F_2(z-z_{tg})+F_3(z-L_T)+F_4\left(z-L_T-\frac{L_S}{2}\right)\right]^2}{2E_TI_T}dz\end{aligned} \tag{80}$$

Accordingly, by taking the derivative of the strain energy with respect to each force shown in Figure 10, the corresponding displacement values can be obtained as expressed in Equations (81) through (84).

$$\begin{aligned}\Delta_{F_1}=&\frac{F_1z_1^3}{3E_TI_T}+\frac{1}{2E_TI_T}\left[\frac{2(F_1+F_2)}{3}\left(L_T^3-z_{tg}^3\right)-F_2z_1\left(L_T^2-z_{tg}^2\right)\right]+\frac{1}{2E_PI_P}\left[\frac{2A_1}{3}D_3-B_1D_2\right]\\ &+\frac{1}{2E_PI_P}\left[\frac{2A_2}{3}D_3-B_2D_2\right]\end{aligned} \tag{81}$$

$$D_1=v-u,\ D_2=v^2-u^2,\ D_3=v^3-u^3,v=L_T+0.5L_S,u=L_T,\ A_1=F_1+F_2+F_3,\ A_2=F_1+F_2+F_3+F_4,$$

$$B_1=F_2z_1+F_3L_T,\ B_2=F_2z_1+F_3L_T+F_4\left(L_T+\frac{L_S}{2}\right)$$

$$\Delta_{F_2}=\frac{1}{2E_TI_T}\left[\frac{2(F_1+F_2)}{3}\left(L_T^3-z_{tg}^3\right)-(F_1+2F_2)z_1\left(L_T^2-z_{tg}^2\right)+2F_2z_{tg}^2(L_T-z_{tg})\right]+\frac{1}{2E_PI_P}\left[\frac{2A_1}{3}D_3-(B_1+A_1z_{tg})D_2+2B_1z_{tg}D_1\right]+\frac{1}{2E_PI_P}\left[\frac{2A_2}{3}D_3-(B_2+A_2z_{tg})D_2+2B_2z_{tg}D_1\right] \quad (82)$$

$$\Delta_{F_3}=\frac{1}{2E_PI_P}\left[\frac{2A_1}{3}D_3-(B_1+A_1L_T)D_2+2B_1L_TD_1\right]+\frac{1}{2E_PI_P}\left[\frac{2A_2}{3}D_3-(B_2+A_2L_T)D_2+2B_2L_TD_1\right] \quad (83)$$

$$\Delta_{F_4}=\frac{1}{2E_PI_P}\left[\frac{2A_1}{3}D_3-\left(B_1+A_1\left(L_T+\frac{L_S}{2}\right)D_2+2B_1L_T\left(L_T+\frac{L_S}{2}\right)D_1\right] \quad (84)$$

When these additional displacement values are incorporated into the deformation, the overall deformation profile of the system changes, leading to a recalculation of the natural frequency based on the updated profile. This iterative process continues until the natural frequency value converges to a stable result. The corresponding computational loop used for this procedure is illustrated in Figure 11.

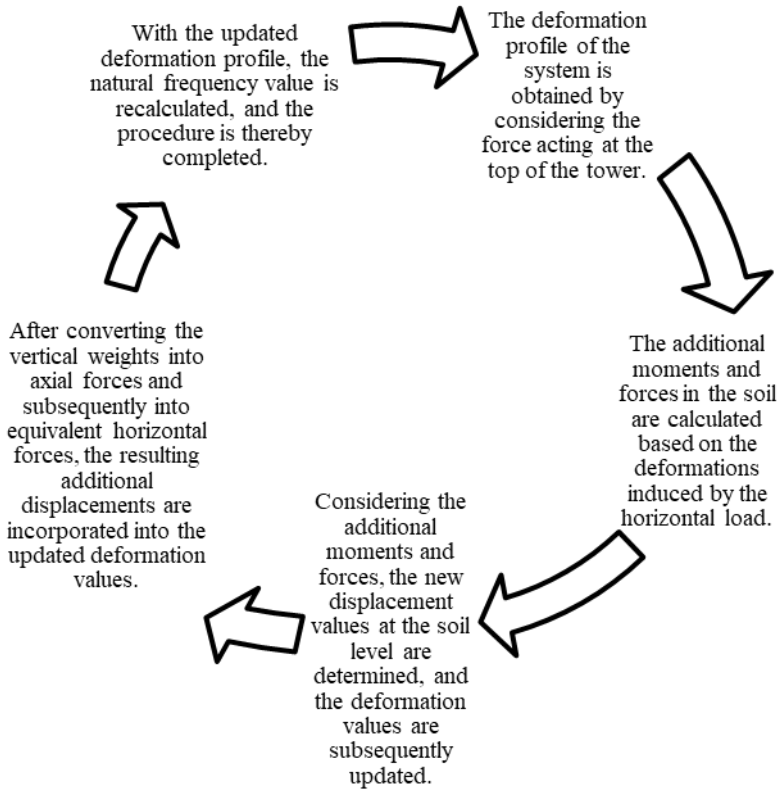


Figure 11. computational loop developed in this study to evaluate the effect of the P–Δ phenomenon on the natural frequency

The iterative loop shown in Figure 11 can be described step by step as follows.

- The deformations induced by the lateral load are calculated.
- Based on these deformations, the variations in the loads and bending moments at the foundation are determined.
- Using the additional moments and forces, the deformation values of the structure are updated.
- The vertical weights are converted first into axial forces and then into equivalent horizontal forces, from which new deformation values are obtained.

Finally, the natural frequency is calculated using the updated deformation profile.

RESULTS AND DISCUSSION

The hybrid offshore wind–hydrokinetic configuration used for model validation combines an NREL 5 MW wind turbine and a SEAGEN S 2 MW hydrokinetic turbine, as summarized in Table 2 (HoWAT, 2019). This configuration was deliberately selected because it represents a widely referenced benchmark in the literature, featuring moderate tower slenderness and a well-documented monopile foundation. The main parameters—such as the tower height (80 m), rotor–nacelle–assembly weight (350 t), and pile embedment length (36 m)—reflect a realistic balance between stiffness and flexibility. The soil profile corresponds to a medium-dense cohesionless sand located below the groundwater level; thus, the subgrade reaction coefficient was taken as n_h=4848 kN/m^3 based on the relative density of 55 % reported by (Jonkman, 2010).

Table 2. Turbine and geometric properties of the hybrid wind–hydrokinetic system (HoWAT, 2019)

Wind Turbine (NREL 5 MW) (HoWAT, 2019)		
Rotor–nacelle–assembly weight	m_{RNA}	350 t
Tower top diameter	D_t	3.87 m
Tower base diameter	D_b	6.00 m
Tower weight	m_{tower}	347.46 t
Tower material density	r_{tower}	8500 kg/m^3
Tower elastic modulus	E_T	210 GPa
Tower length	L_T	80 m
Distance between tower base and seabed	L_S	38 m
Transition piece weight	$m_{transition\ piece}$	172 t
Wind load	F_1	0.79 MN
Hydrokinetic Turbine (SEAGEN S 2 MW) (HoWAT, 2019)		
Hydrokinetic turbine weight	m_{hydRNA}	120 t
Distance between hydrokinetic turbine and tower base	L_C	24 m
Pile elastic modulus	E_P	210 GPa
Pile diameter	D_P	6.00 m

Pile wall thickness	t_T	70 mm
Pile material density	r_{pile}	7850 kg/m^3
Hydrokinetic turbine load	F_2	1.05 MN
Embedded pile length	L_P	36 m
Soil Properties (HoWAT, 2019)		
Subgrade reaction coefficient	n_h	4848 kN/m^3

In the reference study by HoWAT (2019), the same configuration was modeled in ANSYS, where the tower, transition piece, and monopile were represented using 3-D solid and shell elements. The analytical model developed in this study was validated against those numerical results by comparing the first natural frequency, both with and without consideration of the P–Δ (second-order) effect, as shown in Table 3.

Table 3. Comparison between the natural frequency values from the proposed method and the literature

Research	**Frequency (Hz)**	**Difference (%)**
HoWAT (2019)	0.218	-
Proposed method w/o P-Δ effect	0.213	2.35
Proposed method w P-Δ effect	0.210	3.67

As seen in Table 3, the analytical results exhibit strong agreement with the reference model. Including the P–Δ effect increases the deviation from 2.35 % to 3.67 %, producing a 1.41 % relative reduction in frequency. This difference arises from the additional flexibility caused by axial-load-induced bending, which slightly decreases the global stiffness of the coupled tower–pile system. The magnitude of this reduction is consistent with the nonlinear stiffness-degradation trends reported by Burgos and Silva (2023) and similar studies (Kühn, 2001). Overall, the proposed analytical approach predicts the first natural frequency within ±4 % of high-fidelity FEM results—adequate for preliminary design and dynamic assessment of hybrid offshore structures. After validation, the analytical model was applied to a conceptual DTU 10 MW + SEAGEN S 2 MW hybrid system proposed for installation off the Kıyıköy coast in the Western Black Sea (Figure 12) (Demir and Balas, 2024).

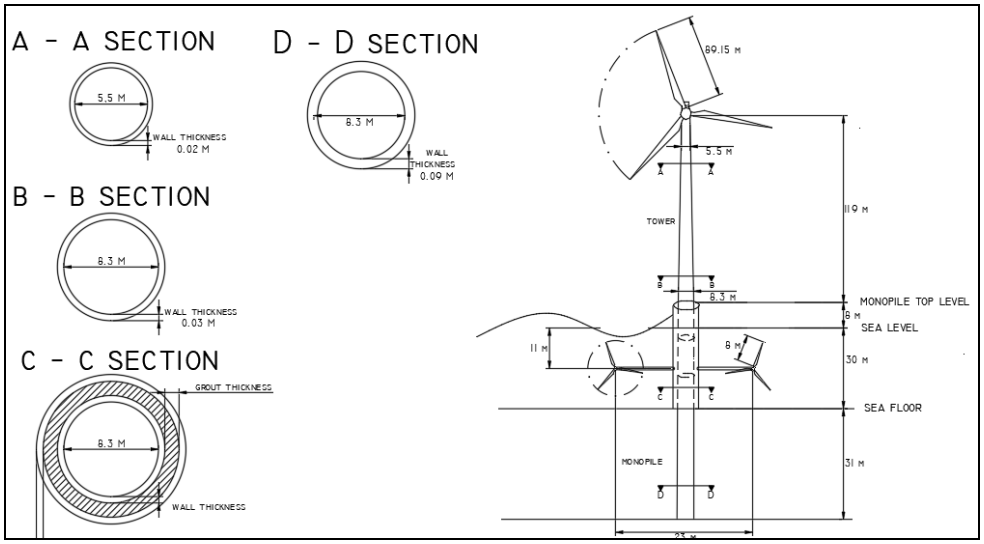


Figure 12. Schematic representation of the hybrid wind–hydrokinetic turbine system designed for the Western Black Sea region (Demir and Balas, 2024)

The structural and soil parameters used are summarized in Table 4.

Table 4. Turbine, geometric, and soil properties for the hybrid system designed for the Western Black Sea region (Demir and Balas, 2024)

Wind Turbine (DTU 10 MW)		
Rotor–nacelle–assembly weight	m_{RNA}	679.85 t
Tower top diameter	D_t	5.50 m
Tower base diameter	D_b	8.30 m
Tower weight	m_{tower}	673.65 t
Tower material density	r_{tower}	8500 kg/m^3
Tower elastic modulus	E_T	210 GPa
Tower length	L_T	115.63 m
Distance between tower base and seabed	L_S	38.19 m
Wind load	F_1	2.19 MN
Hydrokinetic Turbine (SEAGEN S 2 MW)		
Hydrokinetic turbine weight	m_{hydRNA}	120 t
Distance between hydrokinetic turbine and tower base	L_C	24 m
Pile elastic modulus	E_P	210 GPa
Pile diameter	D_P	8.3 m
Pile wall thickness	t_T	100 mm
Pile material density	r_{pile}	7850 kg/m^3
Hydrokinetic turbine load	F_2	1.05 MN
Embedded pile length	L_P	31 m
Soil Properties		
Subgrade reaction coefficient	n_h	4848 kN/m^3

Compared with the NREL 5 MW system, this configuration features a taller tower (115.6 m), larger monopile diameter (8.3 m), and heavier top mass (~ 680 t)—conditions that increase both axial load and slenderness ratio.

The calculated natural frequencies, obtained with and without inclusion of the P–Δ effect, are compared in Table 5.

Table 5. Comparison of natural frequency values for the hybrid system designed for the Western Black Sea region

Research	Frequency (Hz)	Difference (%)
Proposed method w/o P-Δ effect	0.135	-
Proposed method w P-Δ effect	0.130	3.71

The inclusion of geometric nonlinearity results in a 3.71 % reduction in the fundamental natural frequency. This decrease stems from amplified bending moments and increased deflections under combined lateral and axial loading, effectively reducing the overall stiffness. The trend agrees with the moment-amplification behavior reported by Burgos and Silva (2023), confirming that P–Δ influence intensifies with increasing turbine capacity and tower slenderness. Physically, the additional curvature induced by axial loads lowers resistance to dynamic bending, producing a measurable frequency shift. For large-capacity turbines such as the DTU 10 MW, this shift can move the structural frequency closer to environmental excitation ranges (e.g., wave 0.1–0.3 Hz or 1P/3P bands). Neglecting this effect may therefore lead to overestimated stiffness and underpredicted resonance risk. In conclusion, accounting for second-order geometric effects is essential in the dynamic analysis of hybrid offshore systems, especially for turbines exceeding 10 MW, where axial forces and tower flexibility dominate the response. Even a few-percent reduction in natural frequency can have significant implications for fatigue life, serviceability, and operational safety in offshore environments.

CONCLUSION

This study developed an analytical framework to evaluate the influence of the P–Δ (second-order) effect on the natural frequency of hybrid offshore wind–hydrokinetic turbine systems. A deterministic two-degree-of-freedom formulation was established by coupling structural dynamics, geometric non-linearity, and soil–structure interaction effects through Castigliano's energy theorem. The model consistently captures stiffness reduction induced by increasing axial loads arising from turbine mass and tower slenderness.

Validation against the HoWAT (2019) benchmark combining an NREL 5 MW wind turbine and a SEAGEN S 2 MW hydrokinetic unit yielded less than 4 % deviation from numerical results, confirming the analytical model's reliability. Application to the Kıyıköy-based 10 MW hybrid configuration revealed that the inclusion of the P–Δ effect decreases the fundamental frequency by approximately 3.7 %, indicating a significant influence on structural stiffness and dynamic behavior for large-capacity turbines.

The present formulation assumes linear-elastic soil behavior, neglects damping and cyclic loading effects, and is restricted to free-vibration conditions. These simplifications limit its use under fully dynamic operating loads. Future work should focus on extending the model to include damping mechanisms, variable soil stiffness, and combined loading scenarios (wind–wave–current interactions). Site-specific calibration of soil parameters and experimental validation would further enhance the model's applicability to real offshore environments.

REFERENCES

Alkhoury, P., Soubra, A.-H., Rey, V., Ait–Ahmed, M., 2020. A full three-dimensional model for the estimation of the natural frequencies of an offshore wind turbine in sand. Wind Energy 24, 699–719. https://doi.org/10.1002/we.2598.

Amel, D., Djillali, A.B., Bhattacharya, S., Nasreddine, A., 2022. Evaluation of sand p–y curves by predicting both monopile lateral response and OWT natural frequency. Studia Geotechnica Mech. 44, 66–81. https://doi.org/10.2478/sgem-2022-0003.

Andersen, O.J., Løvseth, J., 1992. The maritime turbulent wind field. Measurements and models. Phase 2–Extension 2–Phase 4. Extended analysis of the Frøya database, Statoil and ALLFORSK AVH.

Arany, L., Bhattacharya, S., MacDonald, J.H.G., Hogan, S.J., 2016. Closed-form solution of Eigen frequency of monopile supported offshore wind turbines in deeper waters incorporating stiffness of substructure and SSI. Soil Dynam. Earthq. Eng. 83, 18–32. https://doi.org/10.1016/j.soildyn.2015.12.011.

Bhattacharya, S., 2014. Challenges in design of foundations for offshore wind turbines. Eng. Technol. Ref. 1. https://doi.org/10.1049/etr.2014.0041.

Burgos, R. B., Silva, L. E., 2023. Evaluation of the P-Δ (P-Delta) effect in columns and frames using the two-cycle method based on the solution of the beam-column differential equation. MethodsX . 11. https://doi.org/10.1016/j.mex.2023.102248.

Caceoğlu, E. (2023) Offshore Wind turbines in Marmara Region, Türkiye: Site selection and preliminary geotechnical design of monopiles, Master of Science Thesis, Middle East Technical University, Graduate School of Natural and Applied Sciences, Ankara.

Demir, A K.., 2025. Türkiye için optimum açık deniz üzeri kombine rüzgar ve mavi enerji santrali geliştirilmesi (in Turkish) Doctorate Thesis. Gazi Üniversitesi Fen Bilimleri Enstitüsü, Ankara, Türkiye.

Demir, AK, Balas, CE, Balas, L., 2024. Enhancing Türkiye's Renewable Energy Capacity: An Advanced Hybrid Model for Combined Offshore Wind and Wave Turbines Design Utilizing Hydrodynamic and Monte Carlo Simulations. Journal of Coastal Research, 113(SI), 793-798.

Demir, A. K., Balas, C. E., 2025a. Frequency response of multi-degree-of-freedom hybrid offshore systems integrating wind and hydrokinetic turbines. Results in Engineering, 25. https://doi.org/10.1016/j.rineng.2025.105631.

Demir, A. K., Balas, C. E., 2025b. Dynamic frequency behavior of hybrid offshore systems under stochastic variations. Ocean Engineering, 340. https://doi.org/10.1016/j.oceaneng.2025.122232.

ESMAP, 2020. Going global: Expanding offshore wind to emerging market,. Energy Sector Management Assistance Program.

GWEC, 2025. Global wind report 2025, Global Wind Energy Council.

HoWAT, 2019. https://www.esru.strath.ac.uk/ EandE/Web_sites/16-17/WindAndTidal/ (accessed 30 August 2024).

Jiang, Y., Zhou, X., Liu, Y., 2023. Simplified calculation method for the natural frequencies of the offshore wind turbine structures with monopile foundations based on euler–Bernoulli beam theory. Adv. Civ. Eng. https://doi.org/10.1155/2023/ 8262901. Article ID 8262901.

Jonkman, J., 2010. Definition of the floating system for Phase IV of OC3. Tech. Rep. NREL/TP – 500 – 47535.

Lande-Sudall, D., Stallard, T. Stansby, P., 2018. Co-located deployment of offshore wind turbines with tidal stream turbine arrays for improved cost of electricity generation, Renewable and Sustainable Energy Reviews, 104, 492–503. https://doi.org/10.1016/j.rser.2019.01.035.

Loken, I.B., 2017. Dynamic Response and Fatigue of Offshore Wind Turbines - Effect of Foundation Type and Modelling Method Using Software FAST, Master of Science Thesis. Norwegian University of Science and Technology Faculty of Engineering Department of Structural Engineering, Trondheim.

Lui, E., M, 1988. A practical P-Delta analysis method for type FR and PR frames, 25, 85-98. Engineering Journal.

Ma, Y., Cui, L., Bhattacharya, S., 2025. A novel foundation design for the hybrid offshore renewable energy harvest system, Ocean Engineering, 323, 120519. https://doi.org/10.1016/j.oceaneng.2025.120519

Offshorewind (2025). https://www.offshorewind.biz/2023/12/13/mingyang-rolls-out-worlds-largest-offshore-wind-turbine-in-capacity-and-rotor-diameter/ (accessed 23 January 2025).

P. Passon, OC3 memo from SWE, memorandum: derivation and description of the soil-PileInteraction models, IEA – Annex XXIII Subtask, 2006.

Pierson Jr, W. J., Moskowitz, L., 1964. A proposed spectral form for fully developed wind seas based on the similarity theory of SA Kitaigorodskii. Journal of geophysical research, 69(24), 5181-5190.

Poulos, H. G., Davis, E. H., 1980. Pile foundation analysis and design, Rainbow – Bridge Book Co, Canada.

Republic of Türkiye Ministry of Energy and Natural Sources (2025) https://enerji.gov.tr/bilgi-merkezi-enerji-elektrik. (accessed 13 September 2025).

Sahu, S. K., Dutta, S. C., 2025. Influence of P-Δ effect on the dynamic response of offshore wind turbines under environmental loads and seismic ground motions. International Journal of Mechanical Sciences, 110638. https://doi.org/10.1016/j.ijmecsci.2025.110638.

Samsó, R., Crespin, J., García-Olivares, A., Solé, J., 2023. Examining the Potential of Marine Renewable Energy: A Net Energy Perspective. Sustainability, 15(10), 8050. https://doi.org/10.3390/su15108050.

Şahin, M. E., 2020 Açık Deniz Rüzgar Sistemleri Üzerine Bir İnceleme ve Danimarka Modeli. Recep Tayyip Erdoğan Üniversitesi Fen ve Mühendislik Bilimleri Dergisi, 1(1), 54 – 67.

Terzaghi, K., 1955. Evaluation of coefficients of subgrade reaction, Géotechnique, 5, 297 – 32. https://doi.org/10.1680/geot.1955.5.4.297.

Timoshenko, S., 1937. Vibration Problems in Engineering, second ed. D. Van Nostrand Company, New York.

Vesic, A., 1961. Bending of Beams Resting on Isotropic Elastic Solid, Journal of the Engineering Mechanics Division, 87, 35-53. https://doi.org/10.1061/JMCEA3.0000212.

Vught, H. 2000. Considerations on the dynamics of support structures for an offshore wind energy converter. Ph.D thesis. The Netherlands: Delft University of Technology

WFO, 2024. Global offshore Wind report 2024, World Forum Offshore Wind.

Yıldırım, B. (2022) Hydrodynamic analysis of floating offshore wind turbine concepts: A case study in Black Sea, Master of Science Thesis, Middle East Technical University, Graduate School of Natural and Applied Sciences, Ankara.

YER FISTIĞI KABUĞU BIYO-KÖMÜRÜ ÜZERINDE SÜREKLI PB(II) ADSORPSİYONU İÇIN SABIT YATAKLI KOLON DINAMIKLERI: GIRIŞ KONSANTRASYONUNUN ETKISI VE KINETIK KIRILMA MODELLEMESI

FIXED-BED COLUMN DYNAMICS FOR CONTINUOUS PB(II) SEQUESTRATION ONTO PEANUT SHELL BIOCHAR: INFLUENCE OF INFLUENT CONCENTRATION AND KINETIC BREAKTHROUGH MODELING

Muhammed ONAY
Assist. Prof. Dr., Malatya Turgut Özal University, Faculty of Engineering and Natural Sciences, Department of Engineering Basic Sciences
ORCID NO: 0000-0002-4276-0425

ÖZET

Hızlı sanayileşme ve kontrolsüz atık su deşarjı, su ekosistemlerindeki ağır metal kirliliğini küresel ölçekte kritik bir çevre tehdidi haline getirmektedir. Bu bağlamda yaygın tarımsal atıkların yüksek değerli biyokömür adsorbanlarına dönüştürülmesi büyük oranda ilgi görmektedir. Bu çalışmada, yer fıstığı kabuğu biyo-kömürü üzerine sürekli akışlı sabit yataklı kolonda Pb(II) adsorpsiyonu, giriş çözünen derişiminin (C_0 = 0.5-2.0 mg L^{-1}) dinamik kırılma hidrodinamiği ve kütle aktarım kinetiği üzerindeki belirleyici etkisini ortaya koymak amacıyla sistematik olarak değerlendirilmiştir. Deneysel kırılma eğrileri, besleme derişimindeki artışın kütle transferi sürükleyici kuvvetini güçlendirerek denge adsorpsiyon kapasitesini (qtotal) 27.72'den 34.05 mg g^{-1}'a çıkardığını göstermiştir. Aksine, seyreltik koşullarda çalışma biyo-kömür yatağının işletim ömrünü önemli ölçüde uzatmış ve %50 kırılma süresini (τ) 202.79'dan 504.57 dakikaya ötelemiştir. Kolon kırılma profillerinin matematiksel simülasyonu Adams–Bohart, Thomas ve Yoon–Nelson modelleri kullanılarak gerçekleştirilmiş ve tüm modeller yüksek korelasyon katsayıları (R^2 > 0.90) sergilemiştir. Thomas ve Yoon–Nelson modelleri, kolon doygunluk davranışını ve işletim performansını öngörmede üstün hassasiyet sunmuştur. Yoon–Nelson hız sabiti (kYN), orta derişim seviyesinde (1.0 mg L^{-1}) 0.039 dak^{-1} ile tepe noktasına ulaşan monotonik olmayan bir eğilim göstererek, dış film kütle transferinin ana hız sınırlayıcı mekanizma olduğunu doğrulamıştır. Sonuç olarak, modifiye edilmiş yer fıstığı kabuğu biyo-kömürü, merkezi olmayan ağır metal atıksu arıtma sistemleri için sürdürülebilir ve düşük maliyetli bir dolgu malzemesi olarak yüksek potansiyel sunmaktadır.

Anahtar kelimeler: Yer fıstığı kabuğu biyo-kömürü; Pb(II) giderimi; Sabit yataklı kolon; Kırılma kinetiği.

ABSTRACT

Rapid industrialization and uncontrolled wastewater discharge are turning heavy metal pollution in aquatic ecosystems into a critical environmental threat on a global scale. In this context, the conversion of abundant agricultural wastes into high-value biochar adsorbents is

attracting significant interest. In this study, continuous-flow fixed-bed column adsorption of Pb(II) onto peanut shell biochar was systematically evaluated to decipher the key influence of influent solute concentration (C_0 = 0.5-2.0 mg L^{-1}) on dynamic breakthrough hydrodynamics and mass transfer kinetics. Experimental breakthrough curves demonstrated that increasing feed strength enhanced the concentration gradient driving force, escalating the equilibrium uptake capacity (qtotal) from 27.72 to 34.05 mg g^{-1}. Conversely, operation under dilute conditions significantly extended the service longevity of the biochar bed, shifting the 50% breakthrough time (τ) from 202.79 to 504.57 min. Mathematical simulation of the column breakthrough profiles was conducted using Adams–Bohart, Thomas, and Yoon–Nelson formulations, all exhibiting strong correlation coefficients (R^2 > 0.90). The Thomas and Yoon–Nelson models delivered superior accuracy in predicting column saturation behavior and service performance. The Yoon–Nelson rate constant (k_{YN}) displayed a non-monotonic trend, peaking at 0.039 min-1 at an intermediate concentration of 1.0 mg L^{-1}, confirming that boundary-layer film mass transfer acts as the primary rate-controlling mechanism. Overall, engineered peanut shell biochar demonstrates substantial potential as a sustainable, low-cost packing media for decentralized heavy metal wastewater purification systems.
Keywords: Peanut shell biochar; Pb(II) removal; Fixed-bed column; Breakthrough kinetics.

INTRODUCTION

Rapid industrialization coupled with unregulated wastewater discharge has escalated heavy metal contamination in aquatic ecosystems into a critical global environmental threat (Thorat et al., 2025). Lead (Pb(II)), widely emitted from battery manufacturing, mining, electroplating, pigment, and petrochemical industries, represents a primary non-biodegradable pollutant exhibiting severe bioaccumulation and extreme toxicity. Exposure to Pb(II) exceeding threshold levels induces severe physiological damage in humans, including renal failure, neurological disorders, cardiovascular dysfunction, and developmental delays in children (Younas et al., 2024). Consequently, regulatory bodies such as the World Health Organization (WHO) and the United States Environmental Protection Agency (USEPA) have imposed stringent maximum contaminant levels for Pb(II) in drinking water at 0.01 mg L-1 and 0.015 mg L-1, respectively (Jaiswal et al., 2025). Therefore, the efficient removal of Pb(II) ions from industrial effluents and contaminated water bodies is paramount for environmental protection and public health.

Although conventional remediation techniques (such as chemical precipitation, ion exchange, membrane filtration, and electrochemical treatment) are widely employed, they suffer from inherent drawbacks including high capital/operational costs, energy intensive operations, toxic sludge generation, and inadequate efficiency at low concentrations. In contrast, adsorption technology offers superior design flexibility, economic feasibility, ease of operation, and freedom from hazardous secondary byproducts (Ghalhari et al., 2023). While extensive research has focused on batch adsorption configurations, batch systems fail to capture the dynamic fluid hydrodynamics and mass transfer limitations characteristic of full-scale

continuous treatment facilities. Fixed-bed column operations overcome these constraints by offering continuous flow management, high volumetric processing efficiency, optimal sorbent utilization, and straightforward scalability for industrial water purification systems.

In line with circular economy paradigms and green chemistry principles, the valorization of ubiquitous agricultural waste into high-value biochar adsorbents has garnered significant attention (Li and Zhai, 2023). Peanut shells represent an abundant lignocellulosic agricultural residue generated globally in millions of tons annually, which is typically underutilized, open-burned, or landfilled. Pyrolytic conversion of peanut shells into biochar yields a highly porous carbonaceous material endowed with a large specific surface area and abundant oxygenated surface functional groups (e.g., carboxyl, hydroxyl, and phenolic units) that provide active binding sites for divalent heavy metal cations. Transforming peanut shell waste into engineered biochar concurrently addresses solid waste management challenges while delivering a sustainable, low-cost adsorbent for aquatic remediation.

Despite growing interest in biochar-mediated heavy metal sequestration, the dynamic breakthrough behavior, mass transfer zone (MTZ) propagation, and continuous kinetics under low-to-moderate influent Pb(II) concentrations (C0 = 0.5-2.0 mg L-1) remain insufficiently elucidated for fixed-bed systems. In realistic effluent polishing applications, fluctuations in feed concentration profoundly dictate bed service longevity and saturation kinetics. Herein, this study systematically investigates the continuous-flow retention performance of Pb(II) onto a peanut shell biochar packed bed as a function of initial solute strength (0.5, 1.0, and 2.0 mg L-1). Furthermore, breakthrough parameters and dynamic hydrodynamic behavior were analyzed using Adams–Bohart, Thomas, and Yoon–Nelson kinetic formulations to decipher rate-limiting mass transfer mechanisms and validate the scalability of the packed-bed reactor.

MATERIALS AND METHODS

Preparation of Biochar

All chemical reagents utilized in this study were of analytical grade and procured from Merck (Germany). A primary stock solution of Pb(II) (1000 mg L-1) was prepared by dissolving high-purity lead nitrate [Pb(NO3)2, 99%] in double-distilled water. Peanut shell biomass, sourced from Osmaniye Province, Turkey, served as the raw lignocellulosic precursor for biochar synthesis. The collected biomass was air-dried, pulverized, and passed through a standard sieve to isolate a uniform particle size fraction (<2 mm). Subsequently, thermal conversion was conducted under oxygen-limited conditions at 300 °C for a residence time of 2 h at a controlled heating rate. The resulting peanut shell-derived material was packed into a continuous fixed-bed column to systematically evaluate the influence of initial solute concentration on Pb(II) sequestration kinetics. Standard laboratory equipment, including a ball mill for particle size reduction and a muffle furnace for thermal processing, was utilized during sample preparation. To ensure experimental accuracy and reproducibility, all parametric measurements were performed in triplicate, and the reported data represent the arithmetic mean values.

Removal Experiments

Dynamic continuous-flow sorption experiments were carried out in a vertically oriented borosilicate glass column (60 cm in height and 2.5 cm in internal diameter). The column was packed with the synthesized peanut shell biochar to constitute a stable stationary sorbent matrix. To achieve uniform hydrodynamics and prevent fluid channeling, an inert sand layer (5 cm depth) was positioned at the column base. Furthermore, glass wool plugs were fitted at both column ends to retain the packing material and safeguard bed integrity throughout the operational runs. To investigate the governing role of initial solute loading on breakthrough kinetics, column operations were systematically tested across three distinct Pb(II) concentrations (C0 = 0.5, 1.0, and 2.0 mg L-1). The metal-bearing influent was introduced in a top-to-bottom (downflow) mode utilizing a precision pump. Effluent aliquots were periodically collected at designated time intervals to monitor residual unadsorbed Pb(II) concentration as a function of time.

Breakthrough and Fixed-Bed Column Efficacy

Establishing the breakthrough curve allows for the systematic evaluation of fixed-bed hydrodynamic dynamics by tracking temporal or volumetric shifts in effluent Pb(II) levels. Furthermore, this profile elucidates crucial operational metrics, including The active sorption zone, breakthrough and exhaustion intervals, and the cumulative sorptive capacity of the fixed-bed material. The cumulative volume of Pb(II) solution processed from the initial breakpoint to complete bed exhaustion (Vs, mL) was quantified via Equation (1):

$$V_S = Q \times t_S \quad (1)$$

Here, Q signifies the volumetric feed flow rate (mL min^{-1}), and t_S corresponds to the total operational duration required to achieve complete bed saturation (min).

The total mass of lead uptake (q_{total}, in mg) retained within the fixed-bed column was calculated via numerical integration of the area circumscribed beneath the breakthrough profile according to Equation (2):

$$q_{total} = \frac{Q}{1000} \int_{t=0}^{t=t_{total}} C_s \, dt \quad (2)$$

where Cs (mg L^{-1}) denotes the quantity of sequestered Pb(II) at time t, and t_{total} corresponds to the total operating duration of the column system. The numerical factor of 1000 is incorporated to handle the transformation of units from milliliters (mL) to liters (L).

The cumulative amount of Pb(II) introduced into the packed bed through the influent stream (X, mg) was determined according to Equation (3):

$$X = \frac{C_o Q_t}{1000} \quad (3)$$

where C_0 represents the initial Pb(II) feed concentration (mg L^{-1}), Q denotes the volumetric flow rate (mL min^{-1}), and t refers to the total operation time of the column (min). The overall removal efficiency of the column (%) was then determined using Equation (4):

$$Removal\ (\%) = 100\ (\frac{q_{total}}{X})$$

(4)

Collectively, these mathematical formulations facilitate the quantitative assessment of column dynamics and overall adsorption performance across diverse operational parameters.

Mathematical Models for Breakthrough Prediction

The Adams–Bohart kinetic model is widely utilized to describe early-stage breakthrough dynamics in packed-bed sorption systems and to forecast column operational lifespan under specific process conditions. By incorporating both adsorption rate kinetics and maximum bed saturation capacity, this formulation relates the effluent Pb(II) concentration to the elapsed operational runtime. The expression of the Adams–Bohart model is formulated as follows:

$$\ln\frac{C_t}{C_o} = k_{AB}C_o\,t - k_{AB}N_o\frac{Z}{U_o}$$

(5)

In this formulation, C_t and C_0 represent the effluent and influent Pb(II) concentrations (mg L^{-1}), respectively; k_{AB} denotes the Adams–Bohart kinetic rate constant (L mg^{-1} min^{-1}); where N_0 signifies the bed volumetric saturation capacity (mg L^{-1}), Z refers to the packing depth (cm), U_0 indicates the linear superficial velocity of the feed (cm min^{-1}), and t denotes the elapsed run time (min).

The fundamental premise of this model assumes that the rate of adsorption is proportional to both the unexhausted capacity of the adsorbent and the concentration of the sorbate species. Experimentally, the parameters N_0 and k_{AB} are derived from the slope and y-intercept of the linear regression plot of $\ln(C_t/C_0)$ versus time (t), evaluated across varying flow rates and bed depths.

The Thomas kinetic formulation is widely utilized to simulate fixed-bed breakthrough curves and extract the corresponding rate constants under different process conditions. According to Roy et al. (2013), this mathematical framework is governed by three primary premises: negligible axial dispersion along the packed column, compliance of the uptake process with pseudo-second-order reaction mechanisms, and the validity of the separation factor under both favorable and unfavorable isotherm scenarios. The linear representation of the Thomas kinetic formulation is given by Equation (6):

$$\ln\left(\frac{C_t}{C_o} - 1\right) = \frac{k_{Th}q_o M}{Q} - k_{Th}C_o t$$

(6)

Determining the model parameters relies on the linear regression of $\ln[(C_t/C_0)\ -1]$ plotted against operational duration (t) under a constant solution feed rate. From this linear plot, the maximum adsorption capacity (q_0, mg g^{-1}) and the Thomas rate constant (k_{TH}, mL min^{-1} mg^{-1}) are derived using the y-intercept and the slope, respectively. The remaining mathematical terms are defined as follows: m signifies the total mass of the adsorbent packed into the column (g), Q refers to the volumetric feed flow rate (mL min^{-1}), and t represents the total contact time (min).

Underlying the Yoon-Nelson theoretical framework is the stipulating that the decay rate of adsorption probability for each sorbate molecule scales directly with both the uptake rate and the breakthrough progression of the adsorbate (Biswas, S., & Mishra, U. 2015). The linearized form of the Yoon-Nelson model is defined by Equation (7):

$$ln\frac{C_t}{C_o - C_t} = k_{YN}\,(t - \tau)$$

(7)

where τ signifies the operational duration required to reach 50% Pb(II) breakthrough (min), and k_{YN} corresponds to the Yoon-Nelson kinetic rate parameter (min^{-1}). Experimentally, evaluating the slope and y-intercept of the linear regression plot of $ln[C_t / (C_0 - C_t)]$ against contact time (t) allows for the direct computation of k_{YN} and τ, respectively.

RESEARCH FINDINGS AND DISCUSSION

Effect of Initial Concentration

To evaluate the effect of initial Pb(II) strength (0.5-2.0 mg L^{-1}) on the fixed-bed sorption behavior of peanut shell biochar, continuous experiments were conducted under fixed hydrodynamic conditions (Z = 10 cm, Q = 7.5 mL min^{-1}). As illustrated in Figure 1 and summarized in Table 1, the feed solute concentration plays a decisive role in shaping the breakthrough profiles and bed saturation rates. At the lowest concentration tested (0.5 mg L^{-1}), the fixed bed achieved an extended service duration of 499 min before breakthrough, treating roughly 402 mL of solution while attaining an uptake capacity of 27.72 mg g^{-1} alongside a 75.54% total retention rate. Escalating the influent load to 1.0 mg L^{-1} reduced both the breakthrough onset to 223 min and the processed volume to 199 mL; nevertheless, the adsorption capacity increased to 30.85 mg g^{-1} with a modest reduction in overall efficiency (70.91%). A further rise to C_0 = 2.0 mg L^{-1} triggered rapid bed breakthrough at 157 min (65 mL treated volume), where despite achieving the highest sorption capacity (34.05 mg g^{-1}), the global removal efficiency fell significantly to 58.45%.

At higher solute concentrations, the steepened concentration gradient between the bulk fluid and the sorbent interface amplifies the concentration driving force, facilitating greater mass transfer per unit mass of biochar (Razzak et al., 2021). However, this intensified influx of Pb(II) ions accelerates the occupation of active surface binding sites, triggering premature breakthrough and lowering the overall fraction of metal ions removed from the feed (Brion-Roby et al., 2018). Furthermore, the shortened residence time at elevated concentrations restricts intraparticle diffusion the rate-controlling step during heavy metal retention onto porous carbonaceous matrices (Kumar and Bhattacharya, 2022). Consequently, only a fraction of the internal pore network is effectively utilized before a rapid concentration breakthrough ensues. Similar phenomena were reported by Shan et al. (2020) for other ionic species, where high influent concentrations diminished removal efficiency due to mass transfer zone compression and restricted internal site accessibility. These observations underscore that while higher feed concentrations enhance apparent uptake capacity through elevated driving forces, they simultaneously compromise bed service life and overall removal efficiency. Thus,

optimizing initial concentration is imperative to maximize sorbent utilization and treatment efficiency in continuous column applications.

Table 1. Fixed-bed column parameters.

Initial Concentration Co (mg/L)	Adsorption Capacity (q_{total}) (mg/g)	Removal (%)	Treated Volume (Vs) (mL)	Breakthrough Time (ts) (min)
0.5	27.72	75.54	402	499
1	30.85	70.91	199	223
2	34.05	58.45	65	157

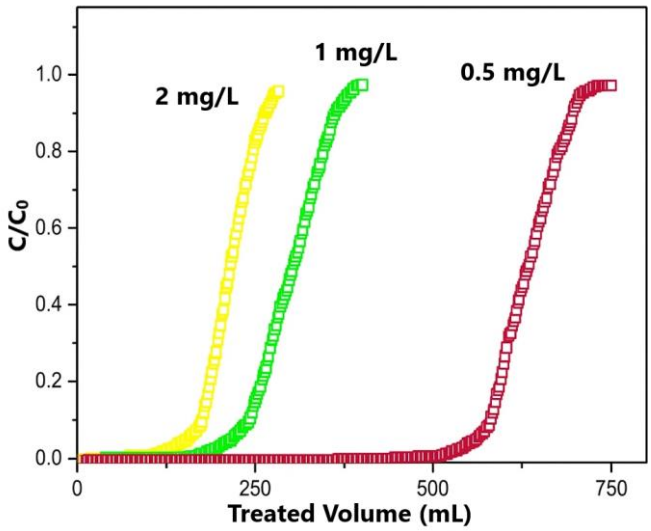


Figure 1. Breakthrough curves for ash derived from peanut shell biomass as the sorbent at different initial concentrations.

Adams Bohart Model

To elucidate the initial dynamic sorption kinetics, the Adams–Bohart model was applied to the experimental breakthrough profiles. As depicted by the linearized regression plots (Figure 2) and compiled parameters (Table 2), the model accurately describes the initial breakthrough region ($C_t/C_0 < 0.5$), signifying that the early adsorption stage is predominantly governed by surface reaction kinetics. Elevating the influent solute concentration from 0.5 to 2.0 mg L^{-1} enhanced both the volumetric sorptive capacity (N_0, rising from 180.53 to 238.58 mg L^{-1}) and the Adams–Bohart rate constant (k_{AB}), increasing from 0.014 to 0.042 L mg^{-1} min^{-1}). This ascending trend is attributed to the steeper concentration gradient across the phase boundary, which imparts a stronger thermodynamic driving force for mass transport and accelerates solute accumulation rates; indeed, elevated feed strengths suppress film diffusion resistance and promote mass transfer rates (Apiratikul, R., & Chu, K. H. 2021). Overall, the Adams–Bohart formulation demonstrated robust applicability (R^2 = 0.90-0.92) in predicting the early breakthrough onset in the peanut shell biochar-packed column, validating that regulating initial concentration effectively tunes adsorption kinetics and bed throughput performance.

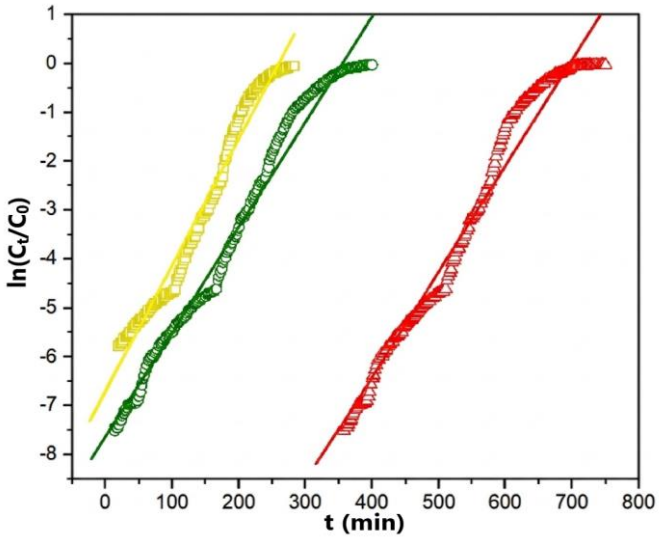


Figure 2. Linearized regression fits of the Adams–Bohart model evaluated at different initial concentrations.

Thomas Model

Mathematical evaluation of the dynamic column profiles via the Thomas kinetic model yielded exceptional agreement, with the derived parameters and linearized regression curves compiled in Table 2 and Figure 3, respectively. High determination coefficients (R^2 = 0.96-0.98) substantiate that the Thomas formulation provided the superior fit to the breakthrough data, confirming that Pb(II) sorption follows second-order reversible kinetics under negligible axial dispersion limitations. Interestingly, operating at a lower initial feed concentration (0.5 mg L^{-1}) enhanced both the rate constant (k_{TH} = 0.067 L mg^{-1} min^{-1}) and maximum volumetric capacity (q_0 = 122.62 mg L^{-1}). This phenomenon indicates greater sorptive efficiency in dilute streams, where a higher availability of functional active sites per target ion minimizes competitive site saturation. Consequently, these findings signify that external boundary-layer film resistance (rather than intraparticle pore diffusion) acts as the primary rate-limiting step governing column performance (Chaudhry et al., 2017).

Yoon-Nelson Model

The applicability of the Yoon–Nelson model to describe the dynamic breakthrough behavior of Pb(II) onto the peanut shell biochar bed was evaluated, with the fitted kinetic parameters and linearized regressions compiled in Table 2 and Figure 4, respectively. High determination coefficients (R^2 = 0.95-0.97) verify superior model agreement, corroborating the validity of the Yoon–Nelson formulation in predicting column saturation dynamics. Diluting the influent concentration from 2.0 to 0.5 mg L^{-1} led to a substantial prolongation of the time required for 50% column breakthrough (τ), which expanded from 202.79 to 504.57 min. This extension signifies delayed bed exhaustion and extended service longevity under lower solute loads. Interestingly, the Yoon–Nelson rate constant (k_{YN}) displayed a non-monotonic trend with respect to feed strength, recording its maximum value (0.039 min^{-1}) at an intermediate concentration of 1.0 mg L^{-1}. In alignment with reported literature an elevated k_{YN} reflects

intensified sorbate–sorbent affinity alongside a compressed mass transfer zone, indicating minimized mass transport resistance and enhanced kinetic control (Saravanakumar et al., 2020).

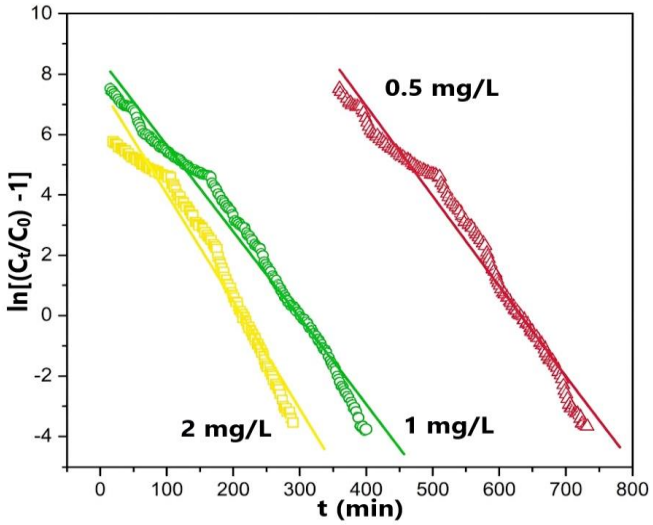


Figure 3 Linearized regression fits of the Thomas model evaluated at different initial concentrations.

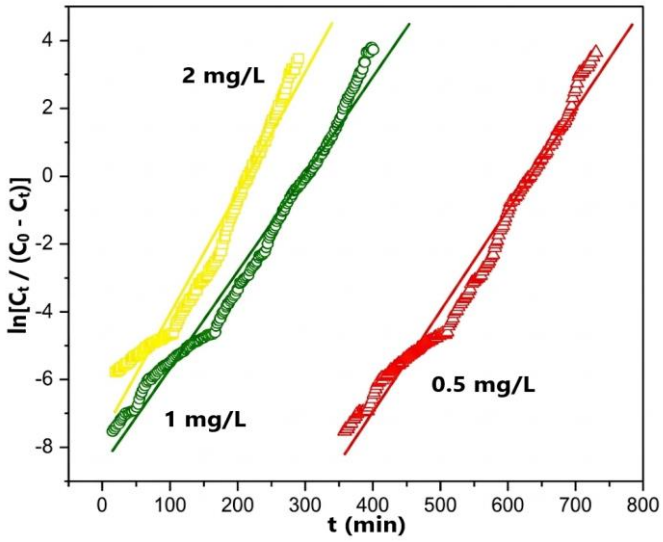


Figure 4 Linearized regression fits of the Yoon-Nelson model evaluated at different initial concentrations.

Table 2. Estimated model parameters derived from fixed-bed column studies.

Initial Concentration Co (mg/L)	**Adams Bohart model**			**Thomas model**			**Yoon Nelson model**		
	k_{AB}	N_0	R^2	k_{TH}	q_0	R^2	k_{YN}	τ	R^2
0.5	0.014	180.53	0.91	0.067	122.62	0.96	0.034	504.57	0.97
1	0.024	210.48	0.90	0.027	82.29	0.98	0.039	278.55	0.95
2	0.042	238.58	0.92	0.014	43.05	0.97	0.031	202.79	0.96

CONCLUSION

This study demonstrates that peanut shell biochar serves as a highly efficient, sustainable, and cost-effective packing media for continuous Pb(II) sequestration in fixed-bed column reactors. The dynamic column hydraulics and breakthrough kinetics were strongly governed by the influent solute concentration (C_0 = 0.5-2.0 mg L^{-1}); elevating the feed strength enhanced the driving force for mass transfer, raising the maximum uptake capacity from 27.72 to 34.05 mg g^{-1}, albeit at the expense of shortened service times and lower overall removal ratios. Mathematical fitting using the Adams–Bohart, Thomas, and Yoon–Nelson models yielded exceptional correlation (R^2 > 0.90), confirming the technical reliability of these dynamic formulations for fixed-bed process design. Specifically, the Thomas and Yoon–Nelson models provided superior predictive accuracy for bed saturation capacity and 50% breakthrough time (τ), confirming that boundary-layer film mass transfer acts as the primary rate-limiting mechanism.

From a practical standpoint, valorizing ubiquitous agricultural peanut shell waste into a functionally active biochar aligns directly with circular economy objectives, offering an accessible wastewater purification solution for resource-constrained regions. The robust sorptive capacity and favorable column kinetics highlight this biochar media as a viable candidate for point-of-use household filtration units, community-scale water purification systems, decentralized treatment facilities, and industrial effluent polishing processes. Nevertheless, to bridge bench-scale findings with commercial implementation, future investigations must prioritize multi-cycle desorption–regeneration studies, detailed techno-economic assessments, and continuous evaluations under complex real-world groundwater matrices containing competing co-existing ions.

ACKNOWLEDGMENT

The study was supported by Malatya Turgut Ozal University Scientific Research Projects Coordination Unit with project number **26G11**.

REFERENCES

Apiratikul, R., & Chu, K. H. (2021). Improved fixed bed models for correlating asymmetric adsorption breakthrough curves. Journal of Water Process Engineering, 40, 101810.

Biswas, S., & Mishra, U. (2015). Continuous fixed-bed column study and adsorption modeling: removal of lead ion from aqueous solution by charcoal originated from chemical carbonization of rubber wood sawdust. Journal of chemistry, 2015(1), 907379.

Brion-Roby, R., Gagnon, J., Deschênes, J. S., & Chabot, B. (2018). Investigation of fixed bed adsorption column operation parameters using a chitosan material for treatment of arsenate contaminated water. Journal of environmental chemical engineering, 6(1), 505-511.

Chaudhry, S. A., Zaidi, Z., & Siddiqui, S. I. (2017). Isotherm, kinetic and thermodynamics of arsenic adsorption onto Iron-Zirconium Binary Oxide-Coated Sand (IZBOCS): Modelling and process optimization. Journal of Molecular Liquids, 229, 230-240.

Ghalhari, M. R., Sanaei, D., Nabizadeh, R., & Mahvi, A. H. (2023). Cellulose-based hydrogel beads derived from wastepapers: application for organic dye adsorption. Cellulose, 30(15), 9669-9691.

Jaiswal, V. K., Gupta, A. D., Kushwaha, R., Kumar, R., Singh, K., Singh, H., ... & Singh, R. S. (2025). Arsenic removal from water using an acid-modified biochar. Journal of Molecular Structure, 1324, 140904.

Kumar, A., & Bhattacharya, T. (2022). Removal of arsenic by wheat straw biochar from soil. Bulletin of Environmental Contamination and Toxicology, 108(3), 415-422.

Li, X. D., & Zhai, Q. Z. (2023). Study on the adsorption of Cr3+ by peanut shell: Adsorption kinetics, thermodynamics, and isotherm properties. Chemistry & Biodiversity, 20(6), e202201095.

Razzak, A., Shafiquzzaman, M. D., Haider, H., & Alresheedi, M. (2021). Arsenic removal by iron-oxidizing bacteria in a fixed-bed coconut husk column: Experimental study and numerical modeling. Environmental Pollution, 272, 115977.

Roy, P., Mondal, N. K., Bhattacharya, S., Das, B., & Das, K. (2013). Removal of arsenic (III) and arsenic (V) on chemically modified low-cost adsorbent: batch and column operations. Applied Water Science, 3(1), 293-309.

Saravanakumar, K., Sathyamoorthy, M., Prasad, D. M. R., Senthilkumar, R., & Prasad, B. S. N. (2022). Continuous removal of cadmium and lead ions by biochar derived from date seeds in a packed column reactor. Desalination and Water Treatment, 250, 126-135.

Thorat, D. S., Ushir, Y. V., & Singh, S. (2025). Value-added-peanut shell as potential source for biofilters: an eco-friendly way to clean water and manage nutrients. Biotechnology for Sustainable Materials, 2(1), 12.

Younas, F., Younas, S., Bibi, I., Farooqi, Z. U. R., Hameed, M. A., Mohy-Ud-Din, W., ... & Niazi, N. K. (2024). A critical review on the separation of heavy metal (loid) s from the contaminated water using various agricultural wastes. International journal of phytoremediation, 26(3), 349-368.

FINITE ELEMENT INVESTIGATION OF CFRP TEXTILE WRAPPING GEOMETRY AND STRIP WIDTH EFFECTS ON THE FLEXURAL BEHAVIOR OF REINFORCED CONCRETE BEAMS

Ali DOGAN
Department of Civil Engineering, Iskenderun Technical University, Iskenderun, Hatay, Türkiye

Mohammad Bilal JALALI
Department of Civil Engineering, Sakarya University, Serdivan, Sakarya, Türkiye

ABSTRACT

In this study, the effects of wrapping geometry, strip width, and CFRP coverage continuity on the flexural behavior of reinforced concrete (RC) beams strengthened with externally bonded carbon fiber-reinforced polymer (CFRP) textile sheets were parametrically investigated. For this purpose, RC beams with a cross-section of 150 × 200 mm and a total span of 1240 mm were modeled using nonlinear finite element analysis (FEA) in Abaqus. The finite element model was first verified against the load-displacement response of a reference RC beam, after which a total of 15 models were developed and analyzed under four-point bending based on three distinct wrapping geometries (Bottom-Only Wrapping, Half U-Wrapping, and Full U-Wrapping) and five strip configurations (100, 150, 200, 250 mm, and continuous Full wrapping). The load-displacement curves extracted from the numerical analyses showed that continuous CFRP coverage was associated with more continuous load-transfer paths and reduced stress concentration effects near the repeated termination regions of segmented strips. While the gaps in segmented strip applications interrupted the continuity of CFRP load-transfer paths, the Full U-Wrapping (Full) model, which continuously jacketed the beam web, exhibited the highest load-carrying capacity, exceeding approximately 21,500 kgf. This response was associated with continuous CFRP coverage and enhanced lateral restraint of the concrete core.

Keywords: CFRP Strengthening, Finite Element Analysis, Abaqus, CFRP Wrapping Geometry, Strip Width, Load-Transfer Continuity.

1. Introduction

The deployment of externally bonded Carbon Fiber Reinforced Polymer (CFRP) systems for retrofitting reinforced concrete (RC) elements represents one of the most prominent fields in modern structural engineering due to its superior strength-to-weight ratio and corrosion immunity **[1]**. However, the Achilles' heel of these composite systems lies in the high shear and peeling stresses generated at the CFRP-concrete interface. Pioneering numerical and experimental studies in the literature have robustly documented that unanchored, flat CFRP strips suffer from sudden detachment from the concrete substrate well before the composite reaches its theoretical tensile limit, yielding highly brittle failure modes **[2], [3]**. This

premature interface debonding problem severely mitigates fiber efficiency and restricts overall strengthening optimization **[4]**.

To circumvent this limitation, U-wrap (U-jacket) configurations are utilized to wrap the beam web, extending the CFRP coverage onto the side faces and thereby improving load-transfer continuity and restraint near the termination regions **[5]**. International design guidelines, particularly ACI 440.2R-17, recognize U-wrap configurations as externally bonded FRP strengthening systems that can provide additional shear reinforcement and improve the anchorage and load-transfer conditions of externally bonded FRP systems **[6]**. The structural layout, strip positioning, and directional orientation of the composite layer drastically influence the failure behavior and stress trajectory **[7]**. When deployed specifically as web side-bonded reinforcement, CFRP networks directly intercept diagonal tension lines, effectively upgrading the shear capacity of shear-deficient structural elements **[8]**. Furthermore, comparative structural investigations evaluating alternative materials, such as basalt fiber sheets, indicate that anchorage configuration and bond integrity are important factors governing the effectiveness of externally bonded strengthening systems **[9]**.

While segmented strip designs are frequently advocated in contemporary research for their cost-efficiency, material savings, and ductility benefits, the adverse effects of breaking the geometric continuity on stress paths and localized stress concentrations remain insufficiently clarified **[10]**. This disruption of load path continuity is particularly critical when retrofitting high-strength matrices, such as ultra-high-performance concrete beams retrofitted with continuous strip layouts **[11]**. Accordingly, this study aims to investigate the influence of CFRP wrapping geometry, strip width, load-path continuity, and lateral confinement on the structural response of strengthened RC beams through a systematic nonlinear finite element analysis of 15 strengthening configurations.

2. Materials

In this investigation, plain concrete, conventional internal steel reinforcing bars, and externally bonded carbon fiber-reinforced polymer (CFRP) textile fabrics were utilized as the primary constituents for the structural modeling. These materials were combined in different configurations to construct and parametrically analyze fifteen numerical beam specimens within the Abaqus finite element framework.

2.1 *Concrete*

In this investigation, the non-linear constitutive behavior of concrete was numerically modeled using the Concrete Damaged Plasticity (CDP) framework within the ABAQUS platform. This continuum damage mechanics model primarily incorporates tensile cracking and compressive crushing as the two dominant failure mechanisms. Under uniaxial tension, the concrete matrix initially exhibits a linear elastic stress-strain response until the ultimate tensile strength is reached. Beyond this peak value, stress-induced degradation triggers macro-cracking, which is represented by a softening stress-strain relationship that dictates progressive micro-crack evolution. Consequently, specifying the initial elastic modulus

alongside post-peak behavior is mandatory to establish the complete numerical constitutive envelope.

To ensure high simulation accuracy, numerical input properties were derived directly from compression tests performed on concrete cube specimens cast using the mixture specifications listed in Table 1. The representative experimental stress-strain profiles for the synthesized concrete matrix are illustrated in Figure 1. The essential mechanical parameters required to govern the constitutive behavior include the elastic modulus E_c and the ultimate tensile strength f_t. The experimental cubic compressive strength f_c' values are systematically compiled in Table 2. Utilizing these baseline experimental results, the structural elastic modulus E_c and tensile strength f_t were analytically calculated using the established empirical formulations proposed in **[12], [1].**

In this study, for beam specimen, three 150 × 150 × 150 mm concrete cube specimens were produced and cured under the same conditions as the corresponding beam specimen. These specimens were cured for 28 days and then tested to calculate the concrete strength and modulus of elasticity **(Figure 1)**.

Table 1. Mix proportions and physical properties of the concrete constituents.

Material	**Type / Size**	**Density (g/cm³)**	**Mix Proportion (kg/m³)**
Cement	OPC Type I	3.15	500
Coarse Aggregate	Max size < 11 mm	2.70	909
Fine Aggregate	Max size < 4 mm	2.65	595
Water	Potable	—	250*
Water-to-Cement (W/C) Ratio	—	—	0.50

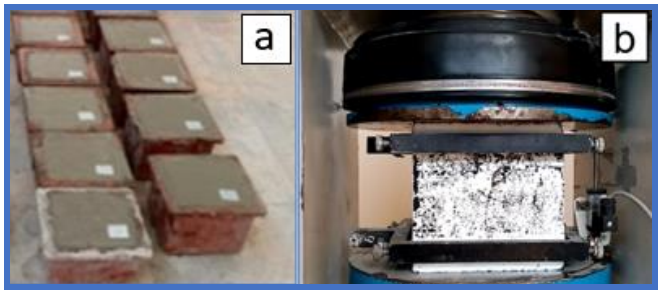


Fig. 1. Samples produced for experiments (a), and compressive test (b)

Elastic modulus (Ec), compressive strengths values (fc′) and tensile strength curve (f_t), peak value of tensile strength (ft′) are shown in Table 2 and Figures 1. E_c, f_t' and f_t were then calculated by using Equation 1, 6 and 7.

$$E_c = 14000 + 3250\sqrt{f_c'} \quad (1)$$

The uniaxial compressive stress-strain curve (σ) for concrete was constructed using Saenz's stress-strain relationship [13].

$$\sigma_c = \frac{E_c \varepsilon_c}{1 + (R + R_E - 2)\frac{\varepsilon_c}{\varepsilon_0} - (2R - 1)\left(\frac{\varepsilon_c}{\varepsilon_0}\right)^2 + R\left(\frac{\varepsilon_c}{\varepsilon_0}\right)^3} \quad (2)$$

$$R = \frac{R_E(R_\sigma - 1)}{(R_\sigma - 1)^2} - \frac{1}{R_\varepsilon} \quad (3)$$

$$R_E = \frac{E_c}{E_0} \quad (4)$$

$$E_0 = \frac{f_c'}{\varepsilon_0} \quad (5)$$

Here, ε_0 = 0.0025, R_ε = 4, R_σ = 4, as indicated in [14]. The Poisson's ratio of concrete was considered to be 0.2. The peak tensile strength (ft′) and the tensile stress-strain relationship (f_t) were determined using Equations (6) and (7), respectively.

$$f_t' = 1.4\left(\frac{f_c' - 8}{10}\right)^{2/3} \quad (6)$$

$$f_t = f_t'\left(\frac{f_t'/E_c}{\varepsilon_t}\right)^{0.4} \quad (7)$$

Table 2. Mechanical properties of three type concrete

Type	**Materials**	Young modulus E_c(MPa)	Poisson Ratio ν	f_c' (MPa)	f_t (MPa)
C	Concrete strength at 28th day	34095	0.2	38.232	2.927

2.2 *Steel reinforcement*

S420 coded rebar was used in this study. The longitudinal reinforcement with a diameter of 10 mm was used in the tension region of the beam and 8 mm in diameter in the compression region. Steel stirrups with a diameter of 8 mm were used on each beam, spaced 100 mm apart. Mechanical properties of steel are given in Table 3.

Table 3. Mechanical properties of steel

Materials	Young modulus (MPa)	Poisson ratio	Yield stress (MPa)
Steel tension strength	210000	0.3	650

In this study, the steel was assumed to be an elastic-perfectly plastic material with identical tension and compression properties. The experimentally determined elastic modulus, E_s, and yield stress, f_y, were 210 GPa and 650 MPa, respectively, and these values were applied in the

FEM model. The steel reinforcement has a Poisson's ratio (v) of 0.3. The bond between steel-reinforcement and concrete was presumed to be perfect.

2.3 *Carbon fibre reinforced polymer textile (CFRP)*

In this study, 0°/90° CFRP textile was used. The carbon fibre reinforced polymer textile was modeled as a linear elastic orthotropic material. Because the textile consisted of orthogonally oriented 0° and 90° fiber directions, an orthotropic constitutive formulation was adopted to represent its directional stiffness characteristics. The orthotropic material model's E_{11} was set at 165 GPa. Using the rule of mixtures [15], with an epoxy modulus of E_{epoxy} = 2.5 GPa and and a fiber volume fraction of 75%, the corresponding fiber elastic modulus was calculated as E_{fibre} =220 GPa The Poisson's ratios were defined as $\nu_{12} = \nu_{13} = 0.3$. Using the inverse rule of mixtures [14], the remaining orthotropic elastic constants were obtained as E_{22} = 9.65 GPa, E_{33} = 9.65 GPa, G_{12} = 5.2 GPa, G_{13} = 5.2 GPa, G_{23} = 3.4 GPa, and ν_{23} = 0.45, as summarized in Table 4.

Table 4. Mechanical properties of CFRP textile

Material	**E_1(Mpa)**	**E_2(Mpa)**	**E_3(Mpa)**	**ν_{12}**	**ν_{13}**	**ν_{23}**	**G_{12}(Mpa)**	**G_{13}(Mpa)**	**G_{23}(Mpa)**
CFRP	165000	9650	9650	0.3	0.3	0.45	5200	5200	3400

2.4 *Epoxy Adhesives and Interface Properties*

In the numerical modeling framework, the interface interaction between the structural concrete core and the external CFRP textile layers was governed using the specific mechanical properties of commercial epoxy systems. In this context, MasterBrace® P 3500 and MasterBrace® SAT 4500 epoxy-based materials were defined to characterize the primer coating and structural binding phases, respectively.

The baseline bonding surfaces were engineered to be primed with MasterBrace® P 3500, which is a two-component, low-viscosity, solvent-free epoxy primer explicitly designed to optimize surface conditioning and enhance concrete-to-composite adhesion. The primary structural bonding and reinforcement matrix impregnation were simulated using the mechanical parameters of MasterBrace® SAT 4500, a two-component, high-strength, epoxy-based structural adhesive designed for performance validation in externally bonded composite profiles. The specific engineering constants and manufacturing thresholds for both epoxy constituents are compiled in Table 5 and Table 6. These adhesive properties were considered as material information associated with the experimental strengthening system; however, the CFRP–concrete interaction in the finite element model was implemented using a Tie constraint rather than an explicit cohesive-zone or adhesive constitutive formulation.

Table 5. Technical properties of MasterBrace® SAT 4500 structural epoxy adhesive.

Technical Property	**Value / Specification**
Material Structure (Component A / B)	Epoxy Resin / Epoxy Hardener
Color	Blue

Mixture Density	1.02 kg/L
Viscosity	1500–2500 mPa·s
Compressive Strength (7 days)	> 60 MPa [16]
Flexural Strength (7 days)	> 50 MPa [16]
Adhesion Strength to Concrete (7 days)	> 3.0 MPa
Applicable Substrate Temperature Range	+5 °C to +30 °C

Table 6. Technical properties of MasterBrace® P 3500 epoxy-based primer.

Technical Property	**Value / Specification**
Material Structure (Component A / B)	Epoxy Resin / Epoxy Hardener
Color	Transparent
Mixture Density	1.08 ± 0.024 kg/L
Solid Content Ratio	100%
Flexural Strength (7 days)	> 20 MPa [16]

In this study, three CFRP wrapping configurations were modeled in Abaqus (Table 7): BCSC1, in which the CFRP textile was applied to the bottom surface; BCSC2, in which the CFRP textile was applied to the bottom and half of the side surfaces; and BCSC3, in which the CFRP textile was applied to the bottom and full side surfaces (Figures 6–11). The length of the beams is 1240 mm, and the distance between supports, i.e., the net span of the beam, is 1040 mm. The width of the beam is 150 mm, and the height is 200 mm. The beam was subjected to a four-point loading test. Two concentrated loads were applied at 347 mm intervals. The reinforced beam specimen contains two ϕ10 mm diameter longitudinal tensile reinforcement bars and two ϕ8 mm diameter longitudinal compression reinforcement bars. Sufficient shear reinforcement was provided and produced from ϕ8 diameter reinforcement bars at 100 mm intervals, as shown in Figure 2. The beams have been loaded until the point of fracture.

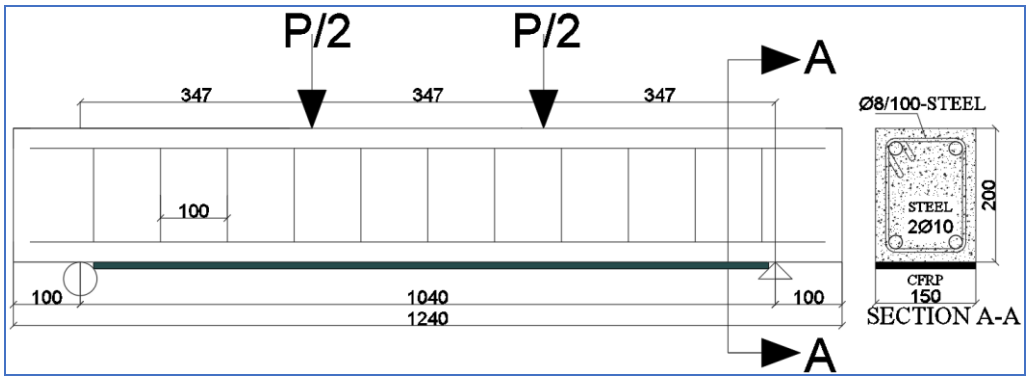


Fig. 2. The geometry, cross-sections and rebars of beams subjected to four-point loading tests.

Table 7. Classification of beam specimens.

Beam Type	Explanation
BCSC1	Steel bar reinforced beam control sample and coated with carbon textile on the bottom surface of the beam.
BCSC2	Steel bar reinforced beam control sample and coated with carbon textile on the bottom and half side surfaces of the beam.
BCSC3	Steel bar reinforced beam control sample and coated with carbon textile on the bottom and full side surfaces of the beam.

3. Finite element modeling

In this stage of the study, the response of composite beams with rectangular cross-section geometries under four-point bending was numerically examined. Finite element models of all test samples were created in the ABAQUS/Static [17] program. In this study, the concrete is modeled with the three-dimensional (3D) solid element C3D8R, the longitudinal and transverse reinforcements are modeled with the three-dimensional (3D) rod element T3D2 and the CFRP textile is modeled using the shell element S4R. In the numerical investigation, nonlinear static analyses were carried out. In these studies, the Concrete Damage Plasticity (CDP) mechanical material model from the ABAQUS library was used to investigate the nonlinear and damage response of concrete. CDP is a continuous, plasticity-based damage material model capable of simulating tensile and compression fractures, as well as damage to concrete samples under various loads [17]. The CDP element's characteristics were established using concrete mechanical properties obtained during sample tests.

The steel reinforcement was modeled using an elastic-perfectly plastic constitutive response based on the experimentally determined properties reported in Section 2.2. For each reinforcement, a separate curve was obtained using the average of the stress-strain curves of 10 mm and 8 mm diameter longitudinal and 8 mm diameter transverse reinforcement obtained from the tests. Traditionally, these curves were referred to as engineering stress-strain curves. The mesh spacing for longitudinal reinforcement rod elements is 50 mm and for transverse reinforcement is 15 mm. The mesh spacing was 25 mm for the concrete solid element and 25 mm for the CFRP shell element (Figure 3 and 4).

In the model used for verification, the mesh interval for longitudinal reinforcements was set to 50 mm for bar elements, and 15 mm for transverse reinforcements. For the solid concrete elements, a mesh interval of 25 mm was applied, and for the CFRP shell elements, a mesh interval of 25 mm was also used. The numerical and experimental responses showed good agreement in terms of the initial stiffness, peak load, and post-peak response, supporting the suitability of the adopted finite element modeling strategy. The numerical model was subsequently compared with the experimental results obtained in the present study. Figure 5 compares the experimental and numerical load-displacement responses of representative beams, showing close agreement over the principal loading range. This comparison supports

the use of the developed FEM model for the subsequent parametric investigation of CFRP wrapping configurations.

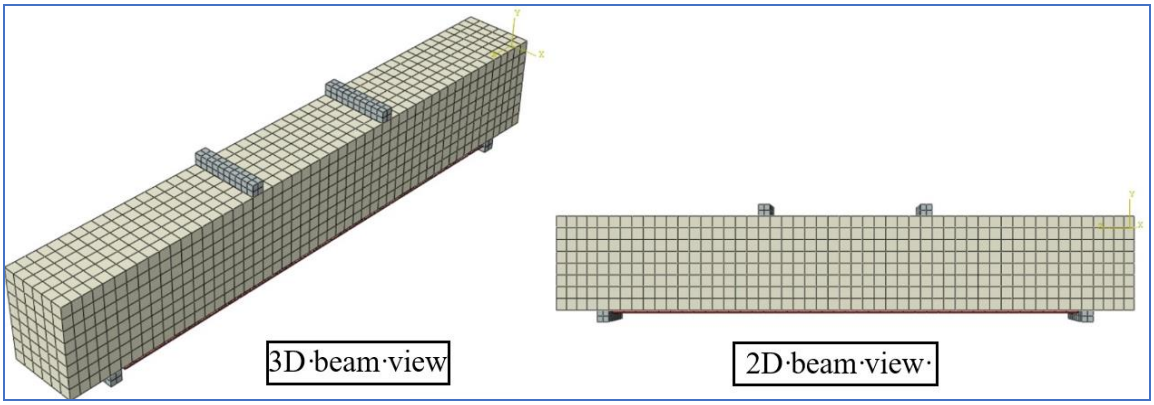


Fig. 3. 3D and 2D view of beam

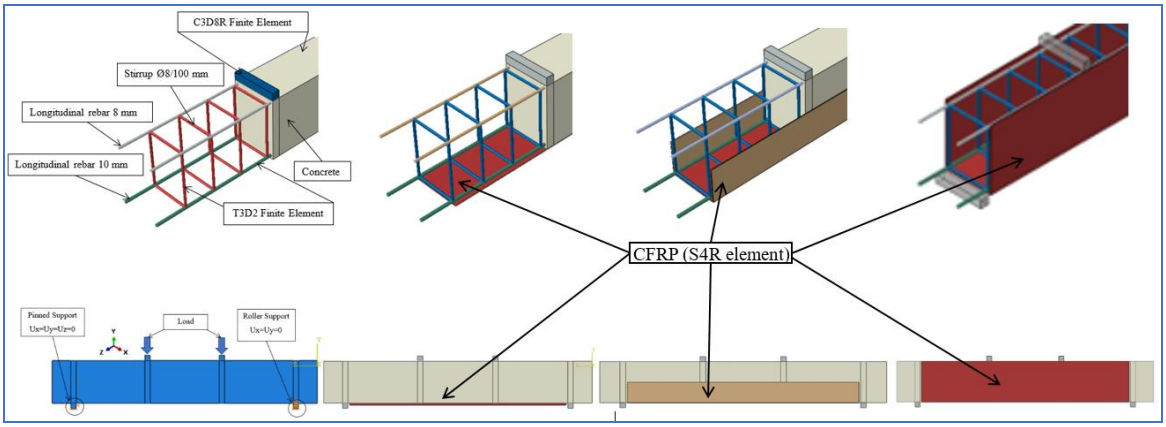
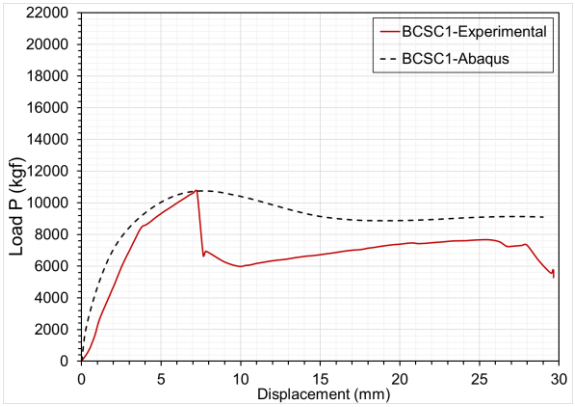


Fig. 4. Abaqus simulation model of beam



a



b

Fig. 5. Comparison of experimental and finite element analysis results and validation of the numerical model: (a) comparison of load–displacement curves, (b) appearance of the beam after testing.

4. Numerical modeling and methodology

In this study, the structural and mechanical responses of reinforced concrete (RC) beams strengthened with externally bonded CFRP textile sheets were parametrically investigated via the finite element method. The numerical simulations were established within the Abaqus software environment.

The concrete, steel reinforcement, CFRP textile, and interface properties used in the numerical models were defined according to the material descriptions given in Section 2. The concrete model was based on the experimentally determined compressive and tensile properties, while the steel reinforcement was modeled using the experimentally determined elastic modulus and yield stress. The CFRP textile was defined as an orthotropic linear-elastic material with E_1 = 165 GPa and the remaining elastic constants listed in Table 4.

The CFRP textile was bonded to the concrete surface using a Tie constraint in Abaqus, which enforced displacement compatibility and direct transfer of stresses between the CFRP and concrete surfaces. Therefore, the numerical model did not incorporate an independent cohesive-zone damage or interface debonding formulation. The influence of CFRP wrapping geometry and strip continuity was consequently evaluated in terms of load-transfer continuity, stress concentration at strip termination regions, and lateral restraint of the concrete core.

During the modeling phase, the widths of the CFRP strips applied to the bottom tensile face of the beams were designated as 100 mm, 150 mm, 200 mm, 250 mm, and a continuous longitudinal jacket representing Full wrapping. In addition to these strip widths, three main configurations were defined to isolate the influence of CFRP wrapping geometry and load-transfer continuity on the overall structural response.

In the first configuration, the CFRP elements were bonded solely to the bottom face of the beam as flat strips (Figure 6). In the second configuration, the textile strips were extended onto half of the beam's side faces, establishing a Half U-wrapping model and increasing the CFRP-covered side-face region (Figure 8). In the third and final series, the CFRP textile was designed to fully jacket the beam web up to the top surface, converting the reinforcement into a full U-wrapping geometry (Figure 10).

All numerical prototypes were sized with a cross-sectional area of 150x200 mm and a total span of 1240 mm. To monitor the flexural and shear performance of the systems under loading, the setup was supported according to a four-point bending test configuration containing two symmetrical point loads (P/2).

The dimensional details, reinforcement layouts, and cross-sectional properties of the bottom-only wrapped specimens are illustrated schematically in Figure 7. The tensile zone of the beams consists of 2Ø10 longitudinal rebars (bottom), accompanied by 2Ø8 assembly rebars (top), and Ø8/100 mm stirrups (shear reinforcement) along the span. The geometric dimensions and strip spacing of the half U-wrapping configuration are detailed in Figure 9, while the structural and geometric parameters of the full U-wrapping models jacketing the beam web continuously are presented in Figure 11.

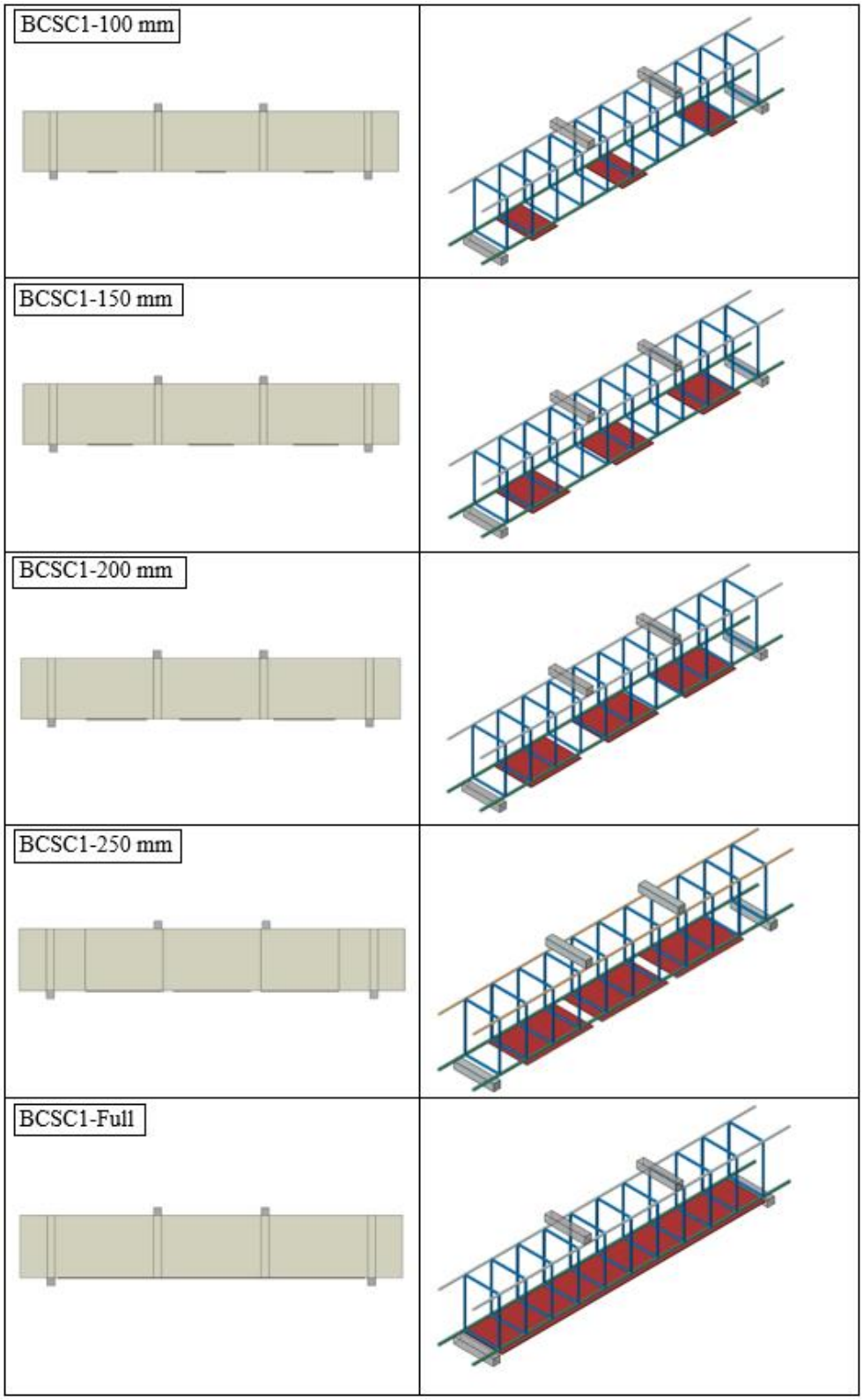


Figure 6. 3D Abaqus reinforcement cages and wrapping models of the beams strengthened with bottom-only segmented and full CFRP textiles.

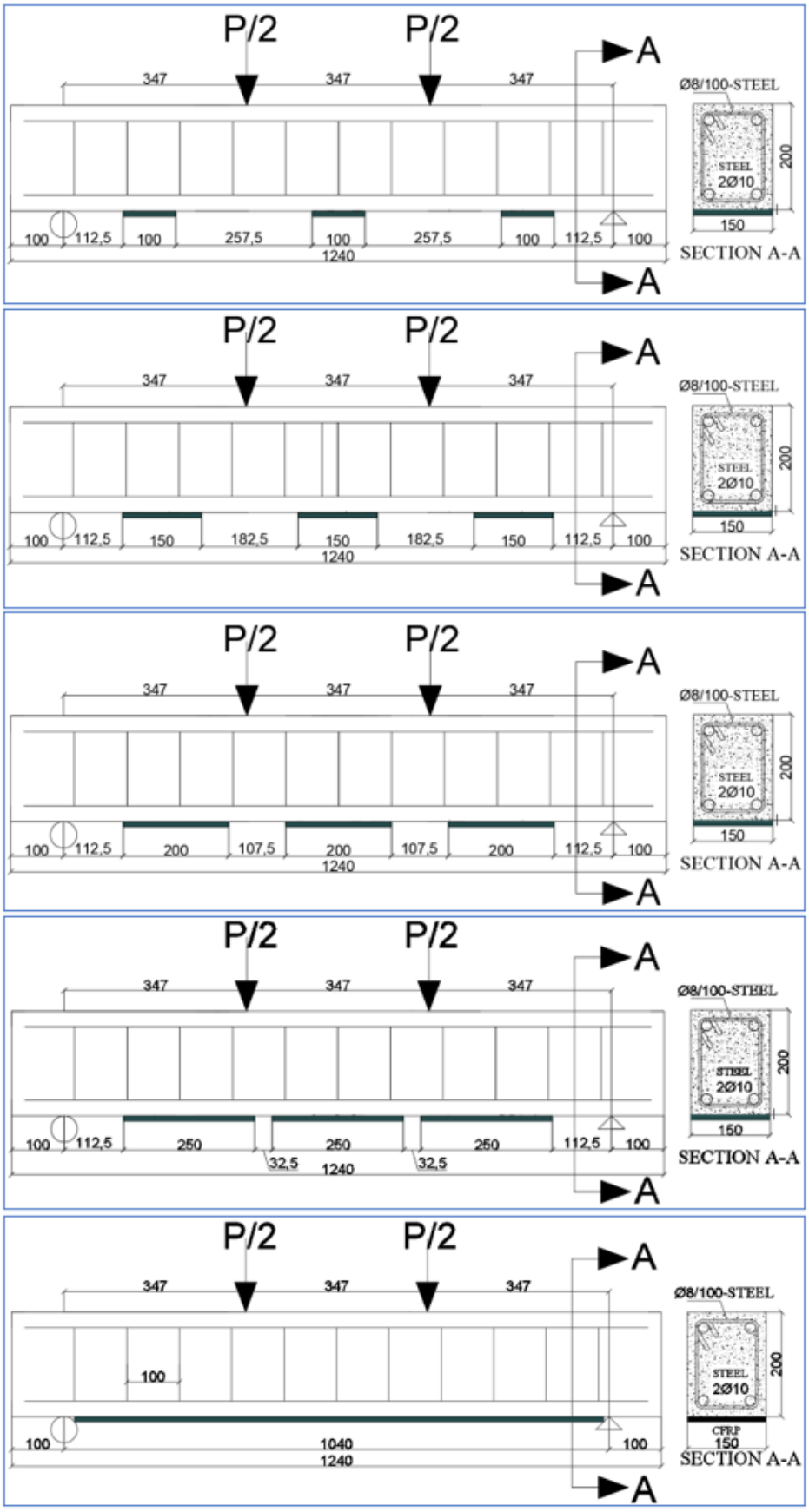


Figure 7. Four-point bending test setup, strip arrangement scheme, and Section A-A reinforcement details of bottom-only wrapped beams (State 1).

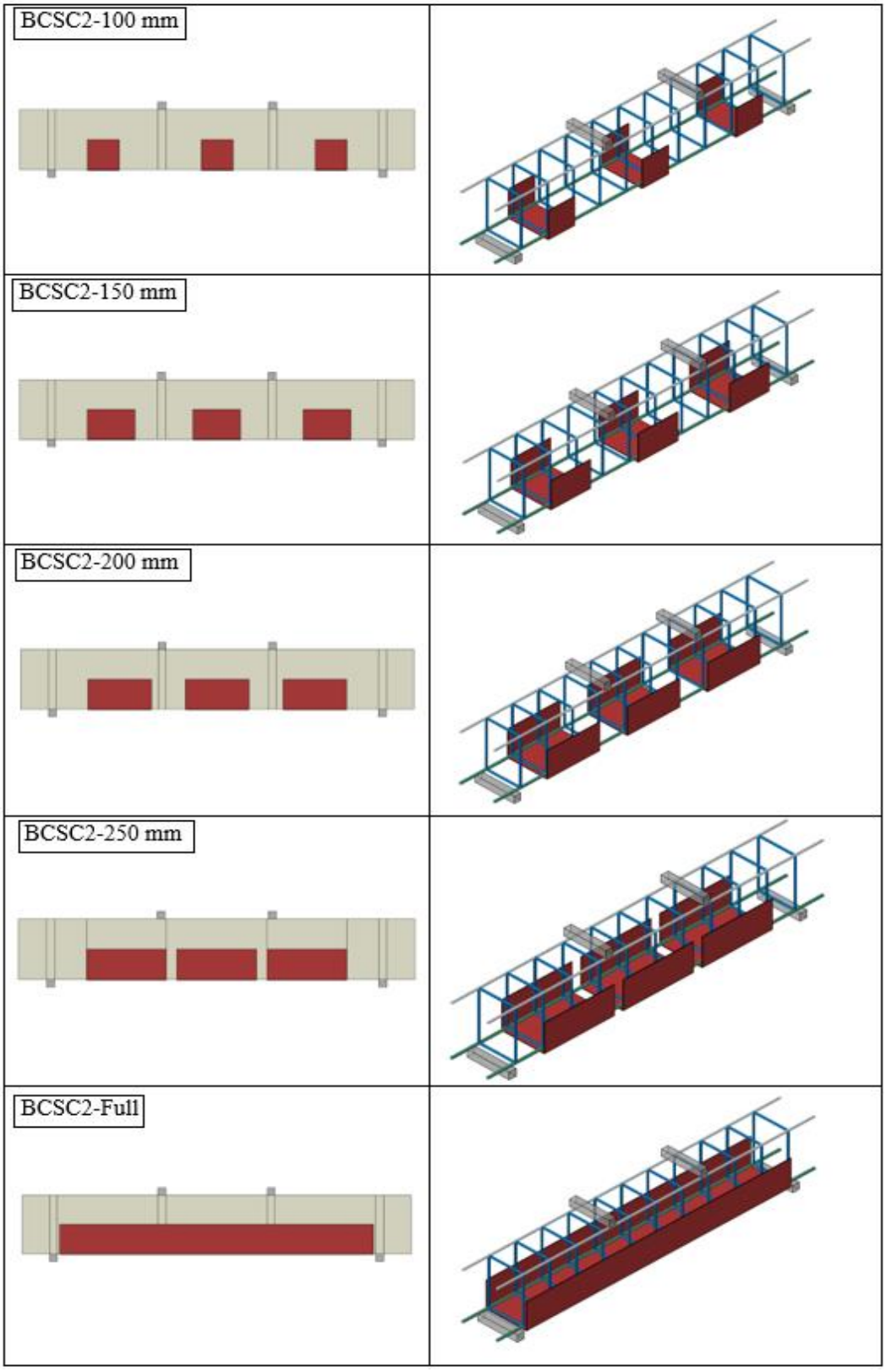


Figure 8. 3D Abaqus reinforcement cages and wrapping models of the beams strengthened with half U-wrapped CFRP textiles.

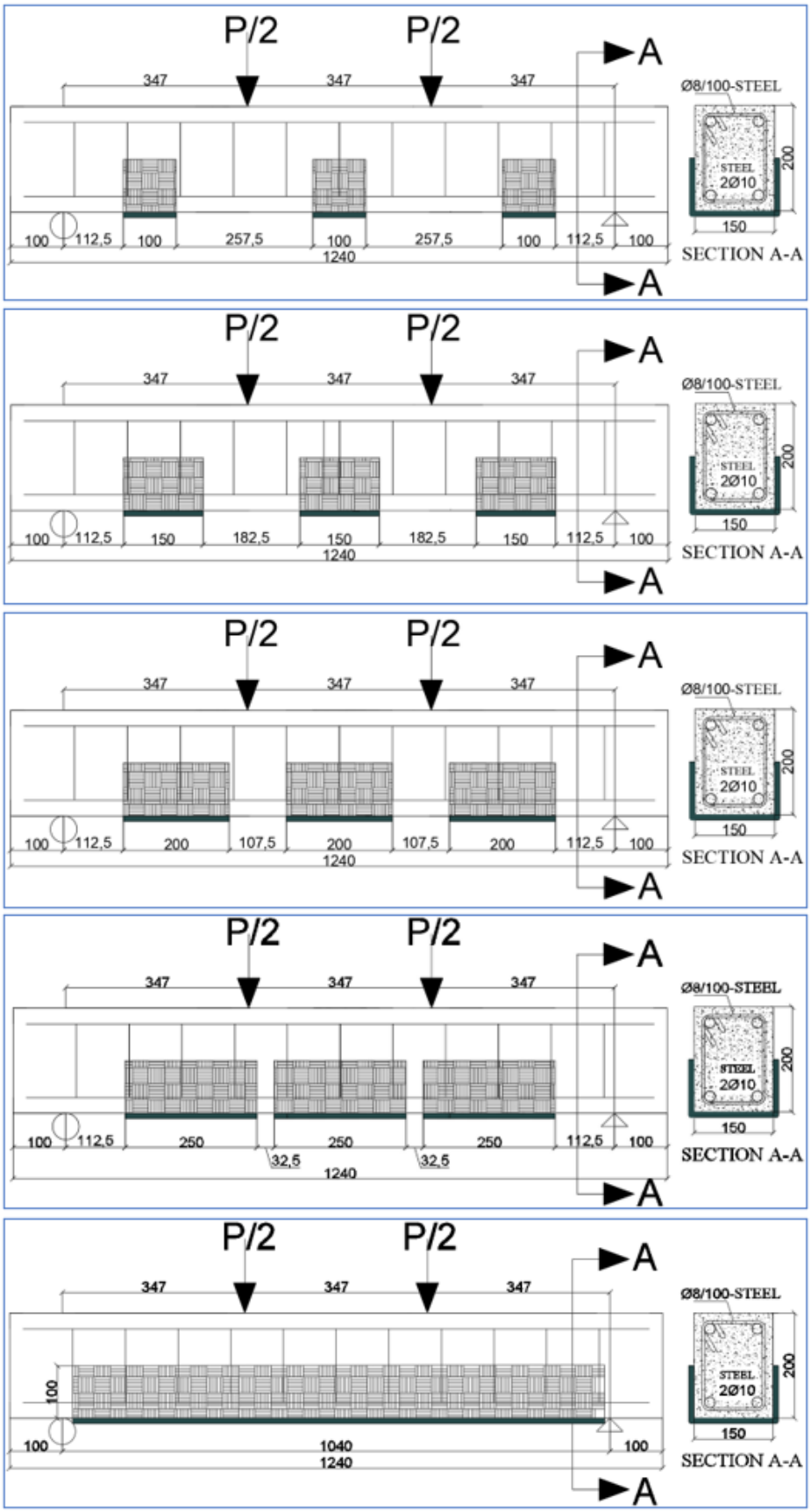


Figure 9. Four-point bending test setup, strip arrangement scheme, and Section A-A reinforcement details of half U-wrapped beams (State 2).

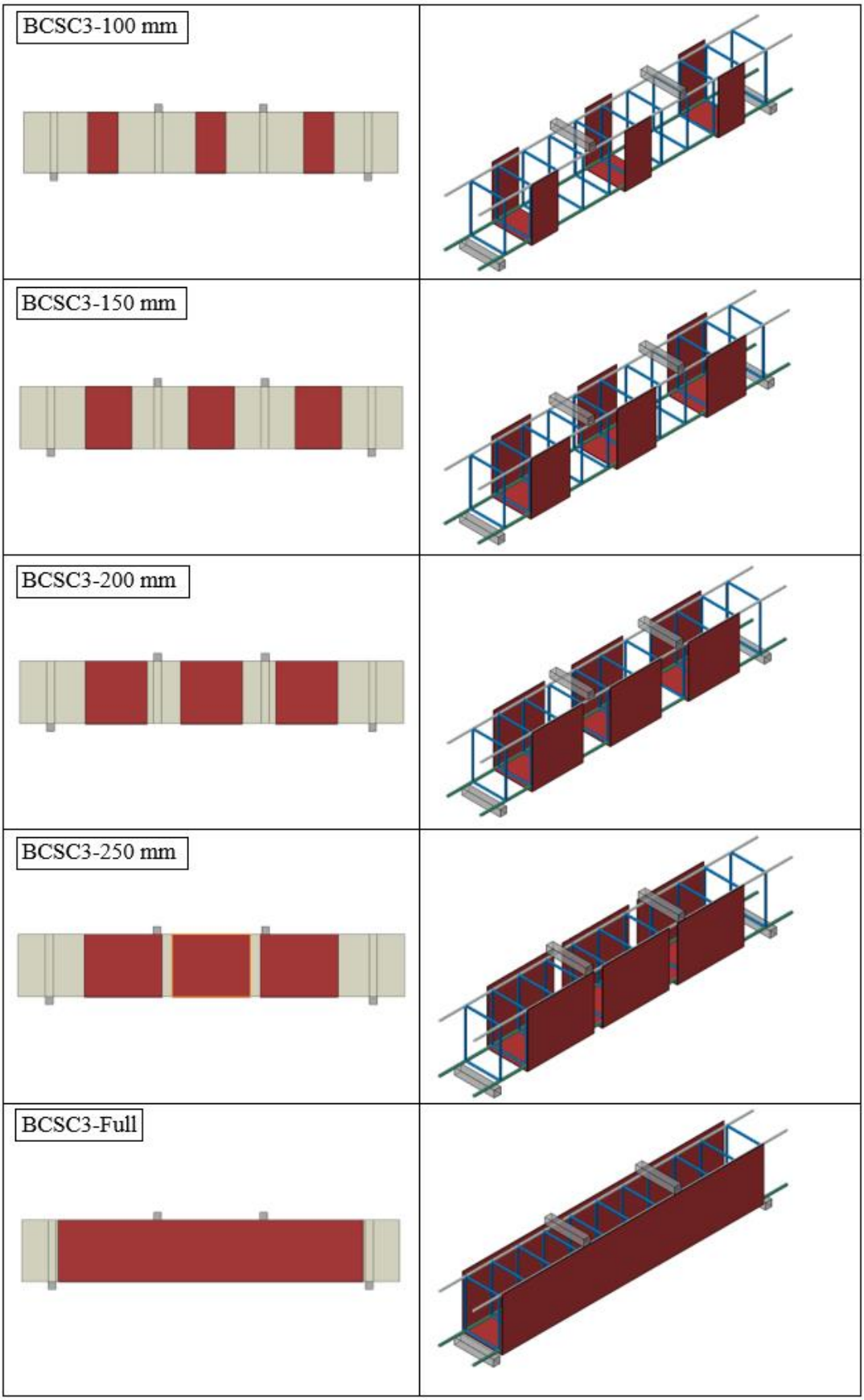


Figure 10. 3D Abaqus reinforcement cages and wrapping models of the beams strengthened with full U-wrapped CFRP textiles.

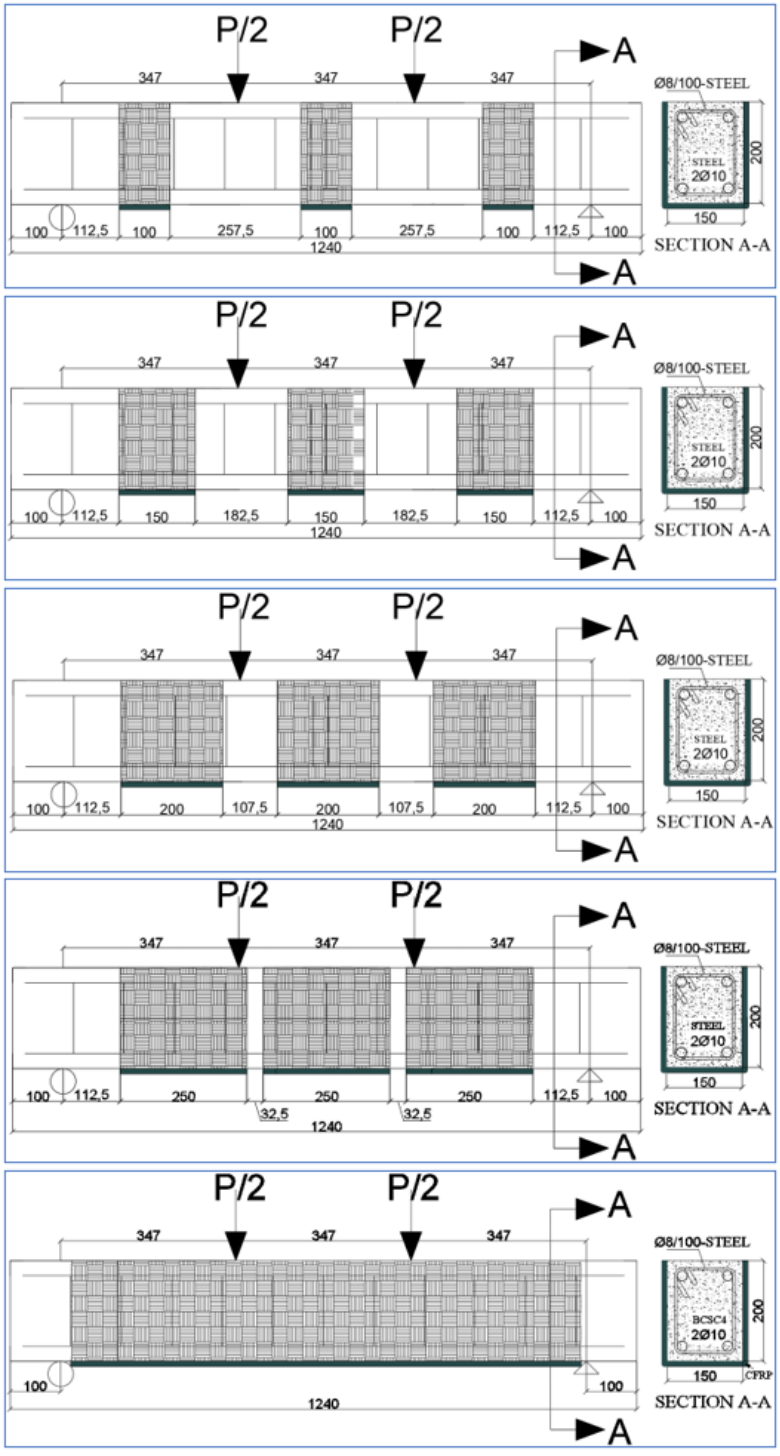


Figure 11. Four-point bending test setup, strip arrangement scheme, and Section A-A reinforcement details of full U-wrapped beams (State 3).

5. Results and discussion

As a result of the non-linear finite element analyses conducted in Abaqus, the Load-Displacement curves of the 15 modeled beams were successfully extracted. These results, compiled into three separate plots corresponding to their strengthening configurations, are presented together in Figure 12. Evaluating the curves reveals that the CFRP strip width and

the wrapping geometry strongly influenced the ultimate load-bearing capacity, initial stiffness, and deformation response of the beams.

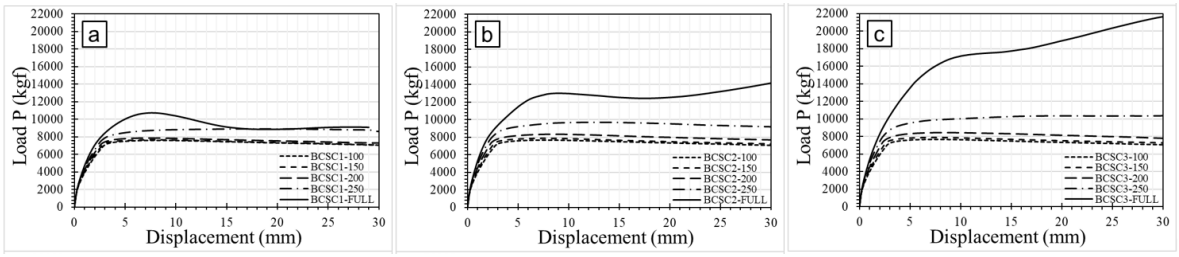


Figure 12. Load-Displacement curves obtained from Abaqus finite element analysis: (a) BCSC1: State 1 (Bottom-Only Wrapping), (b) BCSC2: State 2 (Half U-Wrapping), (c) BCSC3: State 3 (Full U-Wrapping).

5.1. Evaluation of BCSC1 Series Curves (Bottom-Only Wrapping)

In the BCSC1 series (Figure 12-a), where the CFRP sheets were applied exclusively to the bottom tension face of the beams, expanding the strip width from 100 mm to 250 mm yielded negligible enhancements in the ultimate load capacity. All strip models reached a distinct threshold at approximately 8000 kgf, exhibiting a relatively stable load level. This response indicates that increasing the bottom CFRP strip width alone was insufficient to produce a substantial increase in the overall load-carrying capacity of the modeled beams. Because the CFRP–concrete connection was defined using a Tie constraint, the present numerical model does not explicitly simulate interface debonding. Instead, the observed response is interpreted in terms of the load-transfer configuration and the stress concentration observed near the termination regions of the bottom CFRP strips. The BCSC1-FULL specimen leveraged its continuous CFRP coverage to reach a higher load level of approximately 11000 kgf; however, it experienced a sharp post-peak load drop, indicating a relatively abrupt loss of load-carrying capacity following the peak response.

5.2. Evaluation of BCSC2 Series Curves (Half U-Wrapping)

In the BCSC2 series (Figure 12-b), where the CFRP strips were extended up to half of the beam's web height, the additional CFRP coverage on the side faces provided a more continuous load-transfer configuration and increased lateral restraint compared with the bottom-only arrangement [4]. The extension of the CFRP strips onto the side faces increased the effective load-transfer region and reduced the concentration of stresses associated with the termination of the bottom-only configuration. The additional CFRP coverage on the side faces and the resulting change in wrapping geometry contributed to the observed increase in ultimate load capacity as the strip width increased from 100 mm toward 250 mm. Notably, the BCSC2-FULL model exhibited a sustained load-carrying response beyond a displacement of 20 mm, maintaining its structural stiffness and exceeding the 14000 kgf capacity mark.

5.3. Evaluation of BCSC3 Series Curves (Full U-Wrapping) and Continuity Analysis

The BCSC3 series (**Figure 12-c**), featuring complete jacketing of the beam web, exhibited the highest load-carrying response among the investigated configurations [6]. The full U-

wrapping geometry provided continuous CFRP coverage over the beam web and enhanced the load-transfer path between the bottom and side regions of the strengthened beam.

The most prominent finding within this series is the substantial difference in load-carrying capacity observed between the **BCSC3-250** segmented strip model and the **BCSC3-FULL** continuous wrapping model. Although the two configurations provide nearly identical CFRP-covered surface areas, except for the small gaps between the segmented strips, the BCSC3-250 model was limited to approximately 10000 kgf, whereas the BCSC3-FULL model maintained a steadily rising stiffness, surpassing the 21500 kgf threshold. This substantial difference highlights the influence of CFRP coverage continuity and the associated load-transfer paths on the numerical load-carrying response of the two configurations [10].

Discontinuity of axial and lateral load paths in the BCSC3-250 model. Although 250 mm represents a significant strip width, the 32.5 mm local gaps maintained between the strips interrupt the continuity of the CFRP reinforcement along the beam length. Consequently, the continuity of CFRP load-transfer paths is interrupted across these gap regions, leading to localized stress concentrations near the strip termination regions. Furthermore, diagonal tension (shear) cracks that may develop during four-point bending can propagate through these locally unreinforced 32.5 mm pathways, contributing to the observed reduction in load-carrying capacity [8].

Material and confinement continuity in the BCSC3-FULL model. Conversely, the continuous material layout in the FULL model eliminates the repeated gaps and intermediate termination regions present in the segmented configuration, thereby reducing the occurrence of the same type of periodic stress concentration [10]. The CFRP textile can contribute to bridging shear cracks across the strengthened region while providing continuous lateral restraint to the concrete core as it undergoes deformation under compression [5]. This continuous restraint can contribute to enhanced confinement of the concrete core and increased deformation capacity; however, the present finite element results do not by themselves justify quantifying this effect as an exponential increase in compressive strength. The resulting response enables the system to sustain higher load levels and deformation before the final loss of structural capacity.

6. Conclusions

In this study, the effects of different CFRP wrapping geometries and strip widths on the flexural behavior of reinforced concrete beams were parametrically investigated using non-linear finite element analysis in Abaqus. Based on the numerical findings, the following conclusions can be drawn:

- Increasing the width of bottom-bonded CFRP strips applied solely to the tension face did not produce a substantial increase in the ultimate load capacity within the investigated range, indicating that increasing the CFRP strip width alone was insufficient to substantially enhance the load-carrying response of the modeled beams.

- Half and Full U-wrapping geometries provided more continuous load-transfer paths and greater lateral restraint between the bottom and side CFRP regions compared with bottom-only configurations.
- Although the BCSC2-250 and BCSC2-FULL configurations provide nearly identical CFRP-covered surface areas save for the small gaps between the discrete strips the continuous FULL jacketing exceeded a load of approximately 14000 kgf, whereas the 250 mm discrete BCSC3 configuration reached approximately 9800 kgf. Thus, the continuous configuration sustained a load approximately 1.4 times that of the discrete configuration. This difference is attributed to the continuity of the CFRP coating and the associated load transfer paths. The 32.5 mm local gaps in the discrete layout interrupt the continuity of the CFRP reinforcement and create localized stress transfer zones that can facilitate crack propagation across the locally unreinforced areas.
- Although the BCSC3-250 and BCSC3-FULL configurations provide nearly identical CFRP-covered surface areas, except for the small gaps between the segmented strips, the continuous FULL jacket exceeded approximately 21500 kgf, whereas the 250 mm segmented BCSC3 configuration reached approximately 10000 kgf. Thus, the continuous configuration carried approximately 2.15 times the load level of the segmented configuration. This difference is associated with the continuity of CFRP coverage and the associated load-transfer paths. The 32.5 mm local gaps in the segmented layout interrupt the continuity of the CFRP reinforcement and create localized stress-transfer regions that may facilitate crack propagation through locally unreinforced zones.
- The continuous jacketing provided in the BCSC3-FULL model reduced the repeated termination-related stress concentrations associated with the segmented layout and provided continuous lateral restraint to the concrete core. These characteristics were associated with the increased load-carrying and deformation capacity observed in the numerical response.
- Within the investigated numerical configurations, the continuous Full U-wrapping arrangement provided the highest load-carrying capacity, while the segmented Half U- and segmented Full U-wrapping configurations provided intermediate responses with reduced material continuity. Therefore, the selection of a segmented configuration should be based on the desired balance between CFRP continuity, wrapping geometry, and material usage rather than being described categorically as an “ideal” solution.

7. References

[1] Uz M.E., Guner Y., Avci E. (2024). Strengthening of Reinforced Concrete Beams via CFRP Orientation. *Buildings*, 14(1), 82. https://doi.org/10.3390/buildings14010082.

[2] Hawileh, R. A., Naser, M.Z., Abdalla, J. A. (2013). Finite element simulation of reinforced concrete beams externally strengthened with short-length CFRP plates. *Composites Part B: Engineering*, 45(1), 1722–1730. https://doi.org/10.1016/j.compositesb.2012.09.032.

[3] Siddika, A., Saha, K., Mahmud, M.S., Roy, S. C. Performance and failure analysis of carbon fiber-reinforced polymer (CFRP) strengthened reinforced concrete (RC) beams. *SN Appl. Sci.* **1(12)**, 1617 (2019). https://doi.org/10.1007/s42452-019-1675-x.

[4] Ayyobi, P., Barros, J.A.O., & Dias, S.J.E. (2024). Numerical assessment of the effect of CFRP anchorages on the performance of strengthened RC beams. *Journal of Composites Science*, 8(9), 348. https://doi.org/10.3390/jcs8090348.

[5] ACI Committee 440. (2017). *Guide for the Design and Construction of Externally Bonded FRP Systems for Strengthening Concrete Structures (ACI 440.2R-17)*. American Concrete Institute, Farmington Hills, MI, USA.

[6] Ishfaq, M., Kanitkar, R., Harries, K., Oller, E., Shapack, G., Alkhrdaji, T., Tatar, J. (2026). Shear strengthening and anchorage effects of CFRP U-wraps in flexurally strengthened reinforced concrete beams. *Journal of Composites for Construction*, 30(2). https://doi.org/10.1061/JCCOF2/CCENG-5320.

[7] Cazacu C.E., Dimitriu, C.Ş., Bărbulescu A. (2024). Concrete CFRP-Reinforced Beam Performances, Tests and Simulations. *Sustainability*, 16(7), 2614. https://doi.org/10.3390/su16072614.

[8] Thamrin, R., Zaidir and Sabril Haris. Shear capacity of reinforced concrete beams strengthened with web side bonded CFRP sheets. *MATEC Web of Conferences 258*, 04010 (2019), SCESCM 2018. https://doi.org/10.1051/matecconf/201925804010.

[9] Kashash M.D., Khalid N.N. (2025). Evaluation of the Shear Strength of RC Beams Strengthened by Basalt Fiber Sheets. *Engineering, Technology & Applied Science Research*, 15(2), 22187-22195. https://doi.org/10.48084/etasr.10284.

[10] Moon, J.S., Kim, D.Y., Ko, M.S., Kim, C. (2023). Performance of reinforced concrete beams strengthened by bidirectional carbon-fiber-reinforced polymers based on numerical models. *Polymers*, 15(4), 1012. https://doi.org/10.3390/polym15041012.

[11] Ahmed A.K., Al-Allaf M.H. (2025). Strengthening of ultra-high performance concrete beams with CFRP strips. *Civil and Environmental Engineering, 22(1), 221-244*. https://doi.org/10.2478/cee-2026-0015.

[12] Dogan A., Jalali M.B. Nonlinear finite element analysis on the flexural behavior of RC beams strengthened with CFRP sheets and internal GFRP bars: Effects of CFRP laminate length and GFRP reinforcement ratio. *5th Internatıonal Ege Congress On Scıentıfic Research July 22-23, (2026), Marmaris, Muğla.* ISBN: 979-8-89695-504-7.

[13] Saenz, LP. Discussion of ‘‘Equation for the stress-strain curve of concrete” by Desayi P, Krishnan S. ACI Journal 1964;61:1229–35.

[14] Hu H-T, Schnobrich WC. Constitutive modelling of concrete by using nonassociated plasticity. *Journal of Materials in Civil Engineering*, 1(4):199-216. https://doi.org/10.1061/(ASCE)0899-1561(1989)1:4(199).

[15] Piggott M. Load bearing fibre composites. 2nd ed. Boston/Dordrecht/London: Kluwer Academic Publishers; 2002.

[16] Methods of Testing Cement - Part 1: Determination of Strength, TS EN 196-1 standard, 2016.

[17] Hibbitt, Karlsson, and Sorensen, Inc. ABAQUS Theory manual, User manual and Example Manual, Version 6.7. Providence, RI; 2000.

ÇOK KRİTERLİ KARAR VERME TEKNİKLERI İLE ÜRETİM, ARGE VE SATIŞ SONRASI PROJELERİNDE KRİTİK BAŞARI FAKTÖRLERİNİN ÇEVİKLİĞE KATKISI VE SEKTÖREL ANALİZİ

CONTRIBUTION OF CRITICAL SUCCESS FACTORS TO AGILITY IN PRODUCTION, R&D AND AFTER-SALES PROJECTS AND SECTORAL ANALYSIS WITH MULTI CRITERIA DECISION TECHNIQUES

Yiğithan YILMAZ
Oyak Renault Otomobil Fabrikaları, Mühendislik Direktörlüğü, Sistem Mühendisliği Departmanı
Oyak Renault Automobile Factories, Engineering Directorate, Department of System Engineering
ORCID ID: 0000-0002-8019-5316

ÖZET

Bu çalışmada günümüzün rekabetçi ve hızla değişen iş dünyasında proje yönetimi organizasyonlarının başarıyı ne derece ve nasıl etkilediği tartışılmaktadır. Yeterince net olmayan ve karışık süreçlerin yoğun olduğu projelerde, çeviklik ile etkisi yüksek çözümler sunmak ve rakipler karşı avantaj sağlamak mümkündür. Projelerde değişime ve müşteri beklentilerine uyum sağlama becerisi çeviklik olarak tanımlanmaktadır. Bu çalışma, otomotiv, savunma sanayi ve tüketici elektroniği sektörlerinde üretim, ARGE (Araştırma-Geliştirme) ve satış sonrası projelerinde çevik anlayışı ve çevikliğe katkı sağlayan kritik başarı faktörlerini incelemektedir. Bu çalışmada altı farklı şirkette ve üç farklı sektörde görev alan alanında uzman profesyonellerden, literatürde bulunan kritik başarı faktörlerinin çevikliğe katkısı açısından değerlendirilmesi istenmiş ve Analitik Hiyerarşi Prosesi tekniği kullanılarak kritik başarı faktörlerinin ağırlıkları belirlenmiştir. Bu teknikle belirlenen kriter ağırlıkları ve profesyonellerden alınan değerlendirmeler kullanılarak TOPSIS, VIKOR ve MOORA yöntemleri ile nümerik ve metodolojik analiz yapılmıştır. Elde edilen sonuçlar karşılaştırılarak sektörlerin ve firmaların çeviklik performansları değerlendirilmiş, incelenen sektörlerde çevikliği etkileme konusunda en başarılı faktörler tespit edilmiştir. Elde edilen sonuçlar, firmaların proje yönetiminde hangi kritik başarı faktörüne daha çok önem verilirse çevikliğin ve dolayısıyla başarının artacağını gözler önünde sermektedir. Bu sonuçlara istinaden firmalar rakiplere karşı avantaj elde edebilecektir. Yapılan çalışmanın sektörel bazda çevik proje yönetimi literatürüne ve çevik proje yönetim uygulamalarına yüksek katkıda bulunması hedeflenmektedir.

Anahtar Kelimeler: Çeviklik, Proje Yönetimi, Çok Kriterli Karar Verme, Otomotiv, Savunma Sanayi, Tüketici Elektroniği

ABSTRACT

This study discusses the extent to which project management organizations affect success in today's competitive and rapidly changing business world. In projects with unclear and complex processes, it is possible to offer high-impact solutions and gain advantage over

competitors with agility. The ability to adapt to change and customer expectations in projects is defined as agility. This study examines the agile approach and critical success factors that contribute to agility in production, R&D and after-sales projects in the automotive, defense industry and consumer electronics sectors. In this study, experts in the field working in six different companies were asked to evaluate the critical success factors found in the literature in terms of their contribution to agility and the weights of the critical success factors were determined using the Analytical Hierarchy Process. Numerical analysis was performed using the TOPSIS, VIKOR and MOORA methods using the determined weights and the evaluations received from the professionals. The obtained results were compared and the agility performances of the sectors and companies were evaluated, and the most successful factors in affecting agility in the examined sectors were determined. The results reveal that which critical success factor is given more importance in the project management of the companies will increase agility and therefore success. In this way, companies will be able to gain advantage over their competitors. The study is aimed to contribute to the agile project management literature and practices on a sectoral basis.

Keywords: Agility, Project Management, AHP, TOPSIS, VIKOR, MOORA, Automotive, Defense Industry, Consumer Electronics.

BEYOND ARTIFICIAL INTELLIGENCE: EXPLORING THE RISE OF SYNTHETIC INTELLIGENCE

S. Suresh Krishna
Second year B.Sc. Computer Science (Artificial Intelligence) Department of Computer Science (Artificial Intelligence) Nadar Mahajana Sangam S. Vellaichamy Nadar College,
Nagamalai, Madurai-19

F. Joshwa Santhosh
Second year B.Sc. Computer Science (Artificial Intelligence) Department of Computer Science (Artificial Intelligence) Nadar Mahajana Sangam S. Vellaichamy Nadar College,
Nagamalai, Madurai-19

Dr. S. Selvam
Head and Assistant Professor, Department of Computer Science (Artificial Intelligence) Nadar Mahajana Sangam S. Vellaichamy Nadar College, Nagamalai, Madurai-19

ABSTRACT

Artificial Intelligence (AI) has significantly transformed the way machines perform tasks that require human intelligence. As technology advances, a new concept called Synthetic Intelligence (SI) is emerging, aiming to develop systems with greater adaptability, reasoning, and autonomous decision-making capabilities. This paper explores the concept of Synthetic Intelligence and compares it with traditional AI in terms of learning, problem-solving, and adaptability. While AI mainly relies on data-driven models, SI focuses on creating more flexible and intelligent systems capable of handling complex situations. The study also examines potential applications of SI and discusses key challenges such as ethics, security, and transparency. The findings suggest that Synthetic Intelligence could represent the next stage in the evolution of intelligent systems, offering new possibilities for future technological development.

KOREA'S CULTURAL RENAISSANCE: THE EVOLUTION OF CINEMA AND K-POP

B. DHARSHINI
Second year B.Sc CS(Artificial Intelligence), Department of Computer Science(Artificial Intelligence), Nadar Mahajana Sangam S.Vellaichamy Nadar College Nagamalai Madurai-19 Tamilnadu, India

S. Selvam
Dr., Head and Assistant Professor, Department of Computer Science(Artificial Intelligence)
Nadar Mahajana Sangam S. Vellaichamy Nadar College Nagamalai Madurai-19, Tamilnadu, India

ABSTRACT
This paper examines South Korea's transformation from a war-torn nation with a GDP per capita lower than Ghana in 1965 to the world's 12th largest economy and a global cultural superpower. Focusing on two pillars of the Korean Wave or Hallyu — cinema and K-Pop — it traces the evolution from a regional phenomenon in the late 1990s to a global cultural force worth $13.2 billion in exports in 2022. The study argues that Korea's Cultural Renaissance is not accidental but the product of five converging factors: democratization and lifting of cultural censorship in the late 1980s, strategic state investment in culture as an export industry after the 1997 Asian financial crisis, rapid adoption of high-tech infrastructure, a unique narrative of "dynamic and turbulent" modern history, and the professionalized idol and studio system.

INTRODUCTION
Hallyu, meaning "Korean Wave," is the global spread of Korean pop culture — dramas, K-pop, film, and more recently beauty and food. The term itself was not coined by Koreans, but by Chinese journalists in 1999 to describe the sudden surge of Korean cultural content. 60e26014

The phenomenon is generally divided into four phases: Hallyu 1.0 (late 1990s - TV dramas), Hallyu 2.0 (late 2000s - K-Pop), Hallyu 3.0 (Korean culture), and Hallyu 4.0 (K-Style). This paper focuses on the two most influential products: cinema and K-Pop, which together have redefined Korea's national image from an industrial exporter to a cultural powerhouse. 08d4

HISTORICAL CONTEXT: FROM CENSORSHIP TO CREATIVE LIBERATION
Hallyu is used to describe Korean pop culture's international diffusion after the end of military rule in the late 1980s: a period of modernization and the liberation of the culture industry from state-controlled media. 6014

Two critical policy shifts enabled the renaissance:

a) Lifting of Travel Bans: In the early 1990s, the government lifted the ban on foreign travel for Koreans. Many Koreans pursued education in the US and Europe and returned in the late 1990s with western production and management knowledge.

b) The 1997 IMF Crisis as Catalyst: Following the Asian financial crisis, the Kim Dae-jung administration (1998-2003) explicitly designated culture as a strategic export industry to earn foreign revenue. This led to the Basic Law for Cultural Industry Promotion (1999). 9da9

Simultaneously, the foundation of a hi-tech infrastructure laid in the mid-1990s was enabling Koreans to leverage the Internet and mobile telecommunications more efficiently than anyone else. 4ebe

EVOLUTION OF KOREAN CINEMA: FROM REGIONAL BLOCKBUSTERS TO OSCARS

***Phase 1:** The Genesis of Hallyu Cinema (1999-2003)*

The public face of Hallyu is often attributed to movies and TV dramas released in 1999. _Shiri (1999)_, a North-South espionage thriller, was the first true Korean blockbuster to succeed across Southeast Asia. It was followed by romantic comedies like _My Sassy Girl (2001)_. 9da95f8e

***Phase 2:** Auteur Recognition and Genre Innovation (2003-2019)*

Filmmakers like Park Chan-wook and Bong Joon-ho built global prestige. Park's violent noir thriller _Oldboy (2003)_ captured the Grand Prix at Cannes. Bong Joon-ho explained the creative secret: South Korea "provides creators with ample inspiration and stimulation. It's such a dynamic and turbulent place," referring to the lived experience of Korean War, military dictatorship, rapid economic transformation, and democratic transition. 4ebe315c

This period created "slick production with professional marketing, underpinned by a key local ingredient - the raw emotion Koreans express so passionately". 4ebe

***Phase 3**: The Global Breakthrough*

Parasite (2019) winning the Palme d'Or and the Academy Award for Best Picture marked the apex. It proved that Korean stories, rooted in specific class anxieties of "dynamic Korea," had universal resonance. This was followed by the streaming era where _Squid Game_ became Netflix's most-watched non-English show. 315c

4. EVOLUTION OF K-POP: FROM H.O.T. TO BTS

***Phase 1**: First Generation Idols (1992-2007)*

The K-pop fad at the time was led by figures like CLON, a powerful male duo, and H.O.T, the first-generation of K-pop idol groups. Agency SM Entertainment, founded in 1995, invented the trainee system — recruiting children, training them for years in singing, dancing, languages, and media manners. 5f8e

***Phase 2:** Second Generation and the Asian Expansion (2007-2012)*

Groups like TVXQ, Big Bang, Girls' Generation, and Wonder Girls expanded Hallyu 2.0 beyond East Asia to Vietnam, Singapore and Thailand. Fast personalization of digital media technology played a significant role in this circulation. 5f8e

***Phase 3**: The Global Breakthrough — Psy and BTS*

While Hallyu started in Asia, it wasn't until Psy's breakout hit "Gangnam Style" that Hallyu hit the West. Psy demonstrated YouTube's power as a distribution channel. This paved the way for the third generation: BTS and BLACKPINK. 315c

BTS represents the culmination of the system: perfection through bodies and visuals, combined with direct fan engagement via social media, narrative-driven albums, and self-production. K-Pop exports expanded from music to encompass fashion, beauty, and lifestyle. 08d4

__Phase 4__: The Industrial Model

Today's K-Pop is a highly professionalized industry:

- *360-degree production:* Agencies control music, choreography, music videos, fashion, and global touring.
- *Fandom economy:* Official lightsticks, photocards, Weverse/ Bubble platforms.
- *Hybridity:* Songs blending Korean lyrics with English hooks, hip-hop, EDM, and Afrobeats to maximize global appeal.

THE STATE AND SOFT POWER

Hallyu as a form of soft power in Korea's foreign relationship started with spreading K-dramas in Asia. The South Korean government now has an explicit goal to become the world's leading exporter of popular culture. 08d49c80

Cultural exports were worth some $13.2 billion in 2022, more than home appliances or electric cars, and the government is targeting $25 billion by 2027. The Hallyu effect had already contributed an estimated USD 12.3 billion boost to the Korean economy in 2019.

COMPARISON

ON CINEMA:

1. Parasite Effect: How Bong Joon-ho Broke the One-Inch Barrier of Subtitles

Why did the West suddenly accept non-English cinema? Study the class narrative of Korea.

2. From Censorship to Cannes: The Role of Democratization (1987) in Korean Cinema

How the end of military dictatorship unlocked violent, political, emotional storytelling.

3. Trauma as Content: How the Korean War, IMF Crisis, and Sewol Ferry Influence Film Plots

Bong's own quote - Korea is "dynamic and turbulent" - why Korean movies can't help but be different.

4. The Netflix Deal: Squid Game and the New Hallyu Business Model

Is Korea losing its culture to US platforms or using them to conquer the world?

5. Women in New Korean Cinema

From _The Handmaiden_ to _Past Lives_ - how female directors are changing the male-dominated Chungmuro industry.

ON K-POP:

6. The Trainee System: Factory or Dream School?

7-10 years of training, no phones, strict diet. Human rights, child labor, and perfection culture behind BTS / BLACKPINK.

7. Why Psy Had to Happen Before BTS Could Happen
How "Gangnam Style" (2012) was the viral bridge that made the West's algorithm ready for K-Pop.
8. Fandom Economy: Lightsticks, Photocards, and Weverse
How K-Pop earns more from fandom merchandise than music sales. The $13.2 Billion export economy.
9. K-Pop's Hybrid Music Formula: Why It Sounds American but Feels Korean
The Swedish producers, American choreographers, and Korean lyrics mix.
10. Military Service vs. World Tour: BTS, EXO, and the National Duty Dilemma
What happens when soft power meets hard military law.
ON BOTH - CINEMA + K-POP TOGETHER:
11. Government as Producer: How Korea Treats Culture Like Samsung
State investment after 1997 crisis - Basic Law for Cultural Industry Promotion (1999). Did the government create Hallyu?
12. Hallyu 1.0 vs Hallyu 4.0 - Drama Fans vs TikTok Fans
Comparison of _Winter Sonata_ ajummas in Japan (2002) vs TikTok Gen Z stans.
13. Cultural Appropriation or Appreciation? K-Pop's Use of Black Culture, Indian Sets, African Beats
14. The Dark Side of Renaissance: Burnout, Cyberbullying, and Sasaeng Culture
Suicides of idols and actors, high pressure - the cost of perfection.
15. India and Hallyu: Why Manipur and Nagaland Fell in Love with K-Pop Before Delhi
Best topic if you are in India - Northeast India as the entry point for Hallyu.
My Top 3 Most Unique for High Grades:
1. *The Trainee System: Factory or Dream School?* - Professors love it, lots of data.
2. *Parasite Effect + Class* - Very academic.
3. *Government as Producer* - Easy to get government documents and prove economic impact.

CONCLUSION: WHY KOREA?

Korea's Cultural Renaissance succeeds because it offers what Bong Joon-ho and Park Chan-wook call "dynamic Korea" — stories that cannot help but be different because everyone has lived through dramatic times. 315c
Cinema provides artistic legitimacy and critical acclaim, while K-Pop provides participatory global fandom and economic scale. Together they have transformed Korea's image: once a nation that exported industrial, but not cultural content, it now exports identity. 4ebe
The future of Hallyu lies in the convergence of these two forms — as seen in K-pop idols becoming actors, films becoming musicals, and both being distributed through the same global streaming platforms. What began with the broadcast of _What is Love (1991)_ on CCTV in 1997 achieving the highest audience share for a foreign drama, has become a permanent feature of global pop culture. 5f8e

REFERENCES

Journal Articles & Research Reports

1. Kim, J. (2015). _The Korean Wave and Media Exchange in Global Culture Industry_. Goldsmiths, University of London. Research report on the evolution of Hallyu from television drama _What is Love (1991)_ to K-Pop expansion.

2. Hallyu: South Korea's Cultural Export Boom. (2019). _World Politics Review_. Analysis of Hallyu's economic impact, noting its contribution of 0.2% of Korea’s GDP in 2004 (USD 1.87 billion) and USD 12.3 billion in 2019.

News & Industry Analysis

3. AJMEDIA English. (2024, October 13). _Hello Hallyu: Why is South Korean culture sweeping the globe?_ AFP Analysis.

- Notes cultural exports worth $13.2 billion in 2022, more than home appliances or electric cars, and the government target of $25 billion by 2027.
- Cites Bong Joon-ho's explanation that Korean creators have lived through "dramatic times".

4. Today Note. (2026). _Hallyu Korean Culture History: Why It Almost Died Twice_.

- Discusses how the name Hallyu was coined by Chinese media, not by Koreans.
- Identifies _What is Love (1991)_ as the source from which the Korean popular culture renaissance originated after airing on CCTV in 1997.
- Describes Hallyu's second phase built on legendary drama _Winter Sonata (2002)_.

Key Primary Sources on Evolution

5. *For Cinema Evolution:*

- _Shiri (1999)_ and _My Sassy Girl (2001)_ as first Korean-style blockbuster films that flooded into Asia.
- Park Chan-wook on Korean cinematic success: "Why don’t you try living in ‘dynamic Korea?’"

6. *For K-Pop Evolution:*

- First-generation groups: CLON and H.O.T, the first-generation of K-pop idol groups.
- Role of fast personalisation of digital media technology in Hallyu circulation.

WAYS TO REDUCE AND RESOLVE MISUNDERSTANDINGS BETWEEN PEOPLE

M. Dhinesh Kumar
Second year BSC.CS (AI), Department of Computer Science (Artificial Intelligence), Nadar Mahajana Sangam S. Vellaichamy Nadar Colllege, Madurai, Tamilnadu, India, Madurai

Dr. S. SELVAM
HEAD and Assistant Professor Department of Computer Science (Artificial Intelligence), Nadar Mahajana Sangam S. Vellaichamy Nadar Colllege, Madurai, Tamilnadu, India MADURAI, Tamilnadu, India

ABSTRACT
Misunderstandings are common in personal, educational, professional, and social relationships. If they are not addressed, misunderstandings may lead to conflict, mistrust, emotional stress, and damaged relationships. This research examines the major causes of misunderstandings and identifies effective ways to prevent and resolve them. The study focuses on active listening, clear communication, empathy, emotional control, clarification, cultural sensitivity, and mediation. Previous research emphasizes that asking questions, restating information, speaking directly, and allowing each person to explain their perspective can reduce confusion and conflict. The findings may help individuals and groups develop healthier communication practices.
Keywords: misunderstanding, communication, active listening, empathy, conflict resolution, clarification.

DEVELOPING LEARNERS' SOFT SKILLS IN A STEM-BASED VIRTUAL LEARNING ENVIRONMENT

STEM TABANLI SANAL ÖĞRENME ORTAMINDA ÖĞRENCILERIN SOSYAL BECERILERINI GELIŞTIRMEK

Kamalbek BERKİMBAYEV
Professor, Khoja Akhmet Yassawi International Kazakh-Turkish University, Turkistan, Kazakhstan
ORCID NO: 0000-0002-5191-8140

Dinara BERDİ
Asist. Prof., Khoja Akhmet Yassawi International Kazakh-Turkish University, Turkistan, Kazakhstan
ORCID NO: 0000-0002-0553-4015

Sherzod RAMANKULOV
Asist. Prof., Khoja Akhmet Yassawi International Kazakh-Turkish University, Turkistan, Kazakhstan
ORCID NO: 0000-0002-0553-4015

Shakhrizada KHIKMATULLA
Master's student, Khoja Akhmet Yassawi International Kazakh-Turkish University, Turkistan, Kazakhstan
ORCID NO: 0009-0007-1481-694X

Kazhymukan KELESBAYEV
PhD, Khoja Akhmet Yassawi International Kazakh-Turkish University, Turkistan, Kazakhstan
ORCID NO: 0009-0008-9605-7138

ABSTRACT

Developing students' soft skills alongside subject-specific knowledge is an important challenge in contemporary physics education. Traditional teaching approaches often provide limited opportunities for collaborative problem-solving, creative thinking, self-regulation and the practical application of scientific knowledge. Integrating STEM education with virtual learning environments offers opportunities to address these challenges through interactive, project-based and collaborative learning activities. This study aims to develop and present a pedagogical model of a STEM-based virtual learning environment designed to support the development and assessment of students' soft skills in Grade 10 physics education. The study adopted a design-based research approach integrating STEM education, project-based learning, gamification, collaborative learning and formative assessment. The Physics•LMS platform was developed around a five-stage instructional sequence consisting of theoretical learning, video materials, problem-solving, testing and virtual laboratory activities. A three-level assessment framework (Foundation, Application and Mastery) was incorporated to evaluate six soft skills: critical thinking, communication, collaboration, creativity, self-

regulation and digital literacy. The study resulted in the development of Physics•LMS, a STEM-based virtual learning environment comprising eight modules, 49 lessons, 147 test questions, 98 physics problems, nine laboratory activities and 72 STEM project stages. The platform integrates gamification, collaborative learning and a three-level assessment system (Foundation, Application and Mastery) for six soft skills: critical thinking, creativity, communication, collaboration, self-regulation and digital literacy. An integrated learning analytics dashboard enables teachers to monitor students' academic progress and soft skills development.

Keywords: STEM education; virtual learning environment; soft skills; physics education; gamification; collaborative learning; learning analytics.

ÖZET

Öğrencilerin alana özgü bilgilerinin yanı sıra sosyal becerilerini (soft skills) geliştirmek, çağdaş fizik eğitiminde önemli bir zorluktur. Geleneksel öğretim yaklaşımları; iş birliğine dayalı problem çözme, yaratıcı düşünme, öz düzenleme ve bilimsel bilginin pratik uygulaması konularında genellikle sınırlı fırsatlar sunmaktadır. STEM eğitiminin sanal öğrenme ortamlarıyla bütünleştirilmesi; etkileşimli, proje tabanlı ve iş birliğine dayalı öğrenme etkinlikleri aracılığıyla bu zorlukların ele alınmasına olanak tanır. Bu çalışma, 10. sınıf fizik eğitiminde öğrencilerin sosyal becerilerinin geliştirilmesini ve değerlendirilmesini desteklemek amacıyla tasarlanmış, STEM tabanlı bir sanal öğrenme ortamına ilişkin pedagojik bir model geliştirmeyi ve sunmayı amaçlamaktadır. Çalışmada; STEM eğitimi, proje tabanlı öğrenme, oyunlaştırma, iş birliğine dayalı öğrenme ve biçimlendirici değerlendirmeyi bütünleştiren, tasarım tabanlı bir araştırma yaklaşımı benimsenmiştir. Physics•LMS platformu; teorik öğrenme, video materyalleri, problem çözme, test etme ve sanal laboratuvar etkinliklerinden oluşan beş aşamalı bir öğretim süreci temel alınarak geliştirilmiştir. Eleştirel düşünme, iletişim, iş birliği, yaratıcılık, öz düzenleme ve dijital okuryazarlık olmak üzere altı sosyal beceriyi değerlendirmek amacıyla üç düzeyli (Temel, Uygulama ve Ustalık) bir değerlendirme çerçevesi sisteme dahil edilmiştir. Çalışma sonucunda; sekiz modül, 49 ders, 147 test sorusu, 98 fizik problemi, dokuz laboratuvar etkinliği ve 72 STEM proje aşamasından oluşan STEM tabanlı bir sanal öğrenme ortamı olan Physics•LMS geliştirilmiştir. Platform; eleştirel düşünme, yaratıcılık, iletişim, iş birliği, öz düzenleme ve dijital okuryazarlık becerilerine yönelik oyunlaştırma, iş birliğine dayalı öğrenme ve üç düzeyli (Temel, Uygulama ve Ustalık) bir değerlendirme sistemini bütünleştirmektedir. Entegre bir öğrenme analitiği paneli, öğretmenlerin öğrencilerin akademik ilerlemelerini ve sosyal beceri gelişimlerini takip etmelerine olanak tanır.

Anahtar kelimeler: STEM eğitimi; sanal öğrenme ortamı; sosyal beceriler; fizik eğitimi; oyunlaştırma; iş birliğine dayalı öğrenme; öğrenme analitiği.

INTRODUCTION

Physics is a discipline that explains natural phenomena through mathematical models, and for this reason students often perceive it as abstract and difficult. When concepts such as velocity, acceleration, force, energy and entropy cannot be linked to everyday experience, misconceptions may become persistent. A study conducted with a large sample of courses showed that interactive-engagement methods considerably increased conceptual gains compared with traditional lecturing (Hake, 1998). Wieman and Perkins (2005) likewise emphasise the importance of research-based teaching and interactive simulations in transforming physics education.

Although laboratory activities are an integral part of physics teaching, hardware, time and safety constraints mean that not every student has the opportunity to carry out experiments. Finkelstein et al. (2005) reported that, in an electric-circuits laboratory where computer simulations replaced real equipment, students who used simulations performed better in conceptual understanding and in building real circuits. This finding suggests that virtual laboratories can be regarded not as an alternative to real experiments but as a means of complementing them and widening access to them.

Contemporary educational approaches, moreover, aim to develop not only subject knowledge but also 21st-century skills such as critical thinking, communication, collaboration and creativity (Trilling and Fadel, 2009). STEM integration is one of the leading approaches for achieving this aim (Bybee, 2010). Project-based learning supports motivation and deep learning by engaging students in research, design and presentation around a real problem (Blumenfeld et al., 1991). The flipped classroom approach allows conceptual content to be delivered digitally outside the lesson, leaving class time for practice and discussion (Bergmann and Sams, 2012).

In terms of motivation, gamification is defined as “the use of game design elements in non-game contexts” (Deterding et al., 2011). Hamari et al. (2014) showed that the effects of gamification vary with context and user, and the meta-analysis by Sailer and Homner (2020) reported small to medium positive effects of gamification on cognitive, motivational and behavioural learning outcomes. These results indicate that gamification should not be a stand-alone solution but part of a well-designed pedagogical model. Self-determination theory, in turn, identifies the satisfaction of the needs for competence, autonomy and relatedness as the basic condition of intrinsic motivation (Ryan and Deci, 2000).

Most existing learning management systems are general-purpose and do not adequately meet physics-specific requirements such as measurement tables, error calculations, virtual experiments and conceptual problems. It is considered that solutions which combine course content, a virtual laboratory, a project process, gamification, soft skills assessment and teacher analytics in a single environment, with a Kazakh-language interface and in line with the Grade 10 physics curriculum, are limited in the literature. This study presents the “Physics•LMS” platform, developed to address this gap.

The aim of the study is to present the design principles, architecture and pedagogical model of the virtual learning management system developed for Grade 10 physics. In line with this aim, the following questions were addressed: (1) Which pedagogical principles underlie the design of the platform? (2) Which components does the platform consist of, and how are they integrated within an architecture? (3) How are gamification, soft skills development, the virtual laboratory and STEM projects operationalised within the platform? (4) What data does the platform generate for evaluating the learning process?

METHOD

Research Design

The study is based on the design-based research approach, in which educational technologies are designed and developed iteratively in real learning environments (Brown, 1992; Design-Based Research Collective, 2003). This article reports the design and development phase of that cycle. The student interface, lesson and laboratory pages, project flow, social modules and teacher dashboard of the platform were examined through descriptive document and product analysis, and the components were classified according to their functions and the pedagogical principles on which they rely. No empirical data on learning outcomes were collected at this stage; an effectiveness study is planned as a later phase.

Design Principles

Five core principles were adopted in designing the platform. **(P1) Management of cognitive load:** Topics are divided into short, sequential steps so that the student's working memory is not overloaded (Sweller, 1988). **(P2) Mastery learning:** A level is unlocked only when sufficient achievement has been reached at the previous level (Bloom, 1968). **(P3) Support for motivation:** Gamification elements are matched with the needs for competence, autonomy and relatedness in self-determination theory (Ryan and Deci, 2000). **(P4) Active and collaborative learning:** Virtual experiments, projects and group tasks aim to let students construct knowledge and learn together with their peers (Vygotsky, 1978; Johnson and Johnson, 2009). **(P5) Data-driven formative assessment:** The data generated throughout the learning process are presented so as to provide feedback to the teacher and the student (Black and Wiliam, 1998).

Technical Infrastructure

Physics•LMS is a web-based platform accessed through a browser and hosted on cloud infrastructure. The interface is in Kazakh. User sessions are managed through a registration and login page, and separate views are provided for student and teacher roles. The landing page gives access to the course content, the virtual laboratory and progress indicators, while the dashboard gives access to the student and teacher views.

Planned Evaluation Design

A pre-test–post-test quasi-experimental design with a control group is envisaged to test the effectiveness of the platform. Students in the experimental group will work with the platform, and those in the control group with the traditional method. A physics achievement test, a soft skills scale, a motivation scale and the System Usability Scale (Brooke, 1996) for platform

usability are planned as data collection instruments. The teacher dashboard is designed to monitor indicators such as weekly activity and skill gains separately for the experimental and control groups.

RESEARCH AND FINDINGS

General Architecture of the Platform

The platform consists of a three-layer structure accessed through the student interface and a teacher dashboard fed by that structure (Figure 1). The learning content layer contains the eight modules, 49 lessons and the test and problem banks. The interaction and project layer covers the virtual laboratory, the STEM projects and the group mission. The motivation and skills layer contains the gamification elements and the soft skills development structure. The data generated in all layers are brought together in the teacher dashboard. The functions of the components and the pedagogical principles on which they rely are summarised in Table 1.

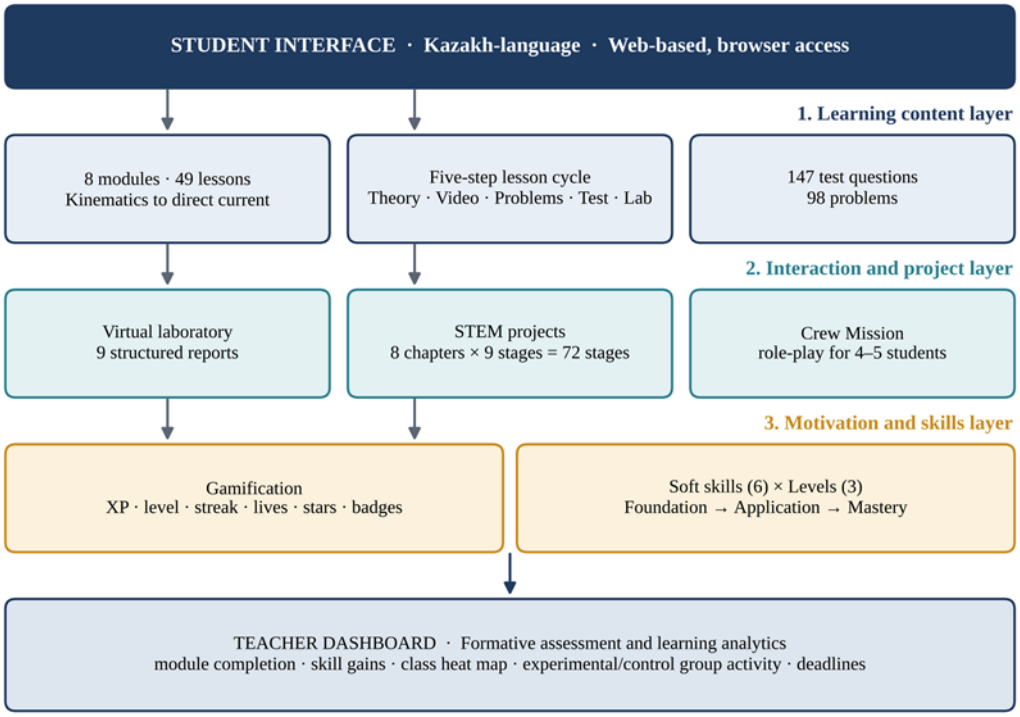


Figure 1. Layered architecture of the Physics•LMS platform

Table 1. Platform components, their functions and pedagogical foundations

Component	Function	Pedagogical foundation
Five-step lesson cycle	Sequential presentation of theory, video, problems, test and virtual laboratory steps	Flipped classroom; cognitive load
Gamification layer	Making progress visible through XP, levels, streaks, lives, stars and badges	Self-determination theory; gamification
Soft skills system	Three-level development and grading for six skills	Mastery learning; 21st-century skills
Virtual laboratory	Structured report; automatic calculation	Simulation-supported laboratory

	of mean, absolute and relative error	
STEM projects	Staged project process from problem definition to defence	Project-based learning; STEM
Crew Mission	Collaborative task in the form of a role-play for four to five students	Collaborative learning; social interdependence
Social module	Friend requests, adding via personal code/QR, permission to be searched by name	Need for relatedness; privacy
Teacher dashboard	Module completion, skill gains, heat map and activity indicators	Formative assessment

Content Structure and the Five-Step Learning Cycle

The course consists of eight modules: kinematics, dynamics, statics and hydrostatics, conservation laws, fundamentals of molecular kinetic theory, thermodynamics, electrostatics and direct current. In the platform interface, the last two modules (electrostatics and direct current) are marked as being at the planning stage. The quantitative structure of the course is given in Table 2.

Table 2. Quantitative structure of the Physics•LMS content

Item	**Number**
Modules	8
Lessons	49
Test questions	147
Problems	98
Structured laboratory reports	9
Virtual experiment activities	24
STEM project stages (8 chapters × 9 stages)	72
Soft skills	6
Achievement badges	8

Every topic is taught with the same structure (Figure 2). The student first learns the concept and the law in the theory step, then reinforces it with a short video summary, applies it by solving problems, receives instant feedback through a test, and makes the topic concrete by taking measurements in the virtual laboratory. The completion status of each step is tracked on the student dashboard by means of counters. A consistent and predictable flow prevents students from losing their orientation within the lesson and reduces cognitive load (Sweller, 1988). The possibility of using the theory and video steps before the lesson and the problem and laboratory steps in class makes it easy to adapt the cycle to the flipped classroom model (Bergmann and Sams, 2012).

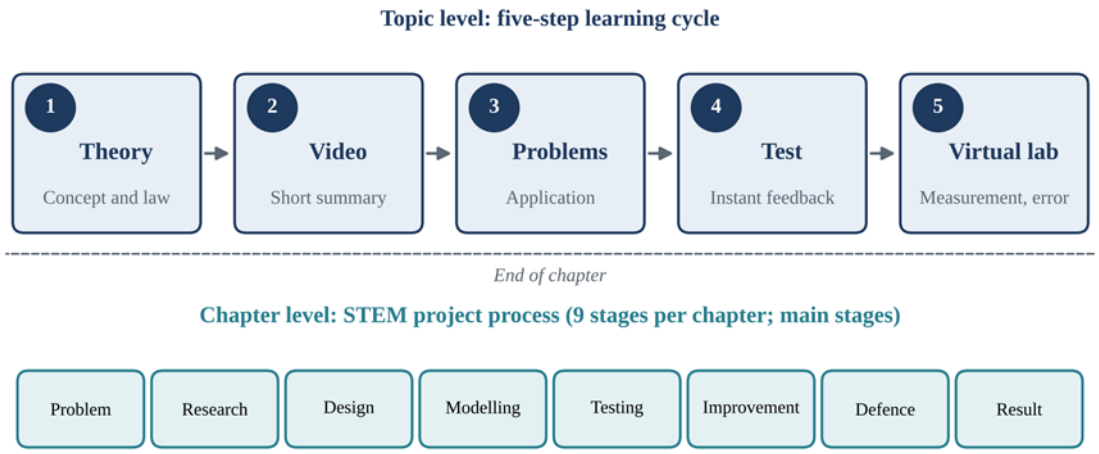


Figure 2. Five-step learning cycle at topic level and the STEM project process at the end of each chapter

Gamification Layer

The top bar of the student dashboard shows the streak (number of consecutive days of study), stars, XP and lives. A daily XP goal (100 XP) is set for the student, and total XP progress is linked to the level system. The dashboard also shows how many of the eight achievement badges have been earned. The greeting "Are you ready for today's journey?" and the presentation of progress as a space journey (Earth–Preparation–Launch–Ascent–Orbit–Deep space) turn the course into an adventure narrative. The match between the gamification elements and the needs in self-determination theory is shown in Table 3.

Table 3. Matching of gamification elements with the needs in self-determination theory

Need	**Counterpart in the platform**	**Expected effect**
Competence	XP, levels, badges, level transitions, instant test feedback	Strengthened sense of achievement
Autonomy	Monitoring one's own progress and daily goal; managing privacy choices such as permission to be searched by name	Taking responsibility for learning
Relatedness	Adding friends, Crew Mission, group project submission	Belonging and collaboration

One point to watch in gamification work is that extrinsic rewards may replace intrinsic motivation (Ryan and Deci, 2000). For this reason, the aim is to link points and badges to learning goals and to use the "lives" indicator not punitively but to encourage repetition and recovery. Since the effect of gamification varies with context (Hamari et al., 2014), the effect of these elements will be examined separately in the planned quasi-experimental study.

Soft Skills and the Levelled Development Structure

The platform monitors six soft skills: critical thinking, communication, collaboration, creativity, self-regulation and digital literacy. Each skill progresses through three levels: Foundation, Application and Mastery. A level is unlocked when achievement at the previous level reaches at least 60%. This mechanism operationalises the basic assumption of mastery learning, namely that adequate command is secured before moving on to subsequent learning (Bloom, 1968). The achievement percentage is converted into a grade out of five according to the criterion shown in Table 4.

Table 4. Soft skills achievement level and corresponding grade

Achievement level (%)	Grade
≥ 85	5
≥ 65 and < 85	4
≥ 40 and < 65	3
< 40	2

Within the self-regulation skill, it is envisaged that students can monitor their own progress, set goals and evaluate their results (Zimmerman, 2002). The daily goal, XP progress and skill percentage indicators on the dashboard make this process visible.

Virtual Laboratory and Structured Report

The virtual laboratory module enables the student to carry out the experiment in an online environment and to record the results in a standard report format. Each report consists of the following sections: aim, theory, equipment, set-up and procedure, measurement table, error calculation, conclusion and control questions. From the values entered in the measurement table, the arithmetic mean, absolute error and relative error are calculated automatically by the system. In this way the student's attention is shifted from the mechanics of calculation to the interpretation of measurement uncertainty. Since simulation-supported laboratory work has been reported to support conceptual learning as well as, and in some contexts better than, work with real equipment (Finkelstein et al., 2005), this module is expected to serve as an equalising tool, especially in schools with limited laboratory facilities.

STEM Project Process

At the end of each chapter the student carries out a STEM project. A total of 72 stages are defined for the eight chapters. The process begins with defining the problem and proceeds through research, design, modelling, testing and improvement, and is completed with the defence and result stages (Figure 2). This structure links the engineering design cycle to physics concepts and enables students to use the laws they have learned to solve a realistic problem. Project-based learning is expected to feature sustained inquiry, a real-life problem, the creation of a product and collaboration (Blumenfeld et al., 1991); the staged structure of the platform aims to provide these features.

Crew Mission and the Social Module

The "Crew Mission" is a role-play with three stations, completed together by four to five students. The game can be played on a single device or on the students' separate phones, and students join the mission through a code or a QR code. The sample mission on the platform, "Faster than Light: Space Mission", combines the topics of kinematics, dynamics and thermodynamics in a single story. Because each station of the mission is devoted to a different topic, crew members need to depend on one another and to explain things to each other. This structure is consistent with the principle of cooperative learning based on positive interdependence (Johnson and Johnson, 2009). In the social module, students can send and receive friend requests, share a personal code and manage the permission to be searched by name themselves. This feature places privacy control in the hands of the student, which matters for young users.

Teacher Dashboard and Learning Analytics

The teacher dashboard consists of the sections "Overview", "Analytics", "Students" and "Tasks". The dashboard shows the completion rate by module, before–after gains for the six soft skills, a class heat map at the intersection of students and modules, the weekly activity of the experimental and control groups, upcoming deadlines and recent activity. By showing at a glance which student is struggling in which module, the heat map allows the teacher to intervene in good time; this function coincides with the core purpose of formative assessment (Black and Wiliam, 1998). The dashboard's support for experimental–control group comparison provides the data infrastructure for the planned quasi-experimental study. In this article, the values shown in the current version of the teacher dashboard are sample (demo) data for demonstration purposes and therefore must not be interpreted as a finding of any learning effect.

Discussion and Limitations

The design of the platform brings together, in a single online environment, approaches that have each been found effective in the literature (interactive teaching, simulation, project-based learning, gamification and formative assessment). This integrated structure makes it possible to monitor the student's cognitive (subject knowledge), affective (motivation) and social (collaboration) development within the same data flow. Presenting soft skills in a levelled and measurable form is a difference from traditional physics lessons, in which these skills often remain implicit.

An important limitation of the study is that empirical data on the effect of the platform are not yet available. The findings presented therefore concern the design and functionality of the platform; the effect on learning achievement or motivation was not tested in this study. Second, the last two modules of the course are at the planning stage and the completion of the content is ongoing. Third, whether gamification elements sustain in the long term the interest they arouse in the short term should be examined separately (Hamari et al., 2014). Finally, the fact that the platform is offered only with a Kazakh-language interface requires adaptation for transfer to other languages and contexts.

CONCLUSION

This study presented the design principles, architecture and pedagogical model of the Physics•LMS virtual learning management system developed for Grade 10 physics. The platform combines a five-step lesson cycle, a virtual laboratory, a STEM project process, a collaborative Crew Mission, a gamification layer and a levelled development structure for six soft skills with teacher analytics. With eight modules, 49 lessons, 147 test questions, 98 problems, nine laboratory reports and 72 project stages, the content has reached a scale that covers the physics curriculum.

The main contribution of the platform is that it integrates cognitive, affective and social dimensions in a single environment and generates measurable learning data. In the next phase, it is planned to complete the last two modules, to carry out a usability evaluation with teacher and student views, and to test the effect of the platform on physics achievement, motivation and soft skills through a pre-test–post-test quasi-experimental study with a control group. In addition, the architecture of the platform offers an adaptable basis for other science subjects and other grade levels.

Funding

This research was funded by the Science Committee of the Ministry of Science and Higher Education of the Republic of Kazakhstan (Grant No. BR28713097).

REFERENCES

Bergmann, J. and Sams, A. 2012. Flip Your Classroom: Reach Every Student in Every Class Every Day. International Society for Technology in Education, Washington, DC.

Black, P. and Wiliam, D. 1998. Assessment and Classroom Learning. Assessment in Education: Principles, Policy & Practice, 5(1): 7–74.

Bloom, B. S. 1968. Learning for Mastery. Evaluation Comment, 1(2): 1–12.

Blumenfeld, P. C., Soloway, E., Marx, R. W., Krajcik, J. S., Guzdial, M. and Palincsar, A. 1991. Motivating Project-Based Learning: Sustaining the Doing, Supporting the Learning. Educational Psychologist, 26(3–4): 369–398.

Brooke, J. 1996. SUS: A “Quick and Dirty” Usability Scale. In: Jordan, P. W., Thomas, B., Weerdmeester, B. A. and McClelland, I. L. (Eds.), Usability Evaluation in Industry. Taylor & Francis, London, 189–194.

Brown, A. L. 1992. Design Experiments: Theoretical and Methodological Challenges in Creating Complex Interventions in Classroom Settings. Journal of the Learning Sciences, 2(2): 141–178.

Bybee, R. W. 2010. Advancing STEM Education: A 2020 Vision. Technology and Engineering Teacher, 70(1): 30–35.

Design-Based Research Collective. 2003. Design-Based Research: An Emerging Paradigm for Educational Inquiry. Educational Researcher, 32(1): 5–8.

Deterding, S., Dixon, D., Khaled, R. and Nacke, L. 2011. From Game Design Elements to Gamefulness: Defining "Gamification". Proceedings of the 15th International Academic MindTrek Conference, 9–15.

Finkelstein, N. D., Adams, W. K., Keller, C. J., Kohl, P. B., Perkins, K. K., Podolefsky, N. S., Reid, S. and LeMaster, R. 2005. When Learning about the Real World is Better Done Virtually: A Study of Substituting Computer Simulations for Laboratory Equipment. Physical Review Special Topics – Physics Education Research, 1(1): 010103.

Hake, R. R. 1998. Interactive-Engagement versus Traditional Methods: A Six-Thousand-Student Survey of Mechanics Test Data for Introductory Physics Courses. American Journal of Physics, 66(1): 64–74.

Hamari, J., Koivisto, J. and Sarsa, H. 2014. Does Gamification Work? A Literature Review of Empirical Studies on Gamification. Proceedings of the 47th Hawaii International Conference on System Sciences, 3025–3034.

Johnson, D. W. and Johnson, R. T. 2009. An Educational Psychology Success Story: Social Interdependence Theory and Cooperative Learning. Educational Researcher, 38(5): 365–379.

Ryan, R. M. and Deci, E. L. 2000. Self-Determination Theory and the Facilitation of Intrinsic Motivation, Social Development, and Well-Being. American Psychologist, 55(1): 68–78.

Sailer, M. and Homner, L. 2020. The Gamification of Learning: A Meta-Analysis. Educational Psychology Review, 32(1): 77–112.

Sweller, J. 1988. Cognitive Load During Problem Solving: Effects on Learning. Cognitive Science, 12(2): 257–285.

Trilling, B. and Fadel, C. 2009. 21st Century Skills: Learning for Life in Our Times. Jossey-Bass, San Francisco.

Vygotsky, L. S. 1978. Mind in Society: The Development of Higher Psychological Processes. Harvard University Press, Cambridge, MA.

Wieman, C. and Perkins, K. 2005. Transforming Physics Education. Physics Today, 58(11): 36–41.

Zimmerman, B. J. 2002. Becoming a Self-Regulated Learner: An Overview. Theory Into Practice, 41(2): 64–70.

STEM-BASED METHODOLOGICAL RECOMMENDATIONS FOR TEACHERS: DEVELOPING SOFT SKILLS IN NATURAL SCIENCE SUBJECTS

ÖĞRETMENLER İÇİN STEM TEMELLİ YÖNTEMSEL ÖNERİLER: FEN BİLİMLERİ DERSLERİNDE SOSYAL BECERİLERİN GELİŞTİRİLMESİ

Yelmurat DOSYMOV
Senior Lecturer, Khoja Akhmet Yassawi International Kazakh-Turkish University, Turkistan, Kazakhstan
ORCID NO: 0000-0003-4258-8669

Serik POLATULY
Senior Lecturer, Khoja Akhmet Yassawi International Kazakh-Turkish University, Turkistan, Kazakhstan
ORCID NO: 0000-0002-0553-4015

Sherzod RAMANKULOV
Assist. Prof., Khoja Akhmet Yassawi International Kazakh-Turkish University, Turkistan, Kazakhstan
ORCID NO: 0000-0002-0553-4015

Shakhrizada KHIKMATULLA
Master's student, Khoja Akhmet Yassawi International Kazakh-Turkish University, Turkistan, Kazakhstan
ORCID NO: 0009-0007-1481-694X

Munisa RAKHMATULLAEVA
Master's student, Khoja Akhmet Yassawi International Kazakh-Turkish University, Turkistan, Kazakhstan
ORCID NO: 0009-0009-3501-3139

ABSTRACT

Alongside subject knowledge, natural science education is expected to develop students' soft skills such as critical thinking, creativity, communication, collaboration, problem solving and digital literacy. STEM-based approaches are widely regarded as a means to this end, yet teachers often lack concrete methodological guidance for translating them into everyday lessons. The aim of this study is to develop and present STEM-based methodological recommendations for teachers that support soft skills development in natural science subjects. Theoretical analysis, comparison, systematisation, generalisation, modelling and pedagogical design methods were used. As a result, a methodological system consisting of four blocks (goal, content, organisational-activity and outcome) and a seven-stage STEM lesson cycle (problem identification, information research, solution proposal, modelling, product development, presentation and reflection) were developed and linked to soft skills, teacher actions and evidence of learning. The system is elaborated through four subject tasks: "An Energy-Saving Smart House" in physics, "Designing an Efficient Recreation Area for the School Yard" in mathematics, and two illustrative tasks designed by the authors for chemistry and biology. The study further offers eight practical recommendations for teachers, a three-level rubric for six soft skills, and strategies for overcoming common implementation barriers

such as limited time, curriculum constraints and scarce resources. The results suggest that the system can be adapted to different natural science subjects without altering their content, while keeping the same methodological logic.
Keywords: STEM education; soft skills; methodological recommendations; natural science education; teacher professional development; project-based learning; problem-based learning.

ÖZET

Fen bilimleri eğitiminde alan bilgisinin yanı sıra öğrencilerin eleştirel düşünme, yaratıcılık, iletişim, iş birliği, problem çözme ve dijital okuryazarlık gibi sosyal becerilerinin (soft skills) geliştirilmesi beklenmektedir. STEM temelli yaklaşımlar bu amaca ulaşmada yaygın biçimde önerilmekle birlikte, öğretmenler bu yaklaşımları günlük derslere uyarlamak için çoğu zaman somut yöntemsel rehberliğe ihtiyaç duymaktadır. Bu çalışmanın amacı, fen bilimleri derslerinde sosyal becerilerin geliştirilmesini destekleyen, öğretmenlere yönelik STEM temelli yöntemsel öneriler geliştirmek ve sunmaktır. Çalışmada kuramsal analiz, karşılaştırma, sistemleştirme, genelleme, modelleme ve pedagojik tasarım yöntemleri kullanılmıştır. Sonuç olarak; amaç, içerik, örgütsel-etkinlik ve sonuç bloklarından oluşan bir yöntemsel sistem ile problemin belirlenmesi, bilgi araştırması, çözüm önerisi, modelleme, ürün geliştirme, sunum ve yansıtma aşamalarından oluşan yedi aşamalı bir STEM ders döngüsü geliştirilmiş; bunlar sosyal becerilerle, öğretmen eylemleriyle ve öğrenme kanıtlarıyla ilişkilendirilmiştir. Sistem; fizikte "Enerji Tasarruflu Akıllı Ev", matematikte "Okul Bahçesi İçin Verimli Bir Dinlenme Alanı Tasarlama" ve yazarlarca kimya ile biyoloji için tasarlanmış iki örnek görevle somutlaştırılmıştır. Ayrıca öğretmenler için sekiz uygulama önerisi, altı sosyal beceri için üç düzeyli bir dereceli puanlama anahtarı ve zaman, program ve kaynak sınırlılığı gibi yaygın engellerin aşılmasına yönelik stratejiler sunulmuştur. Sonuçlar, sistemin ders içeriğini değiştirmeden, aynı yöntemsel mantığı koruyarak farklı fen bilimleri derslerine uyarlanabileceğini düşündürmektedir.
Anahtar kelimeler: STEM eğitimi; sosyal beceriler; yöntemsel öneriler; fen bilimleri eğitimi; öğretmen mesleki gelişimi; proje tabanlı öğrenme; probleme dayalı öğrenme.

INTRODUCTION

Teaching subject knowledge is no longer the only task of the education system. Preparing students to act in a changing environment requires the development of soft skills such as critical thinking, creativity, communication, collaboration, problem solving, decision making and independent learning (Trilling and Fadel, 2009). These skills are related not only to students' academic achievement but also to their future professional and social adaptation. In this respect, STEM education is regarded as a pedagogical approach that links subject content with practical tasks and thereby develops students' cognitive activity and soft skills together. A synthesis of meta-analytic and empirical evidence indicates that STEM-based approaches have the potential to develop teamwork, problem solving, creativity and communication skills (Rizakhojayeva et al., 2025).

What distinguishes STEM education is that science, technology, engineering and mathematics are organised not as a set of separate subjects but as interrelated fields of knowledge directed at solving a real problem. In integrated STEM lessons the student moves from being a recipient of ready-made information to being a researcher, designer and problem solver. Roehrig et al. (2021) offer a detailed conceptual framework of integrated STEM that makes explicit what integration involves, including real-world context, disciplinary content and disciplinary practices. These principles require the teacher to reorganise not only the content of the learning material but also the system of activities in the lesson.

The teacher's methodological readiness plays a decisive role in the effective introduction of STEM approaches. A systematic review of teachers' perceptions of STEM integration shows that teachers evaluate positively the potential of STEM for developing students' interest, engagement, collaboration and problem-solving ability, but that limited time, the structure of the curriculum, material resources and a lack of methodological experience in integrating subjects are named as barriers (Margot and Kettler, 2019). Research on the needs of teachers indicates that they require methodological support in planning interdisciplinary lessons, formulating open-ended problems, organising project work and connecting the content of different subjects around a single task (Shernoff et al., 2017). Practical results also show that professional development programmes that integrate science and engineering practices help teachers to change the structure of their lessons and to introduce inquiry and engineering activity into the learning process (Brand, 2020). Analyses of how science teachers implement integrated STEM units further show that the level of integration depends on how the teacher understands the links between subjects and how the learning task is organised (Dare et al., 2018). Therefore, it is not enough to give teachers a theoretical understanding of STEM; they need tasks adapted to subject content, lesson models, assessment tools and concrete ways of developing soft skills.

The effectiveness of the STEM approach depends on its realisation through specific content and practical activity. For example, the introduction of an interdisciplinary bio-sensor STEM module into the training of teachers demonstrated that scientific, engineering and technological knowledge can be combined within a single learning task (Hsu et al., 2020). Work on the development of primary school students' interest in STEM in supplementary education shows the importance of practical, research and creative tasks (Ibraeva and Shaushekova, 2023), and the theoretical justification of a STEM education base in the training of future biology teachers is considered an important condition for teachers' understanding of interdisciplinary links and their ability to design practice-oriented tasks (Bakirova et al., 2025). This points to the need for the systematic use of the STEM methodology at all stages of teacher education.

Problem-based and project-based learning provide the main pedagogical mechanisms through which STEM tasks develop soft skills. Reviews of curriculum models for interdisciplinary STEM education emphasise the need to combine problem-based, project-based, inquiry and engineering models with the learning content (Joseph and Uzondu, 2024), and project-

oriented problem-based learning has been reported to create an effective environment for developing 21st-century skills (AlAli, 2024). Such an approach requires students to understand the problem, search for information, analyse alternatives, propose and justify a solution and defend it in front of a group (Blumenfeld et al., 1991; Hmelo-Silver, 2004). Each of these actions contributes to the development of a particular soft skill.

Accordingly, developing STEM-based methodological recommendations for teachers of natural science subjects is a timely task. The main idea of the recommendations is to regard STEM not as a separate technology or a form of teaching intended only for certain subjects, but as an interdisciplinary methodological system that enables soft skills to be developed. In this system, the specific content of each subject is preserved, and elements of a problem situation, a research task, project activity, a digital or material product and reflection are added to each lesson. The aim of the study is to develop STEM-based methodological recommendations for teachers aimed at developing students' soft skills in natural science subjects and to demonstrate them through specific tasks in physics, mathematics, chemistry and biology. In line with this aim, the study (1) systematises the theoretical and methodological foundations of STEM-based teaching, (2) identifies the STEM components that contribute to soft skills development, (3) proposes a task model adapted to natural science subjects, (4) develops practical examples for four subjects and (5) defines ways of assessing the soft skills.

The practical significance of the proposed methodological direction is that it enables the teacher to introduce STEM elements into the lesson without radically changing the subject content. As a result, subject learning goals and the goals of soft skills development are achieved in coherence within a single lesson.

METHOD

Research Design

The study is a theoretical and design-oriented study. Methods of theoretical analysis, comparison, systematisation, generalisation, content analysis, modelling and pedagogical design were used. It was carried out in five steps. First, the theoretical and methodological foundations of STEM education, the principles of interdisciplinary integration and the approaches to developing soft skills were analysed. Second, the relationships between the components of STEM teaching (problem situation, research, design, engineering activity, modelling, digital technologies and product creation) were systematised. Third, on the basis of the pedagogical modelling method, the structure of a STEM-based methodological system for developing soft skills was developed, in which goal, content, organisational-activity and outcome blocks were defined, and the motivational, content and activity components, the teaching methods, tools and forms and the stages of soft skills development were specified.

Fourth, to determine whether the system can be adapted to subject content, pedagogical design and task construction were used. STEM tasks were developed for physics and mathematics, and, following the same logic, for chemistry and biology; in each task the manifestation of the Science, Technology, Engineering and Mathematics components in line

with the characteristics of the subject was identified. Finally, a comparative analysis of the tasks was used to determine the main learning activities, the resulting products and the dominant soft skills, and an assessment rubric and a set of strategies for implementation barriers were designed. The physics and mathematics tasks are based on the authors' earlier subject-adapted STEM tasks, whereas the chemistry and biology tasks were designed for this article as illustrations of the same methodology. No participants took part and no empirical data were collected in this study.

Source Base

The analysis relied on eleven core sources on STEM integration, teachers' perceptions and professional development needs, interdisciplinary curriculum models and soft skills development (Rizakhojayeva et al., 2025; Roehrig et al., 2021; Margot and Kettler, 2019; Shernoff et al., 2017; Brand, 2020; Dare et al., 2018; Hsu et al., 2020; Ibraeva and Shaushekova, 2023; Bakirova et al., 2025; Joseph and Uzondu, 2024; AlAli, 2024), supplemented by foundational works on project-based and problem-based learning, formative assessment and curriculum design.

RESEARCH AND FINDINGS

The STEM-Based Methodological System

As a result of the study, a STEM-based methodological system aimed at developing students' soft skills in natural science subjects was developed (Figure 1). The system aims to link subject content with real-life situations, to organise research and design activity, to use digital tools and to develop critical thinking, creativity, communication, collaboration and problem-solving skills.

The structure of the system consists of goal, content, organisational-activity and outcome blocks. The goal block defines the aim of developing soft skills through STEM approaches in natural science subjects. In the content block the motivational, content and activity-based components of the system are considered in interrelation, and for each of them indicators of soft skills development are defined: interest in STEM tasks and readiness for teamwork (motivational); application of subject knowledge, problem analysis and understanding of interdisciplinary links (content); and skills of research, design, modelling, calculation, the use of digital tools, presentation and reflection (activity-based).

The organisational-activity block describes the pedagogical conditions (organising problem-based and project-based learning, linking subject content with real-life situations, and systematically introducing research tasks, group work, digital resources, modelling and reflection) together with the methods (problem-based learning, STEM project, STEM case, research method, engineering design), tools (teaching materials, digital platforms, interactive resources, laboratory and visual aids) and forms (traditional and practical lessons, laboratory work, project defence, exhibition and STEM fair) of teaching. Soft skills develop in three stages: arousing interest, identifying the problem and setting the goal; research, design, modelling and joint activity; and analysis of the result, assessment, presentation and

reflection. The outcome block is characterised by the image of a student who can apply subject knowledge in real-life situations and whose soft skills have been formed.

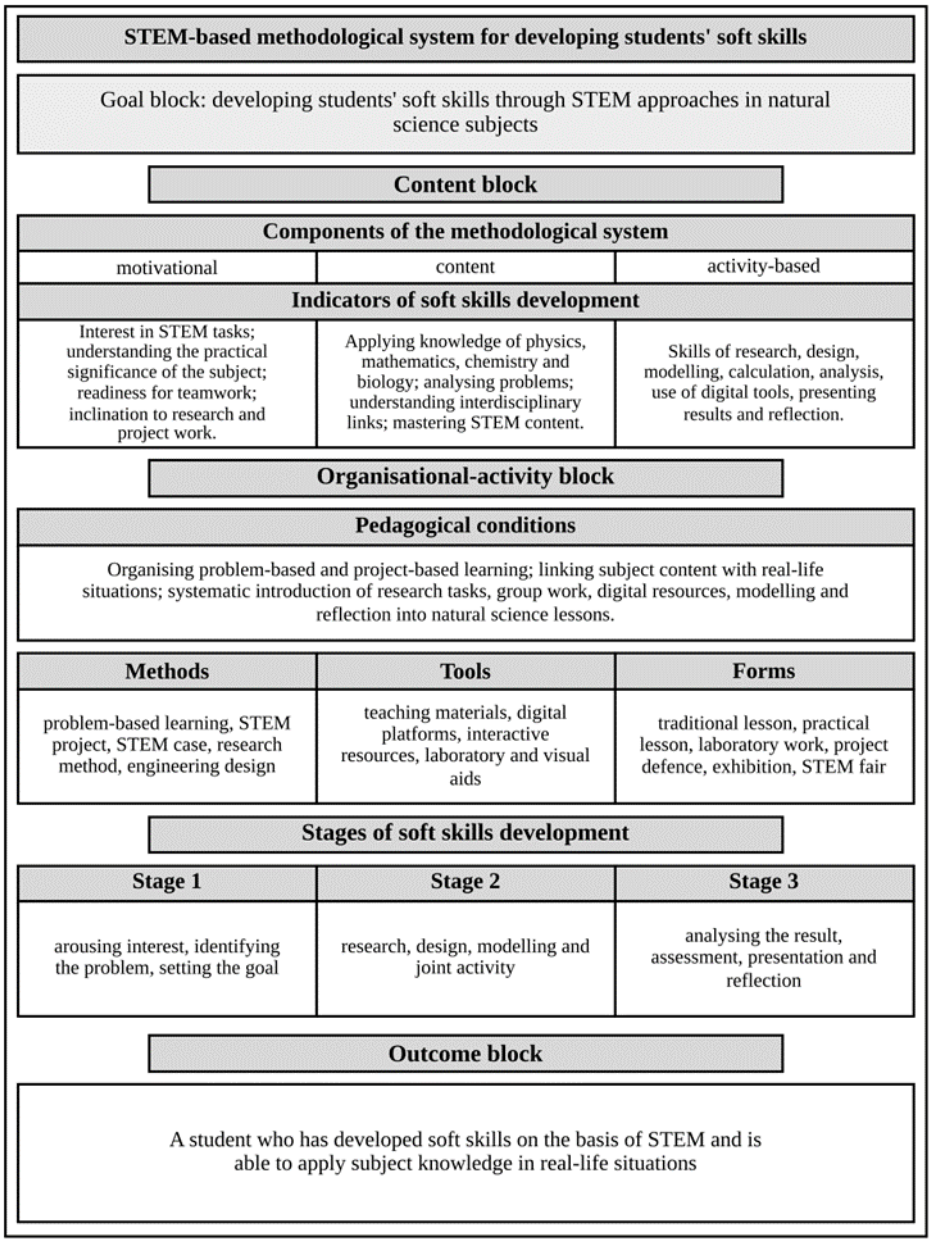


Figure 1. STEM-based methodological system for developing soft skills in natural science subjects

The Seven-Stage STEM Lesson Cycle

To make the system usable in a lesson, a common methodological logic was defined for all tasks: problem identification – information research – solution proposal – modelling – product development – presentation – reflection (Figure 2). The three stages of soft skills development in Figure 1 are detailed in this cycle: stage 1 corresponds to problem identification, stage 2 to information research, solution proposal, modelling and product development, and stage 3 to presentation and reflection. The cycle can be implemented over two to four lessons or, in a shortened form, within a single lesson. Each stage is associated with primary soft skills,

specific student and teacher actions and a form of evidence that the teacher can collect (Table 1).

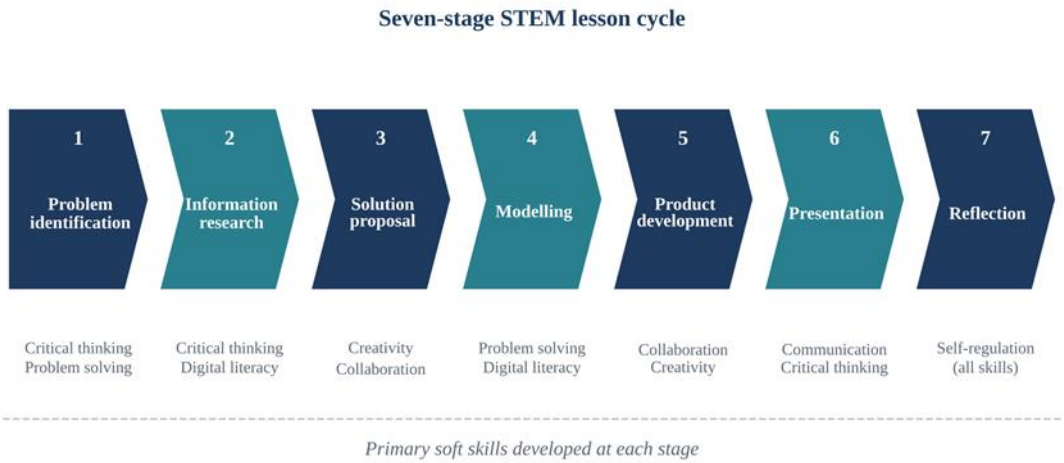


Figure 2. Seven-stage STEM lesson cycle and the primary soft skills developed at each stage

Table 1. Stages of the STEM lesson cycle, teacher actions and evidence of learning

Stage	What students do	What the teacher does	Evidence of learning
1. Problem identification	Analyse a real-life situation, formulate the problem and ask questions	Presents an open-ended problem with constraints; asks a driving question	Problem statement; list of questions
2. Information research	Search, select and compare sources and data	Provides sources; teaches source evaluation and note-taking	Source log; research notes
3. Solution proposal	Generate alternatives and choose one using criteria	Facilitates brainstorming; helps define criteria and constraints	Sketches; table of alternatives with criteria
4. Modelling	Build a physical, mathematical or digital model; calculate and test	Guides the use of tools (spreadsheets, GeoGebra, simulations, sensors)	Model; calculations; graphs
5. Product development	Create the product or prototype in a team with defined roles	Assigns and rotates roles; monitors teamwork	Prototype, plan or digital product
6. Presentation	Present and defend the solution with evidence	Organises the presentation and feedback; asks probing questions	Presentation; peer feedback sheet
7. Reflection	Evaluate the process and the result; set improvement goals	Leads reflection; links the result to the subject outcomes	Reflection notes; self-assessment

Subject Tasks

To adapt the methodological system to specific subject content, four STEM tasks were developed for physics, mathematics, chemistry and biology. All the tasks preserve the common logic of the lesson cycle, which shows that the same system can be applied in different subject contexts. The composition of the STEM components in each task is given in Table 2.

Physics. The task "An Energy-Saving Smart House" links the laws of heat transfer, thermal conduction and convection to engineering design. Students compare heat-insulating materials, build a model of a house, measure temperature changes, and construct tables and graphs, thereby applying theoretical knowledge in a practical situation. Research activity, engineering thinking, teamwork and the ability to present a result with evidence are developed predominantly (Figure 3).

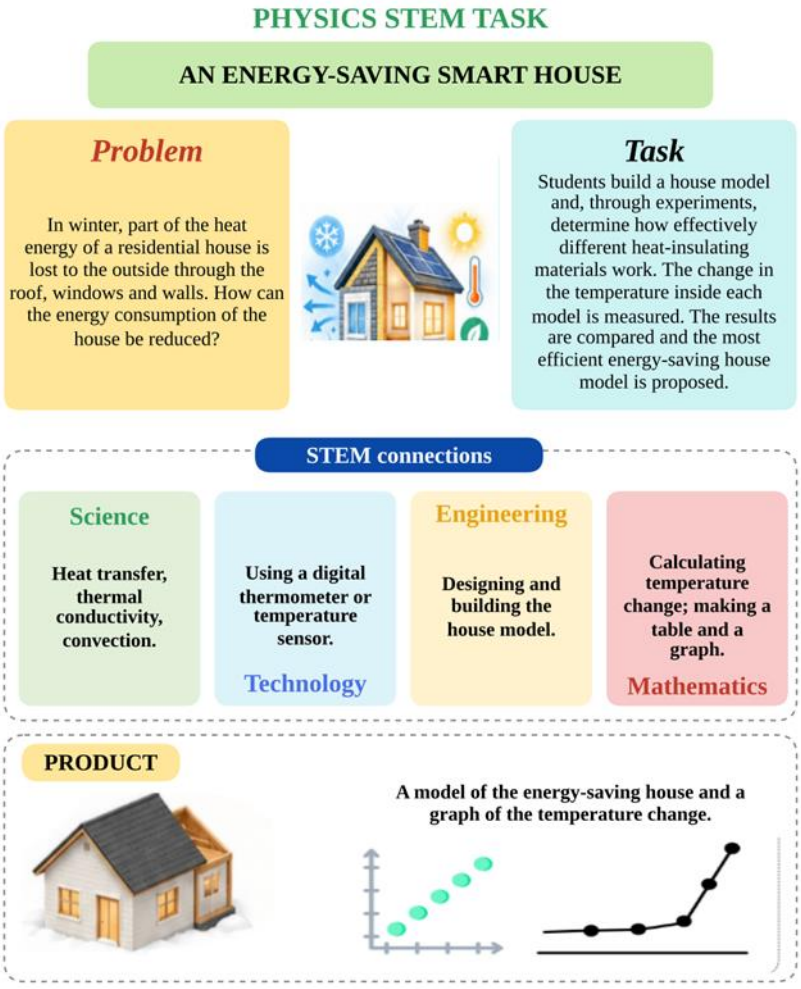


Figure 3. STEM task card for physics: "An Energy-Saving Smart House"

Mathematics. The task "Designing an Efficient Recreation Area for the School Yard" connects knowledge of scale, area, perimeter, percentages and cost calculation with the task of designing a real space. Using GeoGebra, Excel or other digital tools, students draw up a plan of the area and compare several design variants. The final product consists of a scaled

plan, a table of calculations and a 2D or 3D model. The task develops logical thinking, financial literacy, creativity and problem solving (Figure 4).

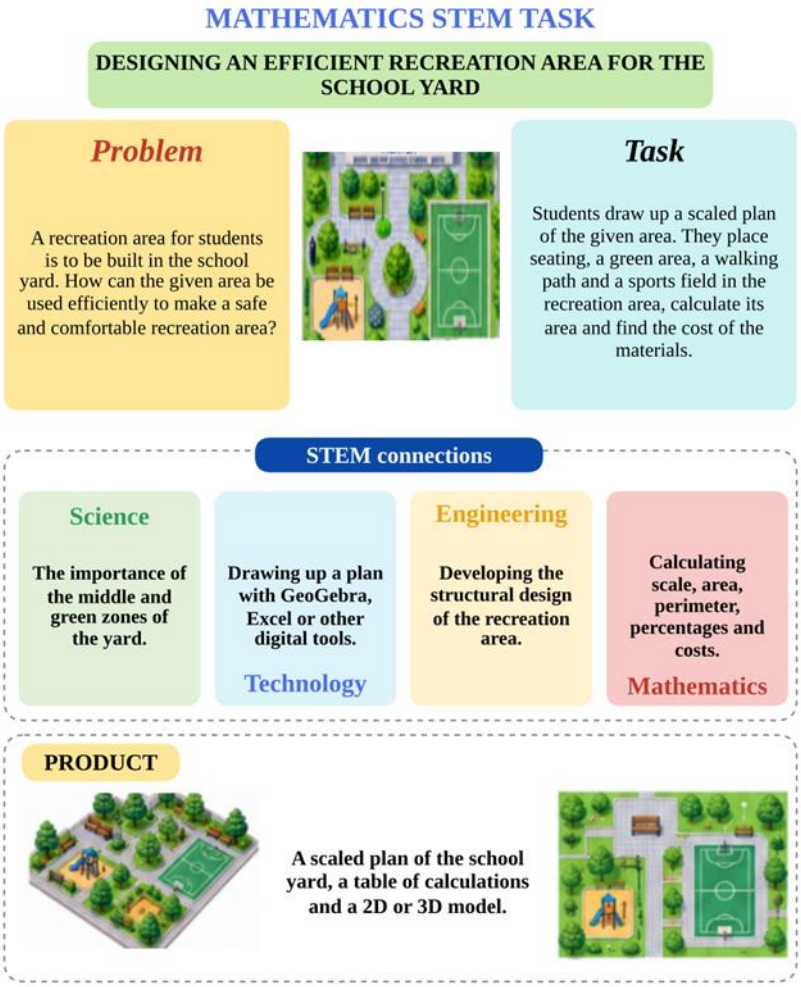


Figure 4. STEM task card for mathematics: "Designing an Efficient Recreation Area for the School Yard"

Chemistry (illustrative task). In "Choosing an Effective Water Filter for a Village Well", students investigate mixtures, filtration and the properties of water, design a filter from layers of gravel, sand and charcoal, test several variants, and calculate the percentage reduction in turbidity achieved by each. The task combines experimental work with data analysis and requires teams to justify the choice of the final design.

Biology (illustrative task). In "Designing a Classroom Greenhouse Microclimate", students study the factors that influence plant growth, build a mini-greenhouse model, monitor temperature and humidity with sensors or a data-logging application, adjust light and ventilation, and present growth data in graphs. The task develops observation, data literacy and the ability to explain results to others.

Table 2. Composition of the STEM components in the subject tasks

Task	Science	Technology	Engineering	Mathematics
Physics: An Energy-Saving Smart House	Heat transfer, conduction, convection	Thermometers or sensors; spreadsheet graphs	Designing and building a house model; selecting insulation	Tables, graphs, comparison of temperature change
Mathematics: Recreation Area for the School Yard	Real space and the needs of its users	GeoGebra, Excel	Layout design; comparing design variants	Scale, area, perimeter, percentage, cost
Chemistry: Water Filter for a Village Well	Mixtures, filtration, properties of water	Turbidity or pH meter, or a simulation	Designing and testing filter layers	Percentage reduction, charts
Biology: Classroom Greenhouse Microclimate	Plant growth factors, photosynthesis	Temperature and humidity sensors, data logger	Mini-greenhouse model; adjusting light and ventilation	Averages, growth graphs

A comparative analysis of the four tasks (Table 3) shows that the methodological system adapts flexibly to subject content. Experiment, measurement, calculation and engineering modelling prevail in the natural science tasks, whereas the common outcome of all the tasks is that the student understands the problem, analyses information, proposes a solution, acts in a team, uses digital tools and presents the result with evidence.

Table 3. Comparison of the subject tasks: activities, products and dominant soft skills

Subject	Core activity	Resulting product	Dominant soft skills
Physics	Experiment, measurement, modelling	House model, temperature graph	Critical thinking, problem solving, collaboration, communication
Mathematics	Calculation, scaling, designing	Scaled plan, calculation table, 2D/3D model	Problem solving, creativity, digital literacy
Chemistry	Testing, comparing, optimising	Filter prototype, efficiency chart	Critical thinking, collaboration, problem solving
Biology	Observing, monitoring, adjusting	Greenhouse model, growth graphs	Critical thinking, digital literacy, communication

Recommendations for Teachers

Based on the methodological system and the tasks, eight practical recommendations were formulated for teachers of natural science subjects.

R1. Start from the subject outcome. Select a learning outcome of the curriculum first and add the STEM task to it, following the logic of backward design (Wiggins and McTighe, 2005). The subject content does not need to be changed; the task is a way of applying it.

R2. Choose a real, open-ended problem. A good problem is connected to students' lives, has more than one acceptable solution and contains constraints such as cost, time or available materials, so that students have to compare and justify alternatives.

R3. Make all four STEM components visible, but in proportion to the subject. Not every task requires a physical device. In some tasks the engineering component appears as the design of a logical structure or of a layout and the choice of the most efficient option among several variants.

R4. Plan the cycle, not a single activity. Distribute the seven stages over two to four lessons; if time is limited, use a shortened version in which stages 1–2 and 3–4 are combined and the presentation and reflection take place in the same lesson.

R5. Target one or two soft skills per task. Name the target skills to students, link each of them to a stage of the cycle (Table 1) and decide in advance what evidence will show their development.

R6. Organise teams with clear roles. Assign roles such as researcher, modeller, designer and presenter, and rotate them between tasks so that each student practises different skills and collaboration does not become an uneven division of labour.

R7. Use accessible digital tools. Spreadsheets, GeoGebra, free simulations, online maps and phone sensors are sufficient for most tasks; the same task can be adapted to a low-resource classroom by replacing devices with simple materials and shared data.

R8. Assess the process and the product and include reflection. Use the rubric in Table 4 together with the evidence collected at each stage, and combine teacher assessment with self-assessment and peer feedback. Reflection helps students to monitor and regulate their own learning (Zimmerman, 2002), while the feedback it generates serves the formative purpose of assessment (Black and Wiliam, 1998).

Assessing Soft Skills

Because soft skills are difficult to measure with traditional tests, a three-level rubric was designed (Table 4). The descriptors are formulated in terms of observable student actions so that they can be applied to the evidence listed in Table 1. A clear rubric helps students to understand what is expected and supports formative feedback (Brookhart, 2013).

Table 4. Three-level rubric for assessing soft skills in STEM tasks

Soft skill	Basic	Developing	Advanced
Critical thinking	Uses the given information without checking it	Compares several sources and selects relevant data	Evaluates the reliability of sources and justifies choices with evidence
Creativity	Reproduces a given solution	Proposes at least two alternative solutions	Proposes an original solution and improves it after testing
Communication	Presents results with limited structure	Presents a clear structure supported by data or graphs	Argues persuasively, answers questions and adapts to the audience
Collaboration	Completes only the assigned part	Shares tasks and listens to team members	Coordinates the team, resolves disagreements and supports others
Problem solving	Applies a familiar procedure	Selects and applies a suitable method	Tests the model, identifies errors and revises the solution
Digital literacy	Uses a digital tool with help	Uses digital tools independently to calculate or visualise	Selects appropriate tools and produces a clear digital product

Overcoming Implementation Barriers

The literature names limited time, the structure of the curriculum, scarce material resources and insufficient methodological experience as the main barriers to STEM teaching (Margot and Kettler, 2019). Table 5 summarises strategies that respond to each barrier within the proposed system.

Table 5. Implementation barriers and corresponding strategies

Barrier	Strategy within the system	Related recommendation
Limited lesson time	Use the shortened one-lesson cycle; integrate the task into existing practical work	R4
Rigid curriculum structure	Link each task to existing learning outcomes and place it after the concept has been taught	R1
Scarce resources	Use free digital tools, simulations and simple materials	R7
Lack of methodological experience	Use ready task templates, plan jointly with colleagues and take part in professional development (Shernoff et al., 2017; Brand, 2020)	R2, R3, R5
Difficulty of assessing soft skills	Apply the rubric and keep an evidence log at each stage	R8

Discussion and Limitations

The proposed system translates the general findings of the STEM literature into steps that a teacher can plan, implement and assess. Its main advantage is that the logic remains the same across subjects while the content of the tasks changes. In the physics and chemistry tasks the experiment, the measurement and the engineering model are the central activities, whereas in the mathematics task calculation and spatial design take this role. The common cycle also gives the teacher a transparent basis for collecting evidence and giving feedback.

The study has limitations. The system and the tasks have not been tested in classrooms, and the chemistry and biology tasks are illustrative designs. The statements on the potential of the approach rely on the literature and do not constitute evidence of effectiveness in the target context. The rubric has not been validated for reliability. These limitations define the next stage of the work.

CONCLUSION

This study developed STEM-based methodological recommendations for teachers aimed at developing students' soft skills in natural science subjects. The system consists of four blocks (goal, content, organisational-activity and outcome) and a seven-stage lesson cycle that links student actions, teacher actions, evidence of learning and primary soft skills. It was elaborated through tasks in physics, mathematics, chemistry and biology, supplemented by eight recommendations for teachers, a three-level rubric for six soft skills and strategies for overcoming implementation barriers.

The comparison of the tasks showed that, while the content changes with the subject, the methodological logic is common: understanding the problem, analysing information, proposing a solution, acting in a team, using digital tools and presenting the result with evidence. The materials allow teachers to develop subject knowledge and soft skills together within a single learning activity through lessons, practical work, STEM projects, cases and interdisciplinary tasks. In the next stage, the effectiveness of the system should be tested with a pre-test–post-test pedagogical experiment in which initial and final soft skills indicators are compared by statistical methods, and the rubric should be validated.

Funding

This research was funded by the Science Committee of the Ministry of Science and Higher Education of the Republic of Kazakhstan (Grant No. BR28713097).

REFERENCES

AlAli, R. 2024. Enhancing 21st Century Skills Through Integrated STEM Education Using Project-Oriented Problem-Based Learning. GeoJournal of Tourism and Geosites, 53(2): 421–430. https://doi.org/10.30892/gtg.53205-1217

Bakirova, A. S., Amanbaeva, M. B. and Mirici, S. 2025. Theoretical Justification of Building a STEM Education Base in the Training of Future Biology Teachers. Bulletin of Toraighyrov University, Pedagogics Series, (1): 128–140. https://doi.org/10.48081/qnxh2139

Black, P. and Wiliam, D. 1998. Assessment and Classroom Learning. Assessment in Education: Principles, Policy & Practice, 5(1): 7–74.

Blumenfeld, P. C., Soloway, E., Marx, R. W., Krajcik, J. S., Guzdial, M. and Palincsar, A. 1991. Motivating Project-Based Learning: Sustaining the Doing, Supporting the Learning. Educational Psychologist, 26(3–4): 369–398.

Brand, B. R. 2020. Integrating Science and Engineering Practices: Outcomes from a Collaborative Professional Development. International Journal of STEM Education, 7(1). https://doi.org/10.1186/s40594-020-00210-x

Brookhart, S. M. 2013. How to Create and Use Rubrics for Formative Assessment and Grading. ASCD, Alexandria, VA.

Dare, E. A., Ellis, J. A. and Roehrig, G. H. 2018. Understanding Science Teachers' Implementations of Integrated STEM Curricular Units Through a Phenomenological Multiple Case Study. International Journal of STEM Education, 5(1). https://doi.org/10.1186/s40594-018-0101-z

Hmelo-Silver, C. E. 2004. Problem-Based Learning: What and How Do Students Learn? Educational Psychology Review, 16(3): 235–266.

Hsu, S., Sung, C. C. and Sheen, H. J. 2020. Developing an Interdisciplinary Bio-Sensor STEM Module for Secondary School Teachers: An Exploratory Study. Voprosy Obrazovaniya / Educational Studies Moscow, (2): 230–251. https://doi.org/10.17323/1814-9545-2020-2-230-251

Ibraeva, E. S. and Shaushekova, B. K. 2023. Development of Interest in STEM Education Among Primary School Children in the System of Supplementary Education. Perspektivy Nauki i Obrazovania, 61(1): 276–290. https://doi.org/10.32744/pse.2023.1.16

Joseph, O. B. and Uzondu, N. C. 2024. Curriculums Development for Interdisciplinary STEM Education: A Review of Models and Approaches. International Journal of Applied Research in Social Sciences, 6(8): 1575–1592. https://doi.org/10.51594/ijarss.v6i8.1371

Margot, K. C. and Kettler, T. 2019. Teachers' Perception of STEM Integration and Education: A Systematic Literature Review. International Journal of STEM Education, 6(1). https://doi.org/10.1186/s40594-018-0151-2

Rizakhojayeva, G., Ramankulov, S., Akeshova, M., Nurizinova, M., Tuyakov, Y. and Abdrakhmanov, R. 2025. STEM-Based Approaches to Soft Skills Development: A Synthesis of Meta-Analytic Findings and Empirical Evidence. Frontiers in Education, 10. https://doi.org/10.3389/feduc.2025.1663155

Roehrig, G. H., Dare, E. A., Ellis, J. A. and Ring-Whalen, E. 2021. Beyond the Basics: A Detailed Conceptual Framework of Integrated STEM. Disciplinary and Interdisciplinary Science Education Research, 3. https://doi.org/10.1186/s43031-021-00041-y

Shernoff, D. J., Sinha, S., Bressler, D. M. and Ginsburg, L. 2017. Assessing Teacher Education and Professional Development Needs for the Implementation of Integrated Approaches to STEM Education. International Journal of STEM Education, 4(1). https://doi.org/10.1186/s40594-017-0068-1

Trilling, B. and Fadel, C. 2009. 21st Century Skills: Learning for Life in Our Times. Jossey-Bass, San Francisco.

Wiggins, G. and McTighe, J. 2005. Understanding by Design, Expanded 2nd Edition. ASCD, Alexandria, VA.

Zimmerman, B. J. 2002. Becoming a Self-Regulated Learner: An Overview. Theory Into Practice, 41(2): 64–70.

AN INTEGRATED CYBERSECURITY FRAMEWORK FOR SECURING CONNECTED DIGITAL ECOSYSTEMS (DE)

Ebole Alpha Friday
Department of Computer Science, College of Basic Sciences, Lagos State University of Science and Technology, Lagos, Nigeria

Aremu Idris Abiodun
Department of Computer Science, College of Basic Sciences, Lagos State University of Science and Technology, Lagos, Nigeria

Ayinde Yusuf Olatunji 3
Information and Communication Unit, Lagos State University of Science and Technology, Lagos, Nigeria

ABSTRACT

Digital Ecosystem integrates people, data, processes, devices and application domain within interconnected ecosystems, enhancing service delivery while simultaneously increasing the cybersecurity attack surface. This study examined cyber threats in GE, evaluated established and emerging controls, and developed a layered conceptual framework for heterogeneous and resource-constrained environments. A qualitative integrative review and design-oriented method were employed, with evidence coded by threat, layer, control, benefit, limitation and deployment condition. The findings show that identity must be managed throughout the device lifecycle, while scale amplifies shared weaknesses. Prompt protection requires coordinated endpoint, edge and cloud controls, and intelligent detection depends on representative data and oversight. Trustworthy operation requires privacy, accountability and recovery. The proposed framework integrates device trust, lightweight authenticated encryption, segmented communication, edge-assisted detection and containment, cloud/application governance, continuous access evaluation and coordinated response, with selective tamper-evident auditing. Conceptual assessment shows coherent security coverage, although the framework has not been experimentally confirmed. The study concludes that digital system security requires coordinated engineering and governance, with Nigerian organisations needing phased implementation, secure procurement, data-protection compliance and sustained cybersecurity capacity development.

Keywords: Internet of Things, cybersecurity, lightweight cryptography, intrusion detection, edge computing, blockchain, Zero Trust Architecture.

CLASSIFICATION OF CLOTHING TYPES USING A CONVOLUTIONAL NEURAL NETWORK: EXPERIMENTAL EVALUATION AND ERROR ANALYSIS ON THE MYNTRA FASHION PRODUCT IMAGES DATASET

Arypzhan ABEN
Khoja Akhmet Yassawi International Kazakh-Turkish University, (Kazakhstan, Turkestan)
ORCID: 0000-0001-8534-3288

Dinmukhammed GABDULLAULY
Master's student, Department of Computer Engineering, Faculty of Engineering, Khoja Akhmet Yassawi International Kazakh-Turkish University (Turkistan, Kazakhstan)

ABSTRACT

Automatic classification of fashion product images is an important task in e-commerce, supporting catalog management, search and recommendation systems. This study experimentally evaluates the ability of a relatively small convolutional neural network (CNN) with three convolutional blocks to classify seven types of clothing. The experiments were conducted on the Myntra Fashion Product Images dataset: from metadata comprising 44,424 records, 19,376 images belonging to the Jeans, Kurtas, Shirts, Tops, Tshirts, Casual Shoes and Sports Shoes categories were selected. The images were resized to 96×96 pixels, normalized to the [0, 1] range in RGB format, and split into training and test sets at a ratio of 80:20. The model was trained with the Adam optimizer for 10 epochs with a batch size of 64. On the test set (3,876 images), the model achieved an accuracy of 90.02%, a Macro-F1 of 0.89 and a Weighted-F1 of 0.90. The highest per-class F1-score was observed for Jeans (0.98) and the lowest for Tops (0.73). Analysis of the confusion matrix showed that 35.4% of all 387 errors occurred between the two footwear categories (Casual Shoes and Sports Shoes), while 63.0% were concentrated within the group of upper-body garments. The results indicate that a small CNN reliably classifies visually distinctive categories but is limited for categories with similar appearance and overlapping semantic boundaries. The contribution of this study is limited to a systematic evaluation of a simple CNN on a well-known dataset and a class-level analysis of the error structure; no new architecture is proposed.

Keywords: convolutional neural network, clothing image classification, computer vision, deep learning, confusion matrix, Fashion Product Images.

ASSESSMENT OF THE EXPLICIT FLEXIBILITY POTENTIAL OF SLOVENIAN BUSINESS CONSUMERS

Jerneja BOGOVIČ
University of Ljubljana, Faculty of Electrical Engineering, Laboratory of Power Systems

ABSTRACT

Due to the growing share of renewable energy sources and the electrification of heating and transport, flexibility is becoming increasingly important for the reliable and stable operation of power systems. The European Union has recognised this trend and is progressively incorporating flexibility into its legislative and regulatory framework. In addition to assessing flexibility needs, the design of effective measures requires a clear understanding of the available flexibility potential. Therefore, this paper estimates the explicit flexibility potential of Slovenian business consumers based on survey results. The estimated explicit flexibility potential depends strongly on activation duration. The highest potential is available for activations of up to one hour, reaching 69.6 MW. As the activation duration increases, the potential decreases to 38.7 MW for activations between one and two hours, 20.7 MW for activations between two and four hours, and 10.1 MW for activations exceeding four hours. Depending on the scenario considered, the estimated annual volume of flexible energy ranges from 20.0 to 29.8 GWh. The average compensation required for participation, expressed as willingness to accept, ranges from 871 to 1,908 EUR/MWh. Energy-intensive industries account for the largest share of the total flexibility potential. Metal production contributes most significantly to short-duration activations, while the paper industry plays a more important role in longer activations. The identified flexibility is primarily provided through adjustments to heating and cooling systems, the use of thermal storage, temporary reductions in non-critical auxiliary processes, and battery energy storage systems. The findings indicate that, alongside technical potential, activation duration, process constraints, and compensation levels are key factors influencing the effective integration of explicit flexibility.

Keywords: Business Consumers, Explicit Flexibility Potential, Willingness to Accept.

INTRODUCTION

The growing share of variable renewable energy sources and the accelerated electrification of various demand segments are significantly changing operating conditions in the power system. To ensure a balance between electricity production and consumption and to manage network constraints effectively, the availability of flexibility sources is becoming increasingly important. In addition to generation units and energy storage systems, electricity consumers can also contribute significantly to providing flexibility. The European Electricity Market Design Framework therefore emphasises the assessment of flexibility needs and the development of non-fossil sources of flexibility, including demand response and energy storage (European Parliament & Council of the European Union, 2024).

In demand response, a distinction is usually made between implicit and explicit flexibility. Implicit flexibility is based on consumers' response to economic incentives, such as time-varying electricity prices, while explicit flexibility means the purposeful adjustment of demand following a request from the system operator or aggregator and under predefined conditions (Saviuc et al., 2022). To evaluate the usefulness of explicit flexibility, it is therefore not enough to know only the available adaptive capacity; the duration and frequency of activations, as well as the amount of compensation required, must also be taken into account.

Business consumers form a heterogeneous group that differs in electricity consumption, operating patterns and constraints on production or business processes. Different methodological approaches have been used in the literature to assess their flexibility potential. Gils (2014) estimated the theoretical demand response potential in Europe based on industrial production statistics, electricity consumption data and typical demand profiles, paying particular attention to the temporal availability and geographical distribution of flexibility potential. Wohlfarth et al. (2020) used a bottom-up approach, supplemented by survey data from service sector companies, which allowed them to distinguish between theoretical, technical and practically feasible flexibility potential. In recent years, data-driven methods for assessing the flexibility of business and industrial consumers have also become increasingly popular. Lee et al. (2020) estimated the demand response potential based on actual electricity consumption data, while Baek et al. (2025) developed a flexibility assessment model based on high-resolution historical energy usage data and classified consumers according to the similarity of their consumption patterns.

The purpose of the paper is to assess the potential for explicit flexibility of business consumers in Slovenia in terms of activation duration, to determine the corresponding annual flexible energy and to evaluate the required level of compensation for participation. Special attention is devoted to the comparison of battery storage with other flexibility measures and to the differences between individual economic sectors. The analysis is based on a survey of business consumerss conducted as part of a Slovenian flexibility assessment study (University of Ljubljana, Faculty of Electrical Engineering, 2026).

METHODOLOGY

The assessment of the potential for explicit flexibility is based on a survey of business consumers that collected data on their willingness to participate in demand response programmes. The surveyed consumers provided information on the company's main sector, annual electricity consumption, peak power and the proportion of power that they would be willing to adapt. They also indicated the expected duration and number of activations, and the requested financial compensation for participation. The analysis was carried out for four activation duration classes: up to one hour, from one to two hours, from two to four hours, and over four hours. Measures related to the adaptation of production and auxiliary processes were considered separately from battery storage.

The explicit flexibility power of an individual consumer *j* in duration class *d* was determined as the product of its peak power and the share of power that it could adjust in the scenario considered and is determinated by (1).

$$P_{EP,j,d} = P_{peak,j} \cdot r_{p,e,j,d} \quad (1)$$

where $P_{peak,j}$ is the peak power of the consumer in MW, and $r_{p,e,j,d}$ is the share of power that the consumer is willing to reduce for a particular activation duration.

Based on the estimated power and duration of the activation, the energy of each activation and the total annual flexible energy were determined by (2) and (3), respecitively.

$$E_{EP,1,j,d} = P_{EP,j,d} \cdot t_{j,d} \quad (2)$$

$$E_{EP,j,d} = P_{EP,j,d} \cdot t_{j,d} \cdot N_{j,d} \quad (3)$$

where $t_{j,d}$ denotes the duration of each activation in hours, and $N_{j,d}$ denotes the annual number of activations. When power is expressed in MW, energy is expressed in MWh.

To convert the results to the level of Slovenia, a weighting approach was used based on the electricity consumption of individual sector. For each sector *i*, an expansion factor was determined by (4)

$$w_i = \frac{E_j}{E_i} \quad (4)$$

where E_i represents the total annual electricity consumption in the sector, and E_j is the total consumption of the surveyed consumerss in the same sector.

The total power of explicit flexibility at the national level was then estimated as the sum of the weighted contributions of individual sectors using (5).

$$P_{EP,SI,d} = \sum_i \left(w_i \cdot \sum_j P_{EP,j,d} \right) \quad (5)$$

The annual flexible energy was also determined using the same procedure. This approach allows for the consideration of differences in the representation of individual sectors in the sample, based on the assumption that the surveyed consumerss are sufficiently representative of the sector they perform in terms of flexibility potential per unit of consumption.

The economic aspect of explicit flexibility was evaluated using the *WTA* (willingness to accept) indicator, which represents the required financial compensation for ensuring demand adjustment. For an individual consumer, it was calculated as the ratio between the required annual compensation and the annual flexible energy by (6).

$$WTA_{j,d} = \frac{C_{j,d}}{E_{EP,j,d}} \quad (6)$$

where $C_{j,d}$ represents the required annual compensation in EUR, and $E_{EP,j,d}$ represents the annual flexible energy in MWh.

RESULTS AND DISCUSSION

The survey questionnaire was sent to more than 200 business consumers in early 2026 and was completed by 48 companies. The total annual electricity consumption of the participating

consumers represented more than a fifth of total business consumption in Slovenia. Special attention was paid to energy-intensive activities, where the sample covered more than 30% of the consumption of individual industries. This level of representation makes it possible to capture a significant share of potential sources of flexibility, but it does not in itself ensure full statistical representativeness of all business consumers in the country.

The results show that the estimated potential for explicit demand reduction at the level of Slovenia varies significantly depending on the required duration of activation. The largest estimated power, 69.6 MW, is available for activations of up to one hour, and the available potential gradually decreases with increasing duration (Table 1). For activations of one to two hours, approximately 56% of the power in the shortest time class remains available, while for activations of more than four hours, only approximately 15% remains. This trend indicates that the number of consumers who can provide longer reductions in demand is significantly smaller, or that they are willing to offer a smaller range of adjustments for longer activations.

Table 1. Estimated potential of explicit flexibility at the level of Slovenia.

Duration of activation (h)	Power (MW)	Annual Energy (GWh)	WTA (EUR/MWh)
≤1h	69.6	20.0	1,908
1h – 2h	38.7	24.9	1,545
2h – 4h	20.7	29.8	871
>4h	10.1	28.4	890

Although the available power decreases as duration increases, the annual flexible energy for activations lasting two to four hours rises. It is 20.0 GWh for the shortest activations, reaches 29.8 GWh for activations lasting two to four hours, and then falls slightly to 28.4 GWh for activations exceeding four hours. This is due to the interaction between the available power, the duration of individual activations, and their frequency throughout the year. The estimated values represent the energy of demand adjustment and not necessarily an actual reduction in annual electricity consumption, as part of the demand can only be shifted to other periods.

The average financial compensation required also varies significantly between the scenarios. The highest values were estimated for activations lasting up to one hour, where the average WTA is 1,908 EUR/MWh. For activations of one to two hours, it is 1,545 EUR/MWh; for activations of two to four hours, it is 871 EUR/MWh; and for the longest activations, it is 890 EUR/MWh. The observed decrease in average WTA values does not necessarily mean that the same consumers would demand lower compensation for longer activations. In individual scenarios, both the composition of participating companies and their relative energy contribution change.

The analysis by type of source shows that, in all scenarios considered, most of the potential is provided by measures related to the adjustment of production and auxiliary processes, while the contribution of battery storage is smaller. For activations of up to one hour, other measures contribute 48.3 MW and battery storage 21.3 MW. As the duration of activation

increases, the contribution of batteries decreases significantly, so that for activations of two to four hours it amounts to only 1.4 MW, while other measures still provide 19.3 MW. Such a distribution is expected due to the limited energy capacity of storage tanks, but it also reflects the fact that companies often use storage tanks primarily for their own needs and are not necessarily prepared to offer their full potential on the flexibility market.

By activity, energy-intensive industries show the greatest potential. Metal production stands out in particular, providing 25.4 MW for activations of up to one hour, but its contribution decreases rapidly with increasing duration and no potential was identified in the survey for activations of more than four hours. In contrast, paper production provides 4.8 MW in all analysed time classes, which increases its importance for longer activations. For the longest duration class, annual flexible energy reaches approximately 21 GWh. When interpreting these results, it should be taken into account that part of the estimated potential relates to planned technological upgrades of production processes, and not solely to existing possibilities for ensuring flexibility. A significant contribution is also made by the production of chemicals and chemical products and by the production of non-metallic mineral products in the case of longer activations. In other activities, the estimated potential is lower. Other manufacturing companies contribute 4.9 MW in the shortest activations, while the contribution of the transport, trade and service sectors and public services is individually less than 1 MW. The structure of explicit flexibility therefore differs from the structure of implicit flexibility, where some other activities usually play a more important role. The surveyed consumers would most often adjust demand by modifying heating and cooling systems, using heat or cold storage, temporarily reducing the operation of non-critical auxiliary processes and using battery storage.

When interpreting the results, it should be borne in mind that this assessment is based on the stated willingness of companies to cooperate under the given conditions. The results therefore do not imply that services have already been established, contracts concluded or pre-qualification procedures successfully completed. The actual use of the potential will depend on verifying resource responsiveness, time availability, the measurability of adjustments and the impact of activations on production processes. In addition, the estimated explicit potential is not entirely additional to implicit flexibility, as some resources may represent the redirection of already existing flexible demand into purpose-driven programmes, while others may represent additional flexibility that would only be activated with appropriate financial compensation.

CONCLUSION

The results of the analysis show that business consumers in Slovenia represent an important source of explicit flexibility, but its actual availability strongly depends on the duration of activation and the participation conditions. The estimated potential for reducing demand gradually decreases as the activation duration is extended, which confirms that flexibility cannot be adequately described with a single power value. For a comprehensive evaluation, simultaneous consideration of the available power, the duration and frequency of activations,

and the economic expectations of consumers is essential for a realistic assessment of the usefulness of such sources.

The analysis showed that the largest share of the potential comes from energy-intensive activities, where, due to higher connection capacities and technological possibilities, larger volumes of demand adjustment are available. At the same time, the results show that measures related to the adjustment of production and auxiliary processes make a significantly greater contribution than battery storage in all the scenarios considered. This suggests that the ability to integrate and adapt existing business processes will play an important role in the further development of explicit flexibility programmes.

The findings provide a basis for planning demand response programmes that must take into account differences between activities, technological limitations of individual processes and varying requirements regarding activation duration. In further developing such mechanisms, in addition to the survey-based flexibility potential, it will be important to verify their actual availability in practice, for example through measurements and trial activations. Special attention will also need to be paid to coordination with other forms of flexibility and to preventing double counting of contributions, especially for sources that can respond to both implicit and explicit incentives.

Since the individual activation duration scenarios consider the same consumers and the same sources of flexibility, their potentials cannot be directly added together. The results therefore do not represent a single assessment of the available flexibility, but a set of scenarios that show how the technical, energy and economic potential change with respect to the required duration of service provision. This approach allows for a more realistic assessment of the contribution of business consumers to ensuring flexibility in the power system.

REFERENCES

Baek, K., Baek, J. & Ko, K. (2025). A data-driven estimation model for industrial demand flexibility potential. Journal of Electrical Engineering & Technology, 20(5), 2849-2857.

European Parliament & Council of the European Union. (2024). Regulation (EU) 2024/1747 of 13 June 2024 amending Regulations (EU) 2019/942 and (EU) 2019/943 as regards improving the Union's electricity market design. Official Journal of the European Union, L, 2024/1747.

Gils, H.C. (2014). Assessment of the theoretical demand response potential in Europe. Energy, 67, 1-18.

Lee, E., Baek, K. & Kim, J. (2020). Evaluation of demand response potential flexibility in the industry based on a data-driven approach. Energies, 13(23), 6355.

Saviuc, I., Zabala López, C., Puskás-Tompos, A., Rollert, K. & Bertoldi, P. (2022). Explicit demand response for small end-users and independent aggregators: Status, context, enablers and barriers. Publications Office of the European Union, Luxembourg, EUR 31190 EN, JRC129745.

University of Ljubljana, Faculty of Electrical Engineering. (2026). Določitev namenskega potenciala prožnosti za potrebe razbremenjevanja prenosnih poti. Technical Report, Study No. ELES 11/2025, Contract No. POG2025/000685, Ljubljana.

Wohlfarth, K., Klobasa, M. & Gutknecht, R. (2020). Demand response in the service sector – Theoretical, technical and practical potentials. Applied Energy, 258, 114089.

IMPACT OF HYDROLOGY AND THERMAL POWER PLANT AVAILABILITY ON RESOURCE ADEQUACY IN SLOVENIA

Jerneja BOGOVIČ
University of Ljubljana, Faculty of Electrical Engineering, Laboratory of Power Systems

ABSTRACT

Due to the transformation of the generation portfolio, the gradual phase-out of coal-fired electricity generation, and the increasing share of renewable energy sources, resource adequacy has become a key challenge for power system development. In this context, a balanced annual electricity budget alone does not guarantee sufficient generation capacity during periods of peak demand. This is particularly evident in systems with a high share of hydropower, where generation and available capacity depend heavily on hydrological conditions. This paper analyses the impact of hydrological conditions and the unavailability of generation units at the Šoštanj Thermal Power Plant on the ability to meet electricity demand in Slovenia. The analysis is based on the 100 hours of highest load on the Slovenian transmission system in 2024, comparing scenarios with favourable and unfavourable hydrological conditions. For each scenario, the capacity of domestic generation sources to meet demand was evaluated against the national adequacy criterion. This criterion requires full coverage of demand for at least 80 of the 100 hours analysed, and at least 80% coverage for the remaining hours. The results demonstrate a significant impact of hydrological conditions on the availability of domestic generation capacity. Assuming the unavailability of units at the Šoštanj Thermal Power Plant, full coverage of demand was achieved in 67 of the 100 hours analysed under favourable hydrological conditions, whereas under unfavourable hydrological conditions, this was achieved in only five hours. Nevertheless, coverage of at least 80% was ensured for 99 hours in the favourable hydrology scenario and for 80 hours in the unfavourable hydrology scenario. The analysis also indicated that, given the stated assumptions, meeting the relevant adequacy criterion would require an additional 84 MW of available capacity under favourable hydrological conditions, or 403 MW under unfavourable hydrological conditions.

Keywords: Hydrological Conditions, Generation Availability, Resource Adequacy.

INTRODUCTION

Resource adequacy refers to the ability of an electric power system to meet electricity demand at any given moment using available generation resources and other available capacities. Consequently, when assessing adequacy, the focus is not merely on total annual generation but primarily on the temporal alignment between available capacity and consumption. While an individual generation resource may contribute significantly to annual electricity production, its role during critical hours may be limited by the availability of the primary energy source, operational constraints, or unplanned outages. Therefore, an increase in annual

generation does not necessarily translate into a proportional improvement in meeting peak demand.

European resource adequacy analyses typically account for uncertainties on both the supply and demand sides by employing various scenarios and probabilistic assessment methods. In this context, the *LOLE* (Loss of Load Expectation) and *EENS* (Expected Energy Not Served) indicators are used to estimate the expected duration of resource inadequacy and the expected volume of unsupplied energy, respectively (Leibowicz et al., 2024). For national-level analyses, a transparent assessment of supply coverage during selected peak-demand hours is also useful, as it provides a better understanding of how individual generation resources contribute to achieving the required level of supply. Although this approach does not replace probabilistic analyses, it facilitates clearer interpretation of the results and of the system's sensitivity to changes in specific input assumptions.

In the Slovenian power system, hydroelectric power plants, the Krško Nuclear Power Plant (NEK) and the Šoštanj Thermal Power Plant (TEŠ) play a significant role in ensuring resource adequacy. While generation from hydroelectric plants depends directly on hydrological conditions and the availability of water resources, changes in the generation portfolio can substantially affect the balance between consumption and available capacity (van Vliet et al., 2016; van der Most et al., 2024).

The aim of this paper is to evaluate the impact of hydrological conditions on the coverage of peak demand hours under the TEŠ unavailability scenario and to assess the additional capacity required to maintain resource adequacy. The research question is how critical-hour demand coverage and additional capacity requirements change between favourable and unfavourable hydrological scenarios, including an assumed reduction in nuclear availability, while maintaining the same demand profile and the same available capacity of the remaining thermal generation.

MATERIALS AND METHOD

Data Basis and Definition of Scenarios

The analysis is based on publicly available data from ELES on electricity consumption and generation connected to the transmission network (ELES, n.d.). To evaluate resource adequacy, a set of 100 hours with the highest load, identified from the data available at the time for the year 2024, was used. The selected hours fall within the winter period, when the system’s peak loads occurred. The average hourly power demand during these hours ranges from 1,948 MW to 2,171 MW, with the peak load recorded on January 22 at 9:00 AM.

In the subsequent analysis, all hourly values are expressed as average power in MW. Since the relationship $P = E/\Delta t$ applies to a one-hour interval, the numerical values for energy (in MWh) and average power (in MW) are identical. This approach allows a direct comparison between system load and available generation capacity. Generation connected to the distribution network is not added separately, since its effect is already reflected in the measured electricity consumption from the transmission network.

To assess the impact of hydrological conditions, two scenarios were developed. The "favourable hydrology" scenario is based on hydrological conditions from 2024, while the "unfavourable hydrology" scenario is based on conditions from 2022. In both cases, the same load profile was used, enabling a direct comparison of how the availability of hydropower resources affects resource adequacy. The hydropower contribution comprises both conventional hydroelectric facilities and pumped-storage hydropower generation. Both scenarios also assume the unavailability of the TEŠ. In the adverse hydrology scenario, in addition to a smaller contribution from hydroelectric power plants, a reduction in the available capacity of the NEK is also taken into account. In the unfavourable hydrology scenario, the available capacity of NEK is reduced from 703 MW to 633 MW. This approximately 10% reduction is a scenario assumption representing potential cooling limitations, rather than an observed reduction during the selected hours. Technology-specific modelling of drought-related generation capacity reductions has been investigated by Shuai et al. (2024). While the contribution from hydroelectric power plants and the NEK decreases in this scenario, the available capacity of thermal power plants and gas-fired power plants remains unchanged at 627 MW(all Combined Cycle Gas Turbine and Open Cycle Gas Turbines).

In the analysis under consideration, battery storage systems are assumed not to provide additional power. This assumption is based on the occurrence of consecutive hours of high load, combined with the limited amount of energy that storage systems can deliver over an extended period. It should be noted that this is a simplification applied specifically in this case. The actual contribution of battery storage systems cannot be assessed solely on the basis of their nominal power; rather, it depends on their energy capacity, operational strategy, and the timing of their activation (Gonzato et al., 2023).

Similarly, solar power plants are not treated as a separate generation source. Their impact on the system's net load is already incorporated into the electricity off-take profile used for the transmission grid; therefore, accounting for their generation separately would result in double-counting the same effect. This approach allows the analysis to focus on the impact of hydrological conditions and the unavailability of the TEŠ, while keeping assumptions regarding other sources and system load constant.

Coverage criterion and mathematical notation

In assessing resource adequacy, the criterion stated on page 74 of the updated 2024 National Energy and Climate Plan was applied (Government of the Republic of Slovenia, 2024). This criterion requires domestic generation capacities to fully cover the system load during at least 80 of the 100 critical hours under consideration, while for the remaining hours at least 80% of the load must be covered.

Load coverage was determined by comparing the system load with the available capacity of domestic generation resources. Here, L_t represents the transmission system load in hour t, and $G_{s,t}$ represents the capacity of the domestic resources under consideration in hydrological scenario s. Based on these assumptions, the relationship for load coverage $C_{s,t}$ and the power balance $B_{s,t}$ is expressed by equations (7) and (8), respectively. A positive balance value

indicates that available domestic production exceeds the load, while a negative value indicates a power deficit that must be covered through imports or additional domestic resources.

$$C_{s,t} = \frac{G_{s,t}}{L_t} \tag{7}$$

$$B_{s,t} = G_{s,t} - L_t \tag{8}$$

For each hydrological scenario, the number of hours with full load coverage and the number of hours with at least 80% load coverage were determined by (9) and (10), respectively.

$$N_{100,s} = \sum_t 1\left(C_{s,t} \geq 1\right) \tag{9}$$

$$N_{80,s} = \sum_t 1\left(C_{s,t} \geq 0.8\right) \tag{10}$$

The summation covers all 100 analysed hours, and the function 1 takes the value one when the condition is met, and zero otherwise. The criterion is satisfied if $N_{100,s} \geq 80$ and, simultaneously, $N_{80,s} = 100$.

The need for additional generation capacity can be illustrated using a simplified assumption of an additional resource that provides a constant power output, ΔP, during all hours under consideration. If we define the deficit in a given hour as the difference between the load and the available domestic generation $d_{s,t} = L_t - G_{s,t}$, the minimum required additional power can be expressed by (11). The 80th-ranked deficit ensures that the condition of full coverage is met for at least 80 hours, while the final term ensures that, in any given hour, coverage does not fall below 80%.

$$\begin{gathered}\Delta P_s = \max\left\{0; d_{s,(80)}; \max_t\left(0.8 \cdot L_t - G_{s,t}\right)\right\} \\ d_{s,(1)} \leq \cdots \leq d_{s,(100)}\end{gathered} \tag{11}$$

RESULTS AND DISCUSSION

The results confirm that hydrological conditions have a significant impact on the adequacy of domestic generation resources and thus on the ability to cover the system's maximum loads. In the favourable hydrology scenario, the entire load was covered in 67 out of 100 analysed hours, while in the unfavourable hydrology scenario there were only five such hours. At the same time, at least 80% coverage was achieved in 99 hours under favourable hydrology and in 80 hours under unfavourable hydrology. The differences between the scenarios are also reflected in the number of hours with a production deficit. Under favourable hydrology, the deficit occurred in 33 hours, while under unfavourable hydrology it occurred in as many as 95 out of 100 analysed hours. This shows that resource adequacy results are strongly dependent on the availability of hydroelectric power plants and other production sources during periods of maximum load.

As a result, the need for additional capacity also increases significantly. To ensure at least 80% coverage in all analysed hours, an additional 7 MW of power would be sufficient in the favourable hydrology scenario, while 345 MW would be needed in unfavourable hydrology. Even greater differences are evident in meeting the entire resource adequacy criterion, which

requires full load coverage in at least 80 hours and at the same time at least 80% coverage in all analysed hours. To meet this criterion, 84 MW of additional capacity would be required under favourable hydrology, and 403 MW under unfavourable hydrology.

The results show that the deterioration of hydrological conditions significantly increases the need for additional power sources. The additional capacity requirement increases by 319 MW between the two scenarios, reflecting the combined effect of the modified hydropower contribution and the assumed 70 MW reduction in nuclear generation availability. Key indicators of load coverage and estimated requirements for additional capacity are presented in Table 1.

Table 1. Comparison of demand coverage and additional capacity requirements in the analysed scenarios.

Indicator	**Favourable hydrology**	**Unfavourable hydrology**
Hours with full demand coverage	67	5
Hours with a generation deficit	33	95
Hours with at least 80% demand coverage	99	80
Additional capacity required to ensure at least 80% coverage in every hour (MW)	7	345
Additional capacity required to ensure full coverage in at least 80 hours (MW)	84	403
Additional capacity required to satisfy both conditions (MW)	**84**	**403**

The identified domestic generation shortfalls do not directly imply electricity supply interruptions, since cross-border electricity availability and transmission constraints are not explicitly modelled. Borbáth and Van Hertem (2024) demonstrated that transmission modelling assumptions substantially influence European resource adequacy results. Further analysis should therefore consider the availability of imports during the identified critical hours. Extending the assessment to chronological simulations over multiple years would allow a more detailed representation of storage operation, generation availability and transmission constraints (Leibowicz et al., 2024; Gonzato et al., 2023).

CONCLUSION

The results of the analysis show that hydrological conditions have a significant impact on the sufficiency of domestic generation resources during periods of maximum system loads. In the favourable hydrology scenario, the entire load was covered in 67 out of 100 analysed hours, while in the un favourable hydrology scenario, there were only five such hours. At the same time, the number of hours with at least 80% coverage decreased from 99 to 80, which confirms the pronounced sensitivity of the results to hydropower availability and the assumed cooling-related reduction in nuclear capacity.

The analysis showed that, given the assumptions taken into account, none of the scenarios considered meet the adopted adequacy criterion without additional capacity. To achieve the

required level of coverage, 84 MW of additional capacity would be needed in the favourable hydrology scenario, and 403 MW in the unfavourable hydrology scenario. The difference between the scenarios shows that un favourable hydrological conditions can significantly increase the need for additional resources to ensure reliable electricity supply.

The findings confirm that when assessing resource adequacy, it is not only the total available generation capacity that is important, but above all the temporal alignment between the load and the availability of individual resources. Both hydrological conditions and assumptions about the availability of other production units play an important role in this. The estimated additional capacities represent a starting point for considering the role of new production sources, energy storage facilities and demand flexibility measures in ensuring resource adequacy in the future.

The presented analysis is based on an overview of selected hours with the highest loads and therefore does not represent a comprehensive probabilistic assessment of resource adequacy. It would be sensible to extend further research to a longer time period and more hydrological years and also include the impact of production unit outages, the operation of energy storage facilities, the demand flexibility potential and the role of cross-border electricity exchanges. Such an approach would enable a more comprehensive assessment of resource adequacy and a better basis for planning the development of the Slovenian electricity system.

REFERENCES

Borbáth, T. & Van Hertem, D. (2024). Appropriate transmission grid representation for European resource adequacy assessments. Applied Energy, 355, 122378.

ELES (n. d.). Prevzem in proizvodnja. ELES, d. o. o., https://www.eles.si/prevzem-in-proizvodnja, accessed October 23, 2024 and October 20, 2024.

Gonzato, S., Bruninx, K. & Delarue, E. (2023). The effect of short term storage operation on resource adequacy. Sustainable Energy, Grids and Networks, 34, 101005.

Government of the Republic of Slovenia (2024). Posodobljeni celoviti nacionalni energetski in podnebni načrt Republike Slovenije. Ljubljana, December 2024.

Leibowicz, B.D., Zhang, N., Carvallo, J.P., Larsen, P.H., Carr, T. & Baik, S. (2024). The importance of capturing power system operational details in resource adequacy assessments. Electric Power Systems Research, 228, 110057.

Shuai, H., Li, F., Zhu, J., Tingen II, W.J. & Mukherjee, S. (2024). Modeling the impact of extreme summer drought on conventional and renewable generation capacity: Methods and a case study on the Eastern U.S. power system. Applied Energy, 363, 122977.

van der Most, L., van der Wiel, K., Benders, R.M.J., Gerbens-Leenes, P.W. & Bintanja, R. (2024). Temporally compounding energy droughts in European electricity systems with hydropower. Nature Energy, 9, 1474-1484.

van Vliet, M.T.H., Wiberg, D., Leduc, S. & Riahi, K. (2016). Power-generation system vulnerability and adaptation to changes in climate and water resources. Nature Climate Change, 6, 375-380.

A GAME-THEORETIC INSIDER THREAT MITIGATION FRAMEWORK: LSTM-AUTOENCODER BASED USER BEHAVIOUR ANALYTICS APPROACH

Olajide O. Ogunbodede
Software Engineering Department, Federal University of Technology, Akure.

ABSTRACT

Insider threats remain one of the most difficult cybersecurity challenges faced by modern organizations. Unlike external attackers, insiders possess legitimate credentials and knowledge of internal systems, making traditional perimeter-based security mechanisms partially ineffective and insufficient. Machine learning approaches have been increasingly applied to detect anomalous user behaviour from enterprise logs; however, most existing approaches stop at detection and do not provide a strategic response mechanism for mitigating insider threats once anomalies are identified. This paper proposes an integrated insider threat detection and mitigation framework that combines user behaviour analytics with deep learning and game theory. First, behavioural features are extracted from enterprise system logs to construct temporal user activity sequences. These sequences are used to train a Long Short-Term Memory (LSTM) Autoencoder capable of learning normal behavioural patterns and detecting anomalies using reconstruction error. The anomaly scores produced by the model are then transformed into risk probabilities that inform a Stackelberg security game between a system administrator and potential insiders. In this game, the administrator commits to an optimal auditing strategy while rational insiders choose whether to attack or remain benign. The equilibrium solution provides an optimal auditing policy that balances monitoring costs and potential security losses. Experiments conducted using a realistic insider threat dataset demonstrate that the proposed framework improves threat detection while enabling cost-effective mitigation strategies. The results highlight the effectiveness of integrating deep learning based anomaly detection with game-theoretic decision making for proactive insider threat defense.

Keywords: Insider Threat Detection, User Behaviour Analytics, LSTM-Autoencoder, Stackelberg Game, Anomaly Detection, Strategic Auditing.

DESIGN AND SIMULATION-BASED EVALUATION OF AN LFSR-DRIVEN BUILT-IN SELF-TEST ARCHITECTURE FOR FAULT DETECTION USING VERILOG HDL

Afaq AHMAD
Professor (Dr.), Faculty of Department of Mathematics and Computer Science
Modern College of Business and Science, [Country: Oman]
ORCID: 0000-0002-8592-1612

M Mohammed Sabir HUSSAIN
Associate Professor (Dr.), Faculty of Department of Electronics and Communication Engineering
Muffakham Jah College of Engineering and Technology, Hyderabad, [Country: India]

ABSTRACT

The increasing complexity of digital systems necessitates efficient and systematic hardware testing techniques for identifying functional faults. This paper presents the design and simulation-based evaluation of a Linear Feedback Shift Register (LFSR)-driven Built-In Self-Test (BIST) architecture for fault detection in digital circuits using Verilog Hardware Description Language (HDL). The proposed architecture integrates an LFSR-based test-pattern generator, a circuit under test (CUT), a fault-injection mechanism, an expected-response reference, and a response comparator. The LFSR generates deterministic test sequences that are applied to both fault-free and fault-injected circuit models. Discrepancies between the reference and observed responses are used to indicate potential faults. A simulation test bench is developed to evaluate representative stuck-at-zero, stuck-at-one, and bit-flip faults under controlled operating conditions. The proposed framework is assessed using fault detection coverage, detection latency, test-pattern count, test completion cycles, and false-positive rate. Different LFSR configurations and test-pattern budgets can also be compared to investigate their influence on fault observability and testing efficiency. The study provides a reproducible RTL-level methodology for analyzing LFSR-based fault detection without requiring physical hardware implementation. The findings are intended to identify the effectiveness and limitations of the proposed architecture and establish a foundation for future extensions to more complex digital systems.

Keywords: Linear Feedback Shift Register (LFSR), Built-In Self-Test (BIST), Verilog HDL, Fault Detection, Fault Injection, Stuck-at Faults, RTL Simulation, Fault Coverage.

ROT BAŞININ SIVANMIŞ KENAR KOROZYON DİRENCİNİN İYİLEŞTİRİLMESİ

IMPROVEMENT OF ROLLED EDGE CORROSION RESISTANCE OF OUTER TIE-ROD

Tuğba Özcan
ZF Lemförder, Ar-Ge, İzmir, Türkiye
ORCID ID: 0009-0007-1758-6043

ÖZET

Bu çalışmanın amacı, dış rot başı üretiminde sıvama işlemi sırasında koruyucu kaplamanın mekanik olarak zarar gördüğü sıvanmış kenar bölgesinin korozyon direncini, ilave ve maliyet odaklı bir montaj sonrası işlem kullanmadan artırmaktır. Dış rot başı, direksiyon hareketini tekerleklere ileten ve doğru tekerlek hizasının korunmasına katkı sağlayan güvenlik açısından kritik bir şasi bileşenidir. Sıvama operasyonunda gövdenin üst kenarı plastik olarak şekillendirilerek uç kapağın üzerine kapatılmakta; bu sırada oluşan aşınma, galvanik kaplamanın yerel bütünlüğünü ve ISO 9227 tuz püskürtme testi performansını azaltmaktadır. Standart proseste sıvanmış kenarda 10 kat saat seviyesinde olan korozyon direncinin 30 kat saate yükseltilmesi hedeflenmiştir. Literatür araştırması ve proses deneyimi doğrultusunda kobalt konsantrasyonu, kromat daldırma süresi, pasivasyon sıcaklığı, sealer konsantrasyonu, sealer daldırma süresi ve kurutma/kürleme süresi olmak üzere altı kaplama parametresi belirlenmiştir. Bu parametreler eş zamanlı olarak optimize edilmiş ve numuneler tuz püskürtme, statik ve dinamik doğrulama testlerine tabi tutulmuştur. Sonuçlar, optimize edilmiş tedarikçi kaplama prosesiyle sıvanmış kenarın korozyon direncinin 10 kat saatten 30 kat saate çıktığını göstermiştir. Kaplama değişiklikleri sonrasında statik ve dinamik doğrulama testlerinde olumsuzluk gözlenmemiş, dış rot başları başarıyla doğrulanmıştır. Böylece ZF tesisinde ek operasyon, ilave çevrim süresi veya montaj sonrası uygulama oluşturmadan daha yüksek korozyon performansı elde edilmiştir

Anahtar Kelimeler: Dış Rot Başı, Sıvanmış Kenar, Korozyon Direnci, Zn-Ni Kaplama, Pasivasyon, Sealer, Tuz Püskürtme Testi, ISO 9227.

ABSTRACT

This study aims to improve the corrosion resistance of the rolled edge area of an Outer Tie-Rod, where the protective coating is mechanically damaged during the rolling operation, without introducing an additional cost-driven post-assembly treatment. The outer tie-rod is a safety-critical chassis component that transfers steering movement to the wheels and supports correct wheel alignment. During rolling, the upper edge of the radial housing is plastically formed over the end cap to close and retain the joint. The associated abrasion locally damages the galvanic coating and reduces performance in the salt spray test conducted according to ISO 9227. The study targeted an increase in rolled-edge corrosion resistance from the 10x-hour level achieved with the standard process to 30x hours. Based on a literature review and process experience, six coating parameters were selected: cobalt concentration, chromate

immersion time, passivation temperature, sealer concentration, sealer immersion time, and drying/curing time. These parameters were optimized simultaneously, and the resulting samples were evaluated by salt spray testing together with static and dynamic validation tests. The results show that the optimized supplier coating process increased rolled-edge corrosion resistance from 10x hours to 30x hours. No adverse effects related to the coating modifications were observed during static or dynamic validation, and the outer tie-rods were validated successfully. Consequently, enhanced corrosion performance was achieved without creating an additional operation, post-assembly application, or cycle-time increase at the ZF facility. The findings demonstrate that coordinated optimization of passivation and sealing parameters can improve the robustness of a mechanically formed coated area while maintaining joint performance.

Keywords: Outer Tie-Rod, Rolled Edge, Corrosion Resistance, Zn-Ni Coating, Passivation, Sealer, Salt Spray Test, ISO 9227.

H07Z-K KABLOLARINDA ALEV GECİKTİRİCİ GRANÜLLERİN İŞLENME PARAMETRELERİNİN OPTİMİZASYONU VE CPR YANGINA TEPKİ PERFORMANSININ İNCELENMESİ

OPTIMIZATION OF FLAME-RETARDANT GRANULE PROCESSING PARAMETERS AND INVESTIGATION OF CPR FIRE REACTION PERFORMANCE IN H07Z-K CABLES

Ebru GÜDÜL
Borsan Ar-Ge Merkezi- Borsan R&D Center

Şükrü SARI
Borsan Ar-Ge Merkezi- Borsan R&D Center

Ayça ÖZEN
Borsan Ar-Ge Merkezi- Borsan R&D Center

Samet DURMUŞ
Borsan Ar-Ge Merkezi- Borsan R&D Center

Onur ADIGÜZEL
Borsan Ar-Ge Merkezi- Borsan R&D Center

Ekrem ALTAN
Borsan Ar-Ge Merkezi- Borsan R&D Center

ÖZET

Elektrik kablolarında yangın güvenliği, özellikle yapı uygulamalarında kullanılan ürünler açısından önemli bir performans kriteridir. Yangın sırasında alev yayılımının sınırlandırılması, ısı açığa çıkışının azaltılması ve kablonun yangına tepki performansının iyileştirilmesi, ürün güvenliği ve Yapı Malzemeleri Yönetmeliği (CPR) kapsamında gerçekleştirilen sınıflandırmalar açısından önem taşımaktadır. H07Z-K kabloları; 450/750 V anma gerilimine sahip, tek damarlı, esnek bakır iletkenli ve halojensiz izolasyon yapısıyla özellikle bina içi elektrik tesisatlarında kullanılan kablo tipleri arasında yer almaktadır. Bu kablolarda yangına tepki performansının geliştirilmesi, uygun malzeme seçiminin yanı sıra üretim süreçlerinin ve hat parametrelerinin optimize edilmesini de gerektirmektedir.

Bu çalışma kapsamında, farklı alev geciktirici özelliklere ve katkı yükleme oranlarına sahip halojensiz izolasyon granülleri kullanılarak H07Z-K kabloların üretim süreçleri incelenmiştir. Granüllerin işlenmesine yönelik üretim hattı parametreleri optimize edilerek proses koşullarının nihai kablo performansı üzerindeki etkisi araştırılmıştır. Bu doğrultuda granüllerin yoğunluk, sınırlayıcı oksijen indeksi (LOI) ve yanma boyu özellikleri belirlenmiş; farklı proses koşullarında üretilen 1,5 mm² ve 10 mm² kesitli H07Z-K kabloların performansları karşılaştırılmıştır. Uygun granül seçimi ve proses parametrelerinin optimizasyonu sonucunda LOI değeri yaklaşık %35'ten %38'e yükselmiştir. 1,5 mm² kesitli kablolarda LOI değerindeki artışla birlikte yanma boyunun azaldığı ve alev ilerlemesinin sınırlandığı belirlenmiştir. 10 mm² kesitli kablolarda ise elde edilen performans iyileşmesi CPR

yangına tepki sınıflandırmasına yansımış ve numunelerin sınıfı Dca seviyesinden B2ca seviyesine kadar yükselmiştir.
Elde edilen sonuçlar, halojensiz granüllerin seçimi ve üretim hattı parametrelerinin optimizasyonunun H07Z-K kabloların yangına tepki performansının iyileştirilmesinde etkili olabileceğini göstermektedir. Ayrıca nihai performansın yalnızca kullanılan granülün özelliklerine değil, üretim koşullarına, kablo kesitine ve kablonun yapısal özelliklerine de bağlı olduğu ortaya konulmuştur. Çalışma, mevcut malzemelerin ve üretim altyapısının etkin kullanımıyla halojensiz kablolarda daha yüksek CPR yangına tepki sınıflarına ulaşılmasına yönelik proses iyileştirme çalışmalarına katkı sunmaktadır.
Anahtar Kelimeler: H07Z-K, alev geciktirici, halojensiz kablo, sınırlayıcı oksijen indeksi, LOI, CPR, yangına tepki

ABSTRACT

Fire safety is a critical performance criterion for electrical cables, particularly those used in building applications. Limiting flame spread, reducing heat release, and improving cable reaction-to-fire performance are essential for product safety and classification under the Construction Products Regulation (CPR). H07Z-K cables are 450/750 V rated, single-core cables featuring flexible copper conductors and halogen-free insulation, and are widely used in indoor electrical installations. Improving the reaction-to-fire performance of these cables requires not only appropriate material selection but also the optimization of manufacturing processes and production line parameters.
In this study, the manufacturing processes of H07Z-K cables were investigated using halogen-free insulation granules with different flame-retardant properties and additive loading ratios. Production line parameters related to granule processing were optimized, and the effects of process conditions on the final cable performance were evaluated. Accordingly, the density, limiting oxygen index (LOI), and burning length characteristics of the granules were determined. The performance of H07Z-K cables with cross-sectional areas of 1.5 mm² and 10 mm², manufactured under different process conditions, was also compared. As a result of appropriate granule selection and process parameter optimization, the LOI value increased from approximately 35% to 38%. For cables with a cross-sectional area of 1.5 mm², the increase in LOI was accompanied by a reduction in burning length and a limitation of flame propagation. For cables with a cross-sectional area of 10 mm², the improvement in performance was reflected in the CPR reaction-to-fire classification, with the classification of the samples improving from Dca to B2ca.
The results demonstrate that the selection of halogen-free granules and the optimization of production line parameters can contribute to improving the reaction-to-fire performance of H07Z-K cables. Furthermore, the final performance was found to depend not only on the properties of the granules used but also on manufacturing conditions, cable cross-sectional area, and structural characteristics. This study contributes to process improvement efforts aimed at achieving higher CPR reaction-to-fire classifications for halogen-free cables through the effective utilization of existing materials and manufacturing infrastructure.
Keywords: H07Z-K, flame retardant, halogen-free cable, limiting oxygen index, LOI, CPR, reaction to fire

VALORIZATION OF SHELL-BASED AGRICULTURAL RESIDUES INTO VALUE-ADDED ENGINEERING MATERIALS THROUGH INDUSTRIAL SYMBIOSIS IN TÜRKİYE: A CRITICAL ASSESSMENT OF TECHNICAL POTENTIAL, REGIONAL RESOURCE DISTRIBUTION, AND IMPLEMENTATION FEASIBILITY

Burcu Nilgün ÇETİNER
Dr., Marmara University, Faculty of Engineering, Department of Metallurgical and Materials Engineering, Istanbul, Türkiye.
ORCID: 0000-0002-3742-4929

Gökçen BAYRAM
Dr., Istanbul Beykent University, Faculty of Engineering – Architecture, Department of Industrial Engineering, Istanbul – Türkiye.
(Responsible Author) **ORCID:** 0000-0001-8892-1020

ABSTRACT

Shell-based agricultural wastes generated from agricultural production and food processing activities in Türkiye are significant secondary raw material sources that can be utilized to produce value-added engineering materials, owing to their lignocellulosic and mineral compositions. Valorizing these wastes within the frameworks of the circular economy and industrial symbiosis offers potential for enhancing resource efficiency, improving waste management, and establishing new value chains across various industrial sectors. However, demonstrating successful material production at the laboratory scale does not, in itself, prove that the associated conversion processes are technically, economically, and logistically feasible at an industrial scale, or that sustainable resource exchange between enterprises can be realized. The aim of this study is to critically evaluate the potential for converting shell-based agricultural wastes generated in Türkiye into value-added engineering materials and to identify the conditions necessary for integrating these conversions into industrial symbiosis systems. In this context, the literature regarding the use of various agricultural by-products—such as hazelnut, walnut, pistachio, almond, sunflower, and rice husks—in the production of activated carbon, biochar, silica-based materials, carbon-based functional materials, and composite fillers is examined using a structured critical review approach. The assessment is conducted within an integrated framework comprising three fundamental dimensions: (i) technical suitability, covering the physical and chemical properties of the waste, conversion technologies, and the performance of the resulting materials; (ii) regional resource and supply suitability, encompassing the geographical distribution of agricultural production, available raw material quantities, seasonality, pre-treatment requirements, and transportation conditions; and (iii) symbiosis feasibility, addressing potential source and user sectors, inter-firm material flows, economic viability, and industrial integration requirements. Findings from the literature indicate that various husk-based agricultural wastes possess technical

potential for the production of carbon- and silica-based materials; however, material properties depend significantly on raw material composition and the conversion processes employed. Furthermore, high laboratory-scale performance does not constitute sufficient evidence of commercial-scale manufacturability or the existence of actual industrial symbiosis relationships between enterprises. Regional variations in agricultural production in Türkiye emerge as variables that must be considered collectively regarding the continuity of raw material supply, the siting of processing facilities, and potential industrial synergies. The study demonstrates that the conversion of husk-based agricultural wastes into value-added engineering materials should be evaluated not solely based on material performance, but also by considering resource supply, supply chain structure, the maturity of conversion technologies, and the conditions for inter-firm collaboration. The proposed integrated assessment framework aims to contribute to identifying potential industrial symbiosis models that could be developed between the agricultural and industrial sectors in Türkiye, as well as to defining the data and research gaps necessary for future regional implementations.

Keywords: Husk/Shell based agricultural waste, Industrial symbiosis, Circular economy, Value-added engineering materials, Regional resource potential, Resource efficiency

GRAFEN VE H-BN HİBRİT NANODOLGU İÇEREN KARBON ELYAF TAKVİYELİ EPOKSİ KOMPOZİTLERİN YÜKSEK SICAKLIK DAVRANIŞLARI

HIGH TEMPERATURE BEHAVIOR OF CARBON FIBER REINFORCED EPOXY COMPOSITES CONTAINING GRAPHENE AND H-BN HYBRID NANOFILLERS

İlayda DEMİR

Yüksek Lisans Öğrencisi, Yıldız Teknik Üniversitesi, Fen Bilimleri Enstitüsü, Metalurji ve Malzeme Mühendisliği Anabilim Dalı

MSc Student, Yildiz Technical University, Graduate School of Natural and Applied Sciences, Department of Metallurgical and Materials Engineering

ORCID ID: 0009-0001-3662-3467

ÖZET

Savunma sanayiinde İHA/SİHA, füze ve roket gövdeleri ile savaş uçakları gibi yüksek performans gerektiren sistemlerde ağırlığın azaltılması; menzil, faydalı yük kapasitesi ve manevra kabiliyeti açısından stratejik önem taşımaktadır. Bu nedenle karbon elyaf takviyeli epoksi (CFRP) kompozitler; yüksek özgül mukavemet, düşük yoğunluk ve korozyon direnci sayesinde alüminyum ve titanyum gibi metalik malzemelerin yerini alarak savunma, havacılık ve uzay sanayiinde birincil yapısal malzeme haline gelmiştir. Ancak epoksi reçineler camsı geçiş sıcaklığı (Tg) civarında rijitliğini kaybetmekte, düşük ısıl iletkenlikleri nedeniyle ısıyı biriktirmekte, elyaf ile matris arasındaki termal genleşme farkı ise arayüzeyde mikro çatlaklara ve delaminasyona yol açmaktadır. Bu durum, özellikle yüksek hızda aerodinamik ısınmaya maruz kalan yüzeylerde CFRP kullanımını sınırlamakta ve kritik bir problem oluşturmaktadır. Epoksi matrisin nanodolgularla modifiye edilmesi bu termodinamik sorunların giderilmesinde ve yapısal bütünlüğün korunmasında önemli bir oynamaktadır.

Grafen nanodolgu; yüksek elastisite modülü, yüksek ısıl ve elektriksel iletkenliği ile geniş yüzey alanı sayesinde matrisi güçlendirmekte ve çatlak ilerlemesini zorlaştırarak kırılma tokluğunu artırmaktadır. “Beyaz grafen” olarak da adlandırılan hekzagonal bor nitrür (h-BN) ise elektriksel olarak yalıtkan, ancak yüksek ısıl iletkenliğe ve kimyasal kararlılığa sahip iki boyutlu bir malzemedir. Grafen ve h-BN’nin birlikte kullanıldığı hibrit nanodolgu sistemlerinde, iki boyutlu nanodolgular matris içerisinde ısı iletim yolları oluşturarak ısıyı daha dengeli dağıtmakta, polimer zincir hareketliliğini kısıtlayarak Tg’yi yükseltmekte ve termal bozunmayı geciktirmektedir. Bu sinerjik etkinin elde edilebilmesi için nanodolguların aglomerasyonunun önlenmesi ve matris içerisinde homojen dağıtılması gerekmektedir. Bu çalışmanın amacı, savunma sanayiindeki yüksek sıcaklık uygulamalarında kullanılmak üzere farklı oranlarda grafen ve h-BN nanodolgu katkılı karbon elyaf takviyeli epoksi kompozitlerin geliştirilmesi ve yüksek sıcaklık altındaki mekanik ve termal davranışlarının incelenmesidir.

Anahtar Kelimeler: Savunma Sanayii, Karbon Elyaf Kompozit, Epoksi Reçine, Grafen Nanodolgu, Hekzagonal Bor Nitrür (h-BN), Yüksek Sıcaklık, Hibrit Nanodolgu.

ABSTRACT

In the defense industry, reducing weight in high-performance systems such as UAVs/UCAVs, missile and rocket airframes, and combat aircraft is of strategic importance for range, payload capacity and maneuverability. Therefore, carbon fiber reinforced epoxy (CFRP) composites have become primary structural materials in the defense, aerospace and space industries, replacing metallic materials such as aluminum and titanium owing to their high specific strength, low density and corrosion resistance. However, epoxy resins lose their stiffness around the glass transition temperature (Tg) and accumulate heat because of their low thermal conductivity, while the thermal expansion mismatch between fiber and matrix leads to interfacial microcracks and delamination. This limits the use of CFRP composites, particularly on surfaces exposed to aerodynamic heating at high speeds, and poses a critical problem. Modification of the epoxy matrix with nanofillers plays an important role in overcoming these thermodynamic problems and preserving structural integrity.

Owing to its high elastic modulus, high thermal and electrical conductivity and large surface area, graphene nanofiller strengthens the matrix and increases fracture toughness by hindering crack propagation. Hexagonal boron nitride (h-BN), often referred to as “white graphene,” is a two-dimensional material that is electrically insulating but has high thermal conductivity and chemical stability. In hybrid nanofiller systems where graphene and h-BN are used together, the two-dimensional nanofillers form heat conduction pathways within the matrix that distribute heat more uniformly, restrict polymer chain mobility to raise Tg, and delay thermal degradation. To achieve this synergistic effect, agglomeration of the nanofillers must be prevented and they must be homogeneously dispersed in the matrix. The aim of this study is to develop carbon fiber reinforced epoxy composites containing different ratios of graphene and h-BN nanofillers for use in high-temperature applications in the defense industry, and to investigate their mechanical and thermal behavior at elevated temperatures.

Keywords: Defense Industry, Carbon Fiber Composite, Epoxy Resin, Graphene Nanofiller, Hexagonal Boron Nitride (h-BN), High Temperature, Hybrid Nanofiller.

KAZICI YÜKLEYİCİ KABİNİ İÇİN TAKOZ SEÇİMİNİN TİTREŞİM İZOLASYONU VE TASARIM ÖLÇÜTLERİ AÇISINDAN DEĞERLENDİRİLMESİ

EVALUATION OF CAB MOUNT SELECTION FOR A BACKHOE LOADER BASED ON VIBRATION ISOLATION AND DESIGN CRITERIA

Yaren DEVİREN
Çukurova Makina İmalat ve Ticaret A.Ş., Mersin, Türkiye
ORCID: 0009-0002-7265-0961

ÖZET

Kazıcı yükleyici kabini, motor kaynaklı titreşimlerin yanı sıra sürüş ve engebeli zemindeki çalışma sırasında oluşan darbe yüklerine maruz kalır. Kabin takozu seçiminde bu etkilerin yanı sıra statik yük dağılımı, kabin hareketi ve montaj koşulları birlikte değerlendirilmelidir. Bu çalışmada Çukurova Makina 885–888 kazıcı yükleyici kabini için yürütülen mühendislik değerlendirmesi ve mevcut 75–80 Shore A sertliğindeki Cone 31 takozunun 60 Shore A sertliğindeki Cone 31 ile değiştirilmesi ele alınmıştır. Karşılaştırmalı tasarım değerlendirmesinde araç geometrisi, kabinin kütle özellikleri, takoz özellikleri ve altı serbestlik dereceli çok cisimli model sonuçları birlikte incelenmiştir. Dört noktadan desteklenen modelde kabin kütlesi 810 kg, sürücü kütlesi 100 kg olarak alınmıştır. Seçim ölçütleri; takozlar arasındaki statik yük dağılımı, hesaplanan doğal frekanslar ve yönlere göre izolasyon, tanımlı şok altındaki kabin hareketi ve mevcut konik bağlantı düzeniyle uyumdur. Varsayılan 30 Hz birinci mertebe uyarımda en yüksek doğal frekans, önceki takozla 27,81 Hz iken seçilen 60 Shore A takozla 25,46 Hz'dir. Boyuna, yanal ve düşey yönlerde hesaplanan izolasyon sırasıyla −%66,31, %75,14 ve %46,20'den %28,86, %84,25 ve %62,49'a yükselmektedir. En yüksek hesaplanan statik yük, takoz için belirtilen nominal kapasitenin altında kalmaktadır. 60 Shore A Cone 31, öngörülen titreşim performansı ile aracın bağlantı düzenine ilişkin gereklilikler arasında dengeli bir seçenek olarak belirlenmiştir. ISO 2017-1, izolasyon sistemi için teknik veri alışverişine bir çerçeve sunar. Çalışma ön yükünde takoz özelliklerinin ve araç üzerindeki operatör maruziyetinin ileride doğrulanması için sırasıyla ISO 10846-2 ve ISO 2631-1 dikkate alınmalıdır. Verilen izolasyon değerleri belirli bir uyarıma ait hesap sonuçlarıdır; ölçülmüş operatör konforunu göstermez.

Anahtar Kelimeler: Kazıcı yükleyici, kabin takozu seçimi, titreşim izolasyonu, çok cisimli analiz, tasarım ölçütleri.

ABSTRACT

A backhoe loader cab is exposed to engine-induced vibration and shock loads arising during travel and operation on uneven terrain. Cab mount selection therefore requires consideration of static load distribution, cab motion and installation constraints. This study presents the engineering assessment conducted for the Çukurova Makina 885–888 backhoe loader cab and

the replacement of the existing Cone 31 mount (75–80 Shore A) with a Cone 31 mount of 60 Shore A hardness. The vehicle geometry, cab mass properties, mount characteristics and six-degree-of-freedom multibody results were considered together in a comparative design evaluation. The model includes an 810 kg cab and a 100 kg driver supported at four locations. Selection criteria were the distribution of static loads among the supports, predicted natural frequencies and directional isolation, cab displacement under a defined shock, and compatibility with the existing conical mounting concept. At the assumed first-order excitation of 30 Hz, the highest predicted natural frequency decreases from 27.81 Hz for the previous mount to 25.46 Hz for the selected 60 Shore A mount. Calculated isolation changes from −66.31%, 75.14% and 46.20% to 28.86%, 84.25% and 62.49% in the longitudinal, lateral and vertical directions, respectively. The maximum calculated static load remains within the nominal capacity specified for the mount. The 60 Shore A Cone 31 was selected as a balance between predicted vibration performance and the requirements of the vehicle mounting concept. ISO 2017-1 provides a framework for exchanging isolation-system design data. Future mount characterization under operating preload and vehicle measurements should be planned with reference to ISO 10846-2 and ISO 2631-1, respectively. The reported percentages are predictions for a specified excitation, not measured operator comfort.

Keywords: Backhoe loader, cab mount selection, vibration isolation, multibody analysis, design criteria.

AN EVALUATION OF IMPEDANCE MATCHING TECHNIQUES FOR SHPB TESTING OF LOW-IMPEDANCE SOFT MATERIALS

Oğuzhan CAN
Istanbul Technical University, Faculty of Mechanical Engineering, Department of Mechanical Engineering, TÜRKİYE

Baran BULUT
Istanbul Technical University, Faculty of Mechanical Engineering, Department of Mechanical Engineering, TÜRKİYE

Safa Melik TÜZÜNER
Istanbul Technical University, Faculty of Mechanical Engineering, Department of Mechanical Engineering, TÜRKİYE

Süreyya Ergün BOZDAĞ
Dr., Istanbul Technical University, Faculty of Mechanical Engineering, Department of Mechanical Engineering, TÜRKİYE

Emin SÜNBÜLOĞLU
Prof. Dr., Istanbul Technical University, Faculty of Mechanical Engineering, Department of Mechanical Engineering, TÜRKİYE

ABSTRACT

Split Hopkinson Pressure Bar (SHPB) systems are used to determine the dynamic mechanical behaviour of materials at high strain rates. However, testing of low impedance soft materials (e.g. foams, rubbers) with conventional metallic bars (e.g. steel, titanium) restricts the specimen from reaching dynamic stress equilibrium due to the phenomenon of “acoustic impedance mismatch”. The high reflections occurring at the rod-specimen interface significantly decrease the amplitude of the stress wave transmitted through the specimen. Consequently, the signals acquired from the rods are obscured by background noise. One of the primary methods employed to mitigate these challenges is the utilization of lower impedance alternatives such as magnesium, aluminum or polymethyl methacrylate (PMMA) as rod materials instead of steel. In addition, hollow transmission bar and applying tapering techniques at the strain-gauge regions are implemented to enhance the signal.

In this study, some impedance matching methods implemented in the literature are examined to overcome the wave transmission limitations encountered in high-rate testing of low impedance materials. Aluminum rods and soft-rubber specimens were used as the trial pair. On the specimen side, introducing a central hole into the rubber specimen was evaluated to reduce additional stresses induced by radial inertia and to attain a uniaxial stress state though the thin-large cross section. Finally, one-dimensional wave propagation was modelled using

the cross-sectional area variation method to balance the impedance at the bar -specimen contact interface.

Numerical analyses revealed that the applications of hollow bars and controlled tapering did not significantly improve the transmitted wave amplitude to the desired extent in low impedance materials. In contrast, altering the cross-sectional area at the bar and specimen contact reduced the impedance mismatch and enhanced wave transmission. This approach enables a more reliable characterization of the mechanical properties of low impedance soft materials at high strain rates using conventional setups.

Keywords: Split Hopkinson Pressure Bar, Low impedance materials, Impedance matching, Wave transmission, Cross-sectional area variation.

DESIGN AND ANALYSIS OF VARIOUS CROSS-SECTION TRANSFORMING HORN DESIGNS FOR TESTING LOW-IMPEDANCE MATERIALS IN SPLIT HOPKINSON PRESSURE BAR SYSTEMS

Baran BULUT
Istanbul Technical University, Faculty of Mechanical Engineering, Department of Mechanical Engineering, TÜRKİYE

Safa Melik TÜZÜNER
Istanbul Technical University, Faculty of Mechanical Engineering, Department of Mechanical Engineering, TÜRKİYE

Oğuzhan CAN
Istanbul Technical University, Faculty of Mechanical Engineering, Department of Mechanical Engineering, TÜRKİYE

Süreyya Ergün BOZDAĞ
Dr., Istanbul Technical University, Faculty of Mechanical Engineering, Department of Mechanical Engineering, TÜRKİYE

Emin SÜNBÜLOĞLU
Prof. Dr., Istanbul Technical University, Faculty of Mechanical Engineering, Department of Mechanical Engineering, TÜRKİYE

ABSTRACT

Split Hopkinson Pressure Bar (SHPB) systems establish a standard methodology for determining the dynamic behaviour of materials at high strain rates. However, the “acoustic impedance mismatch” between conventional metal bars and low-impedance soft materials, such as rubber, remarkably reduces the applicability of specimen characterization. This mismatch prevents dynamic stress equilibrium, as significant wave energy reflects from the interface, highly distorting the transmitted signal's shape and amplitude.

In this study, cross section transformer horn (CSTH) systems are placed at both sides of the specimen to enhance wave transmission. CSTH geometries were developed using Bezier, exponential, and step functions. Their effects on one-dimensional wave propagation were numerically investigated via ABAQUS under a 30 m/s striker bar velocity. Since converging horns failed to improve wave transmission, diverging horn designs were developed to achieve better acoustic impedance matching. Geometric optimization revealed that to prevent wave distortion and reflections, the difference between the horn's inlet and outlet diameters (Δd) must be 10-20% of its total length (L).

The best-performing diverging horn geometry utilizes the Bezier approach, which preserves wave amplitude extensively. This ensures a considerable portion of the incoming pressure

wave transfers to the transmission bar, enabling highly accurate characterization of low-impedance soft materials using conventional metal bars.

Keywords: Split Hopkinson Pressure Bar, Low impedance materials, Acoustic impedance mismatch, Cross section transformer horn (CSTH), Bezier geometry.

GRAVITY-LESS IN ARCHITECTURE AS A DESIGN PROBLEM: CASE STUDIES OF SINGAPORE NATIONAL STADIUM AND MERCEDES-BENZ STADIUM, ATLANTA

Shayan Zulfiqar
Ar. Practicing Architect, IEB Nexus Hub, Dubai

Omer Shujat Bhatti
Ar. Dr., Associate Professor & COD, Dept. of Architecture, School of Architecture & Planning, UMT, Lahore

Usman Raza Kazmi
Ar., Lecturer, Dept. of Architecture, School of Architecture & Planning, UMT, Lahore.

Nouman Zulfiqar
Engr. Practicing Engineer.

Hamza Rashid
Engr. Practicing Engineer, Infrastructure Development Authority, Punjab (IDAP)

ABSTRACT

Sports Stadiums have the capabilities to invite a large crowd, therefore the need to cover a large span to cater to a maximum number of people without affecting the viewpoint and comfortability of the public to enjoy the sports becomes the foremost factor in their structure. In this light stadium Structures are unique in themselves as they require to be column-free, high span, and open plan. Through the help of case studies and comparative analysis of different structures, it can be observed that Gravity-less Structure can be made by using Trusses and Spaceframes Structures. More ever moveable structures can also cover long spans. To conceptualize this problem case study of Singapore National Stadium is chosen for this assignment. The project uses spaces trusses interlinked with louvers that allow the structure to cover a span of 312 m with a height of 80 m and making it the world's largest dome. The upper part of the Roof is Moveable depending upon the use of the Stadium. The structure moves along the outside vault, from the closed to the empty location, the reinforcing framework of the moving areas is planned with adaptable associations, allowing the structure to stop and twist under the activity of gravity. The roof system uses a space truss structure. The structures are arranged like a half-ball dome. Thus, a wide enough distance can still be covered with lightweight and strong materials.

Keywords: Islamic architecture; volumetric forms; structural challenges; domes; arches; minarets; large-span structures; lateral stability; contemporary mosque architecture.

LEVERAGING DIGITAL TRANSFORMATION TO DRIVE SUSTAINABLE FOOD SYSTEMS IN AFRICA: A CASE STUDY OF MKPAT ENIN LOCAL GOVERNMENT AREA OF AKWA IBOM STATE, NIGERIA

AKPAN CHRISTOPHER ANIEKAN
Department of Agricultural Education, Federal College of Education (Technical) Ekiadolor Benin City, Edo State Nigeria.

ABSTRACT

Africa's food systems are under increasing pressure from population growth, climate variability, environmental degradation, food loss, inadequate market infrastructure, limited access to agricultural information and persistent rural poverty. Digital transformation offers opportunities to address several of these challenges by connecting farmers with information, markets, financial services, extension advice, weather intelligence and improved production technologies. This opinion paper examines how digital transformation can contribute to sustainable food-system development in Africa, using Mkpat Enin Local Government Area (LGA) of Akwa Ibom State, Nigeria, as a contextual case. The paper argues that mobile phones, digital extension platforms, geographic information systems (GIS), remote sensing, digital financial services, e-commerce, artificial intelligence (AI), Internet of Things (IoT) technologies and digital traceability systems can improve productivity, resource-use efficiency, and resilience and market participation. Evidence from Akwa Ibom indicates growing acceptance of mobile-based agricultural applications, while research specifically in Mkpat Enin has documented relationships between technology adoption and agricultural production. However, inadequate connectivity, digital illiteracy, affordability, electricity constraints, limited institutional coordination and unequal access may restrict benefits. The paper therefore advocates a locally adapted, farmer-centred digital transformation strategy combining infrastructure, digital literacy, agricultural extension, inclusive finance, data governance and public-private partnerships. Such an approach could help Mkpat Enin and similar rural communities contribute more effectively to sustainable and resilient food systems in Africa.

Keywords: Digital transformation, sustainable food systems, digital agriculture, agricultural extension, smallholder farmers, Mkpat Enin, Akwa Ibom State, Nigeria, food security.

ENHANCING SAFETY AND ACCESSIBILITY IN THE DESIGN OF A PUBLIC TRANSPORTATION HUB IN MINNA, NIGER STATE

Kater Titus
Department of Architecture, School of Architectural Technology, Federal University of Technology, Minna, Nigeria

A.J. Simon
Department of Architecture, School of Architectural Technology, Federal University of Technology, Minna, Nigeria

D.O. Alonge
Department of Architecture, School of Architectural Technology, Federal University of Technology, Minna, Nigeria

ABSTRACT

Public transportation hubs occupy a central position in the social and economic fabric of Nigerian cities, serving simultaneously as transit nodes, commercial centres, and sites of daily interaction. Yet, despite their strategic importance, a significant number of these facilities remain poorly designed - unsafe, inaccessible, and inadequately equipped to meet the needs of all users, particularly the elderly, persons with disabilities, and women travelling with children. This study investigates how targeted design interventions can meaningfully improve safety and accessibility within Minna's public transportation hubs, drawing on empirical evidence gathered through a mixed-methods research approach. Structured questionnaires were administered to 166 respondents across three major terminals - Mobil Roundabout, Chanchaga Motor Park, and Maitumbi Terminal - complemented by field audits using lux meters and inclinometers, as well as in-depth interviews with transport stakeholders. The analytical framework was guided by the WHO Environmental Accessibility Audit Toolkit (2021), ISO 21542:2021 Building Accessibility Standards, and the Nigeria National Building Code (2024). Findings reveal pervasive deficiencies across all sites, including inadequate ramps and tactile paving, unsafe pedestrian–vehicle conflicts, insufficient lighting, poor wayfinding systems, and near-total exclusion of vulnerable users from design consideration. As many as 94% of respondents reported feeling unsafe after dark, while 68% indicated that existing facilities were not designed with vulnerable users in mind. In response to these findings, the study proposes a comprehensive redesign framework grounded in universal design principles - encompassing segregated pedestrian pathways, compliant ramp gradients, tactile guidance surfaces, CCTV-integrated lighting systems, and multilingual wayfinding provisions. Policy recommendations include the strengthened enforcement of national accessibility codes and the integration of participatory planning processes that bring diverse user groups into design decision-making. The framework advanced in this study is intended

not merely as a local intervention, but as a transferable model for upgrading informally evolved transport infrastructure across Nigerian and sub-Saharan African cities.

Keywords: Public transportation hub, Accessibility, Safety, Universal design, Minna, Inclusive urban design.

A DIMENSIONLESS HYDRO-MECHANICAL FRAMEWORK FOR SCREENING RAINFALL-INDUCED SHALLOW SLOPE INSTABILITY: ANALYTICAL THRESHOLDS AND PARAMETRIC SENSITIVITY

Ali Akbar Firoozi
School of Civil, Environmental Engineering and Geomatics, Faculty of Engineering and Built Environment, University of Botswana, Gaborone, Botswana

Ali Asghar Firoozi
Department of Civil Engineering, Faculty of Engineering, National University of Malaysia (UKM), Selangor, Malaysia

ABSTRACT

Rainfall-related instability of shallow soil slopes is governed by interactions among soil shear strength, slope geometry and pore-water pressure, yet screening decisions often rely on a single factor-of-safety estimate without quantifying the pressure threshold at which an initially stable slope becomes critical. This study develops and tests an explicitly dimensionless screening framework derived from the effective-stress infinite-slope formulation. A closed-form expression is obtained for the pore-pressure ratio corresponding to either limiting equilibrium or a selected screening safety level, and analytical derivatives quantify the influence of inclination, effective friction angle, effective cohesion, and prospective failure depth. A fully specified deterministic parameter grid comprising 7,056 scenarios is evaluated; all input ranges are illustrative, and no field or laboratory dataset is claimed. For a reference slope with inclination 26°, friction angle 34°, cohesion 3 kPa, unit weight 19 kN/m³, and vertical failure depth 1.5 m, the computed factor of safety is 1.304 at a normalized pore-pressure ratio of 0.25. The corresponding limiting-equilibrium pressure ratio is 0.470, whereas the ratio associated with a screening factor of safety of 1.30 is 0.253. Across the equally weighted screening grid, the fraction of combinations with a factor of safety below 1.00 increases from 3.57% at zero positive pore pressure to 60.15% at a pressure ratio of 0.60. These fractions describe the selected design space, not observed landslide frequencies or calibrated probabilities. The framework provides auditable threshold charts and intervention comparisons for preliminary engineering assessment, while explicitly identifying the need for site-specific hydraulic characterization, suction-aware analysis, and external stability checks before design use.

Keywords: Instability, Shallow Slope Stability, Effective Stress, Pore-Water Pressure, Parametric Analysis, Rainfall Infiltration.

INTRODUCTION

Shallow landslides commonly develop when the mobilized gravitational shear stress within a near-surface soil layer exceeds the available shear resistance. Rainfall can contribute to this transition through transient infiltration, redistribution of water, loss of matric suction and the

development of positive pore-water pressures. The relevant hydrological processes occur on timescales that depend on permeability, diffusivity, rainfall history and soil-layer thickness rather than on rainfall intensity alone. Iverson (2000) demonstrated the importance of transient pressure transmission for rainfall-triggered landsliding, while Rahardjo et al. (2007) examined the roles of soil properties, rainfall and geometric conditions in homogeneous slopes. These contributions establish that the pore-water-pressure state at the potential failure surface is a central mechanical variable, even when it is not the only process governing instability.

The state of the art now extends substantially beyond static limit-equilibrium calculations. Distributed rainfall-infiltration and stability procedures can connect changing hydraulic conditions to spatially varying factors of safety (Baum et al., 2008; Baum et al., 2010; Anagnostopoulos et al., 2015). Effective-stress approaches for variably saturated soils include suction-related resistance, while field-based investigations show how pressure head and water content can be related to the timing and depth of shallow failure (Lu et al., 2010; Godt et al., 2012; Bordoni et al., 2015). More recent syntheses highlight the importance of antecedent water storage and catchment-scale hydrological memory (Bogaard and Greco, 2018; Greco et al., 2023). Numerical hydro-mechanical studies also demonstrate that permeability, rainfall patterns and vegetation affect pressure development in ways that cannot be recovered from a single normalized pressure parameter (Liu et al., 2023; Guo et al., 2024).

Nevertheless, simplified analytical formulations retain value during the earliest stages of slope appraisal, when complete hydraulic and mechanical characterization may not yet be available. A preliminary model can determine whether a nominally stable section has little tolerance to increasing positive pore-water pressure, whether a reduction in inclination is more effective than a change in shear strength, and which measurements would materially reduce uncertainty. The risk arises when this screening function is confused with a site-specific prediction. A static pore-pressure ratio does not encode rainfall duration, preferential flow, soil-water characteristic behavior, hydraulic anisotropy, changing unit weight or the development of a perched water table. An analytical screening paper should therefore state what is calculated, what is assumed and what remains outside its domain.

The contribution of the present study is a transparent dimensionless reformulation of the classical infinite-slope criterion, followed by an exact threshold analysis and a reproducible multidimensional sensitivity assessment. The purpose is not to present a new constitutive relationship or to claim improved prediction accuracy against an unavailable field dataset. The specific objectives are to derive the pore-pressure limit associated with a user-selected factor of safety; investigate the coupled effects of inclination, effective-stress strength and failure depth; quantify how often sampled combinations cross screening thresholds within a defined parameter grid; and compare mechanically distinct hypothetical improvement measures under identical reference assumptions. The findings are intended for screening shallow translational mechanisms on a plane approximately parallel to the ground surface, not for predicting deep rotational failure or time-dependent rainfall response.

MATERIALS AND METHOD

Mechanical idealization and governing assumptions

A homogeneous soil mantle over a prospective planar slip surface is considered. The slope is sufficiently long relative to the layer thickness for end effects to be neglected, and the slip plane is assumed parallel to the ground surface. The vertical depth z is measured downward from the ground surface to the slip plane, not perpendicular to the ground surface. Effective cohesion c′ and effective friction angle φ′ are treated as fixed material properties for each trial, and γ denotes the bulk unit weight adopted in the stress calculation. The soil is represented as a constant-unit-weight layer, and the available shear resistance follows the effective-stress Mohr–Coulomb criterion. These assumptions deliberately exclude spatial stratification, progressive failure, hydraulic transients, tensile effects and reinforcement. Figure 1 illustrates the assumed geometry and direction of mobilized downslope shear.

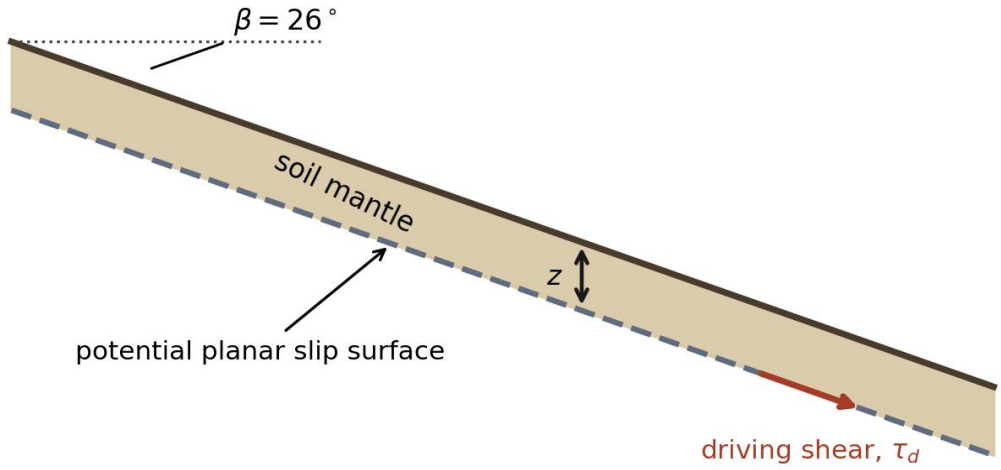


Figure 1. Infinite-slope schematic defining inclination, vertical failure depth, and mobilized downslope shear along a plane parallel to the ground surface.

For a soil column and a prospective failure surface parallel to the ground, the total normal and mobilized shear stresses follow the classical infinite-slope stress resolution. The notation is defined as follows: σ_n denotes the total normal stress on the slip plane (kPa); τ_d is the mobilized downslope shear stress (kPa); τ_f is the available shear resistance (kPa); u is the pore-water pressure at the potential slip surface (kPa); c′ is effective-stress cohesion (kPa); φ′ is the effective friction angle (degrees for reported inputs); β is ground-surface inclination (degrees for reported inputs); γ is bulk soil unit weight (kN/m³); and z is the vertical depth to the slip surface (m). One kilopascal equals 1 kN/m². All trigonometric operations are evaluated using angular arguments in radians, although angles are displayed in degrees for engineering readability.

$$\sigma_n = \gamma z \cos^2\beta \quad (1)$$

$$\tau_d = \gamma z \sin\beta \cos\beta \quad (2)$$

$$\tau_f = c' + (\sigma_n - u)\tan\phi' \quad (3)$$

The factor of safety F (dimensionless) is defined as available shear resistance divided by

mobilized shear stress at the prescribed slip plane. Substituting the stress relationships into the Mohr–Coulomb criterion produces Equation (4). Equation (5) introduces the nonnegative dimensionless pore-pressure ratio r_u, namely the positive pressure u divided by the total normal stress σ_n at that plane. Equation (6) is the resulting working equation. The cases F = 1.00, F > 1.00 and F < 1.00 respectively denote limiting equilibrium, a positive resistance margin and a calculated resistance deficit within the assumed mechanism. An additional F = 1.30 threshold is chosen only to illustrate engineering screening; it is not represented as a general code requirement. Negative r_u values and suction-dependent soil resistance lie outside this positive-pressure model.

$$F = \frac{c' + (\gamma z \cos^2\beta - u)\tan\phi'}{\gamma z \sin\beta \cos\beta} \quad (4)$$

$$r_u = \frac{u}{\gamma z \cos^2\beta} \quad (5)$$

$$F = \frac{c'}{\gamma z \sin\beta \cos\beta} + (1 - r_u)\frac{\tan\phi'}{\tan\beta} \quad (6)$$

Because r_u is the ratio of pore-water pressure to total normal stress, holding r_u fixed while changing inclination or vertical depth changes the corresponding physical pressure u. Each parameter-grid result therefore compares fixed normalized hydraulic conditions, rather than claiming the same pressure head for slopes of different geometry. For the range $0 \le r_u \le 0.60$ assessed in this study, calculated effective normal stress remains positive; extrapolation toward $r_u \ge 1$ would require particular care because zero or negative effective normal stress is incompatible with the present frictional contact idealization. Consequently, a slope-flattening intervention assessed at fixed r_u must be rechecked at the pressure head appropriate to the redesigned site.

Dimensionless cohesion and critical hydraulic state

The dimensionless cohesion number N_c in Equation (7) is defined as the ratio of effective cohesion c′ (kPa) to the overburden stress scale γz (kPa); it consequently has no unit. Equation (8) isolates this cohesion contribution from the geometric and frictional terms. Solving Equation (8) for the target factor of safety F_T (dimensionless) yields the critical pore-pressure ratio $r_u^*(F_T)$ in Equation (9), also dimensionless. A negative threshold means the target is already missed at r_u = 0; a threshold above the prescribed assessment interval means the target is not crossed within that interval. The expression assumes positive β and φ′ such that the denominators are nonzero. The calculated threshold is a mechanical pressure-state criterion, not a rainfall intensity, storm duration, or probability.

$$N_c = \frac{c'}{\gamma z} \quad (7)$$

$$F = \frac{N_c}{\sin\beta \cos\beta} + (1 - r_u)\frac{\tan\phi'}{\tan\beta} \quad (8)$$

$$r_u^*(F_T) = 1 + \frac{c'}{\gamma z \cos^2\beta \tan\phi'} - \frac{F_T \tan\beta}{\tan\phi'} \quad (9)$$

For F_T = 1.00, Equation (9) specifies the limiting-equilibrium pressure ratio; for F_T = 1.30 it specifies the illustrative screening-margin threshold. The same expression could be rearranged

for geometry or strength variables, but the dimensionless pressure ratio is particularly convenient for comparing a measured or simulated slip-plane pressure with the local total normal stress. Neither a critical pressure ratio nor an individual F value represents a calibrated probability of failure without site-specific probability distributions, parameter dependence, and hydraulic loading information.

Analytical sensitivity measures

Equations (10)–(14) provide the partial derivatives of dimensionless F with respect to r_u, c′, z, φ′, and β, respectively, holding the remaining inputs constant. The derivative $\partial F/\partial r_u$ is dimensionless per unit change in r_u; $\partial F/\partial c'$ has units kPa^{-1} when c′ is entered in kPa; $\partial F/\partial z$ has units m^{-1} when z is entered in metres. Both angular derivatives, $\partial F/\partial \varphi'$ and $\partial F/\partial \beta$, have units rad^{-1} because angles must be in radians for differentiation. To obtain the change per degree, multiply an angular derivative by π/180, where π is the mathematical constant pi. In Equations (13) and (14), sec(x) = 1/cos(x) and csc(x) = 1/sin(x); both are dimensionless trigonometric functions. The pressure and depth derivatives are negative for positive c′ and φ′, whereas the cohesion and friction-angle derivatives are positive for $r_u < 1$. The inclination derivative is negative within the investigated range. These relationships hold for the stipulated mechanical assumptions, not for arbitrary coupled variations of real site parameters.

$$\frac{\partial F}{\partial r_u} = -\frac{\tan\phi'}{\tan\beta} \quad (10)$$

$$\frac{\partial F}{\partial c'} = \frac{1}{\gamma z \sin\beta\cos\beta} \quad (11)$$

$$\frac{\partial F}{\partial z} = -\frac{c'}{\gamma z^2 \sin\beta\cos\beta} \quad (12)$$

$$\frac{\partial F}{\partial \phi'} = (1 - r_u)\frac{\sec^2\phi'}{\tan\beta} \quad (13)$$

$$\frac{\partial F}{\partial \beta} = -\frac{c'\cos(2\beta)}{\gamma z \sin^2\beta\cos^2\beta} - (1 - r_u)\tan\phi'\csc^2\beta \quad (14)$$

Reproducible parameter grid and numerical checks

The numerical study uses exclusively disclosed illustrative values; no borehole observations, measured pore-pressure records, rainfall histories, or laboratory shear tests were supplied or simulated as observations. The reference case takes β = 26°, φ′ = 34°, c′ = 3 kPa, γ = 19 kN/m³ and z = 1.50 m, with r_u = 0.25 as the initial normalized hydraulic state. Table 1 specifies the reference inputs, tested levels, and corresponding units. These ranges are deliberately chosen mathematical scenarios rather than reported statistics for a particular soil or location. All sampled grid combinations are counted equally; no probability distribution is fitted.

Table 1. Assumed reference conditions and numerical parameter-grid domains, with units given for each input.

Input parameter	Reference	Discrete grid/interval	Unit
Slope inclination, β	26	15–35 in increments of 1	degrees
Effective friction angle, φ′	34	28–40 in increments of 2	degrees
Effective cohesion, c′	3	0, 2, 4, 6	kPa
Bulk unit weight, γ	19	19 (fixed in grid)	kN/m³

Input parameter	Reference	Discrete grid/interval	Unit
Vertical failure depth, z	1.50	0.75, 1.50, 2.25	m
Pore-pressure ratio, r_u	0.25	0.00, 0.20, 0.40, 0.60	dimensionless
Screening threshold, F_T	1.30	1.00 and 1.30	dimensionless

The factorial grid includes 21 inclinations, 7 friction angles, 4 cohesion levels, 3 slip depths and 4 pore-pressure ratios, giving 21 × 7 × 4 × 3 × 4 = 7,056 individual combinations. At any one pore-pressure level, 1,764 combinations are evaluated. For each combination, F is calculated from Equation (6) and classified according to F < 1.00 and F < 1.30. The reported fraction is the number of classified combinations divided by 1,764; it is a descriptive property of the chosen numerical design grid. A real failure probability would require site-calibrated parameter distributions, hydraulic time histories, correlation structure, and a suitable reliability or inverse framework of the type discussed by Jiang et al. (2024). This distinction prevents an engineered scenario enumeration from being misrepresented as observational evidence.

Three independent checks support reproducibility. Algebraic substitution of Equation (5) into Equation (4) reproduces Equation (6). Substituting the pressure ratio obtained from Equation (9) into Equation (6) recovers the requested F_T to machine precision. Finally, centered finite differences around the reference state were compared with the exact pressure and cohesion derivatives: the computed derivatives are −1.38295 per unit r_u and +0.08905 kPa^{-1}, respectively. Finite differences with increments of 0.0001 for r_u and 0.001 kPa for c′ agree to the displayed precision. These checks establish numerical consistency, not empirical validation. All plotted curves and tabulated values follow directly from the declared equations. Alternative-measure calculations compare isolated changes against an initial wet condition of r_u = 0.45; one combined change is included.

RESULTS AND DISCUSSION

Reference condition and pressure threshold

For the stated reference condition, the calculated factor of safety is F = 1.650 at r_u = 0 and F = 1.304 at r_u = 0.25. The frictional coefficient tan(34°)/tan(26°) equals 1.383, whereas the cohesive term c′/[γz sin(26°) cos(26°)] equals 0.267. At fixed reference geometry and strength, the resulting linear relationship is F = 1.650 − 1.383r_u (rounded coefficients). Equation (9) gives a limiting-equilibrium ratio of 0.470 at F_T = 1.00 and a screening threshold of 0.253 at F_T = 1.30. The reference r_u = 0.25 state therefore lies only slightly above the screening threshold, even though the computed F remains above unity. A slope can have positive resistance relative to limiting equilibrium while possessing little reserve under an independently chosen screening margin.

Increasing r_u from 0.25 to 0.45 lowers F from 1.304 to 1.028; at r_u = 0.60, F decreases to 0.820. These are comparisons of stipulated pressure states rather than of specified rainfall intensities or durations. A relationship between rainfall and the pressure ratio would require hydraulic characterization or direct measurement (Iverson, 2000; Godt et al., 2012). Table 2 tabulates the selected pressure cases, and Figure 2 compares their continuous response across

four slope inclinations at fixed soil properties and depth.

Table 2. Calculated reference-slope factor of safety at six specified dimensionless pore-pressure ratios and two screening levels.

Pore-pressure ratio r_u	**Factor of safety F**	**Relation to F = 1.00**	**Relation to F = 1.30**
0.00	1.650	Above	Above
0.15	1.443	Above	Above
0.25	1.304	Above	Above
0.35	1.166	Above	Below
0.45	1.028	Above	Below
0.60	0.820	Below	Below

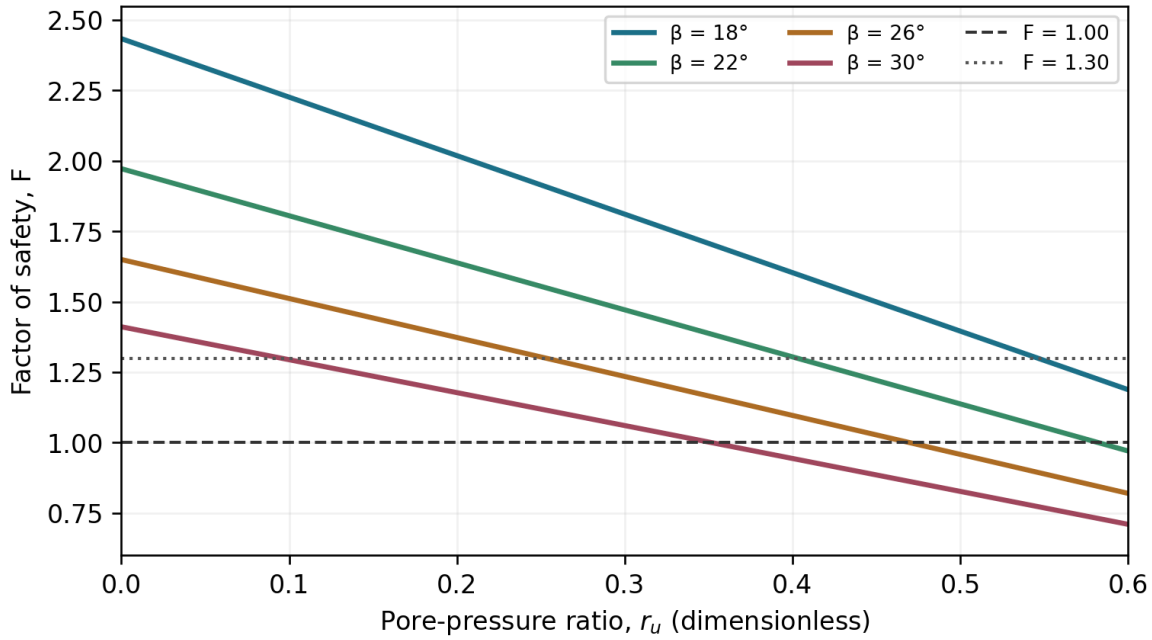


Figure 2. Decline in calculated factor of safety with increasing normalized pore pressure for four illustrative slope inclinations, holding φ′ = 34°, c′ = 3 kPa, γ = 19 kN/m³ and z = 1.50 m fixed.

Figure 2 illustrates how slope geometry changes the magnitude of pressure sensitivity. At β = 18°, F equals 1.500 for r_u = 0.45; at β = 30°, F falls to 0.886 at the identical dimensionless pressure ratio. The derivative magnitude tanφ′/tanβ is approximately 2.08 at 18° and 1.17 at 30°. A shallower slope thus has a larger absolute change in F per unit r_u under this normalization but also begins from a greater safety margin. Sensitivity magnitude alone must not be equated with susceptibility. The steeper slope crosses F = 1.00 at a smaller r_u because of its reduced initial resistance margin. The example distinguishes baseline stability from incremental hydraulic sensitivity.

Critical ratio mapping across cohesion and inclination

Figure 3 traces the limiting-equilibrium pressure ratio over β = 15°–35° for c′ = 0, 3 and 6 kPa at the other reference conditions. In this domain, the pressure threshold decreases monotonically as inclination increases. At c′ = 3 kPa, raising β from 18° to 34° reduces the critical ratio from 0.691 to 0.227. At β = 26°, increasing cohesion from 0 to 3 and 6 kPa raises the corresponding ratio from 0.277 to 0.470 and 0.663, respectively. These are algebraic consequences of Equation (9), not evidence that measured strength intercepts remain constant

during wetting. In particular, apparent cohesion caused by matric suction or weak bonding may not persist as pore pressure rises.

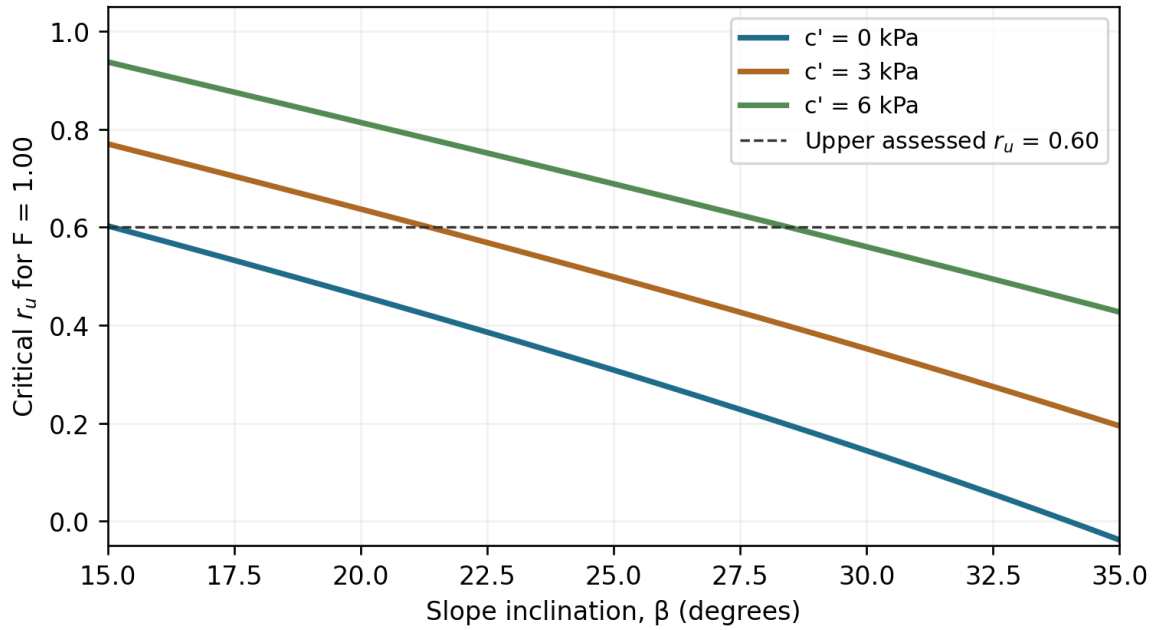


Figure 3. Limiting-equilibrium pressure threshold versus slope inclination for three assumed effective cohesion intercepts; all other model parameters retain their reference values.

The cohesion effect is strongest where c′ is a defensible effective-strength parameter measured for the governing stress and drainage conditions. If a frictional soil has negligible true effective cohesion, adopting a fitted positive intercept from a small set of shear tests without verifying its persistence can produce an optimistic threshold. Similarly, a shallow apparent rupture depth increases the dimensionless cohesion number because the same cohesion is compared against a smaller overburden stress; it does not imply that all near-surface failures are more stable in practice. Vegetation, desiccation, discontinuities, layering and progressive softening can all alter the shallow failure process in ways not represented in the homogeneous model. The appropriate use of Figure 3 is to identify which assumptions require confirmation, rather than to extrapolate a material property from a generic chart.

Combined inclination–pressure response

Figure 4 depicts the combined β–r_u dependence of F at the reference effective strength, unit weight, and depth. Curved contour lines mark F = 1.00 and F = 1.30, reflecting geometric contributions to both cohesive and frictional stresses. The point (β = 26°, r_u = 0.25) falls close to the F = 1.30 contour, in agreement with the computed 1.304. At β = 30° and r_u = 0.25 the factor of safety is 1.119, between the two thresholds; at β = 34° and the same ratio it is 0.977, below unity. Thus the combined-response diagram separates conditions with a mathematical resistance deficit from cases that merely fall below a chosen screening margin. No geographical failure assessment is implied.

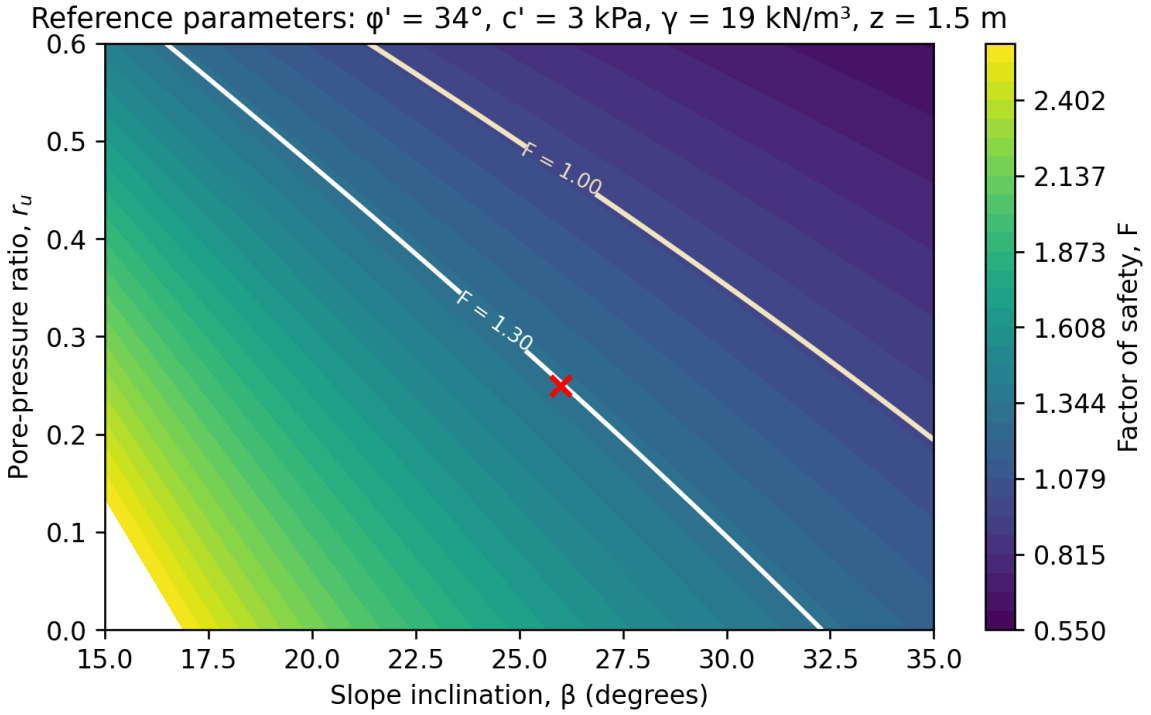


Figure 4. Computed factor-of-safety contours in the inclination–pore-pressure plane for φ′ = 34°, c′ = 3 kPa, γ = 19 kN/m³ and z = 1.50 m; the cross identifies β = 26° and r_u = 0.25.

From a practical screening perspective, the contour geometry can support a sequence of questions. An observed slope may be checked against the geometry and the most defensible available strength parameters; a monitored positive pressure can then be normalized to the actual total normal stress at the hypothesized slip plane. An exceedance of the selected threshold indicates the need for a more detailed appraisal but does not, by itself, predict a landslide. Conversely, a nominally adequate F is not a guarantee of safety where the assumed plane is incorrect or other mechanisms dominate. The full hydrological response must be established through site observations or transient numerical analysis before a pressure trajectory can be forecast. More sophisticated approaches explicitly simulate unsaturated water movement and hydrological feedbacks (Greco et al., 2023; Liu et al., 2023; Guo et al., 2024).

Discrete grid statistics and meaning of the reported fractions

Table 3 enumerates the 7,056 factorial scenarios, divided into 1,764 cases at each of four pressure ratios. At r_u = 0, 63 cases have F < 1.00 (3.57%), increasing to 13.44%, 32.88% and 60.15% at r_u = 0.20, 0.40 and 0.60. The corresponding fractions below F = 1.30 are 18.31%, 35.66%, 57.82% and 79.65%. The trend follows from the negative pressure derivative in Equation (10) for fixed geometry and material properties. These values are counting fractions of a constructed mathematical grid and must not be reported as frequencies of observed landslides or calibrated probabilities of failure. A different grid density, domain or joint parameter distribution would generally change the fractions.

Table 3. Equal-weight classification of 1,764 trial combinations at each of four normalized pressure levels (7,056 cases overall; not failure probabilities).

Pore-pressure ratio	Cases	F < 1.00: cases	F < 1.00: share	F < 1.30: cases	F < 1.30: share	Median F
0.00	1764	63	3.57%	323	18.31%	1.797
0.20	1764	237	13.44%	629	35.66%	1.494
0.40	1764	580	32.88%	1020	57.82%	1.195
0.60	1764	1061	60.15%	1405	79.65%	0.887

The median factor of safety shifts from 1.797 at r_u = 0 to 0.887 at r_u = 0.60. A median is appropriate here only as a compact descriptor of the enumerated mathematical scenarios; it cannot be treated as a measured median property of a geological formation. The results show that a threshold map evaluated over an explicitly documented domain conveys more information than an isolated baseline case. However, the domain remains a modeling choice, and the equal-weight rule has no observational justification. For actual slopes, variability in shear strength, pore-water pressure and geometry is not generally uniform or independent. Jiang et al. (2024) demonstrate that multi-source field and monitoring information can be used within a probabilistic back-analysis framework to improve estimation of uncertain geotechnical parameters. Such calibration is outside the present contribution and should not be inferred from the numerical grid.

Comparative implications of hypothetical remedial measures

An intentionally unfavorable reference state is defined by increasing r_u to 0.45 while retaining β = 26°, φ′ = 34°, c′ = 3 kPa, γ = 19 kN/m³ and z = 1.50 m. Its factor of safety is 1.028. Table 4 contrasts five hypothetical alternatives: reducing r_u to 0.15 as a notional drainage benefit; flattening β to 20°; increasing φ′ to 38°; increasing c′ to 5 kPa; and jointly reducing r_u to 0.15 and β to 20°. These interventions are mathematical tests, not demonstrations that any specific drainage, excavation, or stabilization treatment can achieve the stipulated changes. No site-based cost, constructability, durability or environmental claims are made.

Table 4. Calculated factor-of-safety changes for five assumed modifications relative to the reference wet state (r_u = 0.45).

Trial condition	Changed input(s)	Computed F	Change from 1.028
Unmodified wet state	r_u = 0.45	1.028	—
Lower positive pressure	r_u = 0.15	1.443	+0.415
Flatter inclination	β = 20°	1.347	+0.319
Higher effective friction	φ′ = 38°	1.148	+0.120
Higher effective cohesion	c′ = 5 kPa	1.206	+0.178
Combined modification	r_u = 0.15; β = 20°	1.903	+0.875

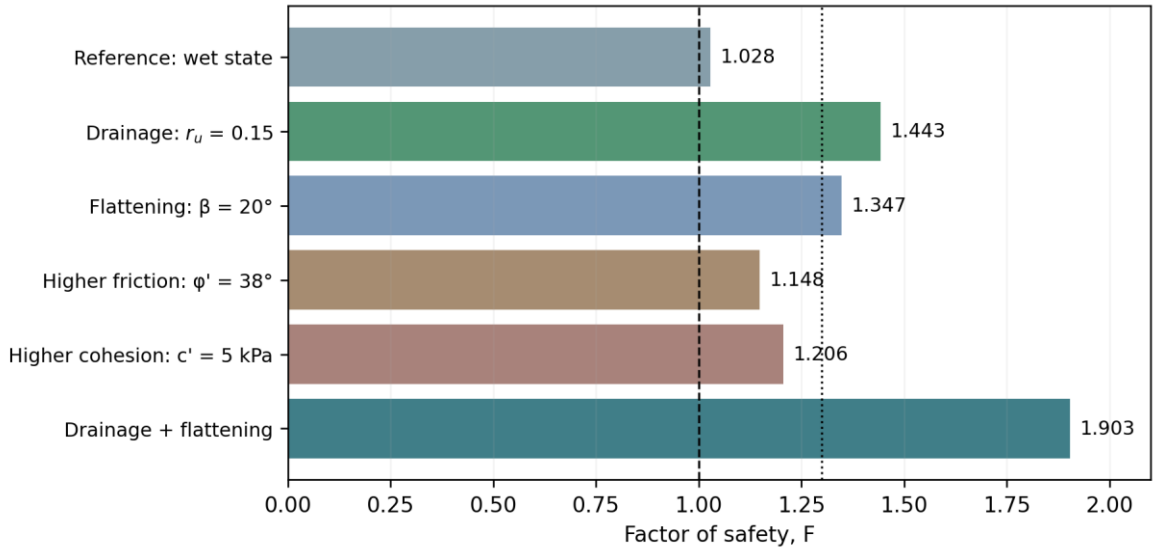


Figure 5. Comparison of idealized drainage, slope-flattening and shear-strength changes with the reference wet state; vertical markers show F = 1.00 and F = 1.30.

Figure 5 juxtaposes the six calculated states against the two screening levels. The idealized pressure reduction yields F = 1.443, while flattening alone gives F = 1.347. The friction-angle change gives F = 1.148 and the cohesion change gives F = 1.206; neither reaches the illustrative screening value of 1.30 under its separate assumed modification. Simultaneous drainage and flattening gives F = 1.903. No ranking of real construction options follows from these values: drainage performance requires hydraulic feasibility and maintenance assessment, flattening depends on property boundaries and excavation stability, and strength increases must be demonstrated through suitable tests. The calculations nonetheless illustrate how analytical screening identifies promising parameter directions without claiming that any one intervention is sufficient. Because r_u is normalized, the flattening case should also be reassessed at a physically consistent pressure head before detailed design.

Scope, limitations and requirements for engineering application

The framework does not compute infiltration or the time needed to reach a critical pressure. Soil suction and associated suction stress are not represented by a negative extrapolation of r_u, because unsaturated effective-stress formulations require additional hydraulic state variables or experimentally characterized suction functions. Lu et al. (2010) provide a theoretical basis for representing suction stress, and Godt et al. (2012) demonstrate its relevance to variably saturated infinite-slope analysis. Consequently, when the starting state is unsaturated and the anticipated failure process involves suction loss before positive pressures develop, the present method should be viewed as a positive-pressure phase screen rather than a full hydro-mechanical simulator. Its role is narrower than coupled infiltration–deformation approaches (Liu et al., 2023) or models resolving vegetation-dependent hydraulic response (Guo et al., 2024).

Potential additional errors arise from the assumption of a prescribed planar slip surface, the neglect of layered soil, root cohesion and reinforcement, fixed density during wetting,

constant effective-strength parameters, and the exclusion of earthquake actions, erosion, toe unloading or three-dimensional confinement. The threshold method does not address progressive failure, strain softening, localized seepage gradients or the connectivity of subsurface flow pathways. Rainfall history is also not an input, even though antecedent conditions often control how the same storm translates into pore-pressure response (Bogaard and Greco, 2018; Greco et al., 2023). These are not minor caveats: using a calculated F as the sole basis for design would require evidence that the assumed mechanism and input stresses are representative, together with checking alternative failure modes and the applicable project-specific design criteria.

For a site-specific extension, the first priority would be a defensible geotechnical section with surveyed slope geometry, stratigraphy, unit-weight measurements and effective-stress shear-strength tests. The slip-depth range should follow geological evidence rather than convenience. Positive pressure conditions should be constrained using instruments or a calibrated seepage model, including rainfall boundary conditions, hydraulic conductivity functions, and antecedent moisture. Site data could then be substituted into the same analytical threshold equation as a transparent first check before performing transient seepage, limit equilibrium, finite-element, or reliability analysis as warranted. A monitored normalized pressure approaching a calculated threshold could help define an investigation trigger, but use in an operational early-warning system would require independent calibration and verification against actual slope behavior.

CONCLUSION

A dimensionless and auditable infinite-slope screening formulation has been developed for shallow translational mechanisms subject to positive pore-water pressure. The principal analytical result is a closed-form expression for the normalized critical pore-water pressure corresponding to any explicitly chosen factor-of-safety level. The associated derivatives distinguish the contributions of slope inclination, friction, cohesion, depth, and hydraulic state, while avoiding reliance on unverified numerical fitting. For the fully disclosed illustrative reference condition, F equals 1.304 at r_u = 0.25; the limiting-equilibrium critical ratio is 0.470, and the ratio for the selected 1.30 screening level is 0.253. These findings are reproducible consequences of the reported input set and should not be generalized to a geographical location or a particular soil without site evidence.

The 7,056-point factorial analysis shows that the share of uniformly enumerated design combinations with F below unity rises from 3.57% to 60.15% as r_u increases from 0 to 0.60. This is a change in an illustrative mathematical design space rather than a change in the measured occurrence probability of landslides. Analytical charts demonstrate that cohesion and inclination jointly determine the tolerable pressure state, and hypothetical improvement calculations illustrate the separate effect of lowering pore pressure, flattening geometry, or increasing effective strength. The principal engineering implication is that preliminary decisions should be framed around transparent thresholds and explicitly uncertain inputs instead of relying on a single unexplained factor of safety. Application to actual projects

requires site-specific investigation, verification of the assumed slip mechanism, suction-aware or transient seepage modeling where relevant, and confirmation against applicable design criteria.

REFERENCES

Anagnostopoulos, G. G., Fatichi, S. and Burlando, P. (2015). An advanced process-based distributed model for the investigation of rainfall-induced landslides: The effect of process representation and boundary conditions. Water Resources Research, 51, 7501–7523. https://doi.org/10.1002/2015WR016909

Baum, R. L., Savage, W. Z. and Godt, J. W. (2008). TRIGRS: A Fortran program for transient rainfall infiltration and grid-based regional slope-stability analysis, Version 2.0. U.S. Geological Survey Open-File Report 2008-1159. https://doi.org/10.3133/ofr20081159

Baum, R. L., Godt, J. W. and Savage, W. Z. (2010). Estimating the timing and location of shallow rainfall-induced landslides using a model for transient, unsaturated infiltration. Journal of Geophysical Research: Earth Surface, 115(F3), F03013. https://doi.org/10.1029/2009JF001321

Bogaard, T. and Greco, R. (2018). Invited perspectives: Hydrological perspectives on precipitation intensity-duration thresholds for landslide initiation: Proposing hydro-meteorological thresholds. Natural Hazards and Earth System Sciences, 18, 31–39. https://doi.org/10.5194/nhess-18-31-2018

Bordoni, M., Meisina, C., Valentino, R., Lu, N., Bittelli, M. and Chersich, S. (2015). Hydrological factors affecting rainfall-induced shallow landslides: From the field monitoring to a simplified slope stability analysis. Engineering Geology, 193, 19–37. https://doi.org/10.1016/j.enggeo.2015.04.006

Godt, J. W., Şener-Kaya, B., Lu, N. and Baum, R. L. (2012). Stability of infinite slopes under transient partially saturated seepage conditions. Water Resources Research, 48(5), W05505. https://doi.org/10.1029/2011WR011408

Greco, R., Marino, P. and Bogaard, T. A. (2023). Recent advancements of landslide hydrology. WIREs Water, 10(6), e1675. https://doi.org/10.1002/wat2.1675

Guo, H., Ng, C. W. W. and Zhang, Q. (2024). Three-dimensional numerical analysis of plant-soil hydraulic interactions on pore water pressure of vegetated slope under different rainfall patterns. Journal of Rock Mechanics and Geotechnical Engineering, 16(9), 3696–3706. https://doi.org/10.1016/j.jrmge.2023.09.032

Iverson, R. M. (2000). Landslide triggering by rain infiltration. Water Resources Research, 36(7), 1897–1910. https://doi.org/10.1029/2000WR900090

Jiang, S.-H., Jie, H.-H., Xie, J., Huang, J. and Zhou, C.-B. (2024). Probabilistic back-analysis of rainfall-induced landslides for slope reliability prediction with multi-source information. Journal of Rock Mechanics and Geotechnical Engineering, 16(9), 3575–3594. https://doi.org/10.1016/j.jrmge.2024.02.008

Liu, C., Yan, Y. and Yang, H.-Q. (2023). Numerical modeling of small-scale unsaturated soil

slope subjected to transient rainfall. Geosystems and Geoenvironment, 2(4), 100193. https://doi.org/10.1016/j.geogeo.2023.100193

Lu, N., Godt, J. W. and Wu, D. T. (2010). A closed-form equation for effective stress in unsaturated soil. Water Resources Research, 46(5), W05515. https://doi.org/10.1029/2009WR008646

Rahardjo, H., Ong, T. H., Rezaur, R. B. and Leong, E. C. (2007). Factors controlling instability of homogeneous soil slopes under rainfall. Journal of Geotechnical and Geoenvironmental Engineering, 133(12), 1532–1543. https://doi.org/10.1061/(ASCE)1090-0241(2007)133:12(1532)

TRANSIENT WETTING AND REPEATED MOISTURE PULSES IN EXPANSIVE SUBGRADES: A DIMENSIONLESS SCREENING FRAMEWORK FOR VERTICAL HEAVE

Ali Akbar Firoozi
School of Civil, Environmental Engineering and Geomatics, Faculty of Engineering and Built Environment, University of Botswana, Gaborone, Botswana

Ali Asghar Firoozi
Department of Civil Engineering, Faculty of Engineering, National University of Malaysia (UKM), Selangor, Malaysia

ABSTRACT

Moisture-driven volume change in expansive soil can cause differential subgrade movement, yet preliminary screening frequently considers swelling potential without representing the duration and sequence of wetting. This paper develops a transparent one-dimensional analytical screening framework linking a prescribed surface moisture perturbation to vertical heave in an expansive active layer. Linear moisture diffusion in a semi-infinite porous domain is coupled to a depth-integrated, mobilized swelling-strain relation. A closed-form dimensionless response is derived for persistent wetting, then superposition is used to evaluate finite-duration moisture pulses and repeated seasonal idealizations. Analytical elasticities quantify how the influence of effective moisture diffusivity and active-layer thickness changes with exposure time. For a hypothetical 1.50 m active layer, effective diffusivity of 2.0×10^{-8} m²/s, volumetric moisture increase of 0.08, strain coefficient of 0.45 and mobilization factor of 0.70, the calculated asymptotic heave is 37.80 mm and the one-year value is 20.19 mm. A single 90-day wetting pulse produces a maximum of 11.18 mm, whereas the five successive 90-day annual pulses result in fifth-cycle maximum of 13.94 mm because some modeled moisture response persists between pulses. The prescribed 20 mm screening threshold is reached after 354.5 days under permanent wetting, but not within the examined five-year periodic-pulse scenario. These outputs are calculated consequences of explicitly assumed coefficients, not measured movements, calibrated site forecasts or evidence of constitutive reversibility. The framework is intended for sensitivity interpretation and screening; geotechnical design requires material-specific testing, nonlinear hydro-mechanical modeling where appropriate, and independent field validation.

Keywords: Expansive Soil; Moisture Diffusion; Subgrade Heave; Wetting–Drying Pulses; Active Layer; Dimensionless Sensitivity

INTRODUCTION

Expansive soils create persistent challenges for lightly loaded structures, pavement subgrades and shallow foundations because changes in pore-water condition can cause significant and

spatially variable volume change. Differential vertical movement is often more disruptive than uniform displacement: a road pavement or ground-bearing slab may tolerate moderate overall uplift yet suffer distress when adjacent portions of the supporting clay are wetted at different rates. Evaluating this behavior requires more than classifying a soil by plasticity or obtaining an isolated laboratory swell measurement. Moisture migration, restraint, wetting history and the depth over which expansivity is mobilized all contribute to the deformation path (Nelson et al., 2015; Fredlund et al., 2012).

Mechanistic treatments of unsaturated flow commonly use constitutive functions for soil-water retention and hydraulic conductivity, together with coupled deformation laws. Richards (1931) provided the foundation for describing capillary moisture transport through unsaturated porous media, while Alonso et al. (1999) demonstrated why expansive clay behavior involves interacting microstructural and macrostructural processes. Such approaches are necessary when accurate predictions are required, particularly for changing suction, hysteresis, crack-induced preferential flow and plastic deformation. At an earlier design stage, however, site-specific soil-water characteristic curves and suction-dependent mechanical parameters may be unavailable. A deliberately reduced formulation can then be valuable, provided that assumptions and inference boundaries are explicit.

Recent evidence underscores the importance of wetting history. Abbas et al. (2023) reported experimental variation of swell pressure, hydraulic conductivity and volume-change behavior with repeated wetting and drying under different mechanical boundary conditions. Oliveira and Cavalcante (2024) documented how successive cycles affect free swelling and swelling pressure in a highly expansive clay. Yu et al. (2024) developed a model for evolving soil-water retention curves during repeated cycles, highlighting changes that cannot be captured by a history-independent linear constitutive relation. These studies do not validate the linear surrogate used here; rather, they motivate a clear separation between transport-driven timing effects and constitutive changes that require additional measurements.

The purpose of the present study is to formulate and examine a narrow but reproducible question: for a prescribed surface change in volumetric water content, how do the active-layer depth, effective diffusivity and wetting duration affect the timing and magnitude of mobilized upward deformation? The study derives a closed-form response for sustained wetting, obtains logarithmic sensitivities, formulates finite and repeated moisture pulses by superposition, and evaluates a simple heave-threshold indicator. All numerical inputs are hypothetical. The contribution lies in combining established diffusion mathematics with an explicit active-layer heave functional, sensitivity identities and transparent exposure schedules; no new experimental law or field calibration is claimed.

MATERIALS AND METHOD

Physical idealization, domain and boundary conditions

An initially uniform soil profile is idealized as a homogeneous one-dimensional medium with a horizontal surface at zero depth and a vertical coordinate increasing downward. Moisture perturbations propagate according to a constant effective diffusivity, and lateral flow is

neglected. An expansive layer extends from the surface to a depth of 1.50 m in the reference example, below which the moisture field may continue but no additional heave strain is counted. This construction distinguishes an active depth for deformation from a hydraulic impermeable boundary: the lower end of the active layer is not a zero-flow boundary, and the diffusion solution is valid in a semi-infinite medium. Changes in groundwater table, roots, cracks, overland runoff, rainfall intensity, evaporation and transport hysteresis are not directly modeled.

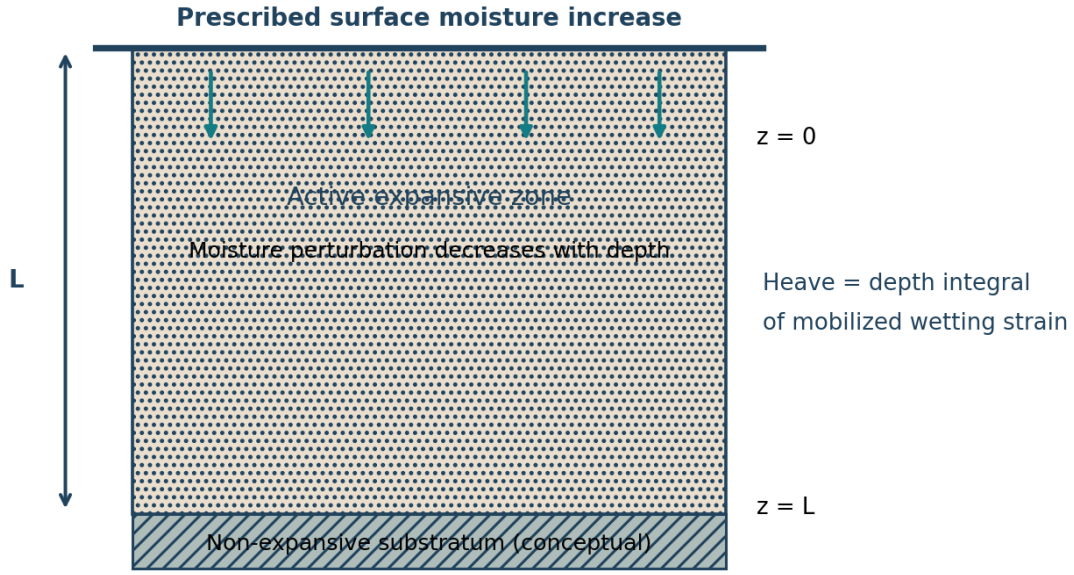


Figure 1. The conceptual soil profile identifies the imposed surface moisture increment, the deformation-active depth and the depth-integrated upward heave.

A surface step is represented by an immediate and sustained increase in volumetric water content. Its use represents a prescribed boundary condition and should not be interpreted as a rainfall depth, infiltration flux or time-resolved climatic forecast. A finite wetting episode is subsequently represented by a positive step followed by an equal negative step at the end of a prescribed duration. Periodic episodes are represented by a train of such step pairs. Because the mathematical diffusion equation is linear, superposition can be performed exactly within the idealized transport model; the resulting mechanical reversibility is an additional assumption rather than an observed property of expansive soil.

Table 1. The hypothetical baseline specifies the physical interpretation, assumed magnitude and units of each moisture–heave input.

Parameter	**Physical meaning**	**Assumed value**	**Reporting unit**
Active depth, L	Thickness of soil counted in vertical heave	1.50	m
Diffusivity, D_θ	Linearized moisture-diffusion coefficient	2.0×10^{-8}	m^2/s
Initial water content, θ_i	Uniform initial moisture content	Not needed separately	m^3/m^3

Parameter	Physical meaning	Assumed value	Reporting unit
Surface moisture increment, $\Delta\theta$	Prescribed change in volumetric content	0.08	m^3/m^3
Moisture–strain coefficient, α_θ	Axial strain per unit volumetric moisture change	0.45	dimensionless
Mobilization factor, λ	Uniform scalar reduction for restraint	0.70	dimensionless
Initial wetting duration, T_w	Length of one prescribed surface pulse	90	days
Repeat period, P	Interval between successive pulse onsets	365	days
Heave limit, $h_{\lim}$	Example screening magnitude only	20	mm
Analysis horizon	Comparison interval for periodic pulses	5	years

Linearized moisture diffusion and exact step response

All notation follows SI conventions. The coordinate z is downward depth (m), t is elapsed time (s), $\theta(z,t)$ is volumetric water content (m^3/m^3), θ_i is its initial value (m^3/m^3), $\Delta\theta$ is the prescribed positive surface increment (m^3/m^3), and D_θ is the constant effective moisture diffusivity (m^2/s). The normalized response χ and the complementary error function erfc are dimensionless, as are the integration arguments u and s. The physical initial state must satisfy $0 \le \theta_i \le 1 - \Delta\theta$.

Let volumetric water content be expressed as cubic metres of pore water per cubic metre of bulk soil and let elapsed time be measured in seconds. The diffusion coefficient is an effective, assumed constant with units of square metres per second; it is not identical to saturated hydraulic conductivity. The one-dimensional moisture-balance surrogate is written as follows.

$$\frac{\partial\theta}{\partial t} = D_\theta \frac{\partial^2\theta}{\partial z^2} \quad (1)$$

The depth coordinate is in metres; the time coordinate is in seconds; the initial water content and subsequent water content are dimensionless volume ratios. For an initially uniform profile, the moisture field satisfies the initial condition in Equation (2) and the constant step boundary in Equation (3). The surface increment is positive under wetting. The semi-infinite lower condition requires the perturbation to vanish with depth at finite time.

$$\theta(z,0) = \theta_i \quad (z > 0) \quad (2)$$

$$\theta(0,t) = \theta_i + \Delta\theta \quad (t > 0) \quad (3)$$

Normalizing the moisture increment by its prescribed surface amplitude defines a dimensionless response in Equation (4). The classical semi-infinite diffusion solution for a constant surface condition is expressed by the complementary error function in Equation (5), which is defined mathematically in Equation (6) (Crank, 1975). The error-function integration variable is dimensionless; the initial and boundary assumptions make the normalized response range from zero to unity.

$$\chi(z,t) = \frac{\theta(z,t) - \theta_i}{\Delta\theta} \quad (4)$$

$$\chi(z,t) = \operatorname{erfc}\left(\frac{z}{2\sqrt{D_\theta t}}\right) \quad (5)$$

$$\operatorname{erfc}(u) = \frac{2}{\sqrt{\pi}} \int_u^\infty \exp(-s^2)\, ds \quad (6)$$

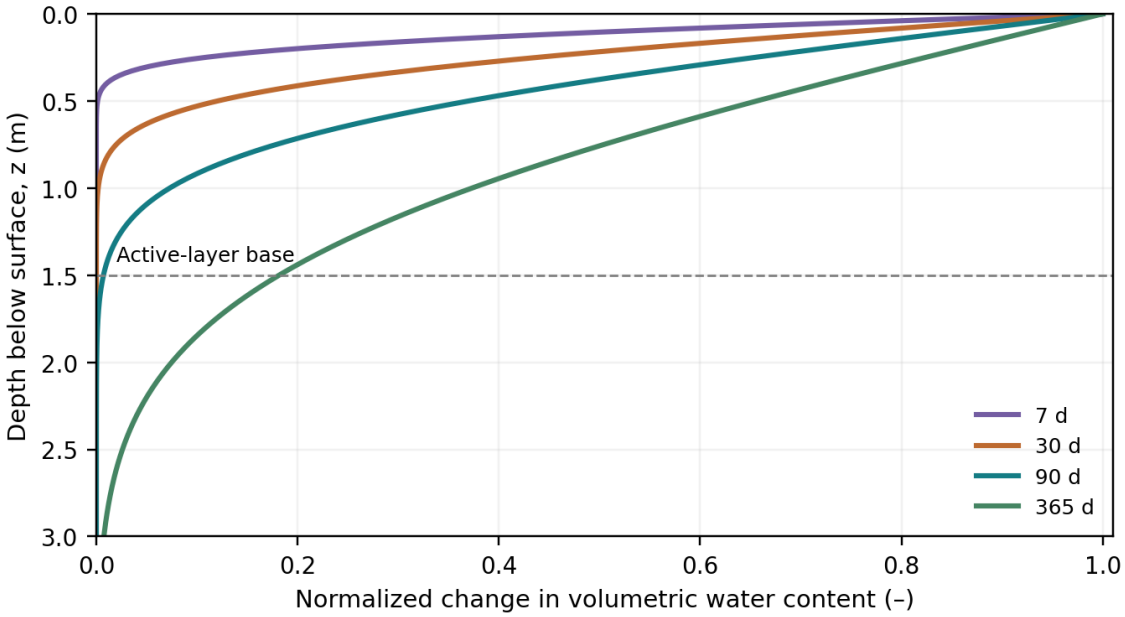


Figure 2. Normalized moisture profiles trace the diffusive response after 7, 30, 90 and 365 days; the dashed horizontal line marks the active-layer base, not a hydraulic boundary.

Moisture-induced strain and active-layer heave

In the heave functional, $\varepsilon_v(z,t)$ is the upward-positive vertical strain (m/m); α_θ is the dimensionless wetting-strain coefficient (m/m per unit volumetric water-content change); and λ is a dimensionless mobilization factor between zero and one. The active depth L and displacement $h(t)$ have units of metres, while the asymptotic displacement h_∞ also has units of metres. The strain coefficient and mobilization factor are assumed rather than experimentally calibrated.

The model assumes that mobilized vertical wetting strain at each depth is proportional to the local increase in volumetric water content. A dimensionless swelling coefficient gives strain per unit moisture change, while a separate dimensionless factor between zero and unity represents a uniform phenomenological reduction associated with restraint or imperfect mobilization. This separation is intended only for sensitivity study. The factor is not derived from stress-dependent swelling pressure and must not replace controlled-suction or oedometer assessment.

$$\varepsilon_v(z,t) = \lambda \alpha_\theta [\theta(z,t) - \theta_i] \quad (7)$$

Vertical heave is defined as the upward-positive depth integral of axial strain across the expansive layer. The resulting displacement is measured in metres when depth is in metres and strain is dimensionless. Equations (8)–(10) provide, respectively, the heave integral, its asymptotic sustained-wetting limit and the closed-form transient expression obtained by integrating the complementary error-function profile over the active layer.

$$h(t) = \int_0^L \varepsilon_v(z,t)\,\mathrm{d}z \quad (8)$$

$$h_\infty = \lambda \alpha_\theta \Delta\theta L \quad (9)$$

$$h(t) = \lambda \alpha_\theta \Delta\theta \left[L\,\mathrm{erfc}\left(\frac{L}{2\sqrt{D_\theta t}}\right) + 2\sqrt{\frac{D_\theta t}{\pi}}\left(1 - \exp\left(-\frac{L^2}{4D_\theta t}\right)\right)\right] \quad (10)$$

The asymptotic value is a mathematical limit for a permanently imposed boundary perturbation and a constant strain coefficient. It does not incorporate hydro-mechanical yielding, cracking, chemical interactions or a physical upper bound imposed by a structural restraint. An infinitely deep diffusive domain combined with a finite expansive depth is therefore a deliberate mathematical construction rather than a physical claim that the full ground profile is homogeneous.

Dimensionless response, analytic sensitivities and limiting behavior

The scaled time τ and response $F(\tau)$ are dimensionless; $F'(\tau)$ denotes their derivative with respect to τ and is likewise dimensionless. The sensitivities S_D and S_L describe changes in h due to proportional changes in D_θ and L, respectively, and have no units. The function $\ln$ denotes a natural logarithm. In the limiting relationships, p is an arbitrary dimensionless fraction strictly between zero and one, z_p is the corresponding iso-response depth (m), and erfc^{-1} denotes the inverse complementary error function.

Scaling time by the diffusive passage time across the active layer produces the dimensionless time in Equation (11). The normalized heave is then a single universal function of this parameter, specified in Equations (12) and (13). These relationships remove the numerical amplitude parameters from the shape of the response, allowing comparisons of different active depths and effective diffusivities without choosing another arbitrary reference water-content increment.

$$\tau = \frac{D_\theta t}{L^2} \quad (11)$$

$$F(\tau) = \mathrm{erfc}\left(\frac{1}{2\sqrt{\tau}}\right) + \frac{2\sqrt{\tau}}{\sqrt{\pi}}\left(1 - \exp\left(-\frac{1}{4\tau}\right)\right) \quad (12)$$

$$\frac{h(t)}{h_\infty} = F(\tau) \quad (13)$$

The exact derivative of the dimensionless response is given in Equation (14), where the prime denotes differentiation with respect to dimensionless time. Logarithmic sensitivities quantify the proportional change in calculated heave arising from a proportional change in an input at fixed physical elapsed time. Equations (15) and (16) yield the diffusivity and active-depth elasticities. At early normalized times, the diffusivity elasticity approaches one-half while thickness elasticity approaches zero; at late normalized times, the diffusivity elasticity tends to zero while thickness elasticity tends to unity. The moisture increment, strain coefficient and restraint factor each have a sensitivity of exactly one under the linear constitutive assumption.

$$\frac{\mathrm{d}F}{\mathrm{d}\tau} = \frac{1-\exp[-1/(4\tau)]}{\sqrt{\pi\tau}} \quad (14)$$

$$S_D = \frac{\partial \ln h}{\partial \ln D_\theta} = \frac{\tau F'(\tau)}{F(\tau)} \quad (15)$$

$$S_L = \frac{\partial \ln h}{\partial \ln L} = 1 - 2S_D \quad (16)$$

The early-time limiting expression in Equation (17) makes the independence from active depth explicit before the diffusion perturbation has reached significant depth. For readers who prefer a moisture-front indicator, Equation (18) gives the depth at which a selected positive fraction of the imposed moisture perturbation remains, using the inverse complementary error function. The prescribed fraction lies strictly between zero and unity; this is a mathematical iso-response depth, not a sharply defined physical wetting front.

$$h(t) \sim \frac{2\lambda \alpha_\theta \Delta\theta}{\sqrt{\pi}} \sqrt{D_\theta t} \quad (\tau \ll 1) \quad (17)$$

$$z_p(t) = 2\sqrt{D_\theta t}\,\mathrm{erfc}^{-1}(p) \quad (18)$$

Finite wetting pulses and repeated annual forcing

The functions $h_s(t)$, $h_p(t)$ and $h_c(t)$ denote the sustained-step, isolated-pulse and repeated-pulse heave responses, each measured in metres. By definition, $h_s(t) = 0$ for nonpositive time. Wetting duration T_w and recurrence period P are in seconds; the number of applied pulses N and summation index j are dimensionless integers, with j ranging from zero to $N - 1$. These time conventions also apply to the delayed arguments in Equations (20) and (21).

For an imposed wet period that ends after a specified number of seconds, linear superposition provides the heave from the sustained step minus the delayed response to an equal surface step of opposite sign. Equation (19) names the sustained step response, and Equation (20) specifies the corresponding single-pulse heave. The step response is defined to be zero at nonpositive elapsed time, so the delayed subtraction is inactive until the wetting interval has ended. The pulse duration is expressed in seconds.

$$h_s(t) = \begin{cases} h_\infty F(D_\theta t/L^2), & t > 0 \\ 0, & t \le 0 \end{cases} \quad (19)$$

$$h_p(t) = h_s(t) - h_s(t - T_w) \quad (20)$$

A series of identical pulses is constructed by adding independent onsets and removals, as written in Equation (21). The repeat period is measured in seconds, the number of pulses is a dimensionless positive integer, and the summation index counts pulse number beginning at zero. This treatment permits transport-driven residual responses from earlier episodes to overlap with later episodes. It deliberately omits irreversible swelling, shrinkage-induced cracks, altered diffusivity, evolving fabric, rainfall-dependent surface moisture and seasonal suction gradients, all of which may affect real expansive soils (Abbas et al., 2023; Oliveira and Cavalcante, 2024).

$$h_c(t) = \sum_{j=0}^{N-1} [h_s(t - jP) - h_s(t - jP - T_w)] \quad (21)$$

Screening limits, numerical implementation and reproducibility

For the screening relationships, t_s is the evaluation time (s), h_{lim} is an illustrative allowable heave (m), $\Delta\theta_{\mathrm{crit}}$ is the limiting prescribed water-content increase (m³/m³), and t_{crit} is the first threshold crossing time (s). The symbol F^{-1} denotes the functional inverse of the

increasing dimensionless response. All displacement values must be converted to metres before substitution into Equations (22)–(24); millimetres are used only for reporting numerical results.

An example serviceability comparison is obtained by selecting a maximum acceptable upward movement and an evaluation time. Equation (22) defines a screening comparison, not an independently justified pavement design criterion. Rearrangement of the sustained-wetting relation yields the critical imposed water-content increment in Equation (23). For limits strictly between zero and the mathematical asymptotic heave, Equation (24) expresses the threshold crossing time through the inverse of the monotonic response. If a limit equals or exceeds the asymptotic heave, no finite threshold crossing exists under the sustained-wetting model. The limit, heave and active depth must all be expressed in consistent length units.

$$h(t_s) \le h_{\lim} \quad (22)$$

$$\Delta\theta_{\text{crit}} = \frac{h_{\lim}}{\lambda \alpha_\theta L\, F(D_\theta\, t_s/L^2)} \quad (23)$$

$$t_{\text{crit}} = \frac{L^2}{D_\theta} F^{-1}\left(\frac{h_{\lim}}{h_\infty}\right) \quad (24)$$

All calculations use the analytic error-function response. Time inputs originally expressed in days are converted using 86,400 seconds per day. One year is defined as 365 days in the periodic loading scenarios. The inverse threshold time is evaluated by a bracketed scalar root-finding method. Evaluations of the closed-form expression use the numerically stable exponential difference, and the limits at zero elapsed time are assigned explicitly. A dense regular grid is used only to illustrate parameter responses; it is not a calibration set or a probabilistic simulation. Independently computed checks include the early-time limit, direct numerical depth integration of the error-function field and the derivative identity for dimensionless sensitivity.

RESULTS AND DISCUSSION

Reference step response and characteristic penetration depth

The reference inputs specified in Table 1 imply an asymptotic upward movement of 37.80 mm. At the beginning of wetting the computed heave is zero, increases with a square-root-of-time trend and gradually approaches its imposed mathematical limit. After 30, 90, 180 and 365 days, the results are 6.47, 11.18, 15.42 and 20.19 mm, respectively. The response does not represent a known field settlement record; it illustrates the combined implications of the assumed diffusion coefficient, active-layer geometry and moisture–strain multiplier. The corresponding moisture profiles in Figure 2 demonstrate that the imposed surface step has not equilibrated through the full active depth on the short time scales, even though the upper part of the profile is strongly perturbed.

Table 2. Computed step-response values quantify the evolution of normalized time, response fraction and upward heave under permanent wetting.

Time (days)	Dimensionless time, τ (–)	Response fraction, $F(\tau)$ (–)	Calculated heave (mm)
7	0.0054	0.0827	3.13
30	0.0230	0.1713	6.47

Time (days)	Dimensionless time, τ (–)	Response fraction, $F(\tau)$ (–)	Calculated heave (mm)
60	0.0461	0.2421	9.15
90	0.0691	0.2958	11.18
180	0.1382	0.4080	15.42
270	0.2074	0.4804	18.16
365	0.2803	0.5342	20.19
730	0.5606	0.6489	24.53
1095	0.8410	0.7068	26.72

The step-response time to a screening magnitude of 20 mm is 354.5 days for the reference assumptions. This crossing time is governed jointly by the amplitude of the asymptotic heave and by the normalized diffusive time. In particular, replacing the actual wetting boundary with the first day of seasonal rainfall would not be justified: the imposed water-content step represents a selected condition at the soil surface, not rainfall volume or a quantified infiltration capacity. Observations of suction and moisture with depth are required to identify an equivalent boundary history for an actual site.

Variation with diffusivity and thickness

Figure 3 distinguishes the timing effect of effective moisture diffusivity from the ultimate heave amplitude. Increasing diffusivity accelerates the response at each finite time but cannot alter the asymptotic heave when the active depth and wetting-strain coefficient remain fixed. For the one-year endpoint, changes from 2×10^{-9} to 1×10^{-7} m²/s increase the heave from 7.14 to 29.05 mm under otherwise identical assumptions. A larger modeled diffusivity should therefore not be interpreted as evidence of a more expansive material; it only produces faster transmission of the imposed moisture perturbation in this linear surrogate.

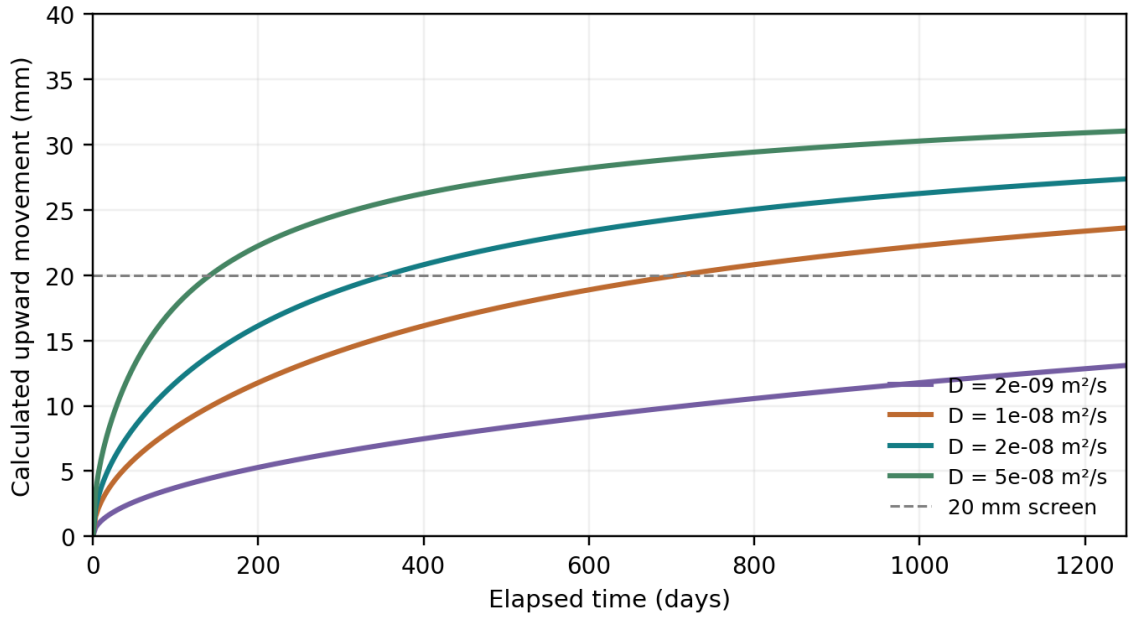


Figure 3. Step-wetting heave curves compare four assumed moisture diffusivities; the dashed horizontal line denotes the illustrative 20 mm screening limit.

Varying active-layer thickness leads to a more nuanced pattern. With the other baseline

quantities unchanged, a 0.75 m active depth gives 14.04 mm at one year, a 1.50 m layer gives 20.19 mm, and a 3.00 m layer gives 22.52 mm. The difference between the deepest alternatives is relatively small at this endpoint because the soil below the depth reached by a strong moisture perturbation contributes little additional strain. At sufficiently long elapsed times, however, the asymptotic heave increases directly with active-layer thickness. The elasticity identities explain the apparent change in influence without attributing it to a change in clay mineralogy.

Table 3. One-year sensitivity calculations contrast changes in diffusivity and deformation-active thickness while holding the remaining inputs constant.

Variable changed	**Test value**	**One-year heave (mm)**	**Ratio to baseline (–)**
Diffusivity	2×10^{-9} m²/s	7.14	0.354
Diffusivity	1×10^{-8} m²/s	15.51	0.768
Diffusivity	2×10^{-8} m²/s	20.19	1.000
Diffusivity	5×10^{-8} m²/s	25.77	1.276
Diffusivity	1×10^{-7} m²/s	29.05	1.439
Active depth	0.75 m	14.04	0.695
Active depth	1.00 m	16.80	0.832
Active depth	1.50 m	20.19	1.000
Active depth	2.25 m	22.11	1.095
Active depth	3.00 m	22.52	1.115

Finite wetting duration and post-pulse relaxation

Finite pulses behave differently from sustained wetting, as Figure 4 shows. A 30-day surface pulse gives a peak displacement of 6.47 mm, whereas the maximum for a 90-day pulse is 11.18 mm and that for a 180-day pulse is 15.42 mm. Because the derivative of the step response decreases with time, the heave after each pulse ends decreases monotonically under the constant-coefficient reversible assumption; therefore the peak is attained at the end of wetting. This peak-time identity is a property of the specific mathematical surrogate. In real expansive soils, delayed swelling, creep, stress changes and hysteresis may shift the peak beyond the surface moisture reversal.

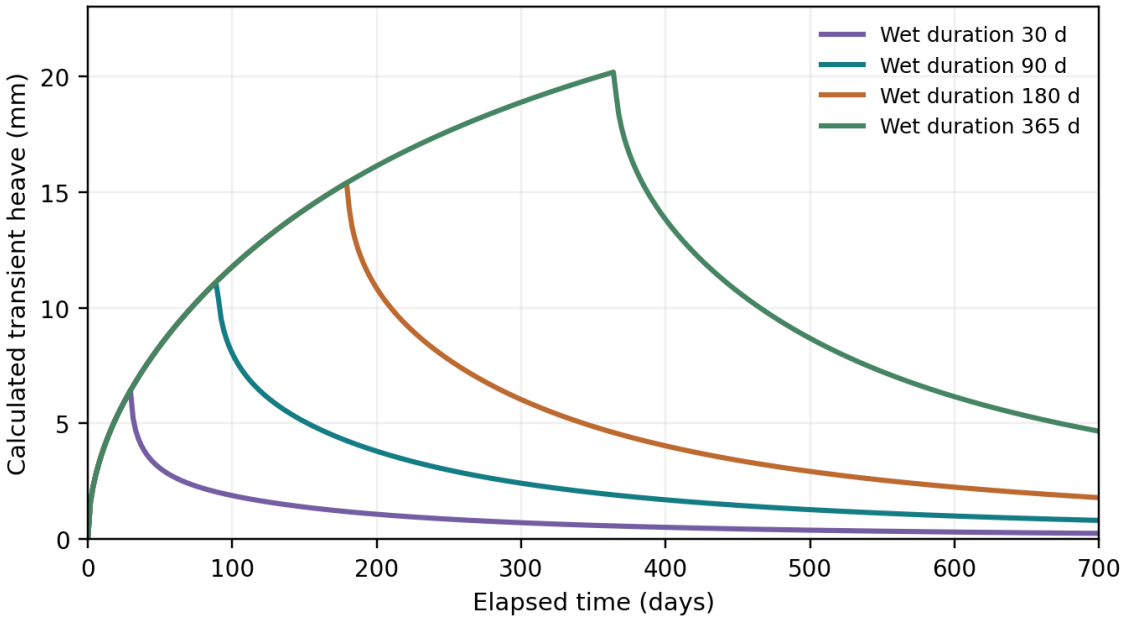


Figure 4. Transient heave histories contrast isolated surface-wetting pulses of 30, 90, 180 and 365 days, including modeled relaxation following each pulse.

At two years after the first onset, the modeled residual heave from a 90-day pulse is only 0.77 mm, compared with 24.53 mm if the moisture step remains imposed without interruption for the same two-year interval. This difference results from boundary-condition history alone; it does not demonstrate recovery of the soil fabric or imply that a wetting episode will be harmless. Desiccation cracking, shrinkage, nonuniform moisture access or an altered strain coefficient would invalidate the reversible-response interpretation. The comparison is nevertheless useful for showing that duration and recurrence must be stated when attributing a calculated heave to climate exposure.

Table 4. Isolated-pulse scenarios report the maximum computed heave and the residual movement two years after wetting begins.

Pulse duration (days)	Peak heave (mm)	Heave at two years (mm)	Peak relative to 20 mm (–)
30	6.47	0.24	0.324
60	9.15	0.50	0.458
90	11.18	0.77	0.559
180	15.42	1.69	0.771
365	20.19	4.34	1.010

Repeated seasonal pulses and carry-over

The annual 90-day sequence depicted in Figure 5 applies five identical pulses separated by 365-day onset intervals. The first-cycle maximum is 11.18 mm, the second-cycle maximum is 12.63 mm, and the fifth-cycle maximum is 13.94 mm. These maxima rise even though the imposed surface amplitude and duration are unchanged. The trend arises because the moisture perturbation remaining at depth from earlier pulses adds to the response to later pulses. Accumulation slows as the diffusive tails of increasingly distant pulses diminish; a five-cycle simulation does not establish a universal stationary seasonal regime.

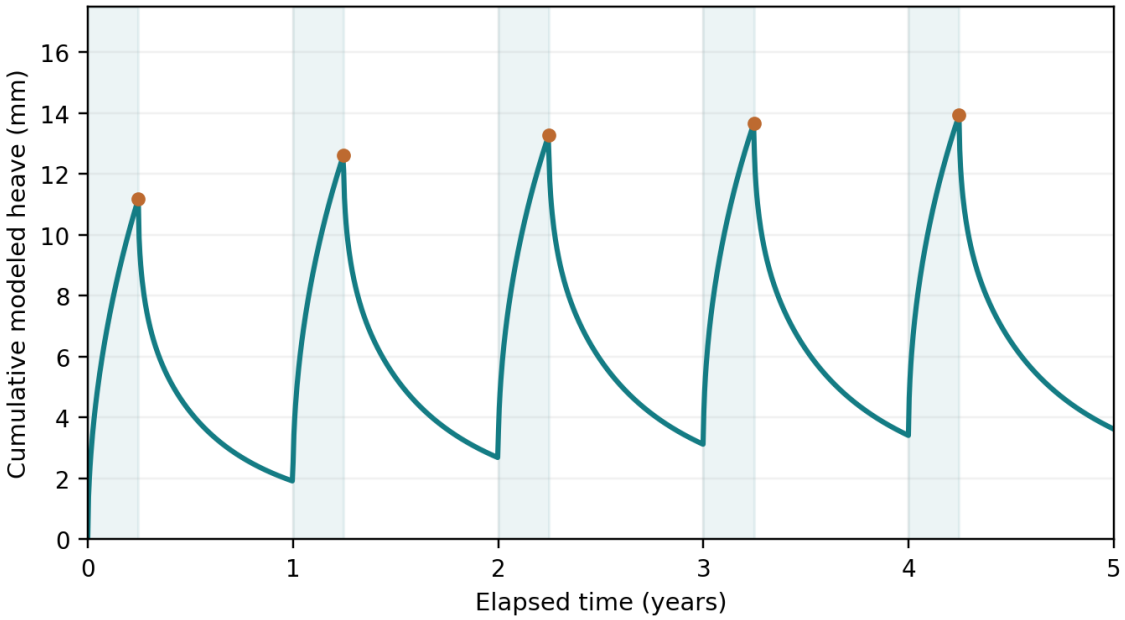


Figure 5. Five annual 90-day pulses produce overlapping heave responses; shaded intervals show prescribed wetting and markers identify each wetting-end maximum.

This apparent carry-over should not be confused with irreversible material degradation. The model returns eventually to zero after all imposed pulses end because its moisture transport and strain relationship are linear and fully reversible. Abbas et al. (2023), Oliveira and Cavalcante (2024) and Yu et al. (2024) provide reasons to expect a more complex response in real clays: stress level, hydraulic history, microstructure and retention properties can evolve with cycling. For practical applications, separate laboratory tests would be required to quantify not only heave in a first wetting event but also contraction, residual strain and alteration of transport parameters following successive drying intervals.

Table 5. The five-cycle sequence tracks the wetting-end maximum and its increment relative to the preceding annual pulse.

Cycle number	Time of wetting-end (days)	Peak heave (mm)	Increment versus prior cycle (mm)
1	90	11.18	—
2	455	12.63	1.45
3	820	13.29	0.66
4	1185	13.68	0.39
5	1550	13.94	0.27

Thresholds, contours and dimensionless sensitivity

The one-year contour in Figure 6 shows joint dependence on active depth and effective diffusivity under the fixed moisture–strain amplitude. Because both parameters influence the normalized time scale, equal-heave contours are curved rather than simple straight iso-products. Near the reference point, the 20 mm screen is marginally exceeded: 20.19 mm after 365 days. The critical prescribed volumetric water-content increment corresponding to exactly 20 mm at that date is 0.07923 when the other baseline parameters are held fixed. This is not a

critical field water content unless the assumed coefficient and restraining factor have been established independently.

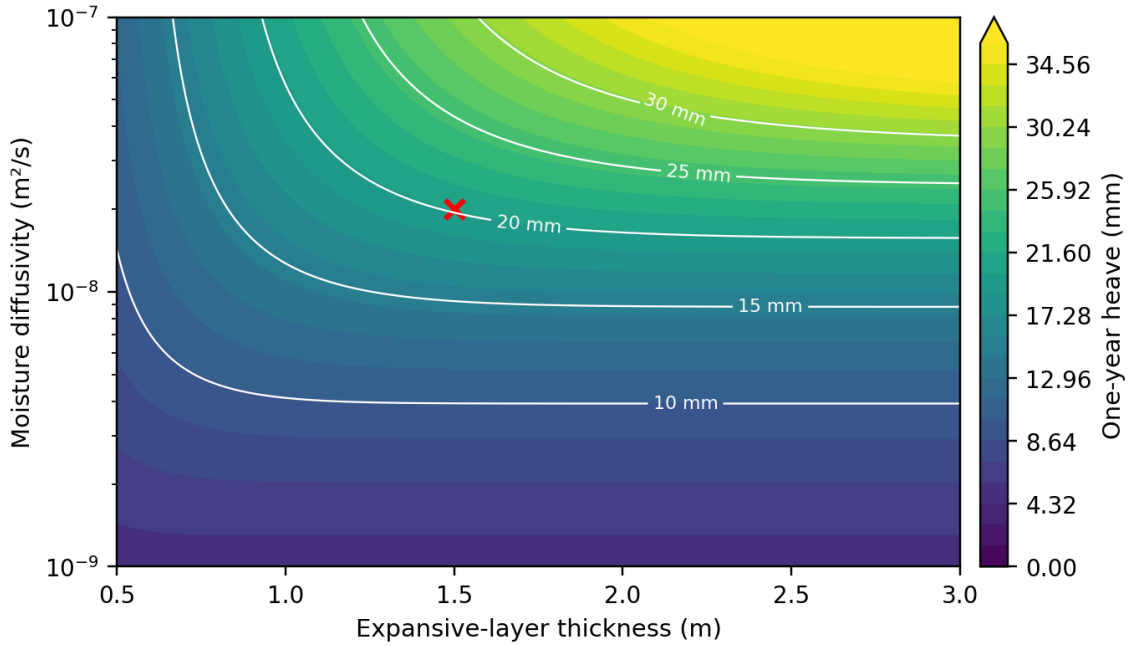


Figure 6. One-year heave contours map the combined influence of assumed diffusivity and active depth; the cross locates the baseline and contour labels give millimetres.

Sensitivity can be quantified without running a large empirical parameter sweep. At the reference one-year dimensionless time, the diffusivity elasticity is determined analytically by the normalized response derivative and the active-thickness elasticity is exactly one minus twice that value. The first elasticity is smaller than the initial-time limiting value of 0.5 because the response has begun to saturate over the finite active depth. Both the moisture increment and the swelling coefficient enter as linear amplitude multipliers; therefore a 10% perturbation of either produces exactly a 10% change in computed heave. This mathematical proportionality should not be extrapolated outside a calibrated strain regime, where swelling pressure, suction-dependent stiffness and mineral interactions can create nonlinear behavior.

Table 6. Local logarithmic elasticities distinguish the timing and amplitude contributions to modeled one-year heave at the reference state.

Input parameter	**Reference value**	**Heave elasticity (–)**	**Interpretation**
Moisture diffusivity, D_θ	2.0×10^{-8} m²/s	0.330	Timing sensitivity
Active-layer thickness, L	1.50 m	0.340	Depth sensitivity
Surface moisture increment, $\Delta\theta$	0.08 m³/m³	1.000	Amplitude proportionality
Moisture–strain coefficient, α_θ	0.45	1.000	Amplitude proportionality
Mobilization factor, λ	0.70	1.000	Amplitude proportionality

Verification and practical limitations

The primary calculations were independently checked by numerical quadrature of the depth-

integrated error-function field, scalar root finding for the reference threshold and finite-difference perturbations of the dimensionless elasticities. The closed-form and direct numerical depth-integral values agree to the numerical quadrature tolerance; this tests the implementation, not the physical adequacy of the linear transport–strain model. The scalar threshold of 354.5 days is recovered whether the root is solved in physical time or in the normalized diffusion time. The response maintains the expected limiting properties: zero heave at the instant of imposed wetting, monotonic increase under a permanent step, and approach to the prescribed asymptotic amplitude.

The strongest limitation is the simplification of coupled unsaturated soil physics. Constant moisture diffusivity neglects variations of hydraulic conductivity with water content and suction, storage nonlinearity, shrinkage cracking, osmotic influences and strongly nonuniform infiltration. A constant linear strain factor neglects expansive mineral chemistry, wetting-induced fabric rearrangement and changes in stiffness with stress. The uniform mobilization factor is not a mechanical constitutive law; vertical strain under a pavement or foundation can be substantially different from unconstrained one-dimensional swell. In addition, a one-dimensional uplift calculation contains no measure of differential settlement or structural damage, and the 20 mm threshold is illustrative only rather than a code requirement.

Before this screening framework could support a site-specific design decision, the active depth should be characterized using trial pits or boreholes and appropriate mineralogical and classification testing; moisture-content or suction profiles should define the relevant initial state and boundary evolution. Controlled wetting and suction-conditioned swell tests under representative stress should estimate the time- and stress-dependent strain relation. Where repeated wetting–drying governs, hydraulic and swelling parameters should be updated by cycling tests, and the conclusions should be compared against field instrumentation or a nonlinear coupled flow–deformation analysis. The analytical method is most defensible as a preliminary sensitivity tool to identify what data should be measured, rather than as a substitute for those measurements.

CONCLUSION

A closed-form dimensionless screening model was developed to connect imposed surface wetting and active-layer swelling with the time evolution of one-dimensional vertical heave. By integrating a semi-infinite moisture-diffusion solution through a finite expansive zone, the framework separates the geometric and strain-amplitude factors from a single normalized temporal response. The resulting sensitivities show that the influence of active-layer thickness is initially small and grows with exposure time, whereas sensitivity to effective moisture diffusivity is greatest during early wetting and declines as the modeled layer approaches its sustained-wetting response. These results are exact within the linear analytical idealization, not experimentally established geotechnical design laws.

For the explicitly hypothetical baseline, asymptotic heave is 37.80 mm and one-year heave is 20.19 mm. The example 20 mm criterion is crossed after 354.5 days under continuous wetting. An isolated 90-day wetting pulse peaks at 11.18 mm, while repeated annual pulses

yield a fifth-cycle maximum of 13.94 mm because nonzero modeled moisture responses persist between episodes. This distinction demonstrates why exposure duration and recurrence must accompany a reported heave magnitude. It does not prove reversible swelling in actual expansive soils or indicate that seasonal moisture pulses can be safely ignored.

The method provides a reproducible basis for screening and for deciding which measurements most strongly reduce uncertainty. Future work should calibrate transient moisture parameters and stress-dependent swelling relations, include hydraulic and mechanical hysteresis, evaluate differential heave over laterally variable wetting fields and compare the analytical predictions with instrumented ground performance. Until these steps are completed, numerical scenarios in this paper should not be represented as measured values or site-specific design recommendations.

REFERENCES

Abbas, M. F., Shaker, A. A., & Al-Shamrani, M. A. (2023). Hydraulic and volume change behaviors of compacted highly expansive soil under cyclic wetting and drying. Journal of Rock Mechanics and Geotechnical Engineering, 15(2), 486–499. https://doi.org/10.1016/j.jrmge.2022.05.015

Alonso, E. E., Vaunat, J., & Gens, A. (1999). Modelling the mechanical behaviour of expansive clays. Engineering Geology, 54(1–2), 173–183. https://doi.org/10.1016/S0013-7952(99)00079-4

Crank, J. (1975). The mathematics of diffusion (2nd ed.). Clarendon Press, Oxford. ISBN 978-0-19-853344-3.

Fredlund, D. G., Rahardjo, H., & Fredlund, M. D. (2012). Unsaturated soil mechanics in engineering practice. John Wiley & Sons. https://doi.org/10.1002/9781118280492

Nelson, J. D., Chao, K. C., Overton, D. D., & Nelson, E. J. (2015). Foundation engineering for expansive soils. John Wiley & Sons. https://doi.org/10.1002/9781118996096

Oliveira, L. da S., & Cavalcante, E. H. (2024). Effects of wetting and drying cycles on the swelling pressure and free swelling of expansive soil. Soils and Rocks, 47(1), e2024011122. https://doi.org/10.28927/SR.2024.011122

Richards, L. A. (1931). Capillary conduction of liquids through porous mediums. Physics, 1(5), 318–333. https://doi.org/10.1063/1.1745010

Yu, M., Gui, Y., & Li, B. (2024). Modelling soil-water retention curves subject to multiple wetting-drying cycles: An approach for expansive soils. Computers and Geotechnics, 171, 106335. https://doi.org/10.1016/j.compgeo.2024.106335

DESIGN-TIME SCREENING OF RESIDUAL PRIMARY CONSOLIDATION IN SOFT CLAY UNDER STAGED EMBANKMENT LOADING: ANALYTICAL SUPERPOSITION AND SENSITIVITY MAPS

Ali Akbar Firoozi
School of Civil, Environmental Engineering and Geomatics, Faculty of Engineering and Built Environment, University of Botswana, Gaborone, Botswana

Ali Asghar Firoozi
Department of Civil Engineering, Faculty of Engineering, National University of Malaysia (UKM), Selangor, Malaysia

ABSTRACT

Embankments founded on saturated soft clay may satisfy an ultimate settlement estimate while retaining sufficient delayed deformation to compromise subsequent pavement or structural serviceability. This analytical study formulates an auditable residual-primary-settlement screening procedure using one-dimensional logarithmic compression, the classical Fourier-series consolidation solution, exact integration for linear-ramp loading, and increment-wise superposition for staged loading. A deliberately hypothetical 6.0 m normally consolidated clay layer with an initial effective stress of 75 kPa, an applied stress increment of 60 kPa, a compression index of 0.30, an initial void ratio of 1.00, and a consolidation coefficient of 1.5 m²/year is examined. The computed ultimate primary settlement is 229.75 mm. Under double drainage, reaching a remaining primary settlement of 25 mm requires 4.883 years for instantaneous loading, 5.137 years for a 0.50-year linear load ramp, and 5.362 years for equal 30 kPa increments applied one year apart. At three years, the predicted remaining settlements are 54.23, 60.21 and 66.03 mm, respectively. For instantaneous loading, replacing double drainage with single drainage increases the modeled time to the 25 mm criterion fourfold, from 4.883 to 19.532 years. The numerical study uses stated assumptions rather than field or laboratory observations and makes no claims of site-specific calibration. Its contribution is a reproducible link between loading schedule, drainage path, parameter sensitivity, and an explicitly defined residual-settlement decision threshold, with limitations identified for nonlinear, multilayer and creep-dominated conditions.

Keywords: Embankments, Soft Clay, Primary Consolidation, Staged Embankment Loading, Residual Settlement, Drainage Path, Analytical Screening.

INTRODUCTION

Construction of embankments, transportation corridors, reclamation platforms and industrial infrastructure over saturated clay poses a coupled deformation and scheduling problem. The final magnitude of primary compression is important, but the relevant engineering decision often concerns how much settlement will remain after the planned commissioning date. If the

pavement structure, culvert connection or other serviceable element is installed while substantial effective-stress redistribution remains unfinished, subsequent deformation may create maintenance difficulties even though the final settlement value itself was anticipated. The time history of load placement must therefore be distinguished from the ultimate compression calculation. Classical consolidation provides a transparent starting point for such assessment when strain is predominantly one-dimensional and soil behavior is represented through constant consolidation properties (Terzaghi et al., 1996; USACE, 1990).

Settlement prediction typically combines a stress-strain description, hydraulic drainage boundaries and a loading timetable. The logarithmic compression model links a normally consolidated clay increment to effective-stress change, whereas the solution to the one-dimensional excess-pore-pressure diffusion equation determines the rate at which a step load produces average primary consolidation. Standard manuals emphasize that drainage conditions and the coefficient of consolidation materially affect prediction (USACE, 1990). However, reporting a single degree of consolidation at a fixed duration can obscure the principal serviceability question: whether the magnitude of residual settlement is sufficiently small for the intended operational requirements. For projects involving staged construction, this question becomes more complex because a later load increment has experienced a shorter period of consolidation than an earlier increment.

Published investigations highlight the physical qualifications needed when extending classical theory to field-scale soft ground. Bjerrum (1967) discussed the importance of delayed consolidation and clay geological history in building-settlement observations. Mesri (1973b) developed a treatment for imperfect drainage boundaries rather than assuming ideal freely draining or impermeable interfaces. Wang et al. (2023) experimentally examined multi-stage loading of soft clay and described stress-dependent consolidation behaviour that is not captured by a constant-coefficient idealization. Mesri (1973a) investigated secondary compression, while Nguyen (2024) addressed long-term settlement of overconsolidated clay under conditions in which creep is important. These contributions establish why a reduced-order model cannot substitute for soil characterization or field monitoring, and identify the mechanisms that should be flagged in preliminary screening.

The purpose of the present paper is to formulate a reproducible decision-time assessment for residual primary consolidation under explicitly prescribed loading histories. The work derives exact finite-ramp expressions from the classical series, connects discontinuous staged loading with nonlinear ultimate compression increments, introduces a user-defined post-construction residual-settlement criterion, and quantifies how construction schedule, drainage path, consolidation coefficient and allowable residual settlement change the forecast. No new soil constitutive law, field experiment, numerical finite-element result, statistical population or validated site-specific prediction is claimed. The added value lies in the transparent comparison of realistic loading-time abstractions through a common remaining-settlement criterion, together with explicit checks and conditions of applicability.

MATERIALS AND METHOD

Soil profile, units and mechanical assumptions

The model consists of a laterally extensive, homogeneous, fully saturated, normally consolidated clay layer beneath a sufficiently wide embankment for the additional vertical stress to be approximated as constant over the modelled depth. Strains are treated as one-dimensional, soil grains and pore water are taken as incompressible for the diffusion idealization, and the compression index, initial void ratio and coefficient of consolidation are held fixed at their illustrative reference values. The formulation excludes shear failure, lateral extrusion, construction-induced destructuration, stress-dependent permeability, small-strain stiffness changes and secondary compression. The one-dimensional approximation is particularly important: narrow embankments, layered drainage systems and appreciable lateral deformation require more complete stress-transfer and coupled hydro-mechanical treatments. Figure 1 depicts the idealized geometry with upper and lower drainage boundaries. In the single-drainage sensitivity case, one of those faces is assumed impermeable, changing the maximum drainage path without changing the thickness of the deposit.

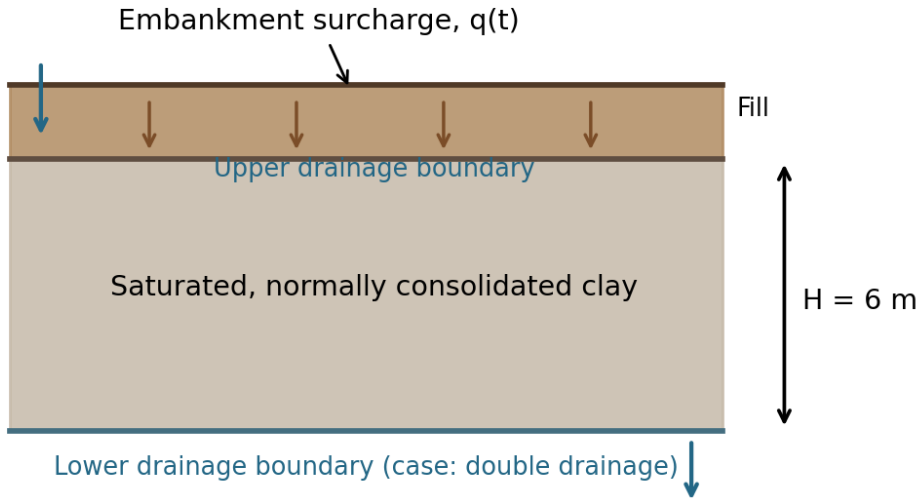


Figure 1. Cross-sectional schematic of the hypothetical embankment and 6.0 m soft-clay layer, showing the upper and lower drainage boundaries active in the reference double-drainage case.

In Equation (1), s_∞ denotes ultimate primary consolidation settlement (m); H denotes clay thickness (m); C_c is the compression index (dimensionless); e_0 is the initial void ratio (dimensionless); σ_0' is the representative initial vertical effective stress (kPa); and $\Delta\sigma$ is the sustained embankment-induced vertical stress increment (kPa). The base-10 logarithm has a dimensionless stress ratio; both stresses must have identical units. Settlement is evaluated in metres when H is specified in metres. The logarithmic compression relationship is restricted to the normally consolidated stress range; an overconsolidated profile additionally requires a preconsolidation stress and a recompression index. Equation (1) is an established analytical approximation, not a fitted correlation derived from measurements in the present study.

$$s_\infty = \frac{HC_c}{1+e_0}\log_{10}\left(\frac{\sigma_0'+\Delta\sigma}{\sigma_0'}\right) \quad (1)$$

One-dimensional hydraulic consolidation response

The excess pore-water pressure u_e (kPa) evolves with elapsed time t (years) and vertical coordinate z (m) in accordance with Equation (2), where c_v (m²/year) denotes the coefficient of consolidation. The coordinate z is a depth coordinate through the clay, whereas H_d (m) denotes its maximum drainage path. The initial excess pore pressure is assumed uniform following a stress step and is assigned zero at each freely draining boundary. Consequently, $H_d = H/2$ for ideal double drainage and $H_d = H$ for ideal single drainage. Equation (3) defines the dimensionless time factor T_v; time and c_v must be expressed in consistent units. The average primary degree of consolidation U is dimensionless and represents the fraction of ultimate primary settlement achieved under the prescribed step-loading assumptions.

$$\frac{\partial u_e}{\partial t} = c_v\frac{\partial^2 u_e}{\partial z^2} \quad (2)$$

$$T_v = \frac{c_v t}{H_d^2} \quad (3)$$

Equation (4) specifies the dimensionless Fourier-series weights a_m and decay factors b_m. Here m is a nonnegative integer (0, 1, 2, …) indexing odd diffusion modes, and π is the mathematical constant pi (dimensionless). Equation (5) expresses the dimensionless average step-load consolidation U as a function of T_v; exp denotes the natural exponential function, and the series tends to $U = 0$ at $t = 0$ and $U = 1$ as t becomes large. Equation (6) defines $s_{\text{step}}(t)$, the accumulated step-load primary settlement (m), while Equation (7) defines $R(t)$, the remaining primary settlement (m), from $s(t)$, the primary settlement accumulated by time t (m). The model intentionally excludes secondary compression, so R is not the remaining total deformation from all mechanisms.

$$a_m = \frac{8}{\pi^2(2m+1)^2}, \qquad b_m = \frac{\pi^2(2m+1)^2}{4} \quad (4)$$

$$U(T_v) = 1 - \sum_{m=0}^{\infty} a_m \exp(-b_m T_v) \quad (5)$$

$$s_{\text{step}}(t) = s_\infty U\left(\frac{c_v t}{H_d^2}\right) \quad (6)$$

$$R(t) = s_\infty - s(t) \quad (7)$$

Exact response to a finite linear load ramp

Instantaneous embankment loading is rarely an exact representation of construction. A finite linear ramp lasting t_r (years) is represented as an accumulation of infinitesimal stress increments, each assigned a delayed step response. In Equation (8), $U_r(t)$ is the dimensionless consolidation fraction obtained under that ramp; τ is a dummy loading-time variable (years); and $\min(t, t_r)$ means the smaller of t and t_r (both in years). The ramp rate of total applied stress is constant. Equations (9) and (10) integrate the step-response series for the periods during and after the ramp, respectively. Equation (11) defines k_m, the modal decay rate (year^{-1}), using the dimensionless b_m, c_v (m²/year) and H_d (m). Equations (8)–(11) are exact within linear time superposition with settlement apportioned in proportion to applied stress. That proportional allocation is an explicit approximation because the logarithmic compression

model is nonlinear with respect to stress.

$$U_r(t) = \frac{1}{t_r}\int_0^{\min(t,t_r)} U\left(\frac{c_v(t-\tau)}{H_d^2}\right)\mathrm{d}\tau \quad (8)$$

$$U_r(t) = \frac{t}{t_r} - \frac{1}{t_r}\sum_{m=0}^{\infty}\frac{a_m}{k_m}[1-\exp(-k_m t)], \quad 0 < t \le t_r \quad (9)$$

$$U_r(t) = 1 - \frac{1}{t_r}\sum_{m=0}^{\infty}\frac{a_m}{k_m}[\exp\{-k_m(t-t_r)\} - \exp(-k_m t)], \quad t > t_r \quad (10)$$

$$k_m = \frac{b_m c_v}{H_d^2} \quad (11)$$

It is necessary to distinguish the temporal approximation from the nonlinear static compressibility relationship. The total ultimate settlement is calculated using Equation (1), while the linear ramp time distribution allocates that same ultimate settlement uniformly over the construction interval. If strictly incremental logarithmic stress allocation were required during a continuous ramp, the settlement contribution would be weighted by the derivative of Equation (1) with respect to applied stress. Equation (16) provides that derivative; it is not constant over a substantial stress change. The present finite-ramp results should consequently be understood as a loading-history screening model with an explicitly declared proportional-settlement approximation, not a nonlinear constitutive integration.

Discrete construction stages and residual-serviceability rule

For a sequence of J construction increments, J is the total number of stages (dimensionless integer), and j = 1, …, J is the stage index. In Equation (12), Q_j and Q_{j-1} (kPa) are the cumulative surcharge immediately after the jth and (j−1)th stages, with Q_0 = 0 kPa; $\Delta s_{\infty,j}$ (m) is the ultimate settlement attributed to stage j. The other terms H (m), C_c and e_0 (both dimensionless), and σ_0' (kPa) retain the definitions given for Equation (1). Logarithmic stage increments telescope to the same ultimate settlement as a single full surcharge. Equation (13) defines $s_{\text{stage}}(t)$, accumulated primary settlement (m), in which t_j (years) is the placement time of increment j and $I(t \ge t_j)$ is the dimensionless indicator equal to one after that stage is placed and zero beforehand. Identical c_v and drainage boundaries are assumed for all stages; real clays can exhibit stress-dependent c_v (Wang et al., 2023).

$$\Delta s_{\infty,j} = \frac{HC_c}{1+e_0}\log_{10}\left(\frac{\sigma_0'+Q_j}{\sigma_0'+Q_{j-1}}\right) \quad (12)$$

$$s_{\text{stage}}(t) = \sum_{j=1}^{J}\Delta s_{\infty,j}\, U\left(\frac{c_v(t-t_j)}{H_d^2}\right) I(t \ge t_j) \quad (13)$$

Equation (14) defines $R_{\text{stage}}(t)$, the forecast residual primary settlement (m) relative to the ultimate settlement under the complete planned loading history. Its first sum represents the residual settlement (m) of stages that have already been placed, and the second sum includes the ultimate settlement (m) of later, not-yet-applied stages; indices satisfying $t < t_j$ are therefore included only in the latter sum. After the last stage is installed, Equation (14) reduces to the sum of the remaining primary settlements of all stages. Equation (15) gives t_{crit} (years), the earliest qualifying time on or after the completion of load placement, $t_{\text{load,end}}$ (years), for which $R(t) \le R_{\text{allow}}$; R_{allow} is the selected allowable residual primary settlement

(m), and inf denotes the infimum or earliest time satisfying the condition. The allowance is illustrative, not a universal code limit; neither immediate elastic settlement nor creep is included.

$$R_{\text{stage}}(t) = \sum_{j=1}^{J} \Delta s_{\infty,j} \left[1 - U\left(\frac{c_v(t-t_j)}{H_d^2}\right)\right] I(t \geq t_j) + \sum_{j:t<t_j} \Delta s_{\infty,j} \quad (14)$$

$$t_{\text{crit}} = \inf\{t \geq t_{\text{load,end}} : R(t) \leq R_{\text{allow}}\} \quad (15)$$

Equation (16) gives the sensitivity of ultimate primary settlement to an additional vertical stress increment. Its derivative $\partial s_\infty / \partial(\Delta\sigma)$ has dimensions of length per stress, specifically m/kPa when H is in metres and the stresses are in kPa. The term ln(10) is the natural logarithm of 10 and is dimensionless. In Equation (17), $T_{v,\text{req}}$ is the dimensionless time factor corresponding to the required mean primary-consolidation fraction for an instantaneous surcharge, while $t_{\text{crit,step}}$ (years) is the associated threshold time. At fixed ultimate settlement and residual allowance, this step-load time varies as H_d^2 (m²) and inversely with c_v (m²/year). Equation (18) defines Θ, the dimensionless screening index, using t_{crit} (years), c_v (m²/year) and H_d (m). For ramp and stage loading, Θ also depends on the dimensionless timing of load placement; it is not a universal soil constant.

$$\frac{\partial s_\infty}{\partial(\Delta\sigma)} = \frac{H C_c}{(1+e_0)\ln(10)(\sigma_0' + \Delta\sigma)} \quad (16)$$

$$t_{\text{crit,step}} = \frac{H_d^2}{c_v} T_{v,\text{req}}, \qquad U(T_{v,\text{req}}) = 1 - \frac{R_{\text{allow}}}{s_\infty} \quad (17)$$

$$\Theta = \frac{t_{\text{crit}} c_v}{H_d^2} \quad (18)$$

Numerical design, calculations and independent verification

All values used here are prescribed analytical examples rather than borehole, consolidation-test or field-instrumentation measurements. The reference clay thickness is 6.00 m, maximum drainage path 3.00 m under double drainage, initial effective vertical stress 75 kPa, embankment-induced stress increment 60 kPa, compression index 0.30, initial void ratio 1.00 and c_v = 1.50 m²/year. A residual primary-settlement allowance of 25 mm (0.025 m) is adopted as a demonstrative serviceability threshold, not as a regulatory acceptance criterion. Three loading programs are assessed: 60 kPa applied at the origin, a linear 60 kPa ramp completed after 0.50 year, and two instantaneous 30 kPa stages placed at zero time and at the end of the first year. The time origin is the initial start of loading in all scenarios. Table 1 summarizes the reference inputs and tested range; the examples are deliberately not attached to any real project location.

Table 1. Illustrative soil parameters, drainage conditions and loading inputs used in the calculations; none represents a measured site property.

Parameter	Reference	Sensitivity cases	Unit
Clay thickness, H	6.00	Fixed in worked examples	m
Initial vertical effective stress, σ_0'	75	Fixed	kPa
Embankment vertical stress increment, $\Delta\sigma$	60	30 + 30 for staged case	kPa
Compression index, C_c	0.30	Fixed	dimensionless

Initial void ratio, e_0	1.00	Fixed	dimensionless
Consolidation coefficient, c_v	1.50	0.75, 1.50, 3.00	m²/year
Maximum drainage path, H_d	3.00	3.00 (double); 6.00 (single)	m
Linear construction ramp duration, t_r	0.50	0.50	year
Separation between equal loading steps	1.00	1.00	year
Allowable residual primary settlement, R_{allow}	0.025	0.015, 0.025, 0.050	m

The infinite series is truncated after 700 terms, with the exact initial-time condition U(0) = 0 explicitly enforced to avoid a small positive truncation bias at the origin. The largest omitted tail under finite truncation for t = 0 is below approximately 0.0003 of the total spectral weight; for positive time its contribution decays rapidly. Each time-to-threshold root is determined numerically from a monotonic residual-settlement function, with a stringent numerical tolerance. The ramp series is independently checked by adaptive quadrature of the convolution integral at four times during and after construction. The ratio between single-drainage and double-drainage times is checked against the analytical square-of-path rule. This verification confirms internal mathematical implementation, not agreement with field measurements.

RESULTS AND DISCUSSION

Ultimate compression and reference time history

Application of Equation (1) to the declared reference conditions gives an ultimate primary settlement of 229.75 mm, or 0.22975 m. The same value results from the two incremental stress contributions: 131.52 mm from raising effective stress from 75 to 105 kPa, and 98.23 mm from raising it from 105 to 135 kPa. These increments are not equal even though both construction stages are 30 kPa, because the logarithmic compression relation gives a diminishing settlement increment as the effective stress rises. This difference is important: splitting the total settlement evenly between stages would be algebraically inconsistent with the specified compression index model. The settlement magnitude is an illustrative consequence of the inputs and should not be interpreted as a measured field prediction.

For the immediate step case, the average degree of consolidation one year after load placement is 46.05%, corresponding to 105.80 mm of primary settlement. By three years, the computed settlement is 175.51 mm, leaving 54.23 mm to develop. The residual 25 mm criterion is met after 4.883 years, whereas the more restrictive 15 mm criterion requires 6.125 years. Table 2 reports the time histories for all three load schedules and establishes that reporting an ultimate settlement alone does not determine a usable serviceability time. Figure 2 displays the gradual convergence of the three calculated curves to the same theoretical limit.

Table 2. Calculated primary consolidation settlement (mm) at selected times for the immediate, ramped and two-stage embankment loading schedules.

Time since start (years)	Instantaneous load	0.50-year linear ramp	Two steps at 0 and 1 year
0.50	74.84	49.89	42.84
1.00	105.80	91.21	60.56
2.00	147.92	138.87	129.91
3.00	175.51	169.54	163.71
5.00	205.92	203.29	200.74

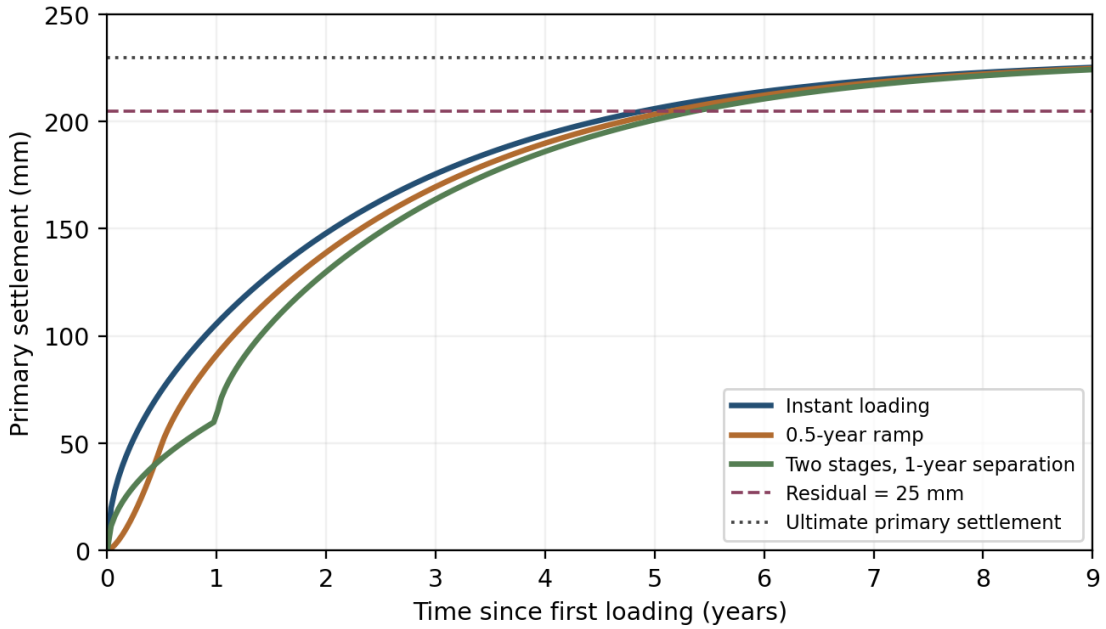


Figure 2. Predicted primary settlement histories for three 60 kPa loading schedules; the horizontal reference lines identify ultimate settlement and the 25 mm residual criterion.

Loading timetable and delayed serviceability

At three years after initial loading, the instant, ramp and two-stage programs produce calculated primary settlements of 175.51, 169.54 and 163.71 mm, leaving 54.23, 60.21 and 66.03 mm of future primary settlement respectively. Despite the identical final surcharge and identical calculated ultimate settlement, the model predicts a larger residual for a load applied later. The two-stage schedule also begins with a smaller ultimate increment, so part of its eventual deformation cannot start consolidating until the second stage is installed. These differences reflect the timing of stress introduction, not a change in soil compressibility, permeability or eventual load.

The calculated times to reach a 25 mm residual are 4.883 years for the immediate load, 5.137 years for the continuous ramp, and 5.362 years for the staged schedule. Relative to immediate loading, the waiting period increases by approximately 3.05 months for the 0.50-year ramp and 5.74 months for the two-stage sequence. Table 3 compares the ultimate compression, three-year residual settlement and threshold time for all three schedules. The calculations demonstrate why elapsed time since commencement of the first lift must not be confused with the consolidation age of the final load increment; in this idealization, changes in time to the criterion arise from stress-placement timing rather than changes in the final load or soil properties.

Table 3. Loading-schedule comparison of ultimate primary settlement, residual settlement after three years and elapsed time to a 25 mm residual.

Loading program	Ultimate primary settlement (mm)	Residual at year 3 (mm)	Time to 25 mm (years)
Instantaneous 60 kPa	229.75	54.23	4.883
Linear ramp, 0.50 year	229.75	60.21	5.137
Two steps, 1-year gap	229.75	66.03	5.362

The absolute waiting times should not be generalized beyond the stipulated values. For a different clay structure, partial drainage, stress-dependent coefficient of consolidation, large strains, variable initial excess pore-pressure distribution, or a nonuniform embankment stress bulb, the curves could change substantially. The 2023 experimental study by Wang et al. specifically reports measurable differences between single-stage and multi-stage consolidation in a tested marine clay. The current paper uses classical linear superposition and should not be interpreted as reproducing those empirical differences or their proposed modified coefficient relation. This distinction is essential for maintaining a scientifically appropriate separation between an illustrative design calculation and a validated material model.

Drainage path and consolidation-coefficient sensitivity

The maximum drainage path enters the time factor as a squared length. Replacing ideal top-and-bottom drainage with single drainage doubles H_d from 3.0 to 6.0 m and therefore increases the calculated time to a specified average degree of consolidation by precisely a factor of four, provided all other model inputs remain unchanged. At c_v = 1.50 m²/year, the 25 mm residual criterion moves from 4.883 to 19.532 years. This relationship is a conditional identity of idealized one-dimensional boundary conditions, not evidence that any particular field treatment reduces consolidation time by 75%. Effective drainage in an actual deposit depends on the permeability and continuity of adjacent layers; partially impeded drainage demands alternative boundary formulations (Mesri, 1973b).

Figure 3 contrasts six scenarios obtained by combining c_v = 0.75, 1.50 and 3.00 m²/year with both ideal drainage geometries. Increasing c_v shortens the consolidation duration, whereas removing a drainage outlet increases the time scale. For example, at c_v = 0.75 m²/year the double-drainage criterion occurs at 9.766 years, whereas at 3.00 m²/year it occurs at 2.442 years. Two curves coincide exactly where the ratio c_v/H_d^2 is equal: double drainage with c_v = 0.75 m²/year and single drainage with c_v = 3.00 m²/year produce the same transient consolidation trajectory. These values deliberately assume that c_v is a model input constant, even though laboratory characterization could show pressure and void-ratio dependence. Table 4 gives corresponding times and settlements at three years. None of the listed c_v values is asserted to represent a characteristic range for a specific Botswana or Türkiye clay deposit.

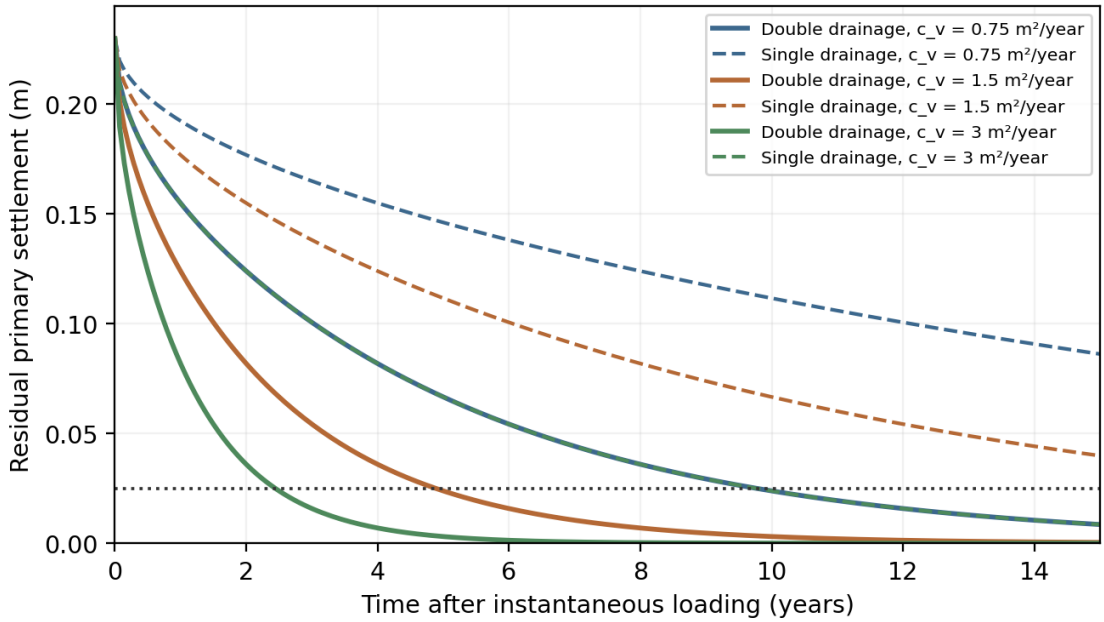


Figure 3. Predicted residual primary settlement for six consolidation-coefficient and drainage-boundary combinations under an instantaneous 60 kPa surcharge; the horizontal line marks 25 mm remaining settlement.

Table 4. Comparison of residual settlement at year 3 and time to a 25 mm residual for specified consolidation coefficients and ideal drainage configurations.

c_v (m²/year)	Boundary condition	Residual at year 3 (mm)	Time to 25 mm (years)
0.75	Double	100.57	9.766
0.75	Single	164.94	39.064
1.50	Double	54.23	4.883
1.50	Single	138.09	19.532
3.00	Double	15.79	2.442
3.00	Single	100.57	9.766

Design-time contour and residual-settlement tolerance

A practical advantage of the time-factor formulation is that a specified maximum residual is first translated into a required consolidation fraction, after which the time scale follows from the drainage path and c_v. For the reference compression magnitude, the 25 mm residual allowance corresponds to a required average consolidation fraction of approximately 89.12%. The relevant threshold time factor is determined directly from the Fourier series rather than taken from a coarse design chart. Figure 4 maps the resulting time-to-criterion as a continuous function of the two independently assigned screening inputs c_v and H_d. The map is intended as a visualization of equation response; it does not imply that the variables are statistically independent in a natural deposit or that a deep clay stratum automatically has a single idealized drainage face.

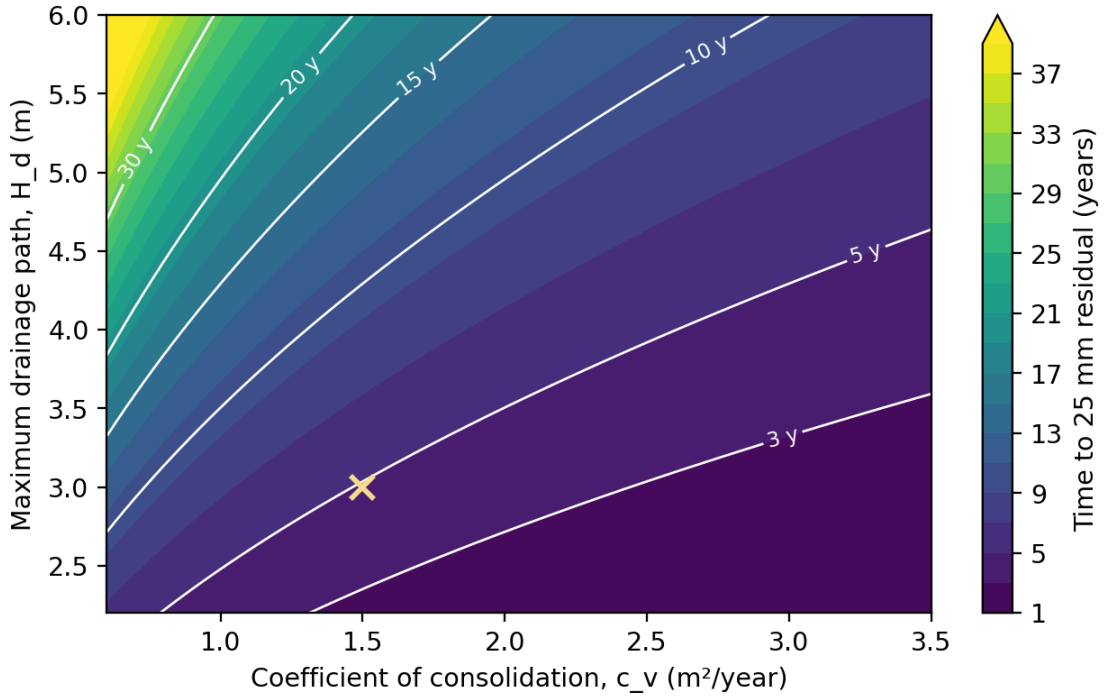


Figure 4. Analytical time (years) to attain 25 mm residual settlement, mapped against coefficient of consolidation and maximum drainage path; the cross indicates the reference case.

A permissible post-construction residual cannot be selected without a project-specific performance requirement. Figure 5 traces the time needed to attain selected allowances from 10 to 70 mm for three c_v values with ideal reference double drainage. Under c_v = 1.50 m²/year, an allowance of 50 mm is reached after 3.198 years, 25 mm after 4.883 years, and 15 mm after 6.125 years. Table 5 tabulates the corresponding required mean consolidation percentages and reference waiting times for these three design limits. Halving an allowance does not halve or double the time because the mean consolidation fraction tends asymptotically towards unity. Requirements for differential settlement may be more restrictive than a total-settlement rule; the present laterally uniform model has no capability to predict the spatial settlement gradients needed for that assessment.

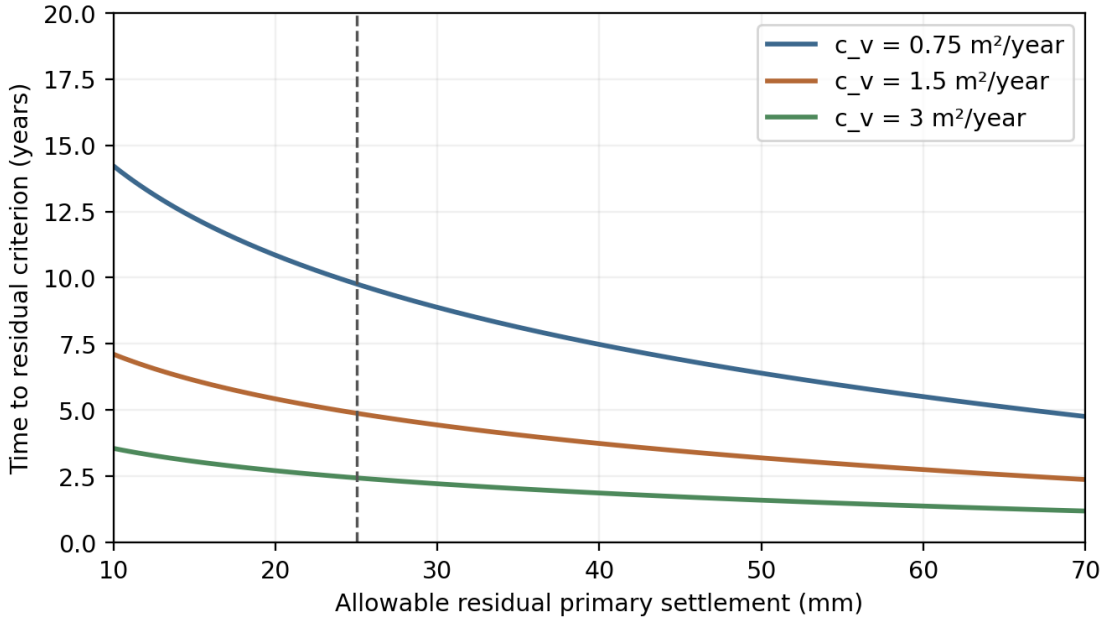


Figure 5. Elapsed time to selected residual primary settlement allowances (10–70 mm) for three assumed consolidation coefficients under ideal double drainage.

Table 5. Required average primary consolidation and time to criterion for three illustrative residual-settlement allowances under immediate loading.

Allowable residual (mm)	**Required mean consolidation (%)**	**Time for c_v = 1.50 m²/year**	**Relative criterion**
15	93.47	6.125 years	Most restrictive
25	89.12	4.883 years	Reference allowance
50	78.24	3.198 years	Least restrictive

Assumption testing, model boundaries and implementation pathway

Internal numerical consistency was checked in three ways. First, the integrated Fourier-series ramp formulation was compared with direct adaptive quadrature of the convolution integral at four elapsed times, both during and after ramp placement; the evaluated differences were below the computational comparison tolerance. Second, the two logarithmically computed stage settlements were summed and reproduced the ultimate compression calculated for the complete 60 kPa surcharge. Third, the time required for the same threshold increased by a factor of four when the maximum drainage path was doubled. These are verification tests of the prescribed equations and implementation, not calibration or validation against field data.

In engineering application the first prerequisite is a defensible ground model. Representative effective stress profiles should be developed from stratigraphy, water levels and unit weights; oedometer tests should identify compression and recompression behavior as well as estimates of c_v over the relevant stress levels. Stratified deposits can be represented by layerwise ultimate settlements, but their transient drainage behavior generally cannot be reproduced accurately by assigning independent H_d values and adding settlements when adjacent layers hydraulically interact. If the deposit exhibits strong stress-dependent permeability, secondary compression, time-dependent destructuration, radial drainage through prefabricated vertical

drains or appreciable large-strain deformation, the use of an advanced consolidation formulation is advisable. For example, Guo et al. (2024) analyze a more complex large-strain process involving vacuum loading and partially penetrating vertical drains, a configuration deliberately excluded here.

A second prerequisite is a construction-stage definition linked to the intended handover event. An engineer should enter the timing and magnitude of fill lifts, distinguish temporary surcharge from the sustained operational load, define which settling components are counted against the performance requirement, and specify when deformation monitoring becomes available. If the field settlement and pore-pressure trajectories depart materially from the proposed model, the input parameters and possibly the governing model should be revised. The appropriate use of the present results is early comparison of scheduling and drainage assumptions, not authorization to proceed without site-specific assessments of global embankment stability, undrained construction response, differential settlement, seepage or traffic-related long-term deformation.

The screening rule also calls attention to an apparent planning paradox: placing the entire load early can accelerate calculated primary settlement, but it can also impose a larger initial undrained stability demand on weak clay. Because shear strength gain and short-term lateral stability are outside the current model, earlier placement cannot be universally recommended. Staged construction may remain necessary to maintain stability while consolidation develops. Any practical selection among schedules must therefore combine the present settlement model with short-term strength and stability analyses and instrumented observational control. The absence of soil-structure interaction and lateral stress redistribution remains a major boundary of the proposed analytical decision map.

CONCLUSION

This study provides an explicitly reproducible residual-primary-consolidation screening procedure for soft clay subjected to immediate, ramped and staged embankment surcharge. For the assumed 6.0 m normally consolidated layer with an initial effective stress of 75 kPa, a 60 kPa stress increment, a compression index of 0.30 and an initial void ratio of 1.00, the calculated ultimate primary settlement is 229.75 mm. At c_v = 1.50 m²/year and ideal double drainage, a residual settlement allowance of 25 mm is reached after 4.883 years for immediate loading, 5.137 years for a 0.50-year ramp, and 5.362 years for two 30 kPa stages separated by one year. These different decision times occur despite the same theoretical final settlement and establish that the construction schedule cannot be omitted from a forecast of remaining primary deformation.

The drainage-path sensitivity is more pronounced than the loading-history sensitivity in the example. Doubling the idealized maximum drainage path from 3.0 to 6.0 m increases the step-load waiting time from 4.883 to 19.532 years, while doubling c_v reduces the waiting time by half. The results are direct consequences of the squared drainage-path and inverse consolidation-coefficient scaling and should not be used as empirical improvement factors for uncharacterized soils. Reducing the allowable residual from 50 to 15 mm increases the

baseline step-load time from approximately 3.198 to 6.125 years. These relationships motivate expressing design screening requirements in millimetres of remaining settlement at a stated date rather than solely in percentage degree of consolidation.

The principal limitation is intentional: all inputs are selected hypothetical values, primary compression alone is modelled, and the adopted theory presumes homogeneous one-dimensional drainage behavior with a constant consolidation coefficient. The finite-ramp treatment additionally distributes ultimate settlement proportionally over the ramp, whereas the staged treatment uses exact logarithmic settlement increments; these approximations should not be conflated with a complete nonlinear time-dependent constitutive simulation. The findings therefore support transparent preliminary comparison and sensitivity identification, not site-specific final design. Future testing should compare the screening criterion against instrumented staged embankments with measured pore pressures, consolidation curves, boundary drainage properties and independently evaluated secondary compression.

REFERENCES

Bjerrum, L. (1967). Engineering geology of Norwegian normally-consolidated marine clays as related to settlements of buildings. Géotechnique, 17(2), 83–118. https://doi.org/10.1680/geot.1967.17.2.83

Guo, W., Zhou, Y., Sun, L., Jiang, H., Lang, R., Chen, H., & Ren, Y. (2024). Large-strain consolidation of vacuum preloading combined with partially penetrating prefabricated vertical drains. International Journal for Numerical and Analytical Methods in Geomechanics, 48(9), 2450–2467. https://doi.org/10.1002/nag.3736

Mesri, G. (1973a). Coefficient of secondary compression. Journal of the Soil Mechanics and Foundations Division, 99(1), 123–137. https://doi.org/10.1061/JSFEAQ.0001840

Mesri, G. (1973b). One-dimensional consolidation of a clay layer with impeded drainage boundaries. Water Resources Research, 9(4), 1090–1093. https://doi.org/10.1029/WR009i004p01090

Nguyen, N. T. (2024). Long-term settlement prediction for over-consolidated soft clay under low embankment. Engineering, Technology & Applied Science Research, 14(6), 18592–18599. https://doi.org/10.48084/etasr.9211

Terzaghi, K., Peck, R. B., & Mesri, G. (1996). Soil mechanics in engineering practice (3rd ed.). John Wiley & Sons. ISBN 9780471086581.

United States Army Corps of Engineers (USACE). (1990). Settlement analysis (Engineer Manual EM 1110-1-1904). Department of the Army. https://www.publications.usace.army.mil/Portals/76/Publications/EngineerManuals/EM_1110-1-1904.pdf

Wang, J., Yuan, W., Yin, X., Li, W., & Li, X. (2023). One-dimensional consolidation properties of soft clay under multi-stage loading. Applied Sciences, 13(18), 10340. https://doi.org/10.3390/app131810340

DIMENSIONLESS SCREENING OF SOLUTE BREAKTHROUGH IN COMPACTED CLAY BARRIERS: HYDRAULIC–DIFFUSIVE COMPETITION AND EQUILIBRIUM SORPTION

Ali Akbar Firoozi
School of Civil, Environmental Engineering and Geomatics, Faculty of Engineering and Built Environment, University of Botswana, Gaborone, Botswana

Ali Asghar Firoozi
Department of Civil Engineering, Faculty of Engineering, National University of Malaysia (UKM), Selangor, Malaysia

ABSTRACT

Compacted clay barriers are often evaluated by hydraulic conductivity, although contaminant migration also depends on molecular diffusion, mechanical dispersion and reversible solute retention. This study develops a dimensionless analytical screening framework for the time needed for a dissolved solute to reach prescribed fractions of a sustained upstream concentration at a specified depth in a saturated, homogeneous clay medium. A one-dimensional advection–dispersion equation with linear equilibrium sorption is reduced to a response governed by the Péclet number and normalized time. Threshold concentrations of 5%, 10% and 50% are obtained using the full Ogata–Banks solution, and analytic scaling identities are supplemented by reproducible root finding and parametric maps. For an explicitly hypothetical reference case with screening depth 0.90 m, hydraulic conductivity 1×10^{-9} m/s, hydraulic gradient 1.0, porosity 0.40, diffusion coefficient 2×10^{-10} m²/s, dispersivity 0.05 m and retardation factor 2.0, the Péclet number is 6.923 and the calculated 10% arrival time is 10.474 years. Reducing hydraulic conductivity by half increases this threshold time to 16.870 years; increasing barrier depth to 1.20 m increases it to 15.568 years. The proposed dimensionless relation shows that equilibrium sorption scales concentration-threshold times linearly, whereas depth and conductivity have nonconstant sensitivities because they also modify the Péclet number. The results are screening estimates, not measured breakthrough, regulatory compliance predictions or simulations of an actual finite-thickness outlet. Verification against independent transport measurements and site-specific lower-boundary conditions is required for design.

Keywords: Hydraulic Gradient; Compacted Clay Liner; Advective–Dispersive Transport; Breakthrough Time; Retardation; Dimensionless Analysis

INTRODUCTION

Compacted clay barriers perform an important containment function within waste-storage facilities, contaminated-ground isolation systems and engineered cutoff arrangements. Their performance is commonly communicated through a target hydraulic conductivity, but low

water permeability alone does not uniquely prescribe how rapidly a dissolved contaminant migrates. Concentration gradients can drive molecular diffusion even when advective flow is small, and the ability of a clay to retain an individual chemical species depends on sorption behavior, solution chemistry and the composition of the porous medium. For this reason, hydraulic and chemical compatibility are closely connected in barrier evaluation (Shackelford, 1991; Rowe, 2005).

Field experience also establishes a practical limitation of single-parameter acceptance. Benson et al. (1999) evaluated 85 full-scale compacted clay liners and found that meeting an intended hydraulic-conductivity target was sensitive to the construction method and field condition. Waste–soil interactions can alter a liner's hydraulic properties after exposure, making it inappropriate to assume that the conductivity or sorption capacity of a compacted clay remains constant under all leachate chemistries (Shackelford, 1994). These observations motivate a transparent representation of the processes governing the time evolution of dissolved concentration, with the understanding that any idealized analysis must be connected to field and laboratory evidence before engineering use.

The classical one-dimensional convective–dispersive equation offers a tractable basis for assessing the competition between advection, diffusion and equilibrium retardation. The solution published by Ogata and Banks (1961), together with subsequent treatments of alternative input and outlet boundary conditions (van Genuchten and Alves, 1982), provides a reliable benchmark for analytical calculations. Laboratory column and diffusion studies have demonstrated why the diffusion coefficient, effective porosity, flow rate and solute retention are material-specific quantities rather than universal values for "clay" (Shackelford and Daniel, 1991; Shackelford and Redmond, 1995). More recent investigations of composite liners include thermodiffusion, geomembrane defects, nonlinear adsorption and coupled thermal–hydraulic processes, emphasizing that simple one-layer models are screening models rather than replacements for full barrier-system assessment (Qiu et al., 2023; Han et al., 2024).

There remains value in an explicitly constrained analytical framework that separates the influence of loading time, hydraulic transport parameters and sorption without hiding them inside a proprietary numerical model. Such a framework permits dimensionless comparison across hypothetical soil scenarios and exposes the exact dependencies of a selected breakthrough threshold. The present study asks three questions: how a concentration threshold changes with the relative strengths of advective and dispersive transport; how its arrival time responds to thickness, conductivity and equilibrium retardation; and where simplified concentration screening may be confused with the actual mass release of a finite liner. The contribution is an independently reproducible dimensionless threshold and sensitivity-map analysis. No laboratory tests, field case history, material-specific sorption measurements or calibration dataset are claimed.

MATERIALS AND METHOD

Physical idealization and parameter selection

The analysis assumes an initially uncontaminated, saturated, homogeneous and isotropic clay medium extending from a constant-concentration upstream plane into a downstream half-space. One-dimensional flow and transport occur along coordinate x, positive in the direction of the hydraulic gradient. The observation coordinate L is a designated screening depth within this homogeneous half-space. It is not treated as a physical free-drainage outlet or impermeable lower boundary. Hydraulic conductivity, porosity, dry density, solute distribution coefficient and hydrodynamic dispersion are held constant. The source concentration is maintained indefinitely from time zero. Temperature, density-driven flow, decay, nonlinear sorption, preferential pathways and chemical reactions other than linear reversible equilibrium sorption are excluded. Figure 1 illustrates the precise interpretation of L and the transport processes retained in the analysis.

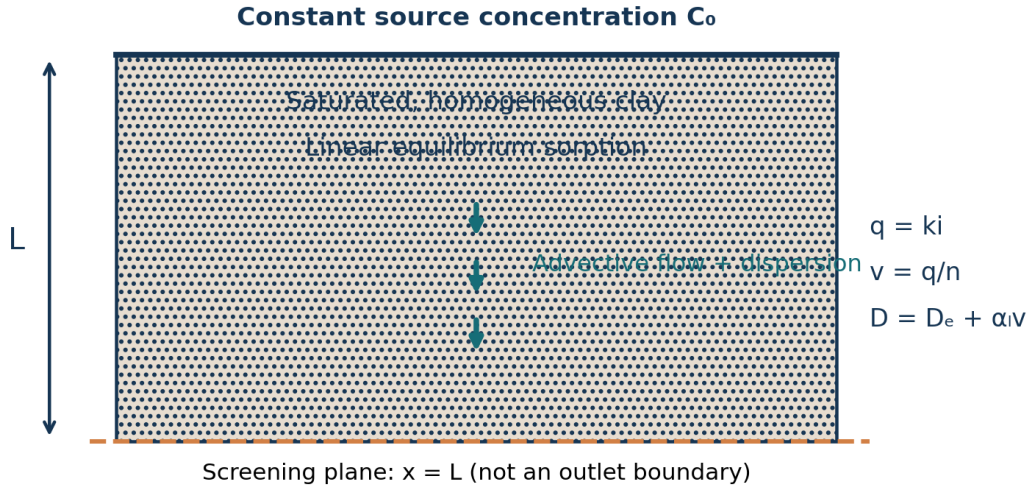


Figure 1. Schematic of the semi-infinite saturated clay domain, the sustained solute source and the in-domain screening location.

The prescribed parameters are selected only to illustrate mathematical behavior over a plausible engineering scale, not to represent a sampled clay deposit or a specific chemical. The dry bulk density, porosity, equilibrium distribution coefficient and transport coefficients are therefore treated as independent scenario inputs and are not claimed to be mutually calibrated measurements. Any application to an individual contaminant requires laboratory determination of the relevant aqueous diffusivity, hydrodynamic dispersion, sorption isotherm and chemical compatibility. Table 1 specifies all dimensional inputs and the baseline scenario, with the distinction between model assumptions and verified material properties maintained throughout.

Table 1. Hypothetical baseline transport inputs, physical meanings and SI units for the analytical screening scenario.

Quantity	Symbol	Baseline value	Unit
Screening depth	L	0.90	m
Hydraulic conductivity	k	1.0×10^{-9}	m/s
Hydraulic gradient	i	1.0	dimensionless
Effective water-filled porosity	n	0.40	dimensionless
Pore-water diffusion coefficient	D_e	2.0×10^{-10}	m²/s
Longitudinal dispersivity	α_L	0.050	m
Dry bulk density	ρ_b	1,600	kg/m³
Linear distribution coefficient	K_d	2.5×10^{-4} (0.25 L/kg)	m³/kg
Retardation factor	R	2.00	dimensionless
Source concentration	C_0	Arbitrary constant > 0	kg/m³

Hydraulic flow, dispersion and reversible sorption

Under one-dimensional saturated flow, the Darcy specific discharge q is obtained from hydraulic conductivity k and hydraulic gradient i. Interstitial or average pore-water velocity v follows by dividing q by the water-filled porosity n. Hydraulic conductivity and velocity are reported in metres per second, whereas the hydraulic gradient and porosity are dimensionless. For simplicity, hydrodynamic dispersion is represented by the sum of a pore-water molecular diffusion coefficient and mechanical dispersion proportional to pore-water velocity, as expressed in Equations (1)–(3). The symbol D_e is defined here as the effective pore-water diffusion coefficient in the pore-scale advection–dispersion equation, in m²/s; its numerical value must not be interchanged uncritically with a bulk-medium diffusion coefficient derived under another porosity convention.

$$q = ki \quad (1)$$

$$v = \frac{q}{n} \quad (2)$$

$$D = D_e + \alpha_L v \quad (3)$$

Linear equilibrium sorption is modeled through an aqueous concentration C (kg of solute/m³ of pore water) and a sorbed concentration S (kg of solute/kg of dry soil). The distribution coefficient K_d therefore has units m³/kg. With constant dry bulk density ρ_b (kg/m³ of bulk soil), the corresponding dimensionless retardation factor is defined by Equations (4) and (5). The assumption implies that the sorbed phase is locally equilibrated with the pore water, and excludes kinetic limitation, competitive ion exchange and nonlinear adsorption. Where tests indicate such effects, the constant-retardation approximation should be replaced by a corresponding coupled reaction-transport model.

$$S = K_d C \quad (4)$$

$$R = 1 + \frac{\rho_b K_d}{n} \quad (5)$$

Governing equation and concentration boundary conditions

For spatially uniform and temporally constant parameters, conservation of dissolved and

reversibly sorbed solute reduces to Equation (6). Time t is measured in seconds, x in metres, and D in m²/s. The left-hand retardation term accounts for reversible storage, while the right-hand terms represent Fickian spreading and net pore-water advection. The problem assumes a zero initial dissolved concentration for x greater than zero (Equation (7)), a prescribed constant source concentration C_0 at the source plane and zero concentration as x approaches infinity at every finite time (Equation (8)). This is a first-type, or Dirichlet, source boundary with a semi-infinite downstream domain. It does not impose a flux continuity condition at a genuine liner–aquifer interface.

$$R\frac{\partial C}{\partial t} = D\frac{\partial^2 C}{\partial x^2} - v\frac{\partial C}{\partial x} \quad (6)$$

$$C(x,0) = 0 \quad (x > 0) \quad (7)$$

$$C(0,t) = C_0, \qquad \lim_{x\to\infty} C(x,t) = 0 \quad (8)$$

For positive velocity and time, the full classical concentration solution is written as Equation (9). The function erfc is the complementary error function defined by Equation (10); its dummy variable u is dimensionless, as is its argument z. The exponential factor in Equation (9) is mathematically important, especially when dispersion cannot be neglected. In numerical evaluation the second term is implemented using the scaled complementary error function to avoid floating-point overflow at large Péclet numbers. Exact reproduction of the full expression, rather than omitting a correction term, is essential for comparison of the low- and moderate-Péclet scenarios considered here (Ogata and Banks, 1961; van Genuchten and Alves, 1982).

$$\frac{C(x,t)}{C_0} = \frac{1}{2}\left[\operatorname{erfc}\left(\frac{Rx-vt}{2\sqrt{DRt}}\right) + \exp\left(\frac{vx}{D}\right)\operatorname{erfc}\left(\frac{Rx+vt}{2\sqrt{DRt}}\right)\right] \quad (9)$$

$$\operatorname{erfc}(z) = \frac{2}{\sqrt{\pi}}\int_z^\infty \exp(-u^2)\,du \quad (10)$$

Dimensionless reduction and breakthrough definitions

The analysis adopts the Péclet number Pe, defined in Equation (11) as the ratio of advective to dispersive transport over screening depth L, and a dimensionless time θ given by Equation (12). At the screening plane x=L, the normalized concentration collapses to the function F in Equation (13), determined entirely by θ and Pe. The retardation factor R influences physical time but not the shape of the response when plotted against θ, as long as equilibrium sorption remains linear and D, n and v remain unaffected by sorption. This separation is the foundation of the proposed screening representation and is not an additional empirically fitted relationship.

$$\mathrm{Pe} = \frac{vL}{D} \quad (11)$$

$$\theta = \frac{vt}{RL} \quad (12)$$

$$F(\theta,\mathrm{Pe}) = \frac{1}{2}\left[\operatorname{erfc}\left((1-\theta)\sqrt{\frac{\mathrm{Pe}}{4\theta}}\right) + \exp(\mathrm{Pe})\operatorname{erfc}\left((1+\theta)\sqrt{\frac{\mathrm{Pe}}{4\theta}}\right)\right] \quad (13)$$

An arrival threshold η is the dimensionless ratio of the selected aqueous concentration to the imposed constant source concentration, between zero and unity. This paper analyzes η = 0.05,

0.10 and 0.50; these values are illustrative comparison criteria, not toxicity limits or statutory acceptance thresholds. The dimensionless arrival time θ_η is obtained by solving Equation (14) for the first positive root, and the physical time t_η then follows from Equation (15). Root solving uses a bracketed Brent algorithm with tight numerical tolerance. The same mathematical approach applies for any positive velocity, screening depth, dispersion coefficient and retardation factor satisfying the model assumptions.

$$F(\theta_\eta, \mathrm{Pe}) = \eta \quad (14)$$

$$t_\eta = \frac{RL}{v}\,\theta_\eta(\mathrm{Pe}) \quad (15)$$

Two limiting time scales aid interpretation. Equation (16) gives the nominal retarded advective transit time, which need not equal any particular concentration-arrival threshold when dispersion is finite. Equation (17) gives the purely diffusive constant-concentration threshold time when v approaches zero and D remains fixed. The inverse complementary error function $\mathrm{erfc}^{-1}(\eta)$ returns the real argument of erfc at η. The diffusion limit is calculated as a separate mathematical check, not as the hydraulic conductivity tending to zero while a mechanically dispersive contribution somehow remains constant.

$$t_{\mathrm{adv}} = \frac{RL}{v} \quad (16)$$

$$t_{\eta,\mathrm{diff}} = \frac{RL^2}{4D\,[\mathrm{erfc}^{-1}(\eta)]^2} \quad (17)$$

Parametric design and logarithmic sensitivities

The variable set comprises screening depth L of 0.45–1.60 m, hydraulic conductivity k of 0.4–4.0 × 10^{-9} m/s, equilibrium retardation R of 1–4, and a Péclet-number range of 0.1–approximately 160. All remaining baseline parameters are fixed unless otherwise stated. These ranges define synthetic comparisons and are not statistical confidence limits. A diagnostic diffusion fraction χ, defined in Equation (18), measures how much of the model dispersion coefficient is associated with the diffusion term rather than mechanical dispersion. The analytical elasticity of threshold time to retardation is exactly unity (Equation (19)), while the logarithmic sensitivities to k and L satisfy Equations (20) and (21). Their derivation follows from t_η = (RL/v)θ_η(Pe), the proportionality of v to k, and Pe = vL/(D_e+α_Lv).

$$\chi = \frac{D_e}{D_e + \alpha_L v} \quad (18)$$

$$E_R = \frac{\partial \ln t_\eta}{\partial \ln R} = 1 \quad (19)$$

$$E_k = \frac{\partial \ln t_\eta}{\partial \ln k} = -1 + \chi\frac{\partial \ln \theta_\eta}{\partial \ln \mathrm{Pe}} \quad (20)$$

$$E_L = \frac{\partial \ln t_\eta}{\partial \ln L} = 1 + \frac{\partial \ln \theta_\eta}{\partial \ln \mathrm{Pe}} \quad (21)$$

The derivatives in Equations (19)–(21) are dimensionless. The notation ∂ln t_η/∂ln k denotes the local change of the logarithm of arrival time with the logarithm of conductivity under fixed values of the remaining inputs; no logarithm of a dimensional absolute magnitude needs to be taken computationally because the elasticities are ratios of changes, or equivalently

logarithms of like-unit ratios. Equation (22) is included to distinguish local concentration from a mass-flux measure: J denotes total dissolved advective–dispersive mass flux through unit bulk cross-sectional area (kg of solute/(m²·s)), and the concentration gradient is required to evaluate its dispersive contribution. Since the benchmark geometry lacks a finite-liner outlet, the downstream-plane concentration in this study must not be mislabeled as a measured or finite-layer leachate effluent concentration.

$$J = n\left(vC - D\frac{\partial C}{\partial x}\right) \quad (22)$$

Notation and SI units. In Equations (1)–(22), q is Darcy specific discharge, k is saturated hydraulic conductivity and v is pore-water velocity (each in m/s); i is hydraulic gradient and n is effective water-filled porosity (both dimensionless). The parameters D and D_e denote the total hydrodynamic dispersion coefficient and the adopted pore-water diffusion coefficient, respectively (m²/s), while α_L is longitudinal dispersivity (m). The parameters ρ_b and K_d are dry bulk density (kg of dry soil/m³ of bulk medium) and equilibrium linear distribution coefficient (m³ of pore water/kg of dry soil); R is the dimensionless linear retardation factor. Both x and L are distances in metres, and L is only an in-domain observation location in this semi-infinite analytical model.

Concentration, time and screening functions. The variables C and C_0 are dissolved and sustained upstream source concentrations (kg solute/m³ of pore water), whereas S is sorbed solute per unit dry soil mass (kg solute/kg dry soil). The independent time t, selected concentration-arrival time t_η, retarded advective time t_{adv} and pure-diffusion limiting arrival time $t_{\eta,diff}$ are in seconds when inserted into the governing equations; values reported in years use 365.25 days/year. The Péclet number Pe, dimensionless time θ, threshold time θ_η, normalized concentration function F, concentration fraction η, diffusion fraction χ and elasticities E_R, E_k and E_L are all dimensionless. The complementary error function erfc and its arguments z and integration variable u are dimensionless. The dissolved total flux J has SI units kg solute/(m²·s); the concentration gradient $\frac{\partial C}{\partial x}$ has units kg solute/m⁴. All source concentrations and fluxes refer to dissolved solute, with adsorption represented separately through S and R.

Numerical verification procedure

For the baseline conditions, the Darcy discharge is 1.000×10^{-9} m/s, pore-water velocity 2.500×10^{-9} m/s and hydrodynamic dispersion coefficient 3.250×10^{-10} m²/s. Accordingly, Pe equals 6.9230769 and the retarded advective transit time is 22.8154 years when a year is defined as 365.25 days. The bracketed Brent root solver uses a dimensionless-time interval of 10^{-7} to 100 and an absolute root tolerance of 2×10^{-13}. Model outputs are calculated by substituting θ_η roots into the exact solution and checking the reconstructed concentration against the target within numerical tolerance. Physical consistency is additionally tested through the expected concentration bounds between zero and one, monotonic increasing concentration with time, exact linear scaling with R, and convergence to the purely diffusive limit as Pe decreases toward zero. The Python/SciPy implementation uses the erfcx stabilization identity to evaluate the second term in the solution, avoiding cancellation and

overflow at extreme inputs.

RESULTS AND DISCUSSION

Baseline transport scales and threshold arrival times

Table 2 brings together the calculated baseline threshold times. The computed 5% and 10% arrivals are 8.814 and 10.474 years, respectively, whereas reaching 50% requires 19.982 years. These times precede the nominal retarded advective transit time of 22.815 years because hydrodynamic spreading transmits nonzero concentration ahead of the average advective front. The difference is important for engineering communication: the quotient of depth and retarded pore velocity is a meaningful benchmark, but it is not a unique definition of breakthrough. An effective barrier assessment must identify the relevant chemical species, boundary conditions, spatial location and concentration criterion before reporting any breakthrough time.

Table 2. Dimensionless and physical arrival times for selected normalized concentration thresholds at the baseline screening plane.

Threshold η	θ_η **(–)**	t_η **(years)**	$\frac{t_\eta}{t_{adv}}$ (–)
0.05	0.38631	8.814	0.38631
0.10	0.45907	10.474	0.45907
0.50	0.87580	19.982	0.87580

Figure 2 traces the temporal concentration histories and reveals the separate impact of the constant equilibrium retardation factor. For R = 1, the 10% threshold occurs after 5.237 years; for R = 1.5, 2 and 4 the corresponding times are 7.855, 10.474 and 20.948 years. These values follow directly from exact linear time scaling and should not be interpreted as field-specific treatment benefits without measuring the solute–soil partition relation over the relevant concentration range. After 20 years, the calculated normalized concentration is 0.911 at R = 1 and 0.084 at R = 4; the apparently large difference is an idealized equilibrium-retardation consequence and does not account for saturation of sorption sites or chemical alteration.

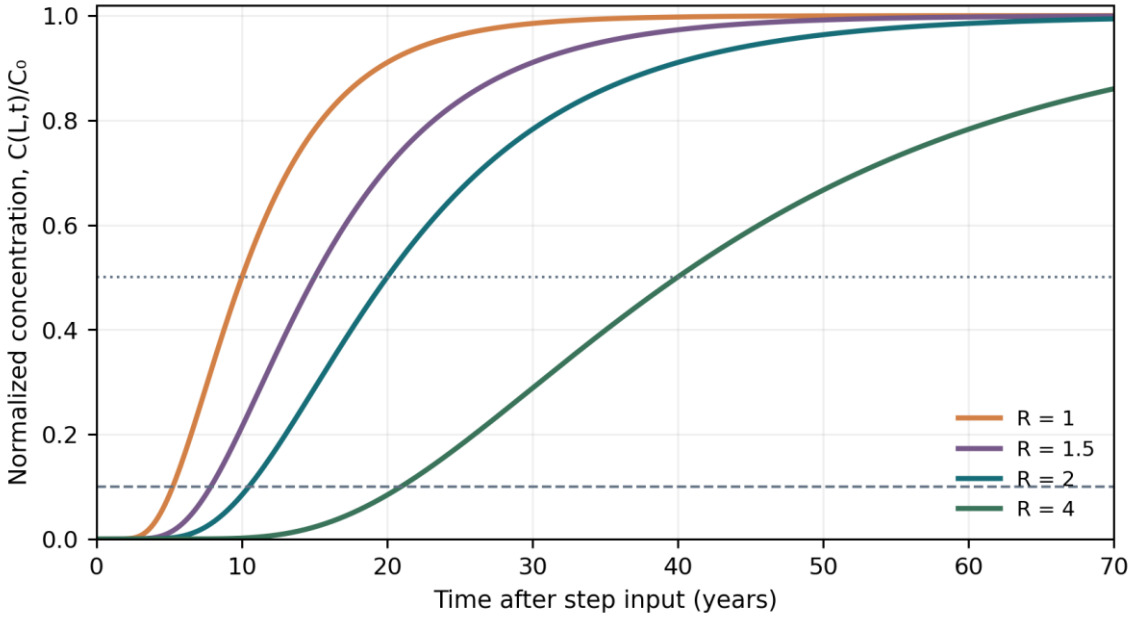


Figure 2. Evolution of normalized concentration at the 0.90 m screening depth for four assumed equilibrium retardation factors.

Dimensionless arrival-time maps and diffusion control

Figure 3 maps the three dimensionless threshold-time curves, while Table 3 tabulates selected numerical roots for comparison. At Pe = 0.2, the 10% normalized arrival time θ_{10} is approximately 0.0349, because diffusive spreading can penetrate the observation depth long before the nominal advective transit. At Pe = 10, the corresponding normalized time is 0.5261; at Pe = 100 it rises to approximately 0.8266. Thus a normalized time close to one is attained only in a relatively advection-dominated limit, and it is not appropriate to equate time to 5% or 10% concentration with retarded advective travel time in a diffusion-influenced liner. The shape of the curves follows solely from Equation (13), rather than from material-specific fitted constants.

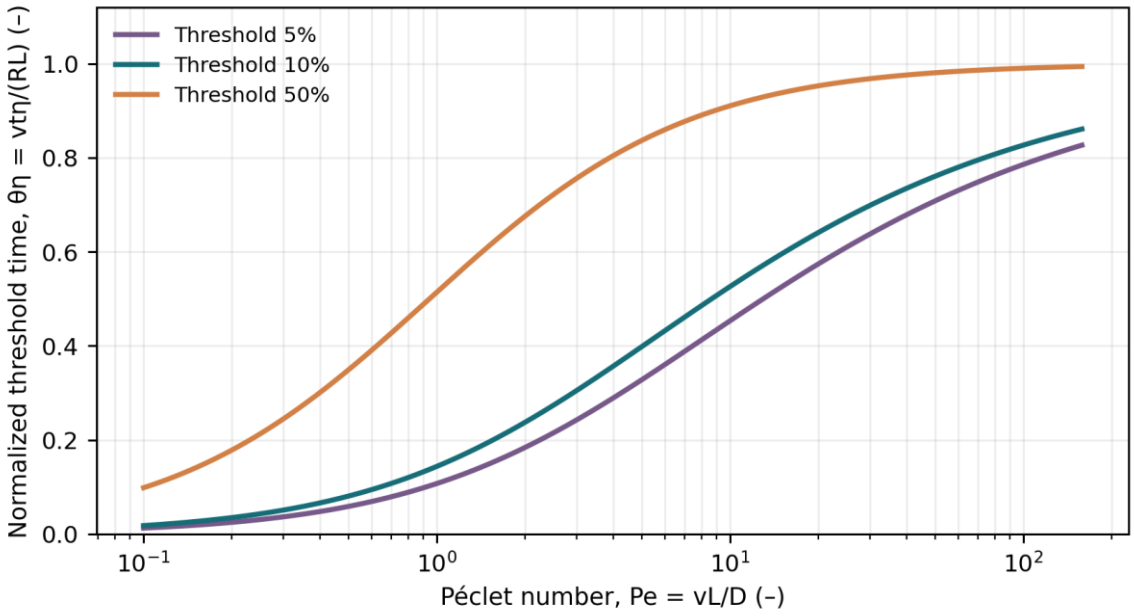


Figure 3. Dimensionless concentration-threshold arrival times over the Péclet-number range for 5%, 10% and 50% source-concentration ratios.

Table 3. Péclet-number-dependent solutions for three dimensionless arrival-time thresholds.

Pe (–)	θ_5 (–)	θ_{10} (–)	θ_{50} (–)
0.2	0.0249	0.0349	0.1785
0.5	0.0588	0.0807	0.3492
1	0.1074	0.1438	0.5142
2	0.1841	0.2376	0.6758
5	0.3279	0.3984	0.8366
10	0.4533	0.5261	0.9102
20	0.5741	0.6409	0.9527
50	0.7080	0.7604	0.9805
100	0.7856	0.8266	0.9901

The original equations show that reducing hydraulic conductivity does not eliminate diffusion. In the hypothetical limit of zero flow, the threshold time remains finite for a fixed D_e and constant boundary concentration, and the governing expression reduces to the erfc diffusion solution. For the baseline L, R and molecular diffusion coefficient D_e, the pure-diffusion 10% threshold is approximately 47.435 years. That limiting number is not comparable to an actual zero-flow finite liner without specifying the lower boundary and source evolution; rather, it demonstrates mathematically why conductivity by itself cannot guarantee zero migration. A hydraulic barrier and a chemical containment barrier must be evaluated through related but non-identical criteria (Shackelford, 1991; Rowe, 2005).

Sensitivity to hydraulic conductivity and screening depth

The conductivity sensitivity is both substantial and nonlinear. Increasing k from 0.5×10^{-9} to 4×10^{-9} m/s reduces the baseline 10% arrival time from 16.870 to 3.250 years. A fourfold increase relative to $k = 1 \times 10^{-9}$ m/s shortens the 10% time from 10.474 to 3.250 years, not exactly to one quarter, because the Péclet number changes at the same time. Figure 4 contrasts

the depth response across four conductivity scenarios; Table 4 quantifies the corresponding threshold times. In this system, increasing the screen depth from 0.90 to 1.20 m at the baseline conductivity increases t_{10} from 10.474 to 15.568 years, a factor of approximately 1.486. Pure advection would predict a depth factor of 1.333, while the purely diffusive limit follows the square of depth; the observed factor therefore lies between the two asymptotic behaviors.

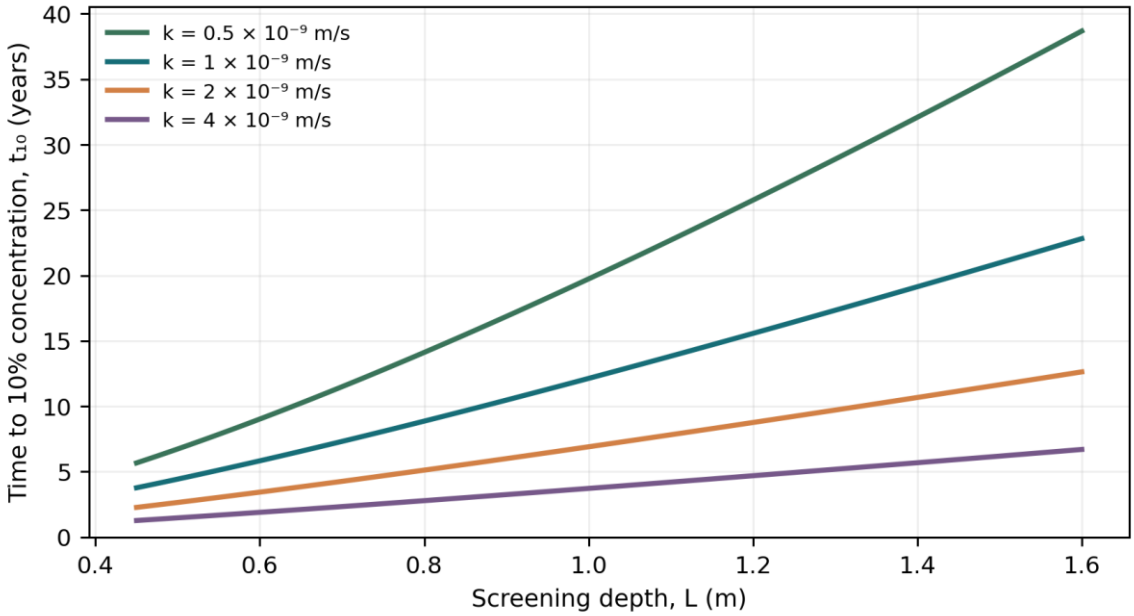


Figure 4. Sensitivity of the calculated 10% concentration-arrival time to screening depth under four hydraulic-conductivity scenarios.

Table 4. Changes in calculated 10% and 50% arrival times with hydraulic conductivity and screening depth.

Varied input	**Level**	**Pe (–)**	t_{10} **(years)**	t_{50} **(years)**
k (m/s)	0.5×10^{-9}	4.286	16.870	37.179
k (m/s)	1×10^{-9}	6.923	10.474	19.982
k (m/s)	2×10^{-9}	10.000	6.001	10.383
k (m/s)	4×10^{-9}	12.857	3.250	5.296
L (m)	0.60	4.615	5.832	12.556
L (m)	0.90	6.923	10.474	19.982
L (m)	1.20	9.231	15.568	27.486
L (m)	1.50	11.538	20.961	35.027

Figure 5 visualizes synthetic combinations of screening depth and hydraulic conductivity under the same chemical and hydraulic assumptions. A reference marker indicates L = 0.90 m and k = 1×10^{-9} m/s. The contours are neither measured performance surfaces nor universal thickness charts: the underlying observation remains a concentration at a plane inside a semi-infinite uniform medium. Nevertheless, the mapping is useful for early-stage sensitivity communication because it identifies how a change in specified screening depth may compensate for a change in permeability within the adopted idealized model, and where the dependence becomes distinctly nonlinear. Site design requires a finite-domain solution that includes the downstream interface and the transport properties of adjacent layers.

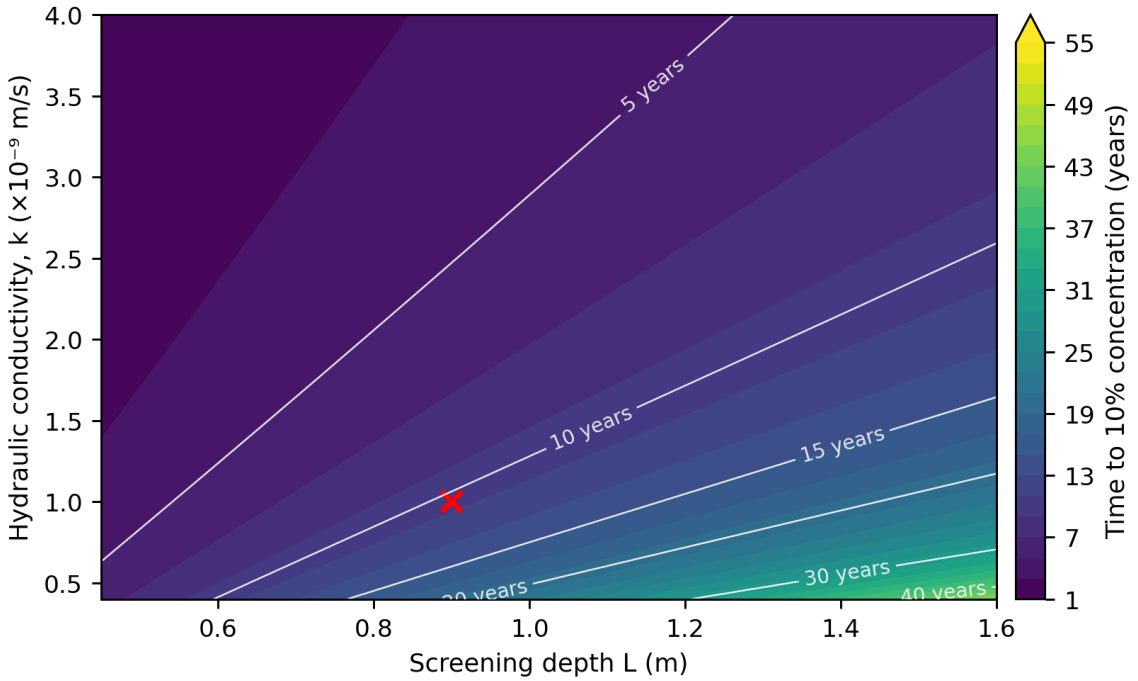


Figure 5. Contours of calculated 10% concentration-arrival time as functions of screening depth and hydraulic conductivity.

Retardation, observation time and combined parameter effects

The exact relation t_η proportional to R is an invariant of the selected equilibrium linear-sorption model. For a ten-percent threshold, doubling R from 2 to 4 doubles the arrival time from 10.474 to 20.948 years without changing the normalized θ_{10} response. Table 5 quantifies this scaling together with calculated concentration levels at fixed service times. Comparing sorption scenarios at a common duration is more informative than comparing threshold times alone when a planning horizon has been selected, because two designs may produce similar threshold dates but different concentrations during the period of operational concern.

Table 5. Retardation-dependent threshold times and normalized concentrations at 20-year and 30-year observation horizons.

R (–)	t_5 (years)	t_{10} **(years)**	$\frac{C}{C_0}$ **at 20 y**	$\frac{C}{C_0}$ **at 30 y**
1	4.407	5.237	0.9106	0.9851
1.5	6.610	7.855	0.7106	0.9106
2	8.814	10.474	0.5007	0.7830
4	17.628	20.948	0.0841	0.2885

Figure 6 charts the combined conductivity–retardation influence on concentration at a fixed 20-year period. Lower permeability and greater sorption both delay penetration, but neither can be considered a universal remedy if solution chemistry changes the soil fabric or shifts the partition relation away from the linear assumption. The contour-like divergence at the same hydraulic conductivity reflects different assumed chemical responses, not experimentally demonstrated performance of a particular clay. This distinction is supported by published

evidence that solution chemistry, interaction mechanisms and measured diffusion coefficients may significantly alter real barrier behavior (Shackelford, 1994; Shackelford and Redmond, 1995).

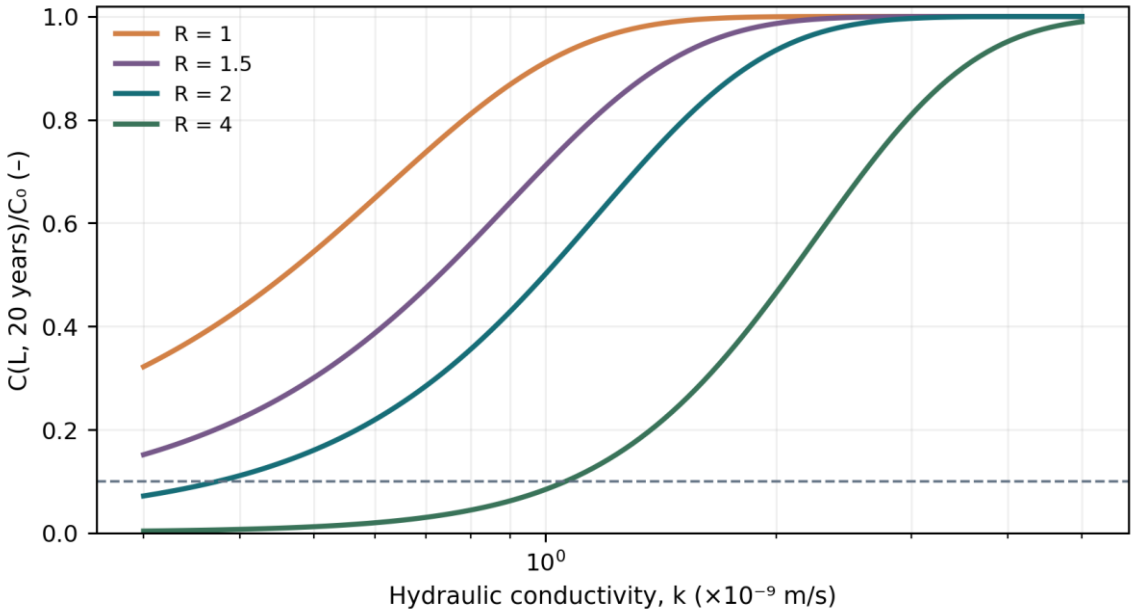


Figure 6. Normalized concentration at 20 years as a function of hydraulic conductivity for four assumed retardation factors.

Local elasticities and numerical consistency checks

The derivative identities permit a quantitative comparison of local design sensitivity that does not require arbitrary changes of scale. At the reference scenario and the 10% threshold, centered finite differences using perturbations of ±0.01% produce a logarithmic elasticity of 1.0000 for retardation, approximately −0.7512 for hydraulic conductivity and approximately +1.4042 for observation depth. The respective values for molecular diffusivity and dispersivity, when changed separately, are approximately −0.2488 and −0.1555. These derivatives describe the local mathematical response of the assumed equation; they are not estimated sensitivity indices inferred from uncertain laboratory data. Table 6 catalogues verification criteria and qualifications intended to prevent misuse of the solution.

Table 6. Internal mathematical verification criteria and limitations on the applicability of the semi-infinite transport model.

Check or assumption	Analytical implication	Required qualification
Linear equilibrium retardation	t_η scales exactly with R	Verify contaminant-specific sorption isotherm.
Constant source concentration	C(0,t) stays at C_0	Finite spill or decaying source needs another input.
Semi-infinite homogeneous medium	L is a screening location	Finite liner effluent requires outlet and layer matching.
No preferential pathways	One-dimensional matrix transport	Inspect cracking, defects and field compaction.

Check or assumption	Analytical implication	Required qualification
Constant transport coefficients	Time-independent Pe and R	Check chemical compatibility and temperature.
Concentration criterion	t_η depends on selected η	Regulatory or risk-based criterion must be defined externally.

The stable implementation reproduces the exact concentration threshold to within numerical solver tolerance when the returned θ_η is substituted into Equation (13). Each concentration curve is nondecreasing with elapsed time and remains between zero and the imposed source concentration. The model approaches the pure-diffusion erfc form as the advective velocity tends to zero with molecular diffusion fixed, and the derived elasticities agree with finite-difference perturbations. These checks support internal arithmetic and mathematical consistency. They do not establish experimental predictive accuracy, because an exact solution to an idealized equation can still be unsuitable for a real cracked, layered, reactive or unsaturated barrier.

Engineering implications and transferability limits

A useful preliminary decision sequence is therefore to identify the transported species and its relevant concentration or flux acceptance criterion; obtain representative saturated hydraulic properties, effective transport coefficients and contaminant-specific retention measurements; characterize credible source loading; and only then select a one-dimensional or multidimensional boundary-value model suited to the actual containment system. Complementary column-test interpretation may use cumulative solute mass as well as concentration histories (Shackelford, 1995). When a physical liner thickness and a downstream aquifer are part of the engineering problem, the finite-liner interface requires an explicit concentration or flux-matching condition. The concentrations presented here at L must not be substituted for a mass flux across that interface. Equation (22) illustrates the additional spatial-gradient information needed even before total mass discharge can be evaluated.

Thermal gradients, geomembrane imperfections, chemical degradation and concentration-dependent adsorption are outside the deliberately restricted analytical scope. Qiu et al. (2023) developed a substantially richer composite-liner solution incorporating effective porosity and thermodiffusion, and Han et al. (2024) treated nonlinear adsorption within coupled hydraulic–mechanical–chemical analysis. The present contribution is not a replacement or claimed experimental improvement over those approaches. Its strength is the exact dimensionless factorization of threshold time for a narrowly defined saturated single-layer transport problem, making the relative roles of diffusion, water flow and equilibrium retention explicit, auditable and suitable for checking or explaining more complex computations.

CONCLUSION

This study developed a dimensionless analytical framework for concentration screening at a specified depth of a homogeneous saturated clay medium subjected to a constant upstream solute concentration. The classical advection–dispersion solution with linear equilibrium

sorption reduces to a normalized response controlled by Péclet number and dimensionless time. For the explicitly illustrative baseline, Pe equals 6.923 and the times to reach 5%, 10% and 50% of the source concentration are 8.814, 10.474 and 19.982 years. The calculated thresholds are properties of the stated mathematical scenario and should not be presented as measured breakthrough of an actual barrier system.

The dimensionless representation establishes three interpretable relationships. First, the equilibrium retardation factor scales all selected concentration-arrival times exactly and proportionally when the transport coefficients are fixed. Second, hydraulic conductivity affects both pore-water travel and mechanical dispersion, so the threshold-time response is not generally inverse-linear in conductivity. Third, screening depth alters both travel distance and Péclet number, yielding thickness sensitivity between simple advective and diffusive limits. The local threshold-time elasticities at the baseline quantify this intermediate regime: +1.404 for observation depth, −0.751 for conductivity and exactly +1 for equilibrium retardation. These identities are suitable for independent numerical verification and transparent scenario ranking.

The primary limitation is the distinction between downstream-plane concentration in a semi-infinite half-space and contaminant effluent or mass release through a finite engineered liner. A barrier-specific assessment should incorporate its actual upstream source history, finite-domain lower boundary, interface conditions, representative field conductivity, diffusion and retardation measurements, and potential pathways created by desiccation, cracking, construction defects or chemical incompatibility. The framework provides a reproducible first-stage comparison, not a stand-alone compliance or design certification method.

REFERENCES

Benson, C. H., Daniel, D. E. & Boutwell, G. P. (1999). Field performance of compacted clay liners. Journal of Geotechnical and Geoenvironmental Engineering, 125(5), 390–403. https://doi.org/10.1061/(ASCE)1090-0241(1999)125:5(390)

Han, L., Zhang, Z. & Zhou, J. (2024). Analytical solutions for a fully coupled hydraulic-mechanical-chemical model with nonlinear adsorption. International Journal for Numerical and Analytical Methods in Geomechanics, 48, 4110–4121. https://doi.org/10.1002/nag.3829

Ogata, A. & Banks, R. B. (1961). A solution of the differential equation of longitudinal dispersion in porous media. U.S. Geological Survey Professional Paper 411-A, A1–A7. https://doi.org/10.3133/pp411A

Qiu, J.-W., Jiang, L.-S., Pu, H.-F., Song, D.-B., Min, M. & Tong, J. (2023). Analytical solutions for contaminant transport through a GMB/CCL composite liner system considering effective porosity and thermodiffusion. Computers and Geotechnics, 163, 105713. https://doi.org/10.1016/j.compgeo.2023.105713

Rowe, R. K. (2005). Long-term performance of contaminant barrier systems. Géotechnique, 55(9), 631–678. https://doi.org/10.1680/geot.2005.55.9.631

Shackelford, C. D. (1991). Laboratory diffusion testing for waste disposal—A review. Journal of Contaminant Hydrology, 7(3), 177–217. https://doi.org/10.1016/0169-7722(91)90028-Y

Shackelford, C. D. (1994). Waste-soil interactions that alter hydraulic conductivity. In Hydraulic Conductivity and Waste Contaminant Transport in Soil (ASTM STP 1142), 111–168. ASTM International. https://doi.org/10.1520/STP23887S

Shackelford, C. D. (1995). Cumulative mass approach for column testing. Journal of Geotechnical Engineering, 121(10), 696–703. https://doi.org/10.1061/(ASCE)0733-9410(1995)121:10(696)

Shackelford, C. D. & Daniel, D. E. (1991). Diffusion in saturated soil. I: Background. Journal of Geotechnical Engineering, 117(3), 467–484. https://doi.org/10.1061/(ASCE)0733-9410(1991)117:3(467)

Shackelford, C. D. & Redmond, P. L. (1995). Solute breakthrough curves for processed kaolin at low flow rates. Journal of Geotechnical Engineering, 121(1), 17–32. https://doi.org/10.1061/(ASCE)0733-9410(1995)121:1(17)

van Genuchten, M. Th. & Alves, W. J. (1982). Analytical solutions of the one-dimensional convective-dispersive solute transport equation. U.S. Department of Agriculture, Agricultural Research Service, Technical Bulletin 1661.

GROUNDWATER-SENSITIVE RELIABILITY SCREENING OF STRIP FOOTINGS ON SAND: A REPRODUCIBLE BEARING-CAPACITY DESIGN MAP

Ali Akbar Firoozi
School of Civil, Environmental Engineering and Geomatics, Faculty of Engineering and Built Environment, University of Botswana, Gaborone, Botswana

Ali Asghar Firoozi
Department of Civil Engineering, Faculty of Engineering, National University of Malaysia (UKM), Selangor, Malaysia

ABSTRACT
Shallow footings supported by cohesionless ground can experience a marked reduction in effective-stress bearing resistance when groundwater rises towards the foundation base. Conventional assessments often present the resulting resistance through a single factor of safety without stating how uncertainties in friction angle and applied pressure affect the probability of exceeding the limit state. This paper develops a reproducible screening framework for a surface strip footing using an explicitly defined unit-weight interpolation, a specified bearing-capacity factor, independent normally distributed effective friction angle and lognormally distributed applied pressure. Bearing-failure probabilities are evaluated through one-dimensional numerical integration and independently checked against a one-million-realization Monte Carlo simulation. For a hypothetical 2.0 m footing with mean friction angle 32 degrees, standard deviation 3 degrees and mean pressure 210 kPa, the calculated probability of bearing failure increases from 1.76% with groundwater at least one footing width below the base to 17.18% when groundwater reaches the base. At 0.5 m groundwater depth, the calculated probability is 9.77%, whereas the nominal factor of safety is 1.80. Under an explicitly illustrative probability-screening level of 5%, the required footing widths are approximately 2.74 m, 2.40 m and 2.06 m for groundwater depths of 0, 0.5 and 1.0 m, respectively. These values are model-dependent demonstrations, not inferred site performance or prescribed design targets. The framework emphasizes consistent hydrological assumptions, uncertainty reporting and the separation of preliminary screening from full geotechnical verification.

Keywords: Geotechnical Engineering; Strip Footings; Groundwater; Bearing Capacity; Reliability; Monte Carlo Simulation; Probability of Failure.

INTRODUCTION
The ultimate bearing resistance of a shallow foundation depends on soil strength, the effective stress field, foundation geometry and the characteristics of the imposed action. For a frictional soil, the self-weight component of the classical bearing-capacity expression is particularly sensitive to both the effective internal friction angle and the soil unit weight contributing to

the assumed failure mechanism. Groundwater introduces an additional design condition because the relevant effective unit weight can change appreciably as the water table approaches the founding level. A foundation assessed only for a relatively deep water table may therefore have a different safety margin after a persistent rise in groundwater, even if its contact pressure and footing geometry remain unchanged.

The influence of groundwater is more complicated than a universally applicable reduction of soil unit weight. Cascone, Biondi and Casablanca (2021) examined strip footing bearing capacity using the method of characteristics and showed that correction factors depend on groundwater depth, friction angle and interface conditions. Showkat and Sivakumar Babu (2023) separately demonstrated how changes in suction during rainfall can affect the response of unsaturated footing soils. These studies provide reasons to describe the assumed hydraulic regime and to distinguish a simplified screening rule from a general solution for coupled transient infiltration, suction and plastic failure. The present contribution intentionally adopts the narrower and auditable case of a steady idealized water table with no suction contribution.

An apparently satisfactory deterministic bearing-capacity ratio also contains no direct information about the distribution of the available resistance. Reliability-oriented work by Griffiths, Fenton and Manoharan (2002), Kayser and Gajan (2014), and Li et al. (2021) demonstrates that uncertainty and spatial variability may materially influence shallow-foundation performance estimates. Motra, Stutz and Wuttke (2016) further examined how selection of a bearing-capacity factor model contributes uncertainty even when conventional input statistics are available. More recently, Li et al. (2024) investigated the relationship between conventional safety factors and reliability for foundations on spatially variable cohesive soil; their configuration differs from the sand strip footing considered here, but the distinction between nominal safety and probability of failure remains relevant.

This study is deliberately limited to a synthetic decision-support model. It does not purport to establish new constitutive parameters from laboratory tests, verify a particular foundation design, or reproduce field histories of groundwater movement. Instead, it asks three narrowly defined questions: how much an assumed rise of the water table changes nominal resistance and conditional failure probability; how footing width can compensate within the selected bearing model; and how sensitive the apparent screening conclusion is to uncertainty in soil friction angle and applied pressure. Reproducibility is strengthened by an independent quadrature and simulation comparison and by publishing the complete numerical assumptions. Because the chosen groundwater and bearing-factor expressions are simplified, their influence on interpretation is discussed explicitly rather than concealed within a purportedly site-calibrated prediction.

MATERIALS AND METHOD

Idealized foundation geometry and effective-stress assumptions

The mechanical idealization is a long, rigid, surface strip footing bearing vertically and centrally on a horizontal, homogeneous, cohesionless granular deposit in plane strain. The footing base is at ground level, so the embedment depth is zero and no surcharge term is

introduced. Groundwater is assigned a steady depth measured vertically below the footing base; no seepage force, capillary suction, uplift action, interface roughness correction, load inclination, load eccentricity or sloping ground is represented. The soil is interpreted as drained, with zero effective cohesion. Consequently, the analysis represents ultimate bearing instability only and does not include immediate or differential settlement, punching through a weak underlying layer, cyclic loading, liquefaction or foundation–structure interaction. Each of these effects would need independent evaluation for engineering design.

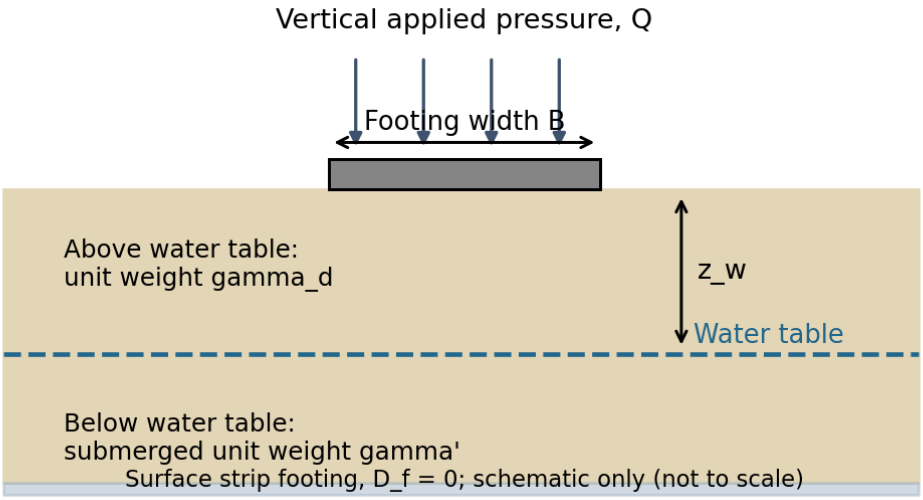


Figure 1. Idealized geometry of the surface strip footing, applied contact pressure and steady groundwater depth (schematic, not to scale).

The theoretical resistance is computed from the self-weight component of a classical strip-footing bearing-capacity expression. An explicit Vesic-type expression for the self-weight bearing factor is selected to ensure that every number can be regenerated. This factor convention follows the bearing-capacity formulation discussed by Vesić (1973); its adoption is a modelling choice: alternative expressions can produce different predictions, and the factor-model uncertainty quantified by Motra et al. (2016) is not embedded in the present random inputs.

$$q_{ult} = 1/2\ \bar{\gamma}(z_w, B)\, B\, N_\gamma(\phi') \quad (1)$$

$$N_q(\phi') = \exp(\pi \tan\phi')\tan^2(\pi/4 + \phi'/2) \quad (2)$$

$$N_\gamma(\phi') = 2\left[N_q(\phi') + 1\right]\tan\phi' \quad (3)$$

In Equations (1)–(3), q_{ult} is the computed ultimate vertical bearing pressure (kPa); $\bar{\gamma}$ is the effective unit weight used by the selected screening correction (kN/m³); B is strip-footing width (m); ϕ' is the effective soil friction angle (degrees when values are reported, converted internally to radians for trigonometric functions); and N_γ and N_q are dimensionless bearing-capacity factors. All trigonometric arguments and the exponential in the computational model use angles in radians. The coefficient 0.5 is dimensionless, and the resulting unit weight multiplied by footing width yields pressure units (kPa). Equation (3) is an adopted factor relationship, not a closed-form solution proven for all roughness conditions.

The water-table correction is implemented through a transparent linear interpolation of soil unit weight over an assumed influence depth equal to one footing width below the base. Above the assigned water table, the dry unit weight is used; below it, the buoyant unit weight is used. When the water table reaches the base, the selected self-weight contribution is completely buoyant. When the water table is one or more footing widths below the base, the correction returns the dry unit weight. This is a conventional simplified type of screening adjustment, not a hydraulic solution of the actual slip-line or plastic zone, whose dimensions depend on the friction angle and boundary conditions.

$$\gamma' = \gamma_{sat} - \gamma_w \quad (4)$$

$$\bar{\gamma}(z_w, B) = \gamma' + (\gamma_d - \gamma')\min(z_w/B\,, 1) \quad (5)$$

$$\alpha = \min(z_w/B\,, 1) \quad (6)$$

Here γ' is buoyant unit weight (kN/m³); γ_{sat} is saturated unit weight (kN/m³); γ_w is water unit weight (kN/m³); γ_d is dry unit weight (kN/m³); z_w is groundwater-table depth below the footing base (m); and α is a dimensionless depth ratio limited to unity. The model does not include partially saturated unit-weight profiles or matric suction. For computations, γ_d = 18.0 kN/m³, γ_{sat} = 20.5 kN/m³ and γ_w = 9.81 kN/m³, giving γ' = 10.69 kN/m³. These are illustrative input values, not results of any soil investigation. In Equation (5), z_w is restricted to non-negative values; scenarios with groundwater above the footing base are outside the model.

Deterministic baseline, uncertain inputs and interpretation

The reference width is 2.0 m. The mean friction angle is assigned as 32 degrees with standard deviation 3 degrees, while the applied contact pressure has mean 210 kPa and coefficient of variation 0.12. The friction angle follows an idealized normal distribution and the contact pressure follows a strictly positive lognormal distribution; the two are assumed independent. The friction-angle variance is expressed in squared degrees, and its input standard deviation must not be mixed with a sensitivity derivative expressed per radian. The practical probabilities of simulated friction angles outside 20–44 degrees total about 0.0063%, so the chosen normal law is effectively bounded over the investigated range for the present numerical precision. These probabilistic descriptions are hypothetical stress tests of the method. They cannot be presented as representative statistical properties of any particular soil deposit or structure without supporting site-specific and loading data.

Table 1. Reference foundation geometry, soil properties, action statistics and units used in the illustrative calculations.

Quantity	**Reference value**	**Distribution or status**	**Units**
Strip-footing width B	2.00	Fixed; varied 1.5–3.0	m
Water table depth z_w	0–3.00	Scenario parameter	m
Mean effective friction angle	32.0	Normal mean	degrees
Friction angle standard deviation	3.0	Normal standard deviation	degrees
Mean contact pressure	210.0	Lognormal mean	kPa
Contact pressure COV	0.12	Lognormal COV	dimensionless
Dry soil unit weight	18.0	Fixed	kN/m³

Quantity	Reference value	Distribution or status	Units
Saturated soil unit weight	20.5	Fixed	kN/m³
Water unit weight	9.81	Fixed	kN/m³
Illustrative probability screen	0.05	Not a code criterion	dimensionless

A nominal factor of safety is obtained by substituting the two arithmetic mean input parameters into the capacity and load expressions. This quantity is deliberately named nominal, rather than mean factor of safety: due to the nonlinear dependence of the bearing factor on the friction angle, the ultimate resistance evaluated at mean friction angle is not identical to the mean of the resistance distribution. Similarly, the ratio of two means is not the mean of a random ratio. The subsequent probabilistic analysis is therefore retained as a separate and necessary computation.

$$F_{\mathrm{nom}} = q_{\mathrm{ult}}(\mu_{\phi}, z_w, B)/\mu_Q \quad (7)$$

$$g(\phi', Q; z_w, B) = q_{\mathrm{ult}}(\phi', z_w, B) - Q \quad (8)$$

$$P_f(z_w, B) = P[g(\phi', Q; z_w, B) < 0] \quad (9)$$

In Equations (7)–(9), F_{nom} is the dimensionless nominal factor of safety; μ_{ϕ} is the arithmetic mean friction angle (degrees); μ_Q is the arithmetic mean contact pressure (kPa); g is the resistance-minus-action limit-state function (kPa); Q is random applied vertical pressure (kPa); and P_f is the dimensionless probability that resistance is less than action. The probabilities are unconditional with respect to these stipulated random inputs, but conditional on the selected bearing-capacity model, groundwater depth, footing width, and assumptions on soil and action distributions. A calculated event g less than zero is an idealized bearing-capacity exceedance rather than an observed foundation collapse.

Probability integral, Monte Carlo verification and moment approximation

The adopted probabilistic description provides a convenient independent verification route. For a given value of the random friction angle, the resistance becomes deterministic at fixed width and groundwater depth. The probability that the lognormal action exceeds that resistance can then be evaluated from a standard normal cumulative distribution function and integrated with respect to the friction-angle density. This removes sampling error from the reported reference probabilities and permits the Monte Carlo procedure to serve as a separate numerical check rather than the only source of the probability estimates.

$$\phi' \sim \mathcal{N}(\mu_{\phi}, \sigma_{\phi}^2), \quad \ln(Q/Q_0) \sim \mathcal{N}(\mu_L, \sigma_L^2) \quad (10)$$

$$\sigma_L = \sqrt{\ln(1 + V_Q^2)}, \quad \mu_L = \ln(\mu_Q/Q_0) - 1/2\,\sigma_L^2 \quad (11)$$

$$P_f \simeq \int_{0.01^{\circ}}^{60^{\circ}} \Phi\left(\mu_L - \ln[q_{\mathrm{ult}}(\phi, z_w, B)/Q_0]/\sigma_L\right) f_{\phi}(\phi)\,\mathrm{d}\phi \quad (12)$$

In Equations (10)–(12), the symbol N denotes a normal distribution; μ_L and σ_L are the dimensionless mean and standard deviation, respectively, of the natural logarithm of contact pressure normalized by a reference pressure Q_0 of 1 kPa; V_Q is the coefficient of variation of Q (dimensionless); f_{ϕ} is the normal probability density of friction angle (degree^{-1} when integration is performed in degrees); Φ is the standard normal cumulative distribution

function; and the integration variable phi denotes friction angle (degrees). For numerical evaluation, friction angle is integrated from 0.01° to 60°, a strictly positive domain for which the adopted resistance and its logarithm are defined. For the reference 3° standard deviation, probability mass omitted outside this interval is negligible; even with the maximum 5° standard deviation used in Figure 5, the excluded tail mass is approximately 1.1×10^{-8}. The bounded integration therefore approximates the stated normal distribution without introducing a material truncation bias into the reported results. The conditional exceedance term is the survival probability of the lognormal action. All logarithms act on dimensionless pressure ratios; the quadrature is an approximation because negligible extreme Gaussian tails are excluded.

Following the broader use of Monte Carlo sampling in foundation reliability studies (Shakir, 2019), one million pairs of normal friction angles and lognormal contact pressures are generated using a fixed random seed, 20261016. The same pairs are reused for alternative groundwater depths and footing widths so that scenario differences are not obscured by different random-number samples. The fraction for which the simulated resistance falls below the simulated action is the crude Monte Carlo failure-frequency estimate. Its estimated binomial standard error is reported alongside the deterministic quadrature result; the latter is used for the figures and sensitivity maps.

$$\hat{P}_{f,\mathrm{MC}} = 1/n \sum_{i=1}^{n} I\left[g\left(\phi_i', Q_i\right) < 0\right] \quad (13)$$

$$\mathrm{SE}\left(\hat{P}_{f,\mathrm{MC}}\right) = \sqrt{\hat{P}_{f,\mathrm{MC}}\left(1 - \hat{P}_{f,\mathrm{MC}}\right)/n} \quad (14)$$

In Equations (13) and (14), n is the number of Monte Carlo realizations (dimensionless count); i indexes the independently generated pairs; the indicator I equals unity when its stated condition is true and zero otherwise; $\hat{P}_{f,\mathrm{MC}}$ is the simulated failure-frequency estimate (dimensionless); and SE is its estimated binomial standard error (dimensionless). The standard error expresses only simulation-count precision. It does not measure bias in the bearing-capacity equation, errors in soil parameter statistics, uncertainty about groundwater position, or incomplete representation of failure modes.

A first-order second-moment (FOSM) estimate is added as a computational comparison. The model is linearized at the mean friction angle, and the load and resistance variances are combined under the stated independence assumption. The friction-angle derivative is evaluated numerically using a centered difference in degrees. A normal approximation for the resulting limit-state function produces a convenient reliability index, although the strongly nonlinear bearing factor and lognormal action make this approximate index different from a calibrated reliability index obtained from the exact failure probability.

$$\sigma_{g,\mathrm{FOSM}}^2 = \left[\partial q_{\mathrm{ult}}/\partial \phi' \,|_{\mu_\phi}\right]^2 \sigma_\phi^2 + \left(V_Q \mu_Q\right)^2 \quad (15)$$

$$\beta_{\mathrm{FOSM}} = q_{\mathrm{ult}}\left(\mu_\phi, z_w, B\right) - \mu_Q/\sigma_{g,\mathrm{FOSM}} \quad (16)$$

$$P_{f,\mathrm{FOSM}} = \Phi\left(-\beta_{\mathrm{FOSM}}\right) \quad (17)$$

In Equations (15)–(17), $\sigma_{g,\mathrm{FOSM}}$ is the approximate standard deviation of the limit state g

(kPa); partial q_{ult}/partial ϕ' has units kPa per degree when friction angle is expressed in degrees; σ_ϕ is the friction-angle standard deviation (degrees); β_{FOSM} is a dimensionless linearized reliability index; and $P_{f,FOSM}$ is the corresponding dimensionless failure-probability approximation. Because σ_ϕ multiplies the derivative in the same angular unit, the first variance term has units of squared pressure (kPa²). These equations support comparison only and are not used to define the probability contours.

Width inversion, sensitivities and reproducibility checks

A final screening question is posed inversely: what footing width would satisfy an illustrative upper bound on the computed failure probability for a specified groundwater depth? This exercise is included to demonstrate a design-map workflow, not to endorse a particular acceptable failure probability for foundation design. In practice, the acceptable reliability level and partial-factor verification would depend on governing design standards, consequence classification, project-specific investigations and the intended design situation. The 5% probability limit used in this study is intentionally a permissive educational screen rather than an adopted ultimate-limit-state code value.

$$B_{req}(z_w) = \inf\{B > 0 : P_f(z_w, B) \le P_{screen}\} \quad (18)$$

In Equation (18), B_{req} is the minimum width identified by the model (m); P_{screen} is the user-specified dimensionless probability threshold, set to 0.05 solely for the present demonstration. The infimum is taken over positive widths and evaluated by root finding in the range 0.8–10 m for the reported cases. The contact pressure is held constant when width is varied, so the implied line load increases with footing width; a real structural redesign at fixed total foundation load would involve a different loading relation. This distinction prevents interpreting the width comparison as a complete fixed-load structural design optimization.

$$\partial q_{ult}/\partial z_w = 1/2\,(\gamma_d - \gamma')N_\gamma, \qquad 0 < z_w < B \quad (19)$$

$$\partial q_{ult}/\partial B = 1/2\,\gamma' N_\gamma, \qquad z_w < B \quad (20)$$

$$\partial q_{ult}/\partial B = 1/2\,\gamma_d N_\gamma, \qquad z_w \ge B \quad (21)$$

In Equations (19)–(21), partial q_{ult}/partial z_w is the nominal bearing-resistance change per unit increase in water-table depth (kPa/m), and partial q_{ult}/partial B is the nominal bearing-resistance change per unit footing-width increase (kPa/m). N_γ is dimensionless and each unit weight is in kN/m³. The width derivatives are evaluated at fixed absolute groundwater depth z_w and fixed friction angle, reflecting the piecewise interpolation in Equation (5). When groundwater lies within the assumed influence zone, the incremental capacity benefit of adding footing width depends only on buoyant unit weight, whereas the portion represented by groundwater depth appears as a constant term. At z_w equal to B, the simplified model is continuous but changes derivative; its sharp transition is a modelling artifact rather than a physical discontinuity.

RESULTS AND DISCUSSION

Groundwater rise and the nominal bearing resistance

The representative capacity varies nonlinearly with the assumed friction angle but linearly

with the effective unit-weight term at a fixed angle. Figure 2 traces these relationships for the 2.0 m footing. The figure does not depict observed variability across test sites, and the full computed ordinate range is displayed: every curve is computed from Equations (1)–(5). For the chosen 32-degree reference angle, the nominal capacity is 543.86 kPa when the water table is at least 2.0 m below the base, falls to 433.43 kPa at 1.0 m and to 322.99 kPa at the base. At unchanged mean applied pressure of 210 kPa, the corresponding nominal factors of safety are 2.59, 2.06 and 1.54. The reduction is significant for the chosen inputs, but its magnitude is not transferable without verification of the site-specific groundwater regime and factor model.

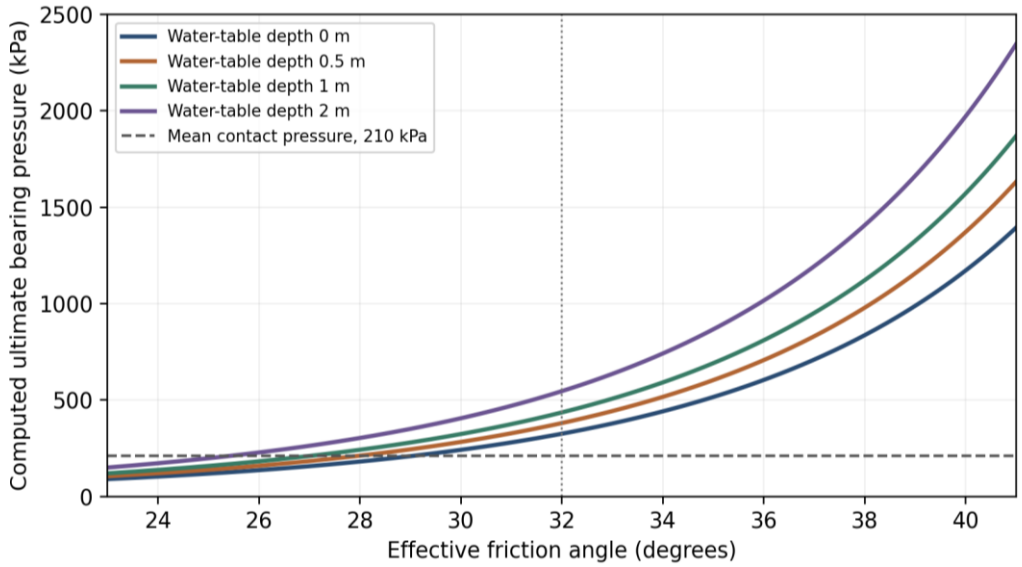


Figure 2. Ultimate bearing-pressure curves across the specified effective friction angles and groundwater depths for a 2.0 m strip footing.

Table 2. Groundwater-dependent effective unit weights, nominal bearing resistance and computed failure probabilities for the 2.0 m footing.

Water depth (m)	**Unit weight (kN/m³)**	**Nominal capacity (kPa)**	**Nominal FS**	**Failure prob. (%)**
0.0	10.69	322.99	1.54	17.18
0.5	12.52	378.21	1.80	9.77
1.0	14.34	433.43	2.06	5.51
1.5	16.17	488.65	2.33	3.11
2.0	18.00	543.86	2.59	1.76
3.0	18.00	543.86	2.59	1.76

Table 2 quantifies the probabilistic consequence of this hydraulic scenario. When water reaches the footing base, the computed failure probability is 17.18%, compared with 1.76% when the water table is at least one footing width below the base. At an intermediate depth of 0.5 m, a nominal factor of safety of 1.80 corresponds to a computed failure probability of 9.77%. These are not two inconsistent definitions of safety; they answer different questions. The deterministic ratio considers only the selected nominal inputs, whereas the probabilistic result integrates many combinations of lower friction angle and higher action, including realizations in which a nominally adequate footing does not have sufficient resistance.

Footing width and hydraulic depth interaction

Figure 3 presents a monotonic reduction in failure probability with increasing depth of the water table for each footing width. Within the chosen interpolation rule, the curves become horizontal once water lies below the nominal influence zone, z_w, at least B. This plateau should not be interpreted as an experimentally established depth beyond which groundwater cannot influence a real failure mechanism; it marks the truncation built into the screening assumption. For a 1.5 m footing, failure probabilities remain greater than 7% even in the deep-water-table scenario, whereas a 3.0 m footing gives approximately 3.25% with water at the base. Thus both footing width and hydraulic state influence whether a specified probability screen is met.

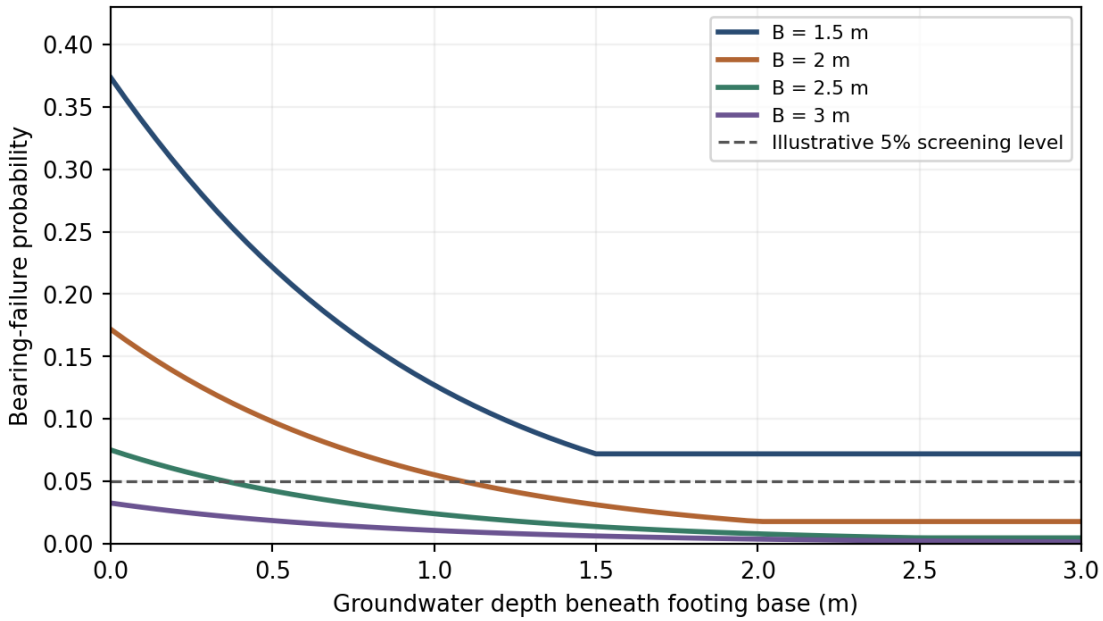


Figure 3. Probability of bearing-capacity exceedance versus groundwater depth at four specified footing widths.

Table 3. Modelled bearing-failure probability (%) across four footing widths and five groundwater depths.

Footing width (m)	z_w **= 0 m**	z_w **= 0.5 m**	z_w **= 1 m**	z_w **= 2 m**	z_w **= 3 m**
1.5	37.36	22.15	12.71	7.19	7.19
2.0	17.18	9.77	5.51	1.76	1.76
2.5	7.50	4.23	2.39	0.78	0.45
3.0	3.25	1.84	1.05	0.35	0.12

Figure 4 maps the two-variable response and is useful for preliminary scenario exploration because it connects footing geometry to groundwater depth without requiring users to infer safety from an isolated factor-of-safety calculation. For instance, a 2.0 m footing with groundwater at 1.0 m has a predicted failure probability of about 5.51%, just above the 5% illustrative screen, while at 2.0 m groundwater depth it falls to 1.76%. The visual boundary is smooth over most of the domain, but it changes curvature as the prescribed influence depth changes relative to the actual water-table depth. This behaviour arises from the simple unit-weight interpolation, not a sudden mechanistic transition in the soil.

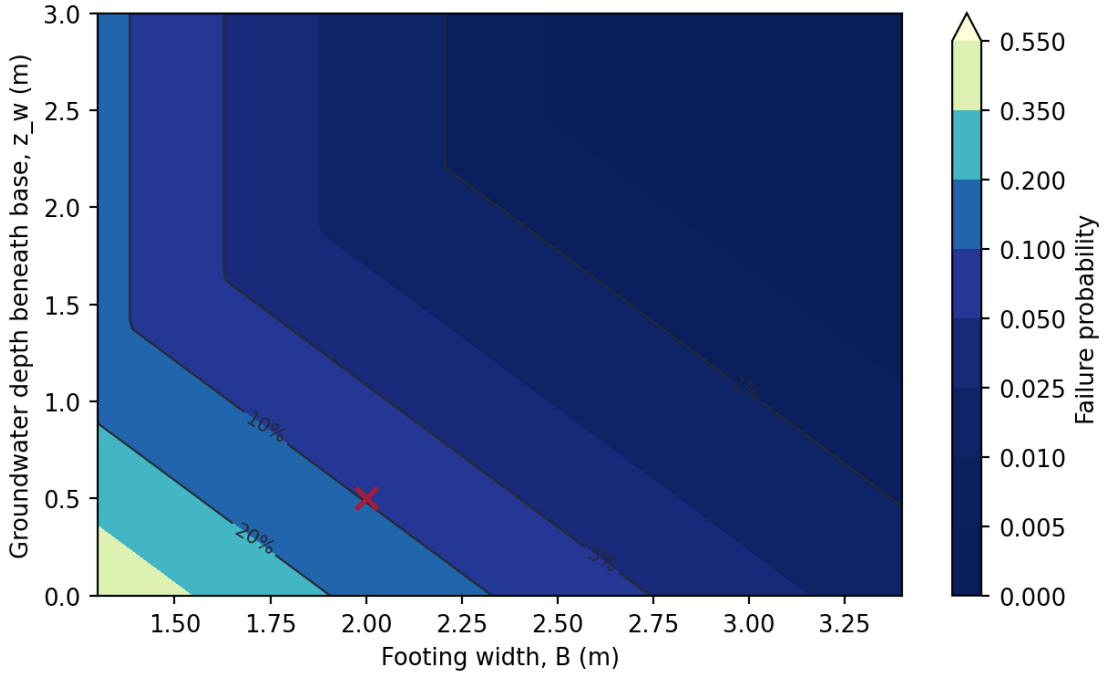


Figure 4. Contours of computed failure probability across footing width and groundwater depth. The cross identifies B = 2.0 m and z_w = 0.5 m.

Distribution assumptions and sensitivity of the probability estimate

Figure 5 visualizes the uncertainty interaction, while Table 4 enumerates the selected numerical combinations. Friction-angle uncertainty is influential because the adopted bearing-capacity factor increases strongly and nonlinearly with friction angle, thereby placing relatively weak realizations in the lower resistance tail. Increasing the standard deviation of effective friction angle from 2 to 4 degrees at z_w = 0.5 m and B = 2.0 m, while holding the action coefficient of variation at 0.12, increases the probability estimate from about 3.13% to 16.20%. Raising the action coefficient of variation from 0.06 to 0.18 at a fixed 3-degree friction-angle standard deviation produces a smaller change, from about 9.39% to 10.35%, for these illustrative means. The comparison is conditional on the stated probability laws and cannot be generalized as proof that load uncertainty is intrinsically unimportant.

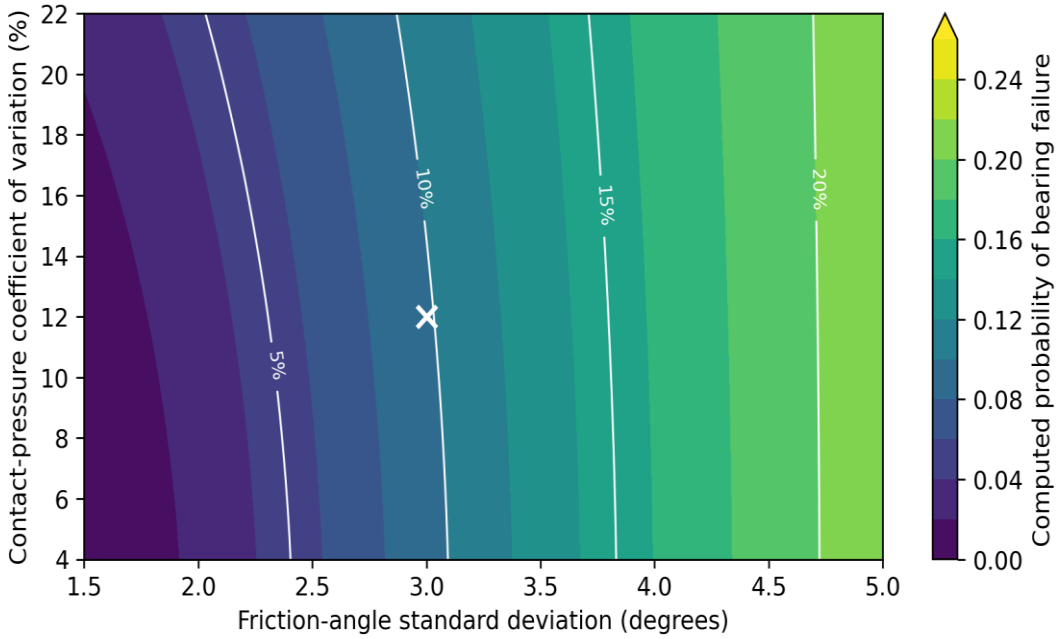


Figure 5. Sensitivity of computed bearing-failure probability to the strength and action dispersions for B = 2.0 m and z_w = 0.5 m.

Table 4. Effect of alternative friction-angle standard deviations and contact-pressure coefficients of variation on failure probability (%).

Pressure COV	**SD phi = 2 degrees**	**SD phi = 3 degrees**	**SD phi = 4 degrees**
0.06	2.54	9.39	16.06
0.12	3.13	9.77	16.20
0.18	4.06	10.35	16.41

The nominal factor of safety cannot reveal this change when the input means remain fixed: changing the standard deviation while preserving the mean friction angle and mean action does not alter Equation (7). This demonstrates why a deterministic and probabilistic comparison must not be reduced to a universal conversion rule between a single factor of safety and a single probability of failure. The selected normal and lognormal laws are also an important simplifying assumption. Correlation between load and soil strength, soil property spatial averaging, multiple soil layers, nonstationary groundwater, and bias in the factor N_γ could alter the distribution of resistance and the resulting exceedance probability. A rigorous project-specific analysis would need measured evidence and a defensible random-field or random-variable representation.

Independent numerical verification and linearization error

The one-million-sample Monte Carlo results agree closely with the deterministic one-dimensional quadrature. Table 5 reports six independently selected geometry–groundwater scenarios, their quadrature estimates, the Monte Carlo frequency and the Monte Carlo standard error. The agreement supports correct implementation of the stated stochastic limit-state equation; it does not validate the chosen geotechnical capacity factor against physical footing tests. Because identical random-number pairs are reused across the compared designs, the exercise also provides coherent scenario differences and avoids presenting simulation noise as a model response. The derivative-based FOSM approximation is included in Figure 6

to show how a convenient normal-limit-state approximation may diverge from the more direct probability evaluation.

Table 5. Agreement of quadrature and seeded Monte Carlo estimates, with sampling precision and FOSM comparison for six scenarios.

B / z_w (m)	Quadrature P_f (%)	Monte Carlo (%)	MC standard error (%)	FOSM P_f (%)
2 / 0	17.179	17.139	0.038	22.387
2 / 0.5	9.773	9.754	0.030	16.629
2 / 1	5.513	5.511	0.023	13.011
2 / 2	1.763	1.769	0.013	8.936
2.5 / 0.5	4.229	4.224	0.020	11.785
3 / 0	3.246	3.239	0.018	10.760

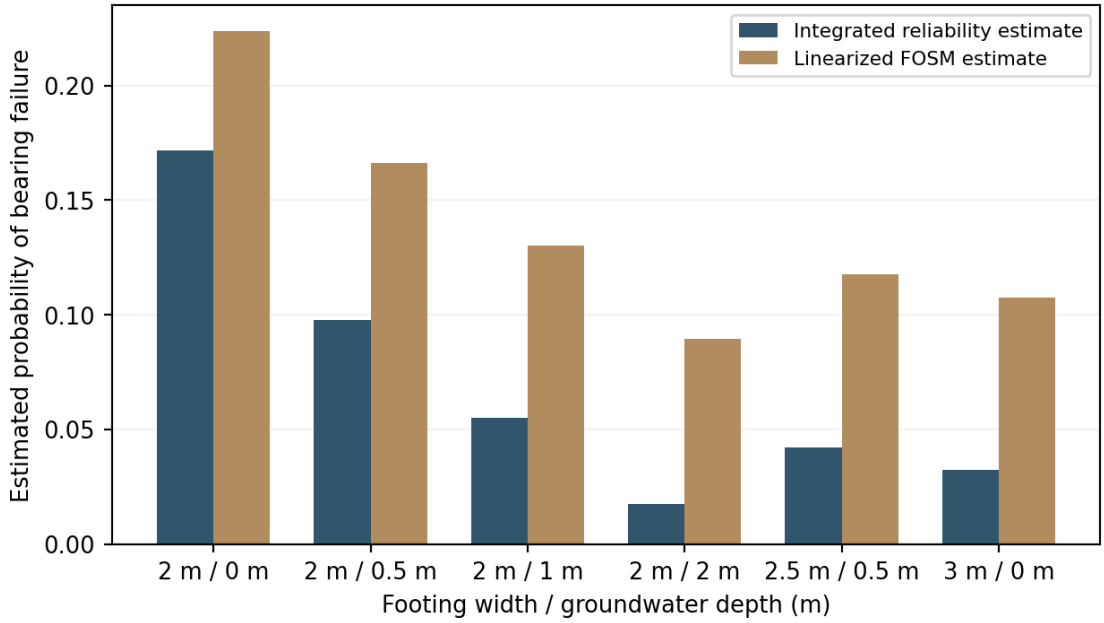


Figure 6. Differences between the integrated bearing-failure probability and its first-order second-moment (FOSM) approximation.

For the 2.0 m footing at 0.5 m groundwater depth, the FOSM approximation yields 16.63%, against 9.77% from integration. At a groundwater depth of 2.0 m, the FOSM result is 8.94%, compared with 1.76% from integration. These deviations, particularly in the smaller-probability tail, arise because nonlinear friction-angle resistance and a lognormal action do not produce a normally distributed limit-state function. Consequently, the FOSM calculation is presented only as a diagnostic comparison, not a substitute for the integrated reliability estimate. In particular, the standard deviation of a friction angle expressed in degrees must be paired with a derivative in kPa per degree; inserting radians into the derivative calculation without converting σ_ϕ would lead to a severe and preventable numerical inconsistency. The completed calculations use degrees consistently in the sensitivity derivative while explicitly converting angles to radians within the bearing-factor trigonometry.

Illustrative width screen and engineering qualifications

Inverting the quadrature probability provides widths of approximately 2.74 m, 2.40 m and 2.06 m for groundwater depths 0, 0.5 and 1.0 m respectively, when the demonstration

threshold is P_f at most 5%. For groundwater at 2.0 m, a width of approximately 1.63 m satisfies the same purely model-based screen. Such a comparison highlights that a footing which is satisfactory under an assumed deep groundwater table can move into a different risk category when groundwater rises, even without any change in structural demand. It also shows that the benefit of footing enlargement is conditional on the loading convention used; the present comparison keeps pressure fixed, not total column or wall load.

Three scientific qualifications constrain interpretation. First, the assumed linear groundwater correction does not resolve the shape of the plastic zone, partially saturated shear strength, groundwater gradients or transient infiltration. It should therefore not substitute for more detailed investigations of water-table effects such as the method-of-characteristics work of Cascone et al. (2021) or unsaturated analyses such as Showkat and Sivakumar Babu (2023). Second, the uncertainty model uses a single global friction angle rather than spatially correlated random fields, a simplification highlighted by random-field research including Griffiths et al. (2002) and Li et al. (2021). Third, the absolute computed probabilities depend strongly on the selected bearing-factor relationship and the hypothetical parameter statistics, meaning that numerical agreement between two integration algorithms does not provide experimental or design-code validation.

For a real project, the proposed workflow would start with a ground investigation that resolves soil stratification, drained shear strength, hydraulic conductivity, unit weights and credible long-term groundwater elevations. Characteristic and design values should be established using the governing local code and the applicable Eurocode 7 provisions where relevant, while imposed actions and serviceability behaviour are evaluated using a structural and geotechnical model consistent with actual loading. A more advanced probability model could then incorporate dependence between geotechnical variables, parameter-estimation uncertainty, resistance-model uncertainty, correlation length and consequence-dependent reliability targets. The present contribution is most valuable as a transparent preliminary sensitivity framework and a means to expose hidden assumptions early in design.

CONCLUSION

A reproducible probability-based screening framework was established for a surface strip footing on hypothetical homogeneous cohesionless soil with a steady water table. Within the selected unit-weight correction and bearing-capacity factor model, the reference 2.0 m footing experiences a reduction in nominal bearing pressure from 543.86 kPa to 322.99 kPa when groundwater rises from at least 2.0 m below the foundation base to the base itself. With a mean applied pressure of 210 kPa, normally distributed effective friction angle of mean 32 degrees and standard deviation 3 degrees, and a lognormal action with 12% coefficient of variation, the computed bearing-failure probability increases from 1.76% to 17.18%. These results represent numerical outcomes under specified assumptions, not empirical foundation failure rates.

The analysis also illustrates the non-equivalence between a nominal factor of safety and

failure probability. At 0.5 m groundwater depth, a nominal factor of safety of 1.80 for the 2.0 m footing corresponds to a conditional bearing-failure probability of 9.77% in the stated stochastic model. The hypothetical 5% probability screening exercise returns footing widths of about 2.74 m, 2.40 m and 2.06 m at groundwater depths of 0, 0.5 and 1.0 m, respectively. These widths are not code-based design recommendations and exclude settlement, eccentricity, transient seepage and resistance-model bias. Uncertainty in the friction angle exerts a strong influence within the investigated range, so selecting a nominal friction angle without reporting its variability obscures a consequential part of the analysis.

One-dimensional probabilistic integration was checked against one million independently sampled friction-angle and action pairs, and the two implementations agree within sampling precision for the benchmark scenarios. This agreement establishes computational reproducibility of the chosen limit-state model, but not its field validity. Future work should evaluate more rigorous groundwater-dependent capacity models, unsaturated-to-saturated transitions, spatially correlated soil properties and field-calibrated parameter distributions. For practice, the principal recommendation is procedural: report groundwater conditions, mathematical assumptions, dimensional units, variability measures and applicable design-limit-state requirements together, rather than interpreting a single nominal bearing-capacity ratio in isolation.

REFERENCES

Cascone, E., Biondi, G. & Casablanca, O. (2021). Groundwater effect on bearing capacity of shallow strip footings. Computers and Geotechnics, 139, 104417. https://doi.org/10.1016/j.compgeo.2021.104417

CEN (2024). EN 1997-1:2024. Eurocode 7: Geotechnical design - Part 1: General rules. European Committee for Standardization, Brussels.

CEN (2025). EN 1997-3:2025. Eurocode 7: Geotechnical design - Part 3: Geotechnical structures. European Committee for Standardization, Brussels.

Griffiths, D. V., Fenton, G. A. & Manoharan, N. (2002). Bearing capacity of rough rigid strip footing on cohesive soil: Probabilistic study. Journal of Geotechnical and Geoenvironmental Engineering, 128(9), 743–755. https://doi.org/10.1061/(ASCE)1090-0241(2002)128:9(743)

Kayser, M. & Gajan, S. (2014). Application of probabilistic methods to characterize soil variability and their effects on bearing capacity and settlement of shallow foundations: State of the art. International Journal of Geotechnical Engineering, 8(4), 352–364. https://doi.org/10.1179/1938636213Z.00000000073

Li, Y., Fenton, G. A., Hicks, M. A. & Xu, N. (2021). Probabilistic bearing capacity prediction of square footings on 3D spatially varying cohesive soils. Journal of Geotechnical and Geoenvironmental Engineering, 147(6), 04021035. https://doi.org/10.1061/(ASCE)GT.1943-5606.0002538

Li, Y., Fu, Z., Zhang, B. & Xu, N. (2024). Reliability-based factor of safety for bearing

capacity of square foundations on 3D cohesive-frictionless soils considering samples. Computers and Geotechnics, 166, 105975. https://doi.org/10.1016/j.compgeo.2023.105975

Motra, H. B., Stutz, H. H. & Wuttke, F. (2016). Quality assessment of soil bearing capacity factor models of shallow foundations. Soils and Foundations, 56(2), 265–276. https://doi.org/10.1016/j.sandf.2016.02.009

Shakir, R. R. (2019). Probabilistic-based analysis of a shallow square footing using Monte Carlo simulation. Engineering Science and Technology, an International Journal, 22(1), 313–333. https://doi.org/10.1016/j.jestch.2018.08.011

Showkat, R. & Sivakumar Babu, G. L. (2023). Deterministic and probabilistic analysis of the response of shallow footings on unsaturated soils due to rainfall. Transportation Geotechnics, 43, 101150. https://doi.org/10.1016/j.trgeo.2023.101150

Vesić, A. S. (1973). Analysis of ultimate loads of shallow foundations. Journal of the Soil Mechanics and Foundations Division, 99(1), 45–73. https://doi.org/10.1061/JSFEAQ.0001846

GRAIN-SIZE COMPATIBILITY AND PRODUCTION TOLERANCE OF GRANULAR FILTERS FOR EMBANKMENT DAMS: A PARAMETRIC SCREENING FRAMEWORK

Ali Akbar Firoozi
School of Civil, Environmental Engineering and Geomatics, Faculty of Engineering and Built Environment, University of Botswana, Gaborone, Botswana

Ali Asghar Firoozi
Department of Civil Engineering, Faculty of Engineering, National University of Malaysia (UKM), Selangor, Malaysia

ABSTRACT

Granular filters are a principal defense against migration of base-soil particles in embankment dams; however, a nominally acceptable particle-size ratio does not by itself describe the available construction gradation window or its robustness to production variability. This analytical study develops a reproducible screening framework for a specific scope: non-dispersive, broadly continuous granular base soils with less than 15% passing the 0.075-mm sieve. The upper filter-percentile bound follows the category-4 retention limit of the USDA Natural Resources Conservation Service (NRCS). Its preliminary lower bound is combined with an explicitly labeled, illustrative drainage-size multiplier. A logarithmic feasible-window width, a geometric-mean target and a maximum symmetric production-tolerance index are derived. Four hypothetical lognormal base gradations and a range of synthetic candidate filters are examined; all numerical values are model inputs or calculated outputs, not laboratory measurements. For the central illustrative case, the base d_{15} and d_{85} are calculated as 0.170 and 0.530 mm, the screening filter D_{15} interval is 0.679–2.122 mm, and the geometric target is 1.200 mm. The symmetric logarithmic tolerance is 0.570, equivalent to a multiplicative bound of 1.768. The analysis reveals that increasing a drainage-size requirement can narrow the feasible window and that passing retention and size screens does not establish full filter suitability. No seepage testing, construction quality assessment or site-specific dam safety claim is made.

Keywords: Embankment Dam; Granular Filter; Particle-Size Distribution; Internal Erosion; Retention; Gradation Tolerance; Parametric Analysis.

INTRODUCTION

Internal erosion is among the mechanisms by which hydraulic gradients may mobilize and transport particles within embankments and their foundations. Once particles are removed from the base soil, changes in hydraulic conductivity, local void structure or flow pathways can initiate or sustain deterioration. Downstream granular filters and drains play complementary roles: a filter must retain potentially mobile particles while offering a pathway

for water discharge. Historic assessments of embankment dam incidents establish the importance of zoning and filter configuration to the occurrence and progression of internal erosion (Foster et al., 2000; Fell et al., 2003). This engineering function cannot be represented by a single bulk permeability comparison, because crack erosion, concentrated leak paths, internal instability and construction defects also influence performance.

Laboratory investigations by Sherard et al. (1984) demonstrated relationships between granular filter size and particle retention, while Sherard and Dunnigan (1989) investigated critical filters for impervious base soils using specialized erosion tests. Foster and Fell (2001) subsequently explained why existing filters that lie outside modern design limits require an assessment of potential erosion behavior rather than a binary label. Kenney and Lau (1985) studied the ability of a granular mixture to retain its own finer grains, distinguishing the internal stability of the filter material from the retention of particles in the soil it protects. These contributions imply that any screening method based on gradation percentiles must explicitly identify the class of soil to which its retention rule applies and must not imply that percentile compliance alone proves filter safety.

Current agency guidance responds to this need by requiring gradation-based classification, regrading where appropriate, consideration of dispersive clay and gap grading, and limits on fines, particle size and constructability. The U.S. Bureau of Reclamation (2011) provides detailed protective-filter design procedures for embankment dams. The Natural Resources Conservation Service (NRCS, 2017), Part 633, Chapter 26, distinguishes lower-case base-soil percentiles from upper-case filter percentiles and adopts different retention rules for base-soil categories defined by fines content. For category 4, comprising sands and gravels with less than 15% fines after required regrading, the maximum allowable filter D_{15} is four times the base-soil d_{85}. The handbook also provides a preliminary minimum D_{15} and cautions that practical band design involves engineering judgment, material availability, internal stability and quality control.

The present contribution addresses a narrower but useful analytical question that arises between preliminary soil screening and the preparation of a material specification: how wide is the numerical interval of candidate D_{15} values after an upper retention bound and explicitly stated lower size screens have been imposed, and how does that interval change with base gradation, a chosen drainage-size multiplier and manufacturing variability? A dimensionless logarithmic window offers a transparent way to compare geometrically different soils without implying equivalence to a full gradation specification. Four deliberately synthetic, continuously graded sands provide examples that can be exactly reconstructed from a two-parameter cumulative distribution, while the candidate filter analysis illustrates the effect of gradation shape on fines and coarse-percentile constraints.

The objectives are to derive explicit size-bound, midpoint and tolerance equations; calculate the resulting design-screening windows for four hypothetical base soils; examine how a heuristic drainage multiplier alters those windows; assess how alternative candidate-filter

gradation shapes intersect with size and fines screens; and identify the additional tests and checks required before translating any screening outcome into a dam-filter design. The contribution is analytical integration and transparent sensitivity quantification, not the invention of a new experimentally calibrated filter retention law.

MATERIALS AND METHOD

Scope, source hierarchy and physical representation

The calculation concerns a conceptual interface between a granular base-soil zone and an adjacent granular filter zone in an embankment dam. Figure 1 depicts this configuration without assigning hydraulic heads, seepage discharge or geotechnical material properties. The filtered base soils are restricted to NRCS category 4 after any required regrading: their passing fraction at 0.075 mm is below 15%, they are not identified as dispersive, and the constructed synthetic gradations are smooth rather than intentionally gap graded. These properties are assumptions used to bound the mathematical exercise. Base soils with more fines, dispersivity, segregation-prone grading or broad gap grading require distinct procedures and are outside the numerical conclusions.

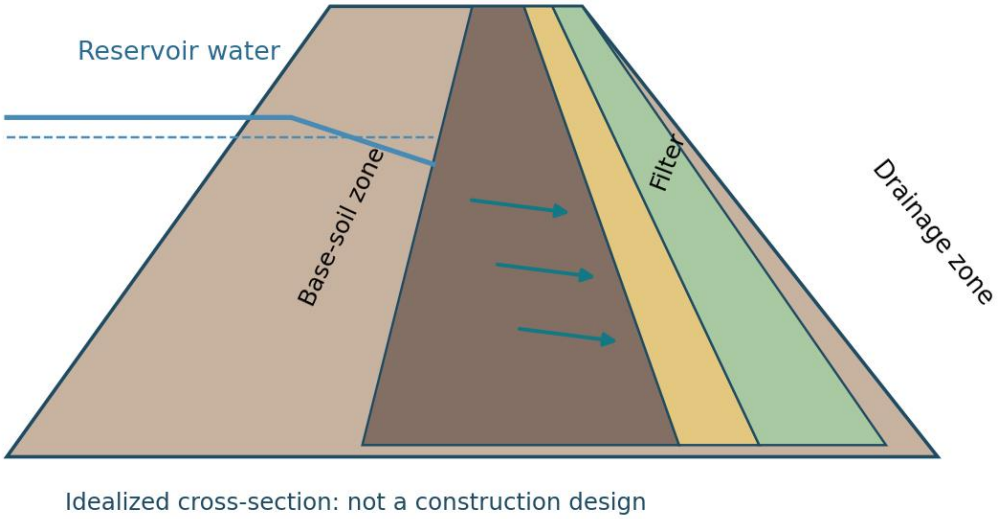


Figure 1. Conceptual embankment zoning identifies the base-soil/filter retention interface and downstream drainage path; geometry is illustrative and not to scale.

Table 1 differentiates the handbook-derived checks from the supplementary assumptions used in this paper. The source hierarchy is deliberately explicit. The category-4 upper D_{15} retention limit and preliminary NRCS lower limit are taken from NRCS (2017). The drainage percentile multiplier K introduced here is an illustrative additional screening assumption, not a universal NRCS acceptance requirement. The synthetic lognormal descriptions and production-tolerance objective are mathematical devices introduced for this study. An optional D_{90} value of 20 mm is used only to show the effect of a chosen coarse-percentile procurement screen; it is not represented as a general agency requirement. Actual design must evaluate full gradation envelopes and all other applicable rules.

Table 1. Origin, engineering purpose and applicability limits of seven filter-screening conditions.

Check	**Origin**	**Use in this paper**
Base category 4: fines <15%	NRCS (2017), classification	Applies the selected retention rule only to granular base soils
Filter $D_{15} \leq 4 \times$ base d_{85}	NRCS (2017), category-4 rule	Upper retention-based percentile bound
Minimum filter $D_{15} \geq$ max(0.1 mm, U/5)	NRCS (2017), preliminary step	Initial lower size bound, subject to detailed design
Filter $D_{15} \geq$ K × base d_{15}	Illustrative drainage-size screen	Variable K (4–9); not a universal design requirement
Filter C_u from 2 to 6 (illustrative)	NRCS upper C_u guidance; illustrative lower limit	Supplementary filter-spread screen, not full agency acceptance
Filter fines ≤ 5%	NRCS (2017), filter-material guidance	Illustrative distribution passing-fraction screen
Filter $D_{90} \leq 20$ mm	Chosen illustrative procurement screen	Not a substitute for maximum-size or segregation criteria

Synthetic base-soil gradations and percentile recovery

To avoid claiming unobserved sieve measurements, every base-soil gradation is described by an idealized lognormal cumulative fraction passing. The positive particle diameter is measured in millimetres; its median and logarithmic dispersion are prescribed parameters. Equation (1) defines the cumulative function in terms of the standard normal distribution function. Equation (2) gives the particle diameter associated with any chosen cumulative passing percentage. These equations are mathematical representations of continuous distributions and do not assert that natural soil samples have exactly lognormal grading or that an unbounded lognormal tail can substitute for a physical maximum size.

$$F_b(d) = \Phi\left(\frac{\ln(d/d_{50})}{\sigma_b}\right) \quad (1)$$

$$d_p = d_{50}\exp(\sigma_b z_p), \qquad z_p = \Phi^{-1}(p/100) \quad (2)$$

In Equation (1), Fb is the dimensionless mass fraction finer than grain diameter d (mm); d_{50} is the model median grain diameter (mm); σ_b is the dimensionless standard deviation of the natural logarithm of d/d_{50}; and Φ is the unit-normal cumulative distribution function. In Equation (2), d_p is the base particle size (mm) corresponding to p percent finer, and z_p is the standard normal quantile at probability p/100, with p in the interval (0,100). The fines percentage passing the 0.075 mm sieve follows Equation (3), where d_s=0.075 mm and f_{200} is reported as a percentage of total mass.

$$f_{200} = 100\Phi\left(\frac{\ln(d_s/d_{50})}{\sigma_b}\right) \quad (3)$$

Four input pairs of median diameter and logarithmic dispersion are selected to produce uninterrupted synthetic granular base gradations. The chosen distributions do not represent materials sampled from Botswana, Türkiye or any other field location. Table 2 specifies these inputs and their analytically derived base-percentile and fines values, while Figure 2 draws the corresponding smooth distribution curves. In each case, the calculated fines content lies

below the category-4 threshold; however, this mathematical property alone does not demonstrate self-filtration under seepage.

Table 2. Assumed lognormal base-soil parameters and calculated sieve-percentile characteristics for four synthetic category-4 scenarios.

Case	d_{50} (mm)	σ_b (–)	d_{15} (mm)	d_{85} (mm)	Fines (%)
B1	0.220	0.58	0.121	0.401	3.177
B2	0.300	0.55	0.170	0.531	0.586
B3	0.350	0.65	0.178	0.687	0.890
B4	0.400	0.50	0.238	0.672	0.041

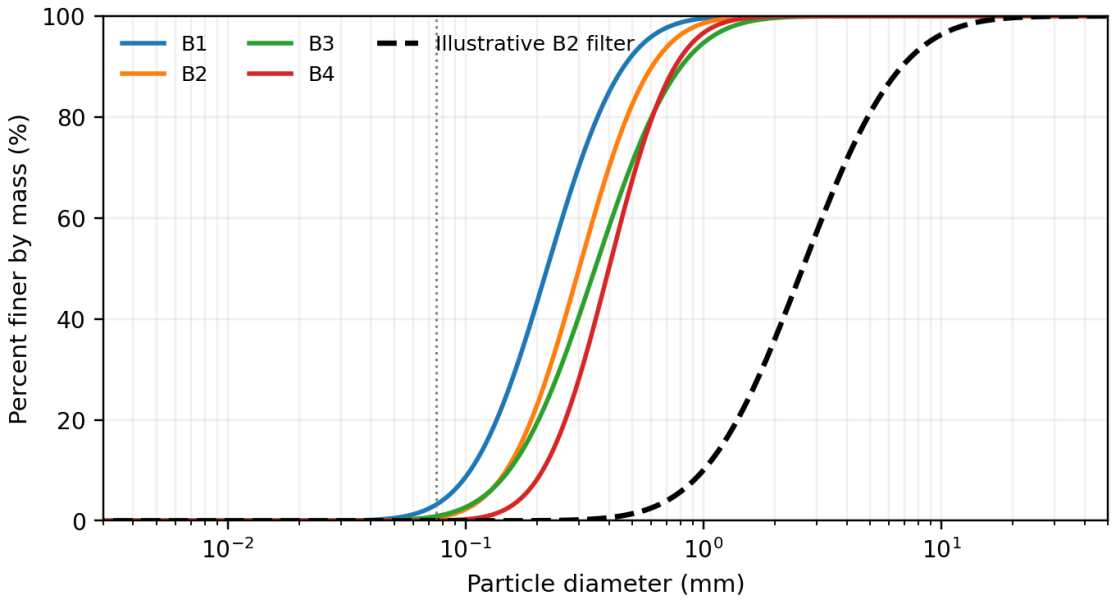


Figure 2. Continuous synthetic grain-size curves for base soils B1–B4 contrasted with an illustrative candidate-filter distribution.

Filter D_{15} interval, screening ratios and dimensionless window

The uppercase particle-size notation refers exclusively to the proposed filter. For category-4 base soils, NRCS (2017) gives the retention upper bound in Equation (4). The preliminary minimum filter size is formed in Equation (5) from the handbook's 0.1-mm floor and one-fifth of the maximum permitted size. The illustrative drainage screen, Equation (6), is stated independently to avoid presenting a hypothetical permeability target as an agency requirement. Its multiplier K is dimensionless; the baseline comparison uses K=4, and the wider study explores K from 3 to 9.

$$U = 4d_{85} \quad (4)$$

$$L_{\mathrm{NRCS}} = \max\left(0.1\ \mathrm{mm}, \frac{U}{5}\right) \quad (5)$$

$$L_h = Kd_{15} \quad (6)$$

Combining these lower screens forms the governing lower candidate percentile in Equation (7), and Equation (8) defines the interval of candidate filter D_{15} values. A nonempty interval exists if its lower endpoint is no greater than its upper endpoint. An empty interval signals

incompatible assumed screening requirements and is not evidence that a safe filter is impossible; the material class, additional constraints and detailed guidance must be reconsidered.

$$L = \max(L_{\mathrm{NRCS}}, L_h) \quad (7)$$

$$\mathcal{I} = [L, U], \qquad L \le U \quad (8)$$

Equation (9) provides separate dimensionless retention and drainage percentile ratios. The retention ratio is compared against the upper limit of four for the category-4 soil, whereas the second ratio depends on the explicitly selected multiplier K and is not a direct laboratory permeability estimate. The logarithmic width in Equation (10) measures the multiplicative breadth of the feasible D_{15} range and is zero where the interval collapses to a single size. Because both endpoints are expressed in millimetres, their ratio is dimensionless and can legitimately appear within the natural logarithm.

$$R_r = \frac{D_{15}}{d_{85}}, \qquad R_h = \frac{D_{15}}{d_{15}} \quad (9)$$

$$W = \ln\left(\frac{U}{L}\right) \quad (10)$$

The geometric midpoint in Equation (11) maximizes the smaller of the two logarithmic distances to the limiting endpoints. Equations (12)–(14) convert this property into a symmetric production-tolerance interpretation: if the filter D_{15} varies multiplicatively by exp(±epsilon) about its nominal geometric midpoint, all such D_{15} values remain inside the two-endpoint screening interval when epsilon does not exceed $\varepsilon_{\max}$. The multiplier rho_max is a positive dimensionless factor rather than a probability or a factor of safety against piping.

For Equations (4)–(14), the base-soil sizes d_{15} and d_{85} and the filter size D_{15} are grain diameters at 15% and 85% passing by dry mass, respectively, expressed in millimetres. U is the maximum allowable candidate-filter D_{15} from the category-4 retention inequality (mm); L_{NRCS} is the preliminary handbook lower size (mm); L_h is the additional illustrative lower size (mm); and L is their controlling maximum (mm). The interval $\mathcal{I}$ contains candidate D_{15} values (mm), whereas the percentile ratios R_r and R_h, logarithmic width W, multiplier K, limiting logarithmic deviation $\varepsilon_{\max}$ and multiplicative tolerance $\rho_{\max}$ are dimensionless. The geometric-center target $D_{15}^{\star}$ and a manufactured-lot value D_{15}^{lot} are diameters (mm); epsilon is the assumed dimensionless magnitude of a multiplicative production deviation. No tolerance parameter represents a measured manufacturing uncertainty.

$$D_{15}^{\star} = \sqrt{LU} \quad (11)$$

$$\varepsilon_{\max} = \frac{1}{2}\ln\left(\frac{U}{L}\right) \quad (12)$$

$$D_{15}^{\mathrm{lot}} \in [D_{15}^{\star}\exp(-\varepsilon), D_{15}^{\star}\exp(\varepsilon)] \quad (13)$$

$$\rho_{\max} = \exp(\varepsilon_{\max}) = \sqrt{U/L} \quad (14)$$

The interpretation is deliberately restricted to a single percentile. Real quarry or borrow pit variability changes the entire particle-size curve, possibly in a nonuniform manner; a D_{15} tolerance cannot ensure compliance with the fines limit, uniformity, stability or segregation

criteria. The selected target also represents an arithmetic design decision in logarithmic size space, not an optimization over cost, resistance to erosion or verified hydraulic conductivity.

Candidate filter gradation shape and auxiliary screens

The retained D_{15} percentile is not a complete filter gradation. To demonstrate this point, the filter grain-size curve is assigned its own independent lognormal dispersion σ_F. Equation (15) relates every filter percentile Dp to its prescribed D_{15} and a pair of standard normal quantiles. Equations (16)–(18) then calculate the standard coefficient of uniformity, the percentage passing 0.075 mm and the filter D_{90} size. This mathematical family is smooth and cannot represent bimodal mixtures, discontinuous grading or particles outside any finite maximum sieve size.

$$D_p = D_{15}\exp\left[\sigma_F\left(z_p - z_{15}\right)\right] \quad (15)$$

$$C_u = \frac{D_{60}}{D_{10}} = \exp[\sigma_F(z_{60} - z_{10})] \quad (16)$$

$$f_{F,200} = 100\Phi\left[z_{15} + \frac{\ln(d_s/D_{15})}{\sigma_F}\right] \quad (17)$$

$$D_{90} = D_{15}\exp[\sigma_F(z_{90} - z_{15})] \quad (18)$$

Filter C_u is the dimensionless D_{60}/D_{10} ratio. The dispersion σ_F is dimensionless, and Dp, D_{15}, D_{90} and d_s are in millimetres. The upper uniformity limit of 6 and the filter-fines ceiling of 5% follow preliminary NRCS guidance; the lower uniformity bound of 2 is an illustrative supplementary screen selected for this comparison. The additional D_{90}≤20 mm screen is a deliberately specified example of a procurement constraint. The uniformity interval in Equation (23) is therefore an assumed screening range, whereas only its upper limit is linked to the cited handbook guidance. Results passing these screens are marked only as screening candidates: the unbounded lognormal tail means they cannot by themselves demonstrate compliance with a maximum physical particle size. Likewise, distribution smoothness is not a substitute for an internal-stability test of the Kenney–Lau type (Kenney and Lau, 1985).

A commonly used dimensional analogy treats hydraulic conductivity as proportional to the square of a characteristic grain diameter if porosity, grading character and fluid properties are otherwise comparable. Equation (19) records the resulting squared-percentile ratio as an illustrative index, not a prediction of true conductivity contrast. The symbol $\hat{k}_r$ is dimensionless; measured hydraulic conductivity and permeability must not be inferred from it. A filter may also fail to provide adequate drainage because of compaction density, fines migration, saturation effects or collector outlet restrictions.

$$\hat{k}_r = \left(\frac{D_{15}}{d_{15}}\right)^2 \quad (19)$$

Manufacturing variation, quantile uncertainty and sensitivity

For a nominally selected D_{15} that is not necessarily the geometric midpoint, Equation (20) defines the smallest logarithmic buffer against violation of either endpoint. Its units are dimensionless. The corresponding maximum two-sided multiplicative deviation is $\exp(\varepsilon_{rob})$. The derivation assumes a uniform multiplicative shift in D_{15} and is therefore a sensitivity

check rather than an empirical production distribution, and no probability model for manufactured material is claimed.

$$\varepsilon_{\mathrm{rob}} = \min\{\ln(D_{15}^{\mathrm{nom}}/L), \ln(U/D_{15}^{\mathrm{nom}})\} \quad (20)$$

To explore uncertainty in the base-soil percentiles, independent lower and upper perturbation amplitudes δ_{85} and δ_{15} are introduced as nonnegative, dimensionless fractions smaller than one. Equation (21) uses an adverse lower value of d_{85} to obtain a conservative retention bound and an adverse upper value of d_{15} to obtain a conservative drainage-size requirement. To make the preliminary NRCS one-fifth lower bound conservative across this uncertainty rectangle, the largest possible base-soil d_{85} is also used in that part of Equation (21), whereas the smallest possible d_{85} controls the retention maximum. The resulting width in Equation (22) is interpreted only as a worst-case rectangular uncertainty screen; it is not a confidence interval, and d_{15} and d_{85} are not statistically independent for a real sampled grading.

$$U_{\min} = 4d_{85}(1-\delta_{85})$$
$$L_{\max} = \max\left(0.1\ \mathrm{mm}, 0.8d_{85}(1+\delta_{85}), Kd_{15}(1+\delta_{15})\right) \quad (21)$$
$$W_{\mathrm{rob}} = \ln(U_{\min}/L_{\max}) \quad (22)$$

Equation (23) defines a binary score equal to one only when all four example checks are satisfied, and zero otherwise. The four screening checks are: candidate size interval, supplementary uniformity range, filter fines limit and optional coarse-percentile ceiling. Its fourth, optional coarse-percentile limit belongs to the present demonstration and must not be read as a universally accepted filter design standard. Equation (24) describes the local sensitivity of logarithmic width to a proportional change in d_{85} only within the branch where the lower bound is fixed by K times d_{15}. Different active bound branches have different derivatives, and transitions may make the piecewise derivative discontinuous.

For Equations (15)–(24), D_p denotes the filter particle diameter (mm) at p% cumulative passing by dry mass; z_p and z_{15} are standard-normal quantiles (dimensionless); σ_F is the dimensionless logarithmic dispersion of the hypothetical filter distribution; and D_{10}, D_{15}, D_{60} and D_{90} are filter diameters in millimetres. C_u=D_{60}/D_{10}, the squared size-ratio index $\hat{k}_r$, the screening indicator $\mathcal{A}$ and the nominal-deviation allowance $\varepsilon_{\mathrm{rob}}$ are dimensionless. The filter fines fraction $f_{F,200}$ is expressed as percent passing the 0.075-mm sieve. D_{15}^{nom} is the nominal candidate filter diameter (mm). $U_{\min}$ is the lowest permissible retention upper bound (mm) over the assumed uncertainty rectangle, whereas $L_{\max}$ is the highest required lower bound (mm), and W_{rob} is their dimensionless logarithmic interval width. The independent fractional perturbation limits δ_{85} and δ_{15} are nonnegative and dimensionless; the partial derivative in Equation (24) is dimensionless and applies only when the specified lower-bound branch is active.

$$\mathcal{A} = \mathbb{1}\{L \le D_{15} \le U,\ 2 \le C_u \le 6,\ f_{F,200} \le 5\%,\ D_{90} \le 20\ \mathrm{mm}\} \quad (23)$$
$$\frac{\partial W}{\partial \ln d_{85}} = 1 \quad \text{if } L = Kd_{15} \quad (24)$$

Numerical implementation and verification

Calculations were performed with double-precision evaluation of normal cumulative and inverse cumulative distributions and direct algebraic evaluation of Equations (1)–(24). For each base case, d_{15} and d_{85} were first recovered analytically and then inserted in the retention and lower-size formulas. The predicted interval endpoints were independently recomputed from the underlying percentiles, and every geometric target was verified to lie between its endpoints. A rectangular grid covering base d_{15} from 0.07 to 0.33 mm and base d_{85} from 0.20 to 0.95 mm was used to display width variation; this grid is a mathematical parameter sweep, not a survey of natural soils. A separate grid varied filter D_{15} and logarithmic dispersion for the B2 base and counted passed example screens. No stochastic Monte Carlo results, physical sieve datasets or validation tests are represented.

RESULTS AND DISCUSSION

Base-gradation controls on the feasible percentile interval

Table 3 reports the principal D_{15} screening results for the four hypothetical base soils at K=4. All four intervals are nonempty. The baseline B2 case gives d_{15}=0.170 mm and d_{85}=0.530 mm. The category-4 retention upper bound is therefore U=2.122 mm. The preliminary NRCS minimum is U/5=0.424 mm, greater than the absolute 0.1-mm floor; however, the illustrative drainage minimum Kd_{15}=0.679 mm is greater still and controls the lower bound. The resulting interval of 0.679–2.122 mm has a ratio U/L of 3.127 and logarithmic width of 1.140. Its geometric-center value is 1.200 mm, and the maximum symmetric logarithmic tolerance is 0.570. These values follow directly from Equations (4)–(14) and do not imply that a filter with D_{15}=1.200 mm has been physically tested.

Table 3. Calculated candidate D_{15} intervals and logarithmic production-tolerance measures use an illustrative multiplier K=4.

Case	L (mm)	U (mm)	Target (mm)	ln(U/L) (–)	e^εmax (–)
B1	0.482	1.605	0.880	1.202	1.824
B2	0.679	2.122	1.200	1.140	1.768
B3	0.714	2.746	1.400	1.347	1.961
B4	0.953	2.686	1.600	1.036	1.679

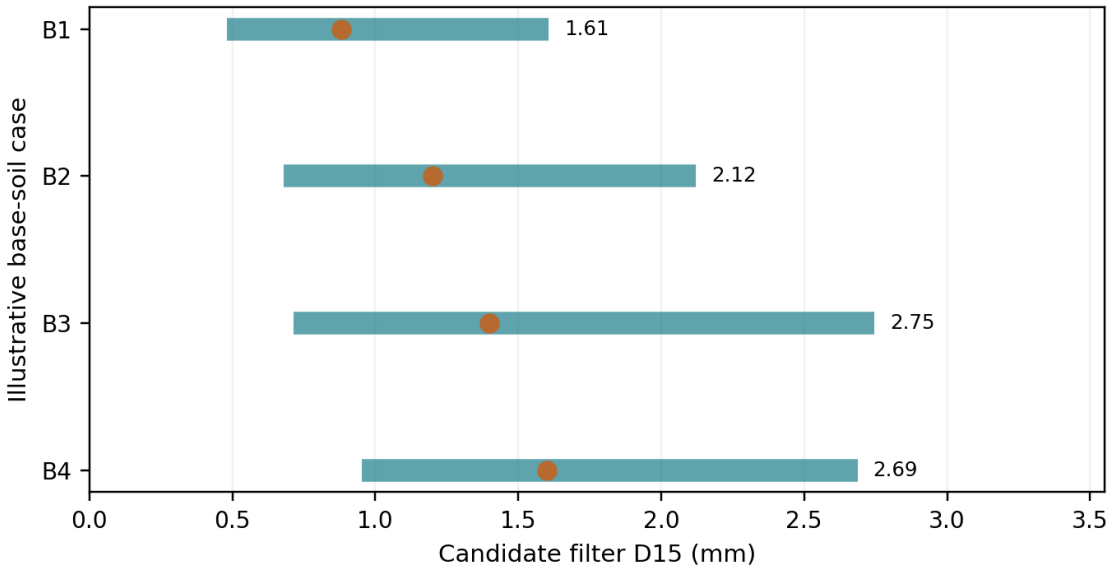


Figure 3. The screening intervals for four synthetic base soils identify the admissible filter D_{15} bands and their geometric midpoint targets for K=4.

The intervals for B1 and B3 are affected differently by median grain size and dispersion, despite both qualifying as category-4 examples. Figure 3 makes this difference evident: a coarser base d_{85} increases the permissible upper filter percentile size, but a coarser d_{15} simultaneously increases the imposed drainage-size floor. The ratio of the two percentiles therefore matters as much as either absolute size alone. This result is especially relevant when comparing supplies at distinct quarries, because an apparently attractive nominal D_{15} may have little construction tolerance once the base characteristic sizes and screening multiplier are fixed.

Dimensionless width map and branch changes

Figure 4 isolates the mathematical dependency on the two base percentiles. Across the displayed parameter grid, the filter upper bound grows directly with d_{85}, whereas the lower bound is the greater of a handbook-based floor and the selected Kd_{15} screen. Where Kd_{15} controls the lower bound, the logarithmic width simplifies to ln(4d85/(Kd_{15})); at K=4 this equals ln(d_{85}/d_{15}), so the window breadth is governed by the base-soil percentile separation. Where the one-fifth upper bound or 0.1-mm floor controls instead, the dependency changes. The labeled points are the four synthetic examples, not samples at known dam sites.

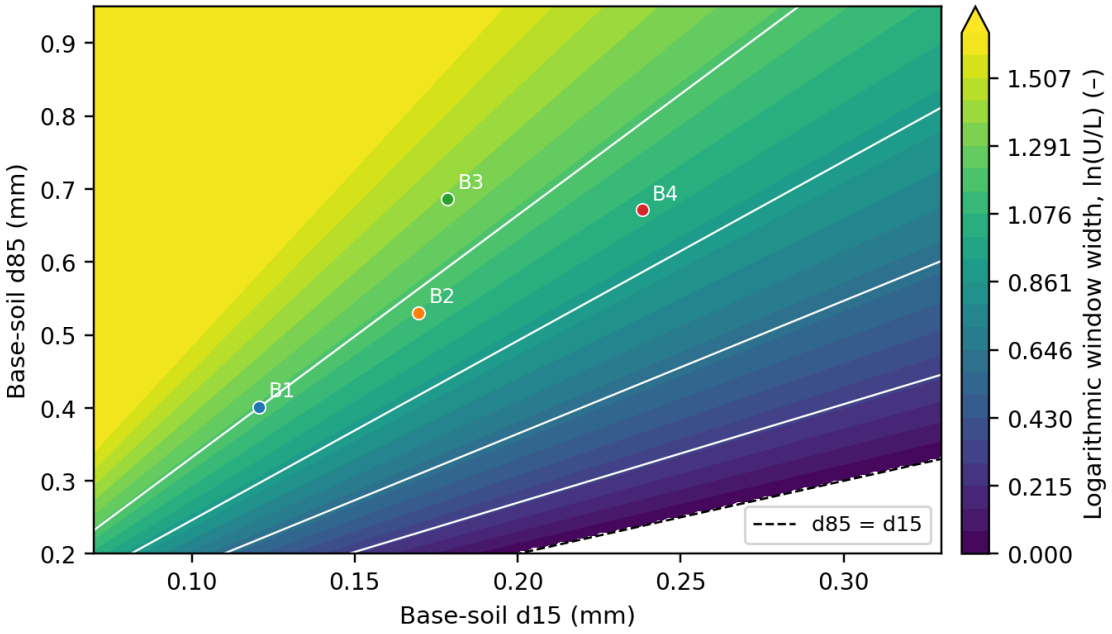


Figure 4. The logarithmic width of the filter D_{15} screening interval varies with base d_{15} and d_{85}; contours are derived from piecewise algebraic bounds rather than fitted performance data.

The analytic structure allows direct identification of a nonempty-interval condition. In the Kd_{15}-controlled branch, a feasible percentile interval requires Kd_{15}≤4d85, or equivalently d_{85}/d_{15}≥K/4. This necessary algebraic condition is not a sufficiency criterion for dam safety. If a more demanding drainage-size multiplier drives K above four times the ratio d_{85}/d_{15}, the example interval disappears even though other filter gradation choices, hydraulic design alternatives or a relaxation of the heuristic assumption may remain available. The branch nature of the problem is a reason to present explicit endpoints rather than conceal the underlying criteria in a single summary score.

Filter gradation dispersion, fines and coarse-percentile screens

Table 4 explores the variation of an illustrative B2 filter at a fixed nominal D_{15} equal to the derived geometric midpoint while increasing the filter logarithmic dispersion. The coefficient of uniformity is controlled by dispersion alone for this lognormal family, even though the retained D_{15} stays constant. As σ_F increases, the coarse-percentile D_{90} rises and the fine tail generally extends toward smaller particle sizes. This demonstrates why one favorable D_{15} retention ratio cannot guarantee that a candidate filter meets a complete gradation specification. The example filter D_{90} constraint is included solely to expose this trade-off.

Table 4. Dispersion sensitivity for a candidate B2 filter at its geometric-center D_{15} shows why complete-gradation screens matter.

σ_F (–)	D_{15} (mm)	C_u (–)	Fines (%)	D_{90} (mm)	All 4 screens
0.50	1.200	2.15	0.000	3.82	Yes
0.70	1.200	2.93	0.000	6.08	Yes
0.90	1.200	3.98	0.002	9.66	Yes

σ_F (–)	D_{15} (mm)	C_u (–)	Fines (%)	D_{90} (mm)	All 4 screens
1.10	1.200	5.41	0.019	15.37	Yes

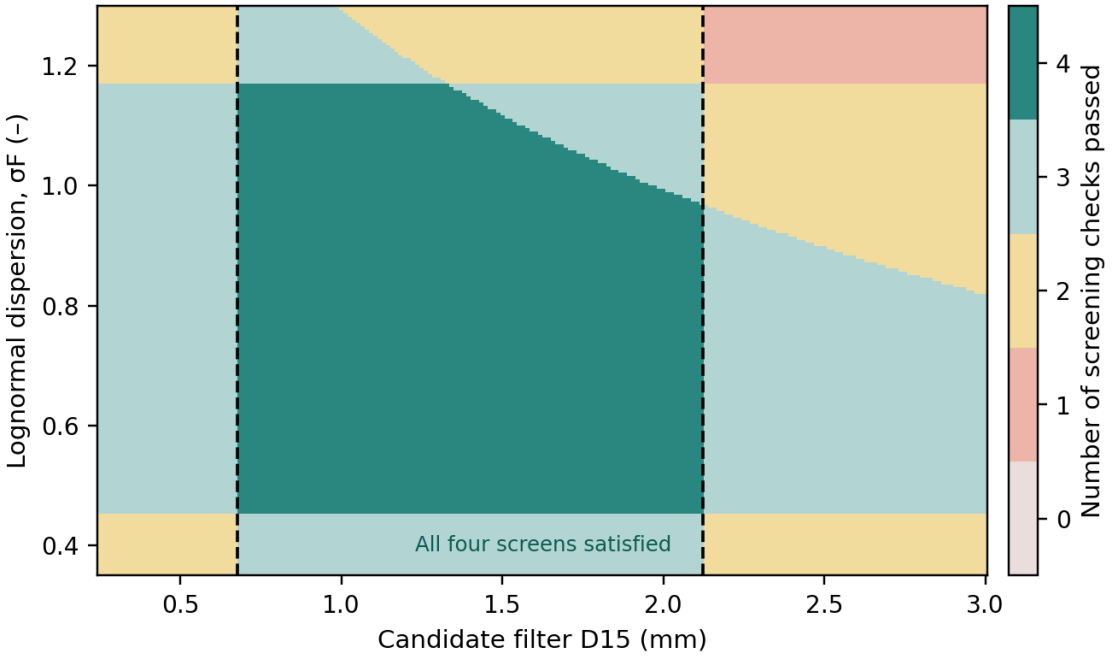


Figure 5. The candidate-filter screening map counts four illustrative requirements: D_{15} interval, uniformity range, fines content and an optional D_{90} procurement limit.

The colored regions in Figure 5 display how many of four explicit screens are satisfied across candidate D_{15} and dispersion values for B2. The figure does not show probabilities, safety factors or predicted erosion. It also does not include the true maximum grain size, geotechnical durability, placement density, effective permeability, self-filtering stability, cracked-core retention or long-term clogging. A map of passed algebraic conditions is useful for rejecting obviously incompatible combinations early in design, but becomes dangerous if interpreted as a replacement for empirical filter testing or agency design review.

Sensitivity to drainage multipliers and percentile uncertainty

Table 5 evaluates B2 over a series of illustrative drainage multipliers. Because the filter retention maximum is unchanged, raising K increases the lower bound once the Kd_{15} constraint becomes controlling and progressively reduces the production interval. Figure 6 generalizes that response to all four synthetic base gradations. The plotted ordinate $\exp(\varepsilon_{\max})-1$ is a one-sided percentage increase implied by the symmetric logarithmic multiplicative tolerance; the permissible reduction is instead $1-\exp(-\varepsilon_{\max})$, and these are not numerically equal. Treating them as symmetric arithmetic percentages would overstate the allowable negative change.

Table 5. The B2 interval contracts when the illustrative drainage multiplier K is increased.

K (–)	Lower L (mm)	Upper U (mm)	Width (–)	Tolerance multiplier (–)
3	0.509	2.122	1.428	2.042
4	0.679	2.122	1.140	1.768
5	0.848	2.122	0.917	1.582

K (–)	Lower L (mm)	Upper U (mm)	Width (–)	Tolerance multiplier (–)
6	1.018	2.122	0.735	1.444
7	1.188	2.122	0.580	1.337
8	1.357	2.122	0.447	1.250
9	1.527	2.122	0.329	1.179

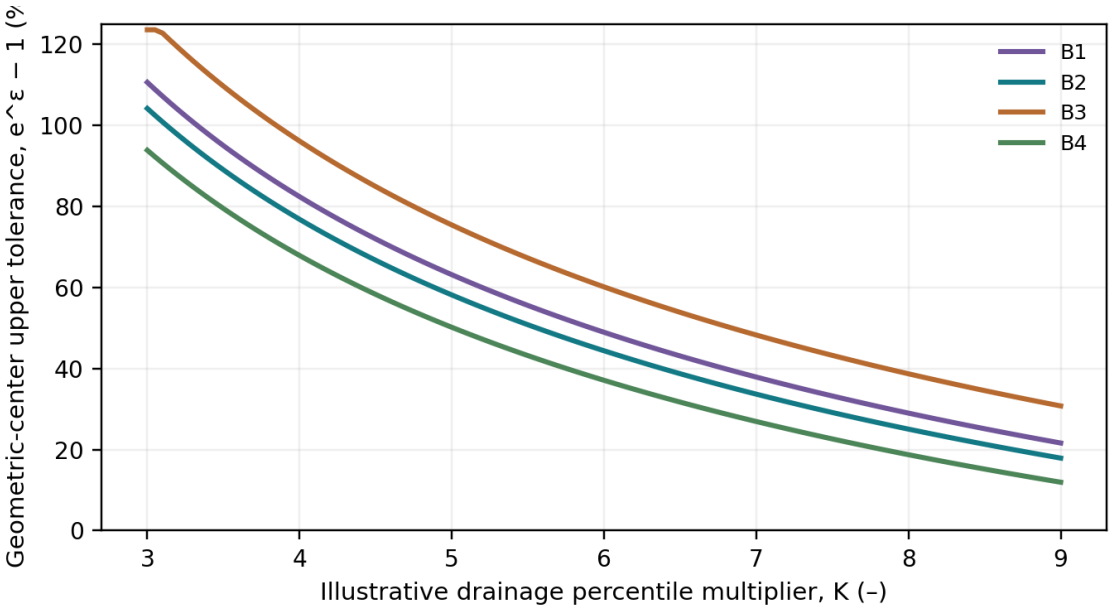


Figure 6. Decline in the admissible upper multiplicative tolerance as the illustrative drainage-size multiplier increases for four base gradations.

The worst-case independent quantile perturbation also yields a clear engineering screening insight: the same nominal filter percentile can become unacceptable if the true base d_{85} is lower than assumed or the true base d_{15} is higher than assumed. Table 6 illustrates this effect for B2 at K=4 using symmetric fractional perturbation bounds. The table should not be interpreted as measured sampling variability: the inputs are artificially selected, and the conservative extremes may not coexist on a physically plausible single particle-size curve. Its value is to make the sensitivity of screening endpoints visible before sieve-testing and quality-control plans are finalized.

Table 6. The illustrative B2 adverse base-quantile perturbation reduces the screening interval without implying measured statistical uncertainty.

Deviation bounds (%)	L_{max} (mm)	U_{min} (mm)	Robust width, W_{rob} (–)	Robust target (mm)
0	0.679	2.122	1.140	1.200
5	0.713	2.016	1.040	1.198
10	0.746	1.910	0.939	1.194
15	0.780	1.804	0.838	1.186
20	0.814	1.698	0.735	1.176
25	0.848	1.592	0.629	1.162

Comparison with established filter practice and engineering implications

Agency design practice goes beyond a percentile window in several decisive respects. NRCS (2017) requires the base material to be classified correctly and potentially regraded, and it provides separate filters for soils containing different proportions of fines. For category-4 material, the upper D_{15} retention limit is a preliminary filter-sizing constraint within a longer design sequence. Filters also require controls over overall gradation, maximum particle size, fines, segregation and constructability; where a collector pipe or double filter is present, compatibility must be checked at every relevant interface. The U.S. Bureau of Reclamation (2011) similarly emphasizes interface conditions, material sources, test procedures and construction controls. These source-derived rules are not replaced by the additional K multiplier or the geometric-center tolerance derived here.

The classical experimental literature further cautions against interpreting the hypothetical drainage-size multiplier as a verified permeability law. Sherard et al. (1984) investigated empirical retention behavior, and Sherard and Dunnigan (1989) provided evidence on fine-grained core filters requiring controlled erosion tests. A filter with satisfactory D_{15} relative to the synthetic base d_{85} may nevertheless be overly broad, gap graded, internally unstable or susceptible to segregation. Kenney and Lau (1985) explicitly related internal stability to grain-size distribution and laboratory seepage response. These mechanisms depend on particle fabric, hydraulic forces and compaction, none of which is contained in the lognormal distribution parameters alone.

For practical engineering interpretation, the proposed framework is best used after the base-soil category and raw gradation have been established and before procurement gradation bands are finalized. First, determine the controlling base-soil gradation, including fine and coarse extremes rather than a single averaged sample. Next, follow the chosen agency procedure to obtain a retention-compatible D_{15} maximum and relevant minimum. The logarithmic screening interval and midpoint may then communicate how far a nominal candidate lies from a potential boundary, while supplementary gradation and material screens expose conflicts that a single D_{15} ratio obscures. Finally, confirm the filter and drain with appropriately selected sieve tests, internal stability assessment, hydraulic measurements, construction quality controls and erosion testing where warranted.

Limitations, reproducibility and future validation

Four limitations determine the scope of the numerical findings. First, the base and filter distributions are synthetic lognormal models, rather than curves from a laboratory gradation dataset. Second, a logarithmic tolerance on a single percentile is not a statistical confidence interval and does not model real quarry-process covariance between percentiles. Third, the additional drainage multiplier K and the lower auxiliary uniformity bound are screening choices rather than universally codified requirements; the squared size ratio is a qualitative index with important material-dependent exceptions. Fourth, the model addresses category-4, non-dispersive continuous grading only and explicitly omits category 1–3 special retention

provisions, cracked core erosion, concentrated flow, fines clogging and segregation mechanisms. The model therefore cannot estimate seepage rate, probability of dam failure, piping progression or guaranteed filter effectiveness.

The method is reproducible because all input distributions, intervals, screening thresholds and algebraic transformations are stated without requiring access to private material records. Independent verification is possible by evaluating the normal-quantile definitions, recomputing d_{15} and d_{85}, applying the piecewise lower and upper bound equations and checking the midpoint identity by substitution. A field-oriented extension would replace the assumed lognormal curves with full measured particle-size distributions from multiple material lots, use the governing current dam safety design procedure for the specific base-soil category, and assess the consistency of gradation envelopes under actual production variation. Experimental filter tests would then be required to evaluate retention under representative hydraulic heads and crack-induced flow, without presupposing agreement with this narrow analytical screening model.

CONCLUSION

A dimensionless screening procedure has been developed for examining candidate granular-filter size compatibility at embankment-dam interfaces, with the retention maximum grounded in the category-4 NRCS rule and the additional drainage-size multiplier clearly separated as an illustrative assumption. The procedure transforms upper and lower D_{15} bounds into a logarithmic interval width, a geometric-center target and a symmetric multiplicative tolerance measure, enabling different synthetic base gradations to be compared transparently. For the hypothetical B2 soil, the recovered base-percentile sizes are d_{15}=0.170 mm and d_{85}=0.530 mm; at K=4 the candidate filter D_{15} window is 0.679–2.122 mm, its geometric center is 1.200 mm and the logarithmic tolerance is 0.570. These values are exact consequences of the specified inputs rather than validated material properties.

The parametric analysis shows that a more demanding minimum size requirement reduces the available interval, and adverse uncertainty in the two controlling base percentiles can narrow the interval even before entire candidate gradation curves are considered. Auxiliary calculations also demonstrate that filters with the same nominal D_{15} can possess appreciably different uniformity, fines fractions and coarse percentiles. The proposed indicators are therefore most useful for initial comparison, sensitivity screening and specification discussions. They cannot certify filter performance, replace laboratory erosion or seepage testing, establish maximum particle size from an unbounded mathematical distribution, or substitute for the complete requirements of the selected dam design guidance. Their utility is precisely that the mathematical acceptance conditions and their limitations remain visible to the engineer.

REFERENCES

Fell, R., Wan, C. F., Cyganiewicz, J., & Foster, M. (2003). Time for development of internal erosion and piping in embankment dams. Journal of Geotechnical and Geoenvironmental Engineering, 129(4), 307–314. https://doi.org/10.1061/(ASCE)1090-0241(2003)129:4(307)

Foster, M., & Fell, R. (2001). Assessing embankment dam filters that do not satisfy design criteria. Journal of Geotechnical and Geoenvironmental Engineering, 127(5), 398–407. https://doi.org/10.1061/(ASCE)1090-0241(2001)127:5(398)

Foster, M., Fell, R., & Spannagle, M. (2000). The statistics of embankment dam failures and accidents. Canadian Geotechnical Journal, 37(5), 1000–1024. https://doi.org/10.1139/t00-030

Kenney, T. C., & Lau, D. (1985). Internal stability of granular filters. Canadian Geotechnical Journal, 22(2), 215–225. https://doi.org/10.1139/t85-029

Sherard, J. L., & Dunnigan, L. P. (1989). Critical filters for impervious soils. Journal of Geotechnical Engineering, 115(7), 927–947. https://doi.org/10.1061/(ASCE)0733-9410(1989)115:7(927)

Sherard, J. L., Dunnigan, L. P., & Talbot, J. R. (1984). Basic properties of sand and gravel filters. Journal of Geotechnical Engineering, 110(6), 684–700. https://doi.org/10.1061/(ASCE)0733-9410(1984)110:6(684)

U.S. Bureau of Reclamation. (2011). Design standards no. 13: Embankment dams, chapter 5: Protective filters. U.S. Department of the Interior. https://www.usbr.gov/tsc/techreferences/designstandards-datacollectionguides/designstandards.html

U.S. Department of Agriculture, Natural Resources Conservation Service. (2017). Gradation design of sand and gravel filters (National Engineering Handbook, Part 633, Chapter 26, Amendment 61). https://directives.nrcs.usda.gov/sites/default/files2/1712930680/26895.pdf

SPECTRAL AND NUMERICAL ANALYSIS OF BIFURCATIONS AND COMPLEX DYNAMICS IN FRACTIONAL BURGERS EQUATIONS

Khadija Zair
Laboratory of Applied Mathematics and Scientific Computing, Sultan Moulay Slimane University, Beni Mellal, Morocco.

M'hamed El Omari
Laboratory of Applied Mathematics and Scientific Computing, Sultan Moulay Slimane University, Beni Mellal, Morocco.

ABSTRACT

This study investigates the stability, bifurcation behavior, and nonlinear dynamics of viscous, forced, and fractional Burgers equations. The effects of viscosity, external forcing, and fractional order on the long-term behavior of solutions are systematically analyzed. Stationary solutions are characterized using linear stability analysis, spectral analysis, and energy estimates**. A** Chebyshev spectral collocation method is employed to accurately determine stationary states, eigenvalues, and critical bifurcation parameters. Numerical continuation is used to track solution branches and identify branch points, fold points, and Hopf bifurcations**.** The analysis is further extended to a fractional Burgers model based on the Caputo derivative, allowing memory effects to be incorporated. Although stationary states remain independent of the fractional order, their stability is strongly influenced by this parameter. The **Matignon criterion** is therefore applied to characterize stability transitions and establish the fractional order as an additional bifurcation parameter. Nonlinear dynamics are explored through time-domain simulations, phase portraits, bifurcation diagrams, Poincaré sections, and Lyapunov exponents. The results reveal transitions from stable stationary states to periodic, quasiperiodic, and complex dynamical regimes**,** highlighting the combined influence of dissipation, forcing, and memory effects on Burgers-type systems.

Keywords: Burgers equation; fractional dynamics; Caputo derivative; stability; bifurcation; Hopf bifurcation; Chebyshev spectral method; nonlinear dynamics; Lyapunov exponent.

MICROALGAE: TINY ORGANISMS WITH GREAT ENVIRONMENTAL POTENTIAL

Ouassila Riouchi
Interdisciplinary Laboratory for Research in Environment, Management, Energy and Tourism (LIREMET), School of Technology Essaouira, Cadi Ayyad University, Essaouira, Morocco.

Khalid Elkalay
Interdisciplinary Laboratory for Research in Environment, Management, Energy and Tourism (LIREMET), School of Technology Essaouira, Cadi Ayyad University, Essaouira, Morocco.

ABSTRACT

Microalgae are microscopic organisms that play an important role in aquatic ecosystems. They produce oxygen, absorb carbon dioxide, and serve as a major source of food for many aquatic organisms. In recent years, microalgae have attracted scientific interest because of their potential applications in wastewater treatment, biofuel production, and the removal of certain pollutants. Some species can also produce valuable compounds for food, cosmetics, and pharmaceutical industries. Therefore, studying microalgae is essential for developing sustainable and environmentally friendly technologies.

Keywords: Microalgae, aquatic ecosystems, environmental protection, biotechnology, sustainability

IN SILICO ANALYSIS OF MAJOR CONSTITUENTS OF THYMUS VULGARIS ESSENTIAL OIL AGAINST PENICILLIUM DIGITATUM: MOLECULAR DOCKING, MOLECULAR DYNAMICS, AND TOXICITY PROFILING

Hajar Sadrati
Applied Biology for Health, Environment and Sustainable Development Laboratory, Faculty of Applied Sciences, Sultan Moulay Slimane University, Beni Mellal, Morocco.

Youssef Arif
Biological Engineering Laboratory, Faculty of Science and Technology, Sulatan Moulay Slimane University, Béni Mellal, Morocco.

Younes Abbas
Applied Biology for Health, Environment and Sustainable Development Laboratory, Faculty of Applied Sciences, Sultan Moulay Slimane University, Beni Mellal, Morocco.

Sanaa Sabour-Alaoui
Applied Biology for Health, Environment and Sustainable Development Laboratory, Faculty of Applied Sciences, Sultan Moulay Slimane University, Beni Mellal, Morocco.

Mohammed El idrissi
Processes and Applied Materials Laboratory, Faculty of Applied Sciences, Sultan Moulay Slimane University, Beni Mellal, Morocco.

ABSTRACT

Penicillium digitatum is the primary causal agent of postharvest green mold in citrus, and its control still relies largely on synthetic fungicides, against which resistant populations are increasingly beging reported. Essential oils are considered promising alternatives, yet their molecular targets in this pathogen remain poorly characterized. In this study, thirteen major constituents of Thymus vulgaris essential oil, identified by gas chromatography-mass spectrometry, were evaluated using an in silico approche targeting 14α-demethylase (CYP51) from P. digitatum. A three-dimensional model of CYP51 was constructed by homology modeling using a suitable structural template retrieved from the Protein Data Bank (PDB) and validated through Ramachandran plot analysis and ProSA-web (−8.67). Binding pockets were predicted with AutoDock Vina and the constituents were docked and compared with the reference fungicide imazalil. β-Caryophyllene (−8.5 kcal/mol), caryophyllene oxide (−8.2 kcal/mol), carvacrol (−8.1 kcal/mol), τ-cadinol (−7.9 kcal/mol) and α-humulene (−7.8 kcal/mol) showed the most favorable binding energies. All five ligands occupied a predominantly hydrophobic cavity, with ASP114 acting as a recurrent anchoring residue. Interaction profiling and molecular surface-property analysis were consistent with hydrophobic complementarity as the main driver of binding. Over 100 ns molecular dynamics

simulations, the complexes remained stable (mean backbone RMSD 2.5-3.5 Å; radius of gyration close to 20 Å), with no major secondary-structure rearrangement. ProTox predictions assigned most compounds to toxicity classes 4 and 5. These results identify sesquiterpene constituents as candidate inhibitors warranting in vitro and in vivo validation.

Keywords: Penicillium digitatum; Thymus vulgaris; essential oil; molecular docking; molecular dynamics; ADMET; postharvest green mold.

UNDERSTANDING THE LOW APPEAL OF GEOSCIENCES IN THE MOROCCAN EDUCATION SYSTEM: A SURVEY OF PROSPECTIVE TEACHERS

El Hassania El Hamzaoui
Geomatics, Geo-Resources and Environment Laboratory, Department of Earth Sciences, Faculty of Sciences and Technology, University Sultan Moulay Slimane, B.P 523, Mghila, Beni Mellal 23000, Morocco.

Hind El Hamzaoui
Ibn Zohr University, Higher School of Education and Training – Agadir, Morocco

ABSTRACT
Earth sciences play a crucial role in understanding terrestrial dynamics and addressing contemporary environmental challenges, ranging from natural resource management to geological hazard mitigation. Despite their evident educational and societal value, Earth science education faces significant global disparities. While several educational systems successfully engage students by incorporating inquiry-based approaches and fieldwork, other contexts—particularly in Morocco—struggle with numerous pedagogical, material, and institutional constraints. This research investigates the factors influencing the low appeal of Earth sciences within the Moroccan education system. Based on a survey conducted among 140 science students and future teachers, this study analyzes their perceptions of the discipline, the obstacles encountered during their academic path, and their learning conditions. The findings highlight a critical lack of practical activities and fieldwork, a dominance of traditional teaching methods, and a negative perception of the discipline, which is often viewed as purely reliant on memorization. In light of these insights, the study offers pedagogical and institutional recommendations aimed at elevating the status of Earth sciences and renewing their instruction.

Keywords: Earth sciences, geoscience education, subject attractiveness, Moroccan education system, perceptions, prospective teachers.

EXPLORING UNDERGRADUATE STUDENTS' EXPERIENCES OF PEER TUTORING AT HIGHER EDUCATION INSTITUTES: A QUALITATIVE PHENOMENOLOGICAL STUDY

Minahil Fatima
Ms., University of management and Technology, Pakistan

Irfan Bashir
Dr., University of management and Technology, Pakistan

Yasira Waqar
Dr., University of management and Technology, Pakistan

ABSTRACT

Peer tutoring is an important academic support strategy in higher education that promotes collaborative learning, academic engagement, communication, confidence, and emotional well-being (Topping, 2020; Gamlath, 2022). However, limited qualitative research has explored students' experiences of peer tutoring in Pakistani universities, particularly at the University of Management and Technology (UMT), Lahore.

This study aims to explore undergraduate students' lived experiences and perceptions of UMT's peer tutoring program. It examines the perceived influence of peer tutoring on academic understanding, motivation, classroom participation, confidence, communication, and collaborative learning. Additionally, it investigates the benefits, limitations, and challenges experienced by tutors and tutees.

Grounded in Vygotsky's (1978) Sociocultural Theory, the study emphasizes the role of social interaction in learning and cognitive development. A qualitative phenomenological research design will be employed to understand participants' experiences. Purposive sampling will be used to select approximately 10–15 undergraduate students who have participated as tutors or tutees. Data will be collected through semi-structured interviews and analysed thematically following Braun and Clarke (2021).

The study is expected to address a research gap by providing context-specific insights into peer tutoring within Pakistani higher education. Its findings may help UMT improve its peer tutoring program, strengthen collaborative learning, and develop effective student-centred academic support initiatives. The research may also inform educators, university administrators, and policymakers seeking to enhance peer-assisted learning practices in higher education institutions across Pakistan.

Keywords: Peer tutoring, undergraduate students, collaborative learning, phenomenology, student experiences, higher education, Pakistan

USE OF ARTIFICIAL INTELLIGENCE FOR MEDICATION ADHERENCE ASSESSMENT IN PATIENTS WITH TYPE 2 DIABETES: AN EXPLORATORY STUDY IN MOROCCO USING CHATGPT AND THE VALIDATED GENERAL MEDICATION ADHERENCE SCALE

Maryem Arraji
Laboratory of Health Sciences and Technologies, Higher Institute of Health Sciences, Hassan First University of Settat, Settat, Morocco

Khaoula EL BARBI
Laboratory of Health Sciences and Technologies, Higher Institute of Health Sciences, Hassan First University of Settat, Settat, Morocco

Fatima Zahra BOUCHACHI
Laboratory of Health Sciences and Technologies, Higher Institute of Health Sciences, Hassan First University of Settat, Settat, Morocco

Mohamed Khalis
Laboratory of Biostatistics, Clinical, and Epidemiological Research, Department of Public Health, Faculty of Medicine and Pharmacy, Mohamed V University in Rabat, Rabat, Morocco

Mohamed Chahboune
Laboratory of Health Sciences and Technologies, Higher Institute of Health Sciences, Hassan First University of Settat, Settat, Morocco

ABSTRACT

Objectives: Medication adherence remains a major challenge in the management of type 2 diabetes (T2D), especially in middle-income countries such as Morocco. With the rapid development of artificial intelligence, large language models, including ChatGPT, may offer new opportunities for clinical research through simulated patient profiles. This study examined the feasibility of using ChatGPT to generate culturally contextualized virtual profiles of Moroccan patients with T2D and to apply the validated Moroccan Arabic dialect version of the general medication adherence scale (GMAS).

Methods: This exploratory pilot simulation study used ChatGPT-4 to generate 11 virtual profiles based on representative sociodemographic and clinical characteristics of Moroccan patients with T2D. Each profile was administered the validated Moroccan Arabic dialect version of the GMAS.

Results: Four profiles (36.4%) showed high adherence, 6 (54.5%) displayed moderate adherence, and 1 (9.1%) exhibited low adherence. Expert evaluations were consistent, with all ratings ≥3 on a 4-point scale, supporting the credibility and cultural appropriateness of the profiles. The simulated patterns reflected real-world trends, with higher adherence among

profiles treated with oral antidiabetic drugs, covered by health insurance, and having shorter disease duration, and lower adherence among profiles using insulin, lacking insurance, and having longer disease duration.

Conclusion: ChatGPT generated credible, culturally adapted patient profiles that enabled application of a validated psychometric tool in a simulated environment. This rapid, low-cost approach may support exploratory research, healthcare training, and intervention design. Comparative studies using real patient data are needed to confirm validity.

Keywords: Artificial intelligence; Diabetes mellitus, type 2; Feasibility studies; Medication adherence; Morocco; Psychometrics

THE ENERGY PERFORMANCE GAP IN AFRICAN BUILDINGS: A COMPARATIVE ASSESSMENT OF BUILDING REGULATIONS, CLIMATE ZONES AND ENERGY-EFFICIENCY STRATEGIES IN NIGERIA AND SELECTED AFRICAN COUNTRIES

Salihu SULEIMAN
Department of Architecture, Federal University Birnin Kebbi, Nigeria
ORCID: 0009-0003-2575-6840

Aisha N. SULEIMAN
Department of Building, University of Calabar, Nigeria

ABSTRACT
A growing number of African countries have building energy rules, but little is known about whether buildings built under those rules use the energy their designers predicted. This paper compares building energy regulations, climate treatment and efficiency strategies in Nigeria and six other African countries (South Africa, Ghana, Kenya, Egypt, Morocco and Rwanda) through document analysis and a review of published studies. We treat the energy performance gap as three linked gaps: a regulatory gap, where requirements are poorly matched to climate and users; a compliance gap, where buildings are not built or checked to the requirement; and the performance gap proper, where measured use differs from prediction. Climate treatment ranges from six zones in South Africa to a single hot-humid label in one summary of Nigeria's code, even though recent research proposes five to seven Nigerian zones. The regimes mix prescriptive, performance, certification and audit routes, yet in the sources we reviewed only Rwanda's permit process checks as-built conditions and only Kenya's regulations require audits of buildings in use. Every quantified Nigerian saving we found comes from simulation, and we found no measured-versus-predicted dataset for any of the seven countries. The gap is therefore better described as invisible than absent. We propose a five-element framework for making it visible and closing it, and a research agenda for Nigeria.

Keywords: energy performance gap; building energy codes; climate zones; passive cooling; Nigeria; Africa; compliance

NIGERIA'S ARCHITECTURAL TRANSITION TOWARDS NET-ZERO BUILDINGS: A BIBLIOMETRIC, POLICY AND GLOBAL BENCHMARKING ANALYSIS OF BUILDING ENERGY EFFICIENCY AND SUSTAINABLE DESIGN

Salihu SULEIMAN
Department of Architecture, Federal University Birnin Kebbi, Nigeria
ORCID: 0009-0003-2575-6840

Gambo B. WURMA
Department of Architecture, Federal University Birnin Kebbi, Nigeria

ABSTRACT

Nigeria has promised net-zero emissions by 2060, with cuts of 29% by 2030 and 32% by 2035 against a 2018 baseline, but it has no matching pathway for buildings. Meanwhile a housing deficit of roughly 14.9 million units means a great deal of construction is still to come. We ask how well Nigerian architectural practice and regulation are prepared for net-zero buildings, using three lenses: a synthesis of published Scopus-based bibliometric studies, a reading of seven Nigerian policy instruments, and a comparison with the European Union, Singapore, South Africa, Rwanda and Ghana. The literature shows a global field that has grown steadily since 2006 around energy efficiency, life-cycle assessment and embodied energy, while Nigerian energy research leans towards renewable supply. The only Nigerian instrument with quantified building requirements, the 2017 Building Energy Efficiency Code, began as a voluntary pilot; practitioners describe the National Building Code as poorly enforced; and nothing we reviewed defines a net-zero building or deals with life-cycle carbon. The comparison points to legal force, permit-linked checking, public-sector-first sequencing, life-cycle carbon rules and public progress tracking as what sets the stronger regimes apart. We offer a four-phase roadmap and a Scopus protocol for readers who want to extend the bibliometric work.

Keywords: Net-Zero Buildings; Building Energy Efficiency; Sustainable Architecture; Nigeria; Bibliometric Analysis; Policy Benchmarking; Building Energy Codes.

CONTEMPORARY SEISMIC ISOLATION TECHNIQUES: IMPLEMENTATION UNDER ALGERIAN REGULATION AND COMPARISON WITH INTERNATIONAL CODES

OUNIS HADJ MOHAMED
Department of Civil Engineering/University of Mostefa Ben Boulaid Batna 253, Route de Constantine. Fésdis, Batna, Batna, Algeria

OUNIS ABDELHAFID,
Faculty of Science and technology /Company University Mohamed Khider Biskra, Algeria

ABSTRACT

Seismic isolation has become a well-recognized and increasingly adopted strategy for enhancing the earthquake resilience of structures. Several national seismic codes, including those of Japan, China, Italy, Taiwan, the IBC 2009, and Algeria's RPA 99, have introduced comprehensive provisions governing its application. In this study, a standardized benchmark building model is used to carry out a comparative assessment of these codes, keeping structural parameters constant, namely mass, height, hysteretic behaviour, and soil conditions.
This research introduces an innovative design methodology for Lead Rubber Bearing (LRB) isolators, specifically adapted to the requirements of the Algerian seismic code. The proposed approach relies on the equivalent static method and integrates an iterative procedure to accurately estimate the design displacement of the isolator, accounting for the mechanical and geometric properties of the structure.
To evaluate the effectiveness of the proposed methodology, nonlinear time-history analyses were performed using seismic records and design provisions from several international codes. The findings showed strong agreement in both base shear and design displacement, highlighting the method's reliability and its consistency with internationally recognized standards.

Keywords: Base isolation; lead rubber bearing (LRB); Algerian seismic code (RPA); Seismic excitation; Hysteresis behaviour

ASSESSMENT OF SOIL LOSS FROM CARROT (DAUCUS *CAROTA*) AS INFLUENCED BY NPK 15:15:15 AND POULTRY MANURE

EWETOLA, E. A.
Ladoke Akintola University of Technology, P.M.B. 4000, Ogbomoso, Oyo State, Nigeria

AFOLORUNSO, G.T.
Ladoke Akintola University of Technology, P.M.B. 4000, Ogbomoso, Oyo State, Nigeria

JAYEOBA, A. D.
Ladoke Akintola University of Technology, P.M.B. 4000, Ogbomoso, Oyo State, Nigeria

OKE S. A.
Ladoke Akintola University of Technology, P.M.B. 4000, Ogbomoso, Oyo State, Nigeria

AYENI, B. O.
Ladoke Akintola University of Technology, P.M.B. 4000, Ogbomoso, Oyo State, Nigeria

ABSTRACT

Soil loss due to crop harvesting is a significant erosion process that has contributed to soil degradation around the world. However, fertilizer types can have various effects on soil and crop productivity. Therefore, a field study was carried out to compare the influence of NPK 15:15:15 and poultry manure both sole and combined on carrot yield, and soil loss during harvesting. Treatments applied included, NPK 15:15:15 at 150 kg N/ha, 5ton/ha of poultry manure (PM), ½ NPK + ½ PM and a control arranged in a randomized complete block design with 3 replications. At harvest, soil loss per unit mass (SLCHspec), total soil loss SLCHcrop and nutrient loss were determined. Application of fertilizers increased root yield of carrot compared with control by 70, 53 and 27%, respectively, on NPK+PM, NPK and PM. However, NPK+PM and PM reduced SLCHspec and SLCHcrop compared with control and NPK respectively, by 64 and 13%. Compared to control and NPK, NPK+PM respectively, reduced SLCHcrop by 146 and 72%. Org C, N, K and Mg losses were higher on NPK than other treatments. The higher root yield of carrot and reduction of soil loss on NPK+PM when compared to the control and NPK may be due to synergistic effects of inorganic and organic fertilizers which improved soil structure that reduced soil adherence to the crop roots. Therefore, NPK+ PM can improve crop yield and reduce soil loss due to carrot harvesting.

Keywords: NPK, Poultry manure, Carrot yield, Soil loss and Nutrient loss

AQUACULTURE POTENTIALS of PARENTAL *CLARIAS GARIEPINUS* and BACKCROSS PROGENY DERIVED from FEMALE *CLARIAS–HETEROBRANCHUS* HYBRID and MALE *CLARIAS GARIEPINUS*

Olugbemi Victor EKUNDARE
Department of Biology, Faculty of Sciences, University of Ilesa, Ilesa, Osun State, Nigeria.

Oluwadamilare Emmanuel OBAYEMI
Department of Zoology, Obafemi Awolowo University, Ile-Ife, Osun State, Nigeria

ABSTRACT

This study evaluated the reproductive performance and growth characteristics of progeny produced from a backcross between female *Clarias gariepinus* × *Heterobranchus longifilis* hybrid and male *Clarias gariepinus*, using pure *C. gariepinus* as the control. Artificial propagation was conducted using Ovaprim-induced spawning, and larvae were reared in triplicates for ten weeks under controlled hatchery conditions. Hatchability, growth performance, survival, and length–weight relationships were assessed, while data were analyzed using an independent-samples t-test at a 95% confidence level. The pure *C. gariepinus* cross recorded significantly higher hatchability (80.37 ± 0.20%) than the backcross (9.77 ± 0.14%; $P < 0.05$). Although the backcross larvae had significantly higher initial weight (0.10 ± 0.005 g) and length (2.04 ± 0.016 cm), pure *C. gariepinus* exhibited superior growth throughout the culture period, with significantly higher final weight (23.84 ± 0.45 g), weight gain (23.75 ± 0.45 g), final length (15.60 ± 0.29 cm), length increase (13.65 ± 0.30 cm), average daily growth (0.34 ± 0.004 g day^{-1}), specific growth rate (3.50 ± 0.01% day^{-1}), and survival (100%) ($P < 0.05$). Length–weight analysis revealed positive allometric growth in pure *C. gariepinus* ($b = 4.06$) and negative allometric growth in the backcross ($b = 1.46$), with strong correlations ($R^2 \geq 0.94$). The findings demonstrate that hybrid catfish can successfully backcross with parental *C. gariepinus* to produce viable offspring, although reproductive performance, growth, and survival were substantially reduced. These results highlight potential ecological risks posed by escaped hybrids to the genetic integrity and sustainability of wild *C. gariepinus* populations.

Keywords: Genetic introgression; growth performance; backcross; *Clarias gariepinus*; hybridization;

EFFECTS OF PERSONALISED LEARNING METHOD ON THE ACHIEVEMENT OF STUDENTS IN JOS NORTH LOCAL GOVERNMENT AREA, PLATEAU STATE, NIGERIA

ASABE EDWARD BASH (Ph.D.)
Department of Science and Technology, Faculty of Education, University of Jos.

CHRISTIANA DAVID DALOK
Department of Science and Technology, Faculty of Education, University of Jos.

ABSTRACT

The aim of the study was to determine the effects of Personalized learning on junior secondary II students' achievement in Basic Science and Technology in Jos North Local Government Area, Plateau state, Nigeria. Two objectives, two research questions as well as two null hypotheses were raised to guide the study. A quasi-experimental research design was used. The study population consisted of all 1,9678 male and female JSS II students in 22 Government Secondary Schools in Jos North Local Government Area, Plateau State. A sample of 112 JSS II students was selected for the study. The Basic Science and Technology Achievement Test (BSTAT) was used to collect the data. Reliability coefficient determined using Kuder- Richardson and had a reliability coefficient of 0.69, indicating acceptable internal consistency for the instruments. The data collected was analyzed using mean and standard deviation for answering the research questions, while ANCOVA was used to test the null hypotheses at 0.05 level of significance. The findings of the research showed that: the use of personalized learning was effective in enhancing teaching and learning. The personalized learning approach significantly improved the achievement scores of students in the experimental group compared to the control group that was exposed to the lecture method. The research recommended among other recommendations that; school proprietors should support the integration of the personalized learning approach in Basic science and Technology classrooms by providing necessary resources and fostering an environment conducive to student-centered teaching and learning. Teachers should receive ongoing professional development and training on how to effectively implement personalized learning strategies. Teachers should be equipped with the necessary tools and pedagogical skills to maximize the engagement and learning outcomes of their students through personalized learning approach.

Keywords: Basic Science and Technology, Achievement, Personalized Learning.

E0 VE E20 İLE ÇALIŞAN BİR LOMBARDİNİ LGW 523 MOTORUNUN PERFORMANSINA BOR BAZLI KATKI MADDESİ KONSANTRASYONUNUN ETKİLERİ: OPTİMUM ÇALIŞMA KOŞULLARININ BELİRLENMESİ

EFFECTS OF BORON-BASED ADDITIVE CONCENTRATION ON THE PERFORMANCE OF A LOMBARDINI LGW 523 ENGINE FUELED WITH E0 AND E20: DETERMINATION OF OPTIMUM OPERATING CONDITIONS

Talip AKBIYIK
Asst. Prof. Dr., Aksaray University, Technical Sciences Vocational School, Automotive Technology
ORCID ID: 0000-0001-8580-8890

Nafiz KAHRAMAN
Prof. Dr., Erciyes University, Faculty of Aeronautics and Space Sciences, Space Engineering
ORCID ID: 0000-0002-8698-8632

ÖZET

İçten yanmalı motorlarda yakıt tüketiminin azaltılması, motor performansının iyileştirilmesi ve egzoz emisyonlarının düşürülmesi amacıyla alternatif yakıtların ve yakıt katkı maddelerinin kullanımı giderek önem kazanmaktadır. Benzin-etanol karışımları, sahip oldukları oksijen içeriği nedeniyle yanma sürecini ve egzoz emisyonlarını etkileyebilen alternatif yakıtlar arasında yer almaktadır. Bununla birlikte, etanol ilavesinin yakıtın alt ısıl değerini ve fiziksel özelliklerini değiştirmesi, motor performansı ve yakıt tüketimi üzerinde farklı sonuçlar ortaya çıkarabilmektedir.

Bor esaslı katkılar da içten yanmalı motorlarda performans ve emisyon iyileştirmesi amacıyla araştırılan katkı maddelerindendir. Ancak bu katkıların etkileri kullanılan yakıt türüne ve katkı miktarına bağlı olarak değişebilmektedir. Özellikle benzin ve E20 gibi farklı özelliklere sahip yakıtlarda bor katkısının motor torku, fren özgül yakıt tüketimi (BSFC), termal verim ve egzoz emisyonları üzerindeki etkilerinin karşılaştırılması önem taşımaktadır. Bu kapsamda, mevcut çalışmada katkısız benzin ve E20 yakıtlarına 7, 14 ve 21 cc/L oranlarında bor katkısı ilave edilerek motor performansı ve egzoz emisyonları 1500–5000 d/d motor devri aralığında deneysel olarak incelenmiştir.

Anahtar Kelimeler: Bor bazlı katkı maddeleri; E0 yakıtı; E20 yakıtı; benzinli motor; Lombardini LGW 523; motor performansı; katkı maddesi konsantrasyonu; motor devri; etanol-benzin karışımları

ABSTRACT

The use of alternative fuels and fuel additives in internal combustion engines is gaining increasing importance as a means to reduce fuel consumption, improve engine performance, and lower exhaust emissions. Gasoline-ethanol blends are among these alternative fuels; due to their oxygen content, they can influence the combustion process and exhaust emissions.

However, the addition of ethanol alters the fuel's lower heating value and physical properties, which can lead to varying outcomes regarding engine performance and fuel consumption.
Boron-based additives are also being investigated for their potential to enhance performance and reduce emissions in internal combustion engines. The effects of these additives, however, can vary depending on the type of fuel used and the dosage of the additive. It is particularly significant to compare the impacts of boron additives on engine torque, brake-specific fuel consumption (BSFC), thermal efficiency, and exhaust emissions when used with fuels that possess different characteristics, such as gasoline and E20 (a blend of 20% ethanol and 80% gasoline). In this context, the present study experimentally examines engine performance and exhaust emissions—across an engine speed range of 1500–5000 rpm—by incorporating boron additives at concentrations of 7, 14, and 21 cc/L into both neat gasoline and E20 fuel.
Keywords: Boron-based additives; E0 fuel; E20 fuel; gasoline engine; Lombardini LGW 523; engine performance; additive concentration; engine speed; ethanol-gasoline blends

1. GİRİŞ

İçten yanmalı motorlarda yakıt ekonomisinin iyileştirilmesi, motor performansının artırılması ve egzoz emisyonlarının azaltılması, otomotiv teknolojileri alanındaki araştırmaların temel konuları arasında yer almaktadır. Bu amaçla alternatif yakıtların geliştirilmesinin yanı sıra yakıtın fiziksel ve kimyasal özelliklerini değiştirebilen katkı maddelerinin kullanımı da araştırılmaktadır. Bor esaslı bileşikler, kimyasal yapıları ve bazı bileşiklerin hidrojen içeriği nedeniyle içten yanmalı motorlarda yakıt katkısı olarak incelenen malzemeler arasındadır. Bununla birlikte, bor içeren bileşiklerin motor performansı ve emisyonlar üzerindeki etkileri; bileşiğin kimyasal yapısına, katkı konsantrasyonuna, yakıtla uyumluluğuna ve motorun çalışma koşullarına bağlı olarak değişebilmektedir (Sertkaya ve Akbıyık, 2016; Yakın ve Gülcan, 2025; Sofuoğlu ve ark., 2026).

Bor esaslı katkıların motorlardaki etkileri, kullanım alanlarına göre doğrudan yakıta eklenen katkılar ve motor yağlama yağına ilave edilen katkılar olmak üzere iki grupta değerlendirilebilir. Yakıta doğrudan eklenen bor bileşikleri yanma süreci, yakıt özellikleri ve emisyonlar üzerinde etkili olabilirken, yağlama yağına eklenen bor bileşikleri daha çok sürtünme, aşınma ve yağlama özellikleri üzerinden motor performansını etkileyebilmektedir. Bu nedenle iki farklı kullanım biçiminden elde edilen sonuçların aynı mekanizma üzerinden değerlendirilmemesi gerekmektedir. Özellikle yağlama yağına eklenen bor katkılarının tork ve yakıt tüketimi üzerindeki etkileri, doğrudan yakıt katkısı olarak kullanılan bor bileşiklerinin yanma sürecine etkilerinden farklılık göstermektedir (Akbıyık ve ark., 2022; Karataş ve Yüksel, 2023).

Benzinli motorlarda bor esaslı yakıt katkılarının etkilerini inceleyen çalışmalardan biri Sertkaya ve Akbıyık (2016) tarafından gerçekleştirilmiştir. Araştırmada bor katkıları benzin içerisine farklı oranlarda ilave edilerek Lombardini LGW 523 benzinli motorda 1500–5000 d/d motor devri aralığında deneyler yapılmıştır. Motor gücü, tork, yakıt tüketimi, yakıt sıcaklığı ve egzoz emisyonlarının değerlendirildiği çalışma, bor esaslı katkıların kıvılcım

ateşlemeli motorlarda kullanım potansiyelini ortaya koymuştur. Yakın ve Gülcan (2025) ise hidrojen bakımından zengin bir bor bileşiği olan metilamin-boranın (MAB) benzinli motor performansı ve emisyonları üzerindeki etkilerini incelemiştir. Hacimsel %5 ve %10 oranlarında hazırlanan MAB karışımlarında CO ve HC emisyonlarında önemli azalmalar bildirilirken NOx emisyonlarında artış, özgül yakıt tüketiminde yükselme ve termal verimde düşüş gözlenmiştir. Bu sonuçlar, bor esaslı katkıların bazı egzoz emisyonlarını azaltmasına rağmen motor performansının bütün parametrelerinde iyileşme sağlamayabileceğini göstermektedir.

Sofuoğlu ve arkadaşları (2026), benzinli kıvılcım ateşlemeli bir motorda trimetil borat (TMB) ve trietil borat (TEB) bileşiklerini farklı karışım oranlarında incelemiştir. Deneyler 2800 d/d motor devrinde ve %75 ile %100 gaz kelebeği açıklıklarında gerçekleştirilmiştir. Çalışmada elde edilen bulgular, bor içeren organik bileşiklerin motor karakteristikleri üzerindeki etkilerinin yalnızca bor elementinin varlığıyla açıklanamayacağını; bileşiğin kimyasal yapısının ve yakıt içerisindeki oranının da önemli olduğunu ortaya koymaktadır. Çakmak ve Özcan (2022) ise bor oksit (B_2O_3) nanoparçacıklarını %20 kanola yağı biyodizeli içeren B20 yakıtına farklı konsantrasyonlarda ilave ederek dizel motor performansı, yanma ve emisyon özelliklerini değerlendirmiştir. Araştırmada 100 ppm bor oksit konsantrasyonunda özgül yakıt tüketiminde %1,66 azalma ve efektif verimde %0,96 artış bildirilmiştir. CO ve HC emisyonlarında azalma görülmesine karşılık NO ve is emisyonlarında artış belirlenmiştir. Ayrıca nanoparçacık kullanımının yakıt maliyetini önemli ölçüde artırdığı ifade edilmiştir.

Bor esaslı katkıların motor performansına etkileri yalnızca yakıt sistemleriyle sınırlı olmayıp yağlama yağı uygulamalarında da incelenmiştir. Akbıyık ve arkadaşları (2022), benzin ve doğal gazla çalışan kıvılcım ateşlemeli bir motorda bor katkılı yağ kullanımının motor performansı ve emisyonlar üzerindeki etkilerini araştırmıştır. Çalışmada özgül yakıt tüketiminde ve NOx emisyonlarında azalmalar bildirilirken CO ve HC emisyonlarında belirgin bir değişim gözlenmemiştir. Karataş ve Yüksel (2023) tarafından gerçekleştirilen diğer bir çalışmada ise tek silindirli dizel motorun mineral esaslı motor yağına sıvı bor katkısı ilave edilmiştir. Farklı motor devirlerinde yapılan deneylerde tork ve egzoz gazı sıcaklığında artış; özgül yakıt tüketimi, CO_2, HC ve NOx emisyonlarında ise azalma rapor edilmiştir. Bu çalışmalar, bor katkılarının yağlama özellikleri üzerinden motor performansını etkileyebileceğini göstermektedir. Bununla birlikte, elde edilen sonuçlar doğrudan yakıt içerisine eklenen bor katkılarının etkileriyle aynı kapsamda değerlendirilmemelidir.

Bor nanoparçacıklarının alternatif yakıt karışımlarında kullanımı da araştırılan konular arasındadır. Gotewala ve arkadaşları (2026), dizel, deiyonize su ve emülgatörden oluşan su-dizel emülsiyonuna farklı konsantrasyonlarda bor nanoparçacıkları ilave ederek tek silindirli dizel motorda performans ve emisyon deneyleri gerçekleştirmiştir. Çalışmada bor içeren emülsiyonların motor karakteristikleri üzerindeki etkileri değerlendirilmiş ve 150 ppm bor nanoparçacığı içeren karışımda NO emisyonunda azalma ve net dizel tüketiminde iyileşme bildirilmiştir. Bununla birlikte, su-dizel emülsiyonlarının fiziksel ve kimyasal özellikleri

geleneksel yakıtlardan farklı olduğundan, bu sonuçların doğrudan benzin veya dizel yakıtına eklenen katkılara genellenmesi uygun değildir.

Literatürdeki çalışmalar genel olarak değerlendirildiğinde, bor esaslı bileşiklerin içten yanmalı motorlarda performans ve egzoz emisyonları üzerinde etkili olabildiği görülmektedir. Ancak bu etkilerin yönü ve büyüklüğü kullanılan bor bileşiğinin türüne, katkı miktarına, yakıt özelliklerine ve motor çalışma koşullarına bağlı olarak değişmektedir. Bazı çalışmalarda özgül yakıt tüketimi ve CO ile HC emisyonlarında azalma bildirilirken, NOx ve is emisyonlarında artışlar da gözlenmiştir. Bu durum, bor esaslı katkıların değerlendirilmesinde motor performansı ve emisyon parametrelerinin birlikte ele alınmasının önemini ortaya koymaktadır.

Mevcut literatürde farklı bor bileşiklerinin ve ticari katkı ürünlerinin aynı motor, yakıt ve çalışma koşulları altında doğrudan karşılaştırıldığı çalışmaların sınırlı olduğu görülmektedir. Özellikle ticari olarak temin edilebilen farklı bor esaslı yakıt katkılarının değişen konsantrasyonlarda benzinli motor performansı üzerindeki etkilerinin karşılaştırmalı olarak incelenmesine ihtiyaç bulunmaktadır. Bu kapsamda, katkı miktarının motor devrine bağlı tork ve yakıt tüketimi değişimleri üzerindeki etkilerinin belirlenmesi, bor esaslı katkıların kullanım potansiyelinin değerlendirilmesine katkı sağlayabilir.

Bu çalışmanın amacı, iki farklı yakıta bor esaslı yakıt katkısının motor performansı ve emisyonlar üzerindeki etkilerini deneysel olarak karşılaştırmaktır. Bu amaçla, iki silindirli Lombardini LGW 523 MPI benzinli motorda katkısız benzin ve E20 yakıtı referans yakıt olarak kullanılmış;, yakıtın litresine 7, 14 ve 21 oranlarında ilave edilmiştir. Deneyler tam gaz koşulunda 1500–5000 d/d motor devri aralığında gerçekleştirilmiş; motor torku, fren özgül yakıt tüketimi ve hesaplanan termal verim parametreleri ve emisyon değerleri değerlendirilmiştir. Böylece farklı yakıtlardaki bor katkısı konsantrasyonlarının motor performansı ve emisyonlar üzerindeki etkilerinin aynı deney düzeneğinde karşılaştırılması amaçlanmıştır.

2. MATERYAL METOD

2.1. DENEY TEST DÜZENEGİ

Tablo 1'de özellikleri verilen Lombardini LGW 523 MPI 2-silindir benzinli motor özellikleri verilen motorda üzerinde deneysel çalışmalar yapılmıştır. Deneysel motorda piyasadaki benzin istasyonlarından temin edilen benzin yakıtı ve biyoetanol benzin karışımı kullanılarak çalıştırılmıştır.

Yakıtlara litre başı 0, 7, 14 cc yakıt bor katkısı ilave edilmiştir. Motorda 1500, 2000, 2500, 3000, 3500, 4000, 4500 ve 5000 devirlerde performans ve emisyon deneyleri yapılmıştır. Motor her bir devirde 5 dakika çalıştırılmış ve bu değerlerin ortalaması alınmıştır. Motor deneyleri 3 kez tekrarlanmış ve elde edilen verilerin ortalaması alınmıştır.

2.2. DENEY METOROLOJİSİ

Baz ve bor ilaveli yapılan deneysel çalışmalar, birbirini takip eden süreçler şeklinde gerçekleştirilmiştir. Tüm deneyler boyunca ortam sıcaklığı yaklaşık 23 °C olarak ölçülmüştür. Deneylerde motor ısındıktan sonra motor performans deneyleri tam gaz durumunda 1500,

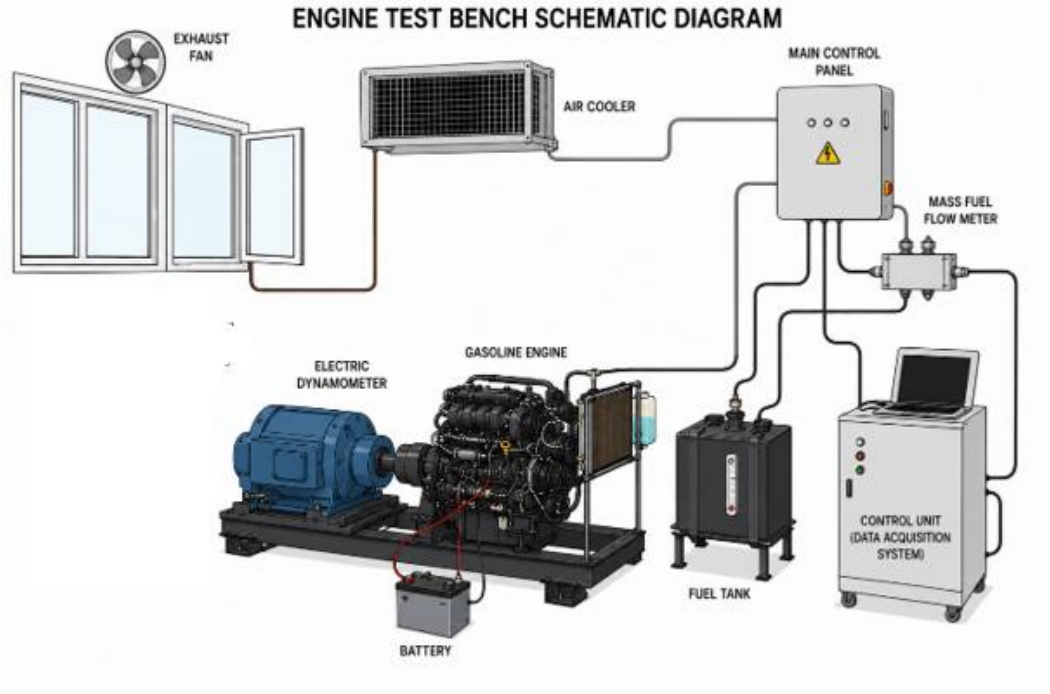
2000, 2500, 3000, 3500, 4000, 4500 ve 5000 devire yüklenerek yapılmıştır. Başlangıçta motor katkısız yakıt ile çalıştırılıp deneyler yapılmış bu değerler baz deger olarak kabul edilmiştir sonra yakıta sırasıyla litre başına 7, 14, 21 cc bor yakıt katkısı ilave edilmiş deneyler yapılmıştır. 2 farklı yakıt ile yapılan deney sonuçları karşılaştırılmıştır.

Table 1. Lombardini LGW 523 engine features [Akbıyık ve ark. 2022]

Motor özelliği	**Birim**	**Değer**
Silindir sayısı	adet	2
Silindir çapı	mm	72
Strok	mm	62
Motor hacmi	cc	505
Sıkıştırma oranı	-	10,7:1
Maksimum motor devri	d/d	5500
Maksimum güç	kW	15
Maksimum tork	Nm	34
Motor ağırlığı	kg	52



Şekil 1. Deney düzeneği

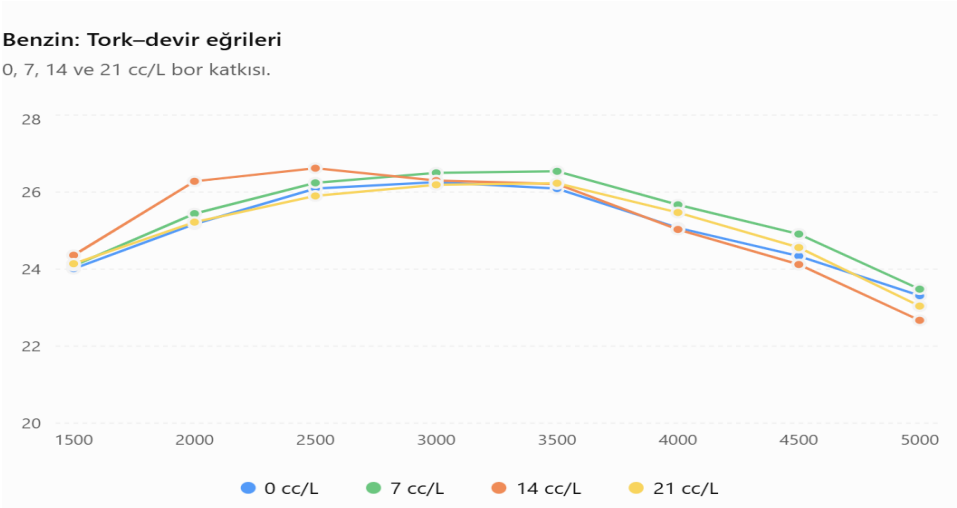


Şekil 2. Deney düzeneği şematik gösterimi.

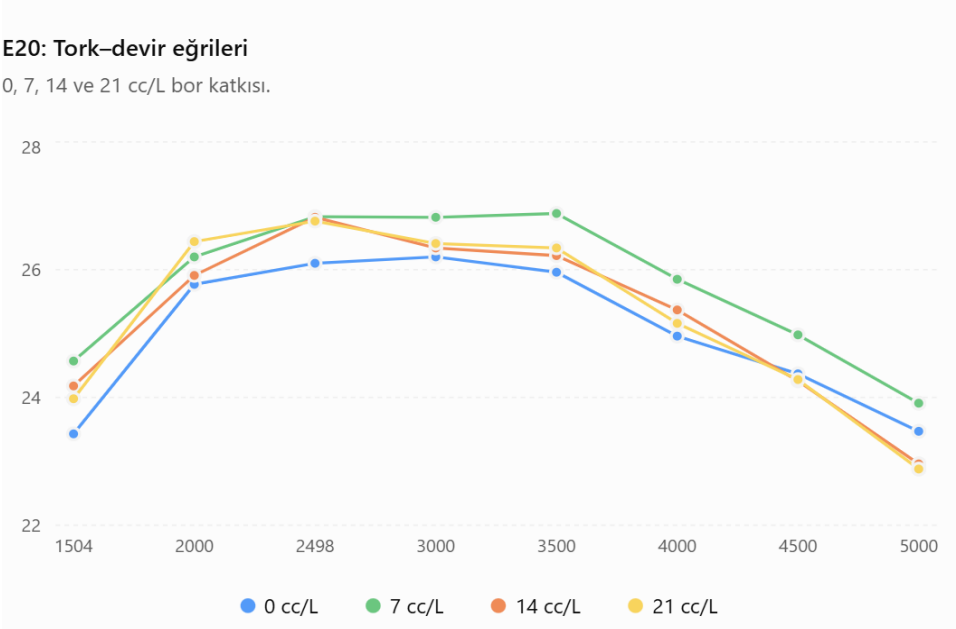
3. DENEY SONUÇLARI

Bu çalışmada, motorda kullanılan iki farklı yakıta farklı oranlarda bor yakıt katkısı katılmıştır. Bor katkılarının karşılaştırması ve en iyi oran oranının belirlenmesi sağlanmıştır. Motorda yapılan karşılaştırma temel performans parametreleri arasında güç, tork, termal verimlilik ve fren özgül yakıt tüketimi (bsfc) ve emisyonlardır. Motor tam yük durumunda 8 farklı motor devrinde (1500, 2000, 2500, 3000, 3500, 4000, 4500 ve 5000) yüklenmiştir. Yakıt olarak ilk çalışma katkısız benzin ile yapılmış ve referans yakıt olarak ele alınmıştır. Sonraki çalışmalar yakıta litre başına 7,4,21 cc yakıt bor katkısı ilave edilerek yapılmıştır. Motor performans ve emisyon değerleri belirlenmiş ve bunların karşılaştırması yapılmıştır.

3.1. Motor Torku



Şekil 3. Benzin yakıtı kullanımında farklı bor katkı oranlarının devire bağlı tork değişimi



Şekil 4. E20 yakıtı kullanımında farklı bor katkı oranlarının devire bağlı tork değişimi

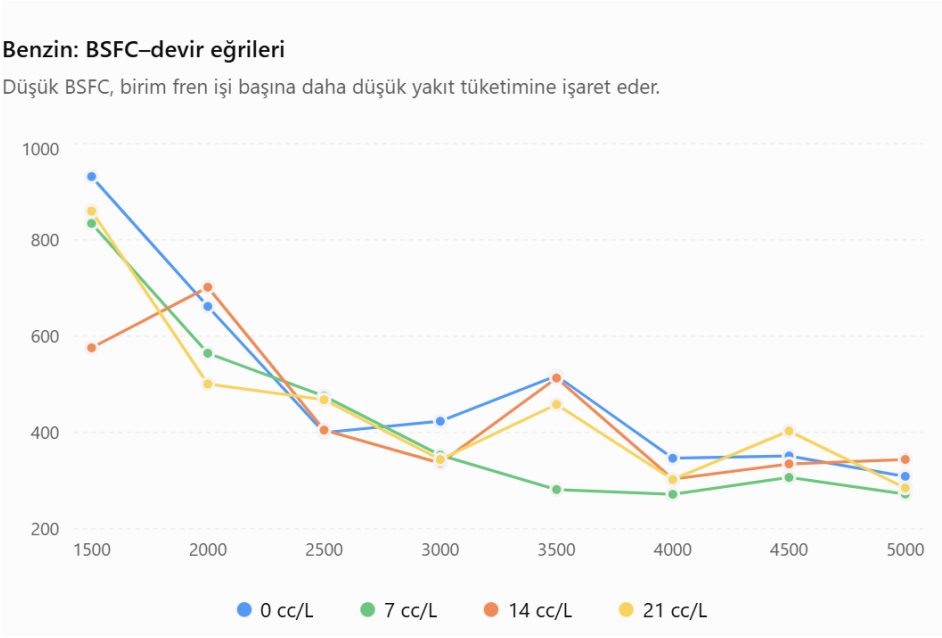
Benzin yakıtında bor katkısının etkisi: Katkısız benzin kullanımında ortalama motor momenti 25,04 Nm olarak belirlenmiştir. Benzine 7 cc/L bor katkısı eklenmesiyle moment 25,36 Nm'ye yükselmiş ve yaklaşık %1,26 artış sağlanmıştır. Katkı miktarının 14 cc/L'ye çıkarılması durumunda ortalama moment 25,20 Nm (%0,62 artış), 21 cc/L seviyesinde ise 25,09 Nm (%0,20 artış) olarak hesaplanmıştır. Bu sonuçlar, benzin yakıtında bor katkısının motor momentine olumlu etkisinin özellikle 7 cc/L seviyesinde ortaya çıktığını, katkı miktarının artırılmasının ise aynı oranda ilave bir performans kazancı sağlamadığını göstermektedir. Dolayısıyla benzin için moment açısından en uygun katkı oranı 7 cc/L olarak değerlendirilebilir.

E20 yakıtında bor katkısının etkisi: Katkısız E20 yakıtında ortalama moment 25,03 Nm iken 7 cc/L bor katkısıyla 25,76 Nm'ye yükselmiştir. Bu değer, katkısız E20'ye göre %2,89 artışa karşılık gelmektedir. Katkı miktarının 14 cc/L'ye çıkarılmasıyla moment 25,26 Nm'ye, 21 cc/L'de ise 25,28 Nm'ye gerilemiştir. Buna göre E20 yakıtında da en yüksek moment 7 cc/L katkı seviyesinde elde edilmiştir. E20+7 yakıtının katkısız E20'ye göre daha yüksek moment üretmesi, bu katkı seviyesinde yakıtın yanma ve enerji dönüşüm süreçlerinde olumlu bir değişim meydana gelmiş olabileceğini düşündürmektedir. Ancak yanma basıncı ve ısı salım hızı ölçümleri bulunmadığından bu durum doğrudan yanma iyileşmesi olarak kesinleştirilemez.

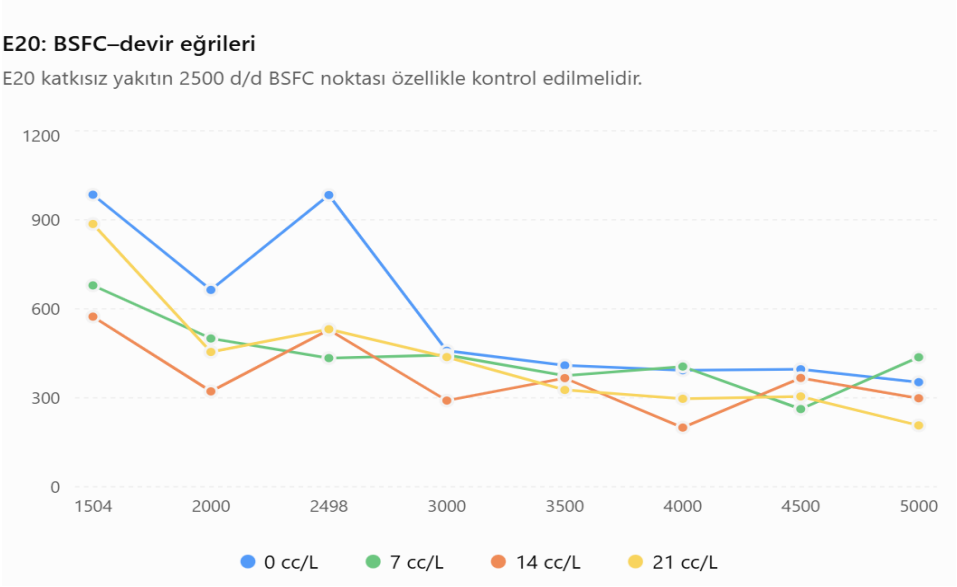
Aynı katkı oranında benzin–E20 karşılaştırması: Katkısız yakıtlarda benzin ve E20'nin moment değerleri birbirine oldukça yakındır. E20'nin momenti benzine göre yalnızca %0,04 daha düşüktür. 7 cc/L katkı seviyesinde E20, benzinden %1,56 daha yüksek moment üretmiştir. 14 ve 21 cc/L katkı seviyelerinde de E20'nin momenti sırasıyla %0,23 ve %0,75 daha yüksektir. Bununla birlikte iki yakıt arasındaki farkların genel olarak sınırlı olduğu görülmektedir. E20'nin özellikle 7 cc/L katkı seviyesinde daha yüksek moment üretmesi, etanolün oksijen içeriği ve yakıtın fiziksel-kimyasal özellikleri ile bor katkısının birlikte

etkisinden kaynaklanmış olabilir. Masum ve arkadaşları (2014), E20 kullanımının benzinli motorlarda performans ve emisyon parametrelerini değiştirdiğini ve bu değişimin yakıt türüne bağlı olduğunu bildirmiştir.

3.2. Özgül yakıt tüketimi (BSFC)



Şekil 5. Benzin yakıtı kullanımında farklı bor katkı oranlarının devire bağlı bsfc değişimi



Şekil 6. E20 yakıtı kullanımında farklı bor katkı oranlarının devire bağlı bsfc değişimi

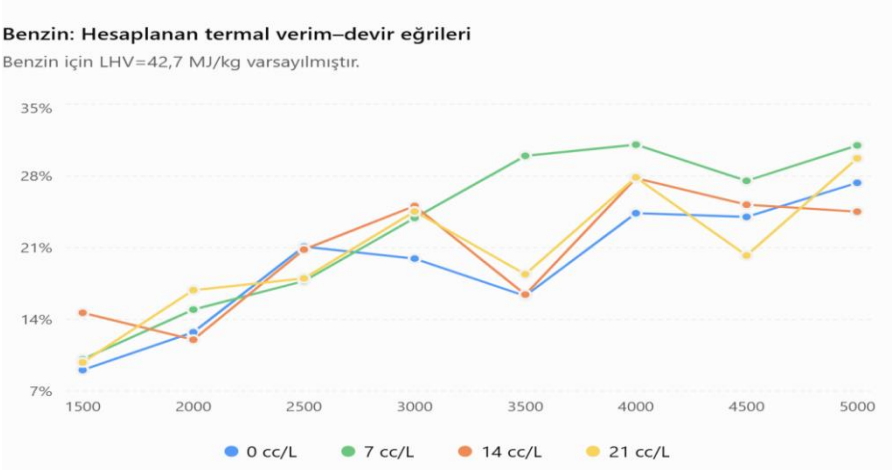
Benzin yakıtında bor katkısının etkisi: Katkısız benzin için ortalama özgül yakıt tüketimi 492,48 g/kWh olarak hesaplanmıştır. 7 cc/L bor katkısı ile bu değer 419,78 g/kWh'ye düşmüş ve %14,76 azalmıştır. 14 cc/L katkı seviyesinde BSFC 439,14 g/kWh (%10,83 azalma), 21 cc/L seviyesinde ise 452,50 g/kWh (%8,12 azalma) olarak belirlenmiştir. Üç katkı seviyesi de katkısız benzine kıyasla özgül yakıt tüketimini azaltmıştır. Ancak en belirgin iyileşme 7 cc/L

katkı oranında gerçekleşmiştir. Katkı miktarının artırılmasıyla BSFC değerinin yeniden yükselmesi, bor katkısının yakıt tüketimi üzerindeki etkisinin doğrusal olmadığını göstermektedir. Bu durum, katkı oranının yakıtın yanma karakteristikleri ve enerji içeriğiyle birlikte değerlendirilmesi gerektiğine işaret etmektedir.

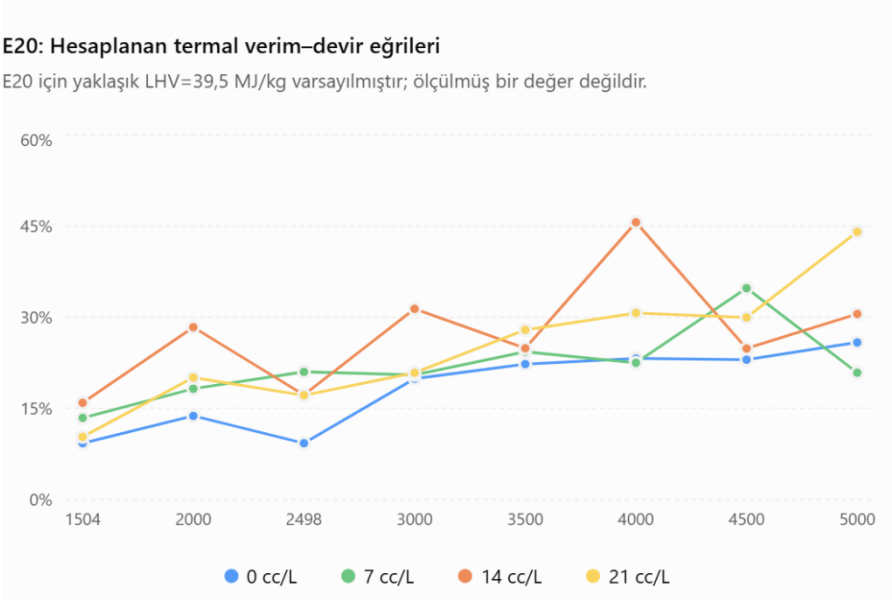
E20 yakıtında bor katkısının etkisi: Katkısız E20 yakıtında BSFC 580,18 g/kWh olarak belirlenmiştir. Bu değer, katkısız benzinin 492,48 g/kWh değerinden %17,81 daha yüksektir. E20 yakıtına 7 cc/L bor katkısı eklenmesiyle BSFC 442,01 g/kWh'ye düşmüş ve katkısız E20'ye göre %23,81 azalma sağlanmıştır. 14 cc/L katkı seviyesinde BSFC 368,35 g/kWh'ye gerileyerek %36,51 azalmış ve bütün yakıt grupları içerisinde en düşük ortalama BSFC değeri elde edilmiştir. 21 cc/L katkı seviyesinde ise BSFC 430,49 g/kWh olarak belirlenmiş ve katkısız E20'ye göre %25,80 azalma gerçekleşmiştir. Bu sonuçlar, E20 yakıtında bor katkısının BSFC üzerinde belirgin bir iyileşme sağladığını, en etkili seviyenin ise 14 cc/L olduğunu göstermektedir. Özellikle E20+14 yakıtının katkısız E20'ye göre sağladığı yüksek azalma, bu karışımın yakıt tüketimi bakımından öne çıktığını ortaya koymaktadır.

Aynı katkı oranında benzin–E20 karşılaştırması: Katkısız durumda E20'nin BSFC değeri benzinden %17,81 daha yüksektir. Bu durum, etanol içeren yakıtların daha düşük alt ısıl değeri nedeniyle aynı faydalı işi üretmek için daha fazla yakıt tüketebilmesiyle ilişkilendirilebilir. 7 cc/L katkı seviyesinde E20'nin BSFC değeri benzinden %5,30 daha yüksektir. Buna karşılık 14 cc/L katkı seviyesinde E20, benzine göre %16,12 daha düşük BSFC değerine ulaşmıştır. 21 cc/L seviyesinde de E20'nin BSFC değeri benzinden %4,86 daha düşüktür. Dolayısıyla bor katkısının özellikle 14 cc/L seviyesinde E20'nin yakıt tüketimi performansını belirgin şekilde iyileştirdiği görülmektedir. Bununla birlikte, benzin ve E20'nin alt ısıl değerleri farklı olduğundan BSFC karşılaştırması tek başına enerji dönüşüm verimliliğini açıklamak için yeterli değildir. Etanol-benzin karışımlarında düşük alt ısıl değer nedeniyle BSFC'nin artabileceği literatürde de belirtilmiştir (Masum vd., 2014; Comprehensive Efficiency Analysis, 2025).

3.3. Termik verim



Şekil 7. Benzin yakıtı kullanımında farklı bor katkı oranlarının devire bağlı termal verim değişimi



Şekil 8. E20 yakıtı kullanımında farklı bor katkı oranlarının devire bağlı termal verim değişimi

Termik verim değerleri, mevcut hesaplamada tüm yakıtlar için 42,7 MJ/kg alt ısıl değer kabul edilerek BSFC üzerinden hesaplanmıştır. Bu nedenle özellikle benzin ve E20 arasındaki karşılaştırmalar, yakıtların gerçek alt ısıl değerleri dikkate alınarak yeniden değerlendirilmelidir.

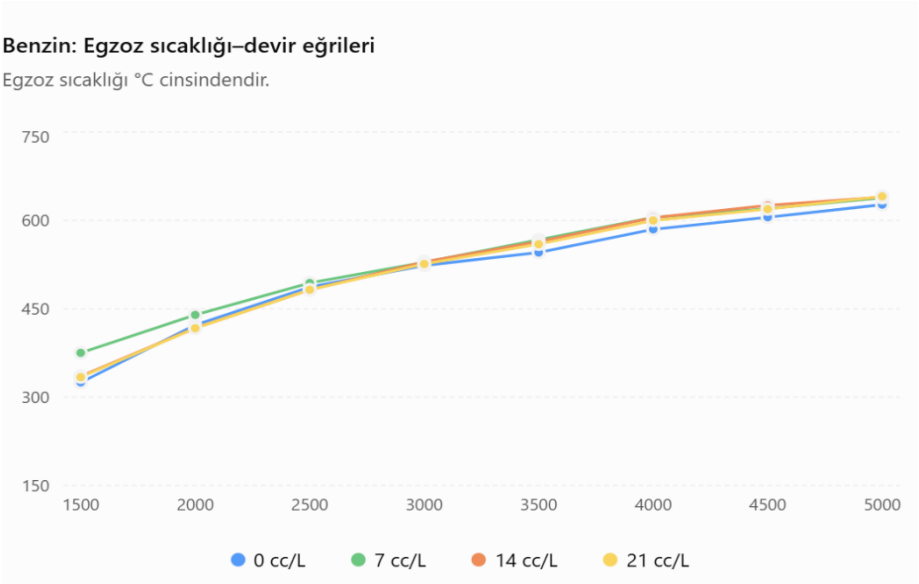
Benzin yakıtında bor katkısının etkisi: Katkısız benzin için ortalama termik verim %19,35 olarak hesaplanmıştır. 7 cc/L bor katkısı ile termik verim %23,28'e yükselmiş ve yaklaşık %20,32 artış sağlanmıştır. 14 cc/L katkı seviyesinde termik verim %20,81, 21 cc/L seviyesinde ise %20,75 olarak belirlenmiştir. Bu sonuçlar, benzin yakıtında 7 cc/L katkının termik verim bakımından en iyi sonucu verdiğini göstermektedir. 14 ve 21 cc/L katkı seviyelerinde de katkısız benzine göre iyileşme görülmekle birlikte, 7 cc/L seviyesindeki artışa ulaşılamamıştır. Bu durum, katkı miktarının artırılmasının termik verim üzerinde sürekli ve doğrusal bir iyileşme oluşturmadığını göstermektedir.

E20 yakıtında bor katkısının etkisi: Katkısız E20 için hesaplanan ortalama termik verim %16,93'tür. 7 cc/L bor katkısıyla bu değer %20,31'e yükselmiş ve %19,92 artış sağlamıştır. 14 cc/L katkı seviyesinde termik verim %25,29'a ulaşarak katkısız E20'ye göre %49,34 artmıştır. 21 cc/L seviyesinde ise termik verim %23,23 olarak hesaplanmış ve %37,20 iyileşme elde edilmiştir. E20 yakıtında en yüksek termik verimin 14 cc/L katkı seviyesinde elde edilmesi, BSFC sonuçlarıyla da uyumludur. Çünkü aynı alt ısıl değer varsayımı altında BSFC'nin azalması termik verimin yükselmesine neden olmaktadır.

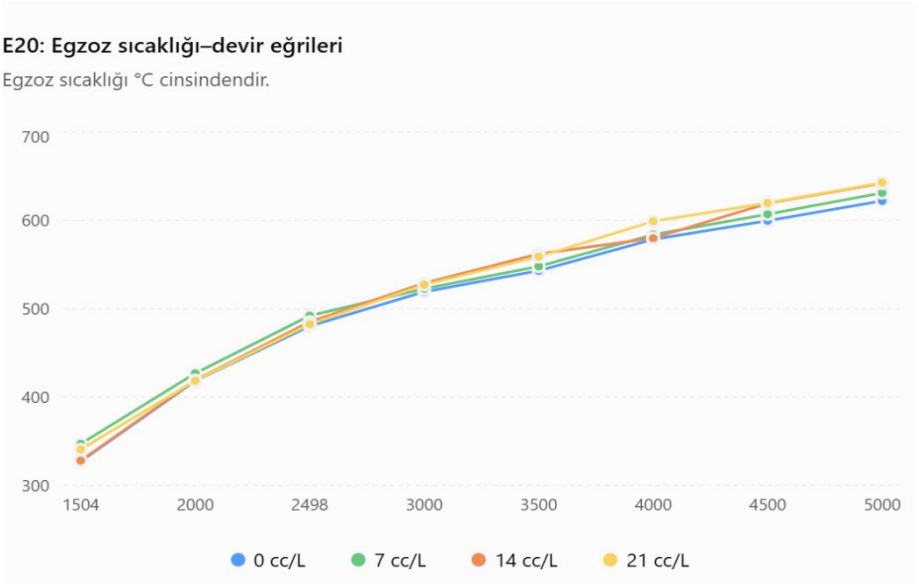
Aynı katkı oranında benzin–E20 karşılaştırması: Katkısız durumda E20'nin hesaplanan termik verimi benzinden %12,47 daha düşüktür. 7 cc/L katkı seviyesinde de E20'nin termik verimi benzinden %12,76 daha düşük bulunmuştur. Buna karşılık 14 cc/L seviyesinde E20'nin hesaplanan termik verimi benzinden %21,49, 21 cc/L seviyesinde ise %11,94 daha yüksektir. Bu sonuçlar, özellikle E20+14 karışımının termik verim bakımından öne çıktığını

göstermektedir. Ancak bu karşılaştırmada bütün yakıtlara aynı alt ısıl değerin atanmış olması önemli bir metodolojik sınırlamadır. E20'nin gerçek alt ısıl değeri benzinden daha düşük olduğundan, termik verim hesaplamalarında her yakıt karışımının kendi alt ısıl değerinin kullanılması gerekir. Bu nedenle burada verilen termik verim sonuçları ön değerlendirme niteliğindedir. Etanol-gasoline karışımlarında alt ısıl değer ve buharlaşma ısısının motor verimi üzerindeki etkisi literatürde de vurgulanmaktadır

3.4. Egzoz gazı sıcaklığı



Şekil 9. Benzin yakıtı kullanımında farklı bor katkı oranlarının devire bağlı eksoz gazı sıcaklığı değişimi



Şekil 10. E20 yakıtı kullanımında farklı bor katkı oranlarının devire bağlı eksoz gazı sıcaklığı değişimi

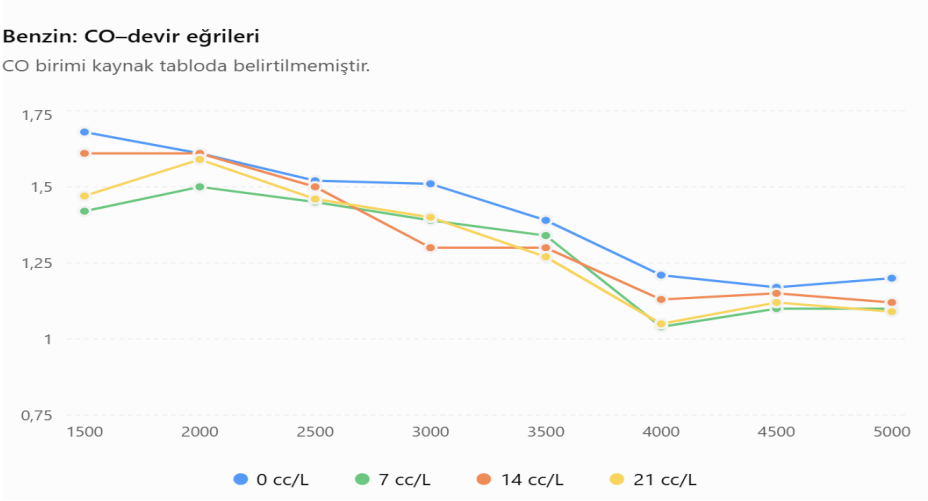
Benzin yakıtında bor katkısının etkisi: Katkısız benzin kullanımında ortalama egzoz sıcaklığı 514,87 °C olarak ölçülmüştür. 7 cc/L bor katkısıyla egzoz sıcaklığı 533,32 °C'ye yükselmiş ve %3,58 artmıştır. 14 cc/L katkı seviyesinde sıcaklık 524,71 °C (%1,91 artış), 21 cc/L

seviyesinde ise 522,20 °C (%1,42 artış) olarak belirlenmiştir. Bütün katkı seviyelerinde egzoz sıcaklığının katkısız benzine göre yükselmesi, bor katkısının yanma ve egzoz gazı sıcaklıkları üzerinde etkili olduğunu göstermektedir. Bununla birlikte en yüksek sıcaklığın 7 cc/L seviyesinde elde edilmesi, katkı oranı arttıkça egzoz sıcaklığının sürekli yükselmediğini ortaya koymaktadır. Egzoz sıcaklığındaki artış, yanma sürecinde açığa çıkan enerjinin egzoz gazlarına taşınan bölümünün artmasıyla ilişkili olabilir; ancak tek başına yanma verimindeki artışın göstergesi olarak değerlendirilmemelidir.

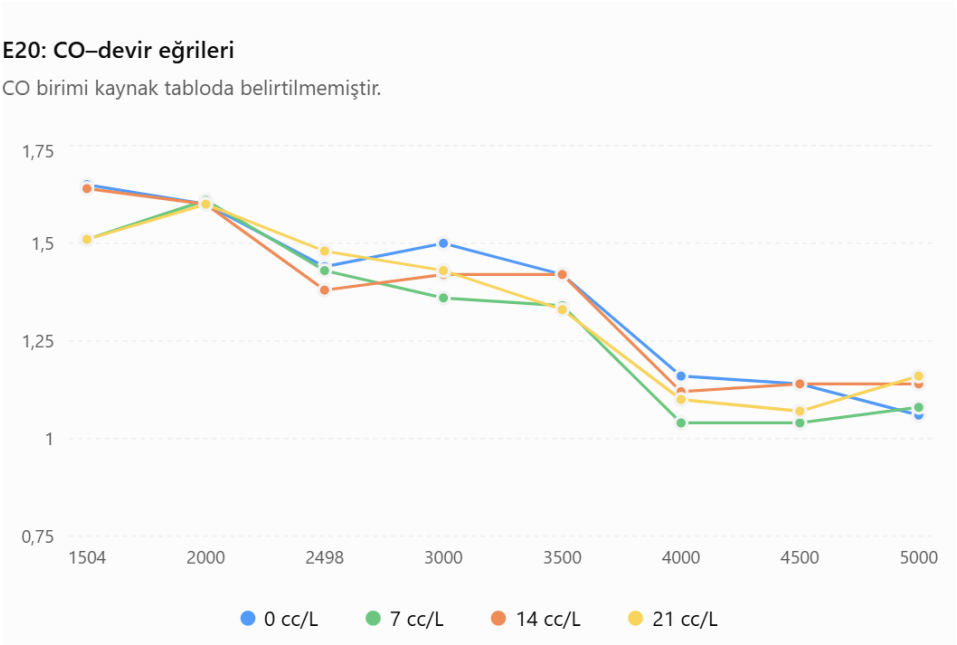
E20 yakıtında bor katkısının etkisi: Katkısız E20 için ortalama egzoz sıcaklığı 511,00 °C olarak belirlenmiştir. 7 cc/L katkı ile sıcaklık 519,79 °C'ye, 14 cc/L katkı ile 520,51 °C'ye ve 21 cc/L katkı ile 523,64 °C'ye yükselmiştir. Bu değerler sırasıyla %1,72, %1,86 ve %2,47 artışa karşılık gelmektedir. E20 yakıtında katkı miktarı yükseldikçe egzoz sıcaklığında kademeli bir artış eğilimi görülmektedir. Bu eğilim, benzin yakıtındaki değişimden farklıdır. Benzinde en yüksek egzoz sıcaklığı 7 cc/L seviyesinde elde edilirken E20'de en yüksek değer 21 cc/L seviyesinde ölçülmüştür. Bu farklılık, etanol içeriğinin yakıtın buharlaşma ve yanma özelliklerini değiştirmesiyle ilişkili olabilir.

Aynı katkı oranında benzin–E20 karşılaştırması: Katkısız E20'nin egzoz sıcaklığı benzinden %0,75 daha düşüktür. 7 ve 14 cc/L katkı seviyelerinde E20'nin egzoz sıcaklıkları benzinden sırasıyla %2,54 ve %0,80 daha düşük bulunmuştur. 21 cc/L seviyesinde ise E20'nin egzoz sıcaklığı benzinden %0,28 daha yüksektir. Dolayısıyla iki yakıtın egzoz sıcaklıkları genel olarak birbirine yakındır. Bor katkısının egzoz sıcaklığı üzerindeki etkisi, yakıt türüne ve katkı oranına bağlı olarak değişmektedir. Yakın tarihli bir çalışmada bor içeren yakıt katkılarının egzoz sıcaklığını düşürebildiği, ancak bu etkinin kullanılan bor bileşiğine ve karışım oranına bağlı olduğu bildirilmiştir (Yakın ve Gülcan, 2025). Bu nedenle farklı kimyasal yapıya sahip bor katkılarından elde edilen sonuçların doğrudan aynı yönde olması beklenmemelidir.

3.5. Karbonmonoksit (CO) emisyonu



Şekil 11. Benzin yakıtı kullanımında farklı bor katkı oranlarının devire bağlı CO değişimi



Şekil 12. E20 yakıtı kullanımında farklı bor katkı oranlarının devire bağlı CO değişimi

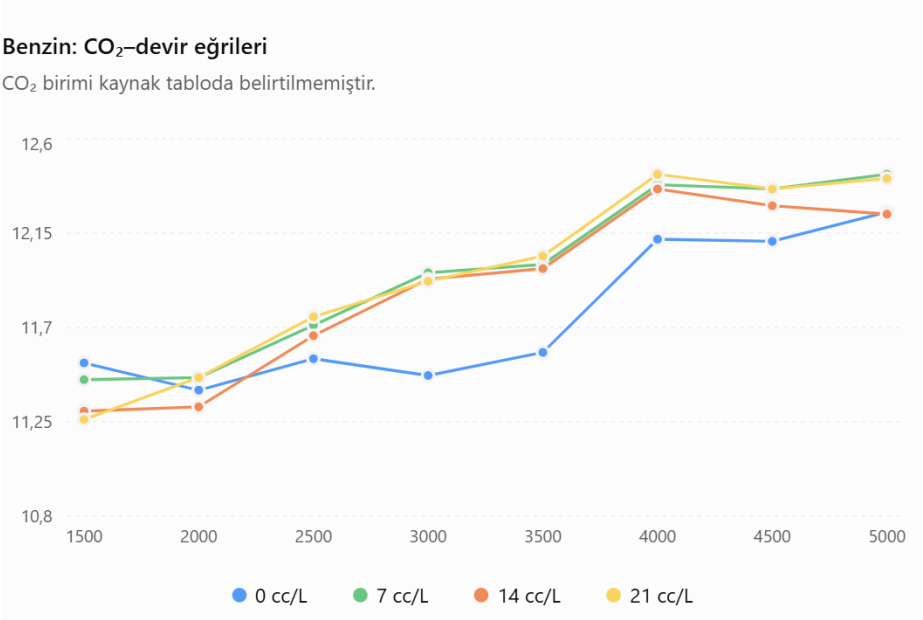
Benzin yakıtında bor katkısının etkisi: Katkısız benzin için ortalama CO emisyonu %1,411 olarak belirlenmiştir. 7 cc/L bor katkısı ile CO emisyonu %1,293'e düşmüş ve %8,41 azalma sağlanmıştır. 14 cc/L katkı seviyesinde CO %1,340 (%5,05 azalma), 21 cc/L seviyesinde ise %1,306 (%7,44 azalma) olarak ölçülmüştür. Bu sonuçlar, bor katkısının benzin yakıtında CO emisyonlarını bütün katkı seviyelerinde azalttığını göstermektedir. En yüksek azalma 7 cc/L seviyesinde elde edilmiştir. CO oluşumu, yakıt içerisindeki karbonun tam olarak CO_2'ye oksitlenememesiyle ilişkilidir. Dolayısıyla CO emisyonundaki azalma, karbon içeren yakıt bileşenlerinin daha ileri oksidasyona uğramasıyla açıklanabilir. Bununla birlikte hava-yakıt oranı, karışım oluşumu ve yanma sıcaklığı gibi faktörler de CO oluşumunu etkiler.

E20 yakıtında bor katkısının etkisi: Katkısız E20 yakıtında ortalama CO emisyonu %1,371 olarak ölçülmüştür. 7 cc/L katkı ile bu değer %1,301'e düşmüş ve %5,10 azalma sağlanmıştır. 14 cc/L katkı seviyesinde CO %1,358 (%1,00 azalma), 21 cc/L seviyesinde ise %1,335 (%2,64 azalma) olarak belirlenmiştir. E20 yakıtında da bütün katkı seviyelerinde CO emisyonu katkısız yakıta göre azalmıştır. Ancak azalma miktarı benzin yakıtındaki kadar belirgin değildir. E20'de en yüksek CO azalmasının 7 cc/L seviyesinde gerçekleşmesi, düşük katkı oranının CO emisyonu açısından daha etkili olduğunu göstermektedir. Etanolün molekül yapısında oksijen bulunması, yanma bölgesinde oksijen mevcudiyetini artırarak CO oluşumunu etkileyebilir. Bununla birlikte mevcut sonuçlarda E20'nin katkısız durumda benzine göre daha düşük CO üretmemesi, emisyon davranışının yalnızca yakıtın oksijen içeriğiyle açıklanamayacağını göstermektedir.

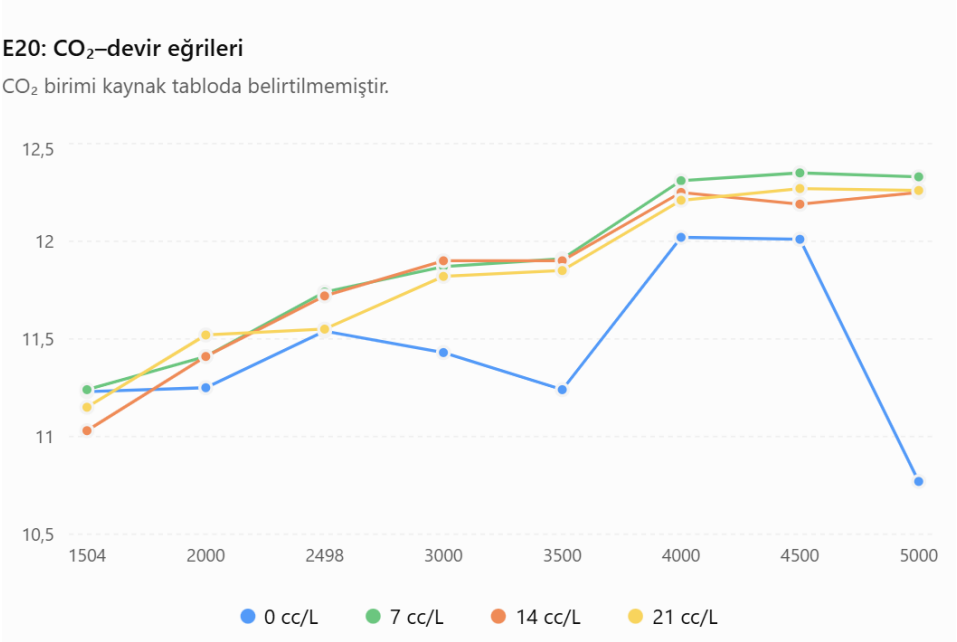
Aynı katkı oranında benzin–E20 karşılaştırması: Katkısız E20'nin CO emisyonu benzine göre %2,83 daha düşüktür. Ancak 7 cc/L seviyesinde E20'nin CO emisyonu benzinden %0,68, 14 cc/L seviyesinde %1,31 ve 21 cc/L seviyesinde %2,20 daha yüksektir. Bu nedenle katkısız durumda E20 küçük bir avantaj gösterirken bor katkılı karışımlarda benzin daha düşük CO

emisyonu üretmiştir. Bu bulgu, bor katkısının CO emisyonu üzerindeki etkisinin etanol içeriğine bağlı olarak değişebildiğini göstermektedir. Sertkaya ve Akbıyık (2016), Lombardini LGW 523 benzinli motorunda bor katkılı yakıtların performans ve egzoz emisyonları üzerindeki etkilerini incelemiş; bor katkısının motorun emisyon karakteristiklerinde değişime yol açtığını ortaya koymuştur. Daha yakın tarihli bir çalışmada ise farklı bor bazlı oksijenli bileşiklerin CO emisyonunu azaltabildiği, ancak bu iyileşmenin motor performansı ve yakıt tüketimi bakımından bazı ödünleşmelerle birlikte görülebildiği bildirilmiştir (Sofuoglu vd., 2026).

3.6. Karbondioksit (CO_2) emisyonu



Şekil 13.Benzin yakıtı kullanımında farklı bor katkı oranlarının devire bağlı CO_2 değişimi



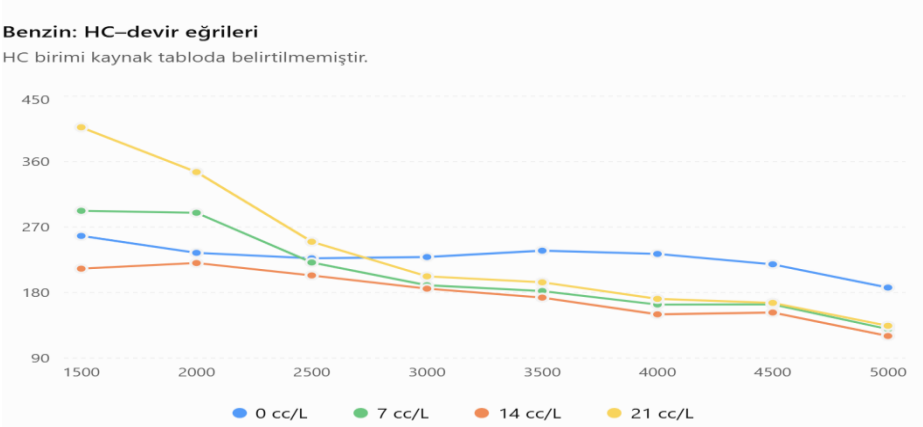
Şekil 14. E20 yakıtı kullanımında farklı bor katkı oranlarının devire bağlı CO_2 değişimi

Benzin yakıtında bor katkısının etkisi: Katkısız benzin için ortalama CO_2 emisyonu %11,751 olarak belirlenmiştir. 7 cc/L bor katkısıyla bu değer %11,969'a yükselmiş ve %1,85 artmıştır. 14 cc/L katkı seviyesinde CO_2 %11,884 (%1,13 artış), 21 cc/L seviyesinde ise %11,954 (%1,72 artış) olarak ölçülmüştür. CO_2 emisyonundaki artış, CO emisyonundaki azalmayla birlikte değerlendirildiğinde yakıt içerisindeki karbonun daha ileri oksidasyona uğramış olabileceğini düşündürmektedir. Başka bir ifadeyle, CO oluşumunun azalmasıyla karbonun daha büyük bölümünün CO_2 formunda egzozdan atılması mümkün olabilir. Ancak CO_2 emisyonundaki artış, tek başına yakıt ekonomisinin veya toplam çevresel performansın kötüleştiğini göstermez; yakıt tüketimi ve yakıtın karbon içeriği de dikkate alınmalıdır.

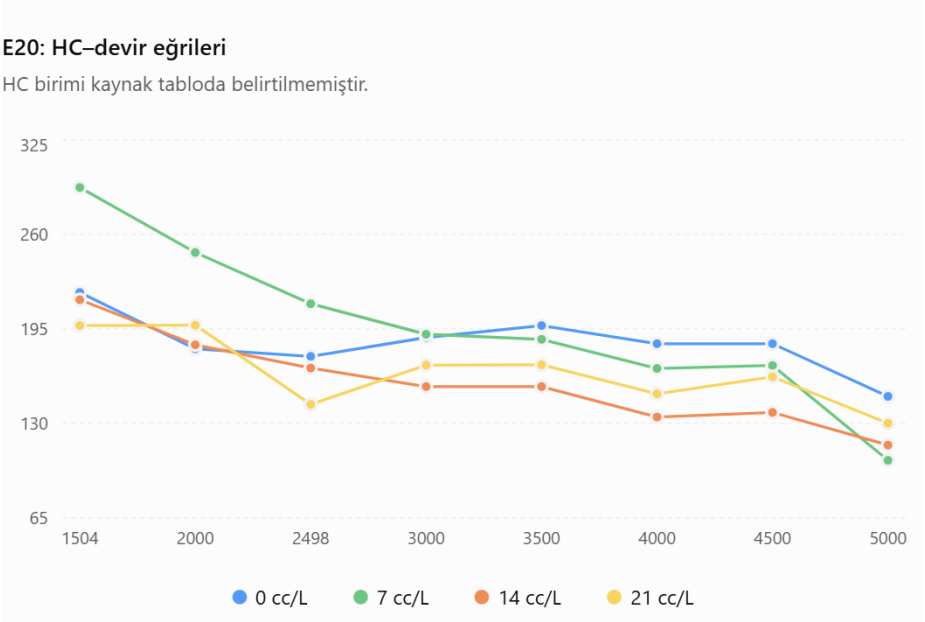
E20 yakıtında bor katkısının etkisi: Katkısız E20 için ortalama CO_2 emisyonu %11,436 olarak belirlenmiştir. 7 cc/L katkı ile %11,895'e yükselmiş ve %4,01 artış göstermiştir. 14 cc/L katkı seviyesinde CO_2 %11,831 (%3,45 artış), 21 cc/L seviyesinde ise %11,829 (%3,43 artış) olarak hesaplanmıştır. E20 yakıtında bor katkısı bütün seviyelerde CO_2 emisyonunu artırmıştır. En yüksek artış 7 cc/L katkı seviyesinde elde edilmiştir. CO_2 artışının CO emisyonundaki azalmayla birlikte görülmesi, karbonlu bileşenlerin oksidasyon derecesindeki değişimle ilişkili olabilir. Bununla birlikte CO_2 emisyonu, egzoz gazındaki konsantrasyon olarak ölçüldüğünden, kütlesel emisyon veya birim faydalı enerji başına karbon salımı ile aynı anlama gelmemektedir.

Aynı katkı oranında benzin–E20 karşılaştırması: Katkısız E20'nin CO_2 emisyonu benzinden %2,68 daha düşüktür. 7, 14 ve 21 cc/L katkı seviyelerinde de E20'nin CO_2 değerleri benzinden sırasıyla %0,62, %0,44 ve %1,05 daha düşük bulunmuştur. Bu sonuçlar, incelenen bütün eşleştirilmiş katkı seviyelerinde E20'nin daha düşük CO_2 konsantrasyonu verdiğini göstermektedir. Bununla birlikte CO_2 konsantrasyonunun düşük olması, doğrudan daha düşük karbon salımı anlamına gelmez. Yakıt tüketimi, yakıtın karbon içeriği ve egzoz debisi birlikte değerlendirilerek g/kWh cinsinden özgül CO_2 emisyonu hesaplanmalıdır. Masum ve arkadaşları (2014), etanol-benzin karışımlarının CO ve HC emisyonlarını azaltabildiğini, ancak CO_2 emisyonunun yakıt bileşimine ve çalışma koşullarına bağlı olarak değişebildiğini bildirmiştir.

3.7. Hidrokarbon (HC) emisyonu



Şekil 15. Benzin yakıtı kullanımında farklı bor katkı oranlarının devire bağlı HC değişimi



Şekil 16. E20 yakıtı kullanımında farklı bor katkı oranlarının devire bağlı HC değişimi

Benzin yakıtında bor katkısının etkisi: Katkısız benzin için ortalama HC emisyonu 228 ppm olarak belirlenmiştir. 7 cc/L bor katkısı ile HC emisyonu 204 ppm'ye düşmüş ve %10,53 azalma sağlanmıştır. 14 cc/L katkı seviyesinde HC 177,22 ppm'ye gerileyerek %22,27 azalmıştır. 21 cc/L seviyesinde ise HC emisyonu 233,72 ppm'ye yükselmiş ve katkısız benzine göre %2,51 artmıştır. Bu sonuçlar, benzin yakıtında 7 ve 14 cc/L bor katkısının HC emisyonlarını azaltmada etkili olduğunu, ancak 21 cc/L seviyesinde aynı iyileşmenin sağlanamadığını göstermektedir. En düşük HC emisyonu 14 cc/L katkı seviyesinde elde edilmiştir. HC emisyonları, yanma odasında yanmadan kalan yakıt, alevin söndüğü bölgeler, silindir duvarı yakınındaki karışım ve yarık hacimlerde hapsolan yakıt gibi mekanizmalarla ilişkilidir. Bu nedenle katkı oranındaki artışın karışım oluşumu ve yanma süreci üzerindeki etkisi HC emisyonlarını farklı yönlerde değiştirebilir.

E20 yakıtında bor katkısının etkisi: Katkısız E20 için ortalama HC emisyonu 185,19 ppm olarak belirlenmiştir. 7 cc/L katkı ile HC 196,63 ppm'ye yükselmiş ve %6,18 artmıştır. Buna karşılık 14 cc/L katkı seviyesinde HC 158,03 ppm'ye düşerek %14,66 azalmıştır. 21 cc/L katkı seviyesinde ise HC 165,03 ppm olarak ölçülmüş ve %10,88 azalma sağlanmıştır. Bu sonuçlar, E20 yakıtında 7 cc/L katkının HC emisyonu bakımından olumsuz sonuç verdiğini, 14 ve 21 cc/L seviyelerinin ise iyileşme sağladığını göstermektedir. En düşük HC emisyonu 14 cc/L seviyesinde elde edilmiştir. E20 içerisindeki etanolün oksijen içeriği, yakıtın buharlaşma ve yanma karakteristiklerini değiştirerek HC oluşumunu etkileyebilir. Ancak 7 cc/L seviyesinde HC'nin artması, etanol içeriğinin tek başına HC emisyonlarını azaltmak için yeterli olmadığını; katkı oranı ve motor çalışma koşullarının da belirleyici olduğunu göstermektedir.

Aynı katkı oranında benzin–E20 karşılaştırması: Katkısız durumda E20'nin HC emisyonu benzinden %18,78 daha düşüktür. 7 cc/L katkı seviyesinde E20'nin HC emisyonu benzinden

%3,62 daha düşük bulunmuştur. 14 cc/L seviyesinde bu fark %10,83'e, 21 cc/L seviyesinde ise %29,39'a yükselmiştir. Böylece bütün eşleştirilmiş katkı seviyelerinde E20 daha düşük HC emisyonu üretmiştir. Özellikle 21 cc/L seviyesinde E20'nin benzin karşısındaki avantajı belirginleşmiştir. Bu sonuç, etanol içeriğinin ve bor katkısının birlikte kullanıldığı yakıtların HC emisyonlarını azaltma potansiyeline işaret etmektedir. Bununla birlikte E20+7 karışımında katkısız E20'ye göre HC artışı görülmesi, katkı etkisinin her seviyede aynı yönde olmadığını ortaya koymaktadır. Masum ve arkadaşları (2014) da E20 dahil alkol-benzin karışımlarının HC emisyonlarında azalma sağlayabildiğini bildirmiştir. Ayrıca 2026 yılında yayımlanan bor bazlı yakıt katkısı çalışmasında, bazı bor bileşiklerinin HC emisyonlarını azaltırken BSFC ve motor momenti üzerinde farklı etkiler oluşturabildiği gösterilmiştir.

4. Sonuçlar ve değerlendirme

4.1. Benzin yakıtına farklı oranlarda bor katkısının etkisi

Benzin yakıtına bor katkısı ilave edilmesiyle ortalama motor torkunda artış meydana gelmiştir. En yüksek ortalama tork artışı 7 cc/L bor katkısında yaklaşık %1,3 olarak belirlenmiştir. Katkı oranı 14 cc/L olduğunda tork artışı %0,6 seviyesinde kalırken, 21 cc/L katkı oranında yaklaşık %0,2 olmuştur. BSFC değerleri incelendiğinde, katkısız benzine kıyasla 7, 14 ve 21 cc/L bor katkılarında sırasıyla yaklaşık %14,8, %10,8 ve %8,1 azalma görülmüştür. Buna bağlı olarak, aynı alt ısıl değer kabulüyle hesaplanan termal verimde en belirgin iyileşmenin 7 cc/L katkı oranında gerçekleştiği söylenebilir.

Egzoz sıcaklığı, bor katkısı kullanılan bütün benzin karışımlarında katkısız benzine göre artış göstermiştir. Ortalama egzoz sıcaklığındaki artış 7 cc/L katkıda yaklaşık %3,6, 14 cc/L katkıda %1,9 ve 21 cc/L katkıda %1,4 olarak hesaplanmıştır. CO emisyonları bütün katkı oranlarında azalmış, en yüksek azalma yaklaşık %8,4 ile 7 cc/L katkıda elde edilmiştir. CO_2 emisyonları ise katkı oranlarının tamamında sınırlı artış göstermiştir. HC emisyonlarında 7 ve 14 cc/L katkı oranlarında sırasıyla yaklaşık %10,5 ve %22,3 azalma belirlenirken, 21 cc/L katkıda yaklaşık %2,5 artış görülmüştür. Bu sonuçlar, benzin yakıtında 7 cc/L bor katkısının tork, BSFC ve CO emisyonları bakımından daha dengeli sonuçlar verdiğini göstermektedir.

4.2. E20 yakıtına farklı oranlarda bor katkısının etkisi

E20 yakıtına bor katkısı ilave edilmesiyle ortalama motor torku katkısız E20 yakıtına göre artmıştır. En yüksek tork artışı yaklaşık %2,9 ile 7 cc/L katkı oranında gerçekleşmiştir. 14 ve 21 cc/L katkı oranlarında ise tork artışları sırasıyla yaklaşık %0,9 ve %1,0 olarak hesaplanmıştır. BSFC değerlerinde 7, 14 ve 21 cc/L bor katkılarıyla sırasıyla yaklaşık %23,8, %36,5 ve %25,8 azalma elde edilmiştir. Buna göre en düşük ortalama BSFC değeri 14 cc/L bor katkısında belirlenmiştir. Aynı yakıt için geçerli alt ısıl değer kullanılarak hesaplanan termal verim açısından da 14 cc/L katkı oranı öne çıkmaktadır.

Egzoz sıcaklığı, E20 yakıtına bor katkısı ilave edilmesiyle bütün oranlarda artış göstermiştir. Ortalama artış 7 cc/L katkıda yaklaşık %1,7, 14 cc/L katkıda %1,9 ve 21 cc/L katkıda %2,5 olarak belirlenmiştir. CO emisyonlarında katkı oranlarına bağlı olarak sınırlı azalmalar görülmüş; en yüksek azalma yaklaşık %5,1 ile 7 cc/L katkıda gerçekleşmiştir. CO_2 emisyonları bütün katkı oranlarında artarken, HC emisyonları 14 ve 21 cc/L katkılarda

sırasıyla yaklaşık %14,7 ve %10,9 azalmıştır. Buna karşılık, 7 cc/L katkı oranında HC emisyonlarında yaklaşık %6,2 artış belirlenmiştir. Bu sonuçlar, E20 yakıtında 14 cc/L bor katkısının BSFC, termal verim ve HC emisyonları açısından daha olumlu sonuçlar ortaya koyduğunu göstermektedir.

4.3. Benzin ve E20 yakıtlarının aynı bor katkı oranlarında karşılaştırılması

Katkısız benzin ve E20 yakıtları karşılaştırıldığında ortalama tork değerlerinin birbirine oldukça yakın olduğu görülmektedir. Buna karşılık E20 yakıtının ortalama BSFC değeri benzine göre yaklaşık %17,8 daha yüksek, HC emisyonu yaklaşık %18,8 daha düşük bulunmuştur. CO ve CO_2 emisyonları da E20 yakıtında sırasıyla yaklaşık %2,8 ve %2,7 daha düşük gerçekleşmiştir.

7 cc/L bor katkısı kullanılan yakıtlar karşılaştırıldığında E20 karışımının ortalama torku benzine göre yaklaşık %1,6 daha yüksek bulunmuştur. Bununla birlikte E20+7 karışımının BSFC değeri benzin+7 karışımından yaklaşık %5,3 daha yüksektir. HC emisyonu ise E20+7 karışımında yaklaşık %3,6 daha düşük gerçekleşmiştir. CO ve CO_2 değerleri iki yakıt arasında birbirine yakın sonuçlar vermiştir.

14 cc/L bor katkısında E20 yakıtının ortalama torku benzin karışımına göre yaklaşık %0,2 daha yüksek bulunmuştur. E20+14 karışımında BSFC yaklaşık %16,1 daha düşük, HC emisyonu ise yaklaşık %10,8 daha az gerçekleşmiştir. Bu katkı oranında E20 yakıtı, yakıt tüketimi ve HC emisyonları bakımından benzine göre daha olumlu sonuç vermiştir.

21 cc/L bor katkısında E20 karışımının ortalama torku benzin karışımına göre yaklaşık %0,7 daha yüksek, BSFC değeri yaklaşık %4,9 daha düşük bulunmuştur. En belirgin fark HC emisyonlarında görülmüş ve E20+21 karışımında HC emisyonu benzin+21 karışımına göre yaklaşık %29,4 azalmıştır. CO ve CO_2 emisyonları ise iki yakıt arasında birbirine yakın değerler göstermiştir.

Bu çalışmada elde edilen ortalama sonuçlara göre bor katkısının benzin ve E20 yakıtları üzerindeki etkileri katkı oranına bağlı olarak değişmiştir. Benzin yakıtında 7 cc/L bor katkısı tork artışı, BSFC azalması ve CO emisyonlarının düşürülmesi bakımından öne çıkarken, E20 yakıtında 14 cc/L bor katkısı BSFC ve HC emisyonları açısından en olumlu sonuçları vermiştir. E20 yakıtı, özellikle 14 ve 21 cc/L bor katkı oranlarında HC emisyonlarının azaltılmasında benzine kıyasla daha başarılı olmuştur. Genel olarak değerlendirildiğinde, bor katkısının motor performansı ve egzoz emisyonları üzerindeki etkisinin yalnızca katkı miktarına değil, temel yakıtın özelliklerine de bağlı olduğu belirlenmiştir.

Kaynakça

Akbıyık, T., Kahraman, N., & Taner, T. (2022). Investigation of the effect of boron additive to lubricating oil on engine performance, exhaust, and emissions. Fuel, 312, 122931. https://doi.org/10.1016/j.fuel.2021.122931

Akbıyık, T., Kahraman, N., Taner, T., (2023) Performance emission, energy and exergy analysis evaluation of gasoline engine using different fuels, Fuel, https://doi.org/10.1016/j.fuel.2023.128189

Akbıyık, T. (2026). Investigating the effect of adding different concentrations of boron to the engine oil of a gasoline engine using bioethanol blends on engine performance. Journal of Thermal Analysis and Calorimetry. https://doi.org/10.1007/s10973-026-16182-z

Çakmak, A., & Özcan, H. (2022). Bor oksit nanoparçacıklarının dizel yakıt katkısı olarak kullanılabilirliğinin araştırılması. Journal of Boron, 7(1), 420–429. https://doi.org/10.30728/boron.1021667

Gotewala, S., Kumar, S. S., Saha, T., Balaji, G., Nandagopalan, P., & Kannan, B. T. (2026). Effect of boron nanoparticles on water-in-diesel emulsion as fuel for CI engine performance and emission characteristics. International Journal of Ambient Energy, 47(1). https://doi.org/10.1080/01430750.2026.2661832

Karataş, Ö., & Yüksel, T. (2023). Experimental investigation of the effects of boron oil additive in internal combustion engine. Fuel, 353, 129234. https://doi.org/10.1016/j.fuel.2023.129234

Sertkaya, A. A., & Akbıyık, T. (2016). Operate With a Gasoline Internal Combustion Engine Evaluation of Different Boron Addition of The Fuel Additive Inside Performance and Emissions Impact. Politeknik Dergisi, 19(4), 633–640. https://izlik.org/JA78ZJ59EM

Sofuoğlu, D., Değirmenci, H., Kantaroğlu, E., & Yontar, A. A. (2026). Effects of boron-based fuel additives on sequential-ignition engine characteristics and emissions. International Journal of Ambient Energy, 47(1). https://doi.org/10.1080/01430750.2026.2730195

Yakın, A., & Gülcan, M. (2025). Effects of boron-based additives on combustion characteristics, emission reduction, and performance improvement in internal combustion engines. Journal of the Energy Institute, 120, 102044. https://doi.org/10.1016/j.joei.2025.102044

İKİ FARKLI TİCARİ BOR ESASLI YAKIT KATKISININ BENZİNLİ MOTOR PERFORMANSINA ETKİSİNİN DENEYSEL İNCELENMESİ

EXPERIMENTAL INVESTIGATION OF THE EFFECTS OF TWO DIFFERENT BORON-BASED ADDITIVES ON THE PERFORMANCE OF A GASOLINE ENGINE AND DETERMINATION OF THE OPTIMUM ADDITIVE CONCENTRATION

Talip AKBIYIK
Asst. Prof. Dr., Aksaray University, Technical Sciences Vocational School, Automotive Technology
ORCID ID: 0000-0001-8580-8890

Nafiz KAHRAMAN
Prof. Dr., Erciyes University, Faculty of Aeronautics and Space Sciences, Space Engineering
ORCID ID: 0000-0002-8698-8632

ÖZET

Bu çalışmada, iki farklı ticari bor esaslı yakıt katkısının benzinli motor performansı üzerindeki etkileri deneysel olarak incelenmiştir. Deneyler, iki silindirli Lombardini LGW 523 MPI benzinli motorda, tam gaz koşulunda ve 1500–5000 d/d motor devir aralığında gerçekleştirilmiştir. Katkısız benzin referans yakıt olarak kullanılmış; A ve B katkıları benzine litre başına 7, 14, 21, 28 ve 35 cc oranlarında ilave edilmiştir. Her motor devrinde elde edilen ölçümler üç kez tekrarlanmış ve ortalama değerler değerlendirilmiştir. Motor performansı tork, fren özgül yakıt tüketimi (BSFC) ve termal verim parametreleri üzerinden karşılaştırılmıştır.

Sonuçlar, bor katkılarının etkisinin katkı türüne, katkı miktarına ve motor devrine bağlı olarak değiştiğini göstermiştir. Ortalama tork artışı A katkısında en yüksek %0,86 ile 7 cc oranında, B katkısında ise %1,00 ile 7 cc oranında elde edilmiştir. A katkısında en düşük ortalama BSFC 28 cc seviyesinde 386,16 g/kWh olarak belirlenirken, B katkısında en düşük değer 35 cc seviyesinde 247,41 g/kWh olmuştur. Katkısız benzine ait ortalama BSFC değeri 492,48 g/kWh'dir. Hesaplanan ortalama termal verim A katkısında 7 cc ile %23,56, B katkısında ise 35 cc ile %34,73 olarak bulunmuştur. Bununla birlikte, bazı ölçüm noktalarında belirgin sapmalar görülmesi ve termal verim hesaplamasında tüm yakıtlar için aynı alt ısıl değerin kullanılması, sonuçların yorumlanmasında dikkate alınmalıdır. Bulgular, B katkısının özellikle 28 ve 35 cc oranlarında yakıt tüketimi ve hesaplanan termal verim bakımından öne çıktığını göstermektedir. Ancak bu sonuçların kesinleştirilmesi için ölçümlerin doğrulanması, yakıtların alt ısıl değerlerinin belirlenmesi ve istatistiksel analiz yapılması gerekmektedir.

Anahtar kelimeler: Bor katkısı, benzinli motor, motor performansı, fren özgül yakıt tüketimi, termal verim, tork.

ABSTRACT

In this study, the effects of two different commercial boron-based fuel additives on gasoline engine performance were experimentally investigated. The experiments were conducted using a two-cylinder Lombardini LGW 523 MPI gasoline engine under wide-open throttle conditions within an engine speed range of 1500–5000 rpm. Gasoline without additives was used as the reference fuel, while additives A and B were blended with gasoline at concentrations of 7, 14, 21, 28, and 35 cc per liter of fuel. Measurements at each engine speed were repeated three times, and the average values were evaluated. Engine performance was compared in terms of torque, brake-specific fuel consumption (BSFC), and thermal efficiency. The results showed that the effects of boron-based additives varied depending on the additive type, concentration, and engine speed. The highest average torque increases were 0.86% at 7 cc for additive A and 1.00% at 7 cc for additive B. The lowest average BSFC for additive A was 386.16 g/kWh at 28 cc, whereas the lowest value for additive B was 247.41 g/kWh at 35 cc. The average BSFC of the reference gasoline was 492.48 g/kWh. The calculated average thermal efficiencies were 23.56% at 7 cc for additive A and 34.73% at 35 cc for additive B. However, noticeable deviations at certain measurement points and the use of the same lower heating value for all fuels in the thermal efficiency calculations should be considered when interpreting the results. The findings indicate that additive B, particularly at concentrations of 28 and 35 cc, exhibited more favorable results in terms of fuel consumption and calculated thermal efficiency. Nevertheless, validation of the measurements, determination of the lower heating values of the fuels, and statistical analysis are required to confirm these findings.

Keywords: Boron-based additive, gasoline engine, engine performance, brake-specific fuel consumption, thermal efficiency, torque.

2. GİRİŞ

İçten yanmalı motorlarda yakıt ekonomisinin iyileştirilmesi, motor performansının artırılması ve egzoz emisyonlarının azaltılması, otomotiv teknolojileri alanındaki araştırmaların temel konuları arasında yer almaktadır. Bu amaçla alternatif yakıtların geliştirilmesinin yanı sıra yakıtın fiziksel ve kimyasal özelliklerini değiştirebilen katkı maddelerinin kullanımı da araştırılmaktadır. Bor esaslı bileşikler, kimyasal yapıları ve bazı bileşiklerin hidrojen içeriği nedeniyle içten yanmalı motorlarda yakıt katkısı olarak incelenen malzemeler arasındadır. Bununla birlikte, bor içeren bileşiklerin motor performansı ve emisyonlar üzerindeki etkileri; bileşiğin kimyasal yapısına, katkı konsantrasyonuna, yakıtla uyumluluğuna ve motorun çalışma koşullarına bağlı olarak değişebilmektedir (Sertkaya ve Akbıyık, 2016; Yakın ve Gülcan, 2025; Sofuoğlu ve ark., 2026).

Bor esaslı katkıların motorlardaki etkileri, kullanım alanlarına göre doğrudan yakıta eklenen katkılar ve motor yağlama yağına ilave edilen katkılar olmak üzere iki grupta değerlendirilebilir. Yakıta doğrudan eklenen bor bileşikleri yanma süreci, yakıt özellikleri ve emisyonlar üzerinde etkili olabilirken, yağlama yağına eklenen bor bileşikleri daha çok sürtünme, aşınma ve yağlama özellikleri üzerinden motor performansını etkileyebilmektedir.

Bu nedenle iki farklı kullanım biçiminden elde edilen sonuçların aynı mekanizma üzerinden değerlendirilmemesi gerekmektedir. Özellikle yağlama yağına eklenen bor katkılarının tork ve yakıt tüketimi üzerindeki etkileri, doğrudan yakıt katkısı olarak kullanılan bor bileşiklerinin yanma sürecine etkilerinden farklılık göstermektedir (Akbıyık ve ark., 2022; Karataş ve Yüksel, 2023).

Benzinli motorlarda bor esaslı yakıt katkılarının etkilerini inceleyen çalışmalardan biri Sertkaya ve Akbıyık (2016) tarafından gerçekleştirilmiştir. Araştırmada bor katkıları benzin içerisine farklı oranlarda ilave edilerek Lombardini LGW 523 benzinli motorda 1500–5000 d/d motor devri aralığında deneyler yapılmıştır. Motor gücü, tork, yakıt tüketimi, yakıt sıcaklığı ve egzoz emisyonlarının değerlendirildiği çalışma, bor esaslı katkıların kıvılcım ateşlemeli motorlarda kullanım potansiyelini ortaya koymuştur. Yakın ve Gülcan (2025) ise hidrojen bakımından zengin bir bor bileşiği olan metilamin-boranın (MAB) benzinli motor performansı ve emisyonları üzerindeki etkilerini incelemiştir. Hacimsel %5 ve %10 oranlarında hazırlanan MAB karışımlarında CO ve HC emisyonlarında önemli azalmalar bildirilirken NOx emisyonlarında artış, özgül yakıt tüketiminde yükselme ve termal verimde düşüş gözlenmiştir. Bu sonuçlar, bor esaslı katkıların bazı egzoz emisyonlarını azaltmasına rağmen motor performansının bütün parametrelerinde iyileşme sağlamayabileceğini göstermektedir.

Sofuoğlu ve arkadaşları (2026), benzinli kıvılcım ateşlemeli bir motorda trimetil borat (TMB) ve trietil borat (TEB) bileşiklerini farklı karışım oranlarında incelemiştir. Deneyler 2800 d/d motor devrinde ve %75 ile %100 gaz kelebeği açıklıklarında gerçekleştirilmiştir. Çalışmada elde edilen bulgular, bor içeren organik bileşiklerin motor karakteristikleri üzerindeki etkilerinin yalnızca bor elementinin varlığıyla açıklanamayacağını; bileşiğin kimyasal yapısının ve yakıt içerisindeki oranının da önemli olduğunu ortaya koymaktadır. Çakmak ve Özcan (2022) ise bor oksit (B_2O_3) nanoparçacıklarını %20 kanola yağı biyodizeli içeren B20 yakıtına farklı konsantrasyonlarda ilave ederek dizel motor performansı, yanma ve emisyon özelliklerini değerlendirmiştir. Araştırmada 100 ppm bor oksit konsantrasyonunda özgül yakıt tüketiminde %1,66 azalma ve efektif verimde %0,96 artış bildirilmiştir. CO ve HC emisyonlarında azalma görülmesine karşılık NO ve is emisyonlarında artış belirlenmiştir. Ayrıca nanoparçacık kullanımının yakıt maliyetini önemli ölçüde artırdığı ifade edilmiştir.

Bor esaslı katkıların motor performansına etkileri yalnızca yakıt sistemleriyle sınırlı olmayıp yağlama yağı uygulamalarında da incelenmiştir. Akbıyık ve arkadaşları (2022), benzin ve doğal gazla çalışan kıvılcım ateşlemeli bir motorda bor katkılı yağ kullanımının motor performansı ve emisyonlar üzerindeki etkilerini araştırmıştır. Çalışmada özgül yakıt tüketiminde ve NOx emisyonlarında azalmalar bildirilirken CO ve HC emisyonlarında belirgin bir değişim gözlenmemiştir. Karataş ve Yüksel (2023) tarafından gerçekleştirilen diğer bir çalışmada ise tek silindirli dizel motorun mineral esaslı motor yağına sıvı bor katkısı ilave edilmiştir. Farklı motor devirlerinde yapılan deneylerde tork ve egzoz gazı sıcaklığında artış; özgül yakıt tüketimi, CO_2, HC ve NOx emisyonlarında ise azalma rapor edilmiştir. Bu çalışmalar, bor katkılarının yağlama özellikleri üzerinden motor performansını

etkileyebileceğini göstermektedir. Bununla birlikte, elde edilen sonuçlar doğrudan yakıt içerisine eklenen bor katkılarının etkileriyle aynı kapsamda değerlendirilmemelidir.

Bor nanoparçacıklarının alternatif yakıt karışımlarında kullanımı da araştırılan konular arasındadır. Gotewala ve arkadaşları (2026), dizel, deiyonize su ve emülgatörden oluşan su-dizel emülsiyonuna farklı konsantrasyonlarda bor nanoparçacıkları ilave ederek tek silindirli dizel motorda performans ve emisyon deneyleri gerçekleştirmiştir. Çalışmada bor içeren emülsiyonların motor karakteristikleri üzerindeki etkileri değerlendirilmiş ve 150 ppm bor nanoparçacığı içeren karışımda NO emisyonunda azalma ve net dizel tüketiminde iyileşme bildirilmiştir. Bununla birlikte, su-dizel emülsiyonlarının fiziksel ve kimyasal özellikleri geleneksel yakıtlardan farklı olduğundan, bu sonuçların doğrudan benzin veya dizel yakıtına eklenen katkılara genellenmesi uygun değildir.

Literatürdeki çalışmalar genel olarak değerlendirildiğinde, bor esaslı bileşiklerin içten yanmalı motorlarda performans ve egzoz emisyonları üzerinde etkili olabildiği görülmektedir. Ancak bu etkilerin yönü ve büyüklüğü kullanılan bor bileşiğinin türüne, katkı miktarına, yakıt özelliklerine ve motor çalışma koşullarına bağlı olarak değişmektedir. Bazı çalışmalarda özgül yakıt tüketimi ve CO ile HC emisyonlarında azalma bildirilirken, NOx ve is emisyonlarında artışlar da gözlenmiştir. Bu durum, bor esaslı katkıların değerlendirilmesinde motor performansı ve emisyon parametrelerinin birlikte ele alınmasının önemini ortaya koymaktadır. Mevcut literatürde farklı bor bileşiklerinin ve ticari katkı ürünlerinin aynı motor, yakıt ve çalışma koşulları altında doğrudan karşılaştırıldığı çalışmaların sınırlı olduğu görülmektedir. Özellikle ticari olarak temin edilebilen farklı bor esaslı yakıt katkılarının değişen konsantrasyonlarda benzinli motor performansı üzerindeki etkilerinin karşılaştırmalı olarak incelenmesine ihtiyaç bulunmaktadır. Bu kapsamda, katkı miktarının motor devrine bağlı tork ve yakıt tüketimi değişimleri üzerindeki etkilerinin belirlenmesi, bor esaslı katkıların kullanım potansiyelinin değerlendirilmesine katkı sağlayabilir.

Bu çalışmanın amacı, iki farklı ticari bor esaslı yakıt katkısının benzinli motor performansı üzerindeki etkilerini deneysel olarak karşılaştırmaktır. Bu amaçla, iki silindirli Lombardini LGW 523 MPI benzinli motorda katkısız benzin referans yakıt olarak kullanılmış; A ve B olarak tanımlanan iki ticari katkı, yakıtın litresine 7, 14, 21, 28 ve 35 cc oranlarında ilave edilmiştir. Deneyler tam gaz koşulunda 1500–5000 d/d motor devri aralığında gerçekleştirilmiş; motor torku, fren özgül yakıt tüketimi ve hesaplanan termal verim parametreleri değerlendirilmiştir. Böylece farklı ticari bor katkılarının ve katkı konsantrasyonlarının motor performansı üzerindeki etkilerinin aynı deney düzeneğinde karşılaştırılması amaçlanmıştır.

2. MATERYAL METOD

2.1. DENEY TEST DÜZENEGİ

Tablo 1'de özellikleri verilen Lombardini LGW 523 MPI 2-silindir benzinli motor özellikleri verilen motorda üzerinde deneysel çalışmalar yapılmıştır. Deneysel motorda piyasadaki benzin istasyonlarından temin edilen benzin yakıt kullanılarak çalıştırılmıştır. Benzin yakıtına 2 farklı bor katkısı farklı oranlarda eklenerek deneyler yapılmıştır. Yakıt içerisine litre başı 0,

7, 14, 21, 28 ve 35 cc yakıt bor katkısı ilave edilmiştir. Motorda 1500, 2000, 2500, 3000, 3500, 4000, 4500 ve 5000 devirlerde performans deneyleri yapılmıştır. Motor her bir devirde 5 dakika çalıştırılmış ve bu değerlerin ortalaması alınmıştır. Motor deneyleri 3 kez tekrarlanmış ve elde edilen verilerin ortalaması alınmıştır.

2.2. DENEY METOROLOJİSİ

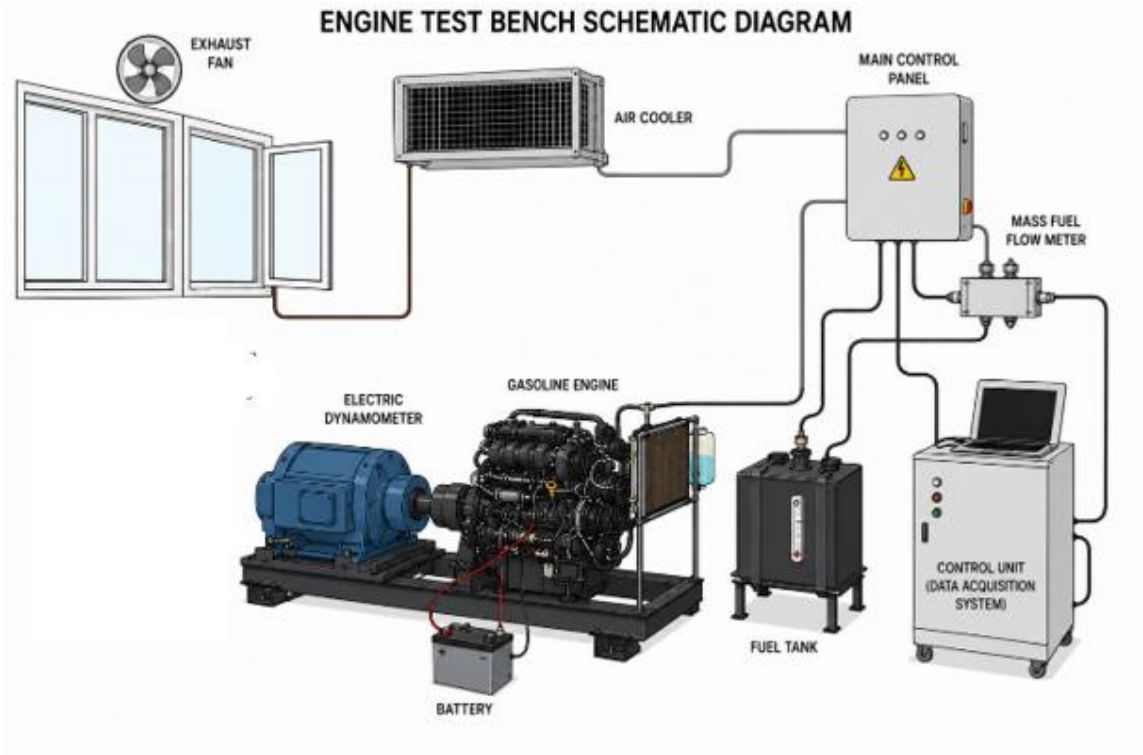
Baz ve bor ilaveli yapılan deneysel çalışmalar, birbirini takip eden süreçler şeklinde gerçekleştirilmiştir. Tüm deneyler boyunca ortam sıcaklığı yaklaşık 23 °C olarak ölçülmüştür. Deneylerde motor ısındıktan sonra motor performans deneyleri tam gaz durumunda 1500, 2000, 2500, 3000, 3500, 4000, 4500 ve 5000 devire yüklenerek yapılmıştır. Başlangıçta motor katkısız yakıt ile çalıştırılıp deneyler yapılmış bu değerler baz deger olarak kabul edilmiştir sonra yakıta sırasıyla litre başına 7, 14, 21, 28 ve 35 cc bor yakıt katkısı ilave edilmiş deneyler yapılmıştır. 2 farklı yakıt ile yapılan deney sonuçları karşılaştırılmıştır.

Table 1. Lombardini LGW 523 engine features [Akbıyık ve ark. 2022]

Motor özelliği	**Birim**	**Değer**
Silindir sayısı	adet	2
Silindir çapı	mm	72
Strok	mm	62
Motor hacmi	cc	505
Sıkıştırma oranı	-	10,7:1
Maksimum motor devri	d/d	5500
Maksimum güç	kW	15
Maksimum tork	Nm	34
Motor ağırlığı	kg	52



Şekil 1. Deney düzeneği

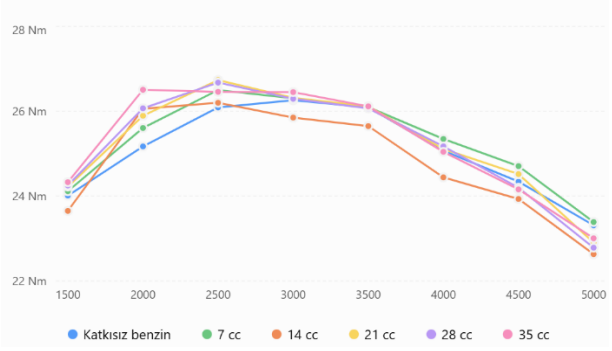


Şekil 2. Deney düzeneği şematik gösterimi.

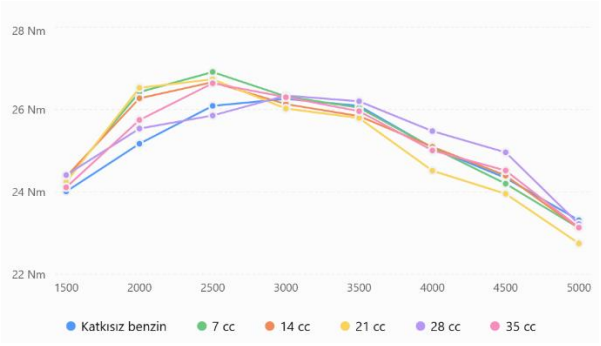
4. DENEY SONUÇLARI

Bu çalışmada, motorda kullanılan yakıta 2 farklı bor yakıt katkısı farklı oranlarda katılmıştır. Bor katkılarının karşılaştırması ve en iyi oran oranının belirlenmesi sağlanmıştır. Motorda yapılan karşılaştırma temel performans parametreleri arasında güç, tork, termal verimlilik ve fren özgül yakıt tüketimi (bsfc) yer almaktadır. Motor tam yük durumunda 8 farklı motor

devrinde (1500, 2000, 2500, 3000, 3500, 4000, 4500 ve 5000) yüklenmiştir. Yakıt olarak ilk çalışma katkısız benzin ile yapılmış ve referans yakıt olarak ele alınmıştır. Sonraki çalışmalar yakıta litre başına 7,4,21,28 ve 35 cc yakıt bor katkısı ilave edilerek yapılmıştır. Motor performans değerleri belirlenmiş ve bunların karşılaştırması yapılmıştır.



Şekil 3. A yakıt katkısının farklı oranlarının devire bağlı tork değişimi



Şekil 4. B yakıt katkısının farklı oranlarının devire bağlı tork değişimi

Aşağıdaki tabloda her katkı miktarı için sekiz farklı motor devrindeki tork değişimlerinin aritmetik ortalaması verilmiştir. Yüzdeler, katkısız benzin verilerine göre hesaplanmıştır.

A bor yakıt katkısı:

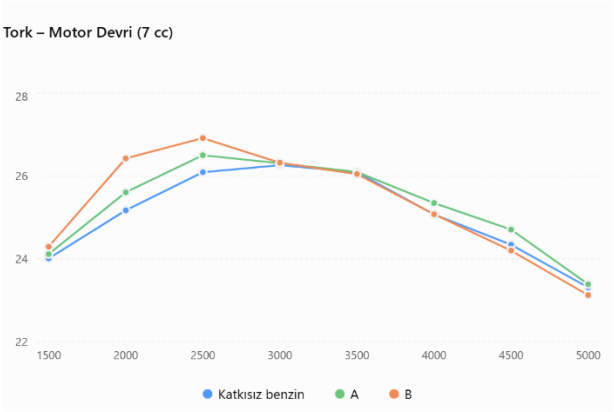
- 7 cc: Ortalama tork artışı %0,86'dır. Artış bütün devir noktalarında pozitif olmakla birlikte 3500 d/d'de fark oldukça küçüktür.
- 14 cc: Ortalama değişim −%0,99'dur. 2000 d/d'de %3,54 artış görülürken 4000–5000 d/d aralığında tork düşüşleri ortaya çıkmaktadır.
- 21 cc: Ortalama artış %0,71'dir. En belirgin artış 2000 d/d'de %2,87 düzeyindedir; 5000 d/d'de ise %1,75 azalma vardır.
- 28 cc: Ortalama artış %0,55'tir. 2000 d/d'de %3,57 artışa rağmen 5000 d/d'de %2,27 düşüş ölçülmüştür.
- 35 cc: Ortalama artış %0,84'tür. En yüksek artış 2000 d/d'de %5,31 olarak hesaplanmıştır. Buna karşılık 4000 d/d'den sonra katkısız referansa göre tork düşüşü görülmektedir.

Dolayısıyla A verilerinde 35 cc katkı, ortalama tork artışı açısından 7 cc'ye yakın sonuç vermiştir; ancak yüksek devirlerde aynı avantaj korunmamaktadır.

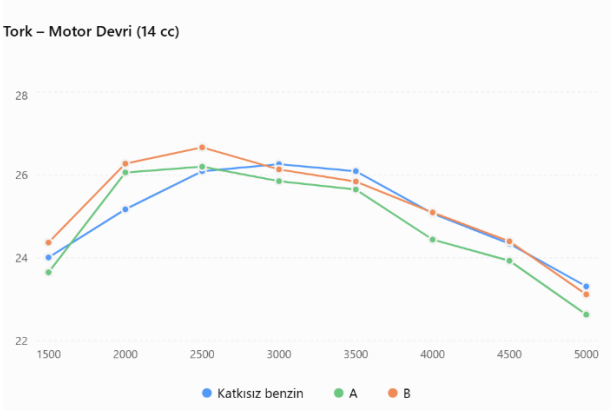
B bor yakıt katkısı:

- 7 cc: Ortalama artış %1,00 ile bu gruptaki en yüksek ortalama değerdir. 2000 d/d'de %4,98, 2500 d/d'de %3,16 artış hesaplanmıştır.
- 14 cc: Ortalama artış %0,77'dir. 2000 d/d'de %4,38 artış görülmesine karşın 3500 d/d'de yaklaşık %0,96 azalma vardır.
- 21 cc: Ortalama değişim yalnızca +%0,07'dir. 2000 d/d'de %5,40 artış ölçülmesine rağmen 3000 d/d ve üzerindeki birçok noktada tork düşmektedir.
- 28 cc: Ortalama artış %0,84'tür. Özellikle 4000 ve 4500 d/d'de sırasıyla yaklaşık %1,62 ve %2,55 artış görülmesi bu katkı düzeyini yüksek devirler bakımından dikkat çekici kılmaktadır.
- 35 cc: Ortalama artış %0,52'dir. Artış 2000–2500 d/d aralığında belirgindir; 4000 d/d'de ise yaklaşık %0,25 düşüş söz konusudur.

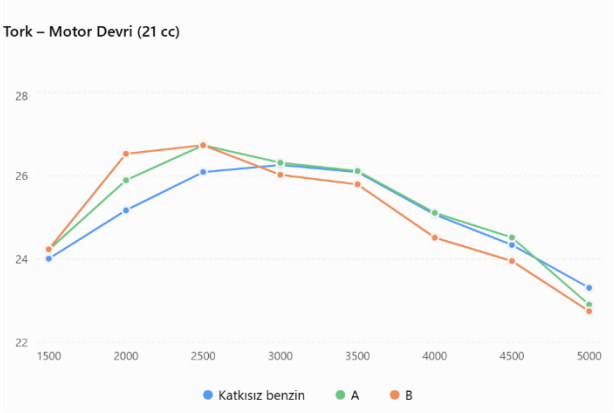
Her iki katkı türünde de sonuçlar katkı miktarına ve motor devrine bağlıdır. Daha yüksek katkı miktarının her koşulda daha yüksek tork sağlayacağı yönünde doğrusal bir ilişki görülmemektedir. Bu durum, bor katkılarının motor performansına etkisinin deney koşulları ve yağlama özellikleriyle birlikte değerlendirilmesi gerektiğini bildiren önceki çalışmalarla uyumludur.



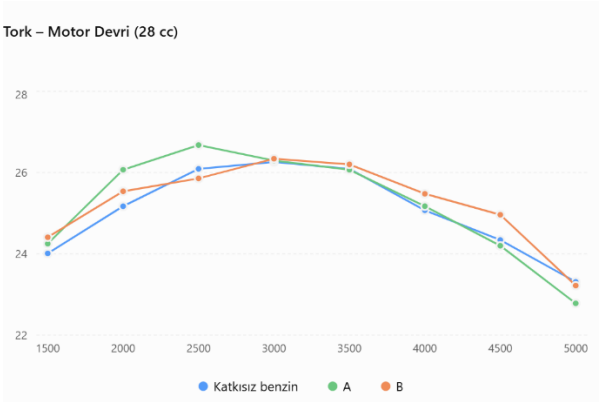
Şekil 5. 7 cc yakıt katkısında torkun devre bağlı değişimi



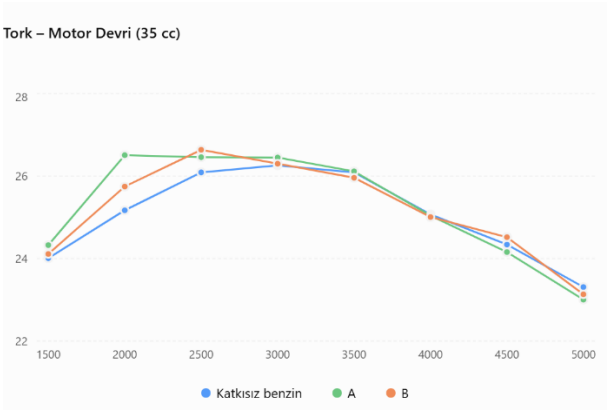
Şekil 6. 14 cc yakıt katkısında torkun devre bağlı değişimi



Şekil 7. 21 cc yakıt katkısında torkun devre bağlı değişimi



Şekil 8. 28 cc yakıt katkısında torkun devre bağlı değişimi



Şekil 9. 35 cc yakıt katkısında torkun devre bağlı değişimi

A ve B katkılarının doğrudan karşılaştırılması:
Bu karşılaştırmada aynı katkı miktarındaki B torku, A torkuyla karşılaştırılmıştır. Pozitif değer B daha yüksek tork verdiğini gösterir.

- 7 cc: İki ürünün ortalama sonuçları birbirine çok yakındır. Bununla birlikte B, özellikle 2000 ve 2500 d/d'de daha yüksek tork üretmiştir.
- 14 cc: B'un en belirgin ortalama avantajı bu düzeyde ortaya çıkmıştır. Sekiz devir noktasının tamamında B torku A değerinden yüksektir.

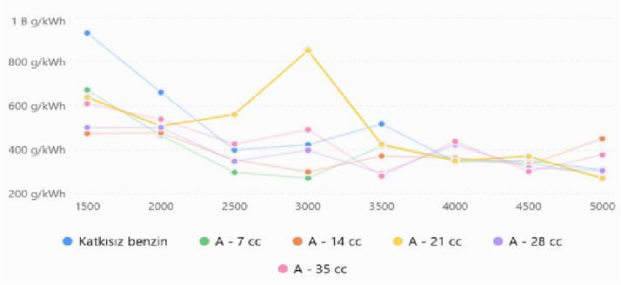
- 21 cc: A'in ortalama torku biraz daha yüksektir. Özellikle 4000 d/d'de A lehine fark görülürken 2000 d/d'de B daha yüksek sonuç vermiştir.
- 28 cc: İki katkının genel sonuçları benzerdir. B'un 4000–4500 d/d aralığındaki avantajı dikkat çekmektedir.
- 35 cc: A'in ortalama sonucu çok az daha yüksektir. Ancak bu fark küçük olduğundan tekrarlı deneyler ve belirsizlik hesabı olmadan kesin üstünlük olarak yorumlanmamalıdır.

Bor katkılarının motor performansına etkisi literatürde çoğunlukla yağlama, sürtünme kayıpları ve yakıt tüketimi üzerinden ele alınmaktadır. Akbıyık ve arkadaşları, benzin ve doğal gazla çalışan kıvılcım ateşlemeli motorda bor katkılı yağ kullanımının özgül yakıt tüketiminde ortalama %2,4–8 azalma sağladığını bildirmiştir. Çalışmada tork sonuçları da incelenmiş ve bor katkılı yağla göreli performans iyileşmesi raporlanmıştır.

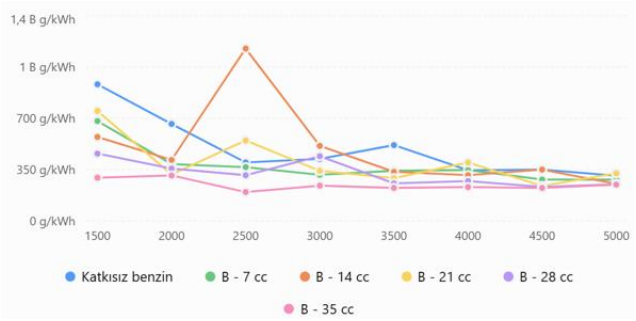
Karataş ve Yüksel'in tek silindirli dizel motor üzerindeki çalışmasında ise %15 bor katkılı yağ kullanımıyla tork ve egzoz sıcaklığının arttığı, özgül yakıt tüketimi ve bazı emisyonların azaldığı belirtilmiştir. Ancak motor tipi, yakıt, katkı oranı ve çalışma koşulları bu çalışmadaki deneylerden farklı olduğundan, sonuçlar doğrudan sayısal eşdeğerlik olarak değerlendirilmemelidir.

Akbıyık 2026 tarihli çalışmanızda da farklı benzin–biyoetanol karışımlarıyla birlikte %5, %10 ve %15 bor katkısı değerlendirilmiş; genel tork sonuçlarında %10 katkı düzeyinin öne çıktığı ve %15 düzeyindeki ek kazanımın sınırlı kaldığı bildirilmiştir. Bu bulgu, mevcut veri setindeki gibi katkı miktarı arttıkça torkun her zaman düzenli biçimde artmadığı yorumunu desteklemektedir. Bununla birlikte, iki deney setinin katkı dozları ve yakıt koşulları aynı olmadığı için bu yalnızca nitel bir karşılaştırmadır.

Deneysel sonuçlar, bor katkısının motor torku üzerindeki etkisinin hem katkı miktarına hem de motor devrine bağlı olduğunu göstermiştir. A katkısında en yüksek ortalama tork artışı %0,86 ile 7 cc ve %0,84 ile 35 cc katkı düzeylerinde elde edilirken, B katkısında en yüksek ortalama artış %1,00 ile 7 cc düzeyinde belirlenmiştir. Devir bazında incelendiğinde, her iki katkı türünde de en belirgin tork artışları 2000 d/d civarında ortaya çıkmıştır. Buna karşılık, özellikle 5000 d/d'de bazı katkı düzeylerinde katkısız benzine kıyasla tork azalmaları gözlenmiştir. Ürünler doğrudan karşılaştırıldığında B, 14 cc katkı düzeyinde A'ya göre daha yüksek ortalama tork sunarken, 21 ve 35 cc düzeylerinde A'in ortalama sonuçları sınırlı ölçüde daha yüksek bulunmuştur. Bu sonuçlar, bor katkılarının motor performansına etkisinin yalnızca katkı miktarıyla açıklanamayacağını ve optimum katkı düzeyinin motor çalışma koşulları dikkate alınarak belirlenmesi gerektiğini göstermektedir. Önceki çalışmalarda bor katkılı yağların sürtünme ve yakıt tüketimi üzerinde olumlu etkileri bildirilmiş olmakla birlikte, bu etkilerin motor tipi ve deney koşullarına bağlı olduğu vurgulanmalıdır .



Şekil 10. A yakıt katkısının farklı oranlarının devire bağlı bsfc değişimi



Şekil 11. B yakıt katkısının farklı oranlarının devire bağlı bsfc değişimi

A katkısında ortalama BSFC bakımından en iyi sonuç 28 cc oranında elde edilmiştir. 7 cc ve 14 cc oranları da birbirine yakın sonuçlar vermiştir. Buna karşılık 21 cc oranında ortalama BSFC katkısız benzinden hafifçe yüksektir.

Bu sonuç, A katkısında katkı miktarı arttıkça BSFC'nin düzenli biçimde azalmadığını göstermektedir. Özellikle 21 cc'de 2500 ve 3000 rpm noktalarında görülen yüksek BSFC değerleri ortalamayı yükseltmiştir. 35 cc oranında ise bazı devirlerde düşük BSFC görülmesine rağmen, 28 cc'ye göre genel sonuç daha zayıftır.

A katkısı için sıralama (en düşük ortalama BSFC'den en yükseğe):

1. 28 cc — 386,16 g/kWh
2. 7 cc — 388,33 g/kWh
3. 14 cc — 390,39 g/kWh
4. 35 cc — 433,19 g/kWh
5. 21 cc — 497,10 g/kWh

28, 7 ve 14 cc sonuçlarının birbirine yakın olması nedeniyle, yalnızca bu ortalamalara bakılarak aralarındaki küçük farkların istatistiksel açıdan anlamlı olduğu söylenemez.

B katkısında en düşük ortalama BSFC 35 cc oranında elde edilmiştir. İkinci en iyi sonuç 28 cc oranındadır. Bu iki oran, özellikle orta ve yüksek motor devirlerinde düşük BSFC değerleriyle öne çıkmaktadır.

7 cc oranı da ortalama BSFC'yi düşürmüştür. 21 cc oranı genel olarak olumlu olmakla birlikte bazı devirlerde referans benzinden daha yüksek BSFC vermiştir. 14 cc oranının ortalaması ise katkısız benzine çok yakındır. Bunun temel nedenlerinden biri, 2500 rpm'de ölçülen 1174,797 g/kWh değeridir; bu nokta deney kayıtlarından doğrulanmalıdır.

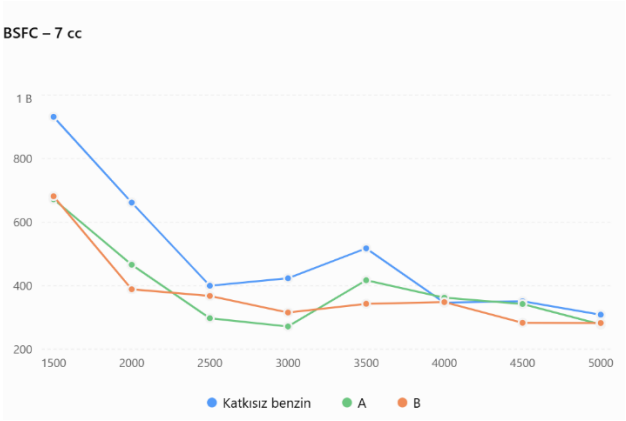
B katkısı için sıralama (en düşük ortalama BSFC'den en yükseğe):

1. 35 cc — 247,41 g/kWh
2. 28 cc — 323,29 g/kWh
3. 7 cc — 376,27 g/kWh
4. 21 cc — 402,10 g/kWh
5. 14 cc — 491,27 g/kWh

B katkısında 28 cc'den 35 cc'ye geçişte ortalama BSFC düşmeye devam etmektedir. Ancak bu eğilim, katkı miktarı daha da artırılırsa aynı şekilde devam edeceği anlamına gelmez; bunun için ilave oranların deneysel olarak incelenmesi gerekir.

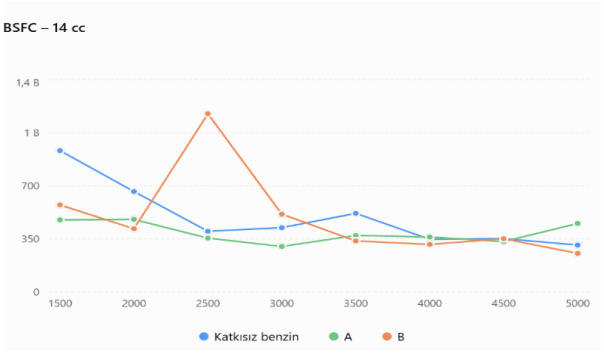
Bu bölümde A ve B katkıları aynı hacim oranında karşılaştırılmıştır. Böylece katkı miktarının etkisiyle katkı türünün etkisini birbirinden ayırmaya yönelik daha doğrudan bir değerlendirme yapılabilir.

Yüzde değişim, aynı katkı oranında A'nın ortalama BSFC değeri referans alınarak hesaplanmıştır. Devir sayımları, her bir motor devrinde A ve B'nin BSFC değerlerinin doğrudan karşılaştırılmasına dayanmaktadır.



Şekil 12. 7 cc yakıt katkısında bsfc devre bağlı değişimi

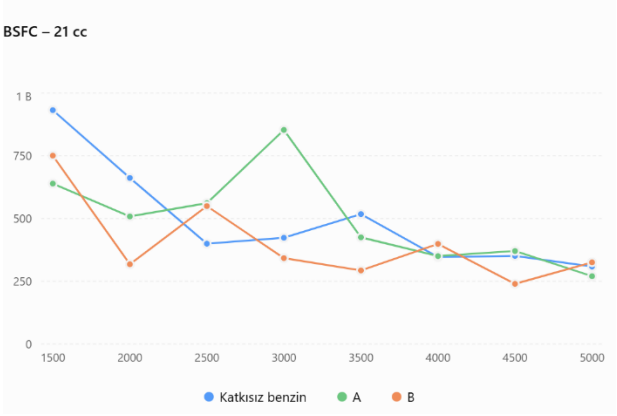
7 cc oranında B katkısının ortalama BSFC'si A'dan yalnızca %3,1 daha düşüktür. Ancak sekiz motor devrinin dördünde A, diğer dördünde B daha düşük BSFC vermiştir. Bu nedenle yalnızca ortalamaya bakarak B'nin her devirde üstün olduğunu söylemek mümkün değildir. 7 cc seviyesinde iki katkının performansları genel olarak birbirine yakındır.



Şekil 13. 14 cc yakıt katkısında bsfc devre bağlı değişimi

14 cc oranında A'nın ortalama BSFC'si B'den daha düşüktür. Ancak B katkısının 2500 rpm'deki 1174,797 g/kWh değeri ortalamayı belirgin biçimde yükseltmektedir. Sekiz devirde A ve B dörder kez daha düşük BSFC vermiştir.

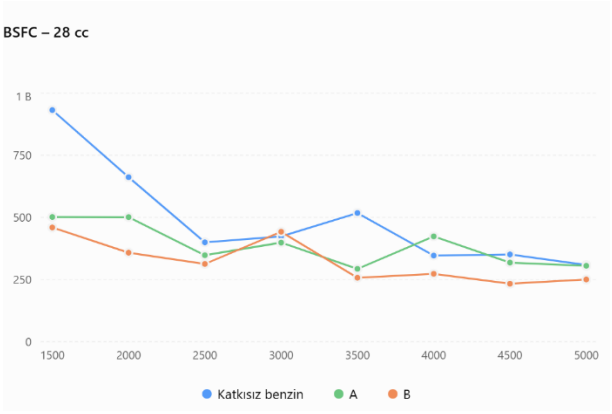
Bu nedenle 14 cc için A katkısının kesin olarak üstün olduğu sonucuna varmadan önce B–14 cc, 2500 rpm ölçümü doğrulanmalıdır. Bu ölçüm hatalıysa ortalama karşılaştırma önemli ölçüde değişebilir.



Şekil 14. 21 cc yakıt katkısında bsfc devre bağlı değişimi

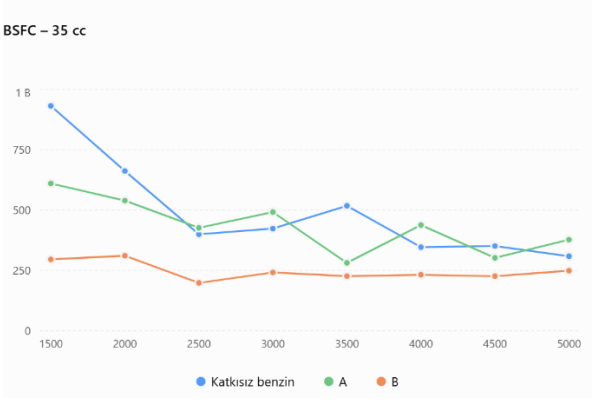
21 cc oranında B'nin ortalama BSFC'si A'dan %19,1 daha düşüktür. B katkısı sekiz devir noktasının beşinde daha düşük BSFC vermiştir. A katkısında özellikle 3000 rpm'deki 852,721 g/kWh değeri, A'nın ortalamasını yükseltmektedir.

Bu sonuç, 21 cc oranında B katkısının mevcut veriler temelinde daha avantajlı olduğunu göstermektedir; ancak devir bazındaki farklılıklar nedeniyle üstünlük bütün çalışma aralığı için aynı düzeyde değildir.



Şekil 15. 28 cc yakıt katkısında bsfc devre bağlı değişimi

28 cc oranında B'nin ortalama BSFC'si A'dan %16,3 daha düşüktür. Ayrıca B, sekiz motor devrinin yedisinde A'dan daha düşük BSFC vermiştir. Bu, 28 cc seviyesinde yalnızca ortalama bakımından değil, devirler boyunca da B lehine daha tutarlı bir sonuç bulunduğunu göstermektedir.



Şekil 16. 35 cc yakıt katkısında bsfc devre bağlı değişimi

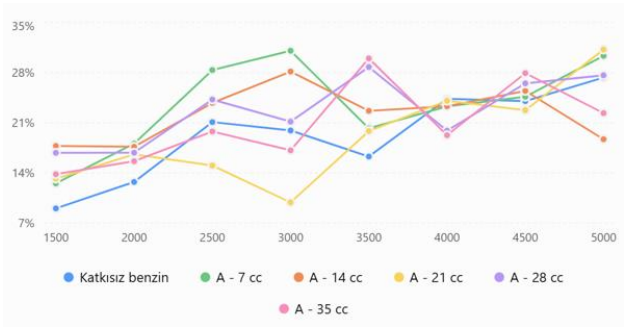
35 cc oranında B'nin ortalama BSFC'si 247,41 g/kWh, A'nınki ise 433,19 g/kWh'dir. B katkısının BSFC'si sekiz motor devrinin tamamında A katkısından düşüktür. İki katkı arasındaki ortalama fark yaklaşık %42,9'dur.

Bu veri setindeki en güçlü A–B farkı 35 cc oranında görülmektedir. Bununla birlikte, farkın büyüklüğü nedeniyle özellikle yakıt debisi, fren gücü hesapları ve ölçüm belirsizliği kontrol edilmeli; sonuç tekrarlı deneylerle desteklenmelidir.

Sonuçlar iki farklı eğilim ortaya koymaktadır:

- A katkısında: En düşük ortalama BSFC 28 cc'de elde edilmiştir. 7 ve 14 cc oranları da benzer sonuçlar vermiştir. Daha yüksek katkı miktarı her zaman daha düşük BSFC sağlamamıştır.
- B katkısında: 28 cc ve özellikle 35 cc oranları öne çıkmıştır. B–35 cc, hem en düşük ortalama BSFC'yi vermiş hem de sekiz motor devrinin tamamında katkısız benzinden daha düşük sonuç göstermiştir.
- A–B karşılaştırmasında: 7 cc'de sonuçlar yakın; 14 cc'de B'nin bir ölçümü nedeniyle karşılaştırma belirsiz; 21, 28 ve 35 cc'de ise B'nin ortalama BSFC'si daha düşüktür. En büyük fark 35 cc'de görülmektedir.

Ortalama, sekiz motor devrinde hesaplanan termal verim değerlerinin aritmetik ortalamasıdır. “Yüzde puan” farkı, iki verim yüzdesinin doğrudan çıkarılmasıyla bulunmuştur.

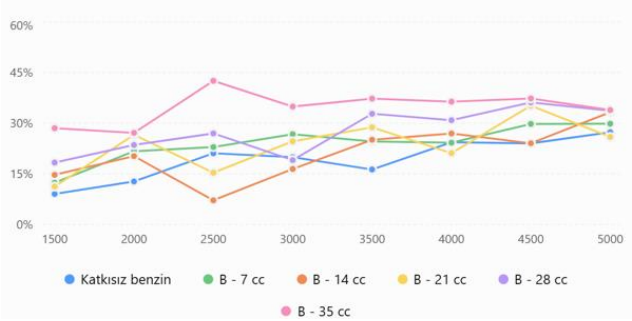


Şekil 17. A yakıt katkısının farklı oranlarının devire bağlı termal verim değişimi

A katkısında en yüksek ortalama termal verim 7 cc oranında (%23,56) elde edilmiştir. 28 cc (%22,73) ve 14 cc (%22,18) oranları bunu takip etmektedir.

- 7 cc: Ortalama termal verim açısından en iyi A oranıdır. Özellikle 2500 ve 3000 rpm'de sırasıyla %28,35 ve %31,04 değerlerine ulaşmıştır. Ancak 4000 rpm'de verim %23,28'e gerileyerek katkısız benzinin %24,34 değerinin altında kalmıştır.
- 14 cc: 1500–3500 rpm aralığında genel olarak katkısız benzinden yüksek verim görülmektedir. 3000 rpm'de %28,14 olan verim, 5000 rpm'de %18,70'e düşmektedir. Dolayısıyla olumlu etki bütün devirlerde devam etmemektedir.
- 21 cc: Ortalama termal verim %19,07 ile katkısız benzinin %19,35 değerinin biraz altındadır. Özellikle 3000 rpm'de %9,89'a düşmesi ortalamayı olumsuz etkilemektedir. Buna karşılık 5000 rpm'de %31,21 ile A grubundaki en yüksek devir noktası sonuçlarından biri elde edilmiştir.
- 28 cc: Ortalama %22,73 ile ikinci sıradadır. 3500 rpm'de %28,77'ye ulaşırken 4000 rpm'de %19,90'a düşmektedir. Bu durum, katkının etkisinin motor devrine bağlı olduğunu göstermektedir.
- 35 cc: Ortalama verim %20,73'tür. 3500 rpm'de %29,97'ye ulaşmasına karşın 3000 ve 4000 rpm'de sırasıyla %17,15 ve %19,26 değerleri görülmektedir.

A katkısı için genel yorum: 7 cc, bu veri setinde ortalama termal verim açısından en avantajlı orandır. Katkı miktarının 7 cc'den 35 cc'ye artırılması, termal verimi sürekli yükseltmemiştir. Özellikle 21 cc oranındaki düşük ortalama, katkı miktarı ile verim arasında doğrusal bir ilişki bulunmadığını göstermektedir.



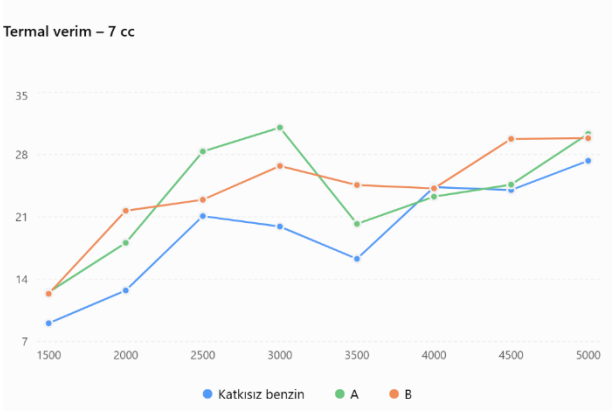
Şekil 18. B yakıt katkısının farklı oranlarının devire bağlı termal verim değişimi

B katkısında en yüksek ortalama termal verim 35 cc oranında (%34,73) elde edilmiştir. 28 cc oranı %27,67 ile ikinci sıradadır. Bu iki oran, diğer B katkı seviyelerinden belirgin biçimde daha yüksek ortalamalar vermiştir.

- 7 cc: Ortalama %24,02'dir. Özellikle 4500 ve 5000 rpm'de %29,77 ve %29,84 değerleri elde edilmiştir. Buna karşılık 1500 rpm'de verim %12,37'dir.
- 14 cc: Ortalama %20,99'dur; ancak 2500 rpm'de termal verim %7,18'e kadar düşmektedir. Bu nokta, BSFC'nin 1174,797 g/kWh olduğu ölçümle aynı noktadır ve deney kayıtlarından doğrulanmalıdır.
- 21 cc: Ortalama %23,59'dur. 4500 rpm'de %35,17 ile yüksek bir değer görülürken 1500 rpm'de %11,24 ve 4000 rpm'de %21,13 elde edilmiştir.

- 28 cc: Ortalama %27,67'dir. 3500–5000 rpm aralığında verim %30,88–36,13 civarına ulaşmaktadır; 3000 rpm'deki %19,07 değeri bu genel eğilimin dışındadır.
- 35 cc: Ortalama %34,73 ile en yüksek sonucu vermektedir. Sekiz devir noktasının tamamında hesaplanan termal verim katkısız benzinin aynı devirdeki değerinden yüksektir. En yüksek değer 2500 rpm'de %42,52'dir.

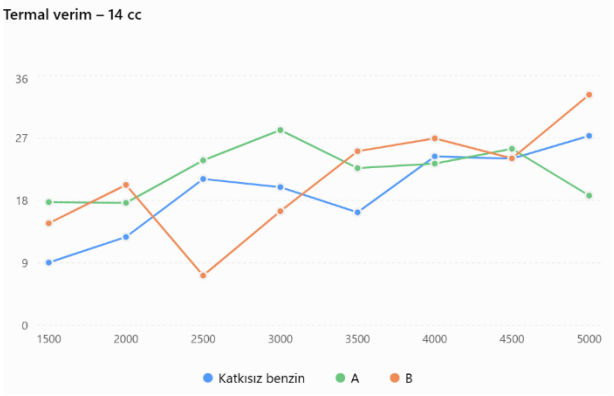
B katkısı için genel yorum: Veriler, özellikle 28 ve 35 cc oranlarında daha yüksek termal verim eğilimi göstermektedir. 35 cc oranı ortalama bakımından açık biçimde öne çıkmaktadır. Ancak %42,52 gibi yüksek bir nokta ve ortalamadaki büyük fark, ölçüm doğrulaması ve belirsizlik analiziyle desteklenmelidir.



Şekil 19. 7 cc yakıt katkısında termal verimin devre bağlı değişimi

B katkısının ortalama termal verimi %24,02, A katkısının ise %23,56'dır. Aradaki fark yalnızca 0,46 yüzde puandır. Ayrıca dört motor devrinde A, diğer dört devirde B daha yüksek verim vermiştir.

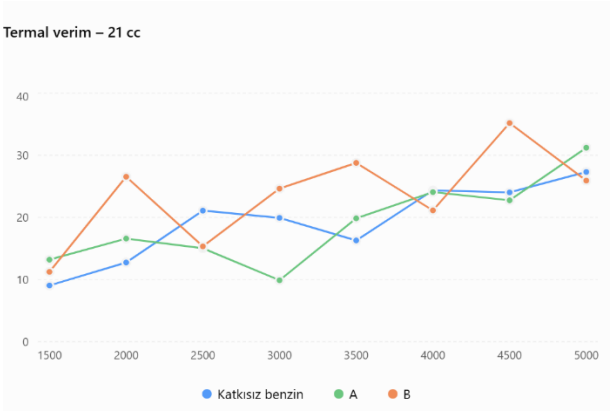
Bu nedenle 7 cc oranında iki katkının ortalama sonuçları birbirine yakındır. Mevcut veriler, B'nin bütün motor devirlerinde belirgin biçimde üstün olduğunu göstermemektedir.



Şekil 20. 14 cc yakıt katkısında termal verimin devre bağlı değişimi

A katkısının ortalama verimi %22,18, B katkısının %20,99'dur. Ancak bu farkın yorumlanmasında B–14 cc'nin 2500 rpm'deki %7,18 termal verim değeri önemlidir. Bu nokta, 1174,797 g/kWh BSFC ölçümünden hesaplanmıştır.

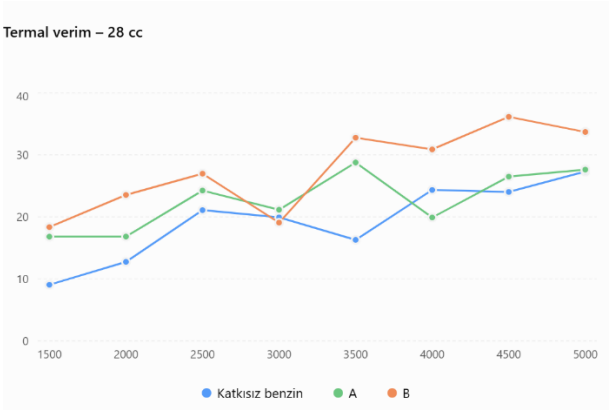
A ve B'nin aynı oranındaki sonuçları dört devirde A, dört devirde B lehinedir. Dolayısıyla A'nın ortalama üstünlüğü, bütün devirlerde daha iyi sonuç verdiği anlamına gelmez. Özellikle B–14 cc'nin 2500 rpm ölçümü doğrulanmadan kesin bir katkı türü üstünlüğü ileri sürülmemelidir.



Şekil 21. 21 cc yakıt katkısında termal verimin devre bağlı değişimi

B katkısının ortalama termal verimi %23,59 iken A katkısında %19,07'dir. B lehine fark 4,52 yüzde puandır. Ayrıca B, sekiz motor devrinin beşinde daha yüksek termal verim vermiştir.

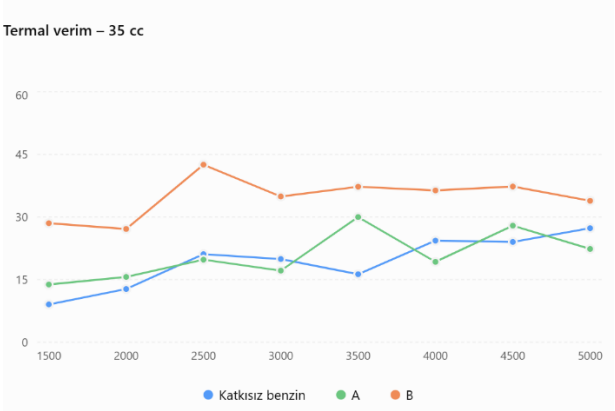
Bu sonuç, 21 cc oranında B katkısının mevcut veri setinde daha avantajlı olduğunu düşündürmektedir. Bununla birlikte 2500 rpm'de A ve B sonuçlarının birbirine yakın olması ve bazı devirlerde sıralamanın değişmesi, katkı etkisinin motor devrine bağlı olduğunu göstermektedir.



Şekil 22. 28 cc yakıt katkısında termal verimin devre bağlı değişimi

B katkısının ortalama termal verimi %27,67, A katkısının %22,73'tür. B lehine fark 4,94 yüzde puandır. B katkısı sekiz motor devrinin yedisinde daha yüksek termal verim sağlamıştır.

Bu oran, A ve B karşılaştırmasında B'nin daha tutarlı biçimde öne çıktığı seviyelerden biridir. Özellikle 3500–5000 rpm aralığında B katkısının yüksek verim değerleri dikkat çekmektedir. Ancak 3000 rpm'de A'nın %21,15 değeri, B'nin %19,07 değerinden yüksektir.



Şekil 23. 35 cc yakıt katkısında termal verimin devre bağlı değişimi

B katkısının ortalama termal verimi %34,73, A katkısının ise %20,73'tür. Aradaki fark 14,00 yüzde puandır. B katkısı sekiz motor devrinin tamamında A katkısından daha yüksek hesaplanan termal verim vermiştir.

B–35 cc'de 2500 rpm'de %42,52, A–35 cc'de ise aynı devirde %19,78 elde edilmiştir. Bu, veri setindeki en belirgin A–B farklarından biridir. Ancak bu büyüklükte bir fark, yayınlanmadan önce özellikle yakıt tüketimi ve fren gücü ölçümlerinin doğrulanmasını, deneylerin tekrarlanmasını ve ölçüm belirsizliğinin raporlanmasını gerektirir.

A katkısı

7 cc

En yüksek ortalama termal verim: %23,56

28 cc (%22,73) ve 14 cc (%22,18) sonraki sıralardadır.

B katkısı

35 cc

En yüksek ortalama termal verim: %34,73

28 cc (%27,67) ikinci sıradadır. 35 cc, bütün devirlerde A–35 cc'den daha yüksek sonuç vermiştir.

Bulgular, A katkısında en yüksek ortalama termal verimin 7 cc'de, B katkısında ise 35 cc'de elde edildiğini göstermektedir. Aynı katkı oranında karşılaştırıldığında B katkısı 7, 21, 28 ve 35 cc seviyelerinde daha yüksek ortalama termal verim verirken, 14 cc seviyesinde A daha yüksek ortalama vermiştir. B'nin avantajı özellikle 28 ve 35 cc oranlarında belirginleşmektedir.

Bununla birlikte, termal verim hesabında kullanılan alt ısıl değer tüm koşullarda 42,7 MJ/kg kabul edilmiştir. Gerçek yakıt veya katkılı karışımların alt ısıl değerleri farklıysa bu varsayım, hesaplanan termal verim karşılaştırmasını etkileyebilir. Fren termal verimi yakıtın alt ısıl

değeri, kütlesel tüketimi ve fren gücüyle ilişkilidir; farklı yakıtların karşılaştırılmasında her yakıtın uygun alt ısıl değerinin kullanılması gerekir.

Bu nedenle mevcut sonuçlar hesaplanan termal verim bakımından B–35 cc ve B–28 cc oranlarının öne çıktığını göstermektedir; ancak kesin bir fiziksel verim artışı iddiası için yakıtların alt ısıl değerlerinin doğrulanması, tekrarlı ölçümler ve istatistiksel analiz gereklidir.

5. SONUÇLAR

Bu çalışmada, iki farklı ticari bor esaslı yakıt katkısının benzinli motor performansına etkileri, farklı katkı miktarları ve motor devirleri için deneysel olarak incelenmiştir. Elde edilen sonuçlardan aşağıdaki çıkarımlar yapılmıştır:

1. **Tork sonuçları:** A katkısında en yüksek ortalama tork artışı 7 cc oranında %0,86, B katkısında ise yine 7 cc oranında %1,00 olarak belirlenmiştir. Aynı katkı miktarlarında yapılan karşılaştırmada B katkısı 14 cc seviyesinde A katkısına göre ortalama %1,78 daha yüksek tork sağlamıştır. Buna karşılık 21 ve 35 cc seviyelerinde A katkısının ortalama torku sınırlı ölçüde daha yüksek bulunmuştur. Genel olarak tork değişimlerinin katkı miktarıyla doğrusal bir ilişki göstermediği belirlenmiştir.
2. **Fren özgül yakıt tüketimi:** Katkısız benzinde ortalama BSFC 492,48 g/kWh olarak hesaplanmıştır. A katkısında en düşük ortalama BSFC 28 cc seviyesinde 386,16 g/kWh ile elde edilmiş ve referans benzine göre %21,6 azalma görülmüştür. B katkısında en düşük ortalama BSFC 35 cc seviyesinde 247,41 g/kWh olarak hesaplanmış; bu değer referans benzine göre %49,8 azalmaya karşılık gelmiştir. B katkısının 28 ve 35 cc seviyeleri, mevcut veri setinde yakıt tüketimi bakımından öne çıkmıştır.
3. **Termal verim:** Katkısız benzin için ortalama hesaplanan termal verim %19,35'tir. A katkısında en yüksek ortalama değer 7 cc seviyesinde %23,56, B katkısında ise 35 cc seviyesinde %34,73 olarak bulunmuştur. B katkısının 28 cc seviyesinde ortalama termal verim %27,67'dir. Aynı katkı miktarlarında yapılan karşılaştırmada B katkısı, 7, 21, 28 ve 35 cc seviyelerinde A katkısından daha yüksek ortalama hesaplanan termal verim vermiştir. En belirgin fark 35 cc seviyesinde görülmüştür.
4. **Katkı türü ve miktarının etkisi:** Sonuçlar, iki ticari katkının aynı hacim oranında kullanılması durumunda dahi benzer sonuçlar vermediğini göstermiştir. A katkısında 7 cc tork ve termal verim bakımından, 28 cc ise BSFC bakımından öne çıkmıştır. B katkısında ise 35 cc, BSFC ve hesaplanan termal verim açısından en avantajlı sonuçları vermiştir.

Sonuç olarak, mevcut deney verileri B katkısının özellikle 28 ve 35 cc seviyelerinde BSFC ve hesaplanan termal verim bakımından daha avantajlı sonuçlar verdiğini göstermektedir. Bununla birlikte, termal verim hesaplamasında bütün yakıtlar için aynı 42,7 MJ/kg alt ısıl değerinin kullanılması nedeniyle bu bulgular, yakıtların gerçek enerji verimliliğindeki artışın kesin kanıtı olarak değerlendirilmemelidir. Nihai sonuçların doğrulanması için yakıt özelliklerinin belirlenmesi, ölçümlerin tekrarlanması ve istatistiksel belirsizliklerin raporlanması gerekmektedir.

Kaynakça

Akbıyık, T., Kahraman, N., & Taner, T. (2022). Investigation of the effect of boron additive to lubricating oil on engine performance, exhaust, and emissions. Fuel, 312, 122931. https://doi.org/10.1016/j.fuel.2021.122931

Akbıyık, T., Kahraman, N., Taner, T., (2023) Performance emission, energy and exergy analysis evaluation of gasoline engine using different fuels, Fuel, https://doi.org/10.1016/j.fuel.2023.128189

Akbıyık, T. (2026). Investigating the effect of adding different concentrations of boron to the engine oil of a gasoline engine using bioethanol blends on engine performance. Journal of Thermal Analysis and Calorimetry. https://doi.org/10.1007/s10973-026-16182-z

Çakmak, A., & Özcan, H. (2022). Bor oksit nanoparçacıklarının dizel yakıt katkısı olarak kullanılabilirliğinin araştırılması. Journal of Boron, 7(1), 420–429. https://doi.org/10.30728/boron.1021667

Gotewala, S., Kumar, S. S., Saha, T., Balaji, G., Nandagopalan, P., & Kannan, B. T. (2026). Effect of boron nanoparticles on water-in-diesel emulsion as fuel for CI engine performance and emission characteristics. International Journal of Ambient Energy, 47(1). https://doi.org/10.1080/01430750.2026.2661832

Karataş, Ö., & Yüksel, T. (2023). Experimental investigation of the effects of boron oil additive in internal combustion engine. Fuel, 353, 129234. https://doi.org/10.1016/j.fuel.2023.129234

Sertkaya, A. A., & Akbıyık, T. (2016). Operate With a Gasoline Internal Combustion Engine Evaluation of Different Boron Addition of The Fuel Additive Inside Performance and Emissions Impact. Politeknik Dergisi, 19(4), 633–640. https://izlik.org/JA78ZJ59EM

Sofuoğlu, D., Değirmenci, H., Kantaroğlu, E., & Yontar, A. A. (2026). Effects of boron-based fuel additives on sequential-ignition engine characteristics and emissions. International Journal of Ambient Energy, 47(1). https://doi.org/10.1080/01430750.2026.2730195

Yakın, A., & Gülcan, M. (2025). Effects of boron-based additives on combustion characteristics, emission reduction, and performance improvement in internal combustion engines. Journal of the Energy Institute, 120, 102044. https://doi.org/10.1016/j.joei.2025.102044

MACHINE LEARNING-BASED DEMAND FORECASTING FOR FOOD WASTE REDUCTION: A CASE STUDY

Meriçsu KARAHAN
Tarsus University, Engineering Faculty, Department of Industrial Engineering, TÜRKİYE

Şölen ZENGİN
Dr., Tarsus University, Engineering Faculty, Department of Industrial Engineering, TÜRKİYE

ABSTRACT

One of the fundamental problems faced by institutions providing mass catering services today is high food waste resulting from demand forecasts based on flawed or traditional methods. This waste leads to significant economic losses for businesses and negatively impacts environmental sustainability. In this study, a data-driven demand forecasting model based on machine learning algorithms was developed to enhance food sustainability and minimize waste for a mass catering institution. A comprehensive dataset covering 522 working days was utilized, combining the selected business's historical portion sales data with environmental and calendar variables such as day, month, season, air temperature, public holiday status, and daily menu contents. The data were processed using the WEKA open-source data mining tool, and the Random Forest, M5P, and Linear Regression algorithms were comparatively evaluated. The forecasting results of the developed model were compared with the business's actual production quantities, and the discrepancy was analyzed. The study revealed that the Random Forest algorithm achieved the highest forecasting accuracy, with values of MAE (Mean Absolute Error) = 18.6 portions, RMSE (Root Mean Square Error) = 23.7, and R^2 (Coefficient of Determination) = 0.942. Air temperature (49.5%) and holiday status (31.2%) were identified as the most decisive factors influencing demand. It has been demonstrated that integrating a machine learning-based forecasting model into daily production planning can contribute to food sustainability and significantly reduce potential portion waste.

Keywords: Demand forecasting, machine learning, random forest, service system management, food sustainability.

SUSTAINABLE RISK MANAGEMENT IN TEXTILE SECTOR: A MULTI-DIMENSIONAL FMEA APPROACH

Yağmur ÇİÇEK
Tarsus University, Engineering Faculty, Department of Industrial Engineering, TÜRKİYE

Şölen ZENGİN
Res. Asst. Dr., Tarsus University, Engineering Faculty, Department of Industrial Engineering, TÜRKİYE

ABSTRACT

By its very nature, the textile industry is a resource-intensive manufacturing sector. When factors such as water and energy consumption, chemical waste generation, and raw material losses are considered, the sector appears to carry significant sustainability risks. A review of the existing literature reveals that these risks have generally been investigated in a fragmented manner. This study evaluates sustainability risks in textile production processes across environmental, operational, and social dimensions using the Failure Mode and Effects Analysis (FMEA) method. Based on expert opinions and process analysis, 22 failure modes were identified. The environmental dimension encompasses water consumption, energy use, and chemical waste; the economic dimension covers production losses, scrap/waste, and machine downtime; and the social dimension includes workplace accidents, dust exposure, and ergonomic risks. A Risk Priority Number (RPN) was calculated for each risk by scoring criteria related to the probability of occurrence, severity, and detectability. An analysis of the results shows that the RPN values are distributed across a wide range, with eight of the identified risks classified as high priority. Chemical wastewater discharge, excessive water consumption in the dyehouse, and chemical exposure in the finishing department emerged as the three most critical risks. Regarding the distribution across dimensions, environmental risks stand out prominently. The study concludes by offering concrete recommendations to enhance sustainable production, particularly addressing the high-priority risks. The findings provide a guiding priority map for enterprises and aim to contribute to the development of safer, more environmentally friendly production conditions within the sector.

Keywords: Risk management, production systems management, sustainable supply chain management, ergonomics and human factors management, failure mode and effects analysis (FMEA).

EKONOMİK GÖSTERGELER VE TAŞINMAZ PİYASASI ARASINDAKİ İLİŞKİNİN AMPİRİK BİR İNCELENMESİ

AN EMPIRICAL EXAMINATION OF THE RELATIONSHIP BETWEEN ECONOMIC INDICATORS AND THE REAL ESTATE MARKET

Şükran YALPIR

Dr., Konya Technical University, Faculty of Engineering and Natural Sciences, Department of Geomatics Engineering

ORCID ID: 0000-0003-2998-3197

ÖZET

Taşınmaz işlemleri, ekonomik büyüme, gelir dağılımı, kentleşme dinamikleri ve sosyal refah üzerinde çok yönlü etkiler yaratan temel bir piyasa bileşenidir. Özellikle gelişmekte olan ülkelerde, taşınmaz piyasasındaki faaliyet, makroekonomik göstergelerle doğrudan ve dolaylı ilişkiler kurarak ekonomik yapının önemli bir belirleyicisi haline gelmektedir. Bu bağlamda, taşınmaz piyasasının dinamiklerinin analizi, hem ekonomik istikrarın değerlendirilmesi hem de sürdürülebilir kentleşme politikalarının geliştirilmesi açısından kritik öneme sahiptir.

Bu çalışma, taşınmaz işlem aktivitesi ile temel ekonomik göstergeler arasındaki ilişkiyi ortaya koymayı amaçlamaktadır. Çalışmada; kişi başına gayri safi yurtiçi hasıla, enflasyon oranı, döviz kuru, konut fiyat endeksi ve nüfus artışı gibi makroekonomik değişkenler ile taşınmaz piyasasındaki işlem hacmi arasındaki ilişkiler istatistiksel olarak analiz edilmiştir. Değişkenler arasındaki doğrusal ilişkilerin yönünü ve gücünü belirlemek için Pearson korelasyon analizi kullanılmıştır. Çalışma alanı olarak Konya ili seçilmiş ve taşınmaz piyasasının ekonomik yapı içindeki rolü bölgesel ölçekte detaylı olarak incelenmiştir. Ayrıca, taşınmaz piyasasında gözlemlenen değişikliklerin sosyal ve ekonomik sonuçları da araştırılmış ve bu değişikliklerin sürdürülebilirliği için öneriler sunulmuştur. Bu çalışma, yerel ve ulusal düzeylerde taşınmaz alım satım politikalarının şekillendirilmesine rehberlik edebilecek bulguları sunmayı amaçlamaktadır.

Anahtar Kelimeler: Taşınmaz İşlemleri, Ekonomik Göstergeler, Konut Fiyat Endeksi, Pearson Korelasyon Analizi.

ABSTRACT

Real estate transactions are a fundamental market component that creates multifaceted impacts on economic growth, income distribution, urbanization dynamics, and social welfare. Particularly in developing countries, the activity in the real estate market becomes a significant determinant of the economic structure by establishing direct and indirect relationships with macroeconomic indicators. In this context, analyzing the dynamics of the real estate market is critically important for both evaluating economic stability and developing sustainable urbanization policies.

This study aims to reveal the relationship between real estate transaction activity and key economic indicators. In this sense, the relationships between macroeconomic variables such as per capita gross domestic product, inflation rate, exchange rate, housing price index, and population growth, and the transaction volume in the real estate market have been statistically analyzed. Pearson correlation analysis was used to determine the direction and strength of linear relationships between the variables. Konya province was chosen as the study area, and the role of the real estate market within the economic structure was examined in detail on a regional scale. Furthermore, the social and economic consequences of changes observed in the real estate market were also investigated, and suggestions for the sustainability of these changes were presented. This study aims to present findings that can guide the shaping of real estate purchase and sale policies at local and national levels.

Keywords: Real Estate Transactions, Economic Indicators, Housing Price Index, Pearson Correlation Analysis.

GİRİŞ

Real estate transactions, as an important part of economic dynamics, are one of the fundamental factors shaping economic well-being and socio-economic structure, especially in developing countries and growing cities (Altıner and Korkmaz, 2023). This market appears not only as one of the financial investment instruments but also as a determinant of social structure and quality of life (Gürünlü, 2011).

The economic implications of real estate transactions are not limited only to the supply and demand relationship, but are directly linked to a number of macroeconomic variables. Factors such as per capita gross domestic product (GDP), inflation rate, exchange rate, interest rates, housing price index (HPI), population growth, and income distribution are the main economic indicators determining the activity in the real estate market (Çetin, 2021). The extent to which these indicators affect real estate transactions can be revealed through macroeconomic analyses. In Turkey, in particular, the housing sector has a significant impact on the economy. Advanced urbanization and population growth increase the demand for real estate; This demand leads to an increase in housing prices and consequently to changes in real estate transactions (Hosseinpour and Dayı, 2024).

Another important factor is the social impact of fluctuations in the real estate market. Real estate transactions affect not only the economic structure of a region but also the living standards, socioeconomic levels, and even social mobility of individuals (Karaçay and Varol, 2015). Rising housing prices can limit homeownership opportunities, particularly for middle and lower income groups, while leading higher income groups to increase their real estate investments. This can deepen income inequality and lead to social disparities.

In the specific context of real estate transactions in Konya, examining the relationship between these transactions and economic indicators is crucial for understanding the dynamics of the real estate market in the region. This study analyzes how real estate transactions in Konya relate to economic indicators and examines the effects of these factors on the real

estate market in detail. It also offers suggestions to contribute to the sustainability of the real estate market.

MATERIALS AND METHODS

This study examines various criteria to investigate the impact of economic and political factors on real estate transactions over time. These criteria include the housing price index, exchange rates (gold, euro, and dollar), CPI, GDP per capita, loan interest rates, neighborhood population, and neighborhood-specific rent index data (TCMB, 2019-2020-2023; URL1-2). Using an annual dataset covering the period 2010-2023, the short-term and long-term relationships between these criteria were investigated. Konya province was selected as the pilot region (Figure 1). The study area encompasses 269 neighborhoods with 82,868 residential plots and 30,395 buildings.

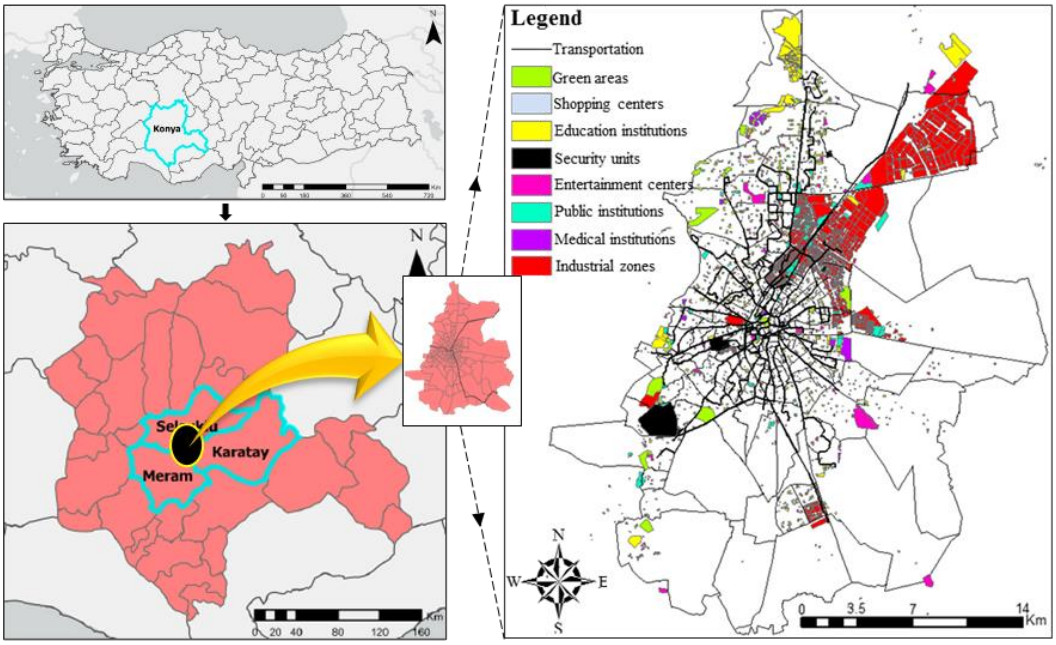


Figure 1. Illustration of the study area.

In this study, population data for the years 2010-2023 was obtained under the headings of province, district, neighborhood, and total population, due to the need for population data living in the neighborhoods of the central districts of Konya. Location information of properties bought/sold (2010-2023) was obtained using the application provided by the General Directorate of Land Registry and Cadastre (TKGM) (Figure 2).

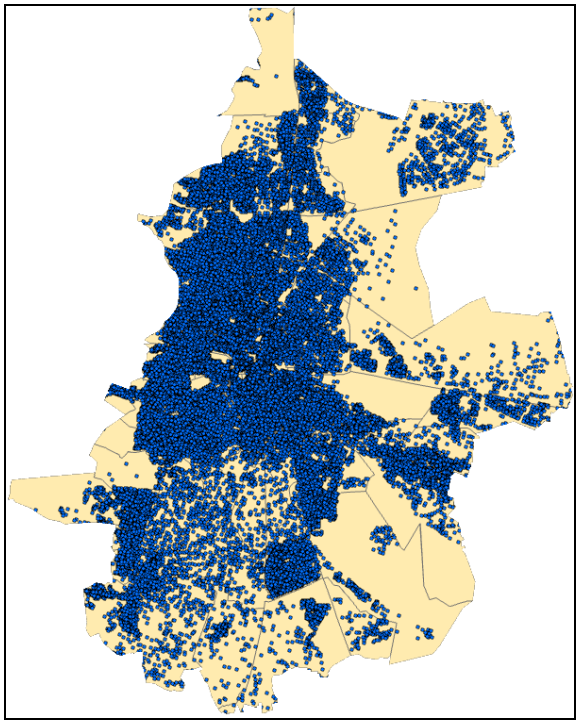


Figure 2. Locations of properties subject to buying -selling (2010-2023)

It can be said that the activity in real estate sales has shown an upward trend since 2014 (especially peaking in 2015). However, the density map shows that the activity has relatively stagnated in 2019, 2020, and 2021. Specifically, the period of high inflation exacerbated by the COVID-19 pandemic, the expansion in the construction cost index, the increase in housing sales to foreigners, and the decrease in the number of households led to the most active period and the highest price increases in recent years (TCMB, 2020). Therefore, we can state that the activity in the buying and selling of real estate has decreased in the opposite direction. These changes can be attributed to economic and political factors, as well as urban transformation projects, infrastructure investments, and changing housing demands after the pandemic. In general, increases in prominent regions in certain years are explained by urban planning and regional development dynamics (Figure 3).

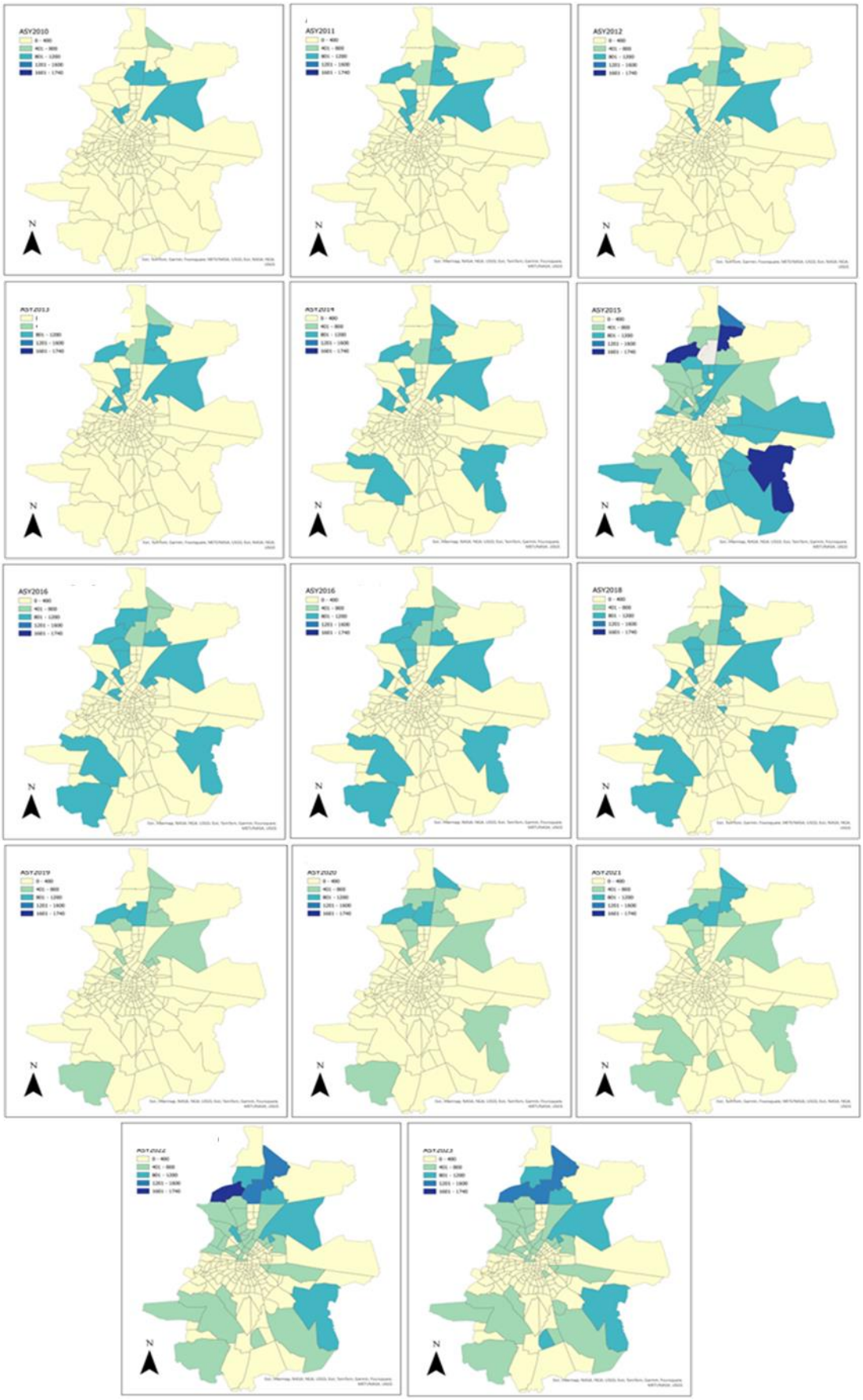


Figure 3. Real estate transaction density in neighborhoods between 2010-2023**.**

Figure 4 shows that economic indicators such as gold, the dollar, and the euro; the housing price index; and GDP have shown an upward trend from 2010 to 2023. Gold and foreign currency are assets that investors consider safe havens. Therefore, when gold and foreign currency rise, the real estate market is generally negatively affected. In this respect, after 2019, there have been significant fluctuating increases in these variables, directly impacting real estate transactions. One reason for the significant divergence in economic variables is, as mentioned earlier, the COVID-19 pandemic.

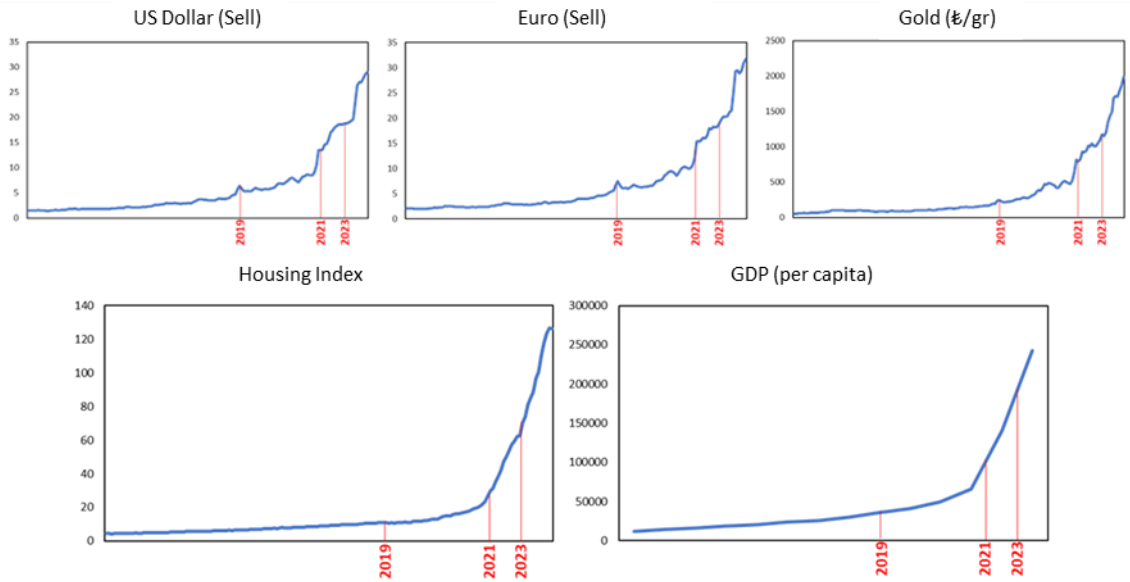


Figure 4. Increasing trend of economic indicators over time

If the Housing Price Index increases, buyers tend to wait. While some investors enter the market with the concern of "Will prices rise even further?", others may postpone their purchase decision due to high prices. On the other hand, sellers gain an advantageous position. Property owners may try to sell their properties at higher prices with the expectation of value appreciation. This means that real estate transactions become stagnant (Paksoy et al., 2014; Uğur and Bingöl, 2021). In particular, while there was a stability in the trend of the graph until 2019, a certain intensity in the buying and selling of real estate was observed here. However, since the stability in the graph was broken, a decrease in buying and selling was observed. Location information was obtained by creating a database by collecting the number of buying and selling transactions within the neighborhood on a yearly basis. Pearson Correlation Analysis was applied to the created database. Pearson correlation analysis is a statistical test to determine the strength and direction of the linear relationship between two continuous variables. The Pearson correlation coefficient (r) is calculated with the following formula (1):

$$r = \frac{\sum(X_i - \bar{X})(Y_i - \bar{Y})}{\sqrt{\sum(X_i - \bar{X})^2}\sqrt{\sum(Y_i - \bar{Y})^2}} \qquad (1)$$

Here, X_i and Y_i are the observed values of the respective variables, $\bar{X}$ and $\bar{Y}$ are the averages of the variables.

CONCLUSIONS AND RECOMMENDATIONS

The study determined that the strongest correlation between the criteria was found among gold, the dollar, and the euro, which are economic indicators crucial for the real estate market (Figure 5). This is an expected result.

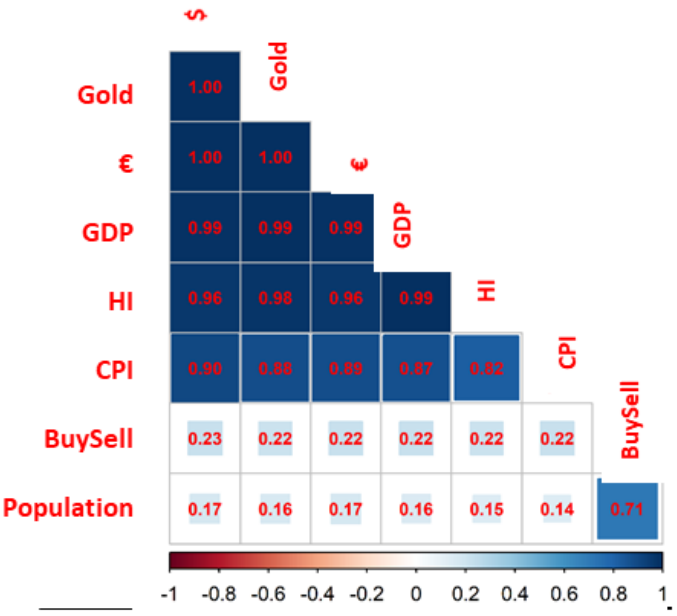


Figure 5. Pearson correlation coefficients for the criteria**.**

Because there is a linear trend between these indicators. On the other hand, a strong positive relationship (0.99) is observed between GDP and HPI. The CPI criterion was found to have strong relationships with the dollar (0.90), gold (0.88), euro (0.89), GDP (0.87), and HPI (0.82) criteria, respectively. A noteworthy point is that there is a positive relationship of 0.71 between the population and the intensity of real estate transactions. The most striking relationship is the 0.71 correlation between real estate transactions and the population. This shows that real estate transactions are quite related to the population.

The findings reveal that macroeconomic factors largely shape the dynamics of the real estate market, with inflation and exchange rates having a decisive impact on transaction volume. Fluctuations in purchasing power and volatility in financial markets affect the overall trend of real estate transactions, causing investors and households to redefine their strategies. Furthermore, population dynamics show a strong correlation with market activity, highlighting the interaction between economic well-being and real estate demand.

In conclusion, this study highlights the need for a multidimensional approach in real estate market analysis, emphasizing the integration of economic indicators with regional and global trends. As economic landscapes change, future research should delve deeper into the links between financial variables and real estate dynamics to ensure resilience and adaptability in an increasingly complex global market.

REFERENCES

Altıner, A., Korkmaz, Y. Ş., 2023, Gelişmekte olan ülkelerde ekonomik büyüme ve yurtiçi tasarruf arasındaki ilişki: ekonometrik bir uygulama, Ekonomi Maliye İşletme Dergisi, 6(1), 22-34.

Çetin, A. C., 2021, Türkiye'de konut fiyatlarına etki eden faktörlerin analizi, Mehmet Akif Ersoy Üniversitesi Uygulamalı Bilimler Dergisi, 5(1), 1-30.

Gürünlü, M., 2011, Finansal piyasaların etkinliği teorisinden davranışsal finansa: finans teorisinin evrimi, Maliye ve Finans Yazıları, 1(92), 31-50.

Hosseinpour, L., Dayı, F., 2024, Konut Talebini Etkileyen Faktörler Üzerine Teorik Bir İnceleme, Quantrade Journal of Complex Systems in Social Sciences, 6(1), 121-129.

Karaçay, H., Varol, Ç., 2015, Sosyo-ekonomik kalkınmada fiziki, beşeri ve sosyal sermaye yatırımları: Vakıflar Genel Müdürlüğü örneği, Gazi Üniversitesi İktisadi ve İdari Bilimler Fakültesi Dergisi, 17(3), 100-121.

Paksoy, S., Yöntem, T., Büyükçelebi, B., 2014, Konut Fiyat Endeksi ve Enflasyon Arasindaki İlişki (Trc1, Trc2 ve Trc3 Düzey Bölgeleri Üzerine Ampirik Bir Çalişma), Assam Uluslararası Hakemli Dergi, 1(2), 54-69.

TCMB, 2019, Yıllık faaliyet raporu 2019. 7 Mayıs 2023.

TCMB, 2020, Enflasyon raporu, 2020-II. 7 Mayıs 2023.

TCMB, 2023, Tüketici Fiyat Endeksi, Mayıs, 2023.

Uğur, A., Bingöl, N., 2021, Konut fiyat endeksi ve yatırımcı duyarlılığı ilişkisinin analizi: Türkiye üzerine ampirik bir uygulama, Uluslararası Ticaret ve Ekonomi Araştırmaları Dergisi, 5(1), 10-21.

URL1, 2024, Gayri Safi Yurt İçi Hasıla (GSYİH).

URL2, 2024, Emlak endeksi.

ERMENEK BÖLGESEL EKONOMİSİNDE MADENCİLİK FAALİYETLERİNİN ROLÜNDEKİ DEĞİŞİKLİKLERİN VE BARAJ İNŞAATININ NEDEN OLDUĞU BÖLGESEL DÖNÜŞÜMÜN EKONOMİK, SOSYAL VE ÇEVRESEL BOYUTLARININ ANALİZİ

AN ANALYSIS OF CHANGES IN THE ROLE OF MINING ACTIVITIES IN ERMENEK'S REGIONAL ECONOMY AND OF THE ECONOMIC, SOCIAL AND ENVIRONMENTAL DIMENSIONS OF REGIONAL TRANSFORMATION CAUSED BY DAM CONSTRUCTION

Handan SOYDABİRCAN
Dr., Konya Technical University, Faculty of Engineering and Natural Sciences, Department of Geomatics Engineering
ORCID ID: 0009-0008-9080-7495

Şükran YALPIR
Dr., Konya Technical University, Faculty of Engineering and Natural Sciences, Department of Geomatics Engineering
ORCID ID: 0000-0003-2998-3197

Vildan ÖNEN
Dr., Konya Technical University, Faculty of Engineering and Natural Sciences, Department of Mining Engineering
ORCID ID: 0000-0002-8139-8385

ÖZET

Bu çalışma, Karaman ili Ermenek ilçesinde meydana gelen maden kazası ve Ermenek Barajı'nın inşa edilmesiyle ortaya çıkan ekonomik, sosyal ve çevresel değişimleri bütüncül bir yaklaşımla değerlendirmeyi amaçlamaktadır. Bölgenin geleneksel ekonomik faaliyetleri arasında yer alan kömür madenciliği, istihdam ve yerel gelir kaynakları açısından önemli bir yere sahipken, Ermenek Barajı ve Hidroelektrik Santrali enerji üretimi ve bölgesel kalkınma bakımından yeni fırsatlar oluşturmuştur. Bununla birlikte, baraj gölünün oluşmasıyla bazı yerleşim alanlarının ve tarım arazilerinin etkilenmesi, yerel yaşam biçimlerinde ve arazi kullanımında değişimlere neden olmuştur. Ekonomik açıdan madencilik faaliyetlerinin büyük ölçüde kapanması; istihdam kaybı, yerel ticaretin daralması ve göç baskısı gibi sorunlarla ilişkilendirilirken, hidroelektrik enerji üretimi ve baraj gölü çevresindeki turizm faaliyetleri alternatif ekonomik olanaklar sunmaktadır. Sosyal açıdan zorunlu yer değiştirme, geçim kaynaklarının dönüşümü ve toplumsal ilişkilerdeki değişimler önem taşımaktadır. Çevresel açıdan ise barajın enerji üretimi yoluyla fosil yakıt kullanımına bağlı emisyonların azaltılmasına katkı potansiyeli bulunmakla birlikte, su altında kalan alanlar, doğal habitatlar ve akarsu ekosistemi üzerindeki etkiler de dikkate alınmalıdır. Sonuç olarak çalışmada, Ermenek örneği, enerji yatırımlarının ve madencilikteki dönüşümün bölgesel kalkınma üzerindeki etkilerinin yalnızca enerji üretimi üzerinden değil; istihdam, toplumsal refah,

çevresel sürdürülebilirlik ve yerel halkın yaşam koşulları birlikte değerlendirilerek ele alınması gerektiğini ortaya koymaktadır. Çalışmada, 2014'teki maden faciası sonrasında ortaya çıkan istihdam kayıpları, barajın yarattığı mikroklimatik değişimler ve nüfus hareketleri ele alınmıştır. Bulgular, madenlerin kapanmasının kırsaldan ilçe merkezine göçü hızlandırdığını; barajın ise kış soğuklarını hafifleterek tarımsal yapıda dönüşüm yarattığını ortaya koymaktadır.

Anahtar Kelimeler: Ermenek Barajı, maden kazası, bölgesel kalkınma, göç, çevresel sürdürülebilirlik.

ABSTRACT

This study aims to assess, through a holistic approach, the economic, social and environmental changes arising from the mining accident in the Ermenek district of Karaman Province and the construction of the Ermenek Dam. While coal mining, one of the region's traditional economic activities, has played an important role in employment and local sources of income, the Ermenek Dam and Hydroelectric Power Plant have created new opportunities for energy generation and regional development. However, the formation of the reservoir has affected some settlements and agricultural land, leading to changes in local ways of life and land use. From an economic perspective, the widespread cessation of mining activities is associated with problems such as employment losses, a contraction in local trade and migration pressure, while hydroelectric power generation and tourism activities around the reservoir offer alternative economic opportunities. From a social perspective, forced displacement, the transformation of livelihoods and changes in social relations are significant. From an environmental perspective, although the dam has the potential to help reduce emissions associated with fossil fuel use through energy generation, its impacts on submerged areas, natural habitats and the river ecosystem must also be considered. In conclusion, the study's examination of Ermenek demonstrates that the effects of energy investments and the transformation of mining on regional development should be assessed by considering employment, social welfare, environmental sustainability and the living conditions of local residents together, rather than energy generation alone. The study examines employment losses following the 2014 mining disaster, microclimatic changes caused by the dam and population movements. The findings reveal that mine closures accelerated migration from rural areas to the district centre, while the dam moderated winter cold and transformed the agricultural structure.

Keywords: Ermenek Dam, mining accident, regional development, migration, environmental sustainability.

INTRODUCTION

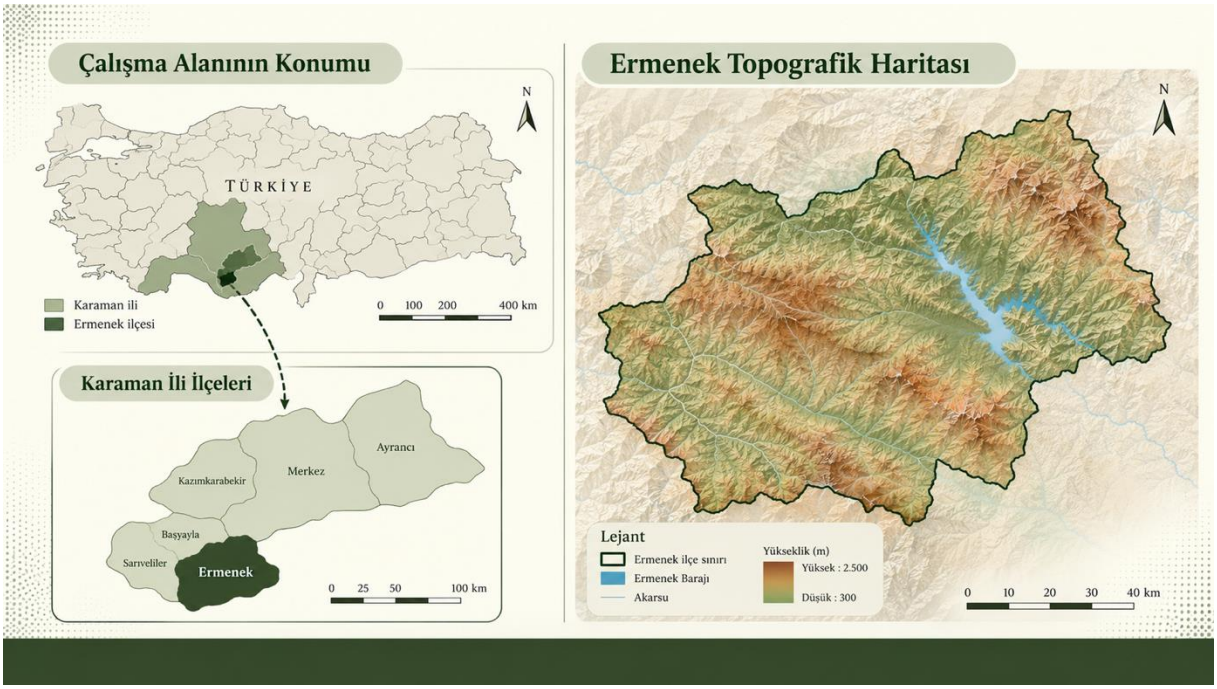
Over the past two decades, the district of Ermenek has undergone a process of radical change in both industrial and hydrographic terms. The data obtained in this study show that the 2014 mining disaster was not merely an occupational accident, but an "economic turning point" for

the region. The loss of income experienced by approximately 1,000 households following the mine closures accelerated migration from rural areas to the district centre and to other provinces.

Meanwhile, the microclimatic effect of the Ermenek Dam is redefining the region's agricultural identity. The "rise in the thermal baseline" observed in temperature data and the decrease in the number of frost days have enabled the cultivation of high-value-added crops such as olives and strawberries. However, an examination of land-use data reveals a reduction of more than 100 km² in agricultural land. This demonstrates that traditional agriculture has been abandoned, but that the transition to modern fruit cultivation has not yet fully filled this gap.

The aim of this study is to examine the social, economic and agricultural dimensions of the changes arising from declining employment in coal mining and the commissioning of the Ermenek Dam in the Ermenek district of Karaman Province.

MATERIALS AND METHODS



Built on the Ermenek River, a tributary of the Göksu, the Ermenek Dam has a body volume of 272,000 cubic hectometres and a height of 210 m above the riverbed. At the normal water level, the reservoir has a volume of 4,582.00 cubic hectometres and a surface area of 55.74 km². It is Türkiye's fourth-largest reservoir (Ermenek Kaymakamlığı, n.d.). A chronological examination of the radical spatial transformation in regional land cover following the construction of the Ermenek Dam shows that, while a riverine regime still prevailed on the valley floor in 2009, the valley rapidly became a reservoir in 2010 after impoundment began on 10 August 2009 (Devlet Su İşleri Genel Müdürlüğü, 2024). In 2012 and 2015, the water level reached the maximum operating level and stabilised. By 2020, this extensive water surface, covering approximately 58 km², had retained its boundaries over the intervening

years and had become an irreversible, permanent feature of the region's geography (Figure 1a).

The Ermenek basin has historically been a strategic region distinguished by its mineral resources. Surveys conducted by the General Directorate of Mineral Research and Exploration (MTA) have revealed that lignite reserves exceed 100 million tonnes (MTA, n.d.). Mining activities in the region came to a tragic halt following the mining accident in 2014. According to official reports, approximately 12,000 m³ of water that had accumulated in an old gallery suddenly flooded the active workings, submerging a 600–700 m gallery within seconds; rescue operations lasted 38 days (Karaman Valiliği, 2014), and 18 miners lost their lives. Following the disaster, all operations were suspended and a rigorous inspection process began (Karaman Valiliği, 2015). At present, Özkar Madencilik (Özkar-2) and Cenne Linyit Kömür İşletmeleri, which holds the region's largest reserve field, continue production. Ermenek Fetih, Özteksan and Özakpınar also remain active (Figure 1b)

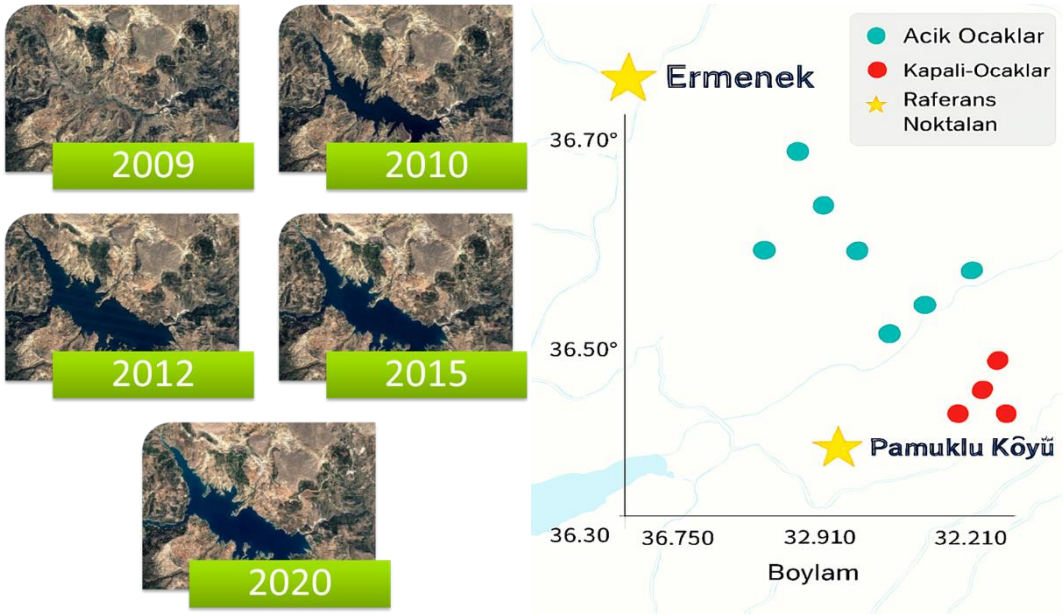


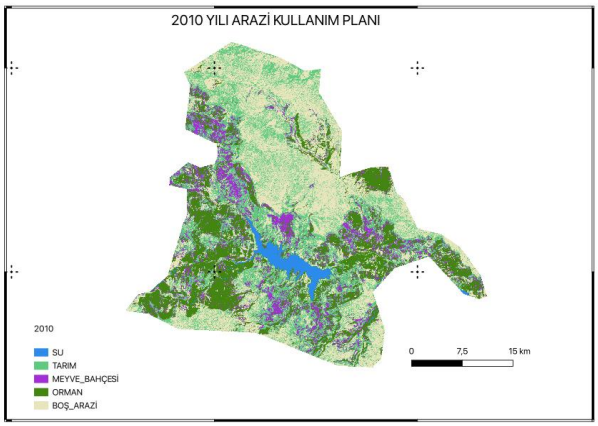
Figure 1. Changes in the Ermenek Dam and Reservoir Area over Time (a), Mines Located in Ermenek (b). Source: Google Earth imagery (a) (Google, n.d.); prepared by the author (b).

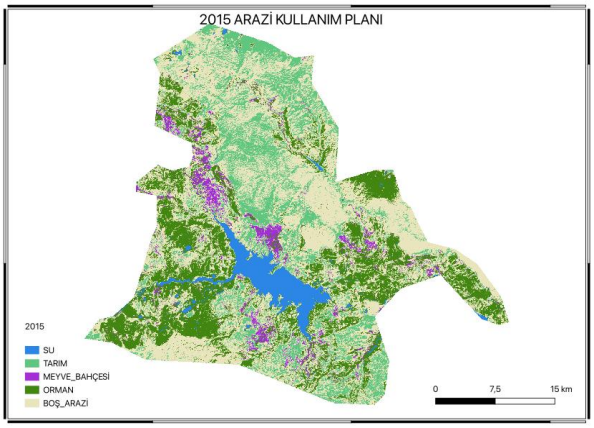
CHANGES IN CLIMATE, POPULATION AND AGRICULTURAL STRUCTURE IN THE ERMENEK REGION OVER TIME

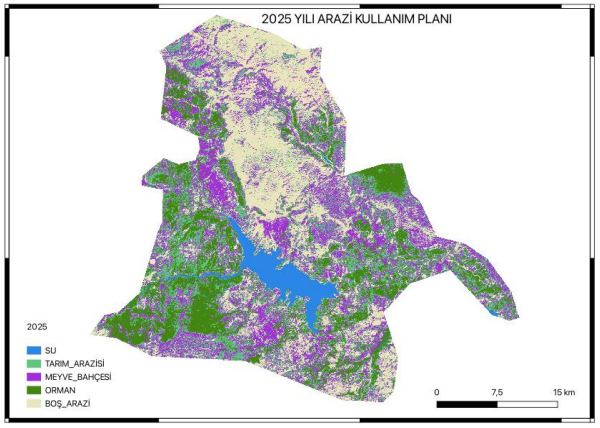
Across Türkiye, the annual mean temperature was recorded as 13.6 °C for the 2003–2013 period, rising to 14.4 °C in the 2014–2024 period (Meteoroloji Genel Müdürlüğü, n.d.). This increase of 0.8 °C corroborates the Mediterranean Basin's sensitivity to climate change. This statistical deviation serves as the principal reference point for microclimatic changes in Karaman and its surroundings, which constitute the study area.

Data obtained from stations within the study area and supplied to the author by the Turkish State Meteorological Service (MGM) via email show that the warming trend is distributed

heterogeneously depending on topographic and hydrographic variables: Ermenek District: Unlike those in the neighbouring district of Hadim, temperature trends in Ermenek remain closer to, and at times above, the national average. The microclimatic modification induced by the extensive body of water created by the Ermenek Dam is the principal determinant of this phenomenon. Owing to its specific heat capacity, the reservoir increases humidity in the surrounding area and alters the radiation balance, particularly by limiting nocturnal radiative cooling. This causes an artificially accelerated rise in annual mean temperatures.

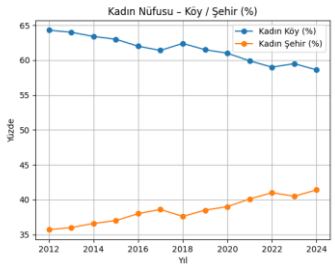


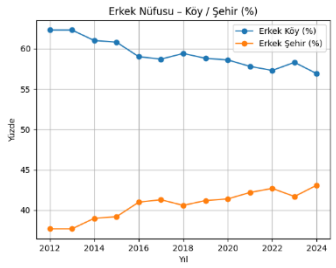


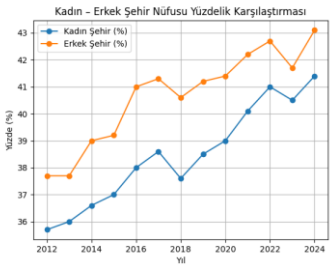


Class	2010	2015	2025	2010→2025 Change (km^2)
Water	31.68	58.44	52.03	+20.35
Farm_ Land	397.47	411.08	295.12	-102.35
Fruit_ Orchard	28.63	70.68	327.62	+298.99
Forest	338.82	92.41	216.42	-122.40
Open_Land	450.46	614.40	355.85	-94.61

Figure 2. Effects of the Dam on Land Use. Source: Calculated and prepared by the author.







Year	Total Population	Annual Change	% Change
2012	30,057	-	-
2013	30,064	7	0,02%
2014	29,957	-107	-0,36%
2015	29,558	-399	-1,33%
2016	29,475	-83	-0,28%
2017	28,903	-572	-1,94%
2018	28,832	-71	-0,25%
2019	28,565	-267	-0,93%
2020	28,417	-148	-0,52%
2021	27,843	-574	-2,02%
2022	27.776	-67	-0,24%
2023	28.103	+327	+1.18%
2024	27.988	-115	-0.41%

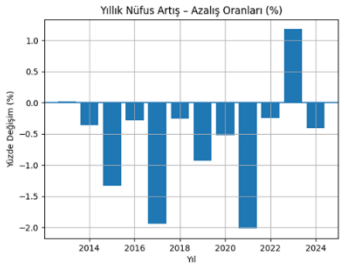


Figure 3. Effects of the Mining Accident and the Dam on Changes in Population Distribution and Demographic Structure in Ermenek. Data source: Türkiye İstatistik Kurumu (TÜİK, n.d.).

Following the construction of the dam, agricultural and forest areas decreased, while fruit cultivation increased substantially (Figure 2). The main reason producers have abandoned wheat and barley cultivation in favour of perennial crops such as olives and cherries is that the presence of the dam has transformed the region's climate from **'harsh continental' to 'mild transitional'** conditions. This change has occurred through a reduction in the frequency and duration of **critically low temperatures (frost events)** that threaten plant survival, rather than through a dramatic increase in mean temperatures. Consequently, the reduced risk posed by extreme cold has encouraged farmers in the region to adopt a higher-value-added cropping pattern.

The decline in mining activities and, consequently, in employment opportunities is one of the factors that may prompt the working-age population, in particular, to seek work in other settlements. As a result, the district's population has been observed to decline from around 30,000 to around 27,000 (Figure 3). However, women, who were largely excluded from economic production processes during the period when mining dominated the economy, have gained the opportunity to participate actively in the labour force through the agricultural transformation accompanying the dam. Strawberry cultivation, greenhouse production, fruit harvesting and processing, in particular, stand out as activities in which women's labour is extensively employed.

CONCLUSIONS AND RECOMMENDATIONS

The study yielded the following key conclusions concerning Ermenek's future: the energy and modern agriculture sectors that have replaced mining have not yet reached an employment level sufficient to maintain the region's population. The decline in population from around 30,000 to around 27,000 is the clearest indication of this.

By increasing humidity, the reservoir has moderated the severity of winter cold, turning the region into a "microclimatic island". The reduced frequency and duration of frost events have

created more favourable conditions for growing crops such as olives and strawberries. Meanwhile, afforestation efforts on former mining sites offer a successful model for reversing the effects of environmental degradation.

Recommendations:

- Tourism Potential: The capacity for outdoor sports and cultural tourism at the Ermenek Dam (Turquoise Lake) and in the surrounding area should be utilised more actively to address the employment gap that emerged following the decline in mining. The cultural heritage and natural products of a region with a long history, such as Ermenek, should be promoted through various events.
- Agricultural Training: Local residents should receive training in modern agricultural techniques for olive and strawberry production suited to the new climatic conditions. Departments focusing on agriculture and agricultural machinery should be established in the region's vocational high schools and vocational college. As a result, knowledgeable farmers would be trained, and the resulting development would bring outward migration to a halt.
- Careful Planning: Changes in land use should be closely monitored to guard against the risk of sedimentation that would shorten the dam's service life.

References

Devlet Su İşleri Genel Müdürlüğü. (2024, December 27). *Dar vadinin gizli hazinesi 15 yaşında!* [The hidden treasure of the narrow valley turns 15!]. https://www.dsi.gov.tr/Haber/Detay/14282

Ermenek Kaymakamlığı. (n.d.). *Ermenek Barajı* [Ermenek Dam]. https://www.ermenek.gov.tr/ermenek-baraji

Google. (n.d.). *Google Earth*. https://earth.google.com/

Karaman Valiliği. (2014, December 11). *Maden ocağında çalışan işçilerle ilgili toplantı yapıldı* [A meeting was held concerning the workers employed at the mine]. https://www.karaman.gov.tr/maden-ocaginda-alisan-iscilerle-ilgili-toplanti-yapildi

Karaman Valiliği. (2015, June 5). *Ermenek'te şartları sağlayan maden ocakları açılıyor* [Mines meeting the requirements are reopening in Ermenek]. https://karaman.gov.tr/ermenekte-sartlari-saglayan-maden-ocaklari-aciliyor

Maden Tetkik ve Arama Genel Müdürlüğü. (n.d.). *MTA*. https://www.mta.gov.tr/

Meteoroloji Genel Müdürlüğü. (n.d.). *Türkiye ortalama sıcaklık* [Mean temperature in Türkiye]. https://www.mgm.gov.tr/FILES/resmi-istatistikler/parametreAnalizi/2024-ortalama-sicaklik.pdf

Türkiye İstatistik Kurumu. (n.d.). *TÜİK*. https://www.tuik.gov.tr/

BÖCEKLERDE SAVUNMA DAVRANIŞLARI

DEFENSIVE BEHAVIOURS IN INSECTS

Nihal Özder
Prof. Dr., Tekirdağ Namık Kemal Üniversitesi, Ziraat Fakültesi, Bitki Koruma Bölümü
Prof. Dr., Tekirdağ Namık Kemal University, Faculty of Agriculture, Department of Plant Protection
ORCID ID: 0000-0002-4637-5364

Esra Tayat
Dr. Öğr. Üyesi, Tekirdağ Namık Kemal Üniversitesi, Ziraat Fakültesi, Bitki Koruma Bölümü
Assistant Professor, Tekirdağ Namık Kemal University, Faculty of Agriculture, Department of Plant Protection
ORCID ID: 0000-0002-4023-7753

ÖZET

Böcekler, avcılarla karşılaşma riskini azaltmak ve saldırı sırasında yakalanmaktan kurtulmak için savunma davranışları sergiler. Tehdit algılandığında hareketsiz kalma, saklanma veya bulunduğu yüzeyden düşme gibi davranışlar, avcıdan kaçmaya ya da yakalanma riskini azaltmaya yardımcı olabilir. Bazı türler hızla uzaklaşır; bazı cırcır böcekleri ise sıkışan bacağını bırakarak kurtulabilir. Ölü taklidi, özellikle avcıyla fiziksel temasın ardından görülebilen savunma tepkilerindendir. Peygamberdevelerinde de görülen irkilme gösterileri avcıda refleks bir geri çekilme tepkisi oluşturabilir. Tepkiler tek başına veya birlikte gerçekleşebilir. Sosyal böceklerde savunma bireysel tepkilerin ötesine geçer: işçi bireylerin saldırması ve birlikte hareket etmesi yuvanın korunmasına katkı sağlayabilir. Tehdit sinyalleri koloni üyelerini uyararak savunma tepkisinin birlikteliğini sağlayabilir. Savunma tepkisinin biçimi, böcek türüne ve karşılaşılan avcının özelliklerine göre değişir. Bir türün aynı tehdide karşı farklı davranış seçenekleri kullanabilmesi, savunmanın tek bir tepkiyle sınırlı olmadığını gösterir. Hareketsiz kalma ve kamuflaj, fark edilme olasılığını düşürmeye yönelikken; kaçış, ototomi ve saldırı, tehdit belirginleştiğinde devreye girebilir. Ancak belirli bir davranışın her türde ya da her avcı karşısında aynı sonucu verdiği söylenemez. Bu değişkenlik, savunma tepkilerinin türler ve tehditler arasında karşılaştırılmasını gerekli kılar. Savunma davranışını değerlendirmek için tür, tehdit ve karşılaşma koşulları dikkate alınmalıdır. Böceklerde savunma, algılanan tehlikeye verilen ve saklanmadan etkin karşı koymaya uzanan tepkiler bütünüdür. Bu çeşitlilik, bireysel kaçıştan grup savunmasına kadar farklı düzeylerde ortaya çıkar; davranışın işlevi ise karşılaşmanın koşulları içinde değerlendirilmelidir.

Anahtar Kelimeler: Böcekler, Savunma Davranışları, Avcı, Kaçış, Ölü Taklidi.

ABSTRACT

Insects use defensive behaviours to reduce predator encounters and avoid capture during attacks. When threatened, insects may remain still, hide, or drop from a surface; these responses may help them evade predators or reduce capture risk. Some species flee rapidly, whereas others, such as field crickets, can escape by shedding a trapped leg. Death-feigning is

observed particularly after physical contact with a predator. Startle displays, which also occur in praying mantises, can cause predators to recoil reflexively. These responses may occur alone or in combination. In social insects, defence also involves coordinated group responses: workers may attack threats and help protect the nest. Threat signals can alert colony members and coordinate their responses. Defensive responses vary with insect species and predator characteristics. A species may use different behaviours in response to the same threat, so defence is not limited to a single response. Stillness and camouflage can reduce detection, whereas escape, autotomy, and attack may follow once a threat becomes apparent. No particular behaviour can be assumed to produce the same outcome across species or predators. Assessment therefore requires considering the species, threat, and encounter conditions. Insects' defence comprises responses to perceived danger, from concealment to active resistance. This range spans individual escape to group defence, and each behaviour's function should be evaluated in context.

Keywords: Insects, Defensive Behaviour, Predators, Escape, Death-Feigning.

GİRİŞ

Böceklerin avcılarla karşılaşması, fark edilme, saldırıya uğrama ve yakalanma aşamalarında farklı savunma tepkilerini gündeme getirir. Savunma davranışları bu aşamaların birinde ya da birkaçında etkili olabilir. Bir böcek tehdidi fark edilmeden önce saklanabilir veya hareketsiz kalabilir; fark edildikten sonra ise kaçabilir, düşebilir, tehdit gösterisi sergileyebilir ya da saldırıya karşı koyabilir. Bu davranışların tüm böceklerde aynı biçimde görüldüğü veya aynı sonucu verdiği söylenemez. Savunma biçimi, tür ve avcıyla karşılaşmanın özelliklerine göre değişir (Kikuchi et al., 2023; Sugiura, 2020).

Önce saldırı sürecindeki savunma tepkilerinin yeri açıklanmakta; ardından kaçış ve hareketsizlik, ototomi, irkilme gösterileri ile sosyal böceklerdeki birlikte savunma hareketleri incelenmektedir. Amaç, tek bir davranışı bütün böcekler için geçerli bir kural gibi sunmak değil, çalışmalarda bildirilen örnekleri ve bunların bağlama bağlı sınırlarını ortaya koymaktır.

SAVUNMA DAVRANIŞLARININ KARŞILAŞMADAKİ YERİ

Avcı–av karşılaşması tek bir andan ibaret değildir. Avcı–av etkileşimi, karşılaşmadan tüketime kadar uzanan ardışık aşamalar olarak ele alınabilir. Savunma, saldırı başlamadan önce fark edilmeyi veya saldırı olasılığını azaltan tepkileri ve saldırı başladıktan sonra yakalanmayı önlemeye çalışan tepkileri kapsar (Kikuchi et al., 2023).

Saldırı başlamadan önceki tepkilere kamuflajla uyumlu duruş ve hareketsizlik örnek verilebilir (Watanabe & Yano, 2010). Böcek fark edildikten veya avcı yaklaştıktan sonra ise kaçış, irkilme gösterisi ve karşı koyma gibi tepkiler ortaya çıkabilir. Watanabe ve Yano'nun (2010) üç peygamberdevesi türü ve bir doğal düşmanla yürüttüğü deneylerde savunma tepkisi tür, gelişim evresi ve avcıyla mesafeye göre değişmiştir. Bu bulgu, savunma davranışlarının zamanlama ve karşılaşma koşulları gözetilerek değerlendirilmesi gerektiğini gösterir.

Saldırı öncesi savunmalar yalnızca arka planla uyumdan ibaret değildir. Skelhorn ve arkadaşları (2010), maskelemeyi bir organizmanın avcının yemediği bir nesneye benzemesi

olarak tanımlamış ve iki tırtıl türünün, bir kuş avcı tarafından dal parçası sanıldığı için korunduğunu deneysel olarak göstermiştir. Araştırmacılar kuşların tırtıllarla karşılaşmasını sabit tutup dal modeliyle önceki deneyimlerini değiştirdiklerinde, kuşların tırtılları yalnızca fark edememekle kalmayıp onları taklit ettikleri nesneyle karıştırdığını ortaya koymuştur.

KAÇIŞ, HAREKETSİZLİK VE OTOTOMİ

Kaçış, tehdit algılandığında böceğin bulunduğu yerden uzaklaşmasına dayanan etkin bir savunmadır. Uçma veya koşma gibi hareketlerin yanı sıra, bulunduğu yüzeyden düşme de bazı karşılaşmalarda kaçış yolu olabilir. Humphreys ve Ruxton (2019), düşerek kaçmayı farklı böcek gruplarında bildirilen ve avcıyla karşılaşma sırasında hızlı uzaklaşmaya imkân verebilen bir savunma olarak ele alır.

Düşerek kaçma yalnızca avcılara karşı kullanılmaz. Gish ve arkadaşları (2010), bezelye yaprakbitinin (*Acyrthosiphon pisum*) yaklaşan büyük memeli otçulların nefesindeki ısı ve nemi algılayarak bitkiden topluca düştüğünü ve böylece koloninin büyük bölümünün otçul tarafından tüketilmekten kurtulduğunu bildirmiştir. Bitkiden düşmenin yaprakbitini konukçu bitkisini kaybetme, kuruma ve yerde avlanma gibi risklerle karşı karşıya bıraktığını; yaklaşan otçulun nefesindeki ısı ve nemin birlikte algılanmasının ise otçul yokken gereksiz düşmeleri önleyen güvenilir bir uyarı işlevi gördüğünü belirtmiştir. Kaçışın işleyişi türler arasında farklılaşabilir. Larabee ve Suarez (2015), kapançeneli karınca *Odontomachus brunneus* işçilerinin çukur kazan karınca aslanlarıyla karşılaşmalarını incelemiştir. Karşılaşmaların yaklaşık yarısında işçiler koşarak, yaklaşık %15'inde ise çenelerini kullanarak sıçrayıp kaçmıştır. Çeneleri bağlanan işçilerin çeneleri serbest olan işçilere göre daha az kaçabilmesi, bu sıçramanın kaçış başarısına katkı sağladığını göstermiştir. Bu durum, avlanmada kullanılan bir özelliğin savunmada da işlev kazanmasına örnek olarak değerlendirmiştir. Çalışma tek bir tür ve tek bir avcı–av düzeniyle sınırlı olduğundan bulgular diğer karınca türlerine genellenemez.

Kaçışın başarısı hızın yanı sıra hareketin doğru yöne yönlendirilmesine de bağlıdır. Card ve Dickinson (2008), yüksek hızlı video kayıtlarıyla *Drosophila* sineklerinin yaklaşan bir görsel tehdit karşısında kalkıştan yaklaşık 200 ms önce bir dizi duruş ayarlaması yaptığını göstermiştir. Bu ayarlamalar sineğin ağırlık merkezini kaydırmakta ve bacaklar uzatıldığında sineği uyarandan uzağa itmektedir. Ayarlamaların büyüklüğü ve yönü sineğin başlangıçtaki duruşuna göre değiştiğinden, bu kaçış hareketi sabit bir motor programla açıklanamamaktadır.

Kaçış yönünün avcı tarafından öngörülememesi de önem taşır. Domenici ve arkadaşları (2008), Amerikan hamamböceğinde (*Periplaneta americana*) her bireyin, tehdidin yönüne göre belirli açılarda konumlanmış birkaç tercih edilen kaçış yolundan birini kullandığını ve böylece kaçışını öngörülemez kıldığını göstermiştir. Ayrıca, tamamen rastgele kaçış yönlerinin öngörülebilirliği ortadan kaldırsa da bazı kaçışları tehdide doğru yönelteceğine dikkat çekmiştir.

Kaçış, av yakalandıktan sonra da mümkün olabilir. Sugiura ve Sato (2018), bombardıman böceği *Pheropsophus jessoensis* ile iki karakurbağası türü (*Bufo japonicus* ve *B. torrenticola*) arasındaki etkileşimleri laboratuvarda incelemiştir. Karakurbağalarının tamamı böcekleri

yutmuş, ancak yaklaşık %43'ü böcekleri 12–107 dakika sonra kusmuş ve kusulan böceklerin tümü canlı kalmıştır. Böceğin karakurbağasının içinde salgıladığı sıcak kimyasal püskürtmenin kusmayı tetiklediği sonucuna varmıştır. Büyük böceklerin daha sık kurtulması ve küçük karakurbağalarının daha sık kusması, av ile avcı arasındaki büyüklük oranının kaçış başarısındaki önemine işaret etmektedir.

Ölü taklidi veya tonik hareketsizlikte böcek, tehdit sırasında hareketini durdurur ve hareketsiz kalır. Humphreys ve Ruxton (2018), bu tepkinin birçok hayvan grubunda görüldüğünü ve sıklıkla avcıyla fiziksel temasın ardından ortaya çıktığını bildirir. Ölü taklidi her zaman savunma dizisinin son adımı olarak ortaya çıkmaz. Asakura ve arkadaşları (2022), ölü taklidi süresi yönünde yapay seçilim uygulanmış *Tribolium* hatlarında, uzun süre ölü taklidi yapan hattaki bireylerin pusu kuran avcı *Amphibolus venator* tarafından saldırıya uğradığında donup kaldığını, kısa süre ölü taklidi yapan hattaki bireylerin ise kaçarak tepki verdiğini bildirmiştir. Donma ve ölü taklidinin farklı avcı türlerine karşı kullanılan ayrı stratejiler olabileceğini öne sürülmüştür. Bununla birlikte, hareketsiz kalmanın her avcıyı caydırdığı sonucuna varılamaz; tepkinin etkisi, avcının davranışına ve karşılaşmanın bağlamına bağlıdır.

Ototomi, bir vücut bölümünün kontrollü biçimde bırakılmasıdır. Fleming ve arkadaşları (2007), omurgasızlarda ototomiyi üç ölçütle tanımlar: vücut bölümünün kaybı savunma amaçlıdır, ayrılma içsel bir mekanizmayla belirli bir kırılma hattı boyunca gerçekleşir ve kayıp kontrollüdür. Ototomi, yakalanan bölümün bırakılmasıyla kaçış fırsatı oluşturabilir; fakat tüm türlerde aynı uzvun bırakıldığı veya davranışın aynı biçimde işlediği varsayılamaz. Ototominin sağladığı anlık yarar maliyetsiz değildir. Maginnis (2006), uzuv kaybının hareket, beslenme, hayatta kalma ve üreme üzerinde olumsuz etkiler doğurabildiğini; kaybedilen uzvun yenilenmesinin bu kayıpları kısmen giderse de vücut büyümesi veya üreme pahasına kaynak gerektirebildiğini belirtmiştir. Bateman ve Fleming (2005), doğal bir *Gryllus bimaculatus* popülasyonunda incelenen 110 bireyin %36'sında en az bir bacağın eksik olduğunu saptamıştır. Laboratuvarda sıkıştırılan bacağın ne kadar hızlı bırakıldığı da ölçülmüş; arka bacaklar orta bacaklardan daha hızlı bırakılmıştır. Laboratuvar deneylerinde arka ya da orta bacak çiftinin kaybı kaçış hızını ve kaçış sırasında yapılan sıçrama sayısını azaltmış, dişilerde iki bacak kaybı çiftleşme başarısını anlamlı ölçüde düşürmüş ve orta bacaklarını kaybeden erkeklerin ömrü kısalmıştır. Ototominin yararı yalnızca kaçışla sınırlı olmayabilir. Emberts ve arkadaşları (2017), yaprak ayaklı böcek *Narnia femorata*'da (Hemiptera: Coreidae) yaralanmaya karşı bazı bireylerin bacağını bıraktığını, bazılarının ise bırakmadığını belirtmiş; bu doğal farklılıktan yararlanarak yaralı bacağını bırakmak ile hayatta kalma arasında olumlu bir ilişki bulmuştur. Çalışmada, ototominin yaralanmanın maliyetini azaltan bir yararı olarak değerlendirmiştir. Sugiura (2020), ototomi, düşme ve ölü taklidi gibi davranışsal savunmaların farklı avcı grupları karşısında ayrı ayrı değerlendirilmesi gerektiğine dikkat çeker.

İRKİLME GÖSTERİLERİ VE TÜRE ÖZGÜ TEPKİLER

Umbers ve arkadaşları (2017), irkilme gösterileri olarak da adlandırılan deimatik gösterileri, avcının aldığı duyusal uyaranın aniden değişmesiyle avcıda refleks bir geri çekilme tepkisi

oluşturan davranışlar olarak tanımlar. Deimatizm, aposematizmden farklı olarak avcının öğrenilmiş ya da doğuştan gelen bir kaçınmasına dayanmaz; avcının sahip olduğu sinirsel mekanizmalardan yararlanır.

Peygamberdevelerini inceleyen karşılaştırmalı ve deneysel çalışmalar, savunma tepkilerinin türler içinde bile değişebildiğini ortaya koymaktadır. Watanabe ve Yano (2010), üç türde kriptik (kamuflaj) duruş, subkriptik (daha az örtük) duruş, savunma ve saldırı tepkilerinin gelişim evresi ve avcıya uzaklıkla ilişkili olduğunu bildirmiştir. Vidal-García ve arkadaşları (2020) ise 58 peygamberdevesi türünde irkilme gösterilerinin varlığını ve karmaşıklığını karşılaştırmıştır. Bu araştırmalar, tek bir peygamberdevesi türünden elde edilen bulguların tüm takıma genellenemeyeceğini; gösterinin bileşenleri, tür ve tehdit özelliklerinin ayrı ayrı ele alınması gerektiğini destekler.

Gösteri sergileme olasılığı da türler arasında farklılık gösterebilir. O'Hanlon ve arkadaşları (2018), Avustralya'nın doğusunda yayılış gösteren üç peygamberdevesi türüne (*Archimantis latistyla*, *Hierodula majuscula* ve *Pseudomantis albofimbriata*) avcıyı temsil eden, dokunsal olan ve olmayan beş farklı uyaran uygulamıştır. Üç tür de gösterisini dokunsal uyarana yanıt olarak sergilemiş; *A. latistyla* ve *H. majuscula* bireylerinin yanıt verme olasılığı *P. albofimbriata* bireylerinden yüksek bulunmuştur. En küçük tür olan *P. albofimbriata* benzetilmiş saldırılara nadiren yanıt vermiştir. Bulgular, peygamberdevelerinin avlanma sürecinin erken aşamalarını temsil eden uyaranlara gösteriyle yanıt vereceği öngörüsünü desteklememiştir.

Savunma tepkileri yalnızca görsel avcılara yönelik değildir; ekolokasyonla avlanan yarasalara karşı akustik savunmalar da gelişmiştir. Corcoran ve arkadaşları (2009), ultrasonik kayıtlar ve yüksek hızlı kızılötesi video kullanarak, zehirli olmayan kaplan güvesi *Bertholdia trigona*'nın ürettiği ultrasonik tıklamaların, saldıran büyük kahverengi yarasaların (*Eptesicus fuscus*) sonarını bozduğunu göstermiştir. Barber ve arkadaşları (2015) ise ay güvesinde (*Actias luna*) arka kanatlardaki dönen kuyrukların yarasa saldırılarını vücuttan uzağa, gözden çıkarılabilir kuyruk bölgesine yönelttiğini bildirmiştir. Aynı yarasa türüyle yapılan denemelerde kuyrukları sağlam güvelerin hayatta kalma oranı, kuyrukları kesilmiş güvelere göre yaklaşık %47 daha yüksek bulunmuş; yarasalar sağlam güvelere yönelik saldırıların yaklaşık %55'inde kanat-kuyruk bölgesini hedeflemiştir.

Savunmaya özelleşmiş bireyler bazı yaprakbiti türlerinde de bildirilmiştir. Stern ve Foster (1996), literatürde "asker" (soldier) olarak adlandırılan bu bireylerin yaklaşık 4.400 yaprakbiti türünden yaklaşık 50'sinde görüldüğünü, yalnızca birbirine yakın iki familyada (Hormaphididae ve Pemphigidae) bulunduğunu ve bu özelliğin en az altı ila dokuz kez bağımsız olarak evrimleştiğini belirtmiştir. Asker üreten türlerin çoğu birincil konukçu üzerindeki galleri savunur. Bazı türlerde askerler bir sonraki döneme geçemedikleri için kısırdır; bazılarında ise gömlek değiştirip üreyebilirler.

SOSYAL BÖCEKLERDE EŞGÜDÜMLÜ SAVUNMA

Sosyal böceklerde savunma, tek bir bireyin kaçma veya karşı koyma tepkisinin ötesinde, koloni üyelerinin birlikte hareket etmesini içerebilir. Abbot (2022), savunmanın sosyal

böceklerde iş bölümüyle ilişkisini ve bazı türlerde savunmaya özelleşmiş işçi kastlarını ele alır. Tehdit karşısında işçilerin yuvayı korumaya yönelmesi, bireysel tepkilerin koloni düzeyinde örgütlenebildiğini gösterir. Bal arıları ve karıncalar gibi sosyal böcekler tehlikeyi alarm feromonlarıyla diğer koloni üyelerine iletebilir; bu kimyasal sinyaller grubun tehdide topluca yanıt vermesine olanak sağlar (Kannan et al., 2022). Bal arısında, ana bileşeni izoamil asetat olan sokma alarm feromonunun arıların beynindeki serotonin ve dopamin düzeylerini artırarak saldırma ve sokma olasılığını yükselttiği gösterilmiştir; araştırmacılar feromonun tepkiyi doğrudan tetiklemekten çok bireylerin tepki eşiğini değiştirdiğini ileri sürmüştür (Nouvian et al., 2018). Savunma görevinin kimler tarafından ve hangi biçimde yürütüldüğü türler arasında çeşitlilik gösterir; bu nedenle sosyal böcekleri tek bir savunma düzeniyle tanımlamak uygun değildir.

Toplu savunmanın dikkat çekici bir örneği Japon bal arısında (*Apis cerana japonica*) görülür. Ono ve arkadaşları (1995), dev yaban arısı (*Vespa mandarinia japonica*) kolonilere saldırdığında, yakalanan yaban arısının çevresinde 500'den fazla işçi arının bir top oluşturduğunu ve topun içindeki sıcaklığın yaklaşık 47 °C'ye ulaştığını bildirmiştir. Bu sıcaklık yaban arısı için öldürücü olurken arılar tarafından tolere edilmektedir. Termitlerde ise savunma kimyası, savunma bezlerinin yapısı ve işleyişi ile alarm iletişimi kapsamlı bir derlemede ele alınmıştır (Šobotník et al., 2010).

Asya bal arısı (*Apis cerana*), dev yaban arısı *Vespa soror* saldırılarına karşı farklı bir yöntem kullanır. Mattila ve arkadaşları (2020), işçi arıların hayvan dışkısı toplayarak yuva girişinin çevresine sürdüğünü ve bu davranışın gerçek saldırılar sırasında ya da yaban arılarının koloniyi saldırı için işaretlemekte kullandığı kimyasal sinyallere maruz kalındığında arttığını bildirmiştir. Orta ve yoğun düzeyde dışkı sürülmesi, birden fazla yaban arısının katıldığı saldırıları ve yaban arılarının girişe konup girişi kemirme olasılığını azaltmıştır. Bu davranışı bal arılarında bildirilen ilk alet kullanımı olarak tanımlamıştır.

Açıkta yuva yapan dev bal arısında (*Apis dorsata*) eşgüdümlü savunma dalga biçiminde ortaya çıkar. Kastberger ve arkadaşları (2008), yuva yüzeyindeki çok sayıda arının karınlarını art arda kaldırmasıyla oluşan ve "parıldama" (shimmering) olarak adlandırılan dalga benzeri davranışın, avcı yaban arılarının (*Vespa* sp.) yönünü değiştirmesine yol açtığını göstermiştir. Parıldamanın şiddeti ve sıklığı yaban arısının hızına ve uzaklığına göre değişmiştir. Bu davranışın yuva çevresinde yaklaşık 50 cm'lik bir koruma bölgesi oluşturduğunu ve yaban arılarının arıları doğrudan yuvadan kapmasını engellediğini belirtmiştir.

Bazı sosyal böceklerde savunma bireyin ölümüyle sonuçlanır. Šobotník ve arkadaşları (2012), *Neocapritermes taracua* işçilerinde bakır içeren protein kristallerinin vücut dışındaki bir kesede, tükürük bezlerinin ise vücut içinde bulunduğunu; mücadele sırasında vücut yırtıldığında bu iki bileşenin tepkimeye girerek zehirli bir damla oluşturduğunu göstermiştir. İşçiler yaşlandıkça ve yiyecek arama yetenekleri azaldıkça taşıdıkları savunma kimyasallarının miktarı ve patlamaya hazırlıkları artmaktadır. Tofilski ve arkadaşları (2008) ise Brezilya'da yaşayan *Forelius pusillus* karıncasında, koloni her akşam gün batımında yuva girişini kapatırken bir ila sekiz işçinin dışarıda kalarak kapatma işlemini tamamladığını ve bu

sırada öldüğünü bildirmiştir. Bu davranış, bir saldırı gerçekleşmeden önce ortaya çıkan savunma amaçlı kendini feda etmenin belgelenen ilk örneği olarak tanımlamıştır.

Alarm sinyalleri yalnızca sosyal böceklere özgü değildir. Vandermoten ve arkadaşları (2012), çoğu yaprakbiti türünde alarm feromonunun ana ya da tek bileşeninin (E)-β-farnesen olduğunu; bu sinyalin yaprakbitleri arasındaki iletişime ve bitkiler, yaprakbitleri ile onların avcı ve parazitoitleri arasındaki etkileşimlere aracılık ettiğini belirtmiştir.

DEĞERLENDİRME VE SONUÇ

Böceklerde savunma davranışları; saklanma ve hareketsiz kalmadan kaçışa, ototomiye, irkilme gösterilerine ve grup hâlinde karşı koymaya uzanan çeşitlilikler gösterir. Bu davranışlar saldırı sürecinin farklı aşamalarında ortaya çıkabilir ve bazı türlerde birden fazlası aynı karşılaşmada kullanılabilir. Birden fazla savunmanın birlikte değerlendirilmesi, savunmaların birbirini tamamlayabileceğini veya belirli koşullarda farklı sonuçlar doğurabileceğini incelemeye imkân verir (Kikuchi et al., 2023).

Bulguların kapsamı her zaman incelenen tür ve deney koşullarıyla sınırlıdır. Örneğin peygamberdevelerinde savunma duruşunun gelişim evresi ve avcıya uzaklıkla değişmesi, aynı davranışın sabit bir tepki olmadığını gösterir (Watanabe & Yano, 2010). Düşerek kaçma, ölü taklidi veya alarm sinyalleri üzerine çalışmalar da davranışın etkisini tehdit oluşturan canlının (avcı ya da fitofag) türü ve karşılaşma bağlamı içinde ele alır (Gish et al., 2010; Humphreys & Ruxton, 2018, 2019; Kannan et al., 2022). Savunma davranışları bireyi tehditten korurken bireyin hayatta kalma, hareket ve üreme yeteneği üzerinde olumsuz etkiler de doğurabilir; bacak kaybından sonra kaçış hızının ve çiftleşme başarısının azalması ile bazı sosyal böceklerde savunmanın bireyin ölümüyle sonuçlanması bunun örnekleridir (Bateman & Fleming, 2005; Šobotník et al., 2012; Tofilski et al., 2008).Ayrıca aynı seçilim hattındaki bireyler farklı avcılara karşı farklı tepkiler sergileyebilir (Asakura et al., 2022). Savunmalar avcının algı biçimine göre de farklılaşabilir; ekolokasyonla avlanan yarasalara karşı gelişmiş akustik savunmalar bunun örneğidir (Barber et al., 2015; Corcoran et al., 2009).

Sonuç olarak böcek savunması, tek bir evrensel davranışla değil, tehdidin algılanması ve karşılaşmanın ilerleyişi sırasında ortaya çıkan farklı tepkilerle açıklanabilir. Tür, avcı, gelişim evresi, mesafe ve sosyal bağlam gibi etkenler, hangi davranışın gözlendiğini ve nasıl değerlendirileceğini belirler. Bu nedenle savunma davranışlarına ilişkin sonuçlar, incelenen tür ve karşılaşma koşulları açıkça belirtilerek yorumlanmalıdır.

KAYNAKÇA

Abbot, P. (2022). Defense in social insects: Diversity, division of labor, and evolution. Annual Review of Entomology, 67, 407–436. https://doi.org/10.1146/annurev-ento-082521-072638

Asakura, M., Matsumura, K., Ishihara, R., & Miyatake, T. (2022). Freezing or death feigning? Beetles selected for long death feigning showed different tactics against different predators. Ecology and Evolution, 12(2), Article e8533. https://doi.org/10.1002/ece3.8533

Barber, J. R., Leavell, B. C., Keener, A. L., Breinholt, J. W., Chadwell, B. A., McClure, C. J. W., Hill, G. M., & Kawahara, A. Y. (2015). Moth tails divert bat attack: Evolution of acoustic deflection. Proceedings of the National Academy of Sciences of the United States of America, 112(9), 2812–2816. https://doi.org/10.1073/pnas.1421926112

Bateman, P. W., & Fleming, P. A. (2005). Direct and indirect costs of limb autotomy in field crickets, *Gryllus bimaculatus*. Animal Behaviour, 69(1), 151–159. https://doi.org/10.1016/j.anbehav.2004.04.006

Card, G., & Dickinson, M. H. (2008). Visually mediated motor planning in the escape response of *Drosophila*. Current Biology, 18(17), 1300–1307. https://doi.org/10.1016/j.cub.2008.07.094

Corcoran, A. J., Barber, J. R., & Conner, W. E. (2009). Tiger moth jams bat sonar. Science, 325(5938), 325–327. https://doi.org/10.1126/science.1174096

Domenici, P., Booth, D., Blagburn, J. M., & Bacon, J. P. (2008). Cockroaches keep predators guessing by using preferred escape trajectories. Current Biology, 18(22), 1792–1796. https://doi.org/10.1016/j.cub.2008.09.062

Edmunds, M. (1972). Defensive behaviour in Ghanaian praying mantids. Zoological Journal of the Linnean Society, 51(1), 1–32. https://doi.org/10.1111/j.1096-3642.1972.tb00771.x

Emberts, Z., Miller, C. W., Kiehl, D., & St. Mary, C. M. (2017). Cut your losses: Self-amputation of injured limbs increases survival. Behavioral Ecology, 28(4), 1047–1054. https://doi.org/10.1093/beheco/arx063

Fleming, P. A., Muller, D., & Bateman, P. W. (2007). Leave it all behind: A taxonomic perspective of autotomy in invertebrates. Biological Reviews, 82(3), 481–510. https://doi.org/10.1111/j.1469-185X.2007.00020.x

Gish, M., Dafni, A., & Inbar, M. (2010). Mammalian herbivore breath alerts aphids to flee host plant. Current Biology, 20(15), R628–R629. https://doi.org/10.1016/j.cub.2010.06.065

Humphreys, R. K., & Ruxton, G. D. (2018). A review of thanatosis (death feigning) as an anti-predator behaviour. Behavioral Ecology and Sociobiology, 72(2), Article 22. https://doi.org/10.1007/s00265-017-2436-8

Humphreys, R. K., & Ruxton, G. D. (2019). Dropping to escape: A review of an under-appreciated antipredator defence. Biological Reviews, 94(2), 575–589. https://doi.org/10.1111/brv.12466

Kannan, K., Galizia, C. G., & Nouvian, M. (2022). Olfactory strategies in the defensive behaviour of insects. Insects, 13(5), Article 470. https://doi.org/10.3390/insects13050470

Kastberger, G., Schmelzer, E., & Kranner, I. (2008). Social waves in giant honeybees repel hornets. PLOS ONE, 3(9), Article e3141. https://doi.org/10.1371/journal.pone.0003141

Kikuchi, D. W., Allen, W. L., Arbuckle, K., Aubier, T. G., Briolat, E. S., Burdfield-Steel, E. R., Cheney, K. L., Daňková, K., Elias, M., Hämäläinen, L., Herberstein, M. E., Hossie, T. J., Joron, M., Kunte, K., Leavell, B. C., Lindstedt, C., Lorioux-Chevalier, U., McClure, M., McLellan, C. F., . . . Exnerová, A. (2023). The evolution and ecology of multiple antipredator defences. Journal of Evolutionary Biology, 36(7), 975–991. https://doi.org/10.1111/jeb.14192

Larabee, F. J., & Suarez, A. V. (2015). Mandible-powered escape jumps in trap-jaw ants increase survival rates during predator-prey encounters. PLOS ONE, 10(5), Article e0124871. https://doi.org/10.1371/journal.pone.0124871

Maginnis, T. L. (2006). The costs of autotomy and regeneration in animals: A review and framework for future research. Behavioral Ecology, 17(5), 857–872. https://doi.org/10.1093/beheco/arl010

Mattila, H. R., Otis, G. W., Nguyen, L. T. P., Pham, H. D., Knight, O. M., & Phan, N. T. (2020). Honey bees (*Apis cerana*) use animal feces as a tool to defend colonies against group attack by giant hornets (*Vespa soror*). PLOS ONE, 15(12), Article e0242668. https://doi.org/10.1371/journal.pone.0242668

Nouvian, M., Mandal, S., Jamme, C., Claudianos, C., d'Ettorre, P., Reinhard, J., Barron, A. B., & Giurfa, M. (2018). Cooperative defence operates by social modulation of biogenic amine levels in the honey bee brain. Proceedings of the Royal Society B: Biological Sciences, 285(1871), Article 20172653. https://doi.org/10.1098/rspb.2017.2653

O'Hanlon, J. C., Rathnayake, D. N., Barry, K. L., & Umbers, K. D. L. (2018). Post-attack defensive displays in three praying mantis species. Behavioral Ecology and Sociobiology, 72(11), Article 176. https://doi.org/10.1007/s00265-018-2591-6

Ono, M., Igarashi, T., Ohno, E., & Sasaki, M. (1995). Unusual thermal defence by a honeybee against mass attack by hornets. Nature, 377(6547), 334–336. https://doi.org/10.1038/377334a0

Skelhorn, J., Rowland, H. M., Speed, M. P., & Ruxton, G. D. (2010). Masquerade: Camouflage without crypsis. Science, 327(5961), 51. https://doi.org/10.1126/science.1181931

Šobotník, J., Jirošová, A., & Hanus, R. (2010). Chemical warfare in termites. Journal of Insect Physiology, 56(9), 1012–1021. https://doi.org/10.1016/j.jinsphys.2010.02.012

Šobotník, J., Bourguignon, T., Hanus, R., Demianová, Z., Pytelková, J., Mareš, M., Foltynová, P., Preisler, J., Cvačka, J., Krasulová, J., & Roisin, Y. (2012). Explosive backpacks in old termite workers. Science, 337(6093), 436. https://doi.org/10.1126/science.1219129

Stern, D. L., & Foster, W. A. (1996). The evolution of soldiers in aphids. Biological Reviews, 71(1), 27–79. https://doi.org/10.1111/j.1469-185X.1996.tb00741.x

Sugiura, S. (2020). Predators as drivers of insect defenses. Entomological Science, 23(3), 316–337. https://doi.org/10.1111/ens.12423

Sugiura, S., & Sato, T. (2018). Successful escape of bombardier beetles from predator digestive systems. Biology Letters, 14(2), Article 20170647. https://doi.org/10.1098/rsbl.2017.0647

Tofilski, A., Couvillon, M. J., Evison, S. E. F., Helanterä, H., Robinson, E. J. H., & Ratnieks, F. L. W. (2008). Preemptive defensive self-sacrifice by ant workers. The American Naturalist, 172(5), E239–E243. https://doi.org/10.1086/591688

Umbers, K. D. L., De Bona, S., White, T. E., Lehtonen, J., Mappes, J., & Endler, J. A. (2017). Deimatism: A neglected component of antipredator defence. Biology Letters, 13(4), Article 20160936. https://doi.org/10.1098/rsbl.2016.0936

Vandermoten, S., Mescher, M. C., Francis, F., Haubruge, E., & Verheggen, F. J. (2012). Aphid alarm pheromone: An overview of current knowledge on biosynthesis and functions. Insect Biochemistry and Molecular Biology, 42(3), 155–163. https://doi.org/10.1016/j.ibmb.2011.11.008

Vidal-García, M., O'Hanlon, J. C., Svenson, G. J., & Umbers, K. D. L. (2020). The evolution of startle displays: A case study in praying mantises. Proceedings of the Royal Society B: Biological Sciences, 287(1934), Article 20201016. https://doi.org/10.1098/rspb.2020.1016

Watanabe, H., & Yano, E. (2010). Stage-specific defensive strategies of three mantid species, Tenodera aridifolia, Hierodura patellifera, and Statilia maculata, against a natural enemy, Takydromus tachydromoides. Annals of the Entomological Society of America, 103(2), 293–299. https://doi.org/10.1603/AN09121

FİTOFAG BÖCEKLERDE KONUKÇU BİTKİNİN KİMYASAL YOLLARLA TANINMASI VE BESLENME DAVRANIŞI

CHEMICAL HOST-PLANT RECOGNITION AND FEEDING BEHAVIOR IN PHYTOPHAGOUS INSECTS

Esra Tayat
Dr. Öğr. Üyesi, Tekirdağ Namık Kemal Üniversitesi, Ziraat Fakültesi, Bitki Koruma Bölümü
Assistant Professor, Tekirdağ Namık Kemal University, Faculty of Agriculture, Department of Plant Protection
ORCID ID: 0000-0002-4023-7753

Nihal Özder
Prof. Dr., Tekirdağ Namık Kemal Üniversitesi, Ziraat Fakültesi, Bitki Koruma Bölümü
Professor, Tekirdağ Namık Kemal University, Faculty of Agriculture, Department of Plant Protection
ORCID ID: 0000-0002-4637-5364

ÖZET

Fitofag böceklerin konukçu bitkileri bulma, tanıma ve kabul etme davranışları, beslenme ve üreme başarısıyla ilişkili olmakla birlikte, bu davranışlar tek bir ipucuna indirgenemez. Bitkiden yayılan uçucu bileşikler uzak mesafede yönelme ve konukçu aramada rol oynayabilir; bitkiye temas sonrasında ise yüzey kimyasalları ve tat alma ipuçları, beslenmenin ya da konukçu kabulünün değerlendirilmesine katkıda bulunabilir. Bu süreçlerin önemi, özellikle farklı böcek türlerinde, yaşam evresi, duyusal özellikler ve deney koşullarına göre değişir. Önceki deneyim, larva veya ergin dönemde edinilmesine bağlı olarak daha sonraki kokuya yönelme, beslenme, konukçu kabulü ya da yumurta bırakma tepkileriyle ilişkili olabilir. İncelenen örneklerde deneyim her zaman deneyimlenen bitkiye yönelimi artırmamış; bazı durumlarda kaçınma, bazı durumlarda ise farklı davranışlarda farklı etkiler bildirilmiştir. Bu nedenle bir davranış ölçümünden diğerine doğrudan genelleme yapılamaz. Konukçu tercihi ile yavru performansı arasındaki ilişki de genel eğilimler sunsa da uzmanlaşma ve sistem özellikleriyle değişebilir. Bitki koruma bakımından, koku bileşenlerinin çekici ya da itici etkisini belirlemek tek başına saha başarısını öngörmeye yetmez; doğal koku ortamı, bitki durumu ve böceğin deneyimi de dikkate alınmalıdır. Larva dönemi deneyiminin ergin tercihlerine taşınıp taşınmadığı ve ergin deneyiminin koku tepkilerine etkisi, tür ve koşullara göre farklı örneklerle ele alınmaktadır. Sonuç olarak kimyasal konukçu tanıma ile öğrenme ve davranışsal plastisite birlikte incelenmeli, deneylerde ölçülen davranış açıkça tanımlanmalı ve sonuçlar tür ile deney koşullarının ötesine genellenmemelidir.

Anahtar Kelimeler: Fitofag böcekler, konukçu bitki seçimi, kimyasal ipuçları, davranışsal plastisite.

ABSTRACT

Phytophagous insects locate, recognize, and accept host plants through behaviors linked to feeding and reproduction, but no single cue explains these processes. This review examines

how chemical cues and prior experience shape host recognition and feeding behavior in phytophagous insects. Plant volatiles can guide orientation and host searching at a distance; after contact, surface chemicals and taste cues may influence feeding or host acceptance. These processes vary by species, life stage, sensory traits, and experimental conditions. Experience acquired during larval or adult stages may affect later odor orientation, feeding, host acceptance, or oviposition. Across reported examples, experience did not always increase preference for the experienced plant: some studies found avoidance, and effects differed among behaviors. Thus, findings from one behavioral measure cannot be generalized directly to another. Host preference and offspring performance may be positively related overall, but this relationship varies with feeding specialization and study system. The reviewed literature distinguishes host search, close-range recognition, plant contact, feeding initiation, and oviposition as separate stages. For plant protection, identifying an odor as attractive or repellent is insufficient to predict field effectiveness; ambient odors, plant condition, and insect experience also matter. Studies also examine whether larval experience persists in adult preferences and how adult experience influences subsequent odor responses in different insect species. These distinctions matter when interpreting behavioral choice tests in practice. Overall, chemical host recognition should be considered alongside learning and behavioral plasticity. Experiments should specify the behavior measured, and conclusions should remain bounded by the species and conditions studied.

Keywords: Phytophagous insects, host-plant selection, chemical cues, behavioral plasticity.

Konukçu bitki seçiminin önemi ve çevresel bağlam

Bitkilerle beslenen böceklerde konukçu seçimi; beslenme, gelişme ve üreme ile ilişkili davranışların bir parçasıdır. Dişi fitofag böcekler yumurta bırakacakları yeri seçerken yavruların gelişebileceği bitkilerle karşılaşır. Larvalar da bitki üzerinde beslenme alanı seçebilir veya kısa mesafelerde bitkiler arasında hareket edebilir. Ergin erkekler ise besin aramak veya eş bulma olasılığı bulunan bitkilere yönelebilir. Konukçu bitkiyle kurulan bu ilişkiler, böceğin yaşam evresine ve davranışın işlevine göre farklılaşır (Schoonhoven ve ark., 2005; Jones ve Agrawal, 2017; Jones ve ark., 2022).

Konukçu bitkilerden yayılan uçucu ipuçları birçok fitofag böceğin bitkiye yönelmesine yardımcı olur; bu ipuçları yumurta bırakma davranışını da etkileyebilir. Böcekler uçucu karışımları bitki türlerini ayırt etmek, konukçu ile konukçu olmayan bitkileri ayırmak ve olası konukçuların uygunluğunu değerlendirmek için kullanabilir. Aynı bitki türünün bireyleri arasında da kalite farkı bulunabilir; bitkinin fizyolojik durumu ve biyotik ya da insan kaynaklı çevresel etkenlere maruz kalması bu farklılıklarla ilişkili olabilir (Bruce ve ark., 2005; Dicke ve Baldwin, 2010; Peñuelas ve Staudt, 2010).

Bitki kalitesi, fitofag böceklerin üreme başarısını etkileyen başlıca etkenlerden biridir. Karbon ve azot gibi besin maddeleri ile savunma kimyasalları, böceğin üretebileceği ve fiilen ürettiği yumurta sayısını doğrudan etkiler; kalitesi düşük ya da değişken bitkilere verilen tepkiler beslenme grupları arasında ve içinde farklılık gösterir. Bitki kalitesi ayrıca yumurta büyüklüğünü, kaynakların yumurtalar arasında paylaştırılmasını ve dişinin yumurta bırakma yeri seçimini etkileyebilir. Fitofaglar da beslendikleri bitkiyi değiştirerek hem tür içi hem de türler arası ilişkileri ve avcı ile parazitoit gibi üst trofik düzeyleri etkileyebilir (Awmack ve Leather, 2002).

Fitofag böceklerin çevresi mekânsal ve zamansal bakımdan değişkendir. Konukçu bitkilerin bulunabilirliği ve yoğunluğu yıllar, mevsimler veya kuşaklar arasında farklılaşabilir. Böcekler uygun besin ya da yumurta bırakma alanı seçmeden önce birden fazla bitkiyi örnekleyebilir. Çevredeki duyusal ipuçlarından edinilen önceki deneyim, değişen koşullarda davranışı esnetmenin yollarından biridir. Bununla birlikte böceklerin bilgi işleme kapasitesi ve duyusal sistemleri sınırsız değildir; bu durum konukçu arama ve tercihlerin nasıl oluştuğunu etkileyebilir (Agrawal, 2001; Bernays, 2001; Anderson ve Anton, 2014).

Kimyasal ipuçlarıyla konukçu arama, tanıma ve kabul

Konukçu arama süreci çoğu zaman bitkiden uzaklıkla birlikte değişen aşamalar içerir. Bitki uçucu organik bileşikleri (VOC'ler) uzaktan yön bulmaya katkı sağlayabilir. Ancak böceklerin bu bileşiklere tepki biçimleri aynı değildir: bazı uçabilen türler kokuya doğru etkin biçimde yönelirken, küçük veya uçma kabiliyeti sınırlı türler hava akımıyla taşınabilir; bazı türler ise bitkiyi ancak yakına geldiğinde değerlendirebilir. Köklerle beslenen böceklerde de toprak ortamındaki kimyasal ipuçları köklere yaklaşma ve onları tanımayla ilişkili olabilir (Johnson ve Gregory, 2006; Döring, 2014; Webster ve Cardé, 2017). Bitki koku bulutları (plume) üzerine yapılan bir derlemede, böceklerin bitki uçucularını algılama eşiğinin üzerinde ve nitel ve nicel olarak ayırt edilebilir bir karışım hâlinde bulunduklarında bir kaynağın işareti

olarak tanıyabildiği, koku bulutunun ince yapısını algılayarak bitki kokusunu arka plan kokularından ayırt edebildiği ve koku bulutunu kaynağına kadar izleyebildiği önerilmiştir (Beyaert ve Hilker, 2014).

Uçucu ipuçlarının algılanması, çoğunlukla antenlerdeki duyu kıllarında (sensillum) bulunan koku alma reseptör nöronlarına dayanır (Bruce ve Pickett, 2011). Bu nöronların bir kısmı dar bir bileşik grubuna, bir kısmı ise daha geniş bir bileşik yelpazesine tepki verir; nöronların duyarlılığını böceklere özgü bir reseptör gen ailesi ve yardımcı proteinler belirler. Güvelerde eşey feromonlarının algılanması son derece özelleşmiş nöronlarla gerçekleşirken, birçok böcek bitki sekonder metabolizmasından ve mikrobiyal etkinlikten kaynaklanan kimyasal ipuçlarına da tepki verir (de Bruyne ve Baker, 2008). Böceklerin konukçu ipuçlarını arka plandaki kokulardan ve kısa, değişken maruz kalmalardan ayırt edebilmesi, belirli bileşiklere duyarlı nöronların zamanlaması uyumlu ateşlemesine dayanır; bu sistem esnektir; çevresel reseptörler aynı kalırken sinyallerin işlenme biçimindeki değişimlerle değişen koşullara uyum sağlanabilir (Bruce ve Pickett, 2011).

Birçok durumda böcekler önce daha geniş habitatı işaret eden ipuçlarından, ardından konukçu seçimini daraltan daha özgül ipuçlarından yararlanır. Fitofaglarda farklı bitki uçucuları arasındaki bağlam ve bileşim, tercih edilen konukçuların ayırt edilmesine katkıda bulunabilir. Örneğin, bitki uçucularının belirli oranlardaki karışımları asma güvesinin konukçusunu tanımasıyla ilişkilendirilmiştir (Tasin ve ark., 2006; Silva ve Clarke, 2020). Böcekler bitki uçucularına çoğu zaman tek tek bileşikler yerine karışımlar hâlinde tepki verir; konukçu ipuçları çoğunlukla konukçuya özgü bileşiklerden değil birçok bitkide yaygın bulunan uçucular dan oluşur ve bir karışım içinde konukçuyu işaret eden bir bileşik tek başına aynı etkiyi göstermeyebilir (Bruce ve Pickett, 2011). Konukçu arama ve tanıma mekanizmaları, uzman ve genelci böceklerde farklılaşabilse de her iki grupta da duyusal ipuçlarının birlikte değerlendirilmesi önem taşır (Jones ve ark., 2022).

Bitkiye temas ettikten sonra böcek, temas kimyasalları ve tat alma ipuçlarıyla bitkinin beslenmeye ya da yumurta bırakmaya uygunluğunu değerlendirebilir. Beslenmeyi uyarıcı ve engelleyici maddelerin bileşimi kabul kararını etkileyebilir. İpek böceği larvalarında yaprak yüzeyindeki bileşikler konukçu tanımaya katkıda bulunurken, beslenmenin kabul edilmesi yaprak özsuyundaki şekere verilen tepkiyle ilişkilendirilmiştir (Tsuneto ve ark., 2020). Fitofag böceklerde beslenmeyi yönlendiren tat almaçları genel olarak beslenmeyi uyarıcı ve caydırıcı olarak sınıflandırılır; konukçu seçimi bu iki tür sinyal arasındaki dengeye bağlıdır (Chapman, 2003). Lepidoptera'da yumurta bırakma davranışı ayrıca kapsamlı biçimde derlenmiştir (Renwick ve Chew, 1994). Görsel ve kimyasal ipuçları da bazı türlerde birlikte etkili olabilir; odun delen böceklerde konukçu seçiminde farklı duyu kiplerinin katkısı incelenmiştir (Campbell ve Borden, 2009).

Bitkinin savunma bileşikleri de konukçu tanımada rol oynayabilir. Bitki sekonder bileşikleri genellikle beslenmeyi caydırır; ancak konukçuyu tanıtan ipuçları olarak işlev gördüklerinde beslenmeyi uyarabilir. Bazı oligofag ve monofag türlerde konukçuyla ilişkili tek bir kimyasal, konukçu seçiminde baskın rol oynayabilir (Chapman, 2003). Bu ilişkinin iyi bilinen bir örneği

glukozinolatlardır. Başta Brassicaceae familyasında bulunan ve 120'den fazla türü bilinen glukozinolatlar, özel hücrelerde depolanan mirozinaz enziminin etkisiyle toksik izotiyosiyanatlara dönüştürülür. Fitofag böcekler bu toksisiteyi bileşikleri dışarı atarak, detoksifiye ederek ya da davranışlarını değiştirerek azaltabilir; uzman fitofaglar ise bu bileşikleri kendi savunmaları için depolayabilir. Glukozinolat düzeyleri bitki genotipine, dokusuna ve gelişme evresine göre değişir ve böcek zararı gibi biyotik etkenlerden etkilenir (Hopkins ve ark., 2009).

Konukçu seçimi deneylerinde davranışın hangi aşamasının ölçüldüğü önemlidir. Kokuya yönelme, bitkiye konma, bitkiyi kabul etme, beslenme ve yumurta bırakma birbirinden farklı ölçümler gerektirir; tek bir deney sonucu bu davranışların tümü için kanıt sayılmaz. Fitofag böceklerde konukçu tercihi ve uyum çalışmalarında kullanılan davranış deneylerinin tasarımı ve yorumlanması bu nedenle ayrıca ele alınmıştır (Knolhoff ve Heckel, 2014). Lahanagillerde zarar yapan böcekler için geliştirilen "uygun/uygun olmayan konma" kuramı da konukçu seçimini; uçucu ipuçlarına tepki, görsel ipuçlarıyla bitkiye konma ve konduktan sonra temas ipuçlarıyla değerlendirme gibi ardışık aşamalar hâlinde ele alır (Finch ve Collier, 2000).

Önceki deneyime bağlı davranışsal plastisite

Larva dönemindeki deneyim

Tam başkalaşım geçiren fitofag böceklerde larva dönemindeki beslenme deneyiminin erginlikteki konukçu tercihine taşınıp taşınmadığı uzun süredir incelenmektedir. Bu olası deneyim aktarımı Hopkins'in konukçu seçimi ilkesiyle ilişkilendirilmiştir; farklı türlerde ve deney koşullarında sonuçların aynı yönde olmadığı da bildirilmiştir (Barron, 2001; Anderson ve Anton, 2014). Tam başkalaşım geçiren fitofag böceklerde yapılan nicel bir literatür analizinde, bitki kimyasal ipuçlarıyla edinilen deneyimin konukçu tercihine olumlu etkisinin polifag, oligofag ve monofag türlerde benzer olduğu; bu etkinin konukçu uzmanlaşma derecesinden çok filogeni ve deneyimin edinildiği gelişme evresiyle ilişkili bulunduğu bildirilmiştir (Petit ve ark., 2017).

Larva deneyiminin erginlerin üreme davranışıyla ilişkili örnekleri vardır. Pamuk üzerinde yetiştirilen *Helicoverpa armigera* erginlerinde, eş tercihinin larva döneminde deneyimlenen konukçu ile ilişkisi bir çalışmada incelenmiştir; ancak deneyde sınanan konukçuların tümünde aynı tercih görülmemiştir (Li ve ark., 2005). *Spodoptera littoralis* erkeklerinde de larva döneminde deneyimlenen bitki uçucularının, dişi eşey feromonuna verilen tepkiyle ilişkisi araştırılmıştır (Thöming ve ark., 2013). Bu sonuçlar belirli deneylere ve türlere aittir; tüm fitofag böceklere genellenemez.

Larva deneyimi, yetiştirildiği bitkiye yönelik tercihi artırmak yerine kaçınmayla da ilişkili olabilir (Mader ve ark., 2012). Doğu ladin tomurcuk kurdu *Choristoneura fumiferana* üzerinde yapılan çalışmada, larva döneminde dayanıklı beyaz ladin çeşitlerinde yetiştirilen ergin dişilerin yumurta bırakma tercihi hassas çeşitlere yönelmiş; hassas çeşitlerde yetişenlerde ise karşılaştırmalı seçim testinde belirgin tercih görülmemiştir (Blackiston ve ark., 2008). Bu örnek, larva deneyiminin her zaman deneyimlenen bitkiye yönelimi artırmadığını gösterir. Polifag kelebek *Polygonia c-album*'da larvaların üç farklı doğal

konukçuda yetiştirildiği bir çalışmada larva konukçusunun ergin dişilerin yumurta bırakma kararlarını etkilemediği bulunmuş; yazarlar Hopkins ilkesinin fitofag böceklerde konukçu seçimi için genel bir hipotez olarak kullanılmaması gerektiğini ileri sürmüştür (Janz ve ark., 2009).

Lahana kurdu *Trichoplusia ni* larvalarının gelişimin belirli döneminde bitki lateksine maruz kalmasının, ergin dişilerin lateks içeren bitkilere yumurta bırakma tepkisiyle ilişkili olduğu bildirilmiştir (Shikano ve Isman, 2009). Bu ve benzeri çalışmalar, larva deneyiminin sonraki tepkiler üzerindeki yönünün bitki bileşiğine, maruz kalma zamanına ve deney koşullarına göre değişebileceğini düşündürür; tek bir etki yönü varsayılmamalıdır (Anderson ve Anton, 2014; Jones ve Agrawal, 2017).

Erginlik dönemindeki deneyim

Erginlik döneminde edinilen deneyim de sonraki konukçu arama, beslenme ve yumurta bırakma davranışlarıyla ilişkili olabilir. Bazı davranış değişiklikleri deneyimin hemen ardından, bazıları ise daha sonra ölçülebilir; bu nedenle deneyimin zamanı ve ölçülen davranış birlikte değerlendirilmelidir (Jaenike, 1988; Anderson ve Anton, 2014).

Lahana kurdu *Trichoplusia ni* dişilerinde, belirli bir bitkinin yapraklarıyla önceki gece kurulan kısa süreli temasın ardından o bitkinin kokusuna yönelme bildirilmiştir. Bu bulgu, temasla edinilen bilginin daha sonraki uçucu ipuçlarına verilen tepkiyle ilişkilendirilebildiğini göstermektedir (Landolt ve Molina, 1996). Elma sineği *Rhagoletis pomonella* üzerine yapılan çalışmalarda da konukçu deneyimi ve yumurta bırakma tercihi arasındaki ilişkiler incelenmiştir (Papaj ve Prokopy, 1986).

Konukçu olmayan bitkilerle edinilen deneyim de sonraki tercihleri etkileyebilir. *Plutella xylostella* dişilerinde bezelye gibi konukçu olmayan bitkilerden gelen kokuya maruz kalma ve daha sonraki yumurta bırakma tercihleri arasındaki ilişki deneysel olarak araştırılmıştır (Zhang ve ark., 2007). Bu sonuç belirli bir zararlı tür ve deney düzeniyle ilgilidir; diğer türlerde aynı sonucun görüleceği varsayılamaz.

Deneyimle öğrenme yalnızca yumurta bırakma tercihlerinde değil, beslenme ve nektar arama davranışlarında da araştırılmıştır. Çöl çekirgesi *Schistocerca gregaria* erginlerinde bitki kokusuyla besin ödülünü ilişkilendirme; şahin güvesi *Manduca sexta* erginlerinde koku ve nektar deneyimi; *Helicoverpa armigera* dişilerinde ise çiçek kokusu bileşenlerine verilen tepkiler incelenmiştir (Simões ve ark., 2011; Riffell ve ark., 2008; Cunningham ve ark., 2006). Bu örnekler farklı türleri ve farklı öğrenme düzeneklerini kapsar.

Larva ve erken erginlik deneyimlerinin etkileri aynı davranışta birleşebilir veya farklı davranışlara ayrı ayrı yansıyabilir. Tahıl biti *Sitophilus granarius* çalışmalarında larva ve erginlikte besin kokusuna maruz kalmanın sonraki koku tepkileriyle ilişkisi değerlendirilmiştir. *Liriomyza huidobrensis* için bildirilen deneylerde beslenme tercihi ve yumurta bırakma tercihi aynı biçimde etkilenmemiştir (Rietdorf ve Steidle, 2002; Videla ve ark., 2010). Bu nedenle bir davranıştaki öğrenme bulgusu, başka bir davranış için doğrudan kanıt kabul edilmemelidir.

Depolanmış ürün zararlısı iki güve türünde larva besini ve erken erginlikte besin ortamına maruz kalma karşılaştırılmıştır. *Cadra cautella* ve *Plodia interpunctella* türlerinde larva deneyiminin yumurta bırakma tercihiyle ilişkisi aynı bulunmamış; erginlikten çıkış sırasındaki besin ortamı deneyiminin etkisi de incelenmiştir (Olsson ve ark., 2006). Erken erginlik deneyiminin konukçu tercihine etkisi literatürde "neo-Hopkins ilkesi" adıyla tartışılmıştır (Jaenike, 1983; Anderson ve Anton, 2014).

Konukçu tercihi ve yavru performansı

Konukçu tercihi ile yavruların bitki üzerindeki performansı arasındaki ilişki, fitofag böcek ekolojisindeki temel araştırma konularındandır. Tercih-performans hipotezi, dişi böceklerin yavrularının daha iyi geliştiği bitkilere yumurta bırakma eğiliminin evrimleşebileceğini öne sürer (Thompson, 1988). Bir meta-analiz, incelenen çalışmalarda tercih edilen bitkilerde yavru performansının ve dişilerin yumurta bırakma tercihinin genel olarak olumlu ilişki gösterdiğini; ancak bu ilişkinin beslenme uzmanlaşma derecesiyle değişebildiğini bildirmiştir (Gripenberg ve ark., 2010). Bu sonuç, her tür veya her bitki sistemi için aynı örüntünün geçerli olduğu anlamına gelmez. Çalışmalarda ergin konukçu seçimi ile yavru performansı arasında ilişki bulunamaması genellikle avcılar, konukçu bolluğu, öğrenme veya ergin beslenme alanları gibi ek etkenlerle açıklanır; buna alternatif olarak, koku algılama mekanizmasının kendisinin konukçu seçiminin evrimini sınırlayabileceği ve görünüşte kötü seçimlerin uyumsal bir davranış stratejisinin parçası olabileceği öne sürülmüştür (Cunningham, 2012).

Konukçu tanıma, bitki kimyası, böceğin duyusal ve bilişsel süreçleri, yaşam döngüsü ve deneyim gibi etkenlerin birlikte ele alınmasını gerektirir. Uzman ve genelci fitofagların konukçu tanıma süreçlerini ortak bir çerçevede değerlendiren derlemeler, seçim davranışını tek bir ipucuna veya tek bir evreye indirgememek gerektiğini vurgular (Jones ve ark., 2022; Carrasco ve ark., 2015).

Bitki koruma açısından anlamı

Kimyasal ipuçları, fitofag böceklerin konukçu bitkiyi bulma ve tanıma davranışlarını değiştirmeye yönelik bitki koruma yaklaşımlarında araştırılmaktadır. Ancak bir bileşiğin çekici ya da itici olduğunun belirlenmesi tek başına sahadaki etkililiği garanti etmez: çevredeki diğer kokular, bitkinin durumu, böceğin deneyimi ve fizyolojik durumu tepkinin yönünü veya gücünü değiştirebilir. Davranışsal plastisiteyi dikkate almak, koku aracılı konukçu tanıma ve allelokimyasalların bitki korumada kullanılmasına ilişkin araştırmaların temel önerilerindendir (Anton ve Cortesero, 2022; Thöming, 2021). Davranışı değiştiren itici ve çekici uyarıcıların birlikte kullanıldığı itme-çekme (push-pull) stratejileri bu yaklaşımların bir örneğidir (Cook ve ark., 2007); bitki uçucularına dayalı yöntemlerin tarımdaki uygulamalarında elde edilen başarılar ve karşılaşılan güçlükler de ayrıca değerlendirilmiştir (Pickett ve Khan, 2016). Böceklerin koku ortamı büyük ölçüde bitkilerin yaydığı uçuculardan oluşur; bu uçucular atmosferde taşınır, karışır ve parçalanır. Her türün yalnızca bir bölümünü algılayabildiği bu "koku manzarası" (odorscape) türe özgü, habitata bağlı ve zaman içinde

değişkendir; zararlıların koku ortamının yönlendirilmesi pestisitsiz bitki korumada umut verici bir yol olarak değerlendirilmektedir (Conchou ve ark., 2019).

Fitofag zararıyla uyarılan bitki uçucuları yalnızca fitofagları değil, onların doğal düşmanlarını da etkiler; bu uçucular saldırı altındaki bitkilere avcı ve parazitoitleri çeker. Bu etkinin ekolojik önemi yaklaşık otuz yıldır geniş ölçüde kabul görse de, uçucuların birincil işlevi ve bitki korumada kullanılabilirliği hâlâ tartışmalıdır (Turlings ve Erb, 2018).

Davranışa dayalı yöntemlerin bir diğer örneği tuzak bitki uygulamasıdır. Tuzak bitkilerin başarısı; tuzak ve ana ürünün özelliklerine, bunların mekânsal ve zamansal düzenine, böceğin davranışı ve hareketine ve üretim sisteminin tarımsal ve ekonomik gereksinimlerine bağlıdır. Bu nedenle yöntem, birçok zararlı yönetimi yaklaşımına göre daha fazla bilgi gerektirir (Shelton ve Badenes-Perez, 2006). Bitki uçucularıyla zararlı davranışının yönlendirilmesine ilişkin 34 çalışmada 50 zararlı türüne ait 374 bitki uçucusu–böcek etkileşimini değerlendiren bir meta-analizde, çekici uçucuların fitofag bolluğu üzerinde anlamlı etkisi bulunmuş, itici uçucuların ise anlamlı etkisi bulunmamıştır; yazarlar bunun, itici uçucuları sınayan arazi çalışmalarının azlığından (yaklaşık %3) kaynaklanabileceğini belirtmiştir. Aynı analizde dişilerin uçucu yemlere erkeklerden daha fazla çekildiği, beslenme genişliğinin tepkileri açıklamadığı, uygulama yönteminin zararlı bolluğunu anlamlı biçimde etkilediği ve daha fazla bileşik içeren yemlerin daha fazla birey çektiği bildirilmiştir (Szendrei ve Rodriguez-Saona, 2010). Bu bulgular, laboratuvarda belirlenen çekici ya da itici etkinin arazideki sonuca dönüşmesinin uygulama koşullarına bağlı olabileceğini düşündürmektedir.

Uygulamalı sonuç çıkarırken deneyde ölçülen davranış açıkça belirtilmelidir: uzaktan yönelme, bitkiye konma, beslenmenin başlaması, yumurta bırakma veya yavru gelişimi birbirinin yerine kullanılamaz. Bu ayrım, laboratuvar koşullarındaki tercihin tarladaki zararlı kontrolüne doğrudan aktarılacağı varsayımını önler (Knolhoff ve Heckel, 2014; Thöming, 2021).

Sonuç

İncelenen literatür, fitofag böceklerde konukçu bitki seçiminin tek bir ipucuna ya da tek bir davranış aşamasına indirgenemeyeceğini göstermektedir. Uzak mesafede uçucu karışımlar ve koku bulutlarının yapısı, yakın mesafede görsel ipuçları, bitkiye temas sonrasında ise tat alma ipuçları ile beslenmeyi uyarıcı ya da caydırıcı bileşikler sürecin farklı aşamalarında rol oynar (Finch ve Collier, 2000; Chapman, 2003; Bruce ve Pickett, 2011; Beyaert ve Hilker, 2014).

Önceki deneyim bu süreci değiştirebilir; ancak etkinin yönü ve büyüklüğü türe, deneyimin edinildiği gelişme evresine ve ölçülen davranışa göre farklılaşır. Larva deneyiminin ergin tercihlerine etkisi bazı türlerde bildirilmiş, bazılarında ise görülmemiştir; bazı durumlarda deneyim, deneyimlenen bitkiden kaçınmayla sonuçlanmıştır (Janz ve ark., 2009; Mader ve ark., 2012; Petit ve ark., 2017).

Konukçu tercihi ile yavru performansı arasındaki ilişki genel eğilim olarak olumlu olsa da sistemler arasında değişkendir (Gripenberg ve ark., 2010; Cunningham, 2012). Bitki koruma açısından, koku temelli yöntemlerin sahadaki başarısı yalnızca bileşiklerin çekici ya da itici etkisine değil; doğal koku ortamına, bitkinin durumuna, böceğin deneyimine ve uygulama

biçimine de bağlıdır (Szendrei ve Rodriguez-Saona, 2010; Conchou ve ark., 2019; Anton ve Cortesero, 2022). Bu nedenle davranış deneylerinde ölçülen davranış açıkça tanımlanmalı ve sonuçlar, çalışılan tür ve koşulların ötesine genellenmemelidir (Knolhoff ve Heckel, 2014; Thöming, 2021).

Kaynakça

Agrawal, A. A. (2001). Ecology—phenotypic plasticity in the interactions and evolution of species. Science, 294, 321–326.

Anderson, P., & Anton, S. (2014). Experience-based modulation of behavioural responses to plant volatiles and other sensory cues in insect herbivores. Plant, Cell & Environment, 37(8), 1826–1835. https://doi.org/10.1111/pce.12342

Anton, S., & Cortesero, A.-M. (2022). Plasticity in chemical host plant recognition in herbivorous insects and its implication for pest control. Biology, 11(12), 1842. https://doi.org/10.3390/biology11121842

Awmack, C. S., & Leather, S. R. (2002). Host plant quality and fecundity in herbivorous insects. Annual Review of Entomology, 47, 817–844. https://doi.org/10.1146/annurev.ento.47.091201.145300

Barron, A. B. (2001). The life and death of Hopkins' host-selection principle. Journal of Insect Behavior, 14, 725–737.

Bernays, E. A. (2001). Neural limitations in phytophagous insects: Implications for diet breadth and evolution of host affiliation. Annual Review of Entomology, 46, 703–727.

Beyaert, I., & Hilker, M. (2014). Plant odour plumes as mediators of plant–insect interactions. Biological Reviews, 89(1), 68–81. https://doi.org/10.1111/brv.12043

Blackiston, D. J., Casey, E. S., & Weiss, M. R. (2008). Retention of memory through metamorphosis: Can a moth remember what it learned as a caterpillar? PLOS ONE, 3, e1736.

Bruce, T. J. A., & Pickett, J. A. (2011). Perception of plant volatile blends by herbivorous insects – Finding the right mix. Phytochemistry, 72(13), 1605–1611. https://doi.org/10.1016/j.phytochem.2011.04.011

Bruce, T. J. A., Wadhams, L. J., & Woodcock, C. M. (2005). Insect host location: A volatile situation. Trends in Plant Science, 10(6), 269–274.

Campbell, S. A., & Borden, J. H. (2009). Additive and synergistic integration of multimodal cues of both hosts and non-hosts during host selection by woodboring insects. Oikos, 118(4), 553–563.

Carrasco, D., Larsson, M. C., & Anderson, P. (2015). Insect host plant selection in complex environments. Current Opinion in Insect Science, 8, 1–7. https://doi.org/10.1016/j.cois.2015.01.014

Chapman, R. F. (2003). Contact chemoreception in feeding by phytophagous insects. Annual Review of Entomology, 48, 455–484. https://doi.org/10.1146/annurev.ento.48.091801.112629

Conchou, L., Lucas, P., Meslin, C., Proffit, M., Staudt, M., & Renou, M. (2019). Insect odorscapes: From plant volatiles to natural olfactory scenes. Frontiers in Physiology, 10, 972. https://doi.org/10.3389/fphys.2019.00972

Cook, S. M., Khan, Z. R., & Pickett, J. A. (2007). The use of push-pull strategies in integrated pest management. Annual Review of Entomology, 52, 375–400. https://doi.org/10.1146/annurev.ento.52.110405.091407

Cunningham, J. P. (2012). Can mechanism help explain insect host choice? Journal of Evolutionary Biology, 25(2), 244–251. https://doi.org/10.1111/j.1420-9101.2011.02435.x

Cunningham, J. P., Moore, C. J., Zalucki, M. P., & Cribb, B. W. (2006). Insect odour perception: Recognition of odour components by flower-foraging moths. Proceedings of the Royal Society B, 273, 2035–2040.

de Bruyne, M., & Baker, T. C. (2008). Odor detection in insects: Volatile codes. Journal of Chemical Ecology, 34(7), 882–897. https://doi.org/10.1007/s10886-008-9485-4

Dicke, M., & Baldwin, I. T. (2010). The evolutionary context for herbivore-induced plant volatiles: Beyond the "cry for help". Trends in Plant Science, 15, 167–175.

Döring, T. F. (2014). How aphids find their host plants, and how they don't. Annals of Applied Biology, 165(1), 3–26.

Finch, S., & Collier, R. H. (2000). Host-plant selection by insects – a theory based on 'appropriate/inappropriate landings' by pest insects of cruciferous plants. Entomologia Experimentalis et Applicata, 96(2), 91–102. https://doi.org/10.1046/j.1570-7458.2000.00684.x

Gripenberg, S., Mayhew, P. J., Parnell, M., & Roslin, T. (2010). A meta-analysis of preference–performance relationships in phytophagous insects. Ecology Letters, 13(3), 383–393. https://doi.org/10.1111/j.1461-0248.2009.01433.x

Hopkins, R. J., van Dam, N. M., & van Loon, J. J. A. (2009). Role of glucosinolates in insect-plant relationships and multitrophic interactions. Annual Review of Entomology, 54, 57–83. https://doi.org/10.1146/annurev.ento.54.110807.090623

Jaenike, J. (1983). Induction of host preference in *Drosophila melanogaster*. Oecologia, 58(3), 320–325.

Jaenike, J. (1988). Effects of early adult experience on host selection in insects: Some experimental and theoretical results. Journal of Insect Behavior, 1, 3–15.

Janz, N., Söderlind, L., & Nylin, S. (2009). No effect of larval experience on adult host preferences in Polygonia c-album (Lepidoptera: Nymphalidae): On the persistence of Hopkins' host selection principle. Ecological Entomology, 34(1), 50–57. https://doi.org/10.1111/j.1365-2311.2008.01041.x

Johnson, S. N., & Gregory, P. J. (2006). Chemically mediated host-plant location and selection by root-feeding insects. Physiological Entomology, 31(1), 1–13. https://doi.org/10.1111/j.1365-3032.2005.00487.x

Jones, P. L., & Agrawal, A. A. (2017). Learning in insect pollinators and herbivores. Annual Review of Entomology, 62, 53–71. https://doi.org/10.1146/annurev-ento-031616-034903

Jones, L. C., Rafter, M. A., & Walter, G. H. (2022). Host interaction mechanisms in herbivorous insects—Life cycles, host specialization and speciation. Biological Journal of the Linnean Society, 137(1), 1–14. https://doi.org/10.1093/biolinnean/blac070

Knolhoff, L. M., & Heckel, D. G. (2014). Behavioral assays for studies of host plant choice and adaptation in herbivorous insects. Annual Review of Entomology, 59, 263–278. https://doi.org/10.1146/annurev-ento-011613-161945

Landolt, P. J., & Molina, O. (1996). Host-finding by cabbage looper moths (Lepidoptera: Noctuidae): Learning of host odor upon contact with host foliage. Journal of Insect Behavior, 9, 899–908.

Li, Z., Li, D., Xie, B., Ji, R., & Cui, J. (2005). Effect of body size and larval experience on mate preference in *Helicoverpa armigera* (Hübner) (Lepidoptera: Noctuidae). Journal of Applied Entomology, 129, 574–579.

Mader, B. J., Daoust, S. P., Cardinal-Aucoin, M., Bauce, E., & Despland, E. (2012). Larval experience induces adult aversion to rearing host plants: A novel behaviour contrary to Hopkins' host-selection principle. Ecological Entomology, 37, 204–211. https://doi.org/10.1111/j.1365-2311.2012.01357.x

Olsson, P. O. C., Anderbrant, O., & Löfstedt, C. (2006). Experience influences oviposition behaviour in two pyralid moths, *Ephestia cautella* and *Plodia interpunctella*. Animal Behaviour, 72, 545–551.

Papaj, D. R., & Prokopy, R. J. (1986). Phytochemical basis of learning in *Rhagoletis pomonella* and other herbivorous insects. Journal of Chemical Ecology, 12, 1125–1143. https://doi.org/10.1007/BF01639000

Peñuelas, J., & Staudt, M. (2010). BVOCs and global change. Trends in Plant Science, 15, 133–144.

Petit, C., Dupas, S., Thiéry, D., Capdevielle-Dulac, C., Le Ru, B., Harry, M., & Calatayud, P.-A. (2017). Do the mechanisms modulating host preference in holometabolous phytophagous insects depend on their host plant specialization? A quantitative literature analysis. Journal of Pest Science, 90(3), 797–805. https://doi.org/10.1007/s10340-017-0833-4

Pickett, J. A., & Khan, Z. R. (2016). Plant volatile-mediated signalling and its application in agriculture: Successes and challenges. New Phytologist, 212(4), 856–870. https://doi.org/10.1111/nph.14274

Renwick, J. A. A., & Chew, F. S. (1994). Oviposition behavior in Lepidoptera. Annual Review of Entomology, 39, 377–400. https://doi.org/10.1146/annurev.en.39.010194.002113

Rietdorf, K., & Steidle, J. L. M. (2002). Was Hopkins right? Influence of larval and early adult experience on the olfactory response in the granary weevil *Sitophilus granarius* (Coleoptera: Curculionidae). Physiological Entomology, 27, 223–227.

Riffell, J. A., Alarcón, R., Abrell, L., Davidowitz, G., Bronstein, J. L., & Hildebrand, J. G. (2008). Behavioral consequences of innate preferences and olfactory learning in

hawkmoth–flower interactions. Proceedings of the National Academy of Sciences, 105, 3404–3409.

Schoonhoven, L. M., van Loon, J. J. A., & Dicke, M. (2005). Insect–Plant Biology (2nd ed.). Oxford University Press.

Shelton, A. M., & Badenes-Perez, F. R. (2006). Concepts and applications of trap cropping in pest management. Annual Review of Entomology, 51, 285–308. https://doi.org/10.1146/annurev.ento.51.110104.150959

Shikano, I., & Isman, M. B. (2009). A sensitive period for larval gustatory learning influences subsequent oviposition choice by the cabbage looper moth. Animal Behaviour, 77(1), 247–251. https://doi.org/10.1016/j.anbehav.2008.08.033

Silva, R., & Clarke, A. R. (2020). The "sequential cues hypothesis": A conceptual model to explain host location and ranking by polyphagous herbivores. Insect Science, 27(6), 1136–1147.

Simões, P. M. V., Ott, S. R., & Niven, J. E. (2011). Associative olfactory learning in the desert locust, *Schistocerca gregaria*. Journal of Experimental Biology, 214, 2495–2503.

Szendrei, Z., & Rodriguez-Saona, C. (2010). A meta-analysis of insect pest behavioral manipulation with plant volatiles. Entomologia Experimentalis et Applicata, 134(3), 201–210. https://doi.org/10.1111/j.1570-7458.2009.00954.x

Tasin, M., Bäckman, A. C., Bengtsson, M., Ioriatti, C., & Witzgall, P. (2006). Essential host plant cues in the grapevine moth. Naturwissenschaften, 93(3), 141–144.

Thöming, G. (2021). Behavior matters—Future need for insect studies on odor-mediated host plant recognition with the aim of making use of allelochemicals for plant protection. Journal of Agricultural and Food Chemistry, 69(36), 10469–10479. https://doi.org/10.1021/acs.jafc.1c03593

Thöming, G., Larsson, M. C., Hansson, B. S., & Anderson, P. (2013). Comparison of plant preference hierarchies of male and female moths and the impact of larval rearing hosts. Ecology, 94, 1744–1752.

Thompson, J. N. (1988). Evolutionary ecology of the relationship between oviposition preference and performance of offspring in phytophagous insects. Entomologia Experimentalis et Applicata, 47(1), 3–14. https://doi.org/10.1111/j.1570-7458.1988.tb02275.x

Tsuneto, K., Endo, H., Shii, F., Sasaki, K., Nagata, S., & Sato, R. (2020). Diet choice: The two-factor host acceptance system of silkworm larvae. PLOS Biology, 18(9), e3000828.

Turlings, T. C. J., & Erb, M. (2018). Tritrophic interactions mediated by herbivore-induced plant volatiles: Mechanisms, ecological relevance, and application potential. Annual Review of Entomology, 63, 433–452. https://doi.org/10.1146/annurev-ento-020117-043507

Videla, M., Valladares, G., & Salvo, A. (2010). Differential effects of experience on feeding and ovipositing preferences of a polyphagous leafminer. Entomologia Experimentalis et Applicata, 137, 184–192.

Webster, B., & Cardé, R. T. (2017). Use of habitat odour by host-seeking insects. Biological Reviews, 92(2), 1241–1249.

Zhang, P.-J., Liu, S.-S., Wang, H., & Zalucki, M. P. (2007). The influence of early adult experience and larval food restriction on responses toward nonhost plants in moths. Journal of Chemical Ecology, 33, 1528–1541. https://doi.org/10.1007/s10886-007-9325-y

GREENS FOR A HEALTHIER BRAIN: DIETARY FIBRE, THE GUT–BRAIN AXIS, AND NEUROPROTECTION FROM SPINACH AND AMARANTHUS

K.R. Padma
Department of Biotechnology, Sri Padmavati Mahila Visvavidyalayam (Women's) University, Tirupati, AP.

K. Sri Vidya
Department of Biotechnology, Sri Padmavati Mahila Visvavidyalayam (Women's) University, Tirupati, AP.

K. R. Don
Reader, Department of Oral Pathology and Microbiology, Sree Balaji Dental College and Hospital, Bharath Institute of Higher Education and Research (BIHER), Bharath University, Chennai, Tamil Nadu, India, Email
ORCID NO: 0000-0003-3110-8076.

ABSTRACT
Mental function impairment and cognitive decline pose a concern to worldwide health, especially with the neurodegenerative diseases associated with ageing, including Alzheimer disease, Parkinson disease. Recent research demonstrates that dietary fibre and the gut-brain axis may have an important role in the preservation of cognitive functioning and protecting neurological health. Spinach and Amaranthus species vegetables are types of leafy vegetables which are quite nutritious. Dietary fibre, vitamins, minerals, antioxidants and polyphenolic compounds are included. These substances can guard the nerve cells from harm. Fermentation of dietary fibre by intestinal microbes results in the production of short-chain fatty acids (SCFAs), acetate, propionate and butyrate. Metabolites may protect the integrity of the intestinal barrier, modulate immunity, impede systemic inflammation, and mediate the gut–brain axis. The bioactive compounds a that spinach and Amaranthus contain can furthermore, due to its anti-oxidative and anti-inflammatory properties, ameliorate oxidative stress and inflammation that damage neurons. This review specifically examines the neuroprotective effect of the dietary fibre from these green leafy vegetables with special emphasis on interactions of dietary components, gut microbiota, SCFAs and neurological health. The paper also critically examines animal and human data and distinguishes mechanistic discoveries from observational associations and clinical benefits. Although studies indicate that leafy-green vegetables may confer benefits for healthy cognitive aging, evidence for the neuroprotective effect of the fibre of spinach and Amaranthus is scarce. It is important for future studies to consider species-specific differences, as well as the processing and level of dietary intake. Finally, a line of study should also distinguish between fibre-specific effects and the effects of other nutrients and phytochemicals. The mechanisms involved could potentially justify the establishment of spinach and Amaranthus as useful components of nutritional strategies for cognitive enhancement.

Keywords: Dietary fibre; Gut–brain axis; Spinach; *Amaranthus*; Gut microbiota; Neuroprotection.

Introduction

The progressive dysfunction and loss of neurons, seen in conditions such as Alzheimer's disease, Parkinson's disease, Huntington's disease and amyotrophic lateral sclerosis (ALS), defines neurodegenerative disease. There has been increasing interest, along with drug research, in dietary patterns and their contribution to cognition. Higher consumption of green leafy vegetables is associated with slower cognitive decline, according to observational evidence. This, however, does not mean that any one vegetable or nutrient prevents neurodegenerative disease (Morris et al., 2018). The fermentation of dietary fibre by intestinal microorganisms produces short-chain fatty acids (SCFAs) like acetate and propionate and butyrate. These metabolites can impact gut physiology, immune signaling, and gut-brain communication. Newly available evidence provides a justification for the investigation of dietary fibre as one component of nutritional strategies that could promote brain health. The efficacy may depend on fibre type, diet and individual microbiome (Yadav et al., 2022).

Amaranthus and Spinach (Spinacia oleracea) are popular leafy vegetables that are rich in dietary fiber as well as vitamins, minerals, carotenoids, and phenolic compounds. Parasitic plants have nutrients that can be beneficial to brain health according to studies. Nonetheless, the evidence for the general benefit of leafy vegetables, isolated phytochemicals, and gut effects mediated through fibre (as mentioned earlier) should not be taken to imply that fibre from these vegetables, in particular, prevents neurodegenerative disease. This review will first outline their nutritional composition and plausible biological mechanisms, and subsequently the experimental and human evidence potentially supportive of their neuroprotective role.

2. Nutritional Composition — A Nutrient-Rich Foundation for Brain Health

Spinach, Spinacia oleracea, and Amaranthus species are leafy vegetables with high nutrient content that supply dietary fibre, vitamins, minerals, carotenoids and other phytochemicals. The nutrients in these foods and the consumption of the categories in a day show that essential nutrients found in spices do not merely enhance nutrient intake daily. However, many of these components participate in physiological processes relevant to metabolic regulation, antioxidant defense, gut health, and normal functioning of the nervous system. Compounds of fruit varies on account of species, cultivar, soil conditions, climate, maturity at harvest, part used and post-harvest handling.

Consequently, the nutritional values that are reported for one species or species preparation should not be generalised to all spinach and Amaranth vegetables (Venskutonis and Kraujalis, 2013). Amazing Benefits of Dietary Fibre Leafy vegetables also contain important dietary fibre and other carbohydrate fractions which are not completely digested and or absorbed in human small intestine. In a broad spectrum, the fibre can be said to be soluble and insoluble fraction although the physicochemical properties and physiological effects of these are quite various. Fibers not dissoluble may increase the bulk of the stool and enhance their intestinal transit. Some of the soluble and fermentable fibers are acted on by colonic microorganisms. Fermentability of soluble fibre depends on the structure of the ingredient and the composition of the gut microbiota (Gill et al., 2021). The appropriate fiber substrates are fermented to

generate SCFAs. These substances are involved in communication within the intestines and metabolism and are attracting attention for their potential roles in immune regulation and gut–brain communication. This implies there is a real biological association between fibre-rich foods and the brain. The variety and amount of SCFAs produced depend on the type and amount of fibre consumed, as well as microbial composition, other dietary factors, and specific factors of the intestinal environment. It is impossible to conclude whether spinach or Amaranthus fibre affects human neuroprotection.

Essential Functions of the Vitamins and Minerals – Nervous System

The incorporation of spinach and edible Amaranthus leaves can provide micronutrients such as folate, vitamin C, vitamin K, iron, calcium, magnesium, potassium and more. These substances influence many body processes including cellular metabolism, normal blood formation, neurotransmission and antioxidant defence. In other words, this evidence does not mean that eating the vegetable will protect people from the neurodegenerative disease. We must think instead of the impact on the brain in relation to diet and personal nutrition. One-carbon metabolism includes folate, while iron is an essential part of oxygen transport and many other enzymes.

The vitamin C as an antioxidant defence, is supplemented with magnesium and calcium in neuronal signalling. While Vitamin K is best known for its role in clotting blood and various other biological processes, its potential neuroprotective role is currently being explored in humans. The fact that green leafy vegetables contain nutrients makes them nutritious but does not mean that they have any therapeutic action against Alzheimer’s, Parkinson’s or other neuro-degenerative diseases. Carotenoids and phenolic substances. The dietary sources of carotenoids are lutein and β-carotene. Because of β-carotene presence, they are also thought to be sources of carotenoids. Lutein is gaining a lot of attention due to its study on visual and brain health. β-Carotene is a carotenoid, or provitamin A. The food composition, preparation, dietary fat, and intestinal absorption will decide the biological availability of the vitamin. Research data on the linked carotenoids or their association with cognitive outcomes do not prove the clinical benefit of spinach fibre.

The concentrations and profiles of phenolic compounds and flavonoids are different for the species, cultivars, and plant parts of edible Amaranthus species. The antioxidant exposure and inflammatory effects of these compounds are investigated. Nonetheless, their activity in experimental systems may not represent dietary concentrations achievable from normal food intake. So specialists must perform a chemical characterization and carry out appropriate biological studies before one can identify particular compounds as the main contributors to any neuroprotective effect. The Impact of Processing and Food Preparation Washing, cutting, storing, cooking, and other processing activities change the composition of a vegetable. Heating may destroy some heat-sensitive nutrients while other nutrients may become more extractable or more accessible when heated. Water-soluble compounds may be lost to the cooking water depending on how food is prepared.

The nutritional value of raw leaves can be different from vegetables that have been boiled, steamed, or treated in other ways. The processing techniques can impact the nutritional and phytochemical properties of spinach, according to Sarma and TR (2024). The bulleted differences are particularly important when comparing studies that test food-based interventions compared to tests that use dried powders, concentrated extracts, or isolated compounds. Different preparations contain different active ingredients. Therefore, one preparation's results cannot be extrapolated to another. The fibre and micronutrient combination of the spinach and Amaranthus is relevant to healthy eating patterns and brain function research. Viewing the potential neuroprotective role of dietary compounds as a research question involving several dietary components and physiological pathways and not as an effect proven to prevent disease as a result of a single nutrient is the best way to go about it. **(Shown in Table 1)**

Table 1. Nutritional components of spinach and Amaranthus species and their potential relevance to brain health

Nutritional component	Spinach (S. oleracea)	Amaranthus species	Potential physiological relevance
Dietary fibre	Contributes to total dietary fibre intake	Contributes to dietary fibre intake; composition varies by species and plant part	Supports bowel function; fermentable fractions may promote SCFA production by gut microbiota
Carotenoids	Contains lutein and β-carotene	Carotenoid content varies among species and cultivars	Antioxidant activity; lutein is being investigated for its potential relationship with cognitive health
Vitamin C	Provides vitamin C	Provides vitamin C, with amounts varying by species and preparation	Contributes to antioxidant defence and normal cellular function
Folate	Contributes dietary folate	Folate content varies with species and growing conditions	Supports one-carbon metabolism and normal cellular processes
Vitamin K	Recognised dietary source	Amounts vary by species and plant material	Essential for normal physiological processes, including blood coagulation
Iron	Provides non-haem iron	Can contribute dietary iron; concentration varies	Supports oxygen transport and iron-dependent enzymatic processes
Magnesium	Provides magnesium	Provides magnesium in species-dependent amounts	Contributes to normal neuromuscular function and cellular signalling
Calcium and potassium	Supplies both minerals	Supplies both minerals, with concentrations varying	Supports normal muscle, nerve, and cellular function
Phenolic compounds and flavonoids	Contains various phenolic compounds	Contains phenolics and flavonoids, with profiles varying by species	Potential antioxidant and anti-inflammatory activities under appropriate experimental conditions

3. How Intestinal Microbes May Influence the Brain – The Role of Dietary Fiber and Gut Brain Axis

The gut–brain axis refers to the two-way communication between the gut and the brain. This communication occurs through different neural, endocrine, immune, and metabolic pathways. The biological signaling and inflammatory responses of this interaction will be influenced by the gut microbiota and gut barrier. Nutritional patterns can alter the composition and activity of gut microorganisms. This provides a framework to investigate the relationship between diet and brain health. Nonetheless, gut-brain communication mechanisms are complex, and no one microbial pathway can account for the onset and/or progression of neurodegenerative diseases (Mayer et al., 2022).

The intestinal microflora can metabolize fermentable fiber which is present in foods, such as fruits, vegetables, barley, oats, and wheat, to produce the short-chain fatty acids (SCFAs) acetate, propionate and butyrate. These metabolites are involved in energy metabolism and cellular signalling functions of the host. They have been studied for their possible ability to regulate inflammation, promote intestinal barrier integrity and modulate neurological functions. Nonetheless, the production and biological functions of SCFA depends on different factors including the type of fibre, diet composition, and the gut microbial community structure. As a result, a higher intake of dietary fibre is not going to have the same microbial or neurological effects on everyone. It is worth researching if the fibre from spinach (Spinacia oleracea) and Amaranthus species can influence these pathways and if such effects are relevant to neurodegenerative disease risk (O'Riordan et al., 2022)**. (Shown in figure-1)**

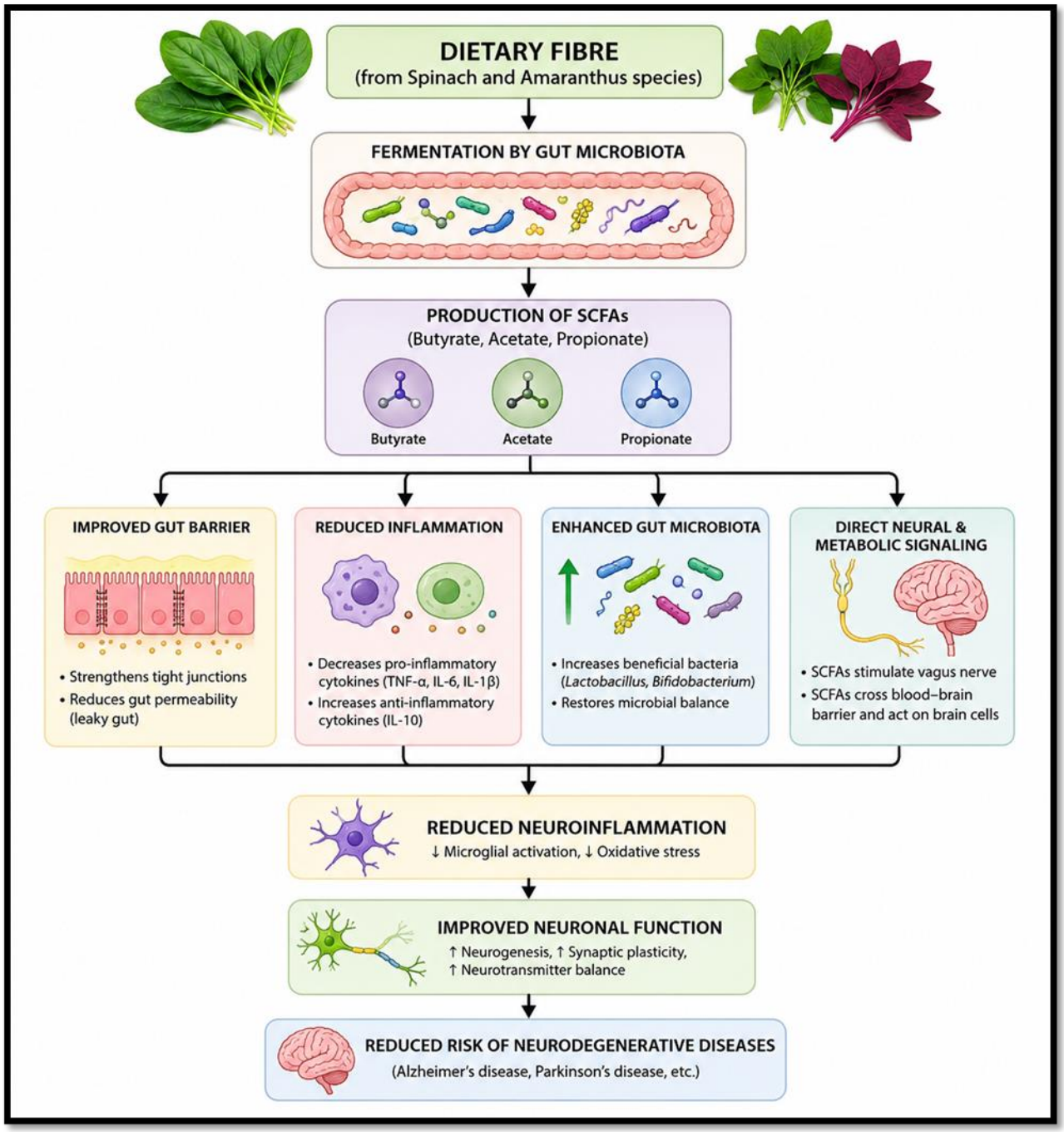


Figure 1: A schematic representation of the fermentation process by gut microbiota to manufacture short-chain fatty acids (SCFAs) from dietary fibre sources like spinach and amaranthus. The risk of neurodegenerative illnesses can be lowered by these SCFAs through promoting gut barrier integrity, reducing inflammation, modulating microbiota, and engaging in neuronal signalling.

4. Bioactive substances other than fiber are antioxidants, inflammation, and neuronal resistance mechanisms

Along with dietary fibre, spinach (Spinacia oleracea) and Amaranthus spp. contain various bioactive constituents which have the potential to affect biological processes associated with neuronal health. Spinach is an acknowledged dietary source of carotenoids, primarily lutein

and beta-carotene while some Amaranthus species have been reported to contain flavonoids and various phenolic substances. Scientists are particularly interested in the antioxidant and anti-inflammatory properties of these compounds. The involvement of oxidative stress and chronic inflammation in the pathogenesis of neurodegenerative disorders may present a utility for these bioactive compounds in the study of brain health. There could be changes in biological effects according to chemical structure, concentration, bioavailability, metabolism, and the experimental conditions (Firozjae et. al., 2025).

Studies conducted on Lutein for association with cognitive performance and neurological outcomes and protecting cells from oxidative damage are examined. Lutein research may confer neuropharmacological effects but their strength varies across experimental models and human studies. Determining whether spinach or Amaranthus consumption protects against neurodegenerative diseases would require human studies to be carried out and not laboratory research on other species. In addition, the bioactive compounds in these vegetables do not indicate that dietary fibre itself is responsible for any neurological indicating observed. To summarize, human studies well designed more, are therefore needed to clarify the contribution of individual compounds, whole-vegetable consumption and associated dietary patterns to cognitive health. **(Shown in Figure-2)**

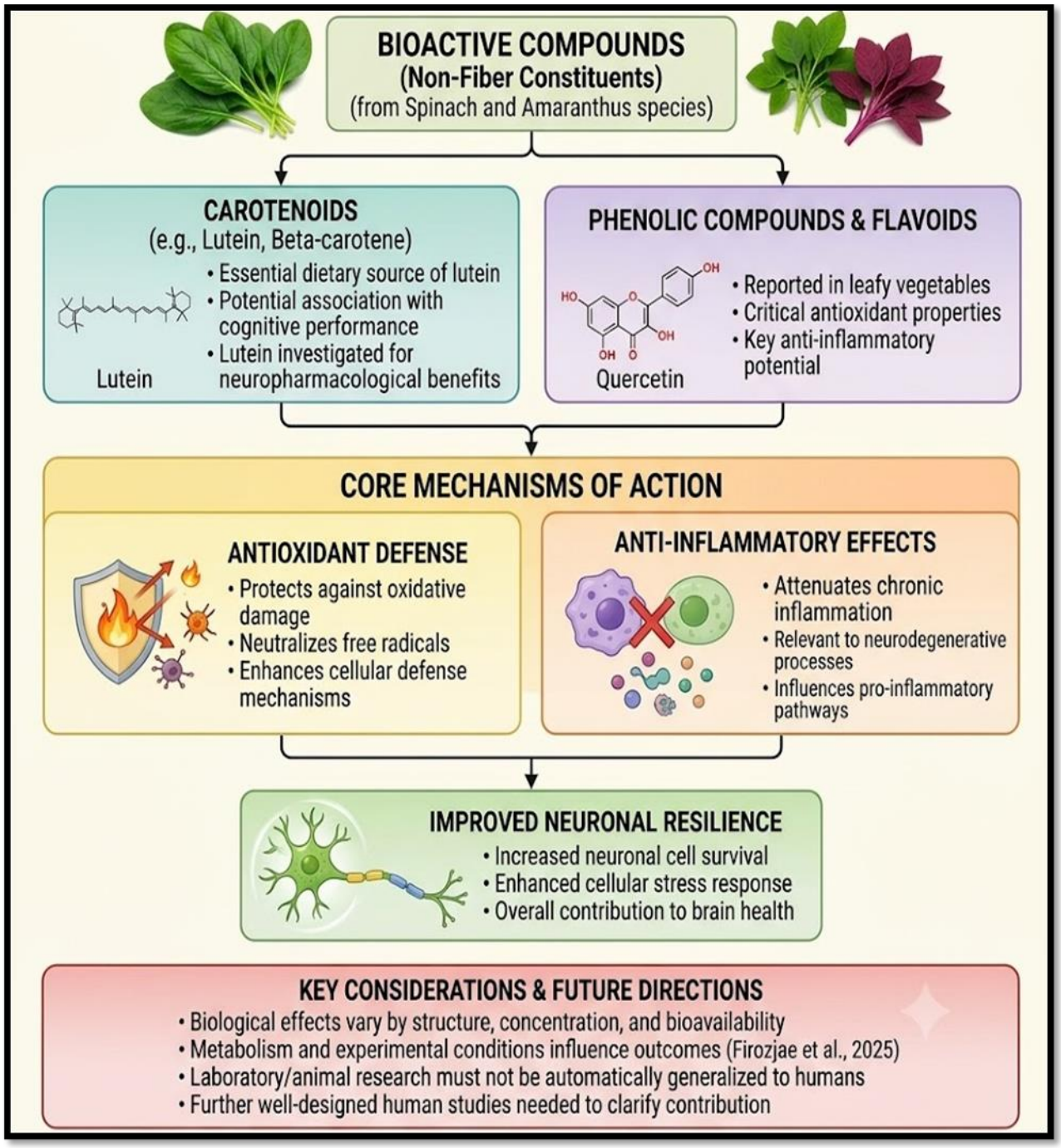


Figure 2: Theoretical framework for the neuroprotective pathways involving non-fiber bioactive components in Amaranthus species and spinach (Spinacia oleracea). Bioactive substances, such as phenolic acids, carotenoids (such as lutein, & β-carotene), and flavonoids, offer protection against oxidative stress and chronic neuroinflammation through their antioxidant and anti-inflammatory capabilities.

5. The Evidence From Animal Studies And Human Studies: What Does It Show In Practice?

Studies done on both “laboratory” and “real life” show that leafy-vegetable consumption may improve brain health. Evidence strength varies by study design, food or compound under

study, and outcome measured. Other health effects. Researchers can investigate neuronal signalling, oxidative stress, inflammation, and cognitive performance via animal studies in a controlled condition. Joseph et al.(1998) looked into the impact of long-term dietary supplementation with strawberry, spinach or vitamin E on age-related neuronal signalling and cognitive behavioural deficits in old animals. As demonstrated in the work of Pezeshki- Nia et al. (2020), the present study provides experimental evidence related to spinach and brain ageing; however, it does not prove that a dietary fibre was responsible for the effect. As spinach has many nutrients and phytochemical, one can't automatically assign any effects from a whole food intervention to one component. Human studies offer corroborating evidence, though the most important distinction is that between observational studies and clinical trials.

Studies have investigated associations between leafy-green vegetable consumption and cognitive decline while those in which dietary fibre, gut microbiota and short-chain fatty acids (SCFAs) have been assessed, observed key physiological processes relevant to brain health. Morris et al, 2018, looked at nutrients and bioactive compounds in green leafy vegetables for cognitive decline. These findings may lead to further inquiries, but it is worth remembering that observation does not equal causation, and the association may depend on other diet, lifestyle and health factors. In addition, evidence relating to leafy vegetables more generally or to particular nutrients, does not directly demonstrate that fibre from spinach (Spinacia oleracea) or Amaranthus species is protective against Alzheimer's disease, Parkinson's disease or other neurodegenerative diseases. Future investigations must compare whole vegetables with isolated fiber, specify the plant species and preparation method, quantify the consumed dose, and evaluate validated cognitive or clinical outcomes over an appropriate follow-up period. **(Shown in Table-2)**

Table-2: Summary of experimental and clinical evidence relevant to leafy vegetables and brain health

Evidence category	Research focus	Main contribution	Key limitation
Animal studies	Spinach, strawberry, and vitamin E supplementation in aged animals	Investigates age-related neuronal signalling and cognitive behavioural performance under controlled conditions	Cannot establish that fibre alone caused the effects or that findings translate directly to humans
Human observational studies	Consumption of green leafy vegetables and cognitive decline	Identifies associations between dietary patterns, nutrients, bioactive compounds, and cognitive outcomes	Associations do not establish causation and may be influenced by confounding factors
Gut microbiota research	Fermentation of dietary fibre and production of SCFAs	Provides plausible mechanisms through which diet and microbial metabolites may influence host physiology	Responses vary with fibre type, microbiota composition, and other individual factors
Whole-food intervention studies	Consumption of spinach or Amaranthus as part of the	Could assess the combined effects of fibre, vitamins,	Effects cannot readily be attributed to one component

	diet	minerals, and phytochemicals	unless the study design separates them
Isolated-fibre studies	Supplementation with quantified fibre fractions from specific vegetables	Could clarify whether particular fibre fractions influence microbial or clinical outcomes	Direct evidence specific to spinach and Amaranthus fibre and neurodegenerative disease outcomes remains limited
Controlled human clinical trials	Dietary interventions with validated cognitive or clinical assessments	Could provide stronger evidence about efficacy and potential causal relationships	Require suitable comparison groups, adequate sample sizes, appropriate follow-up, and reproducible outcome measures

6. Identifying Research Gaps and Future Directions

While it is believed that spinach and Amaranthus species possesses dietary fibre and useful phytochemicals, much is yet to be known. In the future the research ought to consider the plant species, cultivar, edible plant part, and other used preparation. A further analysis of total dietary fibre, and soluble and insoluble fractions of food along with their associated carotenoids, phenolic compound, vitamin and mineral content. Because the nutritional composition changes depending on growing conditions, stage of maturity, storage, cooking, and processing, this information for use. Standardized characterization would enable better comparability between studies. Understanding the biological effects reported are associated with fibre fractions in particular, other bioactive compounds, or both will help by doing this.

Future research will need to include the design of well-designed human studies moving beyond lab and animal studies. Experimental studies are required to observe the gut microbial composition, SCFA production and intestinal barrier function. Controlled human interventions could compare whole spinach or Amaranthus consumption with suitable control diets or characterised fibre preparations. Scholarly researchers should rely on validated cognitive measures and explicit clinical endpoints that are sufficiently followed up to enable suitable sample sizes. Factors that should also be taken into account include participant age, baseline diet, physical activity, drug use and pre-existing conditions. In summary, multi-year studies are critical to establish whether the changes noted in these brain biomarkers have any effect on cognitive function or neurodegenerative disease frequency. Until such evidence becomes available, it should be regarded as a potential research direction rather than a clinical benefit.

7. Conclusion

Spinach (Spinacia oleracea) and Amaranthus species are nutrient-rich leafy vegetables that provide dietary fibre, vitamins, minerals, carotenoids, and other phytochemicals. These components are relevant to research on general health and brain ageing because they may influence physiological processes such as intestinal microbial fermentation, SCFA signalling, oxidative stress, and inflammation. Experimental studies involving spinach supplementation in aged animals and observational research on green leafy vegetables offer a rationale for

further investigation. Nevertheless, evidence concerning whole vegetables, individual bioactive compounds, and general dietary fibre cannot be treated as interchangeable.

At present, the evidence does not establish that fibre isolated from spinach or Amaranthus prevents Alzheimer's disease, Parkinson's disease, or other neurodegenerative conditions. Nor can potential effects be attributed to fibre alone when a whole vegetable contains multiple interacting nutritional components. Future research should therefore prioritise precise nutritional characterisation, mechanistic studies, and well-controlled human interventions. A clearer understanding of these relationships may help establish whether particular vegetables or fibre fractions contribute to measurable improvements in cognitive health. Until stronger direct evidence becomes available, spinach and Amaranthus are best discussed as nutritious components of a balanced diet and promising subjects for further research, rather than proven strategies for preventing neurodegenerative disease.

Author Contributions

Dr.K.R.Padma and K. Srividya contributed to writing, and drawing figures and tables in this research article. KRP and KS solely drafted this review article. Dr.K.R.Padma, and Dr. K.R.Don has done the final editing of the paper.

ACKNOWLEDGEMENTS

The authors gratefully acknowledge Sri Padmavati Mahila Visvavidyalayam, Tirupati, Andhra Pradesh, and the Department of Oral Pathology and Microbiology, Sree Balaji Dental College and Hospital, Bharath Institute of Higher Education and Research (BIHER), Bharath University, Chennai, Tamil Nadu, India, for their constant support and encouragement.

Conflicts of Interest:

"The authors declare no conflict of interest."

DECLARATIONS

Availability of data and materials

"The datasets used and/or analysed during the current study available from the corresponding author on reasonable request."

ETHICS APPROVAL AND CONSENT TO PARTICIPATE

Not applicable

Funding

"This research received no external funding".

Clinical Trial Number

Not applicable

Consent Statement

I have read and understood the study details, including its purpose, procedures, and potential risks or benefits. I understand that participation is voluntary, involves tasting the product, and I may withdraw at any time without penalty. I consent to participate and allow my data to be used for research purposes. We confirm that all research was performed in accordance with relevant guidelines/regulations, and include in their manuscript a statement confirming that informed consent was obtained from all participants and/or their legal guardians.

References

Firozjae, A. A., Shiran, M. R., & Rashidi, M. (2025). The neuropharmacological and clinical effects of lutein: A systematic review. Hormone Molecular Biology and Clinical Investigation, 46(1), 27–38. https://doi.org/10.1515/hmbci-2024-0053.

Gill, S. K., Rossi, M., Bajka, B., & Whelan, K. (2021). Dietary fibre in gastrointestinal health and disease. Nature Reviews Gastroenterology & Hepatology, 18, 101–116. https://doi.org/10.1038/s41575-020-00375-4.

Guo, B., Zhang, J., Zhang, W., Chen, F., & Liu, B. (2025). Gut microbiota-derived short chain fatty acids act as mediators of the gut-brain axis targeting age-related neurodegenerative disorders: A narrative review. Critical Reviews in Food Science and Nutrition, 65(2), 265–286. https://doi.org/10.1080/10408398.2023.2272769.

Joseph, J. A., Shukitt-Hale, B., Denisova, N. A., Prior, R. L., Cao, G., Martin, A., Taglialatela, G., & Bickford, P. C. (1998). Long-term dietary strawberry, spinach, or vitamin E supplementation retards the onset of age-related neuronal signal-transduction and cognitive behavioral deficits. The Journal of Neuroscience, 18(19), 8047–8055. https://doi.org/10.1523/JNEUROSCI.18-19-08047.1998.

Mayer, E. A., Nance, K., & Chen, S. (2022). The gut–brain axis. Annual Review of Medicine, 73, 439–453. https://doi.org/10.1146/annurev-med-042320-014032.

Morris, M. C., Wang, Y., Barnes, L. L., Bennett, D. A., Dawson-Hughes, B., & Booth, S. L. (2018). Nutrients and bioactives in green leafy vegetables and cognitive decline: Prospective study. Neurology, 90(3), e214–e222. https://doi.org/10.1212/WNL.0000000000004815.

O'Riordan, K. J., Collins, M. K., Moloney, G. M., Knox, E. G., Aburto, M. R., Fülling, C., Morley, S. J., Clarke, G., Schellekens, H., & Cryan, J. F. (2022). Short chain fatty acids: Microbial metabolites for gut-brain axis signalling. Molecular and Cellular Endocrinology, 546, 111572. https://doi.org/10.1016/j.mce.2022.111572.

Pezeshki-Nia, S., Asle-Rousta, M., & Mahmazi, S. (2020). Spinacia oleracea L. extract attenuates hippocampal expression of TNF-α and IL-1β in rats exposed to chronic restraint stress. Medical Journal of the Islamic Republic of Iran, 34, Article 10. https://doi.org/10.34171/mjiri.34.10.

Sarma, U., & TR, B. (2024). Dietary phytonutrients in common green leafy vegetables and the significant role of processing techniques on spinach: A review. Food Production, Processing and Nutrition, 6, Article 10. https://doi.org/10.1186/s43014-023-00192-7.

Venskutonis, P. R., & Kraujalis, P. (2013). Nutritional components of amaranth seeds and vegetables: A review on composition, properties, and uses. Comprehensive Reviews in Food Science and Food Safety, 12(4), 381–412. https://doi.org/10.1111/1541-4337.12021.

Yadav, S., Dwivedi, A., Tripathi, A., & Tripathi, A. K. (2022). Therapeutic potential of short-chain fatty acid production by gut microbiota in neurodegenerative disorders. Nutrition Research, 106, 72–84. https://doi.org/10.1016/j.nutres.2022.07.007.

MINERALOGICAL CHARACTERISTICS OF FLOODPLAIN SOILS IN SOUTHERN TARABA STATE NORTHEAST, NIGERIA

Imadojemu, P.E.
Department of Soil Science and Land Resources Management, Federal University Wukari, Taraba State, Nigeria

Imadojemu, O.I.
Department of Agricultural Economics and Extension, Federal University Wukari, Taraba State, Nigeria

ABSTRACT

This study evaluated the mineralogical, morphological, physical and chemical characteristics of fadama (floodplains) soils in Ibi, Wukari and Donga Local Government Areas of southern Taraba State, Nigeria. Three representative pedons were examined within floodplain mapping units delineated according to flooding status and geomorphology. Routine soil analyses and X-ray diffraction (XRD) of the clay fraction were used to assess soil properties and mineral assemblages. The soils were predominantly sandy in the surface horizons, with mean sand contents of 65.00%, 57.20% and 80.41% for the Wukari, Donga and Ibi pedons, respectively. Clay increased in several subsurface horizons, reflecting clay translocation and textural differentiation. Mean pH(H_2O) values were 6.91, 6.76 and 6.28, while mean pH(KCl) values were 5.35, 5.63 and 5.31 for Wukari, Donga and Ibi, respectively. Negative ΔpH values indicate predominantly net negative surface charge. Mean base saturation was high (80%, 74% and 77%), although effective cation exchange capacity was comparatively low in the studied pedons. XRD identified quartz, microcline and kaolinite in all three locations, with phlogopite and gibbsite additionally present in Wukari. The mineral assemblages indicate mixed mineralogy and contrasting stages of weathering, with inherited weatherable minerals occurring alongside kaolinite and gibbsite. The soils therefore retain nutrient-bearing mineral reserves while exhibiting properties typical of seasonally flooded tropical soils. Sustainable management should emphasize erosion control, maintenance of organic matter and site-specific nutrient management.

Keywords: clay mineralogy; fadama soils; X-ray diffraction; soil fertility; weathering; southern Taraba State.

ARTIFICIAL INTELLIGENCE AND MULTI-OMICS INTEGRATION IN PRECISION MEDICINE: DECIPHERING MOLECULAR MECHANISMS OF DISEASE AND ADVANCING BIOMARKER-GUIDED THERAPEUTIC DEVELOPMENT

Ibrahim Sani Dikko
Department of Biochemistry, Umaru Musa Yar'adua University Katsina, Nigeria
ORCID: 0009-0006-1401-5117

ABSTRACT

The development of precision medicine has created new opportunities to understand disease at the molecular level and improve the selection of treatments for individual patients. However, diseases such as cancer, diabetes, cardiovascular disorders, and neurodegenerative conditions involve complex biological processes that cannot always be explained by examining a single molecular pathway. Artificial intelligence (AI) and multi-omics technologies offer complementary approaches to addressing this challenge by integrating large volumes of biological information and identifying patterns that may otherwise remain undetected. This review examines the growing role of AI-driven multi-omics integration in understanding disease mechanisms, discovering clinically relevant biomarkers, and advancing personalised therapeutic development. Multi-omics integrates information from genomics, transcriptomics, proteomics, metabolomics, and other molecular disciplines to provide a broader understanding of biological systems. When combined with machine learning and other AI techniques, these datasets can help identify relationships between genetic variation, gene expression, protein activity, metabolic alterations, and disease progression. Such integration may improve the identification of molecular signatures associated with disease susceptibility, treatment response, and adverse drug reactions. In cancer research, for example, combining molecular profiles with computational analysis may help explain tumour heterogeneity and identify potential therapeutic targets. Similarly, integrating pharmacogenomic and clinical data may support more informed treatment decisions by revealing why patients respond differently to the same medication. Despite these opportunities, important challenges remain. Differences in data quality, limited representation of diverse populations, high computational requirements, difficulties in interpreting complex models, and inadequate independent clinical validation can restrict the reliability and practical application of AI-generated predictions. Addressing these limitations requires multidisciplinary collaboration, transparent analytical methods, robust experimental validation, and appropriate ethical and regulatory oversight. The review further considers the relevance of these developments to Nigeria and other African countries, where locally representative molecular datasets, research infrastructure, and affordable diagnostic technologies are essential for equitable precision medicine. Strengthening regional research capacity and international collaboration could help translate advances in computational

biology into context-appropriate healthcare solutions.

Overall, integrating AI with multi-omics approaches offers a promising pathway towards a deeper understanding of disease biology and more effective, biomarker-guided therapeutic development. However, meaningful clinical progress will depend on rigorous validation, responsible implementation, and equitable access to emerging technologies.

Keywords: Artificial intelligence; multi-omics integration; precision medicine; molecular biomarkers; therapeutic development; pharmacogenomics.

INHIBITORY EFFICACY OF HONEY AGAINST MULTISPECIES BACTERIAL BIOFILM

Iram Liaqat
Dr., Tenured Associate Professor, Department of Zoology, Government College University, Lahore

ABSTRACT

Bacterial biofilms are a major worldwide healthcare problem (urinary tract infections) and are associated with decreasing quality of life and significant patient morbidity. This study is first to test Pakistani honey bess, *Apis dorsata* and *A. cerana* honey samples as anti biofilm, anti quorum sensing (QS) and biofilm dispersal agents honey against multispecies biofilm of bacteria (obtained from obese patients). Briefly, five previously identified isolates *Pseudomonas aeruginosa*, *Escherichia coli*, *Staphylococcus aureus*, *Morganella morganii* and *Klebsiella pneumoniae* (MT448672-MT448676) were selected. Antibiogram study of all five isolates was tested against three antibiotics *viz*., erythromycin (20 µg/mL), lincomycin (100 µg/mL) and rifampicin (100 µg/mL). In order to form multispecies biofilm, identified bacteria were grown in batch culture by mixing equal volumes (OD_{590nm}= 0.1) of 2, 3 and 5 bacterial isolates. In total 11 groups (g1-g11) were made. Crystal violet (CV) staining method was used to evaluate the antibiofilm potential and biofilm dispersal potential of both honey samples. QS inhibition in *P. aeruginosa* was measured following culture supernatant method. Antibiogram study showed significant ($p < 0.05$) resistance by *P. aeruginosa* against tested antibiotics. *E. coli*, *M. morganii* and *K. pneumoniae* were significantly susceptible to erythromycin and *S. aureus* to lincomycin. Minimum inhibitory concentrations (MIC) values of both honey samples showed 2 and 5% concentrations as having significant ($p < 0.05$) inhibition potential of multispecies biofilm by all test groups (g1-g11). Though *A. dorsata* honey significantly inhibited biofilm formation at 2 and 5% against all groups but 2% concentration was highly significant against g2-g4 groups. Regarding *A. cerana* honey, 2% concentration was significantly effective against g1, g4-g7 and g9-g11 groups. Both honey samples significantly inhibited QS at 2 and 5%. The 5% concentration of *A. dorsata* honey significantly dispersed biofilm by all groups compared to 2% which showed dispersal potential only by g2 and g3 groups. Collectively, honey samples showed significant antibiofilm, anti-QS and biofilm dispersal potentials thus can be considered as good alternative to antibiotics.

Keywords: Honey potential as antibiofilm, quorum sensing, antibiotic resistance, resistant isolates

ASSESSMENT OF URBANIZATION DYNAMICS IN SUBURBAN AREAS IN LITHUANIA USING GIS-BASED MONITORING

Vilma Šalkauskienė
Lietuvos Inžinerijos Kolegija, Higher Education Institution, Faculty of Environmental Engineering

Daiva Gudritienė
Lietuvos Inžinerijos Kolegija, Higher Education Institution, Faculty of Environmental Engineering

ABSTRACT

Rapid urbanization in suburban areas poses challenges to sustainable land use, infrastructure development, and environmental quality. This study aims to assess urbanization dynamics and the sustainability of built-up area development in Didvyriai village, Kaunas District Municipality, Lithuania, using Geographic Information Systems (GIS). The research was based on the analysis of ORT10LT orthophoto maps with a spatial resolution of 0.2–0.5 m, enabling detailed identification of buildings and their spatial distribution. The study examined changes in the number, location, and footprint area of buildings over time, compared the observed development with the provisions of the municipal master plan, and applied linear trend extrapolation to forecast future construction trends. The results revealed a substantial increase in the number of buildings, from 3 in 2005–2006 to 133 by 2025. The most intensive development occurred during 2021–2023 and continued in the subsequent period, with new construction concentrated mainly in the southwestern part of the study area. Most residential buildings had a footprint area of 101–200 m². The forecast indicates that the number of buildings could exceed 275 by 2030 if the current trend continues. These findings suggest that the pace of suburban development may exceed the capacity of existing and planned infrastructure, increasing pressure on transport networks, engineering infrastructure, and social services. The study demonstrates the value of high-resolution orthophoto data and GIS-based monitoring for identifying urbanization trends and supporting evidence-based spatial planning. Continuous monitoring and coordinated infrastructure planning are essential to promote more sustainable suburban development.

Keywords: Urbanization, suburban areas, orthophoto maps, spatial planning, Lithuania.

MACHINE LEARNING-ENHANCED CLASSIFICATION AND ANALYSISOF MODIFIED CARBON PASTE ELECTRODES FOR METHANOL FUELCELL APPLICATIONS

Mustapha Oukbab
Molecular Electrochemistry and Inorganic Materials Team, Beni Mellal Faculty of Science andTechnology, Morocco

ABSTRACT

This study presents a comprehensive machine learning approach for theclassification and analysis of modified carbon paste electrodes (CPE) designed for methanolfuel cell anodes. Four electrode configurations were systematically investigated: unmodifiedCPE, zinc-modified CPE (CPE/Zn), polymer-enhanced CPE/Zn with 1,4-cis polymyrcene(CPE/Zn/Polymer), and bio-modified CPE/Zn/Polymer/Bacteria electrodes using Escherichiacoli biofilms. Advanced machine learning techniques including Convolutional NeuralNetworks (CNN), Random Forest, Support Vector Machines, Long Short-Term Memorynetworks, and Bayesian analysis were employed to analyze cyclic voltammetry data and predictelectrode performance for methanol oxidation. The deep CNN achieved superior classificationaccuracy of 98% (AUC = 0.98) compared to Random Forest (91%) and SVM (87%). PrincipalComponent Analysis revealed that electrode modifications systematically alteredelectrochemical properties, with methanol oxidation peak current and potential being the mostdiscriminative features (47% combined importance). Autoencoder-based denoisingsuccessfully reconstructed CV curves with minimal error, while LSTM networks demonstratedpredictive capability for temporal electrode behavior and methanol oxidation efficiency. Theintegration of machine learning with fundamental electrochemical principles provides apowerful framework for automated electrode characterization, quality control, andperformance optimization in methanol fuel cell applications.

Keywords: Machine learning; Methanol fuel cells; Carbon paste electrodes; Cyclicvoltammetry; Deep learning; Electrode modification; Bioelectrochemistry; Zinc catalysis.

NUMERICAL ASSESSMENT OF HYDROGEN EMBRITTLEMENT SUSCEPTIBILITY IN API 5L PIPELINE STEELS FOR HYDROGEN TRANSPORT

DJEBBARA BENZERGA
LSCMI, University of Sciences and Technology of Oran Mohamed Boudiaf (USTO-MB), Faculty of Mechanical Engineering, Oran, Algeria.

FAYCAL SOTEHI[1], NOUREDDINE BOUALEM
LSCMI, University of Sciences and Technology of Oran Mohamed Boudiaf (USTO-MB), Faculty of Mechanical Engineering, Oran, Algeria.

ABSTRACT

The transition toward low-carbon energy systems has accelerated interest in green hydrogen as a sustainable energy carrier. In this context, Algeria has the potential to become a major hydrogen supplier to Europe through emerging export infrastructure, including the SoutH2 Corridor. However, converting existing natural gas pipelines to hydrogen service requires a rigorous assessment of material compatibility and structural integrity, particularly because hydrogen diffusion and trapping can promote embrittlement and compromise pipeline reliability.

This study presents a numerical framework for investigating hydrogen transport and embrittlement susceptibility in API 5L pipeline steels ranging from grade X42 to X80. The approach combines hydrogen diffusion and trapping models with finite element n-defect geometry on hydrogen redistribsimulations to evaluate the effects of steel grade, internal pressure, and corrosioution and local accumulation. A parametric investigation considers seven steel grades, four defect half-lengths ranging from 1 to 7 mm, four defect depths ranging from 1 to 7 mm, and three internal pressure levels between 6.035 and 8.165 MPa. The contribution of stress-driven diffusion is examined separately to identify the role of mechanical loading in hydrogen transport.

The results indicate that stress-driven diffusion governs the pressure-dependent contribution to hydrogen redistribution within the adopted modelling framework. Furthermore, defect geometry strongly influences local hydrogen accumulation, with sharper defect configurations promoting higher concentrations near defect roots. The comparison of steel grades also shows that total hydrogen uptake alone is insufficient to establish material suitability for hydrogen service. Instead, material selection requires a multi-criteria assessment incorporating lattice hydrogen concentration near defects, irreversible trapping, and available mechanical margin. Based on these criteria, grades X52–X60 emerge as promising candidates for further evaluation, whereas X80 presents concerns associated with hydrogen retention and irreversible trapping, and X42 exhibits limitations in mechanical margin under sharp-defect conditions.

These findings provide a numerical basis for comparing API 5L pipeline steels and prioritizing materials for further investigation in hydrogen transport applications. The proposed framework may support the preliminary assessment of existing pipeline infrastructure intended for future hydrogen export from North Africa to Europe.

Keywords: Green hydrogen; Hydrogen embrittlement; API 5L pipeline steels; Hydrogen diffusion and trapping; Finite element analysis; Corrosion defects; Pipeline integrity.

PHYSİCS-INFORMED NEURAL APPROXİMATİON OF DİSCRETE ANİSOTROPİC VARİABLE-EXPONENT PROBLEMS

Ilyasse Joubbi
Laboratory for Monitoring Emerging Technologies (LAVETE), Faculty of Sciences and Technics, Hassan First University, Settat, Morocco

Fatima Aqel
Laboratory for Monitoring Emerging Technologies (LAVETE), Faculty of Sciences and Technics, Hassan First University, Settat, Morocco

Nour Eddine Alaa
Laboratory LAMAI, Faculty of Science and Technology, Cadi Ayyad University, Marrakesh, Morocco

ABSTRACT

Introduction and Purpose: Nonlinear discrete systems with anisotropy and spatial heterogeneity arise in lattice diffusion, networks, and data-driven discretizations of partial differential equations. Variable-exponent p(·)-Laplacian operators provide a flexible framework for such problems, but their nonstandard growth and strong nonlinearities create substantial analytical and computational challenges. This study combines a rigorous discrete variational analysis with physics-informed neural solvers for a two-dimensional anisotropic p(·)-Laplacian Dirichlet problem.

Materials and Methods: We formulate the problem on a two-dimensional discrete Dirichlet space and define the associated energy functional. Existence of a weak solution is established through coercivity and variational minimization under standard growth assumptions, while monotonicity conditions are used for uniqueness. For the numerical approximation, a physics-informed neural network (PINN) is trained directly on the discrete grid by enforcing the governing residual and boundary constraints. Network depth and width, grid resolution, and training with Adam followed by L-BFGS are examined. The PINN results are compared with a Jacobian-free Newton-Krylov solver.

Results: The variational framework yields existence of at least one weak solution when the growth exponent of the nonlinear term remains below the minimal discrete exponent, with uniqueness under suitable monotonicity assumptions. Computational experiments show that the PINN provides stable and robust approximations as the nonlinearity increases or the grid is refined. The Newton-Krylov method is highly efficient in smoother regimes, but it can experience convergence difficulties for larger or nonsmooth nonlinear systems.

Discussion and Conclusion: The results show that discrete variational theory can be effectively combined with physics-informed deep learning for anisotropic variable-exponent lattice problems. Classical Newton-Krylov solvers remain attractive for sufficiently smooth problems of moderate size, whereas PINNs provide a competitive and often more robust

alternative in challenging nonlinear regimes. These findings also motivate hybrid approaches that combine neural approximations with classical iterative solvers, together with improved preconditioning and adaptive PINN training strategies.

Keywords: Discrete Boundary Value Problem; Anisotropic p(·)-Laplacian; Physics-Informed Neural Networks; Variational Methods; Newton-Krylov Methods

KİŞİYE ÖZGÜ GLİOBLASTOMA ORGANOİDLERİ, EKSTRASELÜLER VEZİKÜLLER VE CAR-T HÜCRE TEDAVİSİNDE METODOLOJİK GELİŞMELER

METHODOLOGICAL ADVANCES IN PATIENT-DERIVED GLIOBLASTOMA ORGANOIDS, EXTRACELLULAR VESICLES, AND CAR-T CELL THERAPY

Mediha Gürel
Dr., Çukurova Üniversitesi, Biyoteknoloji Araştırma ve Uygulama Merkezi
Dr., Çukurova University, Biotechnology Research and Application Center
Dr., Bitlis Eren Üniversitesi, Elektronik ve Otomasyon Bölümü
Dr., Bitlis Eren University, Electronic and Automation Department
ORCID ID: 0000-0001-9732-5706

Fatih Özoğul
Dr., Çukurova Üniversitesi, Su Ürünleri Fakültesi, Avlama ve İşleme Teknolojisi Bölümü
Dr., Çukurova University, Faculty of Fisheries, Department of Seafood Processing Technology
ORCID ID: 0000-0002-0655-0105

ÖZET

Glioblastoma (GBM), merkezi sinir sisteminin en agresif primer malignitelerinden biri olup belirgin intra- ve intertümöral heterojenite, infiltratif büyüme, tedavi direnci ve yüksek nüks oranı ile karakterizedir. Maksimal güvenli cerrahi rezeksiyon sonrasında uygulanan radyoterapi ve temozolomid tedavisine rağmen klinik sonuçlar halen sınırlıdır. Bu çalışmada, translasyonel GBM araştırmalarında kullanılan hasta türevi glioblastoma organoidleri (GBO), ekstrasellüler veziküller (EV)/eksozomlar ve kimerik antijen reseptörü taşıyan T hücre (CAR-T) tedavilerine yönelik güncel metodolojik yaklaşımların değerlendirilmesi amaçlanmıştır. Bu kapsamda hasta türevi GBO üretimi, EV/eksozom izolasyonu ve karakterizasyonu, terapötik yüklerin taşınması ve CAR-T hücrelerinin mühendisliği üzerine gerçekleştirilen güncel çalışmalar incelenmiştir. Özellikle enzimatik doku ayrıştırması, mekanik parçalama, minimal manipülasyonla tümör parçalarının kültürü, EV/eksozom temelli terapötik taşıma sistemleri ve tümör mikroçevresini hedefleyen CAR-T yaklaşımları ele alınmıştır. Güncel çalışmalar, GBO üretiminin standardizasyonu, kişiselleştirilmiş ilaç taraması, EV/eksozom aracılı terapötik taşıma ve tümör mikroçevresine yönelik CAR-T stratejilerinde önemli gelişmeler olduğunu göstermektedir. Bu yaklaşımlar, geleneksel iki boyutlu hücre kültürlerine kıyasla tümör heterojenitesi, tedavi direnci ve tümör-immün hücre etkileşimlerinin daha gerçekçi biçimde modellenmesine olanak sağlamaktadır. Sonuç olarak, hasta türevi GBO'lar, EV/eksozom temelli taşıma sistemleri ve CAR-T hücre tedavilerinin birlikte değerlendirilmesi, GBM tedavilerinin kişiye özgü ve fizyolojik açıdan daha uygun üç boyutlu modeller üzerinde araştırılmasına olanak sağlayabilecek tamamlayıcı platformlar sunmaktadır. Bu yaklaşımların metodolojik olarak standardize edilmesi ve disiplinler arası çalışmalarla desteklenmesi, kişiselleştirilmiş GBM tedavi modellerinin geliştirilmesi açısından önem taşımaktadır.

Anahtar Kelimeler: Glioblastoma, kişiye özgü glioblastoma organoidleri, ekstrasellüler veziküller, eksozomlar, CAR-T hücreleri, kişiselleştirilmiş ilaç taraması, üç boyutlu modeller

ABSTRACT

Glioblastoma (GBM) is one of the most aggressive primary malignancies of the central nervous system and is characterized by marked intra- and intertumoral heterogeneity, infiltrative growth, treatment resistance, and a high rate of recurrence. Despite maximal safe surgical resection followed by radiotherapy and temozolomide treatment, clinical outcomes remain limited. This study aimed to evaluate current methodological approaches involving patient-derived glioblastoma organoids (GBOs), extracellular vesicles (EVs)/exosomes, and chimeric antigen receptor T-cell (CAR-T) therapies in translational GBM research. Current studies investigating patient-derived GBO generation, EV/exosome isolation and characterization, therapeutic cargo delivery, and CAR-T cell engineering were reviewed. Particular emphasis was placed on enzymatic tissue dissociation, mechanical fragmentation, minimally manipulated tumor-fragment culture, EV/exosome-based therapeutic delivery systems, and tumor-microenvironment-targeted CAR-T approaches. Recent studies demonstrate substantial advances in the standardization of GBO generation, personalized drug screening, EV/exosome-mediated therapeutic delivery, and CAR-T strategies targeting the tumor microenvironment. These approaches enable more physiologically relevant modeling of tumor heterogeneity, treatment resistance, and tumor-immune cell interactions compared with conventional two-dimensional cell cultures. In conclusion, patient-derived GBOs, EV/exosome-based delivery systems, and CAR-T cell therapies represent complementary platforms with potential to facilitate the investigation of GBM therapies using patient-specific and physiologically relevant three-dimensional models. Methodological standardization and interdisciplinary integration of these approaches are essential for the development of personalized and clinically relevant GBM treatment models.

Keywords: Glioblastoma, patient-derived glioblastoma organoids, extracellular vesicles, exosomes, CAR-T cells, personalized drug screening, three-dimensional models

KÜLTÜRLENMİŞ DENİZ ÜRÜNLERİNDEKİ METODOLOJİK GELİŞMELER VE GIDA ENDÜSTRİSİNDEKİ POTANSİYELİ

METHODOLOGICAL ADVANCES IN THE PRODUCTION OF CULTURED SEAFOOD AND ITS POTENTIAL IN THE FOOD INDUSTRY

Mediha Gürel
Dr., Çukurova Üniversitesi, Biyoteknoloji Araştırma ve Uygulama Merkezi
Dr., Çukurova University, Biotechnology Research and Application Center
Dr., Bitlis Eren Üniversitesi, Elektronik ve Otomasyon Bölümü
Dr., Bitlis Eren University, Electronic and Automation Department
ORCID ID: 0000-0001-9732-5706

Fatih Özoğul
Dr., Çukurova Üniversitesi, Su Ürünleri Fakültesi, Avlama ve İşleme Teknolojisi Bölümü
Dr., Çukurova University, Faculty of Fisheries, Department of Seafood Processing Technology
ORCID ID: 0000-0002-0655-0105

ÖZET

Kültüre edilmiş deniz ürünleri, geleneksel balıkçılık ve su ürünleri yetiştiriciliğine alternatif bir üretim yaklaşımı olarak çevresel sürdürülebilirlik, doğal kaynakların azalması, gıda güvenliği ve hayvan refahına ilişkin sorunlara yönelik potansiyel çözümler sunmaktadır. Bu çalışmada, kültüre edilmiş deniz ürünlerinin üretimine yönelik güncel metodolojik yaklaşımların balık hücrelerinin izolasyonu ve karakterizasyonu, serum içermeyen hücre çoğaltımı, gıda uyumlu biyomürekkep geliştirilmesi, mikroalgler ve deniz kökenli biyoaktif bileşiklerin kullanımı, kişiselleştirilmiş beslenme ve üç boyutlu (3B) biyobaskı uygulamaları kapsamında değerlendirilmesi amaçlanmıştır. Bu doğrultuda, balık hücrelerinin izolasyonunda kullanılan enzimatik sindirim, eksplant kültürü ve mekanik ayrıştırma yöntemleri karşılaştırmalı olarak incelenmiş olup serum içermeyen hücre çoğaltım stratejileri ve gıda uyumlu hibrit hidrojel biyomürekkepler değerlendirilmiştir. Biyomürekkeplerin reolojik, mekanik, fizikokimyasal ve biyolojik özelliklerinin belirlenmesine yönelik yöntemler ile ekstrüzyon, inkjet ve lazer destekli 3B biyobaskı yaklaşımları ele alınmıştır. Ayrıca mikroalgler ve deniz kökenli biyoaktif bileşiklerin besinsel ve fonksiyonel özelliklerin geliştirilmesindeki potansiyeli incelenmiştir. Güncel metodolojik gelişmelerin hücre izolasyonu, biyomürekkep fonksiyonelliği ve 3B doku üretiminde ilerleme sağladığı, mikroalgler ve deniz kökenli biyoaktif bileşiklerin ise besinsel ve fonksiyonel açıdan önemli katkılar sunabileceği görülmektedir. Bununla birlikte, balık türlerine özgü hücre kültürü protokolleri, gıda uyumlu kültür ortamları, biyomürekkep formülasyonları ve analitik yöntemler açısından önemli standardizasyon eksiklikleri bulunmaktadır. Sonuç olarak, standardize üretim protokollerinin geliştirilmesi, gelişmiş biyomalzemelerin kullanımı, ölçeklenebilir biyobaskı teknolojilerinin uygulanması ve disiplinler arası çalışmalar, besinsel

açıdan optimize edilmiş ve ticari olarak uygulanabilir kültüre edilmiş deniz ürünlerinin geliştirilmesi açısından önem taşımaktadır.

Anahtar Kelimeler: 3B biyobaskı, doku mühendisliği, biyomürekkep, kişiselleştirilmiş beslenme, hücresel deniz ürünleri, sürdürülebilirlik

ABSTRACT

Cultured seafood is an emerging alternative to conventional fisheries and aquaculture, offering potential solutions to challenges related to environmental sustainability, resource depletion, food security, and animal welfare. This study aimed to evaluate current methodological approaches for cultured seafood production, focusing on fish cell isolation and characterization, serum-free cell expansion, food-compatible bioink development, the use of microalgae and marine-derived bioactive compounds, personalized nutrition, and three-dimensional (3D) bioprinting. Accordingly, enzymatic digestion, explant culture, and mechanical dissociation methods used for fish cell isolation were comparatively reviewed, while serum-free cell expansion strategies and food-compatible hybrid hydrogel bioinks were evaluated. Methods for assessing the rheological, mechanical, physicochemical, and biological properties of bioinks, together with extrusion-, inkjet-, and laser-assisted 3D bioprinting approaches, were examined. The potential of microalgae and marine-derived bioactive compounds to enhance the nutritional and functional properties of cultured seafood was also assessed. Recent methodological advances have contributed to improvements in cell isolation, bioink functionality, and 3D tissue fabrication. Microalgae and marine-derived bioactive compounds may provide important nutritional and functional benefits, while personalized modulation of nutritional components may support the development of nutritionally optimized cultured seafood products. However, substantial methodological variability remains, particularly regarding fish-specific cell culture protocols, food-compatible culture media, bioink formulations, and analytical methods. In conclusion, the development of standardized production protocols, advanced biomaterials, scalable bioprinting technologies, and interdisciplinary approaches is essential for the development of nutritionally optimized and commercially viable cultured seafood products.

Keywords: 3D bioprinting, tissue engineering, bioink, personalized nutrition, cellular seafood, sustainability

INFLUENCE OF ATMOSPHERIC FACTORS ON THE DYNAMICS OF RADON EMISSION IN SOIL

Azad BAYRAMOV
SD Prof., Republican Seismic Survey Center of the Azerbaijan National Academy of Sciences

Michyil AWTUSHKO
PhD, Institute of Radiobiology of the National Academy of Sciences of Belarus

ABSTRACT

The main objective of this work was: 1) to develop and manufacture an autonomous complex for measuring radon concentrations in the surface region, simultaneously measuring the Earth's magnetic field and studying the correlation of the measured values with the seismic situation of the area; 2) in carrying out monitoring measurements on the basis of which it seems possible to identify patterns of influence of the dynamic characteristics of the air environment and the lithosphere on the emission of radon in soils, and on its concentration in the atmospheric air. The following results were obtained: 1) a joint research program with the Institute of Radiobiology of the National Academy of Sciences of Belarus was developed for joint research into the influence of atmospheric factors on the dynamics of radon emission in soil, 2) an autonomous station for measuring radon emission was developed; 3) systematic monitoring and measurement of levels of various atmospheric factors (precipitation, atmospheric pressure) with parallel observations has begun; 4) GPRS (2G) communication system has been developed to transmit signals to the central post; 5) The Institute of Radiobiology of the National Academy of Sciences of Belarus carried out monitoring measurements in the Gomel region of Belarus, on the basis of which patterns of influence of the dynamic characteristics of the air environment on the concentration of radon in the atmospheric air were identified, as well as certain patterns of their correlations were established.

Keywords: Radon, Atmospheric Factors, Monitoring, Emission Dynamics, Soil.

INTRODUCTION

The geomorphology of the Shamakhi region, where field tests of the radon installation and experiments are planned, is characterized by a complex mountainous terrain located on the southeastern slope of the Greater Caucasus. The area consists of highlands, interalgal basins and foothills of the Main Caucasus Range (Dubrar, Gyulyumdostu, 2200-2700 m), high seismic activity and erosion-denudation processes (landslides, avalanches) are observed here. Main features of the area: High and Middle Highlands: in the northern part the altitude exceeds 2000 m, the terrain is steep, the valleys are deep. Intermountain depressions: in the center of the region there are intermountain depressions (for example, the Shamakhi

depression), belonging to the Shamakhi-Gobustan synclinorium, subject to denudation processes.

Foothills and low mountains: to the southeast the height decreases, the rocks become younger (Neogene clays) and erosional landforms predominate. Rock structure: Cretaceous limestones are common in the north, Paleogene-Neogene clays and sandstones are common in the south, which affects the formation of the relief. Borders: The region's topography is surrounded by mountain ranges in the north (Pirdirey, Giz Galas) and river valleys (Zogalavay) in the south. The Shamakhi region has a fragmented topography, constantly changing under the influence of intense tectonic movements.

The study of the processes of emission of radioactive gas radon in mountainous conditions and comparison with the results obtained for flat conditions is of particular relevance (Feyzullayev et.al., 2014). The processes of radon emission (release) in the mountains and on the plains differ due to the geological structure, the degree of rock destruction and climatic factors. The main difference is that in the mountains convective gas transport through cracks predominates, while on the plains it is dominated by slow diffusion through the soil layer (see Table 1).

Table 1. Main differences in radon emission processes in mountainous and lowland conditions.

Factor	Mountain conditions	Flat conditions
Transfer mechanism	Convection. Gas rises quickly along tectonic fault zones and cracks.	Diffusion. Gas slowly seeps through the pores of the soil layer.
Geological source	Bedrock (granites, shales), often enriched in uranium.	Sedimentary deposits, clays, sands with lower radionuclide content.
Soil permeability	High in crushing and fault zones, but low in monolithic massifs.	Relatively uniform, depends on soil moisture and density.
Effect of pressure	Pressure changes “pump out” radon from deep cracks (pump effect).	Atmospheric pressure can only affect the top layers of soil.
Terrain and wind	Slopes and gorges create air draft, increasing exhalation (gas release).	The release is more stable and depends on weather conditions.

The features of mountain conditions.

1. Tectonic activity: Active faults are much more common in mountains. These act as "highways" through which radon can rise from great depths (tens and hundreds of meters) to the surface in a short time, without having time to decay.
2. The "chimney" effect: Systems of interconnected voids often exist within mountain ranges. The temperature and pressure differences within the range and outside create rising air currents that carry radon to the surface.
3. Local anomalies: In the mountains, radiation levels can change dramatically: at one point they are extremely high (above the fault), and a few meters away they are minimal.

Features of flat conditions.

1. Soil barrier: The layer of sediment and soil on flat plains often serves as a natural barrier. Radon, formed deep below, decays (half-life 3.8 days) as it makes its way through dense clay layers.
2. Dependence on precipitation: On flat plains, soil moisture critically reduces radon emissions, as water fills the pores and blocks the gas's escape. In the mountains, however, water can transport radon over long distances through underground streams.
3. Uniformity: Radon fields on plains are more uniform, and their concentrations often correlate with the type of surface soil rather than with deep structures.

M.I. Avtushko's research examined the influence of precipitation and lunar-solar gravity on radon concentrations in the pore air of dispersed soils in flat areas (Avtushko, 2000). Experimentally confirmed data were obtained characterizing previously unknown migration properties of radon in the surface atmosphere and near-surface soil layers (Avtushko, 2001). It was shown that radon concentrations in the pore air of near-surface dispersed (sandy) soil are formed by two ground-based sources—intrinsic and deep—with the atmospheric source playing a significant role in delivering radon filtered from the atmosphere to the Earth's surface by precipitation.

In Azerbaijan, at the Institute of Geology and Geophysics and the Republican Seismological Survey Center, scientists such as Ch. Aliyev, A.A. Feyzullayev, and A. Karimova conducted studies of radon content in wells and on the soil surface on the Absheron Peninsula using physicochemical methods (Feyzullayev et al. 2012). Work was carried out to compile a map of radon activity distribution in Azerbaijan, create a radon register, and include this map in the European radon map (Feyzullaev et al., 2012), (Feyzullayev et al., 2014).

This paper is devoted to the development of an autonomous station for measuring radon emissions in the mountainous conditions of the Shamakhi region of the Republic of Azerbaijan and monitoring measurements at the Institute of Radiobiology in the flat territory of the Gomel region of Belarus, and the study of the patterns of influence of dynamic characteristics of the air environment on the concentration of radon in outdoor atmospheric air and in indoor air.

MATERIALS AND METHOD

Seismic-fluid-geochemical studies in Azerbaijan were carried out to study the fluid regime in the seismogenic zones of the southern (Shamakhi, Sheki regions) and north-eastern (Khachmaz, Siyazan regions) slopes of the Greater Caucasus megaanticlinorium, the boundaries of seismogenic zones, its south-eastern extremity (Absheron Peninsula) and at the same time in seismically active zones Azerbaijani part of Talish. (Lenkoransky district). made. There are 6 stationary geochemical stations operating in these territories: “Bibi-Heybat” gk/st (Baku city); "Shamakhi" city complex (Shamakhi district); “Sheki” city complex (Sheki district); "Osakuya" gk/st (Lenkoransky district); "Boyuk-Khamya" gk/st (Siyazan district); "Mukhtadir" gk/st (Khachmaz district). Objects of fluid observations differ

in the genesis of hydrogeochemical parameters and migration conditions (Feyzullaev et. al., 2012).

The study of seismic activity and determination of its relationship with parameters measured on the Earth's surface is an important task of seismology (Bayramov et.al., 2016). Over the past decades, scientists have tried to develop methods for predicting earthquakes. Particular attention is paid to the search for precursors, among which radon anomalies and magnetic field variations stand out as potentially important. In addition, the increase in computing power and the development of artificial intelligence methods are opening up new opportunities for analyzing complex multivariate data.

Current research highlights the need for sophisticated systems capable of collecting, processing, and interpreting data in real time. This is especially true for regions with high seismic activity, such as the Caucasus region. The development of autonomous systems capable of operating in remote and hard-to-reach areas is becoming the main focus of modern seismology. Such systems allow for real-time monitoring without human intervention, minimizing risks and increasing response speed.

The measured physical quantities are the concentration of the radioactive gas radon and the intensity of the Earth's magnetic field. Therefore, at the first stage, only two types of detectors were developed: for radon gas and for the Earth’s magnetic field.

The prepared complex consists of detector blocks, an interface, a control unit, a block of Internet channels, a device for receiving data from a seismic center, a device for receiving data on the current state of solar activity, an analysis unit based on artificial intelligence and decision-making, as well as an autonomous power supply for solar panels. Detector units include a detector for the radioactive gas radon and magnetometer devices to measure the magnetic field strength in a given area..

RESULTS AND DISCUSSION

The measured physical quantities of the developed installation are the concentration of the radioactive gas radon and the intensity of the Earth's magnetic field. Therefore, at the first stage, only two types of detectors were developed: for radon gas and for the Earth’s magnetic field.

In a simplified form, the control and analysis software algorithm of the complex consists of the following main blocks that interact with each other (Bayramov, 2026).

The following blocks are discussed below:

- block 1 for receiving, filtering and processing data on radon concentration on the surface of the earth and at a depth of 1-3 meters;
- block 2 for receiving data from the magnetometer;
- block 3 for analyzing and filtering data from blocks 1 and 2;
- block 4 for joint analysis of data from power unit 3 and data from seismic center 5 and solar activity;
- block 6 of the GPRS radio communication modem;

- block 7 for processing and in-depth analysis of block 4 data based on the machine learning method using the Internet channel and the Seismic Center database;
- block 8 for analysis and decision-making based on the results of block 7.

The GPRS radio modem provides wireless data transmission, voice communication over the GSM network, text messaging (SMS) and packet data transmission based on GPRS technology (Bayramov, 2025).

The developed circuit diagram represents the functional architecture of a communication module based on the GSM/GPRS SIM900 chip.

Main chip SIM900 (U4).

The central element of the circuit is the SIM900A integrated circuit - a communication chip that supports quad-band GSM networks and provides interaction with an external microcontroller via a UART interface:

- The UART module is connected to the microcontroller via signals (Tx, Rx). The UART module is connected to the microcontroller via signals (Tx, Rx);
- Control lines PWKEY, STATUS, NETLIGHT are used to control the operating mode and visual control of the modem

SIM card interface (U9).

The SIM card connection is placed in a separate interface block. This interface includes the following signals:

- SIM_VDD – power line,
- SIM_RST – reset signal,
- SIM_CLK – clock signal,
- SIM_DATA – duplex data line,
- SIM_PRE – presence signal.

These lines are connected in series to the SIM card tray through protective resistors and TVS diodes, protecting them from both electromagnetic influence and static charge.

Power cycle.

The module is equipped with an LDO stabilizer type MIC29302WU. Using this stabilizer allows you to reduce the voltage required for SIM900 from 5 V to 4 V.

- filtering of high-frequency pulses is ensured by the use of electrolytic and ceramic capacitors (100 μF and 100 nF) at the input and output;
- The power circuit protects the module from current peaks and can provide the instantaneous ~2A current required during GPRS data transmission.

To control the operating modes of the module, two main LEDs are used:

- STATUS LED – shows the general operating status of the module,
- NETLIGHT LED – indicates the registration status in the GSM network.

Both LEDs are driven by NPN transistors (BC547B), which isolate the signal lines from the voltage level on the module and increase reliability.

The PWKEY signal is controlled by a transistor switch to turn the module on and off using software. This approach is effective both in automated systems and in devices that require energy conservation.

The RF output of SIM900 is connected to the GSM network via the external SMA antenna connector (RF1). The antenna unit ensures stable reception and transmission of the module signal (İbrahimov et.al., 2024).

The developed circuit diagram is distinguished by stable power supply, SIM card interface protection mechanisms, operating mode control via LED indicators and GPRS functionality. This solution is suitable for a wide range of applications in data acquisition and remote monitoring systems, IoT devices and wireless control applications.

SIM900 is a GSM/GPRS module developed by SIMCom. Through this module, microcontrollers can connect to the mobile network and perform the following functions:

- making and receiving calls;
- send and receive SMS;
- connect to the Internet via GPRS (2G);
- data transmission via TCP/IP protocol.
- network support: GSM 850/900/1800/1900 MHz (quad band)
- supply voltage: 3.2 – 4.8 V (optimally 4.0 V)
- current electricity consumption:
- standby mode: ~10 mA;
- during a call: ~250 mA;
- peak current: up to 2 A;
- controlled by AT commands (using UART).
- UART interface: data transfer rate is in the range of 9600 – 115200 baud**.**

Dimensions: about 24x24 mm (chips themselves) and modules (boards) about 40x40 mm. AT commands (attention commands) are standard text commands used to communicate with GSM/GPRS modules via the UART interface. Using these commands, SIM900 allows you to manage calls, SMS, GPRS Internet, TCP/IP and other services.

When measuring radon concentration with the developed complex, two data arrays will be obtained: $y_1 = (x_1,x_2,\ldots,x_n)$ U $y_2 = (z_1,z_2,\ldots,z_n)$ for measurements outside and inside the room, respectively. This data will be transmitted via GPRS communication line along with meteorological data to the central post. There they will be included in the database and analyzed using Machine Learning and Deep Learning algorithms. The software solution to this problem conventionally consists of six main stages:

1) obtaining vectors $y_1 = (x_1,x_2,\ldots,x_n)$ U $y_2 = (z_1,z_2,\ldots,z_n)$ and pre-processing;

2) carrying out analysis, comparison with the norm, calculating average values and comparing them with MPC (maximum permissible concentration), usually the norm in the room is up to 200 Bq/m³;

3) Using the Random Forest, Neural network model to detect anomalies, taking into account the difference between the street and the room;

4) Meteorological data analysis;
5) Data transfer to the central station via GPRS communication line;
6) Seismological data analysis, risk assessment and classification.

Below is a general diagram of the implementation of a processing program in Python:

```
import numpy as np
from sklearn.ensemble import IsolationForest
def analyze_radon(y1, y2):
    # 1. Basic measurement results
    avg_outdoor = np.mean(y1)
    avg_indoor = np.mean(y2)
    limit = 200  # Safety threshold in Bq/m3
        print(f" Average on the street: {avg_outdoor:.2f}, indoors: {avg_indoor:.2f}")
    # 2. Comparison with database (conditional norms)
    status = "Norm" if avg_indoor <= limit else "Excess"
        # 3. Artificial intelligence (search for anomalies)
    # Combining data to look for sharp spikes that are not typical for sensors
    data = np.array(y2).reshape(-1, 1)
    clf = IsolationForest(contamination=0.1, random_state=42)
    anomalies = clf.fit_predict(data)
        has_anomaly = -1 in anomalies
    # Generating a report
    result = {"status": status, "avg_indoor": avg_indoor,
        "anomaly_detected": has_anomaly,
        "alert_level": "High" if status == "Excess" or has_anomaly else "Low"}
     return result # Example data (Bq/m3)
y1 = [10, 12, 15, 11, 14]  # Street
y2 = [150, 160, 450, 155, 158]  # Room (with one release)
report = analyze_radon(y1, y2)
print("AI solution:", report)
```

Isolation Forest: this is an Artificial Intelligence (AI) algorithm that detects anomalies in data. If a sudden spike in concentration occurs in a room that deviates from the overall statistics, the system will flag it as an anomaly. The program can take into account the coefficient of radon gas penetration from the soil (y_1) into the building (y_2).

Below is the program that automatically creates a table of measurements, analyzes new data using AI, and saves the results:

```
import sqlite3
import numpy as np
from sklearn.ensemble import IsolationForest
def init_database():
    """ Creates the database and table if they do not already exist."""
```

```
conn = sqlite3.connect('radon_data.db')
cursor = conn.cursor()
cursor.execute('''Create table ıf not exısts history
(id Integer prımary key autoıncrement,
timestamp Date tıme default current_tımestamp,
 outdoor_avg REAL, indoor_avg REAL, anomaly_flag INTEGER,
 verdict TEXT)''')
conn.commit() return conn def process_and_store(y1, y2):
""" Analyzes data and records the result in history."""
# 1. Calculation of averages
avg_out = float(np.mean(y1))
avg_in = float(np.mean(y2))
   # 2. AI anomaly analysis (Isolation Forest)
model = IsolationForest(contamination=0.1)
# Finding an anomaly in a current series of room measurements
preds = model.fit_predict(np.array(y2).reshape(-1, 1))
has_anomaly = 1 if -1 in preds else 0
   # 3. Making a decision threshold = 200 # Maximum permissible concentration
verdict = "DANGEROUS" if avg_in > threshold or has_anomaly else "NORM"
   # 4. Saving to the Database
conn = init_database() cursor = conn.cursor() cursor.execute('''
   INSERT INTO history (outdoor_avg, indoor_avg, anomaly_flag, verdict)
   VALUES (?, ?, ?, ?)
''', (avg_out, avg_in, has_anomaly, verdict))
   conn.commit() conn.close() return verdict
# Usage example:
y1_measurements = [12.5, 14.2, 13.8, 15.0] # Outdoor data
y2_measurements = [190, 205, 198, 450]  # Indoor data (with ejection 450)
status = process_and_store(y1_measurements, y2_measurements)
print(f" Analysis completed. Status: {status}")
```

This part of the paper presents preliminary results from radon concentration measurements conducted in the Gusar region of Azerbaijan. A calibrated handheld radon detector (radon concentration analyzer, electric ion detection radon, or concentration meter) was used for the measurements (Shenzhen Langdeli Technology Co., Ltd.) Dienmern DM229R. The measurement range is 0–11,000 Bq/m³, with an accuracy of ±10%. Measurements were made indoors and outdoors at altitudes of 700 m, 1,100 m, and 1,710 m.

The main conclusions obtained from the measurements are:

- a radon volume activity in the open air varied from 27 Bq/m^3 to 96 Bq/m^3, and indoors from 13 Bq/m^3 to 113 Bq/m^3;
- a radon emissions are independent of altitude;

- a radon emissions are independent of wind speed;
- a positive correlation is observed between relative humidity and radon concentrations in indoor and outdoor air;
- an outdoor air temperature has no effect on radon concentrations.

Monitoring measurements were carried out on the territory of the Gomel region of Belarus, on the basis of which patterns of influence of the dynamic characteristics of the air environment on the concentration of radon in the atmospheric air were identified (Matveev, 2016; Matveev et.al., 2022). Regular measurements of radon concentration were carried out in a reference indoor room (Rnin) and in outdoor air (Rnout), with accompanying measurements of atmospheric pressure (mmHg), relative air humidity (φ, %) and air temperature (T, °C).

Based on the results of monitoring measurements, positive correlations were established between relative air humidity and radon concentration in indoor air (Rn_{in}) and in outdoor air (Rn_{out}). In both cases, the relationships are described by exponential equations (1) and (3) with average values of regression coefficients (2) and (4) (Figure 1).

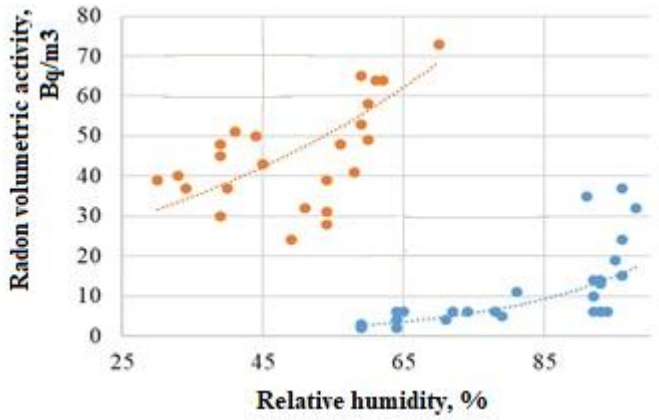


Figure 1. Dependence of radon concentration in the air on air humidity: red point - Rn_{in} ; blue pointy- Rn_{out}.

$$y = 17{,}7 \cdot e^{0{,}0193x} \quad (1)$$

$$R^2 = 0{,}403 \quad (2)$$

$$y = 0{,}1586 \cdot e^{0{,}0478x} \quad (3)$$

$$R^2 = 0{,}4654 \quad (4)$$

A moderate negative correlation has been established between the concentration of radon in indoor air (Rnin) and air temperature (5) and (6). The temperature of the outside air does not affect the concentration of radon in it (Figure 2).

$$y = 276{,}04 \cdot e^{-0{,}0853x} \quad (5)$$

$$R^2 = 0{,}4197 \quad (6)$$

$$y = -0{,}1736x + 12{,}925 \quad (7)$$

$$R^2 = 0{,}0059 \quad (8)$$

Analysis of the results of monitoring measurements shows that atmospheric pressure does not affect the concentration of radon in the air (9), (10), (11) and (12) (Figure 3).

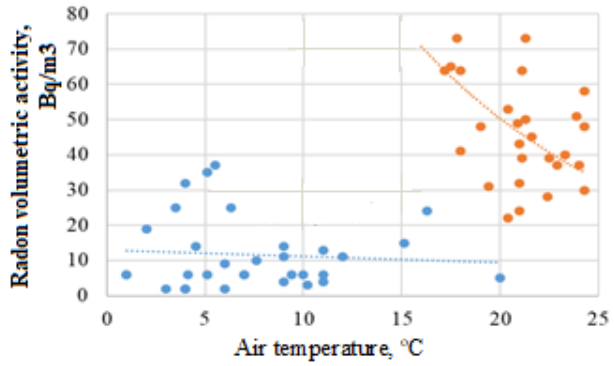


Figure 2. Dependence of radon concentration in the air on temperature: red point - Rn_{in} ; blue pointy- Rn_{out}.

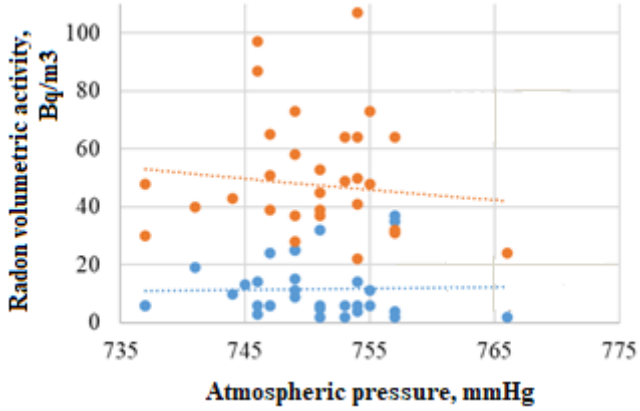


Figure 3. Dependence of radon concentration in the air on atmospheric pressure: red point - Rn_{in}; blue pointy- Rn_{out}.

$$y = 19598 \cdot e^{-0,008x} \quad (9)$$

$$R^2 = 0,0038 \quad (10)$$

$$y = 0,0393x - 17,876 \quad (11)$$

$$R^2 = 0,0006 \quad (12)$$

Monitoring studies will be continued and their results are planned to be used to adjust the established dependencies and for comparison with the results obtained in the mountainous conditions of the Shamakhi region.

CONCLUSION

Thus, an autonomous complex has been developed, designed for the simultaneous analysis of seismic processes in the territory of Azerbaijan and neighboring regions, as well as for the simultaneous measurement of the concentration level of the radioactive gas radon and the

level of the Earth's magnetic field strength. The GPRS radio modem is designed to provide Internet connection, apply machine learning method and connect to the center. A software algorithm has been developed to control the complex, carry out measurements and analyze the obtained data using machine learning. The purpose of development and research is to study the relationship of measured physical quantities with seismic activity. Monitoring measurements of radon emissions were carried out in the Gusar region of Azerbaijan and correlations between the dynamic characteristics of the atmosphere and radon concentration were investigated. Also, monitoring measurements were carried out at the Institute of Radiobiology on the flat territory of the Gomel region of Belarus, and the patterns of influence of the dynamic characteristics of the air environment on the dynamics of radon emission in soils and its concentration in the atmospheric air were studied. Positive correlations have been established between relative air humidity and radon concentration in indoor and outdoor air. On the other hand, atmospheric pressure has no effect on the concentration of radon in the air. The results of measurements obtained in Azerbaijan do not contradict the results obtained by Belarusian scientists.

REFERENCES

Avtushko M.I., Matveev A.V. (2010) Concentration of radon in near-surface soils on the territory of the Soligorsk geodynamic test site (Belarus). Litasfera. No.2(33). P. 98–105.

Avtushko M.I., Matveev A.V., Isachenko S.A. (2021) New data on the entry of radon into the human environment. Dokl. National acad. Sciences of Belarus. Vol. 65, No.3. P.355–360.

Bayramov A.A., Keremova A.D., Tagıyeva M. (2026) Radon emission investigation in the Shamakhi district of the Azerbaijan. Danish Scientific Journal. Vol.1 (105). pp.27-29.

Bayramov A.A., Suleymanov S.S. (2025) GPRS Radio Communication For AI-Based Measurement And Control Complex. Modeling, control and information technologies. N8, pp. 353-356.

Bayramov A.A. (2026) Development and creation of an automated station based on artificial intelligence for the study of the radon problem in the environment. Innovation and sustainable development: new ideas and solutions. Ist International scientific conference. 01-02 October 2025. Nakhchivan. Vol. I. 1139 p. pp.942-948.

Feyzullaev A.A., Bagirli R.J., Velieva F.F. (2012) Factors controlling the level of volumetric activity of radon in Azerbaijan. Xeberler Yer Elmleri, №1, pp. 42-48.

Feyzullaev A.A., Bagirli R.J., Velieva F.F., Alieva A.R. (2012) The radon problem: geodynamic and environmental aspects. Geology Institute of ANAS Republican Seismic Survey Center of ANAS. Seismoforecasting researches carried out in the Azerbaijan territory. 7-12 October, Baku, Azerbaijan. pp. 97-106.

Feyzullayev A.A., Aliyev Ç.S., Valsangiacomo C., Baghirli R.J., Hoffmann M., Mahmudova F.F. (2014) The Prospects of Solving of the Radon Problem in Azerbaijan. 12th

International Workshop on the Geological Aspects of radon Risk Mapping. Proceedings. Czech geological Survey, Radon v.o.s., Prague. pp. 7-10.

İbrahimov B.G., Hasanov A.H., Hashimov E.G. (2024) Research and analysis of efficiency indicators of critical infrastructures in the communication system. Advanced Information Systems. Kharkov. Vol. 8, No. 2. pp.58-64.

Matveev A.V. (2016) Zoning of the territory of Belarus according to the degree of radon hazard of soils. Reports of the National Academy of Sciences of Belarus. Vol. 60, No. 5. pp.108-112.

Matveev A.V., Avtushko M.I., Isachenko S.A. (2022) On the influence of atmospheric precipitation and lunar-solar gravitational influence on the concentration of radon in the pore air of dispersed soils. Reports of the National Academy of Sciences of Belarus. Vol. 66, No. 2. pp.223–228.

This work was supported by the Azerbaijan Sciences Foundation (Grant № AEF-BQM-BRFTF-4-2024-5(53)-06/03/2-M-03, and by the support of the Belarusian Republican Foundation for Fundamental Research (Grant BRFFR № X25A32-029»).

STATİK BASINÇ DEĞİŞİMİ ALTINDA DİNGİL KALDIRMA KÖRÜĞÜNÜN 3B LAZER TARAMA VE KESİTSEL SİMETRİ MERKEZİ YER DEĞİŞTİRMESİ YÖNTEMİYLE GEOMETRİK DAVRANIŞININ DENEYSEL OLARAK İNCELENMESİ

EXPERIMENTAL INVESTIGATION OF THE GEOMETRIC BEHAVIOR OF AN AXLE LIFT AIR SPRING UNDER STATIC PRESSURE VARIATION USING 3D LASER SCANNING AND CROSS-SECTIONAL SYMMETRY CENTER DISPLACEMENT METHOD

Recep GÜNENÇ
PEGA Otomotiv Süspansiyon Sistemleri A.Ş, Bursa, Türkiye
PEGA Automotive Suspension Systems Inc., Bursa, Türkiye
ORCID ID: 0009-0002-2058-8801

Hasan KASIM
PEGA Otomotiv Süspansiyon Sistemleri A.Ş, Bursa, Türkiye
PEGA Automotive Suspension Systems Inc., Bursa, Türkiye
ORCID ID: 0000-0002-3024-5207

ÖZET

Bu çalışmanın amacı, ağır ticari araçlarda (kamyon, çekici, treyler vb.) kullanılan bir dingil kaldırma körüğünün farklı statik iç basınç seviyelerindeki geometrik davranışını üç boyutlu (3B) lazer tarama ve kesitsel simetri merkezi yer değiştirmesi yöntemiyle deneysel olarak incelemektir. Çalışma kapsamında dingil kaldırma körüğü, 350 mm sabit bağlama yüksekliğinde ve 1–7 bar iç basınç aralığında değerlendirilmiştir. Her basınç seviyesinde körüğün geometrisi, Hexagon Absolute Arm 83 üç boyutlu ölçüm sistemi kullanılarak lazer yöntemiyle taranmış ve elde edilen veriler Geomagic Control X yazılımında analiz edilmiştir. 1 bar basınç seviyesinde elde edilen tarama referans geometri olarak kabul edilmiş, diğer basınç seviyelerine ait taramalar ise basınç değişiminden etkilenmeyen rijit fikstür geometrileri esas alınarak aynı koordinat sistemine hizalanmıştır. Kauçuk gövdenin üst, orta ve alt bölgelerinde sabit kesitler oluşturularak kesit profillerinin simetri merkezleri belirlenmiştir. Bu merkezlerin 1 bar referans konumuna göre X ve Y eksenlerindeki yer değiştirme bileşenleri (ΔX ve ΔY) Geomagic Control X yazılımı aracılığıyla belirlenmiş ve elde edilen bileşenlerden bileşke simetri merkezi yer değiştirme (ΔR) değerleri hesaplanmıştır. Ayrıca karakterizasyon testi kapsamında ölçülen körük çapı ve taşıma kuvveti değerleri değerlendirilmiştir. Deneysel sonuçlar, iç basınç artışıyla birlikte üst ve orta kesitlerde bileşke simetri merkezi yer değiştirmesinin genel olarak arttığını, alt kesitte ise daha sınırlı ve dalgalı bir değişim meydana geldiğini göstermiştir. Tüm basınç seviyeleri arasında en yüksek ΔR değeri, 7 bar basınçta üst kesitte 1,02 mm olarak hesaplanmıştır. Aynı basınç aralığında ve 350 mm sabit bağlama yüksekliğinde körük çapı 140,1 mm'den 165,1 mm'ye yükselerek toplam 25,0 mm artış göstermiştir. Sonuç olarak, 3B lazer tarama ve sabit kesit analizi yaklaşımının, dingil kaldırma körüklerinin farklı statik iç basınç seviyelerindeki

bölgesel geometrik davranışlarının nicel olarak değerlendirilmesine olanak sağladığı belirlenmiştir.

Anahtar Kelimeler: Dingil Kaldırma Körüğü, 3B Lazer Tarama, Statik Basınç, Kesitsel Simetri Merkezi, Geometrik Yer Değiştirme, Karakterizasyon.

ABSTRACT

This study aimed to experimentally investigate the geometric behavior of an axle lift air spring used in heavy commercial vehicles (trucks, tractor units, trailers, etc.) under different static internal pressure levels using three-dimensional (3D) laser scanning and the cross-sectional symmetry center displacement method. The axle lift air spring was evaluated at a constant installation height of 350 mm over an internal pressure range of 1–7 bar. At each pressure level, the geometry of the air spring was scanned using the Hexagon Absolute Arm 83 three-dimensional measurement system with laser scanning technology, and the acquired data were analyzed using Geomagic Control X software. The scan obtained at 1 bar was defined as the reference geometry, while scans acquired at the other pressure levels were aligned within the same coordinate system using rigid fixture geometries unaffected by pressure variations. Fixed cross-sections were established in the upper, middle, and lower regions of the rubber body, and the symmetry centers of the cross-sectional profiles were determined. The displacement components of these centers along the X and Y axes (ΔX and ΔY), relative to their reference positions at 1 bar, were determined using Geomagic Control X software, and the resultant symmetry center displacement (ΔR) values were calculated from these components. In addition, the air spring diameter and load-bearing force values measured during the characterization test were evaluated. The experimental results showed that the resultant symmetry center displacement generally increased with increasing internal pressure in the upper and middle cross-sections, whereas the lower cross-section exhibited a more limited and fluctuating variation. The maximum ΔR value across all pressure levels was calculated as 1.02 mm in the upper cross-section at 7 bar. Over the same pressure range and at a constant installation height of 350 mm, the air spring diameter increased from 140.1 mm to 165.1 mm, corresponding to a total increase of 25.0 mm. In conclusion, the findings demonstrated that the combined use of 3D laser scanning and fixed cross-sectional analysis enables the quantitative evaluation of the regional geometric behavior of axle lift air springs under different static internal pressure levels.

Keywords: Axle Lift Air Spring, 3D Laser Scanning, Static Pressure, Cross-Sectional Symmetry Center, Geometric Displacement, Characterization.

ŞEKER PANCARI ATIKLARININ TEKSTİL ENDÜSTRİSİNDE YENİDEN KULLANIMI: BOYAR MADDE OLARAK DEĞERLENDİRİLMESİ

REUSE OF SUGAR BEET WASTE IN THE TEXTILE INDUSTRY: EVALUATION AS A DYEING AGENT

Keziban ÇAKMAKTAŞI
Ilsan Tekstil San. ve Tic. A.Ş.
ORCID ID: 0009-0009-9127-6873

HULUD BAYRAM
Ilsan Tekstil San. ve Tic. A.Ş.
ORCID ID: 0009-0003-5106-6114

ÖZET

Tekstil endüstrisinde sentetik boyar maddelerin kullanımından kaynaklanan çevresel etkiler, sürdürülebilir ve çevre dostu alternatiflerin geliştirilmesini önemli hâle getirmiştir. Bu çalışma, şeker pancarı atıklarının doğal boyar madde kaynağı olarak değerlendirilmesini ve tekstil endüstrisinde kullanılabilirliğinin araştırılmasını amaçlamaktadır. Tarımsal ve endüstriyel atıkların katma değerli ürünlere dönüştürülmesi, döngüsel ekonomi yaklaşımına katkı sağlayabilecek bir çözüm sunmaktadır.

Çalışma kapsamında, şeker pancarı atıklarından doğal pigmentlerin elde edilmesi amacıyla su bazlı, etanol bazlı ve ultrasonik destekli ekstraksiyon yöntemlerinin değerlendirilmesi planlanmaktadır. Elde edilen ekstraktların pamuklu kumaşlarda boyar madde olarak uygulanabilirliği; boyar madde konsantrasyonu, pH, sıcaklık ve işlem süresi parametreleri dikkate alınarak incelenecektir. Bu doğrultuda %5, %10 ve %20 konsantrasyonlar, pH 3–10 aralığı, 40, 60 ve 80 °C sıcaklıklar ile 30, 60 ve 120 dakikalık işlem süreleri değerlendirilecektir. Ayrıca alüminyum sülfat, demir sülfat, tanen ve pektin gibi farklı mordanların renk oluşumu ve dayanıklılığı üzerindeki etkilerinin araştırılması hedeflenmektedir. Boyanmış kumaşların performansı, yıkama (ISO 105-C06), sürtme (ISO 105-X12) ve ışık haslığı (ISO 105-B02) testleriyle değerlendirilecektir.

Çalışmanın, şeker pancarı atıklarının tekstil sektöründe alternatif bir hammadde olarak kullanılabilirliğine ilişkin bilimsel veriler sağlaması beklenmektedir. Elde edilecek bulguların, doğal boyar maddelerin kullanım alanlarının genişletilmesine, tarımsal atıkların değerlendirilmesine ve çevresel açıdan daha sürdürülebilir tekstil boyama süreçlerinin geliştirilmesine katkı sunması hedeflenmektedir.

Anahtar Kelimeler: Şeker pancarı atıkları, doğal boyar madde, sürdürülebilir tekstil, pamuklu kumaş, renk haslığı.

ABSTRACT

The environmental impacts associated with the use of synthetic dyes in the textile industry have increased the importance of developing sustainable and environmentally friendly alternatives. This study aims to evaluate sugar beet waste as a source of natural dyes and investigate its potential for reuse in the textile industry. Converting agricultural and industrial waste into value-added products offers an innovative approach that can contribute to the circular economy.

Within the scope of the study, water-based, ethanol-based, and ultrasound-assisted extraction methods will be evaluated to obtain natural pigments from sugar beet waste. The applicability of the resulting extracts as dyes for cotton fabrics will be investigated by considering parameters such as dye concentration, pH, temperature, and processing time. In addition, the effects of different mordants, including aluminum sulfate, iron sulfate, tannin, and pectin, on color development and durability will be examined. The performance of the dyed fabrics will be evaluated through washing, rubbing, and light fastness tests.

The study is expected to provide scientific data on the use of sugar beet waste as an alternative raw material in the textile industry and contribute to the development of more sustainable dyeing processes. It also aims to promote waste valorization and support approaches that reduce environmental impacts.

Keywords: Sugar beet waste, natural dye, sustainable textiles, cotton fabric, color fastness.

1. GİRİŞ

Tekstil endüstrisi, üretim süreçlerinde yüksek miktarda su, enerji ve kimyasal madde tüketen sektörlerden biridir. Özellikle kumaş boyama ve terbiye işlemlerinde kullanılan sentetik boyar maddeler, atık su yükü ve çevresel etkileri nedeniyle önemli bir araştırma konusu oluşturmaktadır. Bu nedenle tekstil üretiminde daha sürdürülebilir yöntemlerin geliştirilmesi, doğal kaynakların verimli kullanılması ve alternatif boyama sistemlerinin araştırılması gerekmektedir.

Doğal boyar maddeler; bitkilerin yaprak, kök, kabuk, çiçek ve meyve gibi farklı kısımlarından elde edilebilmektedir. Bu maddeler, uygun ekstraksiyon ve uygulama koşulları sağlandığında tekstil yüzeylerine renk kazandırabilmektedir. Bununla birlikte doğal boyar maddelerin elyafla etkileşimi; sıcaklık, pH, işlem süresi ve kullanılan mordan türü gibi çeşitli parametrelere bağlıdır. Özellikle pamuk gibi selülozik elyaflarda boyar maddenin kumaşa tutunmasını ve renk dayanımını artırmak amacıyla farklı uygulama yöntemleri araştırılmaktadır (Shahid ve Mohammad, 2013).

Doğal boyama işlemlerinde alüminyum sülfat ve demir sülfat gibi metal tuzları mordan olarak kullanılabilmektedir. Bunun yanında tanen ve pektin gibi doğal kaynaklı maddeler de alternatif mordanlama yaklaşımları açısından değerlendirilmektedir. Kullanılan mordanın türü, boyama sonucunda elde edilen renk tonunu ve haslık özelliklerini etkileyebilmektedir (Nambela vd., 2020; Batool vd., 2024).

Tarımsal üretim ve gıda işleme süreçlerinde ortaya çıkan atıkların yeniden değerlendirilmesi, döngüsel ekonomi ve kaynak verimliliği açısından önemli fırsatlar sunmaktadır. Bu kapsamda şeker pancarı, şeker üretiminde kullanılan temel tarımsal hammaddelerden biridir. İşleme sürecinde şeker pancarı küspesi, melas ve bitkisel yapraklar gibi farklı yan ürünler ortaya çıkmaktadır. Bu yan ürünlerin yalnızca atık olarak değerlendirilmesi yerine, içerdikleri doğal bileşenlerin farklı endüstriyel alanlarda kullanılabilirliğinin araştırılması önem taşımaktadır.

Şeker pancarı yaprakları ve diğer bitkisel kısımlar, doğal renk verici bileşenler bakımından araştırılabilecek kaynaklar arasında yer almaktadır. Bu bileşenlerin uygun çözücüler ve ekstraksiyon yöntemleriyle elde edilmesi, tekstil boyamacılığında alternatif hammadde kullanımına katkı sağlayabilir.

Bu çalışmanın temel amacı, şeker pancarı işleme atıklarından ve yapraklarından elde edilen ekstraktların doğal boyar madde kaynağı olarak değerlendirilmesidir. Bu doğrultuda farklı ekstraksiyon yöntemleri ve çözücüler denenmiş, ekstraktların pH değişimlerine karşı gösterdiği renk davranışları incelenmiştir. Elde edilen ön bulgular doğrultusunda, ilerleyen aşamalarda pamuklu kumaşlara uygulanabilirliğin ve renk haslığı özelliklerinin araştırılması hedeflenmiştir.

2. ARAŞTIRMA VE BULGULAR

2.1. Kullanılan Hammaddeler

Çalışmada kullanılan şeker pancarı atıkları iki farklı kaynaktan temin edilmiştir. Şeker pancarı küspesi Malatya Şeker Fabrikası'ndan sağlanırken, yaprak örnekleri Malatya'nın Yazıhan bölgesindeki şeker pancarı tarlalarından toplanmıştır.

Deneylerde yaş küspe, taze yaprak ve kurutulmuş yaprak örnekleri kullanılmıştır. Yaprak örnekleri ekstraksiyon öncesinde küçük parçalara ayrılmış, bazı örnekler ise kurutularak hazırlanmıştır.

2.2. Şeker Pancarı Küspesinden Su Ekstraksiyonu

Çalışmanın ilk aşamasında şeker pancarı küspesinin doğal renk verici bileşenlerini belirlemek amacıyla su ekstraksiyonu gerçekleştirilmiştir.

Bu kapsamda yaş küspe örneği alınarak su içerisinde ekstraksiyona tabi tutulmuştur. Elde edilen ekstraktın başlangıç pH değeri 5 olarak ölçülmüştür. Ekstraktın asidik ve bazik koşullardaki davranışını incelemek amacıyla pH değişimleri gerçekleştirilmiştir.

Yapılan gözlemlerde pH değişimine rağmen ekstraktın renginde belirgin bir farklılık meydana gelmemiştir. Bu sonuç üzerine araştırmanın devamında şeker pancarı yapraklarının doğal renk verici bileşenler açısından değerlendirilmesine ağırlık verilmiştir.



Şekil 1.1. Şeker pancarı küspesinden elde edilen su ekstraktının asidik ve bazik koşullardaki görünümü.

2.3. Ultrasonik Banyo Yöntemiyle Ekstraksiyon

Şeker pancarı atıklarında bulunan renk verici bileşenlerin çözücü ortamına aktarılmasını sağlamak amacıyla ultrasonik banyo yöntemi kullanılmıştır.

Deneylerde öğütülerek toz hâline getirilen şeker pancarı atıklarıyla çözücü balon içerisine aktarılmıştır. Ekstraksiyon işlemi yaklaşık 4 saat boyunca ultrasonik banyoda gerçekleştirilmiştir.

Çözücü olarak etil asetat ve metanol ayrı ayrı denenmiştir. Her iki çözücüyle gerçekleştirilen çalışmalarda renkli ekstraktlar elde edilmiştir. Ancak etil asetatın su içerisinde sınırlı çözünürlüğe sahip olması nedeniyle ekstraktın bekletilmesi sonucunda faz ayrımı meydana gelmiştir.

Tekstil kumaşlarının boyama işlemleri ağırlıklı olarak sulu ortamda gerçekleştirildiğinden, ekstraktın suyla uyumlu olması önemli bir kriter olarak değerlendirilmiştir. Metanolün suyla karışabilir olması dikkate alınarak sonraki çalışmalarda metanol ekstraktlarıyla devam edilmesine karar verilmiştir.



Şekil 2.3. Ultrasonik Banyoda Şeker Pancarının Küspesinin Ekstraksiyonu

2.4. Soxhlet Yöntemiyle Şeker Pancarı Atıklarının Ekstraksiyonu

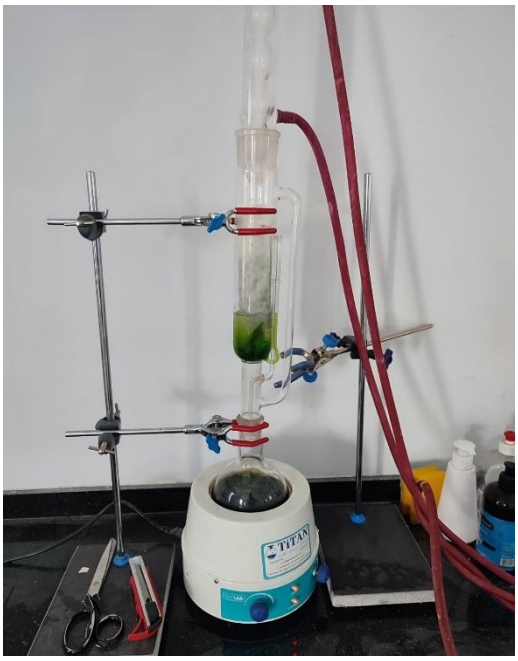
Ultrasonik banyo çalışmalarına ek olarak Soxhlet ekstraksiyon yöntemi de uygulanmıştır. Bu yöntemde şeker pancarı yaprakları küçük parçalara ayrılmış ve bazı örnekler kurutularak ekstraksiyona hazırlanmıştır.

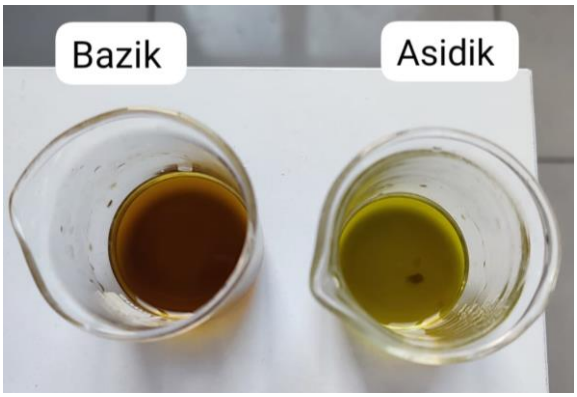
Yaprak örnekleri filtre kâğıdına yerleştirilerek Soxhlet düzeneğine alınmış ve çözücü olarak metanol kullanılmıştır. Böylece yapraklarda bulunan çözünebilir bileşenlerin ekstrakte edilmesi amaçlanmıştır.

Ayrı bir deneyde ise öğütülmüş şeker pancarı atığı metanol ile Soxhlet düzeneğinde ekstrakte edilmiştir. İşlem sonrasında ekstraktın yoğunluğunu artırmak amacıyla metanolün bir kısmı damıtılarak geri kazanılmış ve yaklaşık metanol geri elde edilmiştir.

Bu deneyde elde edilen ekstraktın pH değeri değiştirilerek renk davranışı incelenmiş, ancak belirgin bir renk değişimi gözlenmemiştir. Bu örnek üzerinde gerçekleştirilen çalışmada mordanlama aşamasına geçilememiştir.

Burada belirtilen sonuç, öğütülmüş şeker pancarı atığıyla gerçekleştirilen ayrı Soxhlet deneyine aittir. Yaprak ekstraktında gözlenen pH kaynaklı renk değişimiyle karıştırılmamalıdır.





Şekil 2.4. Alınan ekstraktların pH değişmesi ile renk değişimine bakıldı. Bazik ve asidik ortamlarda farklı renk verdiği gözlemlenmiştir

2.5. Şeker Pancarı Yaprak Ekstraktının pH Değişimlerine Karşı Davranışı

Çalışmanın önemli aşamalarından biri, şeker pancarı yapraklarından elde edilen ekstraktın farklı pH koşullarındaki renk davranışının incelenmesidir.

Bu kapsamda şeker pancarı yaprağından 250 mL metanol ekstraktı elde edilmiştir. Ekstraktın asidik ve bazik ortamlardaki renk değişimini belirlemek amacıyla farklı pH koşulları oluşturulmuştur.

Gerçekleştirilen gözlemlerde ekstraktın pH değerine bağlı olarak farklı yeşil tonlarına dönüştüğü belirlenmiştir. Bu durum, şeker pancarı yapraklarından elde edilen ekstraktın pH koşullarına duyarlı renk verici bileşenler içerebileceğini göstermektedir.

Küspe ekstraktında belirgin bir renk değişimi gözlenmemesine karşın yaprak ekstraktında farklı yeşil tonlarının ortaya çıkması, kullanılan bitki kısmının ve ekstraksiyon koşullarının elde edilen ekstraktın özellikleri üzerinde etkili olabileceğini düşündürmektedir.

2.6. Deneysel Bulguların Genel Değerlendirilmesi

Çalışmada gerçekleştirilen ekstraksiyon deneyleri sonucunda elde edilen ön bulgular aşağıda özetlenmiştir. Elde edilen sonuçlar, ekstraksiyon yönteminin, çözücü türünün ve kullanılan şeker pancarı bölümünün ekstraktın özelliklerini etkileyebileceğini göstermektedir.

Özellikle yaprak örneğinden elde edilen metanol ekstraktında pH değişimine bağlı farklı yeşil tonlarının gözlenmesi, çalışmanın sonraki aşamaları açısından önemli bir başlangıç bulgusudur. Bununla birlikte gözlenen renk değişiminin hangi kimyasal bileşenlerden kaynaklandığının belirlenmesi için ileri analizlerin yapılması gerekmektedir.

3. SONUÇ

Bu çalışmada şeker pancarı işleme sürecinde ortaya çıkan atıkların ve şeker pancarı yapraklarının tekstil endüstrisinde doğal boyar madde kaynağı olarak değerlendirilebilirliği araştırılmıştır. Çalışma kapsamında su ekstraksiyonu, ultrasonik banyo ve Soxhlet yöntemleri kullanılarak farklı ekstraktlar elde edilmiştir.

İlk aşamada yaş şeker pancarı küspesinden su kullanılarak ekstrakt hazırlanmış ve başlangıç pH değeri 5 olarak belirlenmiştir. Ekstraktın asidik ve bazik koşullardaki incelenmesinde belirgin bir renk değişimi gözlenmemiştir. Bu nedenle araştırma yaprak örnekleri üzerinde yoğunlaştırılmıştır.

Ultrasonik banyo yöntemiyle gerçekleştirilen çalışmalarda etil asetat ve metanol kullanılarak renkli ekstraktlar elde edilmiştir. Ancak etil asetatın suyla sınırlı çözünürlüğü nedeniyle faz ayrımı meydana gelmesi ve tekstil boyama işlemlerinin sulu ortamda gerçekleştirilmesi dikkate alınarak metanol ekstraktlarıyla devam edilmesine karar verilmiştir.

Soxhlet yöntemiyle gerçekleştirilen çalışmalarda ise farklı deney koşullarına bağlı olarak farklı sonuçlar elde edilmiştir. Özellikle şeker pancarı yaprağından elde edilen metanol ekstraktında, farklı pH koşullarında yeşil tonlarının değiştiği gözlemlenmiştir. Bu bulgu, şeker pancarı yapraklarının doğal renk verici bileşenler açısından araştırılmaya değer bir kaynak olduğunu göstermektedir.

Çalışmanın mevcut aşamasında ekstraktların pamuklu kumaşlara uygulanması, mordanlama işlemleri ve renk haslığı testleri henüz tamamlanmamıştır. Bundan sonraki aşamada ekstraksiyon koşullarının geliştirilmesi, pH değişimlerinin sistematik olarak incelenmesi ve elde edilen ekstraktların pamuklu kumaşlara uygulanması planlanmaktadır.

Boyama işlemlerinin ardından ISO 105-C06 yıkama haslığı, ISO 105-X12 sürtme haslığı ve ISO 105-B02 ışık haslığı standartlarına göre değerlendirmeler yapılması hedeflenmektedir. Ayrıca farklı mordan türlerinin renk oluşumu ve kumaşa tutunma üzerindeki etkilerinin araştırılması planlanmaktadır.

Sonuç olarak şeker pancarı yapraklarının ve işleme atıklarının tekstil sektöründe doğal boyar madde kaynağı olarak kullanılabilirliği konusunda umut verici ön bulgular elde edilmiştir. Çalışmanın ilerleyen aşamalarında yapılacak kumaş uygulamaları ve haslık testleriyle bu potansiyelin teknik açıdan değerlendirilmesi amaçlanmaktadır.

4. KAYNAKÇA

1. Shahid, M., & Mohammad, F. (2013). Recent advancements in natural dye applications: A review. Journal of Cleaner Production, 53, 310–331

4. ISO 105-C06. Textiles — Tests for colour fastness — Part C06: Colour fastness to domestic and commercial laundering.

5. ISO 105-X12. Textiles — Tests for colour fastness — Part X12: Colour fastness to rubbing.

6. ISO 105-B02. Textiles — Tests for colour fastness — Part B02: Colour fastness to artificial light: Xenon arc fading lamp test.

PVA TABANLI ELEKTROSTATİK EĞİRME NANOLİFLERİNDE ZnO VE MnO KATKISININ MORFOLOJİ VE LİF ÇAPI DAĞILIMINA ETKİSİ

THE EFFECTS OF ZnO AND MnO ADDITIONS ON THE MORPHOLOGY AND FIBER DIAMETER DISTRIBUTION OF PVA-BASED ELECTROSPUN NANOFIBERS

Berkay ARSLAN
Yıldız Teknik Üniversitesi, Kimya-Metalurji Fakültesi, Metalurji ve Malzeme Mühendisliği Bölümü, İstanbul, Türkiye

Nilüfer DUYGULU
Yıldız Teknik Üniversitesi, Kimya-Metalurji Fakültesi, Metalurji ve Malzeme Mühendisliği Bölümü, İstanbul, Türkiye

ÖZET

Enerji depolama sistemlerinde elektrot içi temas direncinin azaltılması ve aktif yüzey alanının en üst düzeye çıkarılması amacıyla bağlayıcısız (binder-free) elektrot tasarımları kritik öneme sahiptir. Bu çalışmada, süperkapasitör elektrotlarının üretiminde karbon öncüsü olarak kullanılan ağırlıkça %10 polivinil alkol (PVA) matrisine farklı oranlarda (%10, %15 ve %20 w/w) çinko oksit (ZnO) ve mangan oksit (MnO) nanoparçacıkları eklenerek elektro eğirme yöntemiyle nanolif membranlar üretilmiştir. Üretim öncesinde çözeltilerin viskozitesi ölçülmüş; elektro eğirme işlemi 9 kV gerilim ve 5 mL/saat akış hızında gerçekleştirilmiştir. Elde edilen nanoliflerin yüzey morfolojileri Taramalı Elektron Mikroskobu (SEM) ile incelenmiştir. Her numuneden ImageJ kullanılarak elde edilen 100 bağımsız lif çapı verisine OriginPro yazılımında Gauss normal dağılım fonksiyonu uygulanmış ve karşılaştırmalı istatistiksel analizler gerçekleştirilmiştir.

Elde edilen sonuçlar, katkı türünün ve derişiminin lif çapı üzerinde belirleyici bir rol oynadığını ortaya koymuştur:

• %10 ZnO-PVA nanoliflerinde 359,71 ± 94,55 nm olan ortalama çap, katkı oranının %15'e çıkarılmasıyla çözelti iletkenliğinin artması sonucunda 294,16 ± 67,75 nm'ye gerilemiştir. Katkı oranının %20'ye yükseltilmesiyle, artan çözelti viskozitesine bağlı olarak çap 427,44 ± 112,19 nm'ye ulaşmıştır.

• MnO katkılı seride, %10 katkı oranında 293,90 ± 48,11 nm olarak ölçülen ortalama lif çapı, %15 MnO katkısında serinin en düşük değerine gerilemiş ve en homojen dağılımı göstermiştir (227,44 ± 58,19 nm). %20 MnO katkısında ise lif çapı 299,71 ± 58,65 nm olarak ölçülmüştür.

Deneysel ve istatistiksel bulgular, %15 metal oksit katkı oranının lif inceliği ve mikroyapısal homojenlik açısından optimum bileşim olduğunu ve karbonizasyon sonrasında yüksek performanslı süperkapasitör elektrotlarında kullanılmaya uygun bir öncü yapı sunduğunu göstermektedir.

Anahtar Kelimeler: Elektrostatik eğirme, nanolif morfolojisi, PVA, ZnO/MnO nanoparçacık, lif çapı dağılımı.

ABSTRACT

Binder-free electrode designs are essential in energy storage systems because they reduce intra-electrode contact resistance and maximize active surface area. In this study, zinc oxide (ZnO) and manganese oxide (MnO) nanoparticles were incorporated into a 10 wt.% polyvinyl alcohol (PVA) matrix at concentrations of 10, 15, and 20 wt.%. The PVA matrix served as a carbon precursor to produce supercapacitor electrodes, which were fabricated using electrospinning. Solution viscosity was measured before fabrication, and electrospinning was conducted at a voltage of 9 kV and a flow rate of 5 mL/h. The surface morphology of the resulting nanofibers was examined using scanning electron microscopy (SEM). For each sample, we analyzed 100 independent fiber-diameter measurements obtained using ImageJ in OriginPro with a Gaussian normal distribution function, followed by comparative statistical analysis.

The results demonstrate that the type and concentration of the additive play a decisive role in determining fiber diameter:

• For 10% ZnO-PVA nanofibers, the average diameter of 359.71 ± 94.55 nm decreased to 294.16 ± 67.75 nm when the additive concentration was increased to 15%, owing to increased solution conductivity. At an additive concentration of 20%, the diameter increased to 427.44 ± 112.19 nm, likely due to increased solution viscosity.

• In the MnO-doped series, the average fiber diameter decreased from 293.90 ± 48.11 nm at a 10% doping ratio to the series' lowest value at 15% MnO doping, which also yielded the most homogeneous distribution (227.44 ± 58.19 nm). At 20% MnO doping, the fiber diameter was 299.71 ± 58.65 nm.

The experimental and statistical findings indicate that 15% metal oxide loading represents the optimal composition for fiber fineness and microstructural homogeneity. Following carbonization, this composition produces a precursor structure suitable for high-performance supercapacitor electrodes.

Keywords: Electrospinning, nanofiber morphology, PVA, ZnO/MnO nanoparticles, fiber diameter distribution.

GREEN SYNTHESIS OF BIMETALLIC ZIRCRONIUM-COPPER NANOPARTICLES USING *BAUHINIA MONANDRA* LEAF EXTRACT: INVESTIGATION OF ITS ANTIBACTERIAL PROPERTIES

Oduntan. A.S.
Department of Biotechnology, School of Life Sciences, Federal University of Technology, Akure, Ondo State, Nigeria.

Adewale. V.O.
Department of Biotechnology, School of Life Sciences, Federal University of Technology, Akure, Ondo State, Nigeria.

ABSTRACT

The increasing danger of antimicrobial resistance has led to the need for new and environmentally friendly nanomaterials that have better antibacterial effects. This study reports the green synthesis of bimetallic zirconium-copper (Zr-Cu) nanoparticles using *Bauhinia monandra* leaf extract as both reducing and stabilizing agent. Fresh leaves were air-dried and subjected to aqueous extraction, followed by qualitative and quantitative phytochemical screening, which revealed the presence of bioactive compounds such as saponins, flavonoids, and polyphenols in appreciable amounts, indicating their role in nanoparticle formation and stabilization. Synthesis was achieved by adding the extract to a mixed $ZrOCl_2$ and $CuSO_4$ solution, resulting in a color change from milky blue to coffee brown (pH 4.22) under magnetic stirring for 60 min. The mixture was kept for 24h at room temperature, decanted, oven-dried at 80°C, and calcined at 700°C for 3h to enhance crystallinity. Characterization was carried out using UV-Visible spectroscopy, FTIR, XRD, SEM, and EDX analyses. FTIR confirmed functional groups such as hydroxyl and carbonyl, indicating biomolecule involvement in reduction and capping. XRD revealed crystalline and polycrystalline structures with nanoscale crystallite sizes (5.2-50.8 nm) and zirconium oxide phases. SEM showed irregular, agglomerated particles with rough morphology, while EDX confirmed the presence of zirconium, copper, and oxygen. Antibacterial activity was evaluated against three Gram-positive (*Staphylococcus aureus*, *Streptococcus pneumoniae*, and *Enterococcus faecalis*) and three Gram-negative (*Klebsiella oxytoca*, *Escherichia coli*, and *Proteus vulgaris*) clinical isolates using the agar well diffusion method at 100 mg/mL. Broad-spectrum activity was observed, with inhibition zones ranging from 25.00 to 43.00 mm. Gram-negative isolates showed higher susceptibility, particularly *E. coli* (42.00 mm) and *P. vulgaris* (43.00 mm), comparable to the amoxicillin control. MIC values ranged from 12.5 to 25 mg/mL. These findings demonstrate that *B. monandra*-mediated synthesis is an effective and sustainable approach for producing Zr-Cu nanoparticles with promising antibacterial applications.

Keywords: Zr-Cu bimetallic nanoparticles; *Bauhinia monandra*; antibacterial activity; phytochemical screening; characterization.

CONTRIBUTION TO THE MATHEMATICAL ANALYSIS OF SOME NONLINEAR PDES ARISING FROM ELECTRORHEOLOGICAL FLUIDS MODELING

Kamal BOUCHIT
Doctorant., Hassan II University, Faculty of Sciences and Technologies Mohommedia, Laboratory of Mathematics and Physical Sciences Applied to Engineering Sciences, Casablanca, MOROCCO

Jilali ABOUIR
Dr., Hassan II University, Faculty of Sciences and Technologies Mohommedia, Laboratory of Mathematics and Physical Sciences Applied to Engineering Sciences, Casablanca, MOROCCO

Abderrahim CHARKAOUI
Dr., Hassan First University, Higher School of Education and Training of Berrechid, Laboratory of Education, Sciences and Techniques, Berrechid, MOROCCO

Anouar BEN-LOGHFYRY
Dr., Hassan II University, Faculty of Sciences and Technologies Mohommedia, Laboratory of Mathematics and Physical Sciences Applied to Engineering Sciences, Casablanca, MOROCCO

ABSTRACT

This work focuses on the mathematical analysis of some nonlinear partial differential equations (PDEs) arising from electrorheological fluids modeling. Variable exponent diffusion mechanisms characterize these models and exhibit a non-standard growth structure. The main objective is to investigate the mathematical properties of these equations, particularly the existence, uniqueness, and regularity of solutions. The study includes an in-depth analysis of the underlying mathematical models, analytical techniques, and relevant boundary conditions to understand the behavior and characteristics of the solutions. Additionally, it aims to develop efficient numerical methods for solving these equations.

Keywords: Nonlinear partial differential equations, Electrorheological fluids, Variable exponent, Boundary conditions, Numerical methods

THE INFLUENCE OF DIGITAL MARKETING CAPABILITIES ON CUSTOMER LOYALTY: THE MEDIATING EFFECTS OF CUSTOMER ENGAGEMENT AND BRAND TRUST

Faruk AHMETI
Prof. Asoc. Dr.**,** University "Isa Boletini" Mitrovica, Faculty of Mechanical and Computer Engineering, Mitrovica, Kosovo
ORCID: 0000-0003-3529-7919

Kushtrim GASHI
Prof. Asoc. Dr.**,** University "Ukshin Hoti" Prizren, Faculty of Economics, Prizren, Kosovo
ORCID: 0000-0002-3349-4102

ABSTRACT
This study explores the link between digital marketing capabilities and customer loyalty by studying customer engagement and brand trust as the mediators. In order to gain insights into the problem, 341 questionnaires were received and analyzed using a quantitative cross sectional design, in which reliability test and multiple regression were used. The inter-item correlations of all constructs were in the acceptable ranges (Cronbach's $\alpha = 0.814$-0.853). The results indicate strong positive relationships between the digital marketing capabilities and customer engagement ($B = 0.514$, $p < 0.001$) and brand trust ($B = 0.544$, $p < 0.001$). The results revealed positive relationship of customer engagement ($B = 0.320$, $p < 0.001$) and brand trust ($B = 0.335$, $p < 0.001$) with customer loyalty, and also a significant direct relationship of digital marketing capabilities and customer loyalty ($B = 0.170$, $p < 0.001$). The model accounts for 46.9% of the variation in customer loyalty. The findings underscore the need for engagement and trust when it comes to making digital marketing more effective in customer relationships.

Keywords: Digital Marketing Capabilities; Customer Loyalty; Customer Engagement; Brand Trust; Digital Consumer Behavior.

GLOBAL HEALTH CHALLENGES AND OUR RESPONSE: SPECIAL FOCUS TO PAKISTAN

Tabussam Tufail
[1] Department of Food Sciences, Government College University Faisalabad, Pakistan.
[2] College of Pharmaceutical Science, Zhejiang University of Technology, Hangzhou, P. R. China

Huma Bader Ul Ain
Department of Food Sciences, Government College University Faisalabad, Pakistan.

Farhan Saeed
Department of Food Sciences, Government College University Faisalabad, Pakistan.

Muhammad Afzaal
Department of Food Sciences, Government College University Faisalabad, Pakistan.

Tanazzam Tufail
Tufail Medical Complex, Shehzad Colony Faisalabad, Pakistan.

Muhammad Umair Arshad
Department of Food Sciences, Government College University Faisalabad, Pakistan.

ABSTRACT
Global health challenges encompass complex issues that affect communities worldwide and require coordinated action across multiple sectors. The main challenges encompass infectious illnesses, non-communicable diseases (NCDs), maternity and child health, healthcare accessibility, health emergencies, antimicrobial resistance, and climate change. The issues are influenced by factors such as socioeconomic conditions, environmental factors, political instability, insufficient healthcare infrastructure, population growth, urbanization, globalization, and lifestyle changes. Pakistan faces distinct issues such as a rapid increase in population, nutritional emergencies, and the adverse effects of climate change, which worsen the problems of food insecurity and poverty. These problems underscore the need for comprehensive responses across multiple sectors and well-planned actions. To tackle these global health issues, it is crucial to adopt a comprehensive approach that involves participation from various parties at the local, national, regional, and international levels. Strategies encompass lifestyle modifications, dietary adjustments, preventive measures, technology-driven initiatives, and the promotion of collaborations across multiple sectors. Key advancements such as digitalization, next-generation healthcare, and the One Health concept play a crucial role in improving healthcare outcomes, optimizing resource allocation, and adapting to new technologies. These methods are designed to address global health concerns and improve health outcomes for populations worldwide.

Keywords: Health challenges, Nutrition, Health Care, Pakistan.

SUSTAİNABLE WATER MANAGEMENT UNDER CLİMATE STRESS: EVİDENCE FROM MARRAKECH ON TREATED WASTEWATER IRRİGATİON, SOİL FERTİLİTY, AND MAİZE AGRO-PHYSİOLOGY

Ahmed Osmane
Laboratory of Organic Chemistry and Physical Chemistry (Fundamental and Applied Chemistry)Faculty of Sciences, Agadir University Ibn Zohr
Laboratory of Biomolecular and Medicinal Chemistry, Faculty of Science Semlalia, University Cadi Ayyad, Marrakech, Morocco.
ORCID ID: 0000-0003-0246-2885

Khadija Zidan
National Center for Studies and Research on Water and Energy (CNEREE), Cadi Ayyad University, Marrakech, Morocco.
Laboratory of Water, Biodiversity and Climate Change, Faculty of Sciences Semlalia, Cadi Ayyad University, Marrakech, Morocco

Hasnae Sabri
Laboratoire Interdisciplinaire de Recherche en Envirenement, Management, Energie et Tourisme Ecole supérieure de Technologie de Essouira Cadi Ayyad University, Essaouira, Morocco

Moustapha Belmouden
Laboratory of Organic Chemistry and Physical Chemistry (Fundamental and Applied Chemistry)Faculty of Sciences, Agadir University Ibn Zohr
ORCID ID: 0000-0002-3083-2620

ABSTRACT

The aim of this work was to investigate the effect of treated wastewater irrigation on the physiological and agronomic properties of *Zea mays*. An experimental reuse study was performed using raw (RWW) and treated urban wastewater (TWW) by Trickling Filter (TF) process to irrigate maize *(Zea mays)* in comparison to well water (WW) as a control over a period of 5 months. The water quality was determined for irrigation based on sodium adsorption ratio (SAR), sodium percentage (Na %) and residual sodium carbonate (RSC) indicating that all treatments were suitable for irrigation purposes. In this study, we also assessed the agro-physiological and biochemical proprieties of the crops. Hence, the highest productivity of maize and leaf area were obtained in response to irrigation with RWW and TWW compared to WW; while macro-elements (TP, TKN, and K) were also affected in maize irrigated with RWW compared to TWW and WW. However, the plants irrigated with well water accumulate more Ca, Na, and Mg than those irrigated with RWW and TWW. All the crops irrigated with three water treatments showed a relatively similar concentration of micro-nutriments. The prevalence of total chlorophyll content in the plants increased with well water irrigation. Nevertheless, the biochemical parameters (protein and sugar content)

were adversely affected in maize irrigated with RWW as compared to TWW and WW. Moreover, the use of treated urban wastewater improves the physicochemical properties and fertility of the soil compared to well water and enhances crop productivity.

Keywords: *Zea mays;* irrigation; treated wastewater reuse; physiological proprieties; agronomic properties ; Trickling Filter.

SYNTHESIS AND ADSORPTION PERFORMANCE OF POZZOLAN–ALGINATE COMPOSITE BEADS TOWARD OLIVE OIL POLYPHENOLS

Ahmed Osmane
Laboratory of Organic Chemistry and Physical Chemistry (Fundamental and Applied Chemistry)Faculty of Sciences, Agadir University Ibn Zohr
Laboratory of Biomolecular and Medicinal Chemistry, Faculty of Science Semlalia, University Cadi Ayyad, Marrakech, Morocco.
ORCID ID: 0000-0003-0246-2885

Khadija Zidan
National Center for Studies and Research on Water and Energy (CNEREE), Cadi Ayyad University, Marrakech, Morocco.
Laboratory of Water, Biodiversity and Climate Change, Faculty of Sciences Semlalia, Cadi Ayyad University, Marrakech, Morocco

Hasnae Sabri
Laboratoire Interdisciplinaire de Recherche en Envirenement, Management, Energie et Tourisme Ecole supérieure de Technologie de Essouira Cadi Ayyad University, Essaouira, Morocco

Moustapha Belmouden
Laboratory of Organic Chemistry and Physical Chemistry (Fundamental and Applied Chemistry)Faculty of Sciences, Agadir University Ibn Zohr
ORCID ID: 0000-0002-3083-2620

ABSTRACT

Adsorption experiments confirmed that the adsorption reaction of phenol ions on AS/PZ was strongly dependent on pH, adsorbent dose and initial phenol concentration, with a maximum adsorption capacity of 244 mg/g at 25°C and pH equal to 6.2. The adsorption isotherm showed a better fit with the Freundlich model and the kinetic studies demonstrated that the adsorption data correlated with a pseudo-second order model. Finally, the phenol regeneration results show that the adsorbed phenol remains almost unstable and can be desorbed using distilled water alone. The kinetic studies showed that the desorption data correlated with a pseudo-second-order model and a pore diffusion model. After six cycles of the adsorption-desorption process, the adsorbent retained its high adsorption capacity, which decreased in the seventh cycle, to 60 mg/g, due to non-reversible saturation of the adsorption sites

Keywords: adsorption,phenol, sodium alginate, bead ,pozzolan, column.

ROS-GAZEBO SİMÜLASYON ORTAMINDA OTONOM İHA'LAR İÇİN ENGELDEN KAÇINMA VE YOL PLANLAMA ALGORİTMALARININ KARŞILAŞTIRMALI DEĞERLENDİRİLMESİ

COMPARATIVE EVALUATION OF OBSTACLE AVOIDANCE AND PATH PLANNING ALGORITHMS FOR AUTONOMOUS UAVS IN A ROS-GAZEBO SIMULATION ENVIRONMENT

Seyit AKPANCAR
Lecturer, Ph.D., Isparta University of Applied Sciences, Atabey Vocational School, Isparta, Türkiye
ORCID NO: 0000-0002-4217-9032

Eyüp ÇAKI
Lecturer, Ph.D., Gaziantep University, Naci Topçuoğlu Vocational School, Gaziantep, Türkiye
ORCID NO: 0000-0002-1980-3810

ÖZET

İnsansız hava araçlarının (İHA) otonom navigasyonunun başarılı bir şekilde gerçekleştirilebilmesi; çevresini doğru algılama, yol planlama, dinamik ve statik engellerden kaçınma süreçlerinin aynı anda yürütülmesine bağlıdır. Bu çalışmada Yapay Potansiyel Alan (Artificial Potential Field - APF), Hızla Keşfeden Rastgele Ağaç (Rapidly-exploring Random Tree - RRT) ve iki boyutlu düzlemde çalışan geleneksel Dinamik Pencere Yaklaşımı'nın (DWA) 3D ortamlarda hareket eden robotlar için uyarlaması (3D-DWA) olmak üzere 3 farklı algoritmanın karşılaştırılabilmesi amacıyla tekrarlanabilecek nitelikte ROS 2-Gazebo simülasyon ortamı oluşturulmuştur. Bu 3 algoritma aynı 6 rotorlu X4 multikopter kullanılarak ROS 2-Gazebo sahnesinde statik engeller, dar geçit engelleri ve yanal hareket eden engellerin bulunduğu 3 farklı senaryoda test edilmiştir. Her algoritma bu üç senaryoda 10'ar kez test edilmiş ve toplam 90 test gerçekleştirilmiştir. Statik engeller ve dar geçit engelleri içeren senaryolarda üç yöntem de 10 testin tamamında hedefe başarıyla ulaşmıştır. Fakat yanal hareket eden engelin bulunduğu senaryoda APF ve 3D-DWA algoritmaları herhangi bir ciddi irtifa kaybı yaşamadan 10 testin tamamını başarıyla tamamlarken, RRT algoritması 10 testin yalnızca 5'ini bu ölçütü ihlal etmeden tamamlayabilmiştir. Sonuç olarak; görev süresi, yörünge geometrisi, algılanan engel mesafesi ve hesaplama özellikleri açısından senaryoya bağlı farklılıklar ortaya çıkmıştır. Bu bulgular, küresel ve reaktif navigasyon yaklaşımlarını tek bir başarı ölçütüne göre değerlendirmek yerine farklı çevresel koşullar ve performans ölçütleri altında değerlendirmenin önemini göstermiştir.

Anahtar kelimeler: Otonom İHA, ROS 2, Gazebo, engelden kaçınma, yol planlama, APF, RRT, 3D-DWA.

ABSTRACT

The successful autonomous navigation of unmanned aerial vehicles (UAVs) depends on the simultaneous execution of environmental perception, path planning, and dynamic and static obstacle avoidance processes. In this study, a reproducible ROS 2–Gazebo simulation environment was created to compare three different algorithms: Artificial Potential Field (APF), Rapidly-exploring Random Tree (RRT), and a three-dimensional adaptation of the conventional Dynamic Window Approach (DWA), referred to as 3D-DWA. The three algorithms were tested using the same six-rotor X4 multicopter in three different ROS 2–Gazebo scenarios involving static obstacles, narrow passages, and a laterally moving obstacle. Each algorithm was tested 10 times in each scenario, resulting in a total of 90 tests. In the static obstacle and narrow passage scenarios, all three methods successfully reached the goal in all 10 tests. However, in the scenario with a laterally moving obstacle, APF and 3D-DWA successfully completed all 10 tests without any serious loss of altitude, whereas RRT completed only 5 of the 10 tests without violating this criterion. The results also showed scenario-dependent differences in mission time, trajectory geometry, detected obstacle distance, and computational characteristics. These findings demonstrate the importance of evaluating global and reactive navigation approaches under different environmental conditions and using multiple performance metrics rather than relying on a single measure of success.

Keywords: Autonomous UAV, ROS 2, Gazebo, obstacle avoidance, path planning, APF, RRT, 3D-DWA.

GİRİŞ

İnsansız hava araçları (İHA) teknolojinin gelişimi ve yaygınlaşmasıyla birlikte çevresel izleme ve denetimlerde, haritalamada, arama-kurtarma çalışmalarında, insanlar için zor veya tehlikeli görevlerde daha aktif bir şekilde kullanılmaktadır. Görev karmaşıklığı arttıkça da otonom hareket eden İHA navigasyonu ile çevrenin daha ayrıntılı algılanması ve engelden kaçınma yöntemlerinin birleştirilmesi gerekmektedir. Bu gereksinim, hava aracının değişen engel yapılarına tepki vermesi gerekirken karmaşık veya dinamik ortamlardaki kararlı bir uçuşun gerçekleşmesi ve kabul edilebilir görev verimliliğinin artırılmasında daha da önem kazanmaktadır (Chen ve ark., 2026).

Engelden kaçınma ve yol planlama yöntemleri, varsayımları ve çalışma prensipleri bakımından önemli farklılıklar göstermektedir. APF (Yapay Potansiyel Alan) algoritması; belirlenen hedefi çekici bir potansiyel, engelleri ise itici bir potansiyel olarak temsil ederek gerçek zamanlı olarak engellerden kaçınılması amacıyla Khatib tarafından geliştirilmiştir (Khatib, 1986). LaValle tarafından önerilen RRT (Hızla keşfeden Rastgele Ağaçlar) algoritması ise; büyük konfigürasyon uzaylarını etkin bir şekilde araştırmak için rastgele örneklemeler kullanmaktadır. Bu algoritma bu özelliğiyle de örnekleme tabanlı hareket planlamanın temel yaklaşımlarından birini oluşturmaktadır (LaValle, 1998). Fox, Burgard ve Thrun tarafından geliştirilen DWA (Dinamik Pencere Yaklaşımı) algoritması ise; aday

komutları dinamik erişilebilirlik ve güvenli durma problemlerine göre kısıtlayarak doğrudan hız uzayında arama yapmaktadır (Fox ve ark., 1997). Dolayısıyla bu üç yöntem sırasıyla reaktif, örnekleme tabanlı küresel ve hız uzayı tabanlı yerel planlama yaklaşımlarını temsil etmektedir.

Bu çalışma aynı zamanda yazarların ROS tabanlı İHA modelleme, simülasyon, otonom navigasyon ve 3D çevresel algılama alanındaki araştırmalarının devamı niteliğindedir. Çakır ve Akpancar daha önce DJI M100 platformunu Gazebo ortamında modellemiş ve simüle edilen aracı ROS üzerinden kontrol etmiştir (Çakır ve Akpancar, 2018). Daha sonraki çalışmalarında ise DJI Matrice 100 platformu, lazer algılama, ultrasonik sensörler ve ROS tabanlı yazılım kullanarak karanlık ve kapalı ortamlarda 3D eş zamanlı konumlama ve haritalama gerçekleştiren otonom bir uçan robot sistemi geliştirmişlerdir (Çakır ve Akpancar, 2020). Bu çalışmalar, mevcut araştırmanın ROS tabanlı İHA simülasyonu, otonom uçuş ve çevresel algılama açısından altyapısını oluşturmaktadır.

Bu çalışmanın amacı; APF, RRT ve DWA'nın 3D ortamlara uyarlanmış biçimi olan 3D-DWA olmak üzere üç farklı algoritmayı ortak bir ROS 2-Gazebo deneysel ortamında karşılaştırmaktır. Yöntemler yalnızca tek bir ortamda değerlendirilmek yerine statik engeller, geometrik olarak kısıtlanmış dar geçit engelleri ve yanal hareket eden bir engelin yer aldığı üç senaryoda incelenmiştir. Her algoritma-senaryo birleşimi için 10 test tekrarı gerçekleştirilmiştir. Algoritmaların performansı hedefe ulaşma başarısı, çarpışma ile ilişkili uçuş başarısızlığı, görevin tamamlanma süresi, yörünge uzunluğu, algılanan minimum engel mesafesi ve hesaplama maliyeti kullanılarak değerlendirilmiştir.

İLGİLİ ÇALIŞMALAR

Bu çalışmada değerlendirilen üç algoritma, hareket planlamanın farklı yaklaşımlarından ortaya çıkmıştır. Khatib'in Yapay Potansiyel Alan formülasyonu, hareket üretmek için çekici ve itici potansiyellerin birleştirildiği gerçek zamanlı bir engelden kaçınma stratejisi sunmuştur (Khatib, 1986). İlk çalışmada hareketli engeller için zamana bağlı potansiyel alanlar da ele alınmıştır. Hesaplama açısından basit ve reaktif olmasına rağmen klasik APF; yerel minimumlar, hedefe ulaşılamayan durumlar ve kısıtlı geometrilerde salınım davranışı gibi problemlere açıktır. Bu sınırlamalar, değiştirilmiş potansiyel fonksiyonlarının, kaçış stratejilerinin ve hibrit planlayıcıların geliştirilmesini teşvik etmiştir.

LaValle, RRT algoritmasını holonomik olmayan ve kinodinamik kısıtlara sahip sistemler de dahil olmak üzere geniş bir yol planlama problemi sınıfına yönelik rastgeleleştirilmiş bir veri yapısı olarak önermiştir (LaValle, 1998). RRT algoritması, durum uzayının keşfedilmemiş bölgelerine doğru hızlı biçimde genişlemekte ve bu nedenle örnekleme tabanlı planlamanın temel çerçevelerinden biri haline gelmiştir. Bununla birlikte İHA uygulamalarında geleneksel RRT çözümleri düzgün olmayan yörüngeler üretebilmekte ve ilk yol oluşturulduktan sonra engeller hareket ettiğinde genellikle ek mekanizmalara ihtiyaç duymaktadır.

Fox ve ark. (1997), reaktif çarpışmadan kaçınma için komut aramasını doğrudan hız uzayında gerçekleştiren Dinamik Pencere Yaklaşımını geliştirmiştir. Aday hızlar, robotun dinamikleri ve çarpışmadan önce güvenli biçimde durabilme gereksinimi ile sınırlandırılmaktadır. Özgün

DWA kara mobil robotları için geliştirilmiş olsa da sonraki çalışmalar hız uzayı kavramını 3D navigasyona genişletmiştir. Güncel İHA çalışmalarında DWA, 3D uçuş ve kapalı ortamlar için yeniden formüle edilmiş (Bes ve ark., 2025); bazı çalışmalarda ise statik ve dinamik İHA yol planlaması için 3D DWA, kayan ufuk optimizasyonu ile birleştirilmiştir (Hu ve ark., 2026). Bu çalışmalar, burada kullanılan 3D-DWA'nın özgün kanonik algoritmadan ziyade DWA ilkesinin 3D bir uyarlaması olarak değerlendirilmesini desteklemektedir.

Karşılaştırmalı ve hibrit İHA çalışmaları, küresel örnekleme tabanlı ve yerel reaktif yöntemlerin birbirini tamamlayan güçlü yönlere sahip olduğunu göstermektedir. Potential-Field-RRT, İHA'larda ilk yolun elde edilmesini ve yol kalitesini geliştirmek amacıyla potansiyel alan yönlendirmesini rastgele ağaç genişlemesine dahil etmektedir (Huang ve ark., 2023). Benzer şekilde Bi-APF-RRT*, geliştirilmiş APF'yi çift yönlü RRT* ile birleştirmekte ve karmaşık 3D ortamlarda geleneksel RRT* ile karşılaştırmalar sunmaktadır (Huang ve ark., 2024). Parçacık sürü optimizasyonu ve APF tabanlı güncel bir 3D İHA yol planlama çalışmasında önerilen yöntem, farklı engel koşullarında geleneksel APF, RRT ve çeşitli geliştirilmiş APF türevleri ile karşılaştırılmıştır (Zhang ve ark., 2025). Bu çalışmalar APF ve RRT algoritmalarının birbirinin alternatifleri olarak görülmesi yerine karşılaştırılması veya birlikte kullanılmasına yönelik ilginin sürdüğünü göstermektedir.

Wang ve ark. (2024), daha önce şekli bilinmeyen karmaşık ortamlarda A*, RRT ve APF algoritmalarını karşılaştırmış, yol uzunluğu ve planlama süresi ölçütlerini raporlamışlardır. Mashkov ve ark. (2026), RRT, RRT* ve APF algoritmaları ile klasik, hibrit ve pekiştirmeli öğrenme tabanlı 3D yörünge planlamasına ilişkin bir çalışma gerçekleştirmişlerdir. Bu çalışmalarda algoritmalar yalnızca tek bir ölçüte göre değerlendirilmemiş; yol kalitesi, engel mesafesi, hesaplama ve başarı gibi farklı ölçütler birlikte ele alınmıştır.

Bir algoritmanın geliştirilmesine ya da algoritmaların tek bir ortamda karşılaştırılmasına yönelen çalışmalardan farklı olarak bu çalışmada APF, RRT ve 3D-DWA algoritmaları ROS 2-Gazebo çerçevesinde statik engeller, dar geçit engelleri ve yanal hareket eden engelin bulunduğu üç farklı koşulda değerlendirilmiştir. Bu çalışmadaki karşılaştırmalar tekrarlı test süreçleri üzerinden gerçekleştirilmiş; başarı, görev süresi, yörünge uzunluğu, algılanan engel mesafesi ve hesaplama özellikleri dikkate alınmıştır. Algoritmalar farklı çevresel bilgi gösterimlerini kullandığından gerçekleştirilen çalışma, matematiksel olarak özdeş girdilere sahip bir kıyaslamadan ziyade uygulanan navigasyon yaklaşımlarının sistem düzeyinde karşılaştırılması olarak ele alınmıştır.

MATERYAL VE YÖNTEM

Simülasyon Ortamı ve İHA Modeli

Deneyler ROS 2 Lyrical ve Gazebo Sim 10.5.0 simülatörü kullanılarak gerçekleştirilmiştir. ROS 2, Windows tabanlı bir Pixi ortamında kaynak koddan derlenmiş ve ROS 2 ile Gazebo arasındaki veri iletişimi ros_gz_bridge kullanılarak sağlanmıştır. Ortak İHA platformu olarak altı rotorlu X4 multikopter kullanılmıştır. Hız komutları /X4/gazebo/command/twist topic'i üzerinden gönderilirken, araç durum bilgileri /model/X4/odometry topic'inden alınmıştır.

Her bir test sürecinin başlangıcında Gazebo simülatörü yeniden başlatılmış olup İHA yeniden etkinleştirilmiştir. İHA 2,0 m yüksekliğe çıkması için programlanmış ve bu koşulu sağlamasının ardından kararlı bir uçuş için 2 saniyelik bekleme süresi uygulanmıştır. Veri toplama işlemi bu aşamadan sonra başlatılmıştır. Dolayısıyla kalkış aşaması, görev süresi ve yörünge ölçümlerine dahil edilmemiştir. Senaryolarda (0, 0, 2) koordinatı ortak navigasyon başlangıç noktası olarak belirlenmiş, hedef ise (17, 0, 2) koordinatı olarak tanımlanmıştır.

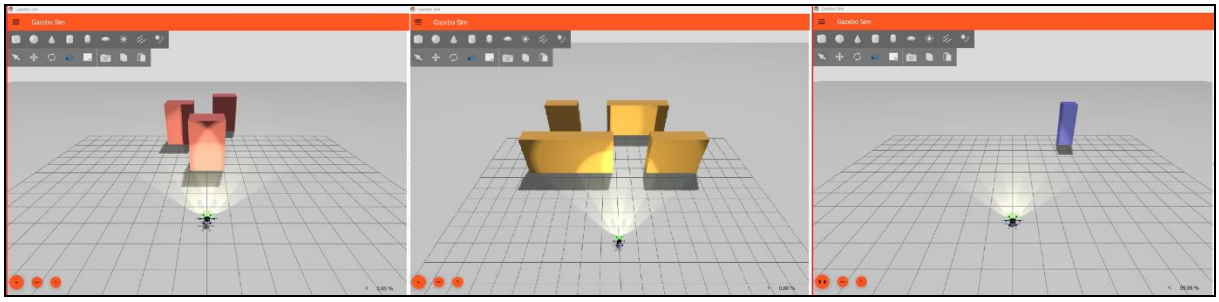
Sensör Yapısı

Simülasyon ortamında X4 modeline LiDAR sensör yerleştirilmiştir. Sensör yaklaşık 160° yatay görüş alanında 640 yatay örnek ve yaklaşık 30° dikey görüş alanında 16 dikey kanal kullanmıştır. Ölçüm aralığı 0,08-10 m ve nominal güncelleme hızı 10 Hz'dir. Böylece tam bir nokta bulutu 10.240 nokta içermektedir.

APF algoritması iki boyutlu LaserScan mesajını kullanırken 3D-DWA algoritması doğrudan PointCloud2 mesajını kullanmaktadır. RRT algoritması statik ve dar geçit senaryolarında önceden tanımlanmış küresel engel gösterimini kullanmıştır. Hareketli engel senaryosunda ise LaserScan ölçümleri RRT'nin yeniden planlanmasını tetiklemiştir. Böylece algoritmalar yapay olarak aynı çevresel gösterimi kullanmaya zorlanmak yerine kendi karakteristik bilgi gereksinimlerini korumuştur.

Deney Senaryoları

Deneysel değerlendirme için Şekil 1'deki farklı çevre koşullarına sahip üç Gazebo simülasyon ortamı oluşturulmuştur. İlk ortam, başlangıç-hedef doğrultusu boyunca farklı konumlara yerleştirilmiş üç sabit engelden oluşmaktadır [Şekil 1(a)]. İkinci ortam, S şeklinde navigasyon problemini temsil eden iki kaydırılmış dar geçitten oluşmaktadır [Şekil 1(b)]. Üçüncü ortamda ise İHA'nın nominal rotasını yanal olarak kesen hareketli bir engel bulunmaktadır [Şekil 1(c)]. Her üç senaryoda kullanılan engellerin yükseklikleri 3 m olarak belirlenmiştir. Böylelikle nominal uçuş irtifasında engellerin üzerinden doğrudan geçiş önlenmiştir.



Şekil 1. Gazebo simülasyon ortamları: (a) statik engel senaryosu, (b) dar geçit senaryosu ve (c) hareketli engel senaryosu.

Senaryo 1'de engel merkezleri Gazebo sahnesinin (5, 0), (9, 2) ve (12, -1,5) konumlarına yerleştirilmiştir. Senaryo 2'de kaydırılmış iki geçit yapısı kullanılmıştır. İlk geçit x=6 konumunda ve geçit açıklığının merkezi yaklaşık y=-1 olacak şekilde, ikinci geçit ise x=11 konumunda ve geçit açıklığının merkezi yaklaşık y=2 olacak şekilde yerleştirilmiştir. Her iki geçit açıklığı yaklaşık 2,5 m genişliğindedir. Duvar yapıları sonlu olduğundan hedefe başarılı biçimde ulaşmak için açıklıklardan geçmek zorunlu tutulmamıştır.

Senaryo 3'te x=8,5 konumunda kinematik olarak tanımlanmış 1 × 1 × 3 m boyutlarında hareketli bir engel kullanılmıştır. Engel, 0,50 m/s hedef hızla y=-4 ile y=+4 arasında yanal olarak salınmıştır. Her test süreci, engelin y=-4 konumundan pozitif y yönünde hareket etmesiyle başlatılmıştır.

APF Tabanlı Engelden Kaçınma

APF algoritması, hedefe yönelik çekici bileşeni LiDAR sensör verilerinden elde edilen itici bileşenlerle birleştirilmiştir. Çekici ve itici kazançlar sırasıyla 0,45 ve 1,20; engel etki mesafesi ise 4,0 m olarak belirlenmiştir. Maksimum yatay ve dikey hızlar sırasıyla 1,0 m/s ve 0,40 m/s ile sınırlandırılmıştır. Hedef toleransı 0,50 m olarak kullanılmıştır. Yerel minimum problemini gidermek amacıyla konumsal ilerlemenin yetersiz olduğu tespit edildiğinde deterministik bir kaçış mekanizması etkinleştirilmiştir. Bu nedenle yöntem, tamamen klasik APF yerine değiştirilmiş APF olarak tanımlanmıştır.

RRT Tabanlı Yol Planlama

RRT algoritması, İHA'nın hedef uçuş yüksekliğinde hareket edeceği şekilde iki boyutlu küresel yol planlayıcı olarak uygulanmıştır. Algoritmanın çalışma alanı x ekseninde -1 ile 18 m, y ekseninde ise -6 ile 6 m arasında sınırlandırılmıştır. Yol planlama sırasında adım büyüklüğü 0,75 m, hedef örnekleme olasılığı 0,15 ve maksimum iterasyon sayısı 5000 olarak belirlenmiştir. İHA'nın engellere fazla yaklaşmasını önlemek amacıyla engellerin çevresinde 0,50 m güvenlik mesafesi bırakılmıştır. RRT algoritmasının rastgele örnekleme yapısından dolayı her test sürecinde farklı, ancak gerektiğinde aynı testin tekrar gerçekleştirilebilmesine olanak sağlayan önceden belirlenmiş bir rastgele sayı başlangıç değeri kullanılmıştır.

Statik engel ve dar geçit senaryolarında RRT tarafından izlenecek yol, İHA navigasyona başlamadan önce oluşturulmuş ve İHA bu yol üzerindeki noktaları takip ederek hedefe ilerlemiştir. Yanal hareket eden engelin bulunduğu senaryoda ise statik ortamlar için kullanılan bu yapı yeterli olmadığından RRT algoritmasına yeniden yol planlama özelliği eklenmiştir. İHA'nın LaserScan verileri kullanılarak hareketli engelin algılanması durumunda mevcut konumundan hedefe doğru yeni bir yol oluşturulmuştur. Böylece RRT algoritmasının hareketli engel senaryosunda algılanan engele göre yolunu yeniden planlayabilmesi sağlanmıştır.

3D-DWA Tabanlı Engelden Kaçınma

3D-DWA algoritmasında çevredeki engellerin algılanması amacıyla LiDAR sensöründen elde edilen PointCloud2 verileri kullanılmıştır. Algoritma bu verileri kullanarak İHA'nın 3D ortamda uygulayabileceği farklı hız komutlarını değerlendirmekte ve uygun hareket yönünü belirlemektedir. İHA'nın maksimum yatay ivmesi 1,0 m/s², maksimum dikey ivmesi ise 0,60 m/s² olarak belirlenmiştir. İHA'nın hareketinin belirlenmesinde 1,5 saniyelik ileriye dönük hareket tahmini yapılmış, 4,0 m mesafe içerisindeki engeller dikkate alınmış ve engellere karşı 0,60 m güvenlik mesafesi kullanılmıştır. Oluşturulan hareket seçenekleri; hedefe ilerleme, engellere olan mesafe, hız, uçuş yüksekliğinin korunması, hareketin yumuşaklığı ve hareket yönünün uygunluğu dikkate alınarak değerlendirilmiştir. Kullanılan yöntem, iki

boyutlu düzlem için geliştirilen geleneksel DWA algoritmasının 3D ortamda hareket eden İHA'lar için uyarlanmış biçimi olarak uygulanmıştır.

Deneysel Prosedür ve Ölçütler

Her algoritma üç farklı senaryoda 10'ar kez test edilmiş ve böylece 3 algoritma × 3 senaryo × 10 tekrar olmak üzere toplam 90 test süreci gerçekleştirilmiştir. Algoritmaların geliştirilmesi ve sistemin kontrol edilmesi sırasında yapılan ön testler değerlendirmeye dahil edilmemiştir. Her test sürecinde navigasyon için maksimum 120 saniyelik süre belirlenmiş ve bu süre içerisinde hedefe ulaşamayan testler başarısız olarak değerlendirilmiştir.

Algoritmaların karşılaştırılmasında hedefe ulaşma başarısı, uçuş başarısızlığı, görevin tamamlanma süresi, yörünge uzunluğu, algılanan minimum engel mesafesi ve hesaplama süresi dikkate alınmıştır. Görev süresi, İHA'nın aktif navigasyona başladığı andan testin tamamlandığı ana kadar Gazebo odometri verilerindeki simülasyon zaman bilgileri kullanılarak hesaplanmıştır. Yörünge uzunluğu ise navigasyon sırasında ardışık olarak elde edilen İHA konumları arasındaki 3D mesafelerin toplanmasıyla belirlenmiştir. Algılanan minimum engel mesafesi, LiDAR verilerinden elde edilen en küçük geçerli mesafe olarak belirlenmiştir. Bu değer İHA'nın engellere ne kadar yaklaştığının değerlendirilmesinde kullanılmış ancak İHA gövdesi ile engel arasındaki kesin fiziksel mesafe olarak kabul edilmemiştir.

APF ve 3D-DWA algoritmalarında hesaplama süreleri navigasyon sırasında gerçekleştirilen her hesaplama döngüsü için ölçülmüştür. RRT algoritmasında ise hesaplama süresi yolun planlanması ve hareketli engel senaryosunda gerekli olduğunda yolun yeniden planlanması için geçen süreyi ifade etmektedir. Bu nedenle RRT için elde edilen hesaplama süreleri ile APF ve 3D-DWA için elde edilen değerler aynı işlemleri ifade etmediğinden ayrı olarak değerlendirilmiştir.

Hareketli engel senaryosunun hazırlanması sırasında Gazebo tarafından üretilen temas bilgilerinin hareketli engelle gerçekleşen çarpışmaları belirlemek için tek başına yeterince güvenilir olmadığı görülmüştür. Bu nedenle hareketli engel senaryosunda gerçekleştirilen testlerde, aktif navigasyon sırasında İHA'nın uçuş yüksekliğinin 1,0 m'nin altına düşmesi çarpışma ile ilişkili uçuş başarısızlığı olarak kabul edilmiştir. İHA'nın başlangıçta 2 m hedef uçuş yüksekliğine çıkması sırasında gerçekleşen kalkış aşaması bu değerlendirmenin dışında tutulmuştur.

BULGULAR VE TARTIŞMA

Genel Bulgular

Tablo 1 temel deney sonuçlarını özetlemektedir. Tamamlanan test süreçleri için değerler ortalama ± örneklem standart sapması olarak verilmiştir. Hareketli engel senaryosunda RRT'ye ait sürekli ölçütler yalnızca başarıyla tamamlanan beş test süreci kullanılarak hesaplanırken, başarı oranı on test sürecinin tamamı üzerinden hesaplanmıştır.

Tablo 1. Genel deneysel sonuçlar.

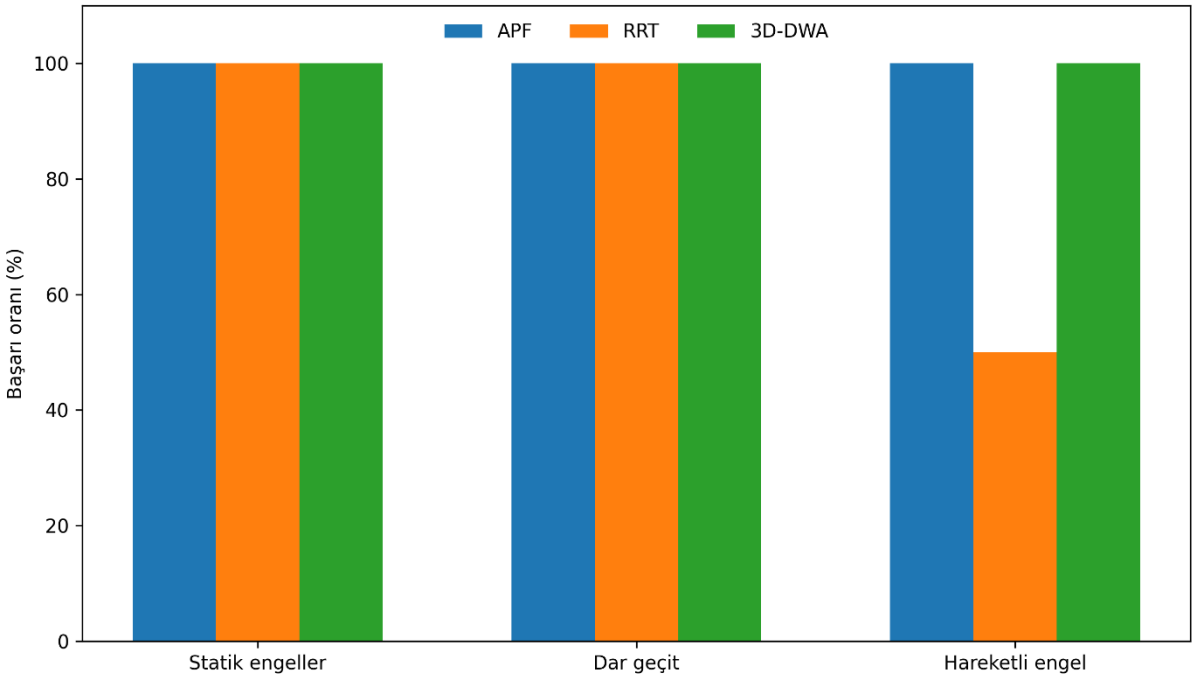
Senaryo	Algoritma	Başarı	Görev	Yörünge	Min. mesafe	Hesaplama

			süresi (s)	(m)	(m)	(ms)
Statik	APF	10/10	51,21 ± 0,12	22,02 ± 0,03	0,969 ± 0,021	5,85 ± 1,20*
Statik	RRT	10/10	44,65 ± 3,44	20,19 ± 1,57	0,682 ± 0,060	4,94 ± 1,81†
Statik	3D-DWA	10/10	35,20 ± 5,14	22,21 ± 0,77	1,051 ± 0,045	35,87 ± 6,74*
Dar geçit	APF	10/10	61,05 ± 0,19	26,87 ± 0,06	0,767 ± 0,017	4,39 ± 0,50*
Dar geçit	RRT	10/10	45,74 ± 1,96	20,61 ± 0,87	0,735 ± 0,099	13,17 ± 9,59†
Dar geçit	3D-DWA	10/10	48,49 ± 7,16	24,31 ± 1,58	0,933 ± 0,083	47,61 ± 9,18*
Hareketli	APF	10/10	57,08 ± 1,13	23,39 ± 0,37	0,669 ± 0,008	5,38 ± 2,85*
Hareketli	RRT	5/10	50,54 ± 12,93‡	27,79 ± 16,89‡	1,411 ± 0,938‡	6,45 ± 6,10†‡
Hareketli	3D-DWA	10/10	23,03 ± 1,78	17,71 ± 0,82	1,772 ± 1,026	8,69 ± 5,12*

* Ortalama kontrol çevrimi hesaplama süresi.

† RRT planlama/yeniden planlama süresi.

‡ Yalnızca başarılı RRT test süreçleri (n=5).



Şekil 2. Üç senaryodaki hedefe ulaşma başarı oranları.

Statik Engel Senaryosu

Statik engel senaryosunda APF, RRT ve 3D-DWA algoritmalarının her biri 10 kez test edilmiş ve üç algoritma da testlerin tamamında herhangi bir uçuş başarısızlığı yaşamadan hedefe ulaşmıştır. APF algoritması testleri 51,21 ± 0,12 s ortalama görev süresi ve 22,02 ± 0,03 m ortalama yörünge uzunluğu ile tamamlamıştır. RRT algoritmasında ortalama görev süresi 44,65 ± 3,44 s ve ortalama yörünge uzunluğu 20,19 ± 1,57 m olarak ölçülmüştür. 3D-DWA algoritmasında ise bu değerler sırasıyla 35,20 ± 5,14 s ve 22,21 ± 0,77 m olarak elde edilmiştir. Algılanan minimum engel mesafeleri APF için ortalama 0,969 m, RRT için 0,682 m ve 3D-DWA için 1,051 m olarak ölçülmüştür. Elde edilen sonuçlar üç algoritmanın da hedefe ulaşma açısından aynı başarıyı göstermesine rağmen görev süresi, yörünge uzunluğu ve engellere yaklaşma mesafeleri açısından farklı sonuçlar ortaya koyduğunu göstermektedir.

Dar Geçit Senaryosu

Dar geçit senaryosunda da APF, RRT ve 3D-DWA algoritmalarının üçü de gerçekleştirilen 10 testin tamamında hedefe başarıyla ulaşmıştır. APF algoritması testleri 61,05 ± 0,19 s ortalama görev süresi ve 26,87 ± 0,06 m ortalama yörünge uzunluğu ile tamamlamıştır. Ancak APF algoritmasının bazı testlerde oluşturulan iki dar geçitten geçmek yerine duvarların dış tarafından dolaşarak hedefe ulaştığı görülmüştür. Bu çalışmada başarı ölçütü olarak İHA'nın belirlenen geçitlerden geçmesi değil, herhangi bir uçuş başarısızlığı yaşamadan hedefe ulaşması kabul edildiğinden bu testler başarılı olarak değerlendirilmiştir.

RRT algoritmasında ortalama görev süresi 45,74 ± 1,96 s ve ortalama yörünge uzunluğu 20,61 ± 0,87 m olarak ölçülmüştür. 3D-DWA algoritmasında ise ortalama görev süresi 48,49 ± 7,16 s, ortalama yörünge uzunluğu 24,31 ± 1,58 m olarak elde edilmiştir. 3D-DWA'nın testler arasında APF ve RRT'ye göre daha fazla değişkenlik gösterdiği görülmüştür. Bu sonuçlar, algoritmaların yalnızca hedefe ulaşıp ulaşmadığına göre değerlendirilmesinin navigasyon sırasında ortaya çıkan farklı davranışları açıklamak için yeterli olmadığını göstermektedir.

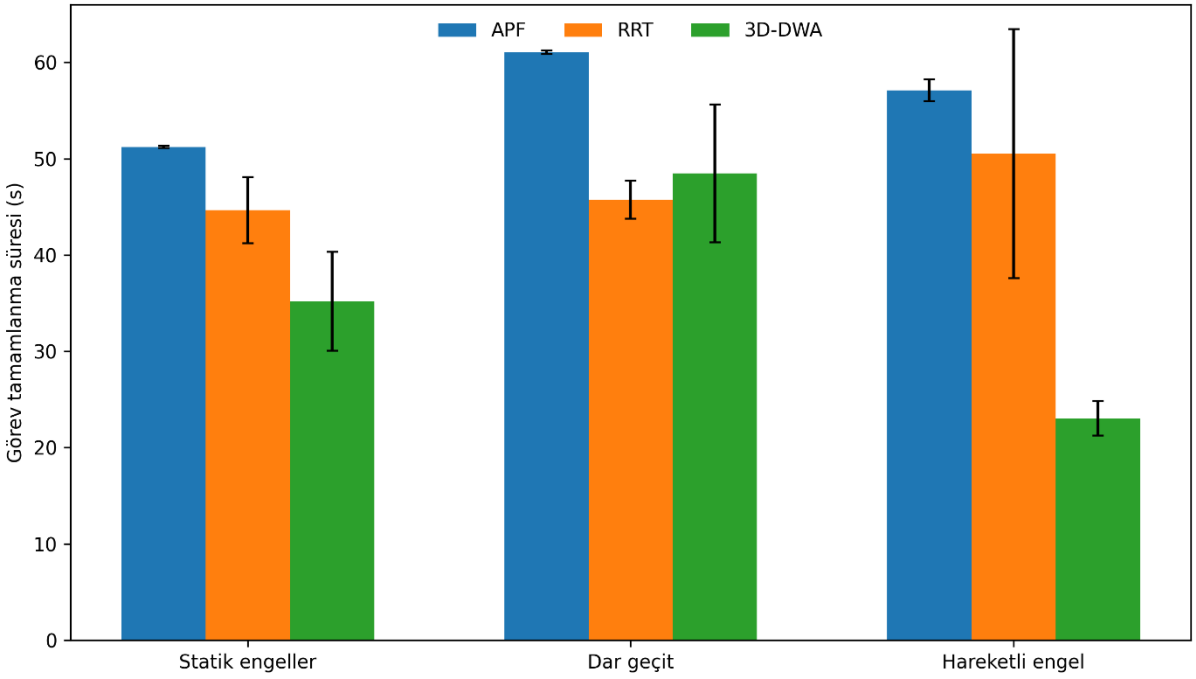
Hareketli Engel Senaryosu

Hareketli engel senaryosunda algoritmalar arasında statik engel ve dar geçit senaryolarına göre daha belirgin farklılıklar ortaya çıkmıştır. APF algoritması gerçekleştirilen 10 testin tamamında hedefe ulaşmış ve ortalama görev süresi 57,08 ± 1,13 s, ortalama yörünge uzunluğu ise 23,39 ± 0,37 m olarak ölçülmüştür. 3D-DWA algoritması da 10 testin tamamını başarıyla tamamlamış ve ortalama görev süresi 23,03 ± 1,78 s, ortalama yörünge uzunluğu ise 17,71 ± 0,82 m olarak elde edilmiştir.

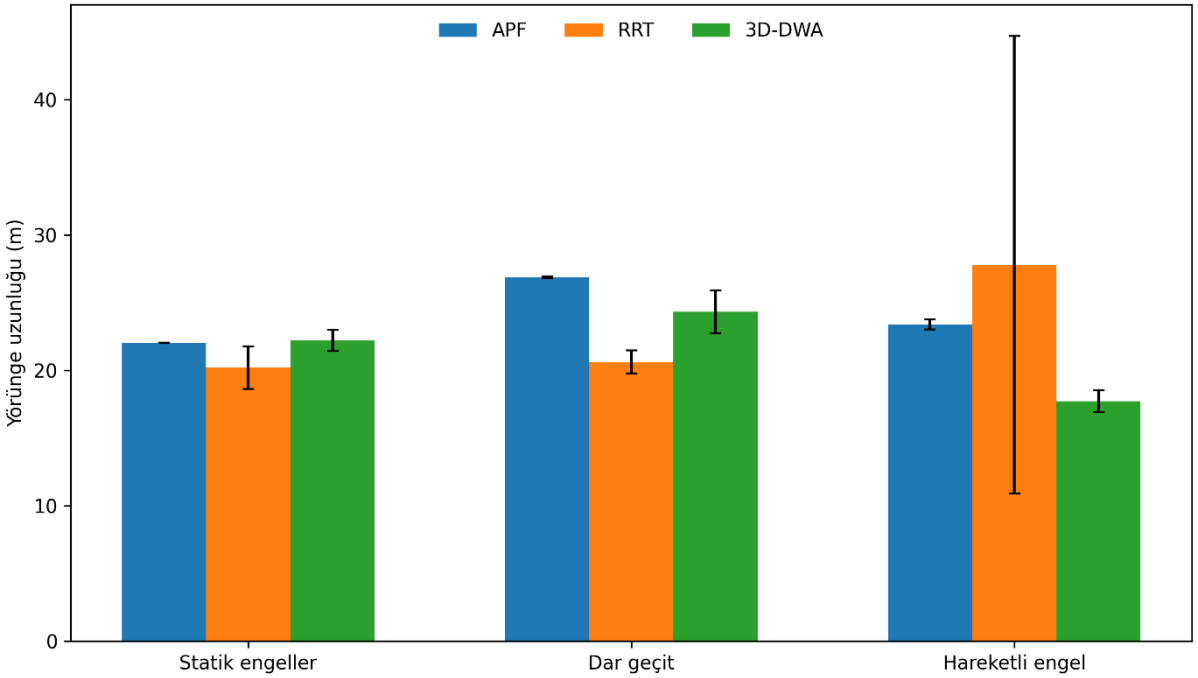
Hareketli engelin algılanması durumunda yeniden yol planlama özelliği eklenen RRT algoritması ise gerçekleştirilen 10 testin 5'inde ciddi bir irtifa kaybı yaşamadan hedefe ulaşabilmiştir. Diğer 5 testte İHA'nın aktif navigasyon sırasında uçuş yüksekliği 1,0 m'nin altına düştüğünden bu testler uçuş başarısızlığı olarak değerlendirilmiştir. Başarısız olan testler deney sonuçlarına dahil edilmiş ve tekrar edilmemiştir.

Başarısız olan beş RRT testinde görev tamamlanamadığından bu testlere ait görev süresi ve yörünge uzunluğu gibi sonuçlar tamamlanmış bir test olarak kayıt altına alınamamıştır. Bu nedenle Tablo 1'de RRT algoritmasına ait görev süresi, yörünge uzunluğu ve diğer sürekli ölçümlerin ortalama değerleri yalnızca başarıyla tamamlanan 5 test kullanılarak hesaplanmıştır. Bu değerlerin RRT algoritmasının gerçekleştirilen 10 testinin tamamına ait ortalama değerler olmadığı dikkate alınmalıdır. Ayrıca başarıyla tamamlanan RRT testlerinden birinde yaklaşık 58 m uzunluğunda bir yörünge oluşması, RRT sonuçlarındaki değişkenliğin artmasına neden olmuştur.

Bu çalışmada kullanılan hareketli engel senaryosunda APF ve 3D-DWA algoritmaları gerçekleştirilen 10 testin tamamında hedefe ulaşırken, yeniden yol planlama özelliği kullanılan RRT algoritması 10 testin 5'inde hedefe ulaşabilmiştir. Ancak elde edilen bu sonuçlar çalışmada kullanılan algoritma parametreleri, sensör yapıları ve hareketli engel senaryosuna bağlıdır. Bu nedenle elde edilen sonuçların genel olarak tüm RRT tabanlı İHA navigasyon sistemlerinin performansını temsil ettiği şeklinde değerlendirilmemesi gerekmektedir.



Şekil 3. Üç farklı senaryoda algoritmaların görev tamamlanma süreleri. Sütunlar ortalama değerleri, hata çubukları ± standart sapmayı (SS) göstermektedir. Hareketli engel senaryosunda RRT değerleri yalnızca başarılı testlere aittir (n=5).



Şekil 4. Üç farklı senaryoda algoritmaların yörünge uzunlukları. Sütunlar ortalama değerleri, hata çubukları ± standart sapmayı (SS) göstermektedir. Hareketli engel senaryosunda RRT değerleri yalnızca başarılı testlere aittir (n=5).

Hesaplama Özellikleri

Algoritmaların hesaplama süreleri değerlendirilirken çalışma yapılarının birbirinden farklı olduğu dikkate alınmıştır. APF ve 3D-DWA algoritmalarında hesaplama süresi, aktif navigasyon sırasında gerçekleştirilen her hesaplama işlemi için ölçülmüştür. RRT algoritmasında ise bu süre yolun planlanması veya gerekli durumlarda yeniden planlanması için geçen süreyi ifade etmektedir. Statik engel senaryosunda APF ve 3D-DWA algoritmalarının ortalama hesaplama süreleri sırasıyla 5,85 ± 1,20 ms ve 35,87 ± 6,74 ms olarak ölçülmüştür. Dar geçit senaryosunda ise bu değerler APF için 4,39 ± 0,50 ms, 3D-DWA için 47,61 ± 9,18 ms olarak elde edilmiştir. RRT algoritmasının ortalama planlama süresi statik engel senaryosunda 4,94 ± 1,81 ms, dar geçit senaryosunda ise 13,17 ± 9,59 ms olarak ölçülmüştür. APF ve 3D-DWA için elde edilen süreler navigasyon sırasında tekrarlanan hesaplama işlemlerini, RRT için elde edilen süreler ise yol planlama işlemini ifade ettiğinden bu değerler doğrudan birbirleriyle karşılaştırılmamıştır.

Genel Tartışma

Elde edilen sonuçlar algoritmaların performanslarının kullanılan senaryoya göre değiştiğini göstermiştir. Statik engel senaryosunda üç algoritma da gerçekleştirilen testlerin tamamında hedefe ulaşmış ancak görev süresi, yörünge uzunluğu ve algılanan minimum engel mesafesi açısından farklı sonuçlar elde edilmiştir. Dar geçit senaryosunda da üç algoritma hedefe ulaşma açısından aynı başarıyı göstermiştir. Bununla birlikte APF algoritmasının bazı testlerde belirlenen dar geçitlerden geçmek yerine duvarların dışından dolaşarak hedefe ulaştığı görülmüştür. Hareketli engel senaryosunda ise algoritmalar arasındaki fark daha

belirgin hale gelmiş; APF ve 3D-DWA gerçekleştirilen testlerin tamamında hedefe ulaşırken, hareketli engel algılandığında yeniden yol planlama özelliği kullanılan RRT algoritması testlerin yarısında hedefe ulaşabilmiştir.

Algoritmaların karşılaştırılmasında kullandıkları çevresel bilgilerin birbirinden farklı olduğu da dikkate alınmalıdır. APF algoritmasında LaserScan verileri, 3D-DWA algoritmasında PointCloud2 verileri kullanılmıştır. RRT algoritmasında ise statik engel ve dar geçit senaryolarında önceden bilinen çevre bilgileri kullanılarak yol oluşturulmuş, hareketli engel senaryosunda LaserScan verileri kullanılarak gerektiğinde yolun yeniden planlanması sağlanmıştır. Bu nedenle gerçekleştirilen karşılaştırma, üç algoritmaya tamamen aynı verilerin verilerek matematiksel olarak karşılaştırılmasından ziyade, algoritmaların kendi çalışma yapılarını korudukları ortak bir İHA navigasyon sistemi içerisindeki performanslarının karşılaştırılması olarak değerlendirilmiştir. Bu durum elde edilen sonuçların herhangi bir algoritmanın genel olarak diğerlerinden üstün olduğu şeklinde yorumlanmasını sınırlandırmaktadır.

SONUÇ

Bu çalışmada otonom bir İHA'nın engellerden kaçınması ve hedefe ulaşması amacıyla kullanılan APF, RRT ve 3D-DWA algoritmalarının karşılaştırılabilmesi için ROS 2-Gazebo tabanlı bir simülasyon ortamı oluşturulmuştur. Aynı 6 rotorlu X4 multikopter kullanılarak statik engel, dar geçit ve hareketli engel olmak üzere üç farklı senaryoda toplam 90 test süreci gerçekleştirilmiştir.

Statik engel ve dar geçit senaryolarında üç algoritma da gerçekleştirilen 10 testin tamamında hedefe başarıyla ulaşmıştır. Hareketli engel senaryosunda APF ve 3D-DWA algoritmaları 10 testin tamamını ciddi bir irtifa kaybı yaşamadan başarıyla tamamlarken, hareketli engelin algılanması durumunda yeniden yol planlama özelliği kullanılan RRT algoritması 10 testin 5'inde hedefe ulaşabilmiştir. Yapılan testlerde algoritmalar arasında görev süresi, yörünge uzunluğu, algılanan minimum engel mesafesi ve hesaplama süreleri açısından da farklılıklar olduğu görülmüştür. Elde edilen sonuçlar, engelden kaçınma ve yol planlama algoritmalarının değerlendirilmesinde yalnızca hedefe ulaşma başarısının yeterli olmadığını, farklı çevresel koşulların ve performans ölçütlerinin birlikte değerlendirilmesi gerektiğini göstermektedir.

Gelecek çalışmalarda oluşturulan simülasyon ortamının daha karmaşık 3D ortamları ve birbirinden bağımsız hareket eden birden fazla engeli içerecek şekilde geliştirilmesi planlanmaktadır. Ayrıca küresel yol planlama ile yerel 3D engelden kaçınma yöntemlerinin birlikte kullanıldığı hibrit yapıların araştırılması ve simülasyon ortamında elde edilen sonuçların gerçek bir İHA platformunda test edilmesi hedeflenmektedir.

KAYNAKLAR

Bes, J., Dendarieta, J., Riazuelo, L., & Montano, L. 2025. DWA-3D: A reactive planner for robust and efficient autonomous UAV navigation in confined environments. Robotics and Autonomous Systems, 195, 21p. https://doi.org/10.1016/j.robot.2025.105196

Chen, J., Zheng, R., & Liu, J. 2026. Towards UAV Path-Planning Algorithms and Obstacle Avoidance Methods: A Comprehensive Review. Robotics and Autonomous Systems, 21p. https://doi.org/10.1016/j.robot.2026.105636

Çakır, A., & Akpancar, S. 2018. Modeling DJI M100 Robot in Gazebo and Controlling with ROS V. International Multidisciplinary Congress of Eurasia (IMCOFE'18), Barcelona, Spain.

Çakır, A., & Akpancar, S. 2020. 3D simultaneous positioning and mapping in dark, closed spaces with an autonomous flying robot. Acta Polytechnica Hungarica, 17(7), 7–23. https://doi.org/10.12700/aph.17.7.2020.7.1

Fox, D., Burgard, W., & Thrun, S. 1997. The dynamic window approach to collision avoidance. IEEE Robotics & Automation Magazine, 4(1), 23–33. https://doi.org/10.1109/100.580977

Hu, L., Ma, J., & Zang, S. 2026. A 3D dynamic window approach with receding horizon optimization for real-time UAV path planning. Complex & Intelligent Systems, 12(170), 16p. https://doi.org/10.1007/s40747-026-02299-z

Huang, T., Fan, K., Sun, W., Li, W., & Guo, H. 2023. Potential-field-RRT: A path-planning algorithm for UAVs based on potential-field-oriented greedy strategy to extend random tree. Drones, article 331, 7(5), 18p. https://doi.org/10.3390/drones7050331

Huang, Y., Li, H., Dai, Y., Lu, G., & Duan, M. 2024. A 3D path planning algorithm for UAVs based on an improved artificial potential field and bidirectional RRT. Drones, article 760, 8(12), 26p. https://doi.org/10.3390/drones8120760

Khatib, O. 1986. Real-Time Obstacle Avoidance for Manipulators and Mobile Robots. The International Journal of Robotics Research, 5(1), 90–98. https://doi.org/10.1177/027836498600500106

LaValle, S. 1998. Rapidly-exploring random trees: A new tool for path planning. Research Report 9811, Department of Computer Science, Iowa State University.

Mashkov, I., Kochetkova, A., Serpiva, V., Yashin, G., & Golikov, P. 2026. Comparative Evaluation of Classical, Hybrid, and RL-Based 3D Trajectory Planning for Multi-UAV Systems. Drones, article 452, 10(6), 49p. https://doi.org/10.3390/drones10060452

Wang, J., Zhao, Z., Qu, J., & Chen, X. 2024. APPA-3D: an autonomous 3D path planning algorithm for UAVs in unknown complex environments. Scientific Reports, 14(1), 18p. https://doi.org/10.1038/s41598-024-51286-2

Zhang, W., Sun, Y., Gao, Y., Guo, C., & Miao, R. 2025. UAV 3D path planning based on integrated particle swarm optimization and artificial potential field method. International Journal of Computational Intelligence Systems, article 287, 18(1), 36p. https://doi.org/10.1007/s44196-025-01009-w

SAĞLIK VERİLERİNDE YENİDEN ÖRNEKLEME YÖNTEMLERİNİN MAKİNE ÖĞRENMESİ PERFORMANSINA ETKİSİ: DERMATOLOJİK BİR UYGULAMA

EFFECTS OF RESAMPLING METHODS ON MACHINE LEARNING PERFORMANCE IN HEALTH DATA: A DERMATOLOGICAL APPLICATION

Burcu DURMUŞ
Lecturer, Tekirdağ Namık Kemal Üniversitesi, Rectorate
ORCID NO: 0000-0002-0298-0802

ÖZET

Bu çalışmada, dengesiz çok sınıflı dermatolojik verilerde yeniden örneklemenin makine öğrenmesi performansına etkisi incelenmiştir. Özgün çalışmadaki 1.119 katılımcıdan hazırlanmış analiz dosyasında kalan 1.091 kayıt kullanılmıştır. Hedef değişkenin dört sınıfında sırasıyla 782, 249, 53 ve 7 gözlem bulunmaktadır. Hedef bilgisini taşıyan değişkenler çıkarılarak 25 açıklayıcı değişkenle karar ağacı, rastgele orman, k-en yakın komşu ve radyal çekirdekli destek vektör makinesi değerlendirilmiştir. Dengeleme uygulanmaması, rastgele aşırı örnekleme ve SMOTENC olmak üzere üç senaryo karşılaştırılmıştır. Analizler, üç kez tekrarlanan tabakalı 5 katlı dış çapraz doğrulama ve 3 katlı iç parametre aramasıyla yürütülmüştür. Ölçeklendirme, kodlama ve yeniden örnekleme yalnızca ilgili eğitim katlarında gerçekleştirilmiştir. En yüksek gözlenen makro-F1, rastgele orman-RAÖ kombinasyonunda 0,282; bu kombinasyonun dengeli doğruluğu 0,281, doğruluğu 0,634 ve MCC değeri 0,103 bulunmuştur. Yeniden örneklemenin etkisi modele ve değerlendirme ölçütüne göre değişmiş; en küçük sınıfta hiçbir gözlem doğru tahmin edilememiştir. Sonuçlar, sınıfların sayısal olarak dengelenmesinin güvenilir azınlık sınıf tahminini tek başına sağlamadığını ve doğruluğun sınıf bazlı ölçütlerle birlikte değerlendirilmesi gerektiğini göstermektedir.

Anahtar kelimeler: Dermatoloji, Makine öğrenmesi, Sınıf dengesizliği, Veri madenciliği, Yeniden örnekleme.

ABSTRACT

This study evaluated the effects of resampling on machine learning performance in imbalanced multiclass dermatological data. The prepared dataset contained 1,091 records from an original study of 1,119 participants, with class sizes of 782, 249, 53 and 7. After excluding target-related variables, 25 predictors were used to compare decision trees, random forests, k-nearest neighbours and radial-kernel support vector machines under no resampling, random oversampling and SMOTENC. Stratified five-fold outer cross-validation was repeated three times, with three-fold inner hyperparameter selection. Scaling, encoding and resampling were fitted exclusively within training folds. The highest observed macro-F1 was 0.282 for the random forest with random oversampling, with balanced accuracy of 0.281, accuracy of 0.634 and MCC of 0.103. Resampling effects depended on the classifier and

evaluation metric; no observations in the smallest class were correctly classified. Numerical class balance alone did not ensure reliable minority-class prediction. Accuracy should therefore be interpreted together with class-sensitive metrics.
Keywords: Dermatology, Machine learning, Class imbalance, Data mining, Resampling.

GİRİŞ

Sağlık verilerinde sonuç kategorilerinin örneklem büyüklükleri önemli ölçüde değişebilir. Bu durumda çoğunluk sınıfını tahmin etmeye yönelen bir sınıflandırıcı yüksek genel doğruluk üretirken daha az temsil edilen sınıfları gözden kaçırabilir. Yeniden örnekleme, bu sorunu eğitim verisinin sınıf dağılımını değiştirerek ele alan veri düzeyindeki yaklaşımlardan biridir. Sağlık verilerinde kullanılan yöntemlerin, veri yapısı ve değerlendirme tasarımıyla birlikte incelenmesi gerektiği vurgulanmaktadır (Salmi vd., 2024).

Rastgele aşırı örnekleme mevcut azınlık gözlemlerini çoğaltırken Synthetic Minority Over-sampling Technique (SMOTE) ailesi azınlık gözlemlerinin komşuluklarından sentetik örnekler üretir (Chawla vd., 2002). Bu işlemler eğitim setinin büyüklüğünü artırsa da bağımsız katılımcı sayısını artırmaz. Dolayısıyla yöntemin başarısı, yeniden örneklenmemiş gözlemler üzerinde ve tüm sınıfları dikkate alan ölçütlerle değerlendirilmelidir.

Bu çalışmanın amacı, dengesiz dört sınıflı bir dermatoloji veri setinde rastgele aşırı örnekleme ve Synthetic Minority Over-sampling Technique for Nominal and Continuous (SMOTENC) yöntemlerinin dört makine öğrenmesi sınıflandırıcısının performansına etkisini karşılaştırmaktır. Araştırma sorusu, yeniden örneklemenin makro-F1, dengeli doğruluk ve sınıf bazlı duyarlılığı hangi ölçüde değiştirdiğidir. Çalışma, mevcut beyaz saç sayısı kategorilerinin eşzamanlı sınıflandırılmasına odaklanan yöntemsel bir uygulama olmakla birlikte, ileriye dönük klinik sonuç tahmini amacı taşımamaktadır.

YÖNTEM

Veri Kaynağı ve Analiz Örneklemi

Veriler, Belli ve arkadaşlarının kesitsel dermatoloji çalışmasına dayanmaktadır (Belli vd., 2016). Özgün araştırmaya Şubat-Temmuz 2015 döneminde dermatoloji polikliniğine başvuran bireyler ve uygun hastane çalışanlarından oluşan 14-20 yaş aralığındaki 1.119 katılımcı dahil edilmiştir. Özgün çalışmada araştırma öncesinde etik kurul onayı alındığı bildirilmiştir. Bu ikincil analizde sağlanan hazırlanmış dosya, 1.091 gözlem ve 29 sütun içermektedir.

Veri hazırlama sürecine ilişkin sağlanan kayıt karşılaştırmasına göre 28 kayıt dışlanmıştır: 18 kayıtta boş/eksik veri, 10 farklı kayıtta ise “********” biçiminde veri giriş eksikliği veya hatası bulunmaktadır. Eksik veri grubunda boy, kilo ve BMI bilgileri aynı 10 kayıtta; stres skoru 6, geçmiş sigara kullanım süresi 1 ve hastaneye yatış nedeni ayrıca 1 kayıtta eksiktir. Yatış nedeni toplam 2 kayıtta boş olup bunlardan biri ölçüm eksikliği grubunda yer almaktadır. Yıldızlı kayıtların 6’sı yatış nedeni, 4’ü kronik hastalık adı alanındadır ve iki dışlama grubu örtüşmemektedir.

Hazırlama kuralında, açıklayıcı değişken seçilmeden önce özgün kayıtların bütünlüğü esas alınmıştır. Modelde kullanılmayan yatış nedeni ve kronik hastalık adı metin alanlarını da kapsamıştır. Hazırlanan örneklem korunmuş, bu yeniden analizde ek kayıt dışlanmamış veya performansa dayalı eleme uygulanmamıştır. Verilen karşılaştırma bilgisine göre 1.091 kaydın tamamı 27 ortak alanda özgün dosyayla eşleşmektedir. Mevcut hazırlanmış dosyada eksik değer ve tamamen aynı yinelenen satır bulunmamıştır.

Hedef değişkenin dört kategorisine ait gözlem sayıları ve yüzdeleri Tablo 1'de sunulmuştur.

Tablo 1. Hedef değişkenin sınıf dağılımı (N=1.091)

Kod	Beyaz saç sayısı kategorisi	n	%
1	0	782	71,68
2	<10	249	22,82
3	10-100	53	4,86
4	>100	7	0,64

Çoğunluk/en küçük sınıf oranı 782/7 = 111,71'dir. Kategoriler, analiz dosyasındaki kod ve tanımlar korunarak kullanılmıştır. Yaş ortalaması 17,41 ± 1,77 yıl, BMI 21,30 ± 3,06, stres skoru 28,18 ± 6,72 bulunmuştur. Tablo 1'de ilk iki kategorinin örneklemin %94,50'sini, son iki kategorinin ise yalnızca %5,50'sini oluşturduğu görülmektedir. Özellikle >100 kategorisinin %0,64 ile temsil edilmesi, bu sınıfın performansının çok az sayıda gözleme dayanmasına yol açmaktadır. Bu dağılım, genel doğruluğun çoğunluk sınıfındaki başarıdan güçlü biçimde etkilenmesini açıklamaktadır.

Açıklayıcı Değişkenler ve Ön İşleme

Dört sınıflı hedef, aynı sonuçtan türetilmiş iki ikili hedef ve "ilk beyaz saç yaşı" model girdilerinden çıkarılmıştır. Böylece 6 sayısal ve 19 kategorik olmak üzere 25 açıklayıcı değişken kullanılmıştır. Sayısal değişkenler yaş, geçmiş sigara kullanım süresi, kilo, boy, BMI ve stres skorudur. Kategorik değişkenler cinsiyet, kepek, saç seyrelmesi, saçta bölgesel açılma, ciltte beyazlama, annede ve babada erken beyazlama, sigara kullanımı, alkol, egzersiz, beslenme, yatarak tedavi, kronik hastalık, öğrenim durumu, meslek, medeni durum, çocuk sahibi olma, aylık gelir ve cilt tipidir.

Sayısal özelliklere z-skor standardizasyonu uygulanmıştır. Kategorik ve dereceli değişkenler, kodlar arasında eşit aralık varsaymamak için yeniden örnekleme sonrasında one-hot kodlama ile temsil edilmiştir. Dönüşümlerin tamamı yalnızca eğitim verisinden öğrenilmiş ve doğrulama verisine uygulanmıştır. Hazırlanmış dosyada eksik değer bulunmadığından değer atama yapılmamıştır. Özellik seçimi veya normalizasyon yöntemleri arasında ayrı bir performans taraması yapılmamıştır.

Yeniden örnekleme ve sınıflandırıcılar

Üç senaryo kullanılmıştır: dengeleme yok, rastgele aşırı örnekleme (RAÖ) ve SMOTENC. RAÖ azınlık sınıflarını yerine koymalı rastgele çoğaltır. SMOTENC, sayısal ve kategorik değişkenleri birlikte işlemek için kullanılan SMOTE varyantıdır (Chawla vd., 2002; imbalanced-learn). Her iki yöntemde de eğitim katındaki azınlık sınıfları çoğunluk sınıfı büyüklüğüne çıkarılmıştır. En küçük sınıftaki örnek sayısı nedeniyle SMOTENC komşu

sayısı k=2 olarak sabitlenmiştir. Kategorik özellikler sentetik üretim sırasında açıkça tanımlanmıştır. Doğrulama katlarının özgün sınıf dağılımı korunmuştur.

Karar ağacı (KA), rastgele orman (RO), kNN ve RBF çekirdekli destek vektör makinesi (DVM) kullanılmıştır. Yeniden örneklemenin etkisini ayrı değerlendirmek için sınıf ağırlığı uygulanmamıştır. Her model-senaryo çifti aynı parametre alanında bağımsız olarak ayarlanmıştır. Rastgele ormanda 200 ağaç kullanılmış ve diğer ayarlar yazılımın varsayılan değerlerinde tutulmuştur.

Tablo 2'de her sınıflandırıcı için dört aday parametre kombinasyonu tanımlanmıştır. Sunulan değerler, tüm katlarda seçilmiş tek bir nihai parametre setini değil, iç çapraz doğrulamada taranan aralıkları göstermektedir. Aynı modelin üç dengeleme senaryosunda aynı arama alanıyla değerlendirilmesi, karşılaştırmaların farklı parametre arama kapsamlarından etkilenmesini azaltmaktadır.

Tablo 2. İç çapraz doğrulamada değerlendirilen parametre alanları

Model	Aranan parametreler	Kombinasyon
KA	Maksimum derinlik: 3, sınırsız; yaprak minimumu: 2, 10	4
RO	max_features: sqrt, 0,5; yaprak minimumu: 1, 5	4
kNN	Komşu sayısı: 5, 11; ağırlık: eşit, uzaklık	4
DVM (RBF)	C: 1, 10; gamma: scale, 0,01	4

Doğrulama ve performans ölçütleri

İç içe çapraz doğrulama kullanılmıştır: dış değerlendirme tabakalı 5 kat, parametre seçimi dış eğitim setinde tabakalı 3 kattır (Cawley ve Talbot, 2010). Dış değerlendirme 42, 2026 ve 31415 tohumlarıyla üç kez tekrarlanmıştır. Tüm kombinasyonlar aynı dış ve iç katları kullanmıştır. Her dış eğitim katında en küçük sınıfta 5-6 gözlem, dış doğrulama katında 1-2 gözlem bulunurken iç eğitim katlarında en az 3 gözlem bulunmaktadır. İç arama makro-F1'i en büyükleyen parametreleri seçmiş ve seçilen pipeline dış eğitim verisinde yeniden eğitilmiştir.

Her tekrarda dış kat tahminleri birleştirilerek her katılımcı için yalnızca bir kat dışı tahmin elde edilmiştir. Doğruluk, dengeli doğruluk, makro-kesinlik, makro-F1 ve çok sınıflı MCC bu 1.091 tahmin üzerinden hesaplanmıştır. Makro-F1, dört sınıfın ayrı F1 değerlerinin aritmetik ortalamasıdır. Makro-kesinlik ve makro-duyarlılığın harmonik ortalaması olarak hesaplanmamıştır. Dengeli doğruluk makro-duyarlılığa eşittir ve yinelenen bir sütun kullanılmamıştır. Tanımsız kesinlik/F1 değerleri 0 alınmıştır. Sonuçlar üç tekrarın ortalaması ± örneklem standart sapmasıdır. Standart sapmalar kat bölünmesi duyarlılığını gösterir, güven aralığı değildir. Tekrarlar aynı katılımcıları içerdiğinden bağımsız örneklemler gibi test edilmemiş ve p değeri üretilmemiştir. Analizler Python, scikit-learn 1.8.0 ve imbalanced-learn 0.14.2 ile yürütülmüştür (Pedregosa vd., 2011; Lemaître vd., 2017).

ARAŞTIRMA BULGULARI VE TARTIŞMA

Genel ve sınıf bazlı performans

Yalnızca çoğunluk sınıfını tahmin eden referansın doğruluğu 0,717, dengeli doğruluğu 0,250, makro-F1'i 0,209 ve MCC değeri 0,000 bulunmuştur. Bu referans, doğruluğun tek başına

yorumlanmasının sınırını göstermektedir. On iki model-senaryo kombinasyonunun sonuçları Tablo 3'te sunulmuştur.

Tablo 3. Tekrar bazında birleştirilen kat dışı tahminlerin performansı (ortalama ± SS)

Model	Senaryo	Doğruluk	Dengeli doğruluk	Makro-kesinlik	Makro-F1	MCC
KA	Dengeleme yok	0,617 ± 0,032	0,250 ± 0,011	0,275 ± 0,051	0,246 ± 0,011	-0,005 ± 0,032
KA	RAÖ	0,537 ± 0,014	0,264 ± 0,019	0,259 ± 0,012	0,258 ± 0,014	0,026 ± 0,022
KA	SMOTENC	0,530 ± 0,019	0,251 ± 0,001	0,257 ± 0,005	0,252 ± 0,004	0,029 ± 0,025
RO	Dengeleme yok	0,700 ± 0,004	0,257 ± 0,001	0,259 ± 0,002	0,235 ± 0,003	0,045 ± 0,003
RO	RAÖ	0,634 ± 0,002	0,281 ± 0,012	0,285 ± 0,016	0,282 ± 0,013	0,103 ± 0,014
RO	SMOTENC	0,555 ± 0,017	0,276 ± 0,020	0,271 ± 0,015	0,270 ± 0,016	0,053 ± 0,028
kNN	Dengeleme yok	0,669 ± 0,003	0,254 ± 0,002	0,247 ± 0,004	0,242 ± 0,003	0,027 ± 0,008
kNN	RAÖ	0,466 ± 0,012	0,261 ± 0,016	0,260 ± 0,010	0,246 ± 0,008	0,037 ± 0,020
kNN	SMOTENC	0,414 ± 0,013	0,269 ± 0,005	0,270 ± 0,002	0,244 ± 0,001	0,049 ± 0,005
DVM	Dengeleme yok	0,674 ± 0,005	0,264 ± 0,003	0,274 ± 0,010	0,256 ± 0,005	0,062 ± 0,018
DVM	RAÖ	0,550 ± 0,021	0,291 ± 0,006	0,278 ± 0,006	0,280 ± 0,007	0,062 ± 0,016
DVM	SMOTENC	0,497 ± 0,036	0,270 ± 0,012	0,268 ± 0,009	0,260 ± 0,013	0,050 ± 0,029

Not: KA: karar ağacı; RO: rastgele orman; DVM: destek vektör makinesi; RAÖ: rastgele aşırı örnekleme. SS, 3 tekrarın standart sapmasıdır. Tüm ölçütler 0-1 ölçeğinde verilmiştir.

Tablo 3'te en yüksek gözlenen makro-F1, rastgele orman-RAÖ ile 0,282 ± 0,013 bulunmuştur. Bu kombinasyon aynı zamanda en yüksek makro-kesinliği (0,285 ± 0,016) ve MCC değerini (0,103 ± 0,014) sağlamıştır. En yüksek doğruluk, dengeleme uygulanmayan rastgele ormanda 0,700; en yüksek dengeli doğruluk ise DVM-RAÖ kombinasyonunda 0,291 elde edilmiştir. DVM-RAÖ'nün makro-F1 değeri 0,280 ± 0,007 olup rastgele orman-RAÖ'ye oldukça yakındır. İki kombinasyon arasındaki yaklaşık fark 0,002' dir.

Dengeleme uygulanmayan modellerin doğrulukları 0,617-0,700 arasında değişirken yeniden örnekleme sonrasında bütün modellerde genel doğruluk azalmıştır. Bununla birlikte rastgele ormanda RAÖ, makro-F1'i 0,235'ten 0,282'ye ve MCC'yi 0,045'ten 0,103'e yükseltmiştir. Karar ağacı ve kNN'de makro-F1 artışları daha sınırlı kalmıştır. DVM'de RAÖ ile dengeli doğruluk ve makro-F1 yükselirken MCC'nin üç ondalıkla raporlanan değeri 0,062 olarak kalmıştır. Dolayısıyla bir ölçütteki artış, diğer ölçütlerde aynı büyüklükte bir kazanım anlamına gelmemektedir.

Bütün model-senaryo kombinasyonlarının doğruluğu, yalnızca çoğunluk sınıfını tahmin eden referansın 0,717 değerinin altında kalmıştır. Buna karşılık makro-F1 değerlerinin tamamı referansın 0,209 değerinin üzerindedir. Bu ayrışma, modellerin bazı azınlık gözlemlerini ayırabildiğini, ancak bu kazanımın toplam doğru sınıflandırma sayısını artırmaya yetmediğini göstermektedir. MCC değerlerinin en yüksek kombinasyonda dahi 0,103 düzeyinde kalması, genel ayrım gücünün sınırlı olduğunu desteklemektedir.

Tablo 4. Sınıf bazlı duyarlılık (üç tekrarın ortalaması)

Model	Senaryo	0 (n=782)	<10 (n=249)	10-100 (n=53)	>100 (n=7)
KA	Dengeleme yok	0,807	0,166	0,025	0,000
KA	RAÖ	0,656	0,262	0,138	0,000
KA	SMOTENC	0,646	0,276	0,082	0,000
RO	Dengeleme yok	0,953	0,074	0,000	0,000
RO	RAÖ	0,794	0,273	0,057	0,000
RO	SMOTENC	0,684	0,249	0,170	0,000
kNN	Dengeleme yok	0,894	0,123	0,000	0,000
kNN	RAÖ	0,506	0,430	0,107	0,000
kNN	SMOTENC	0,436	0,395	0,245	0,000
DVM	Dengeleme yok	0,894	0,142	0,019	0,000
DVM	RAÖ	0,654	0,313	0,195	0,000
DVM	SMOTENC	0,573	0,343	0,164	0,000

En küçük sınıfta (>100) tüm model-senaryo kombinasyonlarının duyarlılığı sıfırdır. Bu durum, sayısal sınıf dengelemenin bu veri setinde en nadir kategoriye genellenebilir bir ayrım kazandırmadığını göstermektedir. Diğer azınlık sınıflarında elde edilen kazanımlar, çoğunluk sınıfı duyarlılığındaki değişimlerle birlikte değerlendirilmelidir.

Tablo 4'te dengeleme uygulanmayan rastgele ormanın "0" sınıfındaki duyarlılığı 0,953 iken <10 sınıfında 0,074, 10-100 sınıfında ise 0,000'dır. RAÖ sonrasında çoğunluk sınıfının duyarlılığı 0,794'e gerilerken <10 ve 10-100 sınıflarında sırasıyla 0,273 ve 0,057'ye yükselmiştir. SMOTENC, aynı modelde 10-100 sınıfı duyarlılığını 0,170'e çıkarmış; buna karşılık çoğunluk sınıfındaki duyarlılık 0,684'e düşmüştür. Bu örüntü, azınlık sınıflarındaki kazanımın çoğunluk sınıfındaki kayıpla birlikte ortaya çıktığını göstermektedir.

<10 kategorisindeki en yüksek duyarlılık kNN-RAÖ ile 0,430; 10-100 kategorisindeki en yüksek duyarlılık kNN-SMOTENC ile 0,245 bulunmuştur. Ancak kNN-SMOTENC'in çoğunluk sınıfı duyarlılığı 0,436 olduğundan bu sınıf bazlı kazanım, en yüksek genel makro-F1 sonucunu sağlamamıştır. DVM-RAÖ ise <10 ve 10-100 kategorilerinde sırasıyla 0,313 ve 0,195 duyarlılık sağlayarak en yüksek dengeli doğruluğa ulaşmıştır. En nadir kategoride tüm duyarlılıkların sıfır kalması, dört sınıfın tamamında dengeli bir tahmin başarısının elde edilemediğini göstermektedir.

Yeniden örneklemeye bağlı değişim ve hata örüntüsü

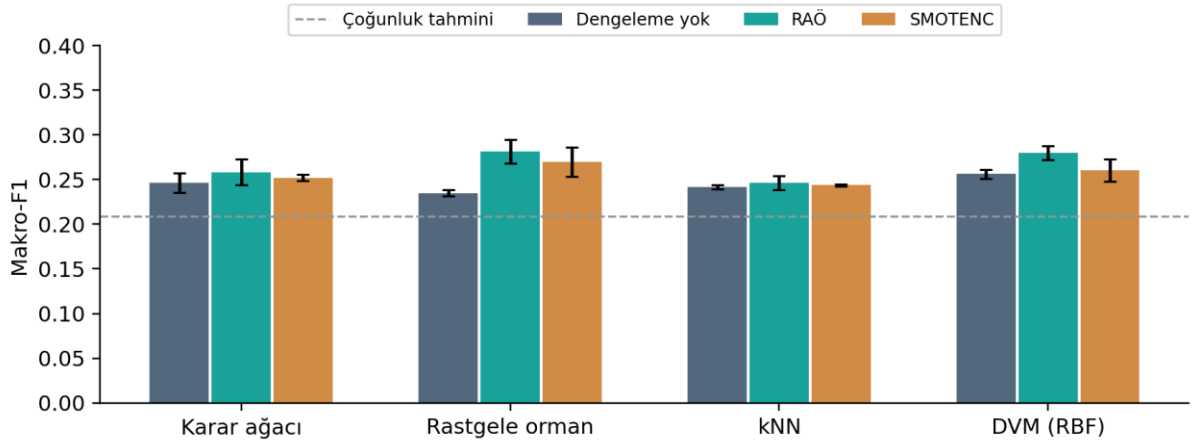
Tablo 5'e göre makro-F1'deki en büyük ortalama artış rastgele orman-RAÖ'de +0,047 ve dengeli doğruluktaki en büyük artış DVM-RAÖ'de +0,027'dir. Rastgele ormanda RAÖ'nün doğruluk kaybı −0,065 iken SMOTENC'in kaybı −0,145'tir; aynı modelde RAÖ, daha düşük doğruluk kaybıyla daha yüksek makro-F1 kazanımı sağlamıştır. En belirgin doğruluk azalması kNN-SMOTENC'te −0,255 olmasına rağmen makro-F1 artışı yalnızca +0,002'dir. Bu sonuç, daha fazla azınlık örneği üretmenin performans ölçütlerine orantılı bir katkı sağlamadığını göstermektedir.

Tablo 5. Dengeleme olmayan senaryoya göre eşleştirilmiş performans değişimi (ortalama Δ)

Model	Yöntem	Δ Doğruluk	Δ Dengeli doğruluk	Δ Makro-F1
KA	RAÖ	-0,080	+0,015	+0,012
KA	SMOTENC	-0,087	+0,001	+0,006
RO	RAÖ	-0,065	+0,024	+0,047
RO	SMOTENC	-0,145	+0,019	+0,035
kNN	RAÖ	-0,203	+0,007	+0,004
kNN	SMOTENC	-0,255	+0,015	+0,002
DVM	RAÖ	-0,124	+0,027	+0,024
DVM	SMOTENC	-0,177	+0,006	+0,004

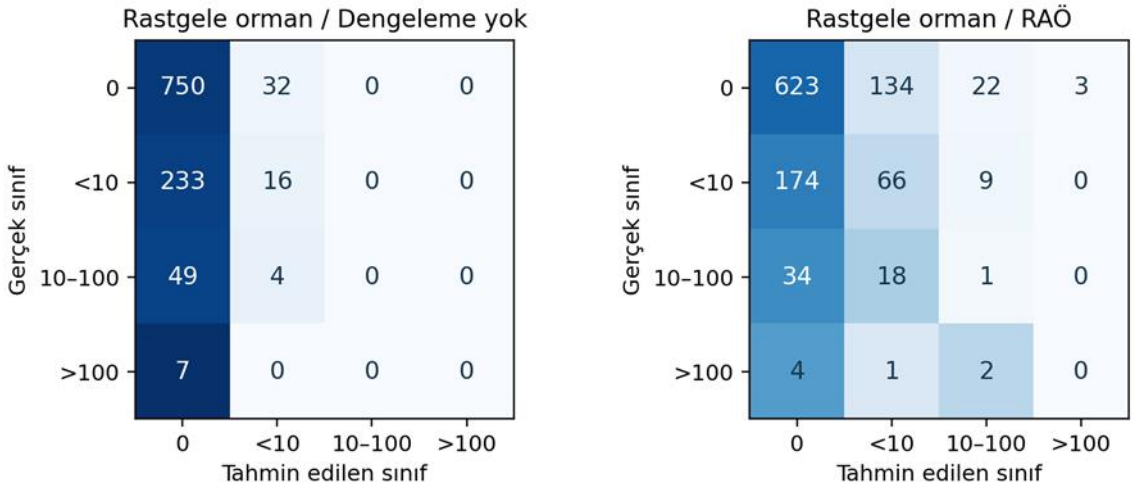
Not: Değişimler aynı tekrarın kat dışı tahminlerinden hesaplanmıştır. Pozitif değer, ilgili ölçütte artışı ifade eder. Değişimler mutlak ölçüt farkıdır, yüzde değişimi değildir.

Şekil 1, RAÖ'nün dört sınıflandırıcının tamamında en yüksek ortalama makro-F1'i verdiğini göstermektedir. Yeniden örneklemeye en belirgin yanıt rastgele ormanda görülürken kNN'de üç senaryonun sütunları birbirine yakın kalmıştır. Bütün kombinasyonlar çoğunluk tahmini referansının üzerindedir; buna rağmen değerlerin yaklaşık 0,24-0,28 aralığında toplanması, mutlak başarının sınırlı kaldığını göstermektedir. Hata çubukları bölünmeye bağlı değişkenliği özetlemekte, yakın sütunlar arasında tek başına bir anlamlılık kararı sağlamamaktadır.



Şekil 1. Makro-F1 karşılaştırması

Şekil 2'de ilk tekrara ait karışıklık matrisleri, rastgele ormanın yeniden örnekleme öncesinde çoğunluk sınıfına yöneldiğini açıkça göstermektedir. Dengeleme uygulanmadığında "0" sınıfındaki 782 gözlemin 750'si doğru tahmin edilmiş; <10 sınıfındaki 249 gözlemin yalnızca 16'sı kendi sınıfına, 233'ü ise "0" sınıfına atanmıştır. Ayrıca 10-100 sınıfında 53 ve >100 sınıfında 7 gözlemin hiçbiri doğru sınıflandırılamamıştır. Bu durumda yüksek görünen genel doğruluk, esas olarak çoğunluk sınıfındaki doğru tahminlerden kaynaklanmaktadır.



Şekil 2. Rastgele orman için dengeleme olmayan senaryo ve RAÖ karşılaştırması (İlk tekrar, tohum=42; N=1.091. Hücreler gerçek gözlem sayılarını, renkler satır içi oranları gösterir.)

RAÖ sonrasında "0" sınıfındaki doğru tahmin sayısı 750'den 623'e düşerken <10 sınıfındaki doğru tahmin sayısı 16'dan 66'ya yükselmiştir. Buna karşılık 10-100 sınıfında yalnızca bir doğru tahmin elde edilmiş, >100 sınıfının yedi gözlemi yine diğer kategorilere atanmıştır. Modelin >100 olarak tahmin ettiği üç gözlemin tamamı gerçekte "0" sınıfındadır. Dolayısıyla bu sınıf için tahmin üretilmesi, gerçek azınlık gözlemlerinin doğru yakalandığı anlamına gelmemektedir.

SONUÇ

Bu çalışmada, dengesiz çok sınıflı dermatolojik verilerde yeniden örnekleme yöntemlerinin makine öğrenmesi performansına etkisi incelenmiştir. Dört sınıflandırıcı, dengeleme uygulanmaması, rastgele aşırı örnekleme (RAÖ) ve SMOTENC senaryolarında karşılaştırılmıştır. Analizler, ön işleme ve yeniden örnekleme işlemleri yalnızca eğitim katlarında uygulanarak tekrarlı iç içe çapraz doğrulama ile yürütülmüştür.

Sonuçlar, yeniden örneklemenin etkisinin sınıflandırıcıya ve değerlendirme ölçütüne bağlı olduğunu göstermiştir. Rastgele ormanda dengeleme uygulanmadığında makro-F1 0,235 iken SMOTENC ile 0,270'e, RAÖ ile 0,282'ye yükselmiştir. Buna karşılık SMOTENC sonrasında doğruluk 0,700'den 0,555'e düşmüştür. En yüksek gözlenen makro-F1 rastgele orman-RAÖ kombinasyonunda elde edilmiştir. Ancak bu değer, yüksek veya klinik kullanıma yeterli bir sınıflandırma başarısı olarak değerlendirilmemelidir.

Çoğunluk sınıfının baskınlığı, yalnızca bu sınıfı tahmin eden referansın bile yüksek görünen doğruluk üretmesine neden olmuştur. Referansın dengeli doğruluğu ve makro-F1'i ise sınırlı kalmıştır. Bu nedenle modellerin doğruluğunun referansın altında olması, azınlık sınıflarında kazanım sağlanmadığı anlamına gelmemektedir. Yeniden örnekleme bazı azınlık sınıflarının duyarlılığını artırırken çoğunluk sınıfının duyarlılığını azaltmıştır. Tablo 4'te görülen bu değişim, eğitim verisinin dengelenmesinin bütün performans ölçütlerinde eşzamanlı iyileşme sağlamadığını ortaya koymaktadır.

En küçük sınıfta yalnızca yedi bağımsız gözlem bulunması, modellerin öğrenebileceği örüntü çeşitliliğini sınırlandırmıştır. Bu sınıfta hiçbir model-senaryo kombinasyonu doğru tahmin sağlayamamıştır. RAÖ mevcut gözlemleri çoğaltırken SMOTENC sınıf içi komşuluklardan sentetik örnekler üretmektedir. Her iki yaklaşım da eğitim setini büyütmesine rağmen bağımsız katılımcı sayısını artırmamaktadır. Bu nedenle sayısal sınıf dengelemesi, yeni bağımsız gözlemlerle sağlanabilecek bilgi artışıyla aynı şekilde değerlendirilmemelidir.

SMOTENC, kategorik değişkenlerde geçersiz ara değerlerin üretilmesini önlemek amacıyla tercih edilmiştir. Ancak yöntem, BMI ile kilo ve boy arasındaki ilişki gibi değişkenler arası fiziksel kısıtların tamamını korumayı garanti etmemektedir. Geçerli kategorik kodların üretilmesi, sentetik gözlemlerin bütünüyle klinik gerçekliği yansıttığını göstermemektedir. Sağlık verilerinde yeniden örnekleme yöntemlerinin veri özellikleriyle birlikte değerlendirilmesi gerektiğine ilişkin uyarılar bu açıdan önemlidir (Salmi vd., 2024).

Çalışmanın başlıca sınırlılıkları, tek bir hazırlanmış örnekleme dayanması, en nadir sınıfta az sayıda katılımcı bulunması ve bağımsız dış doğrulama yapılmamasıdır. Üç tekrar, sonuçların veri bölünmesine duyarlılığını göstermektedir. İç içe doğrulama parametre seçimini dış değerlendirmeden ayırmış olsa da 12 kombinasyon arasındaki karşılaştırma keşifseldir. Ayrıca hazırlama aşamasında model girdisi olarak kullanılmayan metin alanlarının da kayıt bütünlüğü açısından değerlendirilmesi, korunan örneklemin özelliklerini etkilemiş olabilir.

Dengesiz sağlık verilerinde yöntem seçimi, doğrulukla birlikte makro-F1, dengeli doğruluk, MCC ve sınıf bazlı duyarlılık üzerinden yapılmalıdır. Bulgular bütün sağlık verilerine genellenmemelidir. Gelecek çalışmalarda azınlık sınıflarındaki bağımsız gözlem sayısının artırılması ve sonuçların dış veri setlerinde doğrulanması önceliklidir. Hedef kategorilerin sıralı yapısını kullanan ordinal modeller ve algoritma düzeyindeki dengeleme yöntemleri de ayrıca değerlendirilebilir.

KAYNAKLAR

Belli, A. A., Etgu, F., Ozbas Gok, S., Kara, B. ve Dogan, G. (2016). Risk factors for premature hair graying in young Turkish adults. Pediatric Dermatology, 33(4), 438-442. https://doi.org/10.1111/pde.12881

Salmi, M., Atif, D., Oliva, D., Abraham, A. ve Ventura, S. (2024). Handling imbalanced medical datasets: review of a decade of research. Artificial Intelligence Review, 57, 273. https://doi.org/10.1007/s10462-024-10884-2

Chawla, N. V., Bowyer, K. W., Hall, L. O. ve Kegelmeyer, W. P. (2002). SMOTE: Synthetic minority over-sampling technique. Journal of Artificial Intelligence Research, 16, 321-357. https://doi.org/10.1613/jair.953

Cawley, G. C. ve Talbot, N. L. C. (2010). On over-fitting in model selection and subsequent selection bias in performance evaluation. Journal of Machine Learning Research, 11, 2079-2107. https://www.jmlr.org/papers/v11/cawley10a.html

Pedregosa, F. ve ark. (2011). Scikit-learn: Machine learning in Python. Journal of Machine Learning Research, 12, 2825-2830. https://www.jmlr.org/papers/v12/pedregosa11a.html

Lemaître, G., Nogueira, F. ve Aridas, C. K. (2017). Imbalanced-learn: A Python toolbox to tackle the curse of imbalanced datasets in machine learning. Journal of Machine Learning Research, 18(17), 1-5. https://www.jmlr.org/papers/v18/16-365.html

imbalanced-learn. SMOTENC: Synthetic Minority Over-sampling Technique for Nominal and Continuous. https://imbalanced-learn.org/stable/references/generated/imblearn.over_sampling.SMOTENC.html (Erişim: 6 Ekim 2026).

HİBRİT ÇALIŞMA ORTAMLARINDA SIFIR GÜVEN VE YAPAY ZEKÂ TABANLI ANOMALİ TESPİTİ İÇİN KATMANLI BİR SİBER GÜVENLİK MODELİ

A LAYERED CYBERSECURITY MODEL FOR ZERO TRUST AND AI-BASED ANOMALY DETECTION IN HYBRID WORK ENVIRONMENTS

Ömer SEVİNÇ

Dr., Ondokuz Mayıs Üniversitesi, Vezirköprü Meslek Yüksekokulu, Bilgisayar Programcılığı Programı, Samsun, Türkiye

Ph.D., Ondokuz Mayıs University, Vezirköprü Vocational School, Computer Programming Program, Samsun, Türkiye

ORCID: 0000-0003-0006-1682

ÖZET

Hibrit çalışma, kullanıcıların kurumsal kaynaklara farklı ağlardan, cihazlardan ve bulut hizmetlerinden erişmesini mümkün kılarken geleneksel ağ çevresine dayalı güvenlik varsayımlarını zayıflatmaktadır. Ele geçirilmiş kimlik bilgileri, yönetilmeyen cihazlar, aşırı yetkiler ve bulut yapılandırma hataları tek bir oturumun çok sayıda kaynağa sıçramasına yol açabilmektedir. Bu çalışma, sıfır güven ilkelerini yapay zekâ tabanlı anomali tespitiyle birleştiren katmanlı bir siber güvenlik modeli önermektedir. Tasarım bilimi yöntemiyle geliştirilen model; kimlik, cihaz, ağ ve ortam, uygulama ve iş yükü, veri ile görünürlük ve otomasyon olmak üzere altı boyuttan oluşmaktadır. Her erişim isteği kullanıcı kimliği, cihaz durumu, kaynak hassasiyeti, oturum davranışı ve güncel tehdit sinyalleri üzerinden sürekli değerlendirilmektedir. Model, çevre tabanlı yaklaşım, kısmi sıfır güven ve uyarlanabilir sıfır güven–yapay zekâ bütünleşmesi olmak üzere üç analitik senaryoda incelenmiştir. Ağırlıklı olgunluk puanları sırasıyla 1,88, 3,38 ve 4,42 olarak hesaplanmıştır. Yüzde yirmilik ağırlık değişimleri senaryo sıralamasını değiştirmemiştir. Bulgular, anomali puanının doğrudan erişim engelleme kararı olarak kullanılmasının yanlış pozitif ve iş sürekliliği riski doğurabileceğini; açıklanabilir risk göstergeleri, kademeli müdahale, insan gözetimi ve geri alma mekanizmalarının gerekli olduğunu göstermektedir. Model, yapay zekâ çıktısını tek yetkilendirme kararı yapmak yerine denetlenebilir politika kurallarıyla birleştirerek güvenlik, mahremiyet ve operasyonel süreklilik arasında dengeli bir uygulama yolu önermektedir. Çalışma gerçek bir ağ üzerinde performans ölçümü yapmamakta, kurumların mimari planlama ve pilot uygulamalarında doğrulayabileceği analitik bir değerlendirme artefaktı sunmaktadır.

Anahtar Kelimeler: sıfır güven, anomali tespiti, hibrit çalışma, yapay zekâ, erişim kontrolü

ABSTRACT

Hybrid work allows users to access organizational resources from diverse networks, devices, and cloud services, weakening security assumptions based on a trusted network perimeter. Compromised credentials, unmanaged devices, excessive privileges, and cloud

misconfigurations may allow a single session to move across multiple resources. This study proposes a layered cybersecurity model that combines zero trust principles with AI-based anomaly detection. Developed through a design-science method, the model covers six dimensions: identity, devices, networks and environments, applications and workloads, data, and visibility and automation. Each access request is continuously evaluated using user identity, device posture, resource sensitivity, session behavior, and current threat signals. The framework is examined through three analytical scenarios: perimeter-based security, partial zero trust, and adaptive zero-trust–AI integration. Their weighted maturity scores are 1.88, 3.38, and 4.42, respectively. Weight variations of twenty percent do not alter the scenario ranking. The findings suggest that an anomaly score should not automatically become an access-denial decision because false positives may threaten productivity and service continuity. Explainable risk indicators, graduated responses, human oversight, and rollback mechanisms are required. The model therefore uses AI to inform policy decisions while retaining deterministic authorization boundaries and auditable responsibility. The study does not measure performance on a live network. It provides an analytical assessment artifact that organizations can validate through pilots using authentication logs, endpoint posture, application telemetry, and incident outcomes.

Keywords: zero trust, anomaly detection, hybrid work, artificial intelligence, access control

GİRİŞ

Hibrit çalışma modeli, çalışanların kurumsal kaynaklara ofis ağı dışından, kişisel veya yönetilen cihazlardan ve çoklu bulut hizmetleri üzerinden erişmesini olağan hâle getirmiştir. Bu yapı verimlilik ve esneklik sağlarken iç ağın güvenilir, dış ağın güvensiz kabul edildiği çevre tabanlı güvenlik modelini zayıflatmaktadır. Bir kullanıcı sanal özel ağ bağlantısı kurduğunda geniş bir kaynak kümesine erişebiliyor veya cihaz durumu yalnızca oturum başlangıcında kontrol ediliyorsa ele geçirilmiş kimlik bilgisi uzun süre fark edilmeden kullanılabilir.

Sıfır güven, ağ konumuna dayanarak örtük güven vermeyen; kullanıcı, cihaz ve kaynak bağlamını her erişim kararında değerlendiren bir güvenlik yaklaşımıdır. NIST SP 800-207, güvenin sürekli doğrulanması, asgari yetki ve kaynak odaklı politika kararlarını sıfır güven mimarisinin temel ilkeleri arasında tanımlar (Rose vd., 2020). CISA Sıfır Güven Olgunluk Modeli ise kimlik, cihaz, ağ, uygulama ve iş yükü ile veri sütunlarını görünürlük ve analiz, otomasyon ve yönetişim yetenekleriyle birlikte ele almaktadır (CISA, 2023).

Yapay zekâ tabanlı anomali tespiti, sabit kuralların göremediği oturum davranışlarını belirleme potansiyeli taşır. Kullanıcının olağan erişim saati, konumu, cihazı, veri hacmi ve uygulama sırası öğrenilerek beklenmeyen sapmalar risk sinyali olarak sunulabilir. Ancak anomali her zaman saldırı değildir. Seyahat, görev değişikliği, toplu raporlama veya erişilebilirlik aracı kullanımı davranışı değiştirebilir. Anomali puanını doğrudan engelleme kararına dönüştürmek yanlış pozitif ve iş sürekliliği riski yaratabilir.

Bu çalışmanın araştırma sorusu şudur: Hibrit çalışmada sıfır güven ilkeleri ile yapay zekâ tabanlı anomali tespiti, denetlenebilir ve kademeli bir erişim karar sürecinde nasıl birleştirilebilir? Çalışma, altı boyutlu katmanlı model geliştirmekte; çevre tabanlı, kısmi sıfır güven ve uyarlanabilir sıfır güven–AI senaryolarını analitik olarak karşılaştırmaktadır. Sunulan puanlar gerçek ağ ölçümü değildir ve pilot uygulamada doğrulanması gereken tasarım değerleridir.

KAVRAMSAL ÇERÇEVE

Sıfır güven mimarisinin ilkeleri

Sıfır güven tek bir ürün veya yalnızca çok faktörlü kimlik doğrulama uygulaması değildir. Tüm veri kaynakları ve bilgi işlem hizmetleri kaynak kabul edilir; iletişim ağ konumundan bağımsız olarak korunur; erişim oturum başına ve asgari yetkiyle verilir; politika kullanıcı, cihaz, hizmet, davranış ve çevresel niteliklere göre dinamik biçimde belirlenir; varlıkların bütünlük ve güvenlik durumu izlenir; kimlik doğrulama ve yetkilendirme kaynak erişiminden önce uygulanır; kurum güvenlik duruşunu geliştirmek için telemetri toplar (Rose vd., 2020).

CISA modeli olgunluğu geleneksel, başlangıç, ileri ve optimum aşamalarında ele alır. Bu yaklaşım, kurumların bir gecede tam sıfır güvene geçmesi yerine kimlik ve cihaz görünürlüğünü geliştirerek, uygulama erişimini daraltarak ve veriyi sınıflandırarak ilerlemesini sağlar. Ancak sütunların bağımsız projeler şeklinde yönetilmesi boşluk oluşturabilir. Örneğin güçlü kimlik doğrulama, güvenliği bozulmuş cihazdan gelen yetkili kullanıcının hassas veriyi dışarı aktarmasını tek başına önleyemez.

Anomali tespiti ve karar riski

Anomali tespiti denetimli, denetimsiz veya yarı denetimli yöntemlerle gerçekleştirilebilir. Denetimli yöntemler etiketli saldırı verisine ihtiyaç duyarken denetimsiz yöntemler olağan davranıştan sapmayı belirler. Hibrit çalışma ortamında etiketlerin sınırlı, davranışın değişken olması denetimsiz veya kendinden denetimli yöntemleri cazip kılar. Bununla birlikte modelin eğitim dönemi saldırgan davranış içeriyorsa yanlış bir norm öğrenilebilir; yeni çalışanlar veya görev değişiklikleri için soğuk başlangıç sorunu ortaya çıkabilir.

Güvenlik kararının açıklanabilirliği operasyon için kritiktir. “Risk puanı 87” ifadesi analistin veya kullanıcının uygun müdahaleyi seçmesine yetmez. Sistem, yeni cihaz, olağandışı ülke, yüksek veri indirme miktarı, kısa sürede çoklu kaynak erişimi veya ayrıcalık yükseltme gibi katkıda bulunan sinyalleri göstermelidir. Müdahale de ikili olmamalıdır: yeniden kimlik doğrulama, oturumu salt okunur moda alma, hassas işlemi onaya yönlendirme, cihazı izole etme veya erişimi durdurma gibi kademeler kullanılabilir.

YÖNTEM

Araştırma tasarım bilimi yaklaşımıyla yürütülmüştür. NIST SP 800-207, CISA Sıfır Güven Olgunluk Modeli 2.0, NIST Siber Güvenlik Çerçevesi 2.0, NIST AI RMF ve sıfır güven uygulama literatürü incelenmiştir. Gereksinimler hibrit çalışma erişim zinciri boyunca kimlik, cihaz, ağ ve ortam, uygulama ve iş yükü, veri ile görünürlük ve otomasyon boyutlarında birleştirilmiştir. Model, teknik kontrolün yanında yönetişim, açıklanabilirlik ve geri alma gereksinimlerini içermektedir.

Tablo 1. Önerilen katmanlı sıfır güven–AI modeli

Boyut	Örnek kanıt ve kontroller	Ağırlık
Kimlik	Kimlik yaşam döngüsü, MFA, koşullu erişim, ayrıcalıklı hesap yönetimi	%20
Cihaz	Envanter, güvenlik durumu, şifreleme, EDR ve uyumluluk	%15
Ağ ve ortam	Şifreli trafik, mikro bölümleme, oturum bağlamı	%15
Uygulama ve iş yükü	Kimlik tabanlı erişim, hizmet hesabı, güvenli API	%15
Veri	Sınıflandırma, asgari erişim, DLP, şifreleme ve kayıt	%20
Görünürlük ve otomasyon	Ortak telemetri, açıklanabilir anomali, kademeli müdahale	%15

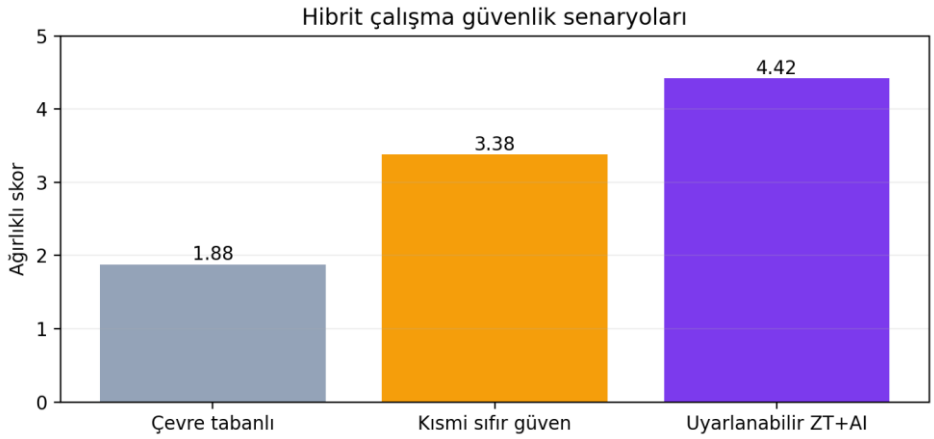
Her boyut 1 ile 5 arasında puanlanmıştır. Bir puan ağ konumu ve statik kurallara dayalı parçalı güvenliği, beş puan politika kararlarının sürekli bağlam, ölçülen performans ve olay geri bildirimiyle güncellendiği olgunluğu göstermektedir. Kimlik ve veri boyutlarına yüzde 20; diğer dört boyuta yüzde 15 ağırlık verilmiştir. Ağırlıklar analitik tercihlerdir ve kurumun görevine, veri hassasiyetine ve mevzuatına göre kalibre edilmelidir.

Üç senaryo tanımlanmıştır. Çevre tabanlı senaryo, sanal özel ağ ve ağ içi geniş güvene; kısmi sıfır güven, MFA, cihaz uyumluluğu ve bazı uygulamalarda koşullu erişime; uyarlanabilir sıfır güven–AI senaryosu, sürekli risk değerlendirmesi, mikro bölümleme, veri odaklı politika ve açıklanabilir anomali analizine dayanmaktadır. Duyarlılık analizinde her ağırlık yüzde 20 değiştirilmiş ve kalan ağırlıklar yeniden normalize edilmiştir.

ARAŞTIRMA VE BULGULAR

Tablo 2. Hibrit çalışma senaryolarının boyut puanları

Boyut	Çevre tabanlı	Kısmi ZT	Uyarlanabilir ZT+AI
Kimlik	2	4	5
Cihaz	2	3	4
Ağ ve ortam	2	3	4
Uygulama ve iş yükü	2	3	4
Veri	2	3	5
Görünürlük ve otomasyon	1	4	4



Şekil 1. Hibrit çalışma güvenlik senaryolarının ağırlıklı puanları.

Çevre tabanlı senaryo 1,88 puan üretmiştir. Kullanıcı VPN üzerinden kimlik doğruladıktan sonra ağ içindeki birden fazla kaynağa erişebilmekte, cihaz durumu ve oturum davranışı düzenli olarak yeniden değerlendirilmemektedir. Günlükler farklı sistemlerde tutulduğu için ele geçirilmiş hesabın hareketi uçtan uca görülememektedir. Bu yapı dış çevreyi güçlendirse de kimlik hırsızlığı ve iç yatay hareket riskine karşı sınırlı kanıt üretmektedir.

Kısmi sıfır güven senaryosu 3,38 puana ulaşmıştır. MFA, cihaz uyumluluğu ve uygulama bazlı erişim saldırı yüzeyini azaltmaktadır. Ancak politikalar bazı uygulamalarda uygulanmakta, veri sınıflandırması tamamlanmamakta ve anomali sinyalleri çoğunlukla yalnızca güvenlik operasyon merkezine bildirim üretmektedir. Kullanıcının rol değişikliği veya cihazın risk durumundaki değişim tüm kaynaklarda aynı hızla yetkiye yansımamaktadır.

Uyarlanabilir sıfır güven–AI senaryosu 4,42 puanla en yüksek sonucu vermiştir. Politika motoru kimlik güvencesi, cihaz durumu, kaynak hassasiyeti ve açıklanabilir davranış sinyallerini birleştirmektedir. Düşük riskte erişim sürmekte, orta riskte yeniden doğrulama veya yetki daraltma uygulanmakta, yüksek riskte hassas işlem durdurularak insan incelemesine yönlendirilmektedir. Anomali modeli yetkilendirme politikasının yerine geçmemekte; denetlenebilir bir risk sinyali sağlamaktadır.

Yüzde 20 ağırlık değişimlerinin hiçbirinde senaryo sıralaması değişmemiştir. En büyük değişim kimlik ve veri ağırlıklarında görülse de uyarlanabilir senaryo en yüksek olgunlukta kalmıştır. Bu bulgu modelin dar ağırlık değişimlerine dayanıklı olduğunu göstermektedir. Ancak puanların güvenlik etkinliğini kanıtlaması için kimlik ele geçirme tatbikatları, yanlış pozitif oranı, ortalama müdahale süresi, yatay hareket mesafesi ve kullanıcı iş kesintisi ölçülmelidir.

Politika karar akışı ve operasyonel denetimler

Önerilen karar akışında erişim isteği önce kimlik ve cihaz politikasından geçer. Ardından kaynak ve veri hassasiyeti belirlenir. Anomali motoru davranış sinyallerini üretir; politika karar noktası bu sinyali kurumsal risk eşiğiyle birleştirir. Politika uygulama noktası erişime izin verir, yeniden doğrulama ister, yetkiyi daraltır veya işlemi engeller. Her kararın girdileri, uygulanan politika sürümü ve sonuç işlemi denetim kaydına yazılır. Böylece modelin aynı koşulda tutarlı davranıp davranmadığı incelenebilir.

Yanlış pozitif yönetimi güvenlik kadar önemlidir. Sağlık, kamu hizmeti veya üretim gibi sürekliliğin kritik olduğu ortamlarda erişimin hatalı engellenmesi de zarar yaratır. Bu nedenle kritik iş rollerinde acil durum erişimi, zaman sınırlı yetki, ikinci kişi onayı ve sonradan zorunlu inceleme mekanizmaları tasarlanmalıdır. Model performansı yalnızca yakalanan saldırıyla değil, meşru kullanıcı üzerindeki sürtünme ve geri alma başarısıyla ölçülmelidir.

Hibrit çalışma cihazları farklı yönetim düzeylerinde olabilir. Kurumsal cihazda ayrıntılı güvenlik telemetrisi kullanılabilirken kişisel cihazda mahremiyet ve veri minimizasyonu sınırları vardır. Kurum, tam cihaz takibi yerine işletim sistemi güncelliği, şifreleme, ekran kilidi ve zararlı yazılım koruması gibi erişim için gerekli asgari durumu ölçmelidir. Davranış analitiği, çalışan performans gözetimine dönüştürülmemeli; amaç, saklama süresi ve erişim yetkileri açıkça belirlenmelidir.

Uygulamaya geçişte en yüksek değeri sağlayan dar kullanım durumları seçilebilir. Ayrıcalıklı yönetici erişimi, hassas veri deposu, finansal işlem ve dış tedarikçi hesabı pilot kapsamına alınabilir. Pilot öncesi temel performans kaydedilir; sonrasında müdahale süresi, gereksiz doğrulama sayısı, engellenen oturum ve kullanıcı desteği talebi karşılaştırılır. Başarılı sonuçlar diğer kaynaklara genişletilirken politika istisnaları ve teknik borç merkezi kayıtta izlenir.

SONUÇ

Hibrit çalışma, güvenlik kararının ağ konumundan kimlik, cihaz, uygulama, veri ve davranış bağlamına taşınmasını gerektirmektedir. Sıfır güven bu dönüşüm için mimari ilkeleri, yapay zekâ tabanlı anomali tespiti ise değişen davranışı görünür kılabilecek ek sinyalleri sağlar. Ancak anomali puanının tek başına erişim kararı olması açıklanabilirlik, yanlış pozitif ve sorumluluk sorunları doğurur.

Önerilen altı boyutlu model, yapay zekâ sinyalini deterministik politika, asgari yetki, kademeli müdahale ve insan gözetimiyle birleştirmektedir. Analitik değerlendirme uyarlanabilir sıfır güven–AI senaryosunun çevre tabanlı ve kısmi sıfır güven senaryolarından daha yüksek olgunluk ürettiğini göstermiştir. Sonuçların gerçek ortama genellenebilmesi için model, farklı sektörlerde pilot uygulamalarla; saldırı yakalama, yanlış pozitif, erişim gecikmesi, kullanıcı deneyimi ve olaydan kurtarma ölçütleri üzerinden doğrulanmalıdır.

KAYNAKÇA

Cybersecurity and Infrastructure Security Agency (CISA). 2023. Zero Trust Maturity Model Version 2.0. https://www.cisa.gov/zero-trust-maturity-model

Do, J., & Kang, K. 2023. A study on applying zero trust architecture: Focusing on implementing remote work system. Journal of the Korea Institute of Information Security and Cryptology, 33(6), 1001–1020. https://doi.org/10.13089/JKIISC.2023.33.6.1001

National Institute of Standards and Technology (NIST). 2023. Artificial Intelligence Risk Management Framework (AI RMF 1.0) (NIST AI 100-1). https://doi.org/10.6028/NIST.AI.100-1

National Institute of Standards and Technology (NIST). 2024. The NIST Cybersecurity Framework (CSF) 2.0 (NIST CSWP 29). https://doi.org/10.6028/NIST.CSWP.29

National Institute of Standards and Technology (NIST). 2025. Implementing a Zero Trust Architecture: High-Level Document (NIST SP 1800-35). https://pages.nist.gov/zero-trust-architecture/

Rose, S., Borchert, O., Mitchell, S., & Connelly, S. 2020. Zero Trust Architecture (NIST SP 800-207). National Institute of Standards and Technology. https://doi.org/10.6028/NIST.SP.800-207

Syed, N. F., Shah, S. W., Shaghaghi, A., Anwar, A., Baig, Z., & Doss, R. 2022. Zero trust architecture (ZTA): A comprehensive survey. IEEE Access, 10, 57143–57179. https://doi.org/10.1109/ACCESS.2022.3174679

ÜRETKEN YAPAY ZEKÂ DESTEKLİ OLTALAMA SALDIRILARINA KARŞI İNSAN–MAKİNE İŞBİRLİĞİNE DAYALI KURUMSAL SAVUNMA MODELİ

A HUMAN–MACHINE COLLABORATION MODEL FOR ORGANIZATIONAL DEFENSE AGAINST GENERATIVE AI-ENABLED PHISHING

Ömer SEVİNÇ

Dr., Ondokuz Mayıs Üniversitesi, Vezirköprü Meslek Yüksekokulu, Bilgisayar Programcılığı Programı, Samsun, Türkiye

Ph.D., Ondokuz Mayıs University, Vezirköprü Vocational School, Computer Programming Program, Samsun, Türkiye

ORCID: 0000-0003-0006-1682

ÖZET

Üretken yapay zekâ, düşük maliyetle dil bilgisi yüksek, kişiselleştirilmiş ve bağlama uyarlanmış oltalama iletileri üretilebilmesini kolaylaştırmaktadır. Geleneksel savunmalar çoğunlukla alan adı itibarı, bilinen kötü amaçlı göstergeler ve kullanıcıların yazım hatalarını fark etmesi gibi sinyallere dayanırken, yapay zekâ destekli iletiler bu ipuçlarını azaltabilmektedir. Bu çalışma, üretken yapay zekâ destekli oltalama saldırılarına karşı teknik denetimleri, insan kararını ve olay geri bildirimini birleştiren beş katmanlı bir kurumsal savunma modeli önermektedir. Tasarım bilimi yaklaşımıyla geliştirilen model; ileti kaynağı ve kimlik doğrulama, içerik ve bağlam analizi, risk tabanlı kullanıcı arayüzü, bağımsız kanal üzerinden işlem doğrulama ve olaydan öğrenme katmanlarından oluşmaktadır. Modelin işleyişi geleneksel, katmanlı ve uyarlanabilir olmak üzere üç analitik senaryo üzerinde değerlendirilmiştir. Kaynak güveni, içerik analizi, insan desteği, yüksek riskli işlem kontrolü ve öğrenme döngüsü boyutlarının ağırlıklı değerlendirmesi sırasıyla 2,05, 3,72 ve 4,48 puan üretmiştir. Ağırlıkların yüzde yirmi değiştirilmesi senaryoların sıralamasını değiştirmemiştir. Bulgular, tek başına yapay zekâ tabanlı sınıflandırmanın yeterli olmadığını; güvenli tasarlanmış uyarıların, bağlama duyarlı eğitimin, çok faktörlü doğrulamanın ve ödeme ya da kimlik bilgisi değişikliği gibi kritik işlemlerde bağımsız kanal doğrulamasının birlikte uygulanması gerektiğini göstermektedir. Öneri, çalışanı güvenlik zincirinin tek hata noktası olarak görmek yerine açıklanabilir uyarılar ve doğrulanabilir süreçlerle desteklenen aktif bir savunma katmanı olarak konumlandırmaktadır. Çalışma gerçek kullanıcı deneyi sunmamakta, kurumlar tarafından saha verisiyle doğrulanabilecek analitik bir karar destek modeli ortaya koymaktadır.

Anahtar Kelimeler: üretken yapay zekâ, oltalama, sosyal mühendislik, insan faktörü, siber güvenlik

ABSTRACT

Generative artificial intelligence enables attackers to produce grammatically convincing, personalized, and context-aware phishing messages at low cost. Traditional defenses often

rely on domain reputation, known malicious indicators, and users noticing spelling or stylistic errors, while AI-generated messages can reduce these cues. This study proposes a five-layer organizational defense model that combines technical controls, human judgment, and incident feedback against generative-AI-enabled phishing. Developed through a design-science approach, the model consists of message-source authentication, content and contextual analysis, risk-based user-interface support, out-of-band transaction verification, and incident-driven learning. Its operation is demonstrated through three analytical scenarios representing traditional, layered, and adaptive defense. A weighted assessment of source trust, content analysis, human support, high-risk transaction control, and learning-loop capabilities produces scores of 2.05, 3.72, and 4.48, respectively. Varying each weight by twenty percent does not change the ranking of the scenarios. The findings indicate that AI-based classification alone is insufficient. Securely designed warnings, context-sensitive training, multi-factor authentication, and independent-channel verification for critical actions such as payments or credential changes should be implemented together. The proposed framework treats employees neither as the sole cause of security failure nor as passive recipients of warnings; instead, it makes them supported participants in a measurable defense process. The study does not report a real-user experiment. It provides an analytical decision-support artifact that organizations can calibrate and validate using phishing exercises, security-operations data, and user-centered evaluation.

Keywords: generative artificial intelligence, phishing, social engineering, human factors, cybersecurity

GİRİŞ

Oltalama saldırıları, kullanıcıyı güvenilir görünen bir ileti üzerinden bağlantıya tıklamaya, dosya açmaya, kimlik bilgisi paylaşmaya veya ödeme gerçekleştirmeye yönlendiren sosyal mühendislik saldırılarıdır. NIST, oltalamayı kurumların her tür ve büyüklükte karşılaştığı yaygın bir siber tehdit olarak tanımlamakta; iletilerin e-posta, kısa mesaj ve sosyal medya gibi kanallardan gelebileceğine dikkat çekmektedir (NIST, 2021). ENISA Tehdit Görünümü 2025, oltalama, zararlı e-posta, sesli oltalama ve kötü amaçlı reklamları birlikte ele aldığında oltalamanın gözlenen ilk erişim vektörleri içinde baskın konumda olduğunu bildirmektedir (ENISA, 2025).

Üretken yapay zekâ saldırganın maliyet yapısını değiştirmektedir. Büyük dil modelleri farklı dillere uyarlanmış, kurumsal üslubu taklit eden, yazım hatası içermeyen ve hedefin rolüne göre kişiselleştirilmiş içerikleri hızla üretebilir. Metin üretiminin yanı sıra ses klonlama, sentetik görüntü ve otomatik keşif araçları da yöneticiyi taklit etme veya tedarikçi yazışmasına sızma senaryolarını güçlendirmektedir. Bu dönüşüm, yalnızca şüpheli kelime ve yazım hatası arayan filtrelerin ve farkındalık eğitimlerinin etkisini sınırlayabilir.

Bununla birlikte çözümün yalnızca daha güçlü bir yapay zekâ sınıflandırıcısı olmadığı açıktır. Sınıflandırıcılar yeni saldırı biçimlerinde hata yapabilir, saldırgan tarafından yanıltılabilir veya meşru iletileri engelleyerek kullanıcı güvenini azaltabilir. İnsanlar da güvenlik zincirinin

zayıf halkası biçiminde etiketlendiğinde, uyarı yorgunluğu ve olay bildirmeme davranışı gözden kaçmaktadır. İnsan-merkezli güvenlik yaklaşımı, kullanıcı bağlamı ile ileti özelliklerini birlikte değerlendirir. NIST Phish Scale, bir iletinin insan tarafından fark edilme güçlüğünü kullanıcı bağlamı ve oltalama ipuçları üzerinden ölçmeyi önermektedir (Steves vd., 2020; NIST, 2023).

Bu araştırmanın sorusu şudur: Üretken yapay zekâ destekli oltalama saldırılarına karşı teknik tespit, insan kararı ve kritik işlem doğrulaması nasıl tek bir ölçülebilir savunma modelinde birleştirilebilir? Çalışmanın amacı, kurumların yalnızca iletiyi sınıflandırmak yerine saldırının ödeme, parola sıfırlama veya hassas veri paylaşımı gibi iş sonuçlarına ulaşmasını engelleyen katmanlı bir artefakt geliştirmektir. Çalışma gerçek çalışanlardan veri toplamamakta; literatür ve standartlardan türetilen gereksinimleri analitik senaryolarla değerlendirmektedir.

KAVRAMSAL ÇERÇEVE

Üretken yapay zekâ ve dijital aldatma

Üretken yapay zekâ sosyal mühendislikte üç yetenek sağlar: ölçek, kişiselleştirme ve uyarlama. Saldırgan, kamuya açık profil ve kurum bilgisini kullanarak hedef rolüne uygun ileti üretebilir; yanıt geldikçe konuşmayı sürdürebilir ve farklı dil ya da üsluba geçebilir. Mouton ve arkadaşları (2024), üretken yapay zekânın sosyal mühendislik ve oltalamada içerik kalitesini ve saldırı ölçeğini artırabileceğini, savunmanın teknik ve insani önlemleri birlikte ele alması gerektiğini vurgulamaktadır.

AI destekli içeriğin yalnızca dil modeline özgü izlerle tespit edileceği varsayımı kırılgandır. Saldırgan metni yeniden yazabilir, meşru bir hesabı ele geçirebilir veya gerçek bir yazışma zincirine yanıt verebilir. Bu durumda iletinin dilsel biçimi normal görünür. Bu nedenle kaynak kimliği, alan adı doğrulaması, hesap davranışı, iletinin iş bağlamı, bağlantı hedefi ve talep edilen işlemin riski birlikte incelenmelidir. İçeriğin yapay zekâ tarafından yazılmış olup olmadığı, eylemin güvenli olup olmadığıyla aynı soru değildir.

İnsan faktörü ve karar desteği

Oltalama başarısı yalnızca bilgi eksikliğiyle açıklanamaz. İş yükü, zaman baskısı, otorite etkisi, alışkanlık, mobil ekran kısıtları ve iletinin alıcı için uygunluğu kararı etkiler. Steves ve arkadaşları (2020), kullanıcı bağlamına uygun iletilerin fark edilmesinin daha zor olabileceğini göstermektedir. Bu nedenle genel ve sık tekrarlanan eğitim yerine role, göreve ve geçmiş tatbikat performansına göre uyarlanmış destek daha anlamlıdır.

Uyarı tasarımı da savunmanın parçasıdır. Kırmızı renkli genel bir “tehlikeli olabilir” etiketi, kullanıcıya hangi kanıtın riskli olduğunu ve ne yapması gerektiğini söylemez. Karar desteği; alan adı benzerliği, yeni gönderici, olağandışı ödeme talebi, dış bağlantı ve aciliyet dili gibi açıklanabilir nedenleri göstermeli; güvenli önizleme, bildir ve bağımsız doğrula gibi eylemler sunmalıdır. Yapay zekâ kararı açıklayamadığında sistem otomatik güven üretmek yerine belirsizliği ifade etmelidir.

YÖNTEM

Araştırmada tasarım bilimi yaklaşımı kullanılmıştır. Birinci aşamada NIST oltalama rehberi, NIST Phish Scale, NIST AI RMF Üretken Yapay Zekâ Profili, ENISA tehdit görünümü ve

hakemli çalışmalar incelenmiştir. İkinci aşamada gereksinimler saldırı zincirinin kaynağa erişim, ileti oluşturma, kullanıcı etkileşimi, kritik işlem ve olay sonrası öğrenme adımlarına eşlenmiştir. Üçüncü aşamada beş katmanlı model ve ağırlıklı değerlendirme matrisi oluşturulmuştur.

Tablo 1. Önerilen savunma modelinin katmanları

Katman	Temel kontroller	Amaç
1. Kaynak ve kimlik	SPF/DKIM/DMARC, alan adı ve hesap davranışı, gönderen doğrulama	Sahte veya ele geçirilmiş kaynağı belirlemek
2. İçerik ve bağlam	Bağlantı/dosya analizi, dilsel ve davranışsal sinyaller, iş bağlamı	İletinin ve talebin riskini açıklamak
3. İnsan karar desteği	Açıklanabilir uyarı, güvenli önizleme, role dayalı mikro eğitim	Kullanıcının güvenli karar vermesini desteklemek
4. İşlem doğrulama	MFA, ayrı kanal, çift onay, işlem limiti	İletinin kritik eyleme dönüşmesini engellemek
5. Öğrenme döngüsü	Tek tık bildirim, olay korelasyonu, geri bildirim ve ölçüm	Yeni saldırılara ve kullanıcı bağlamına uyarlanmak

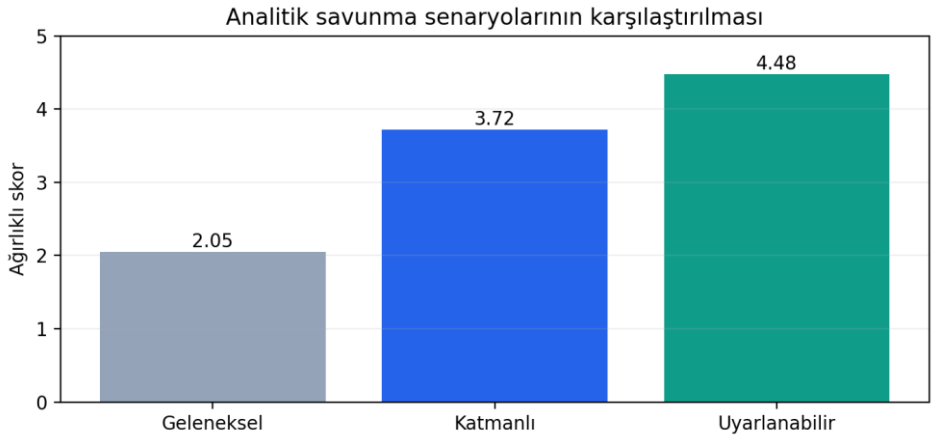
Her katman 1 ile 5 arasında puanlanmıştır. Bir puan kontrollerin parçalı veya yalnızca politika düzeyinde olduğunu, beş puan kontrollerin ölçüldüğünü, düzenli test edildiğini ve olay geri bildirimiyle güncellendiğini göstermektedir. Kaynak güveni yüzde 20, içerik ve bağlam analizi yüzde 20, insan karar desteği yüzde 20, kritik işlem doğrulaması yüzde 25 ve öğrenme döngüsü yüzde 15 ağırlıklandırılmıştır. Ağırlıklar, saldırının doğrudan kurumsal kayba dönüşmesini engelleyen kontrolün önemini yansıtacak biçimde belirlenmiştir; ampirik olarak doğrulanmış katsayılar değildir.

Üç analitik senaryo oluşturulmuştur. Geleneksel senaryo e-posta ağ geçidi ve yıllık farkındalık eğitimine; katmanlı senaryo açıklanabilir uyarılar, MFA ve işlem doğrulamasına; uyarlanabilir senaryo ise sürekli davranış analizi, role dayalı eğitim ve olaydan öğrenmeye dayanmaktadır. Duyarlılık analizinde her ağırlık ayrı ayrı yüzde 20 artırılmış ve azaltılmış, diğer ağırlıklar toplam yüzde 100 olacak biçimde yeniden ölçeklenmiştir.

ARAŞTIRMA VE BULGULAR

Tablo 2. Analitik senaryoların boyut puanları

Boyut	Geleneksel	Katmanlı	Uyarlanabilir
Kaynak ve kimlik güveni	3	4	5
İçerik ve bağlam analizi	2	4	5
İnsan karar desteği	2	4	4
Kritik işlem doğrulaması	2	4	5
Öğrenme döngüsü	1	2	4



Şekil 1. Analitik savunma senaryolarının ağırlıklı puanları.

Geleneksel senaryo 2,05 puan üretmiştir. Bu senaryoda ileti ağ geçidi bilinen zararlı alan adlarını ve dosyaları engelleyebilse de meşru hesabın ele geçirilmesi, yeni alan adı veya dil bilgisi yüksek kişiselleştirilmiş içerik karşısında görünürlük sınırlıdır. Yıllık eğitim kullanıcının bağlamını ve saldırının değişen biçimini izlememektedir. Ödeme veya kimlik bilgisi değişikliği yalnızca ileti içindeki talebe dayanıyorsa tek bir başarılı aldatma yüksek etki oluşturabilir.

Katmanlı senaryo 3,72 puana ulaşmıştır. Kaynak ve içerik sinyalleri birlikte değerlendirilmekte, kullanıcıya risk gerekçesi gösterilmekte ve kritik talepler bağımsız kanal veya çift onayla doğrulanmaktadır. Bu yapı, sınıflandırıcı hatalı biçimde iletiyi güvenli saysa bile saldırının işlem aşamasında durdurulmasını sağlar. Öğrenme döngüsünün görece düşük kalması, olay bildirimlerinin model, eğitim ve politika güncellemesine sistematik olarak bağlanmamasından kaynaklanmaktadır.

Uyarlanabilir senaryo 4,48 puanla en yüksek sonucu vermiştir. Kullanıcı rolü, gönderici ilişkisi, oturum davranışı ve işlem tipi dinamik risk puanına dâhil edilmiştir. Sistem düşük riskte iletiyi normal biçimde sunmakta, orta riskte açıklanabilir uyarı ve güvenli önizleme sağlamakta, yüksek riskte ise işlemi ikinci bir yetkili veya bağımsız iletişim kanalıyla doğrulamaktadır. Böylece her belirsizlik otomatik engellemeye dönüşmemekte ve iş sürekliliği korunmaktadır.

Duyarlılık analizinde hiçbir yüzde 20 ağırlık değişimi senaryoların sıralamasını değiştirmemiştir. En büyük fark kritik işlem doğrulamasının ağırlığında görülmüş, ancak uyarlanabilir senaryo tüm koşullarda en yüksek puanda kalmıştır. Bu sonuç modelin dar ağırlık değişimlerine karşı kararlı olduğunu göstermektedir; modelin gerçek etkinliği için kullanıcı deneyi, yanlış pozitif oranı, bildirim süresi ve engellenen kritik işlem gibi göstergelerle doğrulama gereklidir.

Uygulama ve ölçüm planı

Kurumsal uygulama üç aşamada yürütülebilir. İlk aşamada ödeme, parola sıfırlama, banka hesabı değişikliği, hassas dosya paylaşımı ve ayrıcalıklı erişim gibi yüksek etkili işlemler envanterlenir. İkinci aşamada e-posta, kimlik, uç nokta ve güvenlik operasyonu günlükleri ortak olay kimliğiyle ilişkilendirilir. Üçüncü aşamada uyarı arayüzü küçük kullanıcı

gruplarıyla test edilir. Sistem yalnızca tıklama oranını değil, kullanıcının doğru bildirimi, karar süresi, yanlış pozitif nedeniyle iş kaybı ve olayın finansal sürece ulaşma oranını izlemelidir.

Farkındalık tatbikatları çalışanı cezalandırma aracı olarak kullanılmamalıdır. Mesajın zorluk düzeyi ölçülmeden tıklama oranlarının karşılaştırılması yanıltıcı olabilir. NIST Phish Scale kullanılarak ileti ipuçları ve kullanıcı bağlamı değerlendirilebilir; zor senaryolarda kullanıcıya karar anında destek verilebilir. Tekrarlanan hatalar kişisel kusur olarak değil, arayüz, süreç veya yetki tasarımındaki eksikliğin göstergesi olarak incelenmelidir.

Yapay zekâ bileşeninin yönetişimi ayrıca ele alınmalıdır. Eğitim verisinin kaynağı, model sürümü, karar eşiği, performans sapması ve insan itiraz süreci belgelenmelidir. Saldırganın sınıflandırıcıyı yanıltmak için içeriği değiştirebileceği kabul edilmeli; model tek karar noktası yapılmamalıdır. NIST AI RMF Üretken Yapay Zekâ Profili, ölçme ve yönetme faaliyetlerinin bağlama ve risk toleransına uyarlanmasını önermektedir (NIST, 2024).

SONUÇ

Üretken yapay zekâ, oltalamanın temel amacını değiştirmemekte; saldırının ölçeğini, dil kalitesini ve kişiselleştirme kapasitesini artırmaktadır. Bu nedenle yalnızca içeriğin yapay zekâ tarafından üretilip üretilmediğini belirlemeye çalışan savunma sürdürülebilir değildir. Önerilen model kaynak kimliğini, içerik ve bağlam analizini, insan karar desteğini, kritik işlem doğrulamasını ve olaydan öğrenmeyi tek bir savunma zincirinde birleştirmektedir.

Analitik değerlendirme, işlem doğrulaması ve geri bildirim döngüsü bulunan uyarlanabilir senaryonun geleneksel ve katmanlı senaryolardan daha yüksek olgunluk ürettiğini göstermiştir. Bununla birlikte puanlar gerçek kurum performansı değildir. Gelecek çalışmalarda model kontrollü oltalama tatbikatlarıyla sınanmalı; doğru tespit, yanlış pozitif, bildirim süresi, kullanıcı güveni, iş kesintisi ve engellenen kayıp üzerinden değerlendirilmelidir. İnsan ve makine işbirliği, çalışanı tek hata noktası olmaktan çıkarıp güvenli karar için desteklenen bir aktöre dönüştürdüğünde daha kalıcı bir kurumsal dayanıklılık sağlayabilir.

KAYNAKÇA

European Union Agency for Cybersecurity (ENISA). 2025. ENISA Threat Landscape 2025. https://www.enisa.europa.eu/publications/enisa-threat-landscape-2025

Mouton, F., Leenen, L., & Venter, H. S. 2024. Digital deception: Generative artificial intelligence in social engineering and phishing. Artificial Intelligence Review, 57. https://doi.org/10.1007/s10462-024-10973-2

National Institute of Standards and Technology (NIST). 2021. Phishing. https://www.nist.gov/itl/smallbusinesscyber/guidance-topic/phishing

National Institute of Standards and Technology (NIST). 2023. NIST Phish Scale User Guide (NIST TN 2276). https://doi.org/10.6028/NIST.TN.2276

National Institute of Standards and Technology (NIST). 2024. Artificial Intelligence Risk Management Framework: Generative Artificial Intelligence Profile (NIST AI 600-1). https://doi.org/10.6028/NIST.AI.600-1

Steves, M., Greene, K., & Theofanos, M. 2020. Categorizing human phishing difficulty: A Phish Scale. Journal of Cybersecurity, 6(1), tyaa009. https://doi.org/10.1093/cybsec/tyaa009

Williams, E. J., Joinson, A. N., Lymperopoulos, L., & Spoof, L. 2024. The anatomy of deception: Measuring technical and human factors of a large-scale phishing campaign. Computers & Security, 140, 103780. https://doi.org/10.1016/j.cose.2024.103780

EKSİK VERİ TAMAMLAMA YÖNTEMLERİNİN PERFORMANS ANALİZİ

PERFORMANCE ANALYSIS OF MISSING DATA IMPUTATION METHODS

Cem ALİŞEN
Yüksek Lisans Öğrencisi, Gazi Üniversitesi, Fen Bilimleri Enstitüsü, Veri Bilimi
Master's Student, Gazi University, Graduate School of Natural and Applied Sciences, Data Science
ORCID ID: 0009-0005-5863-9637

Fikri GÖKPINAR
Prof. Dr., Gazi Üniversitesi, Fen Fakültesi, İstatistik
Prof. Dr., Gazi University, Faculty of Sciences, Statistics
ORCID ID: 0000-0002-6310-8727

ÖZET

Veri analizinde ve istatistiksel modelleme süreçlerinde sıklıkla karşılaşılan eksik veri sorunu; parametre tahminlerinde yanlılığa, örneklem varyansının bozulmasına ve analizlerin istatistiksel gücünün azalmasına neden olan temel bir sorundur. Bu çalışmada, farklı eksik veri tamamlama (imputasyon) yöntemlerinin performansları hem kurgulanan deneysel senaryolar hem de gerçek veri setleri üzerinde karşılaştırmalı olarak incelenmiştir. Simülasyon aşamasında farklı veri yapılarını temsil etmek üzere; örneklem büyüklüğü (N = 1000, 6000), değişken sayısı (P = 6, 10), değişkenler arasındaki doğrusal ilişkinin gücü (ρ = 0,2, 0,8), eksiklik oranı (%10, %20) ile homojen/heterojen varyans dağılım senaryoları tasarlanmıştır. Uygulama aşamasında ise yöntemlerin gerçek dünya verilerindeki başarıları, farklı özelliklere sahip "Rice" ve "Combined Cycle Power Plant" veri setleri kullanılarak test edilmiştir. Çalışmada Amelia, Random Hot-deck, Multiple Imputation by Chained Equations (MICE), MissForest, Aritmetik Ortalama (MEAN), k-En Yakın Komşu (kNN), Histogram Tabanlı Gradient Boosting, Extreme Gradient Boosting (XGBoost) ve Predictive Mean Matching (PMM) algoritmaları değerlendirilmiştir. Yöntemlerin hata performansları, Ortalama Mutlak Yüzde Hata (MAPE) ve Normalleştirilmiş Kök Ortalama Kare Hata (NRMSE) ölçütleri birlikte kullanılarak hesaplanmıştır. Elde edilen bulgular, eksik veri tamamlama başarısı üzerinde veri yapısının sistematik etkilere sahip olduğunu göstermiştir. Değişkenler arasındaki doğrusal ilişkinin zayıf seviyeden güçlü seviyeye (ρ = 0,8) çıkması modeller arası bilgi transferini kolaylaştırarak hata değerlerini belirgin biçimde düşüren en temel faktör olurken; varyans (standart sapma) yapısındaki artış performansı olumsuz etkileyen ana etmen olarak kaydedilmiştir. Hem simülasyon hem de gerçek veri uygulamalarında karar ağacı tabanlı topluluk algoritmalarının (MissForest, HistGradientBoosting, XGB) en düşük hata değerlerini üreterek en başarılı ve kararlı yöntemler olduğu, tek değişkenli veya rastgele donör atama yaklaşımlarının (Ortalama, Hot-deck) ise en zayıf performansı sergilediği tespit edilmiştir. Bu çalışma, araştırmacılara uygun eksik veri tamamlama yöntemini seçmelerinde yardımcı olacak bir rehber sunmaktadır.

Anahtar Kelimeler: Eksik veri, imputasyon, MissForest, MICE, Amelia, Random Hot-deck, PMM, Random Forest, kNN, XGBoost, Ortalama, Histogram Tabanlı Gradient Boosting, MAPE, NRMSE

ABSTRACT

Missing data is a common problem in data analysis and statistical modeling, potentially leading to biased parameter estimates, distorted sample variance, and reduced statistical power. This study comparatively evaluated the performance of different missing data imputation methods using both simulated scenarios and real-world datasets. In the simulation phase, various scenarios were designed by considering sample size (N = 1000, 6000), number of variables (P = 6, 10), strength of linear correlation between variables (ρ = 0.2, 0.8), missingness rate (10%, 20%), and homogeneous and heterogeneous variance structures. In the real-data applications, the performance of the methods was evaluated using the Rice and Combined Cycle Power Plant datasets, which have different characteristics. The methods examined included Amelia, Random Hot-deck, Multiple Imputation by Chained Equations (MICE), MissForest, Arithmetic Mean (MEAN), k-Nearest Neighbors (kNN), Histogram-Based Gradient Boosting, Extreme Gradient Boosting (XGBoost), and Predictive Mean Matching (PMM). Imputation performance was assessed using both Mean Absolute Percentage Error (MAPE) and Normalized Root Mean Square Error (NRMSE). The results demonstrated that data structure systematically influences imputation performance. Increasing the correlation between variables from a weak to a strong level (ρ = 0.8) was the most influential factor in reducing imputation errors, as stronger relationships enabled the models to make better use of information across variables. In contrast, increased variability, reflected in higher standard deviations, negatively affected performance. Across both simulation scenarios and real-data applications, tree-based ensemble methods (MissForest, HistGradientBoosting, and XGB) consistently achieved the lowest error values, demonstrating superior accuracy and stability. Conversely, mean imputation and random donor-based approaches (Mean and Hot-deck) generally exhibited the weakest performance. These findings provide practical guidance for researchers in selecting appropriate missing data imputation methods under different data conditions.

Keywords: Missing data, imputation, MissForest, MICE, Amelia, Random Hot-deck, PMM, Random Forest, kNN, XGBoost, Arithmetic Mean, Histogram-based Gradient Boosting, MAPE, NRMSE

TRANSFERABILITY OF SQL SERVER MEMORY SETTINGS ACROSS WORKLOADS

Meral ERGÜN
Doktora Öğrencisi, Marmara Üniversitesi, Fen Bilimleri Enstitüsü, Bilgisayar ve Elektronik Eğitimi Anabilim Dalı
PhD Candidate, Marmara University, Institute of Pure and Applied Sciences, Department of Computer and Electronics Education
ORCID ID: 0009-0003-4453-0898

Mustafa KURBAN
Prof. Dr., Ankara Üniversitesi, Ortez ve Protez Bölümü; Araştırmacı, Texas A&M University at Qatar
Professor, Ankara University, Department of Prosthetics and Orthotics; Research Associate, Texas A&M University at Qatar
ORCID ID: 0000-0002-7263-0234

Erchin SERPEDIN
Prof. Dr., Texas A&M University, Elektrik ve Bilgisayar Mühendisliği Bölümü, College Station, Teksas, ABD
Professor, Texas A&M University, Department of Electrical and Computer Engineering, College Station, TX, USA
ORCID ID: 0000-0001-9069-770X

Buket DOĞAN
Doç. Dr., Marmara Üniversitesi, Teknoloji Fakültesi, Bilgisayar Mühendisliği, Bilgisayar Yazılımı Anabilim Dalı
Assoc. Prof. Dr. Department of Computer Software, Department of Computer Engineering, Faculty of Technology, Marmara University, Istanbul, Türkiye.
ORCID ID: 0000-0003-1062-2439

ABSTRACT

A database memory setting selected under one workload may not remain suitable when the workload changes. This study evaluates the transferability of a SQL Server memory operating point from a transaction-oriented workload to an analytical workload using a controlled cross-workload bridge. Microsoft SQL Server 2022 was deployed in a four-CPU container with 5 GiB of memory. Five explicit max server memory settings between 2048 and 3584 MB were first examined with HammerDB TPROC-C and then replayed under HammerDB TPROC-H while MAXDOP 4 and the cost threshold for parallelism 5 were held constant. In addition to raw performance, a descriptive normalized-loss analysis compared each setting with the best observed value for transaction throughput, p95 transaction latency, analytical query-set time, and geometric-mean query time. The 3072 MB setting produced the highest TPROC-C throughput at 61,616 new orders per minute and the shortest TPROC-H query-set time at 75 s. Its only gap from a within-metric best was a 5.6% p95-latency excess relative to 3328 MB; consequently, it also had the smallest observed worst-case normalized loss across the four

criteria. During the analytical bridge, recorded telemetry contained no non-zero Memory Grants Pending samples or physical low-memory flags, and maximum container memory remained below the 4.75 GiB operational guard. Because the TPROC-H bridge used one matched seed and the formal TPROC-C points were interpreted descriptively, the result is not a universal optimum. The findings support treating cross-workload configuration transfer as a hypothesis that requires controlled validation rather than as an automatic reuse of a previously successful setting.

Keywords: Database configuration, Workload transfer, Memory optimization, SQL Server, Operational telemetry, Normalized loss.

INTRODUCTION

Modern database systems expose configuration controls for memory, parallel execution, caching, and resource management. These controls can materially change throughput and latency, but their effects are rarely constant across workloads. Learning-based tuners such as OtterTune, CDBTune, and QTune were developed because the number and interaction of database knobs make manual tuning difficult (Van Aken et al., 2017; Zhang et al., 2019; Li et al., 2019). Later systems made workload context more explicit. WATuning adapts recommendations to changing workload characteristics, CGPTuner treats the workload as contextual information, and CDBTune+ evaluates adaptation across workloads and hardware environments (Ge et al., 2021; Cereda et al., 2021; Zhang et al., 2021). The common implication is that a configuration is not inherently good; it is good relative to a workload, a metric, and an execution environment.

Memory configuration makes this problem concrete. SQL Server uses max server memory to bound memory managed by the database engine, especially the buffer pool, but the setting is not an absolute cap on every allocation made by the SQL Server process. Microsoft therefore recommends that it be interpreted together with host-level memory needs and allocations outside its direct control (Microsoft, 2026). A larger value can reduce avoidable memory pressure, yet it does not guarantee better workload performance. The response can be non-monotonic because the database state, query mix, parallel execution, and competing resource demands change the value of additional buffer capacity.

A second difficulty is that workload classes reward different behavior. HammerDB TPROC-C represents a derived online transaction processing workload, whereas TPROC-H is a fair-use derivation of the TPC-H decision-support workload and executes a stream of 22 complex analytical queries (HammerDB, 2026a, 2026b). The measurements in this study are therefore HammerDB workload results and are not official TPC-C or TPC-H benchmark scores. Transaction throughput and tail latency may favor a different memory region from large analytical scans and joins. Directly carrying a setting from one workload into the other can consequently create an untested assumption of transferability.

The present study asks a deliberately narrow question: does the memory point selected from a controlled transaction-oriented sweep remain defensible when the workload changes to

analytical processing? This is distinct from searching the full database configuration space. The analysis holds analytical parallelism settings fixed, compares the same five memory levels, and uses operational telemetry to determine whether the observed performance occurred without recorded memory-pressure warnings. A newly derived normalized-loss view then expresses the cost of each memory choice relative to the best observed value in four performance criteria. This worst-case-loss perspective follows the general logic of regret-based decisions, which evaluate an action by its shortfall from the best action under each considered condition (Savage, 1951), while remaining descriptive because the experimental replication is limited.

The contribution is twofold. First, the study provides a controlled bridge between transaction-oriented and analytical evidence instead of assuming that a memory choice transfers automatically. Second, it demonstrates a compact decision rule that preserves multiple performance criteria without collapsing them into an arbitrary weighted average. The aim is not to declare a universal optimum, but to show how an existing configuration can be challenged before it is reused under a different workload.

MATERIALS AND METHOD

Controlled environment and workloads

Experiments were conducted with Microsoft SQL Server 2022 Developer Edition, RTM-CU26 (16.0.4265.3), in a container restricted to four CPUs and 5 GiB of memory. The database engine was evaluated with HammerDB 6.0. Known database states were restored from golden backups before controlled blocks; wait statistics were cleared, and analytical runs started from controlled cold-cache states. These controls were used to reduce contamination from persistent cache contents, accumulated waits, and state drift. The design reflects recent methodological recommendations that auto-tuning results should state the environment, baseline, tuning budget, and treatment of stochastic variation (Willemsen et al., 2024).

Table 1. Controlled testbed and cross-workload memory protocol.

Component	Controlled setting or protocol
Database engine	Microsoft SQL Server 2022 Developer Edition, RTM-CU26 (16.0.4265.3)
Resource envelope	4 CPUs; 5 GiB container memory; SQL Server memory limit 4096 MB
TPROC-C	50 warehouses; 8 active virtual users; 3 min ramp-up; 10 min measurement
TPROC-H	Scale factor 10; rowstore; 22-query set; approximately 32.9 GB allocated database
Compared memory values	2048, 2560, 3072, 3328, and 3584 MB
Analytical controls	Seed 20260913; MAXDOP 4; cost threshold for parallelism 5
State control	Golden-backup restore; cold cache; cleared wait statistics
Operational signals	Memory Grants Pending, physical low-memory flag, CPU p95, runnable tasks, and cgroup memory

Transaction-oriented memory characterization

The transaction-oriented stage evaluated five explicit max server memory values from 2048 to 3584 MB. The primary criterion was new orders per minute (NOPM), with p95 new-order latency retained as a complementary tail-latency criterion. The formal sweep was interpreted descriptively because the retained summary does not support an independent sampling distribution for every explicit point. The memory value with the highest observed throughput was treated as the candidate operating point, while the latency result was preserved to expose any throughput-latency trade-off.

Analytical memory bridge and telemetry

The same five memory values were next evaluated under TPROC-H. Only memory changed: MAXDOP was fixed at 4, the cost threshold for parallelism was fixed at 5, and all runs used seed 20260913. Each run executed the complete 22-query set. The primary analytical outcome was total query-set completion time; the geometric mean of individual query times was used as a second criterion that reduced domination by the longest queries. The bridge was designed as a controlled challenge to the transaction-derived setting, not as a replicated analytical optimization.

Runtime telemetry included CPU utilization, runnable tasks, Memory Grants Pending, the SQL Server physical low-memory flag, and container-level memory consumption. A 4.75 GiB guard was defined inside the 5 GiB container. Because max server memory does not bound every process allocation, the configured value and total container memory were evaluated together (Microsoft, 2026). Safety statements refer specifically to the recorded telemetry samples; they do not imply continuous observation between samples.

Normalized cross-workload loss

To compare metrics with different units, each observation was converted to a percentage gap from the best observed value within that metric. For throughput, the loss was 100 multiplied by the difference between the maximum NOPM and the observed NOPM, divided by the maximum NOPM. For latency and analytical times, the excess was 100 multiplied by the difference between the observed value and the minimum value, divided by that minimum. Four gaps were thus obtained for each memory setting: TPROC-C throughput loss, TPROC-C p95-latency excess, TPROC-H query-set-time excess, and TPROC-H geometric-mean-time excess. The largest of the four was reported as the observed worst-case normalized loss. No weights were introduced, and the statistic was used only as a transparent descriptive screen.

RESULTS AND DISCUSSION

Different workloads produced different memory-response shapes

The TPROC-C sweep showed a non-monotonic memory response. Increasing the setting from 2048 to 3072 MB raised throughput from 48,399 to 61,616 NOPM, a 27.3% increase, while p95 new-order latency fell from 8.968 to 6.524 ms. The lowest tail latency, 6.177 ms, occurred at 3328 MB, but throughput declined to 59,260 NOPM. At 3584 MB, throughput fell further to 55,153 NOPM and p95 latency rose to 6.592 ms. Additional configured memory

therefore did not yield monotonic improvement, and the best transaction throughput and best tail latency occurred at different settings.

The analytical bridge also produced a non-monotonic ordering, but not the same curve. Query-set times were 78, 83, 75, 81, and 79 s at 2048, 2560, 3072, 3328, and 3584 MB, respectively. The corresponding geometric means were 2.414, 2.580, 2.214, 2.495, and 2.442 s. Thus, 3072 MB was the best observed analytical point under the matched seed, while the transaction-latency winner at 3328 MB was 8.0% slower in total analytical time and 12.7% slower in geometric-mean query time. This difference illustrates why transfer should be tested against the target workload rather than inferred from a source-workload metric. Workload-aware tuners reach a similar conclusion: configuration effectiveness depends on the current workload and may change as workload characteristics change (Ge et al., 2021; Cereda et al., 2021).

Table 2. Raw performance, operational telemetry, and observed worst-case normalized loss.

Memory (MB)	NOPM	p95 latency (ms)	TPROC-H total (s)	Geometric mean (s)	Max cgroup memory (GiB)	MGP / physical-low	Worst-case loss (%)
2048	48,399	8.968	78	2.414	3.671	0 / 0	45.2
2560	53,529	7.249	83	2.580	3.549	0 / 0	17.4
3072	61,616	6.524	75	2.214	3.749	0 / 0	5.6
3328	59,260	6.177	81	2.495	3.974	0 / 0	12.7
3584	55,153	6.592	79	2.442	4.052	0 / 0	10.5

MGP: maximum recorded Memory Grants Pending. Physical-low: whether the SQL Server physical low-memory flag was observed.

The normalized-loss view favors 3072 MB without hiding the latency trade-off

Figure 1 compares the gap from the best observed value in each of the four performance criteria. At 3072 MB, the throughput, analytical query-set time, and analytical geometric mean all had zero observed loss. Its only shortfall was a 5.6% p95-latency excess relative to the 3328 MB latency minimum. The resulting worst-case loss was 5.6%, lower than 10.5% at 3584 MB, 12.7% at 3328 MB, 17.4% at 2560 MB, and 45.2% at 2048 MB.

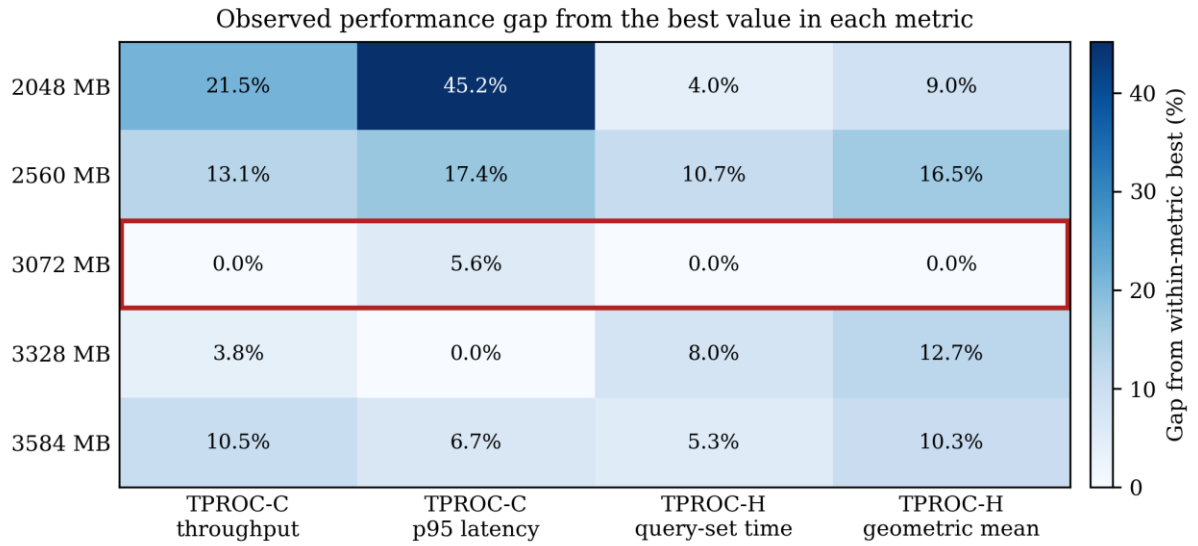


Figure 1. Cross-workload normalized performance loss by memory setting. Each cell is the percentage gap from the best observed value in that metric; lower values are better. The red outline identifies the retained 3072 MB setting. Values are descriptive and do not represent confidence intervals.

This result is stronger than selecting 3072 MB from throughput alone, because the same setting remained close to the best observed value across both workload classes and all four criteria. It also avoids a misleading claim of universal dominance. The 3328 MB setting still had a genuine advantage in TPROC-C p95 latency. If tail latency were the sole service objective, that setting could be preferred despite its lower throughput and slower analytical execution. The worst-case-loss screen instead answers a different question: which tested value had the smallest largest observed penalty when no single performance criterion was allowed to erase the others? Under this descriptive criterion, 3072 MB was the most balanced tested value.

The finding also explains why a single weighted score was avoided. Weights would require an application-specific judgment about the relative value of NOPM, milliseconds, and analytical completion time. The maximum normalized loss is not free of assumptions—it depends on the selected metrics and observed comparison set—but its decision logic remains visible. This transparency is valuable in small experimental budgets, where numerical precision can otherwise suggest more certainty than the data support.

Operational telemetry supports feasibility but not universal safety

Performance transfer is useful only if the target workload remains within an acceptable operating envelope. In the recorded TPROC-H telemetry, Memory Grants Pending remained zero and the physical low-memory flag was not asserted at any of the five memory settings. Maximum observed container memory ranged from 3.549 to 4.052 GiB, remaining below the 4.75 GiB guard (Figure 2). The 3072 MB point combined the shortest query-set time with a maximum recorded container footprint of 3.749 GiB.

The telemetry should be interpreted narrowly. First, absence of a warning in sampled measurements is not proof that no transient event occurred between samples. Second, remaining below a local guard does not demonstrate safety on other hardware or under concurrent production activity. Third, lower memory consumption is not automatically better: the 2560 MB run used the least recorded container memory but produced the slowest analytical completion time. The evidence therefore supports feasibility of the retained point in this controlled testbed, not a general rule that 3072 MB is safe or optimal for SQL Server deployments.

Implications and limitations

The practical implication is a validation sequence rather than a fixed parameter prescription. A source workload can identify a candidate region, but the candidate should be replayed under the target workload while unrelated settings are held constant. Multiple target metrics should then be preserved, and the performance result should be read together with operational telemetry. This sequence complements automatic tuning systems that adapt models or policies to workload context (Zhang et al., 2021; Ge et al., 2021; Cereda et al., 2021). It is especially useful when the evaluation budget is too small to justify a broad claim of global optimality.

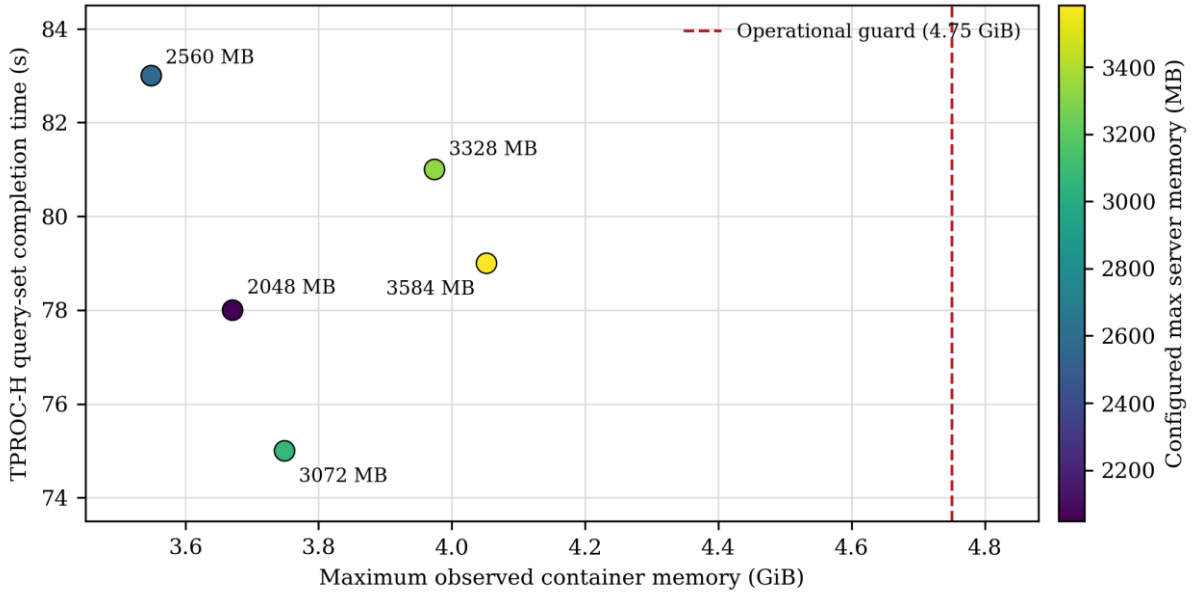


Figure 2. Analytical query-set completion time versus maximum observed container memory in the matched-seed TPROC-H bridge. All five runs had recorded MGP = 0 and no physical low-memory flag. The dashed line shows the 4.75 GiB operational guard within the 5 GiB container.

Several limitations bound the result. The study used one SQL Server version, a four-CPU and 5 GiB container, one TPROC-C protocol, and one TPROC-H scale factor. The analytical bridge used a single matched seed, and the retained formal TPROC-C points were treated descriptively rather than as replicated estimates. The normalized-loss matrix is therefore a secondary analysis of observed values, not an inferential comparison. The memory bridge also fixed MAXDOP at 4 and the cost threshold at 5, so interactions with other parallelism

settings were intentionally outside the scope of this paper. Finally, TPROC-C and TPROC-H are controlled workload models and do not reproduce every property of mixed, time-varying production traffic.

These constraints are central to the interpretation. The analysis shows that 3072 MB survived one carefully defined transfer test; it does not show that the value will transfer to larger servers, other database sizes, different storage systems, or production concurrency. Further validation would normally require additional matched seeds and environments. In the present frozen experimental package, the appropriate scientific conclusion is a conditional operating point supported by converging observations, not a universal optimum.

CONCLUSION

This study examined whether a SQL Server memory setting selected under a transaction-oriented workload could be retained under an analytical workload. The response was not monotonic in either workload, and the best TPROC-C tail-latency setting did not provide the best TPROC-H performance. Nevertheless, 3072 MB produced the highest observed transaction throughput and the shortest analytical query-set and geometric-mean query times. A newly derived normalized-loss analysis made the trade-off explicit: 3072 MB had a 5.6% p95-latency gap from the within-metric minimum but the smallest worst-case loss across all four criteria.

Recorded analytical telemetry contained no non-zero Memory Grants Pending samples or physical low-memory flags, and container memory remained below the local operational guard. These observations support the feasibility of the setting in the defined testbed, while the single-seed bridge and descriptive source-workload sweep prevent a claim of universal optimality. The main conclusion is therefore methodological: a configuration that succeeds under one workload should be treated as a candidate hypothesis and challenged under the target workload with controlled execution, multiple performance criteria, and operational telemetry.

DATA AND CODE AVAILABILITY

The processed benchmark tables, run-level records, analysis scripts, figure-generation code, experiment logs, provenance documentation, and SHA-256 integrity records used for this analysis are retained in the frozen supporting package. Distribution will follow applicable institutional confidentiality, anonymization, and data-sharing permissions.

REFERENCES

Cereda, S., Valladares, S., Cremonesi, P. & Doni, S. (2021). CGPTuner: A contextual Gaussian process bandit approach for the automatic tuning of IT configurations under varying workload conditions. Proceedings of the VLDB Endowment, 14(8), 1401-1413. https://doi.org/10.14778/3457390.3457404.

Ge, J.-K., Chai, Y.-F. & Chai, Y.-P. (2021). WATuning: A workload-aware tuning system with attention-based deep reinforcement learning. Journal of Computer Science and Technology, 36(4), 741-761. https://doi.org/10.1007/s11390-021-1350-8.

HammerDB. (2026a). What is the TPC and the TPROC-C workload derived from TPC-C? https://hammerdb.com/docs/ch03s02.html (accessed 22 October 2026).

HammerDB. (2026b). What is TPROC-H derived from TPC-H? https://hammerdb.com/docs/ch11s01.html (accessed 22 October 2026).

Li, G., Zhou, X., Li, S. & Gao, B. (2019). QTune: A query-aware database tuning system with deep reinforcement learning. Proceedings of the VLDB Endowment, 12(12), 2118-2130. https://doi.org/10.14778/3352063.3352129.

Microsoft. (2026). Server memory configuration options - SQL Server. Microsoft Learn. https://learn.microsoft.com/en-us/sql/database-engine/configure-windows/server-memory-server-configuration-options (accessed 22 October 2026).

Savage, L. J. (1951). The theory of statistical decision. Journal of the American Statistical Association, 46(253), 55-67. https://doi.org/10.1080/01621459.1951.10500768.

Transaction Processing Performance Council. (2026). Current TPC benchmark specifications: TPC-C and TPC-H. https://www.tpc.org/tpc_documents_current_versions/current_specifications5.asp (accessed 22 October 2026).

Van Aken, D., Pavlo, A., Gordon, G. J. & Zhang, B. (2017). Automatic database management system tuning through large-scale machine learning. Proceedings of the 2017 ACM International Conference on Management of Data, 1009-1024. https://doi.org/10.1145/3035918.3064029.

Willemsen, F.-J., Schoonhoven, R., Filipovič, J., Tørring, J. O., van Nieuwpoort, R. & van Werkhoven, B. (2024). A methodology for comparing optimization algorithms for auto-tuning. Future Generation Computer Systems, 159, 489-504. https://doi.org/10.1016/j.future.2024.05.021.

Zhang, J., Liu, Y., Zhou, K., Li, G., Xiao, Z., Cheng, B., Xing, J., Wang, Y., Cheng, T., Liu, L., Ran, M. & Li, Z. (2019). An end-to-end automatic cloud database tuning system using deep reinforcement learning. Proceedings of the 2019 International Conference on Management of Data, 415-432. https://doi.org/10.1145/3299869.3300085.

Zhang, J., Zhou, K., Li, G., Liu, Y., Xie, M., Cheng, B. & Xing, J. (2021). CDBTune+: An efficient deep reinforcement learning-based automatic cloud database tuning system. The VLDB Journal, 30(6), 959-987. https://doi.org/10.1007/s00778-021-00670-9.

THE EFFECT OF USING DIFFERENT TYPES OF BORON FUEL ADDITIVES ON ENGINE PERFORMANCE AND EXHAUST EMISSIONS IN A GASOLINE ENGINE

İbrahim Akdeniz
Selçuk University, Graduate School of Natural and Applied Sciences, Department of Mechanical Engineering, Konya, Türkiye
ORCID ID: 0009-0001-3629-3541

Halil Erdi Gülcan
Assoc. Prof., Selçuk University, Fakulty of Technology, Department of Mechanical Engineering, Konya, Türkiye
ORCID ID: 0000-0002-2328-5809

Samet Çelebi
Assoc. Prof., Sakarya University of Applied Sciences, Arifiye Vocational School, Motor Vehicles and Transportation Technologies Department, Sakarya, Türkiye
Automotive Technologies Application and Research Center, Sakarya University of Applied Sciences, Sakarya, Türkiye
ORCID ID: 0000-0002-4616-3935

Emrah Arda
Asst. Prof., Sakarya University of Applied Sciences, Arifiye Vocational School, Department of Machinery and Metal Technologies, Sakarya, Türkiye
Automotive Technologies Application and Research Center, Sakarya University of Applied Sciences, Sakarya, Türkiye
ORCID ID: 0000-0002-5496-3764

ABSTRACT

The widespread use of internal combustion engines worldwide and the increasing environmental impacts associated with the use of fossil fuels in these engines necessitate the development of alternative fuels and innovative fuel additives. In this study, the effects of using borate esters with different molecular structures as fuel additives on the engine performance and exhaust emissions of a spark-ignition gasoline engine were experimentally investigated. Three different borate esters, namely triethyl borate (TEB), trimethyl borate (TMB), and tri-n-octyl borate (TOB), were used as fuel additives. Each additive was blended with gasoline at a concentration of 1%. The aim of this study was to investigate and compare the effects of borate esters with different molecular structures on specific fuel consumption (SFC), brake thermal efficiency (BTE), and hydrocarbon (HC), carbon monoxide (CO), carbon dioxide (CO2), and nitrogen oxide (NO_x) emissions. The experiments were conducted at a constant engine speed under different engine load conditions. The results showed that the use of TEB in gasoline reduced brake-specific fuel consumption as the engine load increased, achieving an improvement of 7.6% at full load. The highest brake thermal efficiency of 22.7% was also recorded with the TEB-blended fuel under full-load conditions. Although increases

in HC and CO emissions were observed with the use of TEB, TMB, and TOB as fuel additives, the TMB- and TOB-blended fuels resulted in reductions of more than 90% in NO_x emissions.

Keywords: Engine performance, Exhaust emissions, Fuel additive, Triethyl borate, Trimethyl borate, Tri-n-octyl borate.

INTRODUCTION

The continued widespread use of internal combustion engines in transportation and power generation systems underscores the ongoing importance of research aimed at reducing fossil fuel consumption and the associated emissions (Khalili et al., 2019; Malik et al., 2024). The physical and chemical properties of fuels used in spark-ignition engines influence fuel–air mixture formation, combustion characteristics, engine performance, and exhaust emissions (Huo et al., 2022; Heejung et al., 2005; Garrett et al., 2016). Therefore, investigating the effects of fuel additives on fuel properties and engine operating characteristics remains an important research area, particularly for additives that can be implemented in existing engine technologies without requiring significant structural modifications (Bolat et al., 2026).

The addition of fuel additives to the base fuel at specific proportions can alter its physical and chemical properties, thereby influencing the combustion process and modifying the engine's performance and emission characteristics (Zhang et al., 2023). In this context, boron-based compounds have emerged as one of the fuel additive groups investigated due to their high energy content and potential effects on combustion behavior (Hu et al., 2022; Sezer et al., 2025; Ojha et al., 2018). However, the challenges associated with the ignition and combustion of elemental boron when used directly as a fuel have led researchers to investigate alternative boron compounds (Yang et al., 2023). Boron esters are among these compounds and are considered potential fuel additives that may alter combustion characteristics owing to the boron and oxygen atoms in their molecular structures (Gültekin et al., 2023).

The literature contains only a limited number of studies investigating trimethyl borate (TMB) and triethyl borate (TEB) as boron ester-based fuel additives. The available studies are summarized below.

Direct experimental investigations have been conducted on the use of TMB as a fuel additive in gasoline-fueled spark-ignition engines. Gültekin et al. (2023) conducted experiments using a single-cylinder, four-stroke spark-ignition engine fueled with gasoline containing TMB at mass fractions of 1%, 1.5%, 2%, and 2.5%. The experiments were performed at an engine speed of 2500 rpm under 25%, 50%, 75%, and full-load conditions, with combustion characteristics, engine performance, and exhaust emissions evaluated simultaneously. The results showed reductions in CO and HC emissions following TMB addition, while performance parameters, including specific fuel consumption and thermal efficiency, also exhibited variations depending on the additive concentration. The combustion behavior of TMB and TEB has been investigated not only through engine experiments but also at the droplet scale. Yontar et al. (2023) experimentally examined the combustion characteristics of

TMB and TEB droplets, along with those of gasoline and diesel fuel. The results revealed that TMB exhibited a shorter ignition delay and a shorter combustion duration than the other fuels. Furthermore, the highest flame temperature was observed for the TMB droplet. In a recent study directly comparing TMB and TEB in a gasoline-fueled spark-ignition engine, Sofuoğlu et al. (2026) conducted experiments using gasoline blended with each boron ester at concentrations of 1%, 5%, and 10%. The experiments were performed at an engine speed of 2800 rpm and throttle openings of 75% and 100%. The results indicated that the addition of TMB and TEB led to reductions in engine torque and brake mean effective pressure, as well as increases in fuel consumption, depending on the operating conditions investigated. In contrast, considerable reductions in CO and unburned HC emissions were achieved, whereas NO_x emissions exhibited an increasing trend at higher additive concentrations. Furthermore, TMB was reported to have a more pronounced effect on emission reduction than TEB. In another study investigating TMB and TEB in a different engine application, Kutlubay and Gültekin (2025), examined the effects of adding these boron esters to JP-8 fuel on the performance and emission characteristics of a turbojet engine. In addition to neat JP-8 fuel, various fuel blends containing TMB and TEB were tested, and thrust, specific fuel consumption, exhaust gas temperature, and several exhaust emissions were evaluated. The results demonstrated that boron-based additives could influence engine performance and emission characteristics, with the observed effects depending on the operating conditions and the type of additive used. Doğu et al. (2024) examined engine performance and exhaust emissions by blending boron derivatives, including borax pentahydrate, anhydrous borax, and boric acid, with gasoline in a commercial i-DSI spark-ignition engine. The results indicated that fuels containing these boron derivatives produced varying effects on engine parameters, such as engine torque, volumetric efficiency, and specific fuel consumption, compared with the reference gasoline. Furthermore, reductions in HC and NO_x emissions were reported. The available literature on trioctyl borate (TOB) appears to be more limited than that on TMB and TEB. Şimşek et al. (2021) investigated a multicomponent additive system called Octamix, which contains TOB as a boron source, in a gasoline-fueled spark-ignition engine. Octamix was formulated using trioctyl borate, ammonia borane, and ethyl alcohol and was added to gasoline at different volumetric concentrations. The study evaluated brake thermal efficiency, brake-specific fuel consumption, and CO, HC, CO_2, and NO_x emissions. The results indicated that an Octamix concentration of 0.5% generally provided more favorable outcomes.

When the above literature summaries are evaluated, TMB has been directly investigated at different concentrations in gasoline-fueled spark-ignition engines, TMB and TEB have been evaluated together in the same engine study, and TOB has been examined as part of a multicomponent additive system. However, studies comparatively investigating TMB, TEB, and TOB, which possess different alkyl chain structures, as individual additives in the same reference fuel using the same experimental engine and operating conditions appear to be limited. In particular, determining how differences in the alkyl groups of TMB, TEB, and

TOB influence engine performance and exhaust emissions within a common experimental framework would enable a more reliable comparison of the effects of different boron esters.

The aim of this study is to experimentally compare the effects of TMB, TEB, and TOB, which possess different alkyl chain structures, on the engine performance and exhaust emissions of a gasoline-fueled spark-ignition engine. In this context, neat gasoline (100%) was used as the reference fuel, and four test fuels were prepared by individually adding TMB, TEB, and TOB to gasoline at a volumetric concentration of 1%. Brake-specific fuel consumption, brake thermal efficiency, and exhaust gas temperature were evaluated as engine performance parameters, while CO, HC, NO_x, and CO_2 were assessed as exhaust emission parameters. Thus, by investigating TMB, TEB, and TOB as individual additives in the same gasoline engine under identical experimental conditions, this study aims to provide a comparative assessment of the effects of different boron esters on engine performance and exhaust emissions.

MATERIALS AND METHOD

Experimental Setup and Measurement Systems

The experimental studies were conducted using a spark-ignition engine test rig located in the Engine Testing and Simulation Laboratory of Arifiye Vocational School, Sakarya University of Applied Sciences. A Honda GX200 gasoline engine, which is widely used in generator applications, was employed in the experiments. The engine is a single-cylinder, air-cooled, four-stroke engine. The experimental engine setup is presented in Fig. 1, and its technical specifications are provided in Table 1.

Table 1. Technical specifications of the GX200 gasoline engine (Özker and Çelebi, 2025).

Technical specification	**GX200 gasoline engine**
Engine type	Spark ignition, 4-stroke
Cylinder number	1-cylinder
Volume	196 cm^3
Bore diameter	68 mm
Stroke diameter	54 mm
Compression ratio	8.5:1
Max. Torque and power	13.24 N·m @ 2500 rpm and 6.5 Hp @3600 rpm

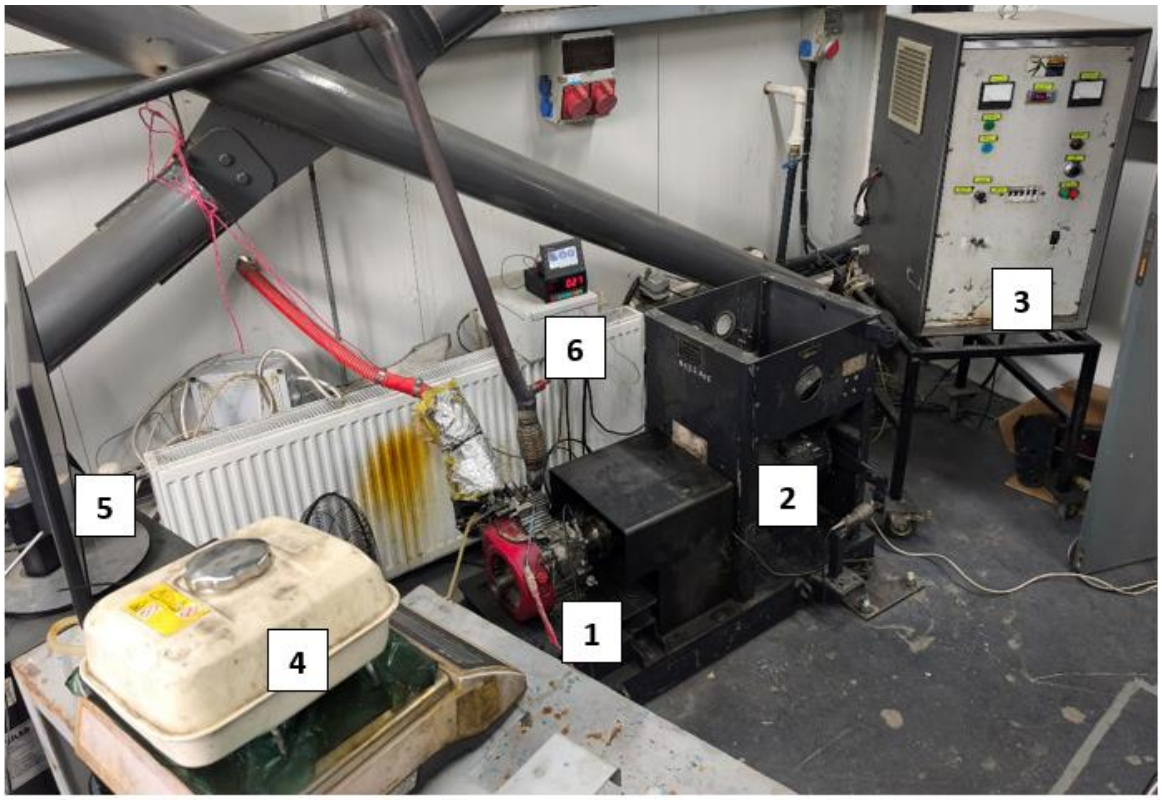


Fig. 1. View of the experimental Honda GX200 engine setup.
(1-Gasoline engine; 2-dynamometer; 3-Control panel; 4-Fuel precision balance; 5-emissions analyser; 6-Temperature measurement system)

A dynamometer was used to apply engine load and determine the engine performance parameters. Exhaust emissions, including CO, CO_2, NO_x, and HC, were measured using a Bilsa exhaust gas analyser. A heated sampling line was employed to prevent condensation, and the analyser was calibrated before each test. Fuel consumption was determined using a high-precision balance with a measurement accuracy of 0.1 g. Exhaust gas temperature was recorded using a K-type thermocouple and a data acquisition system. The measurement accuracies of the instruments used in the experiments are presented in Table 2.

Table 2. Measuring instruments used and their precision.

Measurement systems	**Devices**	**Accuracy**
Dynamometer	Load cell	0.2 Nm
Rotation measurement system	Digital tachometer	0.5%
Exhaust gas analyser	Exhaust emission devices	1% of full scale
Fuel consumption measurement system	Precision balance	0.1 g
Temperature measurement system	K-type thermocouple	0.5%

Test Fuels

Gasoline was used as the base fuel in the experiments and was obtained from a local fuel station. The physical and chemical properties of gasoline are presented in Table 3. Trimethyl borate (TMB), triethyl borate (TEB), and tri-n-octyl borate (TOB) were used as boron-based fuel additives. These boron ester additives were obtained from a chemical supplier.

Table 3. Properties of gasoline fuel (Özer 2021).

Properties	**Gasoline**
Density (kg/m3)	746
Lower Heating Value (KJ/kg)	43590
Octane Rating	95
Stoichiometric Air/Fuel Ratio	14.7

Experimental Procedure

Before each fuel test, the engine was operated on neat gasoline to eliminate any residual fuel from the previous blend in the fuel lines. Prior to testing, the engine was warmed up using neat gasoline for 10 min to reach a stable operating temperature. The experiments were conducted at a constant engine speed of 2500 rpm, corresponding to the engine's maximum torque, while the load was adjusted using a dynamometer in increments of approximately 25%, from no-load to full-load conditions. At each load level, a waiting period of 2 min was allowed for the engine to reach steady-state operation, after which fuel consumption, exhaust gas temperature, and exhaust emissions were recorded. To ensure data reliability, each test was repeated three times, and the results were evaluated using the average values. The experiments were initially conducted using neat gasoline. Subsequently, trimethyl borate was added to gasoline at a volumetric concentration of 1%, and tests were performed at a constant engine speed under different load conditions. The same procedure was then repeated using gasoline containing 1% triethyl borate by volume. Finally, the experiments were completed using gasoline blended with 1% tri-n-octyl borate by volume.

Table 4. Fuels used in experiments, abbreviations, and test matrix.

Case	**Load**	**Main Fuel**	**Fuel additive**	**Mixing ratio**	**Abbreviation**
1	%0, %25, %50, %75 and %100	Gasoline	-	-	Gasoline
2	%0, %25, %50, %75 and %100	Gasoline	triethyl borate ($C_6H_{15}BO_3$)	Gasoline 99% + triethyl borate 1%	TEB
3	%0, %25, %50, %75 and %100	Gasoline	trimethyl borate ($C_3H_9BO_3$)	Gasoline 99% + trimethyl borate 1%	TMB
4	%0, %25, %50, %75 and %100	Gasoline	tri-n-octyl borate ($C_{24}H_{51}BO_3$)	Gasoline 99% + tri-n-octyl borate 1%	TOB

RESULTS AND DISCUSSION

Engine Performance

Figure 2 illustrates the effects of different boron-based fuel additives on the specific fuel consumption (SFC) of a gasoline engine under no-load and loaded operating conditions. The addition of trimethyl borate (TMB) and tri-n-octyl borate (TOB) to gasoline significantly

increased SFC. For instance, at 25% engine load, the highest SFC was recorded for the TMB-blended fuel, representing an increase of approximately 30% compared with neat gasoline. In contrast, the addition of triethyl borate (TEB) to gasoline reduced SFC, particularly at engine loads of 50%, 75%, and 100%. The greatest reduction in SFC was observed with TEB at 100% engine load, where SFC decreased by 7.6% relative to neat gasoline.

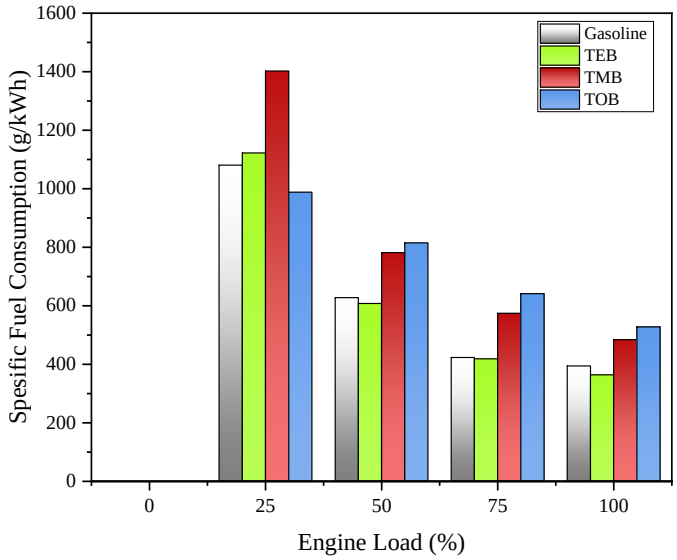


Fig. 2. Variation of SFC with different types of boron fuel additives.

Figure 3 illustrates the effects of different boron-based fuel additives on the brake thermal efficiency (BTE) of a gasoline engine under no-load and loaded operating conditions. The addition of boron-based additives to gasoline had a considerable effect on BTE. The lowest BTE of 4.2% was recorded for the TOB-blended fuel at 25% engine load, whereas the highest BTE of 7.4% was obtained with the TEB-blended fuel under the same load condition. As the engine load increased, BTE increased for all fuel blends, with the highest values observed at 100% engine load. At full load, the BTE values of G100, TEB, TMB, and TOB were 20.9%, 22.7%, 17.1%, and 7.8%, respectively.

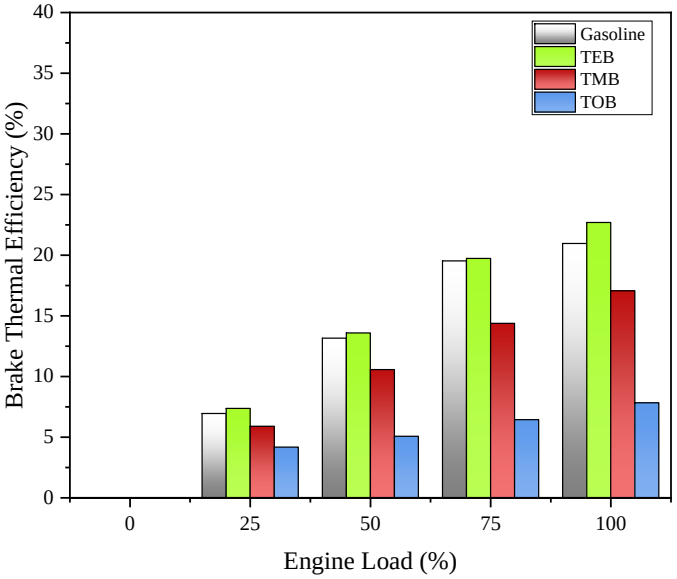


Fig. 3. Variation of BTE with different types of boron fuel additives.

Emissions

Figure 4 illustrates the effects of different boron-based fuel additives on CO emissions from a gasoline engine under no-load and loaded operating conditions. The addition of boron-based fuel additives to gasoline resulted in a considerable increase in CO emissions. The greatest increase was observed with the TOB-blended fuel, followed by the TMB-blended fuel. This increase in CO emissions can primarily be attributed to insufficient oxygen availability during combustion, which prevents the complete oxidation of carbon to CO_2, resulting in higher CO emissions. Furthermore, a decrease in combustion temperature may inhibit the conversion of CO to CO_2 by slowing down the oxidation reaction, thereby contributing to the substantial increase in CO emissions.

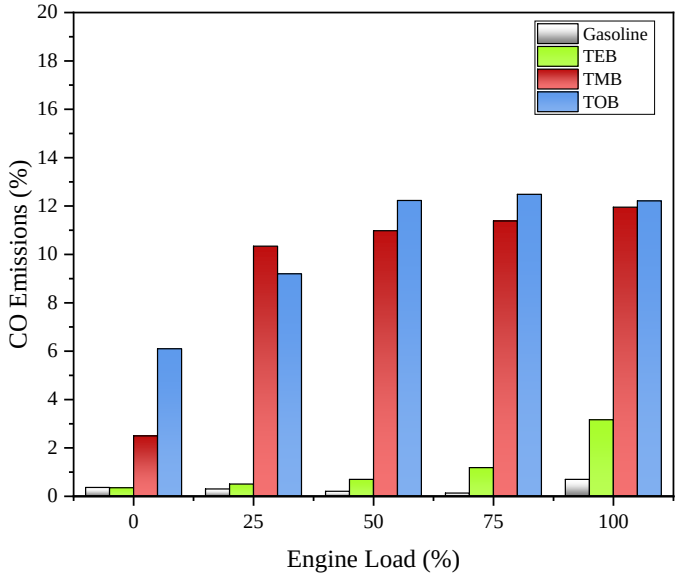


Fig. 4. Variation of CO emissions with different types of boron fuel additives.

Figure 5 illustrates the effects of different boron-based fuel additives on CO_2 emissions from a gasoline engine under no-load and loaded operating conditions. The boron-based additives had a noticeable influence on CO_2 emissions. Overall, the highest CO_2 emissions were recorded for neat gasoline and the TEB-blended fuel, whereas the addition of TMB and TOB to gasoline resulted in substantial reductions in CO_2 emissions. For instance, at 25% engine load, the CO_2 emission level obtained with neat gasoline was 9.54%, while the addition of TMB and TOB reduced CO_2 emissions by 21.5% and 18%, respectively. The reductions in CO_2 emissions achieved with TMB and TOB became even more pronounced at higher engine loads. At 100% engine load, CO_2 emissions decreased by 51.3% and 53.2% with TMB- and TOB-blended fuels, respectively, compared with neat gasoline.

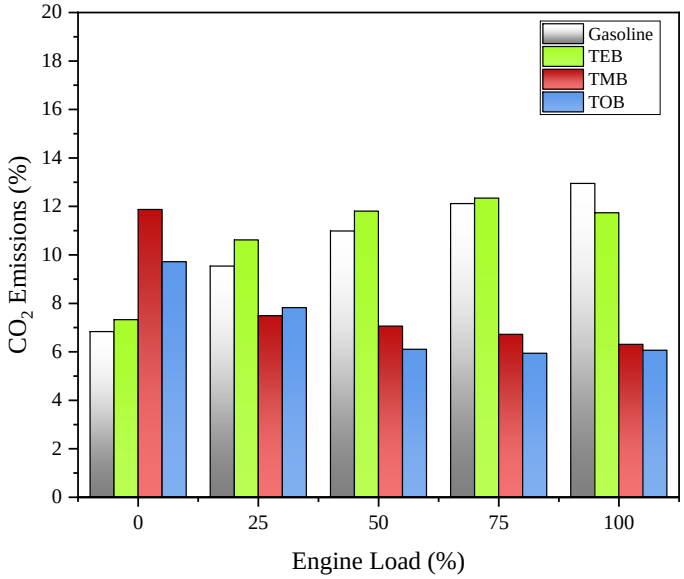


Fig. 5. Variation of CO_2 emissions with different types of boron fuel additives.

Figure 6 illustrates the effects of different boron-based fuel additives on HC emissions from a gasoline engine under no-load and loaded operating conditions. Under no-load conditions, HC emissions increased considerably with neat gasoline and the TEB-blended fuel. This behavior may be attributed to the relatively low combustion temperatures, which can hinder complete fuel oxidation. In contrast, the use of TMB- and TOB-blended fuels did not cause a pronounced increase in HC emissions under no-load conditions. However, as the engine load increased, HC emissions with these fuels became higher than those obtained with the other test fuels. This behavior may be associated with the relatively high fuel density, which could hinder complete vaporization and homogeneous fuel–air mixture formation. At higher engine loads, HC emissions generally remained below 400 ppm, primarily due to the higher combustion temperatures that promote more complete oxidation. Across the engine load range from 0% to 100%, the TEB-blended fuel reduced HC emissions by an average of 1.8% compared with neat gasoline, whereas the TMB- and TOB-blended fuels increased HC emissions by 34.3% and 26.1%, respectively.

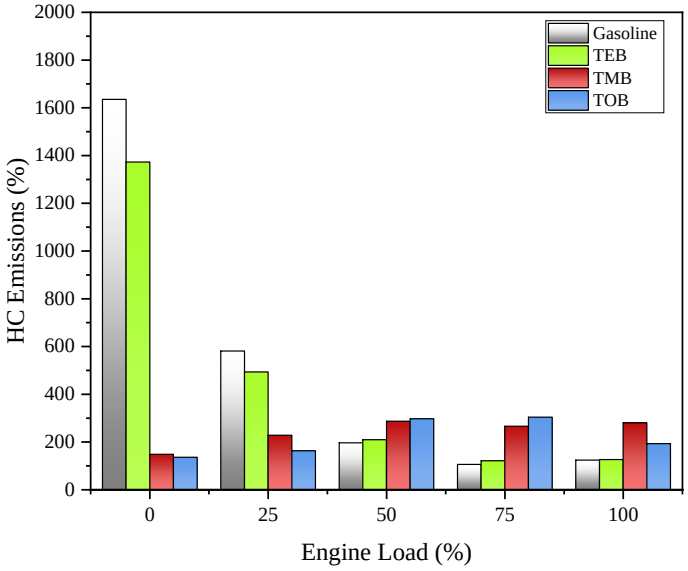


Fig. 6. Variation of HC emissions with different types of boron fuel additives.

Figure 7 illustrates the effects of different boron-based fuel additives on NO_x emissions from a gasoline engine under no-load and loaded operating conditions. As shown in the figure, the lowest NO_x emissions were recorded under no-load conditions, whereas increasing engine load resulted in a noticeable increase in NO_x emissions, particularly for neat gasoline and the TEB-blended fuel. Under no-load conditions, the relatively low local temperatures result in lower peak combustion temperatures, thereby limiting NO_x formation. As the engine load increases, local temperatures rise, leading to higher peak combustion temperatures and accelerating thermal NO_x formation. The highest NO_x emissions were recorded at 100% engine load. However, compared with neat gasoline, NO_x emissions decreased by 66.8%, 98.5%, and 99.1% with the TEB-, TMB-, and TOB-blended fuels, respectively.

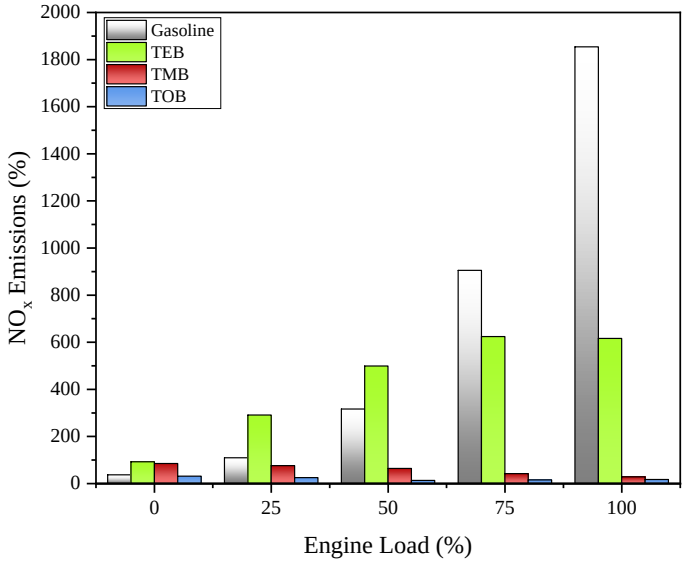


Fig. 7. Variation of NO_x emissions with different types of boron fuel additives.

CONCLUSION

In this study, the effects of different boron ester fuel additives blended with gasoline on engine performance and exhaust emissions were investigated. The main findings of the study are summarized below.

- The use of TEB as a fuel additive in the gasoline engine tended to reduce SFC, whereas the addition of TMB and TOB resulted in an increase in SFC.
- The TEB additive slightly improved BTE, while the use of TMB and TOB considerably reduced BTE.
- All three fuel additives significantly increased CO emissions, whereas TMB and TOB considerably reduced CO_2 emissions.
- The addition of TEB resulted in a slight reduction in HC emissions, while TMB and TOB increased HC emissions.
- The addition of TMB and TOB led to noticeable reductions in NOx emissions.

In conclusion, although the use of TEB as a gasoline additive improved engine performance, it did not provide substantial improvements in exhaust emissions. Therefore, investigating the effects of TEB in combination with oxygen-containing solvent alcohols would be valuable for further understanding its influence on engine performance and emission characteristics.

ACKNOWLEDGMENTS

This study was derived from the master's thesis entitled "*Investigation of the Effects of Different Types of Boron-Based Fuel Additives on the Performance and Emissions of a Spark-Ignition Engine*," prepared by İbrahim Akdeniz under the supervision of Assoc. Prof. Dr. Halil Erdi Gülcan. The authors gratefully acknowledge the Scientific Research Projects Coordination Unit of Selçuk University for its financial support (Project No.26201022) and Sakarya University of Applied Sciences for providing the experimental system and infrastructure support.

CONFLICT OF INTEREST STATEMENT

The authors declare no conflicts of interest.

REFERENCES

Bolat, R. B., Balgabekov, T., Rustembayev, A. ve Zharassov, S., 2026, Improving the performance of a vehicle's internal combustion engine using various types of additives, Eurasian Journal of Applied Engineering and Technology, 155 (2), 173–189.

Doğu, Y., Yontar, A. A., & Kantaroğlu, E. (2024). Experimental investigation of effects of single and mixed alternative fuels (gasoline, CNG, LPG, acetone, naphthalene, and boron derivatives) on a commercial i-DSI engine. Energy Sources, Part A: Recovery, Utilization, and Environmental Effects, 46(1), 12680-12699.

Garrett Parker, Stuart Bartley, Michael Nicholls. Two-Stroke Engine Cleanliness via a Fuel Additive. SAE: 2016-32-0048.

Gültekin, E., Calam, A., & Şahin, M. (2023). Experimental investigation of trimethyl borate as a fuel additive for a SI engine. Energy sources, part a: recovery, utilization, and environmental effects, 45(1), 419-433.

Heejung Jung, David B Kittelson, Michael R Zachariah.The influence of a cerium additive on ultrafine diesel particle emissions and kinetics of oxidation[J]. Combustion and Flame, 2005, 142(3): 276-288.

Hu, Y.; Wang, X.; Zhang, J.; et al. Encapsulated boron–based energetic spherical composites with improved

reaction efficiency and combustion performance. Chem. Eng. J. 2022, 433, 134478.

Huo, Y., Jing, X., Yin, Z., & Wu, M. (2022, June). Study on the effect of fuel additive on PFI gasoline engine performance and emissions. In *E3S Web of Conferences* (Vol. 360, p. 01036). EDP Sciences.

Khalili, S., Rantanen, E., Bogdanov, D., & Breyer, C. (2019). Global transportation demand development with impacts on the energy demand and greenhouse gas emissions in a climate-constrained world. Energies, 12(20), 3870.

Kutlubay, A., & Gültekin, E. (2025). Investigation of TMB and TEB as Fuel Additives for an Aerojet Engine. Fuel, 402, 135970.

Malik, M. A. I., Kalam, M. A., Abbas, M. M., Silitonga, A. S., & Ikram, A. (2024). Recent advancements, applications, and technical challenges in fuel additives-assisted engine operations. *Energy Conversion and Management*, *313*, 118643.

Sezer, İ., 2025, Effects of Boron Additive to Engine Fuels and Oils on Combustion, Performance and Emissions of Internal Combustion Engines, New Energy Exploitation and Application, 4 (1), 1–47.

Sofuoğlu, D., Değirmenci, H., Kantaroğlu, E. ve Yontar, A. A., 2026, Effects of boron-based fuel additives on sequential-ignition engine characteristics and emissions, International Journal of Ambient Energy, 47 (1), 2730195.

Şimşek, S., Uslu, S. ve Şimşek, H., 2022, Evaluation of the effect of a new alternative fuel containing boron and hydrogen on gasoline engine performance and emission responses, International Journal of Environmental Science and Technology, 19 (6), 4913–4922.

Ojha, P.K.; Karmakar, S. Boron for liquid fuel engines–A review on synthesis, dispersion stability in liquid fuel, and combustion aspects. Progress Aerosp. Sci. 2018, 100, 18–45.

Özer, S. (2021). Effects of alternative fuel use in a vehicle with TSI (turbocharged direct-injection spark-ignition) engine technology. *International Journal of Green Energy*, *18*(12), 1309-1319.

Özker, H., & Çelebi, S. (2025). Effect of the use of methanol, toluene and nitromethane mixtures as fuel additives in a gasoline engine on engine performance and exhaust emissions. *Fuel*, *391*, 134819.

Yang, D., Liu, R., Li, W. ve Yan, Q.-L., 2023, Recent advances on the preparation and combustion performances of boron-based alloy fuels, Fuel, 342, 127855.

Yontar, A. A., Sofuoğlu, D., Değirmenci, H., Ayaz, T. ve Üstün, D., 2023, Investigation of combustion characteristics on triethyl borate, trimethyl borate, diesel, and gasoline droplets, Energy, 266, 126440.

Zhang, X., Zhang, S., Zhao, Y., Liu, J., Zhang, S., Wen, M., & Liu, H. (2023). Effects of different additives on physicochemical properties of gasoline and vehicle performance. *Fuel Processing Technology*, *242*, 107668.

Tİ-6AL-4V ELI (GRADE 23) MALZEMENİN HELİSEL DALMA İLE CEP FREZELEME İŞLEMİNDE YÜZEY PÜRÜZLÜLÜĞÜ DEĞİŞİMİ VE TAKIM AŞINMASININ İNCELENMESİ

SURFACE ROUGHNESS AND TOOL WEAR IN HELICAL RAMPING POCKET MILLING OF TI-6AL-4V ELI (GRADE 23)

Deniz ÇOBAN ÖZKAN
Dr., Manisa Celal Bayar Üniversitesi, Hasan Ferdi Turgutlu Teknoloji Fakültesi, Makine Mühendisliği
Dr., Department of Mechanical Engineering, Hasan Ferdi Turgutlu Faculty of Technology, Manisa Celal Bayar University
ORCID ID: 0000-0002-8044-5952

Fikret SÖNMEZ
Dr., Manisa Celal Bayar Üniversitesi, Hasan Ferdi Turgutlu Teknoloji Fakültesi, Makine Mühendisliği
Dr., Department of Mechanical Engineering, Hasan Ferdi Turgutlu Faculty of Technology, Manisa Celal Bayar University
ORCID ID: 0000-0003-1718-892X

ÖZET

Talaşlı imalat sırasında zamana bağlı olarak takım aşınmasının meydana gelmesi ve yüzey pürüzlülüğünün giderek kötüleşmesi birçok durumda olağan bir sonuçtur. Özellikle titanyum alaşımları gibi işlenmesi zor malzemelerin işlenmesinde takım aşınması ve yüzey pürüzlülüğü değişimi daha belirgin olmaktadır. Bu çalışmada titanyum alaşımları arasında önemli bir yere sahip Ti-6Al-4V ELI (Grade 23) alaşımı kullanılarak helisel dalma ile cep frezeleme işlemi gerçekleştirilmiştir. Bu amaçla silindirik iş parçası, Ø4 mm yekpare karbür parmak freze kesici takım ile 70 m/dk kesme hızı, 1 mm eksenel talaş derinliği (ap=1 mm) ve 0,2 mm radyal talaş genişliği (ae=0,2 mm) kullanılarak işlenmiştir. Toplam 7 paso ile yapılan işlemlerde, her paso sonunda kesici takım aşınması incelenmiş ve iş parçası yüzey pürüzlülük değerleri analiz edilmiştir. Paso sayısı arttıkça takım aşınmasının arttığı ve yüzey pürüzlülüğünün kötüleştiği anlaşılmıştır.

Anahtar Kelimeler: Yüzey pürüzlülüğü, takım aşınması, Ti-6Al-4V ELI, helisel dalma, cep frezeleme, talaşlı imalat.

ABSTRACT

Progressive tool wear over machining time and the gradual deterioration of surface roughness are common outcomes in many machining operations. These changes in tool wear and surface roughness become more pronounced when machining difficult-to-cut materials such as titanium alloys. In this study, pocket milling of Ti-6Al-4V ELI (Grade 23), an important titanium alloy, was performed using helical ramping. For this purpose, a Ø4 mm solid carbide end mill was used to machine a cylindrical workpiece at a cutting speed of 70 m/min, with an axial depth of cut of 1 mm (ap = 1 mm) and a radial width of cut of 0.2 mm (ae = 0.2 mm).

The machining operation was carried out in a total of seven passes. Tool wear was examined and the surface roughness of the workpiece was analyzed at the end of each pass. The results showed that tool wear increased and surface roughness deteriorated with an increasing number of passes.

Keywords: Surface roughness, tool wear, Ti-6Al-4V ELI, helical ramping, pocket milling, machining.

GİRİŞ

Talaşlı imalat yüksek yüzey kalitesi erektiren fonksiyonel yüzeylerin üretiminde kullanılan başlıca yöntemlerden biridir. Özellikle fonksiyonel yüzeylerin istenen yüzey karakteristiğine sahip olması gerek endüstriyel olarak gerekse akademik olarak önemli bir araştırma alanıdır. Ancak talaşlı imalat sırasında kullanılan kesici takımlar iş parçası-kesici takım teması nedeniyle doğal olarak aşınma sürecine girer. Aşınma her ne kadar kaçınılmaz olsa da aşınmanın takibi ve mümkünse yavaşlatılması amacıyla yapılan bilimsel araştırmalar devam etmektedir [1].

Titanyum alaşımları yüksek mekanik dayanım özelliklerinin yanında aynı zamanda düşük yoğunluğa sahip olmaları ($d_{Ti\text{-}6Al\text{-}4V}$=4,43 g/cm³) nedeniyle özellikle çelik ($d_{Çelik}$=7,8 g/cm³) gibi endüstriyel metallere karşı çok iyi bir alternatif oluşturmaktadır. Ti6Al4V ELI (Grade 23), yaygın olarak kullanılan Ti6Al4V'nin (Grade 5) bir varyantı olup, daha az ara atom (oksijen ve karbon) içermektedir. Ti6Al4V ELI (Grade 23) üstün biyouyumluluğu ve korozyona karşı direnci nedeniyle biyomühendislik ve havacılıkta kullanılan başlıca malzemelerden biri haline gelmiştir [1-2].

Her ne kadar Ti6Al4V ELI malzeme talaşlı imalata uygun olsa da bu malzemenin işlenmesinde birçok zorlaştırıcı faktörün olması Ti6Al4V ELI malzemeyi işlemesi zor malzeme (hard-to-cut) sınıfına sokmaktadır. Ti6Al4V ELI düşük ısıl iletkenliğe sahip olması nedeniyle ısı birikiminin kesici takım üzerinde yoğunlaşmasına neden olur. Bu olumsuz etkinin yanında Ti6Al4V ELI malzemenin yüksek sıcaklıklarda dayanımını koruması, kimyasal reaktivitesi ve yığma kenar (BUE) oluşumuna yatkınlığı da talaşlı imalat işlemlerini zorlaştırmaktadır [3-5]. Bu nedenle Ti6Al4V ELI malzemenin işlenmesinde optimum değerlerin bulunması gereklidir.

İş parçalarında talaş alırken kullanılabilen birçok farklı talaşlı imalat yöntemi bulunmaktadır. Cep frezeleme işlemi ise kapalı bir alanda gerçekleştirilmesi nedeniyle talaş tahliyesinin zorluğu ve iş parçasına giriş (plunge) gibi birçok zorluğa neden olmaktadır. Bu zorlukları aşmak için kullanılabilecek yöntemlerden biri de helisel dalma (helical ramping) yöntemidir. Bu yöntemde, kesici takım kendi ekseni etrafında dönerken, aynı anda iş parçasına da helisel bir yörünge izleyerek girmektedir. Helisel frezeleme, iş parçasında konik ve karmaşık şekilli ceplerin oluşturulmasında kullanılır. Ayrıca, bu yöntem ile birçok geometri oluşturulabileceğinden takım değiştirme ihtiyacını azaltır [6]. Bu yöntemle daha iyi talaş tahliyesi, daha yüksek yüzey kalitesi ve daha düşük itme kuvvetleri elde edilebilir ve aşınma mekanizması daha iyi izlenebilir ve anlaşılabilir [7]. Helisel frezeleme aynı zamanda helik

delme işlemi içinde kullanılabileceğinden orbital delme olarak da tanımlanabilmektedir. Bu metot geleneksel delik delme işlemleri ile karşılaştırıldığında kompozit malzemelerde tabaka ayrılmasını ve termal hasarı önemli ölçüde azalttığı da görülmüştür [8].

Bir cep frezeleme yöntemi olarak kullanılan helisel frezeleme de yapılan kesme işlemi birçok parametreden etkilenmektedir [9-10]. Örneğin Pereira ve arkadaşları farklı kesme hızlarında 3° helis açısı ve 0,3 mm kesme derinliği ile işlemlerini gerçekleştirmiştir. Artan kesme hızının takım ömrünü ciddi şekilde azalttığını tespit etmişlerdir [10]. Ramezani ve arkadaşları helisel işlemenin, delik delmeye kıyasla çok düşük kesme kuvvetleri ve 2 kat daha iyi yüzey kalitesine ulaşabileceğini rapor etmişlerdir [11]. Wang ve arkadaşları artan kesme derinliğinin yüzey kalitesini kötüleştirdiğini, artan iş mili devir sayısının ise yüzey kalitesi üzerinde olumlu etkiye sahip olduğunu tespit etmişlerdir [12]. Kharka ve arkadaşlarının yapmış olduğu çalışma da ise artan talaşlı imalat işlemlerine bağlı olarak serbest yüzey aşınmasının gittikçe arttığını vurgulamışlardır [13].

Bu çalışmada, Ti-6Al-4V ELI (Grade 23) alaşımının helisel dalma ile cep frezelenmesinde her paso sonunda takım aşınması ve yüzey pürüzlülüğü (Ra ve Rz) incelenerek takım aşınmasının yüzey kalitesine etkisinin ortaya konulması amaçlanmıştır.

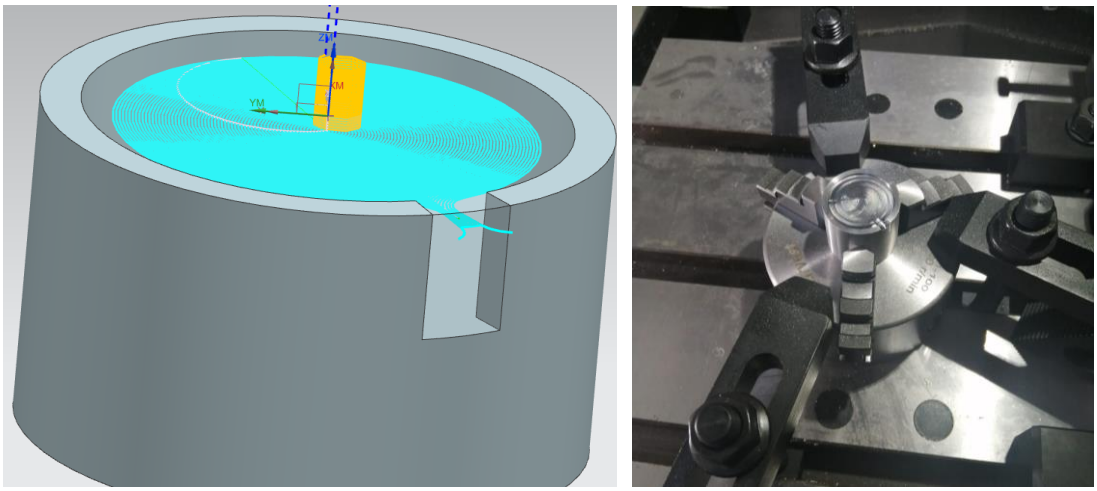
MATERYAL VE METOT

Bu çalışmada Ti6Al4V alaşımlarından olan Ti6Al4V ELI (Grade 23) malzeme kullanılmıştır. Düşük işlenebilirliğe sahip olmasının yanında üstün mekanik özelliklere sahip olması bu malzemeyi birçok sektör için tercih edilebilir bir alternatif haline getirmektedir. Ti6Al4V ELI malzemeye ait kimyasal içerik Tablo 1'de verilmiştir.

Tablo 1. Ti6Al4V ELI Titanyum alaşımına ait kimyasal kompozisyon

Element	Al	C	Fe	H	N	O	V	Ti
%	5.885	0.022	0.1	0.003	0.008	0.101	3.925	Kalan

Talaşlı imalat deneylerinde HPMT marka Ø4 mm çaplı dört ağızlı karbür parmak freze tercih edilmiştir. Genel amaçlı bu karbür parmak freze ile Ø35 mm Ti6Al4V ELI iş parçası frezeleme işlemlerine tabi tutulmuştur. Deneyler öncesi iş parçasının üst yüzeyi takma uçlu tarama freze ile temizlenmiş ve iş parçasından birer mm'lik pasolar halinde 7 paso alınmıştır. Deneylerde kesici takım yana kayma miktarı (a_e) 0,2 mm olarak belirlenmiştir. Kesici takım iş parçasına 1°'lik helisel dalma (rampa) açısı ile girmiş ve her seferinde 1 mm eksenel talaş (a_p) kaldırmıştır. Helisel dalmanın ardından cep, spiral takım yolu ile işlenmiştir. İş parçası 70 m/dk kesme hızı ile işlenmiş ve Şekil 1'de görüldüğü gibi tezgah tablasına sabitlenen bir ayna yardımı ile bağlanmıştır. Talaşlı imalat deneyleri kuru işleme şartlarında tamamlanmıştır. Her paso sonunda iş parçası üzerinden yüzey pürüzlülüğü ölçümleri gerçekleştirilmiştir. Bu ölçümlerin alınabilmesi için yüzey pürüzlülüğü ölçüm cihazının uç (stylus) kısmının girebileceği kadar bir boşluk da oluşturulmuştur.



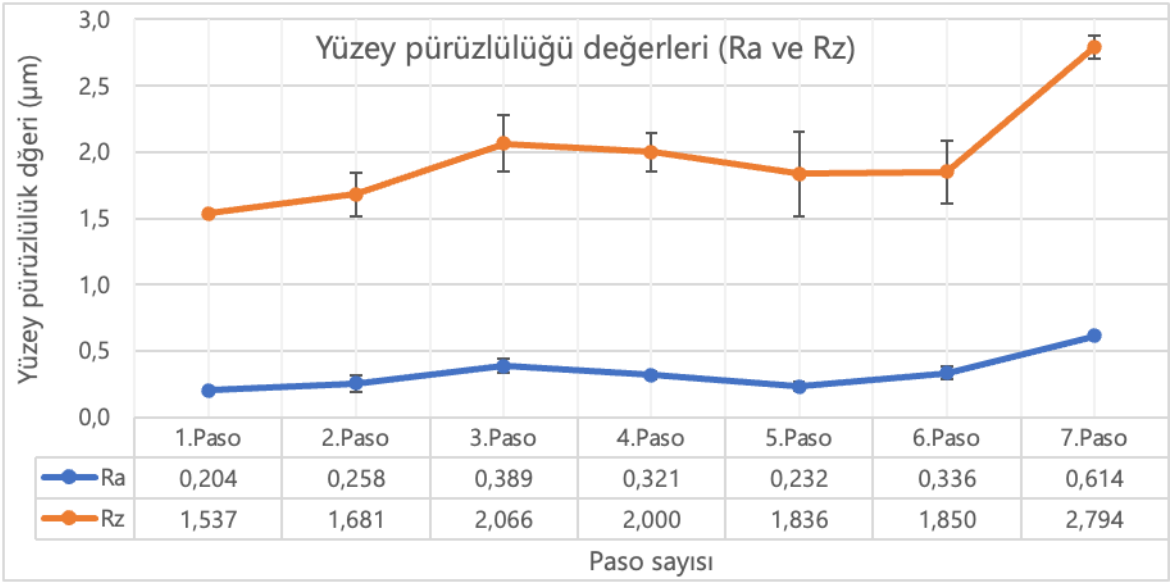
(a) (b)

Şekil 1. Deneylerin gerçekleştirilmesi a) Takım yollarının çıkarılması b) İş parçasının işlenmesi

Yüzey pürüzlülüğü ölçümlerinde her paso için üç adet ölçüm alınmış ve bu ölçüm değerlerinin ortalaması iş parçası pürüzlülük değeri olarak belirlenmiştir. Ayrıca kesici takım aşınması da takip edilmiştir. Bu amaçla kesici takım her paso sonunda sökülerek bir takımcı mikroskobu ile analiz edilmiştir.

BULGULAR VE TARTIŞMA

Yüzey pürüzlülüğü talaşlı imalat işlemlerinde kullanılan en önemli parametrelerden biridir. Yüzey pürüzlülüğü birçok talaşlı imalat faktöründen etkilendiği için dikkatle takip edilmesi gerekmektedir. Deneyler kapsamında yapılan ölçümler sonucunda elde edilen yüzey pürüzlülüğü değerleri (Ra ve Rz) Şekil 2'de sunulmuştur.

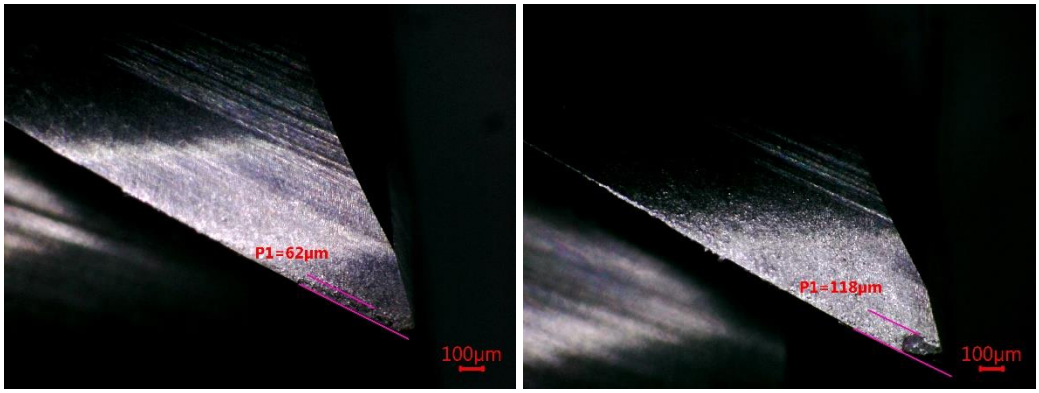


	1.Paso	2.Paso	3.Paso	4.Paso	5.Paso	6.Paso	7.Paso
Ra	0,204	0,258	0,389	0,321	0,232	0,336	0,614
Rz	1,537	1,681	2,066	2,000	1,836	1,850	2,794

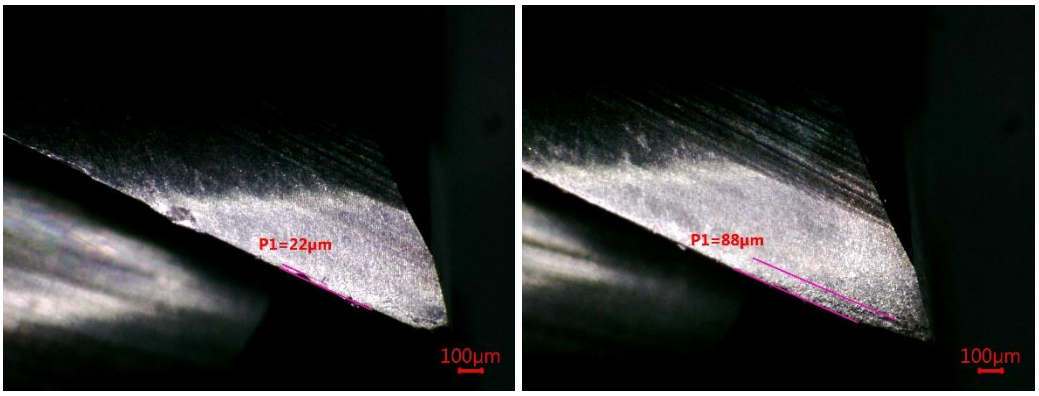
Şekil 2. Yüzey pürüzlülüğü ölçüm sonuçları

Yüzey pürüzlülüğü parametreleri arasından Ra (ortalama yüzey pürüzlülüğü) en temel ölçüttür. Bu çalışma kapsamında yapılan Ra ölçüm sonuçlarına göre (Şekil 2) yüzey pürüzlülüğü değerlerinin en düşük 0,204 µm ve en büyük 0,614 µm aralığında gerçekleştiği, bu değerlerin ise oldukça küçük olduğu görülmektedir. Bununla birlikte Ra değerlerinin 1. pasodan 7. pasoya yaklaşık 3 kat artması takım aşınması ile açıklanabilir. Ancak Ra değerleri pasolar boyunca düzenli bir artış göstermemiş; 3. pasodan sonra azalarak 5. pasoda 0,232 µm'ye düşmüş, 7. pasoda ise en yüksek değerine ulaşmıştır. Bu dalgalanmanın, kesme kenarına yapışan malzemenin (Şekil 4d) oluşup kopmasından ve kenar kırılmalarından kaynaklandığı düşünülmektedir. Ortalama yüzey pürüzlülüğü (Ra), makine parçalarının yüzey pürüzlülüğü hakkında genel bir değerlendirme imkânı sağlamakla birlikte, yüzeyin karakteristik özelliklerini ayrıntılı biçimde ortaya koymak için tek başına yeterli değildir. Bu nedenle, deneyler kapsamında belirlenen ortalama maksimum yüzey pürüzlülüğü (Rz) değerleri kullanılarak malzeme yüzeyinin daha kapsamlı ve detaylı bir şekilde değerlendirilmesi amaçlanmıştır. Rz değerlerinin de genel talaşlı imalat işlemleri açısından düşük pürüzlülük değerlerini gösterdiği Şekil 2'den anlaşılmaktadır. Takım aşınmasına bağlı olarak Rz değerlerindeki artışın (1,537 µm'den 2,794 µm'ye, yaklaşık 1,8 kat) Ra değerlerinde görülen artıştan daha az olması ilgi çekicidir.

Gerek Ra gerekse Rz parametrelerinin deneyler boyunca ciddi değişime uğraması takım aşınmasının belirgin olduğuna işaret etmektedir. Kullanılan karbür parmak frezenin dört ağzının tamamı takımcı mikroskobu ile incelenmiştir. Takım aşınması ölçümlerinde Mahr takımcı mikroskobu kullanılmıştır. Takımcı mikroskobuna daha sonradan eklenen 5 MP bir kamera yardımı ve Imageview yazılımı ile aşınma miktarları analiz edilmiştir. Şekil 3'te ilk paso sonunda meydana gelen aşınma miktarı görülmektedir.



(a) (b)

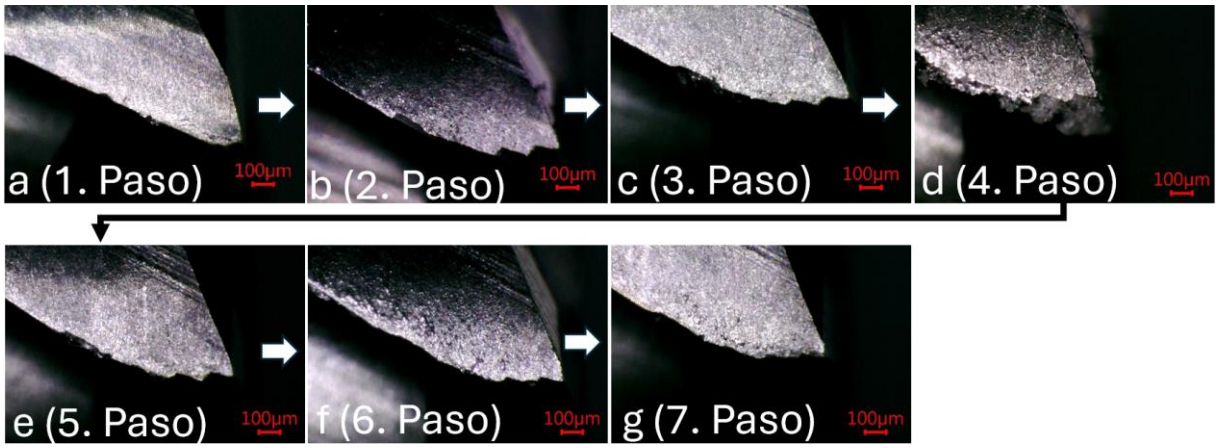


(c) (d)

Şekil 3. İlk paso sonunda takım aşınmasının analizi a) İlk kesme kenarında görülen aşınma b) İkinci kesme kenarında görülen aşınma c) Üçüncü kesme kenarında görülen aşınma d) Dördüncü kesme kenarında görülen aşınma

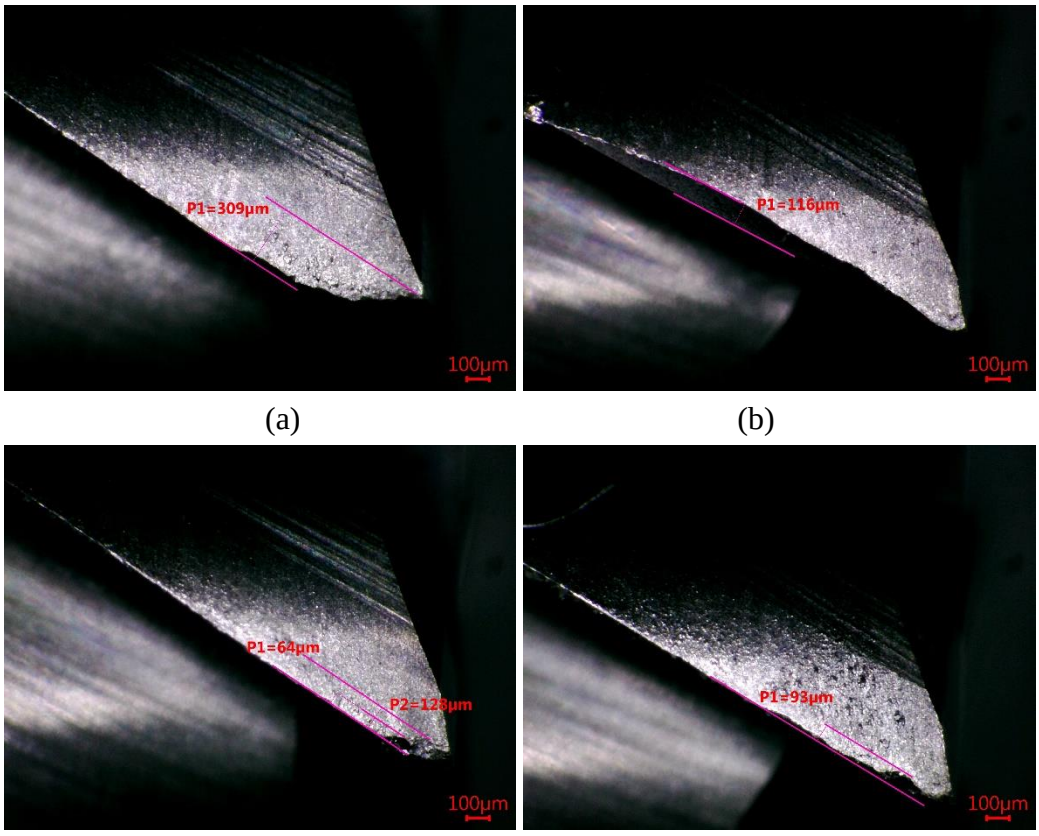
Şekil 3'te görüldüğü gibi yapılan incelemede, ilk talaşlı imalat pasosundan itibaren takım ucunda kırılma ve takım kenarında belirgin aşınma tespit edilmiştir. Bu aşınmanın sebebi kuru işleme şartlarına bağlanabilir. Kuru işleme sırasında soğutma sıvısının hem soğutma hem de yağlama fonksiyonu kullanılmadığından belirgin aşınma görülmüştür.

Takım aşınmasının düzenli olduğu kesme kenarından elde her paso için ayrı ayrı elde edilen aşınma görüntüsü Şekil 4.'de verilmiştir.



Şekil 4. İlk pasodan başlayarak son pasoya kadar aşınmanın değişimi

Şekil 4'te görüldüğü gibi aşınma zaman içinde belirgin şekilde artmıştır. İlk pasoda görülen ve nispeten küçük sayılabilecek uç kırılması 2. pasodan başlayarak gittikçe ilerlemiş ve son paso olan 7. paso'da maksimum boyuta ulaşmıştır. Kesici takımda meydana gelen bu aşınma değişimi her bir kenar için farklı gerçekleşmiştir. Şekil 5'te her bir kesme kenarının son pasoda elde edilmiş aşınma görüntüleri sunulmuştur.



Şekil 5. Son paso (7. paso) sonunda takım aşınmasının analizi a) İlk kesme kenarında görülen aşınma b) İkinci kesme kenarında görülen aşınma c) Üçüncü kesme kenarında görülen aşınma d) Dördüncü kesme kenarında görülen aşınma

Şekil 5 incelendiğinde her bir kenarın farklı miktarlarda aşındığı görülmektedir. Birinci kesme kenarında aşınma ilk pasodaki 62 µm'den son pasoda 309 µm'ye, üçüncü kesme kenarında ise 22 µm'den 128 µm'ye ulaşmıştır. Buna karşın ikinci (118 µm → 116 µm) ve dördüncü (88 µm → 93 µm) kesme kenarlarında belirgin bir değişim görülmemiştir. Bu durum kesme sırasında kesici takımın kenarlarının farklı yüklerle karşılaşması sonucunda farklı aşınma miktarları ile aşındığını göstermektedir.

SONUÇLAR

Düşük özgül ağırlığının yanında yüksek mekanik özelliklere sahip olması ile birçok sektörde kendine yer bulan ve endüstriyel önemi gittikçe artan Ti6Al4V ELI (Grade 23) malzeme üzerinde helisel dalma ile gerçekleştirilen cep frezeleme işleminde aşağıdaki sonuçlara ulaşılmıştır.

- Yüzey pürüzlülüğü değerlerinin bir frezeleme operasyonu için oldukça düşük olmasının yanında artan paso sayılarına bağlı olarak gözlenen aşınma nedeniyle arttığı gözlenmiştir. Yüzey pürüzlülüğü artışı Ra değerleri için 3 kat olurken, Rz değerleri için bu artış yaklaşık 1,8 kat olmuştur.

- Takım aşınması ilk pasodan itibaren belirgin şekilde görülmüştür. Bunun sebebi kuru işleme şartları nedeniyle soğutma/yağlama kullanılmaması olarak açıklanmaktadır.
- Takım aşınması her bir kesme kenarı için farklı şekilde gerçekleşmiştir. Bazı kenarlarda takım ucu kırılmış iken bazı kenarlarda yan yüzeyde kırıklar tespit edilmiştir.
- Takım aşınması en belirgin şekilde birinci kesme kenarında görülmüş ve 62 µm değerinden 309 µm değerine kadar çıkmıştır.

Teşekkür: Bu çalışma Manisa Celal Bayar Üniversitesi Bilimsel Araştırma Projeleri Koordinasyon Birimi tarafından desteklenmiştir. Proje Numarası: 2023-028

KAYNAKLAR

[1] Groover MP. Fundamentals of Modern Manufacturing: Materials, Processes and Systems. USA:John Wiley & Sons; 2010.

[2] Callister WD, Rethwisch DG. Materials Science and Engineering: An Introduction. Wiley; 2013.

[3] Çakır, M. Cemal. "Modern Talaşlı İmalatın Esasları (Modern Metal Cutting), 2." Baskı, Nobel Yayın-Dağıtım, Ankara (2006).

[4] Davim, J. Paulo, ed. "Machining: fundamentals and recent advances." (2008).

[5] Ortner, Hugo M., Peter Ettmayer, and Hans Kolaska. "The history of the technological progress of hardmetals." International Journal of Refractory Metals and Hard Materials 44 (2014): 148-159.

[6] Brinksmeier, E., Fangmann, S., Meyer, I., “Orbital drilling kinematics”, Production Engineering, 2: 277-283, (2008). DOI: https://doi.org/10.1007/s11740-008-0111-7

[7] Iyer, R., Koshy, P., Ng, E., “Helical milling: an enabling technology for hard machining precision holes in AISI D2 tool steel”, International Journal of Machine Tools and Manufacture, 47(2): 205-210, (2007). DOI: https://doi.org/10.1016/j.ijmachtools.2006.04.006

[8] Sadek, A., Meshreki, M., Attia, M.H., “Characterization and optimization of orbital drilling of woven carbon fiber reinforced epoxy laminates”, CIRP Annals, 61(1): 123-126, (2012). DOI: https://doi.org/10.1016/j.cirp.2012.03.089

[9] Qin, X., Gui, L., Li, H., Rong, B., Wang, D., Zhang, H., Zuo, G., “Feasibility study on the minimum quantity lubrication in high-speed helical milling of Ti-6Al-4V”, Journal of Advanced Mechanical Design, Systems, and Manufacturing, 6(7): 1222-1233, (2012). DOI: https://doi.org/10.1299/jamdsm.6.1222

[10] Pereira, R.B.D., Lauro, C.H., Brandão, L.C., Ferreira, J.R., Davim, J.P., “Tool wear in dry helical milling for hole-making in AISI H13 hardened steel”, The International Journal of Advanced Manufacturing Technology, 101: 2425-2439, (2019). DOI: https://doi.org/10.1007/s00170-018-3129-9

[11] Molla Ramezani, N., Rezaei Hajideh, M., Shahmirzaloo, A., "Experimental study of the cutting parameters effect on hole making processes in hardened steel", Journal of Modern Processes in Manufacturing and Production, 6(3): 67-76, (2017).
[12] Wang, H., Tao K., "Study on material removal and cutting analysis in ball helical milling process", Proceedings of the Institution of Mechanical Engineers, Part C: Journal of Mechanical Engineering Science, 236(24): 11493-11504, (2022). DOI: https://doi.org/10.1177/09544062221110463
[13] Kharka, V., Mujumdar, S., Shukla, S., "Study on helical milling of SS 304 with small diameter tools under the influence of minimum quantity lubrication (MQL)", Manufacturing Letters, 35: 1312-1317, (2023). DOI: https://doi.org/10.1016/j.mfglet.2023.08.042

BILIRUBIN IN THE HUMAN BODY: FROM A WASTE PRODUCT TO AN ENDOGENOUS ANTIOXIDANT

Bogdan-Catalin SERBAN
National Institute for Research and Development in Microtechnologies–IMT Bucharest, Voluntari, Romania

Maria Ruxandra SALAGEAN
National College "Saint Sava", Bucharest, Romania

Matei-Gabriel URSACHESCU
National College "B. P. Hasdeu", Buzau, Romania

Vlad DİACONESCU
University of Medicine and Pharmacy "Carol Davila", Bucharest, Romania

Caterina ZETU
International Theoretical High School of Computer Science, Bucharest, Romania

Diana DUMITRAȘCU
National College "Saint Sava", Bucharest, Romania

Maria Ruxandra DİMA
International Theoretical High School of Computer Science, Bucharest, Romania

Marius BUMBAC
Sciences and Advanced Technologies Department, Faculty of Sciences and Arts, Valahia University of Targoviste, 13 Sinaia Alley, 130004 Targoviste, Romania

ABSTRACT

Bilirubin is commonly regarded as a waste product of heme degradation and is best known for its accumulation in jaundice. Yet this yellow pigment has a more complex biological role: at physiological concentrations, it can act as a potent endogenous antioxidant, whereas excessive levels may become cytotoxic and, particularly in newborns, neurotoxic. This paper examines the chemistry behind this dual behavior and follows bilirubin from heme breakdown to elimination. Heme oxygenase first converts heme into biliverdin, which is subsequently reduced by biliverdin reductase to unconjugated bilirubin. Because this form is poorly soluble in water, it circulates mainly bound to albumin before hepatic conjugation increases its polarity and facilitates biliary excretion. The antioxidant properties of bilirubin are discussed in relation to scavenging of reactive oxygen species, inhibition of lipid oxidation, and the biliverdin-bilirubin redox cycle. At the same time, the conditions under which unconjugated bilirubin can accumulate, cross biological barriers, interact with membranes, and disturb

cellular function are considered. Special attention is given to neonatal hyperbilirubinemia, where insufficient conjugation and elimination can transform a normally protective molecule into a serious neurological hazard. The work also addresses the growing interest in mild hyperbilirubinemia and its possible association with reduced oxidative stress and cardiometabolic protection. Bilirubin therefore illustrates how the biological meaning of a molecule depends not only on its structure, but also on concentration, transport, compartmentalization, and metabolism. A substance once dismissed as metabolic waste may, within carefully controlled limits, contribute to the body's own chemical defense system.

Keywords: bilirubin, heme metabolism, antioxidant, hyperbilirubinemia, oxidative stress

D-AMINO ACIDS IN THE HUMAN BODY: EXCEPTIONS TO THE RULE OF BIOLOGICAL HOMOCHIRALITY

Bogdan-Catalin SERBAN
National Institute for Research and Development in Microtechnologies–IMT Bucharest, Voluntari, Romania

Matei-Gabriel URSACHESCU
National College "B. P. Hasdeu", Buzau, Romania

Vlad DİACONESCU
University of Medicine and Pharmacy "Carol Davila", Bucharest, Romania

Caterina ZETU
International Theoretical High School of Computer Science, Bucharest, Romania

Maria Ruxandra SALAGEAN
National College "Saint Sava", Bucharest, Romania

Diana DUMITRAȘCU
National College "Saint Sava", Bucharest, Romania

Maria Ruxandra DİMA
International Theoretical High School of Computer Science, Bucharest, Romania

Marius BUMBAC
Sciences and Advanced Technologies Department, Faculty of Sciences and Arts, Valahia University of Targoviste, 13 Sinaia Alley, 130004 Targoviste, Romania

ABSTRACT

Biological homochirality represents one of the most remarkable features of living systems, with L-amino acids being almost exclusively employed for protein biosynthesis. Nevertheless, increasing evidence demonstrates that D-amino acids are naturally present in the human body and, far from being merely accidental metabolic products, some of them perform important physiological functions. This paper presents a concise overview of the occurrence, origin, metabolism, and biological significance of D-amino acids in humans, with particular emphasis on D-serine and D-aspartate. The different sources of D-amino acids, including diet, intestinal microbiota, enzymatic racemization, and spontaneous age-dependent racemization of amino acid residues in long-lived proteins, are discussed. Particular attention is devoted to D-serine, an endogenous co-agonist of N-methyl-D-aspartate receptors involved in neurotransmission, synaptic plasticity, learning, and memory, as well as to D-aspartate and its possible roles in neuroendocrine regulation. The paper also highlights the importance of

enzymes responsible for the formation and degradation of D-amino acids, particularly serine racemase and D-amino acid oxidase. Furthermore, alterations in D-amino acid homeostasis and their possible relationships with neurological and psychiatric disorders, renal dysfunction, and aging are critically considered. Not least, the accumulation of D-amino acid residues in long-lived proteins and its potential significance as a molecular marker of biological aging are presented. The paper emphasizes the increasingly recognized physiological relevance of D-amino acids and shows that biological homochirality is not an absolute rule, revealing molecular chirality as a dynamic and functionally significant feature of human biochemistry.
Keywords: D-amino acids, D-serine, racemization, human metabolism

CYANIDE IN THE FOODS WE EAT: NATURAL PLANT DEFENSE, HUMAN TOXICITY, AND DETOXIFICATION

Bogdan-Catalin SERBAN
National Institute for Research and Development in Microtechnologies–IMT Bucharest, Voluntari, Romania

Maria Ruxandra SALAGEAN
National College "Saint Sava", Bucharest, Romania

Matei-Gabriel URSACHESCU
National College "B. P. Hasdeu", Buzau, Romania

Vlad DİACONESCU
University of Medicine and Pharmacy "Carol Davila", Bucharest, Romania

Caterina ZETU
International Theoretical High School of Computer Science, Bucharest, Romania

Diana DUMITRAȘCU
National College "Saint Sava", Bucharest, Romania

Maria Ruxandra DİMA
International Theoretical High School of Computer Science, Bucharest, Romania

Marius BUMBAC
Sciences and Advanced Technologies Department, Faculty of Sciences and Arts, Valahia University of Targoviste, 13 Sinaia Alley, 130004 Targoviste, Romania

ABSTRACT

Cyanide is widely recognized as one of the most potent chemical poisons, yet cyanogenic compounds occur naturally in a surprising number of commonly consumed plants. This work explores that apparent contradiction through the chemistry of cyanogenic glycosides, their biological role in plants, and the factors that determine whether dietary exposure becomes hazardous. Amygdalin in bitter almonds and stone-fruit kernels, linamarin in cassava, and related glycosides in sorghum and other edible species are considered as representative examples. Their enzymatic hydrolysis, initiated when plant tissue is damaged, can generate unstable cyanohydrins that decompose to release hydrogen cyanide. The paper compares this natural defense mechanism with the biochemical basis of cyanide toxicity in humans, especially inhibition of mitochondrial cytochrome c oxidase and the resulting disruption of cellular respiration. Attention is also given to detoxification, notably conversion of cyanide to thiocyanate through sulfur-transfer pathways, and to the limited capacity of these mechanisms

during high exposure. Food processing is examined as a decisive factor controlling risk, since soaking, fermentation, drying, boiling, and other treatments can markedly reduce cyanogenic content. The distinction between the mere presence of a toxic chemical and the actual toxicological risk is emphasized throughout. Particular examples from cassava, bitter almonds, apricot kernels, and sorghum illustrate how plant chemistry, preparation practices, dose, and metabolism jointly determine safety. The work shows that naturally occurring cyanide in food is not an anomaly but part of a well-defined chemical defense strategy, whose relevance to human health depends on both molecular transformations and the conditions of consumption.

Keywords: cyanide, cyanogenic glycosides, amygdalin, cassava, detoxification

WHY DOES THE HUMAN BODY PRODUCE FORMALDEHYDE? FROM A TOXIC CHEMICAL TO AN ENDOGENOUS METABOLITE

Bogdan-Catalin SERBAN
National Institute for Research and Development in Microtechnologies–IMT Bucharest, Voluntari, Romania

Matei-Gabriel URSACHESCU
National College "B. P. Hasdeu", Buzau, Romania

Vlad DİACONESCU
University of Medicine and Pharmacy "Carol Davila", Bucharest, Romania

Caterina ZETU
International Theoretical High School of Computer Science, Bucharest, Romania

Maria Ruxandra SALAGEAN
National College "Saint Sava", Bucharest, Romania

Diana DUMITRAȘCU
National College "Saint Sava", Bucharest, Romania

Maria Ruxandra DİMA
International Theoretical High School of Computer Science, Bucharest, Romania

Marius BUMBAC
Sciences and Advanced Technologies Department, Faculty of Sciences and Arts, Valahia University of Targoviste, 13 Sinaia Alley, 130004 Targoviste, Romania

ABSTRACT

Formaldehyde is commonly viewed as an environmental pollutant, industrial chemical, and carcinogenic toxicant. Paradoxically, the same highly reactive molecule is continuously generated inside the human body as a normal product of metabolism. The present work examines this apparent contradiction by reviewing the main endogenous sources of formaldehyde, the chemical reactions in which it participates, and the mechanisms that prevent its accumulation to harmful levels. Endogenous formation may result from methanol oxidation, oxidative demethylation of DNA, RNA, proteins, and small metabolites, as well as from reactions linked to one-carbon metabolism. Because formaldehyde readily attacks nucleophilic sites, its interaction with amino, thiol, and nucleic-acid functionalities can lead to adduct formation and molecular cross-linking. The study also discusses the enzymatic and glutathione-dependent pathways responsible for converting formaldehyde into less reactive products, particularly formate, thereby maintaining cellular homeostasis. The physiological

relevance of this tightly controlled turnover is emphasized, together with the fact that endogenous formaldehyde concentrations reflect a dynamic balance between continuous formation, utilization, and removal. When generation exceeds detoxification capacity, however, the same chemistry that makes formaldehyde metabolically manageable can become damaging, promoting protein modification, genomic instability, and cellular stress. Associations with aging, neurodegenerative processes, and carcinogenesis are therefore considered from the perspective of disrupted formaldehyde balance rather than external exposure alone. By comparing endogenous production with toxicity mechanisms, the work highlights a broader biochemical principle: compounds traditionally regarded only as poisons may also be unavoidable metabolic intermediates whose biological impact depends critically on concentration, localization, and efficient detoxification.

Keywords: formaldehyde, endogenous metabolism, detoxification, one-carbon metabolism, toxicity

WHY CAN GRAPEFRUIT TURN A SAFE MEDICINE INTO A DANGEROUS ONE? CHEMISTRY AND BIOCHEMISTRY OF A CLASSIC FOOD–DRUG INTERACTION

Bogdan-Catalin SERBAN
National Institute for Research and Development in Microtechnologies–IMT Bucharest, Voluntari, Romania

Maria Ruxandra SALAGEAN
National College "Saint Sava", Bucharest, Romania

Matei-Gabriel URSACHESCU
National College "B. P. Hasdeu", Buzau, Romania

Vlad DİACONESCU
University of Medicine and Pharmacy "Carol Davila", Bucharest, Romania

Caterina ZETU
International Theoretical High School of Computer Science, Bucharest, Romania

Diana DUMITRAȘCU
National College "Saint Sava", Bucharest, Romania

Maria Ruxandra DİMA
International Theoretical High School of Computer Science, Bucharest, Romania

Marius BUMBAC
Sciences and Advanced Technologies Department, Faculty of Sciences and Arts, Valahia University of Targoviste, 13 Sinaia Alley, 130004 Targoviste, Romania

ABSTRACT

Grapefruit is generally regarded as a healthy food, yet its consumption can profoundly alter the pharmacokinetics of certain medicines and, in some cases, increase the risk of serious adverse effects. The present work examines the chemical and biochemical basis of this classic food–drug interaction. Particular focus is placed on naturally occurring furanocoumarins, especially bergamottin and 6',7'-dihydroxybergamottin, which can inhibit intestinal cytochrome P450 3A4 (CYP3A4) and thereby reduce the presystemic metabolism of susceptible drugs. As a consequence, compounds that normally undergo extensive intestinal first-pass metabolism may reach unexpectedly high plasma concentrations after grapefruit consumption. The paper discusses why the magnitude of the interaction varies markedly among medicines and among individuals, and why the effect may persist long after the fruit or juice has been consumed. Examples from several therapeutic classes are used to illustrate the

clinical relevance of the phenomenon, including certain statins, calcium-channel blockers, immunosuppressants, and other drugs with narrow therapeutic margins. The role of intestinal transport proteins is also considered, since grapefruit components may influence drug absorption through mechanisms that are not limited to CYP3A4 inhibition. Differences between whole grapefruit, juice, processing conditions, and other citrus fruits are briefly addressed in relation to furanocoumarin content. The work underlines an important lesson in everyday pharmacology: a food considered beneficial from a nutritional perspective can become problematic when its natural constituents modify drug metabolism. Understanding this interaction provides a clear example of how organic chemistry, enzymology, nutrition, and pharmacotherapy intersect in daily life.

Keywords: grapefruit, furanocoumarins, CYP3A4, drug metabolism, food–drug interactions

THE CHEMISTRY OF HUMAN BODY ODOR: WHY DO WE SMELL AND WHY DOES OUR SMELL CHANGE WITH AGE?

Bogdan-Catalin SERBAN
National Institute for Research and Development in Microtechnologies–IMT Bucharest, Voluntari, Romania

Maria Ruxandra SALAGEAN
National College "Saint Sava", Bucharest, Romania

Matei-Gabriel URSACHESCU
National College "B. P. Hasdeu", Buzau, Romania

Vlad DİACONESCU
University of Medicine and Pharmacy "Carol Davila", Bucharest, Romania

Caterina ZETU
International Theoretical High School of Computer Science, Bucharest, Romania

Diana DUMITRAȘCU
National College "Saint Sava", Bucharest, Romania

Maria Ruxandra DİMA
International Theoretical High School of Computer Science, Bucharest, Romania

Marius BUMBAC
Sciences and Advanced Technologies Department, Faculty of Sciences and Arts, Valahia University of Targoviste, 13 Sinaia Alley, 130004 Targoviste, Romania

ABSTRACT

Human body odor is a familiar but chemically complex phenomenon resulting from interactions between secretions of the skin, microbial metabolism, and numerous volatile organic compounds. Interestingly, freshly secreted sweat is largely odorless, while characteristic body odors develop mainly after transformation of its components by microorganisms inhabiting the skin. This paper presents an overview of the chemistry responsible for human body odor, with emphasis on the origin, formation, and chemical diversity of the volatile molecules involved. The different contributions of eccrine, apocrine, and sebaceous secretions are discussed, together with the role of the skin microbiome in converting initially non-volatile or weakly odorous precursors into volatile compounds. Particular attention is devoted to volatile fatty acids, sulfur-containing compounds, steroids, aldehydes, and other molecules responsible for characteristic odors originating from different regions of the human body. The influence of genetic factors, diet, hormonal status, hygiene,

medication, and disease on individual odor profiles is also considered. Furthermore, the paper highlights the chemical changes occurring during aging and their consequences for body odor. Special attention is given to 2-nonenal, an unsaturated aldehyde associated with age-related changes in skin lipid composition and oxidative degradation. Not least, the potential use of characteristic volatile compounds as non-invasive indicators of physiological or pathological processes is presented. The paper emphasizes that human body odor is not simply a consequence of perspiration, but represents a complex chemical signature generated by the interaction of human metabolism, skin chemistry, microorganisms, and environmental factors.
Keywords: body odor, skin microbiome, volatile organic compounds, 2-nonenal, aging

HYDROGEN SULFIDE IN THE HUMAN BODY: FROM A TOXIC GAS TO AN ESSENTIAL BIOLOGICAL MESSENGER

Bogdan-Catalin SERBAN
National Institute for Research and Development in Microtechnologies–IMT Bucharest, Voluntari, Romania

Maria Ruxandra SALAGEAN
National College "Saint Sava", Bucharest, Romania

Matei-Gabriel URSACHESCU
National College "B. P. Hasdeu", Buzau, Romania

Vlad DİACONESCU
University of Medicine and Pharmacy "Carol Davila", Bucharest, Romania

Caterina ZETU
International Theoretical High School of Computer Science, Bucharest, Romania

Diana DUMITRAȘCU
National College "Saint Sava", Bucharest, Romania

Maria Ruxandra DİMA
International Theoretical High School of Computer Science, Bucharest, Romania

Marius BUMBAC
Sciences and Advanced Technologies Department, Faculty of Sciences and Arts, Valahia University of Targoviste, 13 Sinaia Alley, 130004 Targoviste, Romania

ABSTRACT

Hydrogen sulfide is traditionally associated with the characteristic odor of rotten eggs and with severe toxicity resulting from inhibition of cellular respiration. During the last decades, however, this apparently simple toxic gas has emerged as an endogenously produced signaling molecule with important physiological functions. This work discusses the dual chemical and biological identity of hydrogen sulfide, focusing on the mechanisms responsible for its formation, reactivity, signaling activity, and toxicity. In mammalian tissues, H_2S is generated mainly from sulfur-containing amino acids through enzymatic pathways involving cystathionine β-synthase, cystathionine γ-lyase, and 3-mercaptopyruvate sulfurtransferase. Its acid–base equilibrium, particularly the distribution between H_2S and HS^- under physiological conditions, strongly influences its transport and chemical behavior. The biological effects of endogenous H_2S are examined in relation to vascular tone, neurotransmission, inflammation, mitochondrial function, and cellular responses to oxidative stress. Special emphasis is placed

on protein persulfidation, a post-translational modification increasingly recognized as an important mechanism of H_2S-mediated signaling. The interaction of sulfide species with metal centers, reactive oxygen and nitrogen species, and thiol-containing biomolecules is also considered. At elevated concentrations, the same molecule becomes hazardous by interfering with mitochondrial electron transport and oxygen utilization, illustrating the crucial importance of dose and intracellular localization. Hydrogen sulfide therefore represents an intriguing example of a compound whose biological role cannot be classified simply as beneficial or toxic, but must be understood through the balance between endogenous production, chemical reactivity, cellular regulation, and exposure level.

Keywords: hydrogen sulfide, gasotransmitter, persulfidation, sulfur metabolism, toxicity

ZERO-/FEW-SHOT MULTILINGUAL STUDENT FEEDBACK ANALYSIS IN LOW-RESOURCE LANGUAGES USING LIGHTWEIGHT TRANSFORMER VARIANTS FOR MOBILE EDUCATIONAL PLATFORMS

Jatinkumar Bhimjibhai Kotadiya
Research scholar in Computer Science Department, Atmiya University, Rajkot, India

ABSTRACT

Within the era of digital learning, pupil remarks performs a important role in assessing instructional best and enhancing learning experiences. however, the linguistic variety of newcomers and the restrained availability of annotated datasets in low-aid languages pose significant challenges for automated remarks evaluation. This take a look at gives a novel technique titled zero-/Few-Shot Multilingual pupil remarks evaluation in Low-aid Languages the usage of lightweight Transformer variations for mobile academic platforms. The proposed framework integrates zero and few-shot mastering strategies with optimized transformer architectures along with DistilBERT, MobileBERT, and TinyBERT to perform multilingual sentiment type efficaciously, even in resource constrained environments. The methodology emphasizes transfer mastering from excessive-resource to low-resource languages, supported through adaptive first-rate-tuning and set off-primarily based mastering to beautify move-lingual The experimental setup evaluates overall performance throughout various educational feedback datasets, that specialize in metrics along with accuracy, F1-rating, model length, and inference pace. effects exhibit that lightweight transformer variants can attain aggressive accuracy with drastically decreased computational costs, making them appropriate for deployment on mobile and area educational structures. The findings spotlight the capability of zero and few-shot paradigms in democratizing AI-driven feedback evaluation throughout linguistically various academic ecosystems. This studies contributes to the development of inclusive, reachable, and green AI programs in training even as placing the inspiration for destiny work in scalable multilingual sentiment evaluation.

Keywords: Zero-Shot Learning, Few-Shot Learning, Multilingual Sentiment Analysis, Low-Resource Languages, Lightweight Transformers, DistilBERT, Mobile Educational Platforms, Student Feedback Analysis

YÜKSEK YOĞUNLUKLU YAYA ALANLARINDA PİEZOELEKTRİK ENERJİ HASAT SİSTEMLERİ: LİTERATÜR TARAMASI VE MEKANİZMA SINIFLANDIRMASI

PIEZOELECTRIC ENERGY HARVESTING SYSTEMS IN HIGH-DENSITY PEDESTRIAN AREAS: LITERATURE REVIEW AND MECHANISM CLASSIFICATION

Efra KALKAN
İstanbul Sabahattin Zaim Üniversitesi, Mühendislik ve Doğa Bilimleri Fakültesi, Endüstri Mühendisliği Bölümü
Istanbul Sabahattin Zaim University, Faculty of Engineering and Natural Science, Department of Industrial Engineering

Ayşe Nuray CANAT
Dr., İstanbul Sabahattin Zaim Üniversitesi, Mühendislik ve Doğa Bilimleri Fakültesi, Endüstri Mühendisliği Bölümü
Dr., Istanbul Sabahattin Zaim University, Faculty of Engineering and Natural Science, Department of Industrial Engineering
ORCID NO: 0000-0002-8527-550X

ÖZET

Sürdürülebilir akıllı şehirler ve yeşil kampüs vizyonu doğrultusunda, günümüzde kentsel enerji arzını çeşitlendirmek, enerji verimliliğini maksimize etmek ve fosil yakıtlara olan bağımlılığı azaltmak amacıyla insan adımlarından kaynaklanan mekanik kinetik enerjinin elektrik enerjisine dönüştürülmesi üzerine yapılan akademik araştırmalar ivme kazanmıştır. Bu kapsamlı çalışmada, yaya trafiğinin yoğun olduğu kamusal alanlarda ve özellikle turnike gibi stratejik geçiş denetim noktalarında uygulanan piezoelektrik enerji hasat sistemleri sistematik bir literatür taraması eşliğinde detaylıca incelenmektedir. Klasik zemin ve karo uygulamalarında sıkça karşılaşılan, yayaların basmama veya geçiş rotasını değiştirme gibi mekanik kayıp yaratan belirsizlik faktörlerine karşın; metro istasyonları, yoğun kamu binaları, plazalar ve üniversite kampüslerindeki turnike altyapıları, yaya akışını kontrollü bir şekilde tek sıraya indirgeyerek mutlak temas garantisi sağlayan kritik bir "darboğaz" etkisi yaratmaktadır. Bu durum, mekanik enerjinin kayıpsız, kesintisiz ve yüksek verimle yakalanması için eşsiz bir mühendislik potansiyeli barındırmaktadır.

Literatürdeki mevcut teorik ve deneysel çalışmalar, mekanik dönüştürme ve enerji iletim ilkelerine göre tasnif edilmiş olup; doğrudan kompresyon matrisleri, konsol tipi yapılar, frekans yükseltmeli rezonans mekanizmaları, kuvvet yükseltmeli bağlantı yapıları ve kavisli transdüser sistemleri derinlemesine analiz edilmiştir. Bununla birlikte, piezoelektrik elemanlar tarafından üretilen değişken karakteristikli alternatif akımın stabil bir doğru akıma dönüştürülmesi ve müteakiben enerji depolama birimlerinde muhafaza edilmesine yönelik gelişmiş elektriksel arayüz topolojileri ve devre çözümleri değerlendirilmiştir. Mevcut literatür sentezinin bulguları, turnike ve geçiş kontrol altyapılarına entegre edilen piezoelektrik tabanlı enerji hasat çözümlerinin, düşük güçlü nesnelerin interneti sensör

düğümlerini, akıllı sayaçları ve kritik acil durum aydınlatma sistemlerini harici şebeke veya pillere ihtiyaç duymadan besleme kapasitesine sahip olduğunu açıkça kanıtlamaktadır. Sonuç olarak bu akıllı sistemler, geleceğin kentsel enerji yönetimi, mikro-şebeke mimarileri ve yeşil altyapı ekosistemleri için son derece yenilikçi, sürdürülebilir ve ölçeklenebilir bir alternatif yaklaşım sunmaktadır.

Anahtar Kelimeler: Piezoelektrik Enerji Hasadı, Turnike Sistemleri, Literatür Taraması, Akıllı Şehirler.

Not: Bu çalışma 2025-BAP-100-066 nolu proje kapsamında gerçekleştirilmiştir.

ABSTRACT

In line with the vision of sustainable smart cities and green campuses, academic research on converting mechanical kinetic energy generated by human footsteps into electrical energy has gained momentum with the aim of diversifying the urban energy supply, maximizing energy efficiency, and reducing dependence on fossil fuels. In this comprehensive study, piezoelectric energy harvesting systems implemented in public spaces with heavy pedestrian traffic—and particularly at strategic access control points such as turnstiles—are examined in detail through a systematic literature review. In contrast to the uncertainties commonly encountered in traditional pavement and tile applications—such as pedestrians failing to step on the sensors or altering their walking path, which result in mechanical energy loss— turnstile infrastructures in subway stations, high-traffic public buildings, plazas, and university campuses create a critical “bottleneck” effect by controlling pedestrian flow into a single file, thereby ensuring absolute contact. This situation holds unique engineering potential for capturing mechanical energy without loss, continuously, and with high efficiency.

Existing theoretical and experimental studies in the literature have been classified according to the principles of mechanical conversion and energy transmission; direct compression matrices, cantilever-type structures, frequency-amplified resonance mechanisms, force-amplified connection structures, and curved transducer systems have been analyzed in depth. Furthermore, advanced electrical interface topologies and circuit solutions for converting the variable-characteristic alternating current generated by piezoelectric elements into stable direct current and subsequently storing it in energy storage units have been evaluated. The findings of this literature review clearly demonstrate that piezoelectric-based energy harvesting solutions integrated into turnstile and access control infrastructure are capable of powering low-power Internet of Things (IoT) sensor nodes, smart meters, and critical emergency lighting systems without the need for an external grid or batteries. Consequently, these smart systems offer an extremely innovative, sustainable, and scalable alternative approach for future urban energy management, microgrid architectures, and green infrastructure ecosystems.

Keywords: Piezoelectric Energy Harvesting, Turnstile Systems, Literature Review, Smart Cities.

Note: This study was conducted as part of Project No. 2025-BAP-100-066.

İDEAL DÜZGÜN DOĞRUSAL ANTEN DİZİSİNDE FAZ NİCEMLEMESİNİN YÖNLENDİRME HATASINA VE HEDEF YÖNDEKİ GÜÇ KAYBINA ETKİSİ

EFFECTS OF PHASE QUANTIZATION ON POINTING ERROR AND POWER LOSS IN THE TARGET DIRECTION OF AN IDEAL UNIFORM LINEAR ANTENNA ARRAY

Ahmet TURGUT
Ondokuz Mayıs Üniversitesi, Elektrik-Elektronik Mühendisliği Bölümü
ORCID: 0000-0001-6729-0266

Muhammet Rıza KARADAVUT
Ondokuz Mayıs Üniversitesi, Elektrik-Elektronik Mühendisliği Bölümü
ORCID: 0000-0001-6507-3890

ÖZET

Faz nicemlemesinde hedef yöndeki güç kaybının kabul edilebilir olması, yönlendirme hatasının da kabul sınırında kalacağını garanti etmez. Bu çalışmada, 16 elemanlı ve yarım dalga boyu aralıklı ideal düzgün doğrusal bir dizide yönlendirme hatası ile hedef yöndeki güç kaybı birlikte incelenmiştir. Elemanların uyarım genlikleri eşit, ortak faz ofseti sıfır tutulmuştur. Sürekli faz uyarımı, her elemanın fazının en yakın ayrık değere yuvarlandığı 2, 3 ve 4 bit seçenekleriyle karşılaştırılmıştır. Hedef açılar 0°–60° arasında 1° aralıklarla seçilmiştir. Böylece 61 hedef için dört uyarım seçeneği değerlendirilmiş, toplam 244 durumun 183'ünde nicemlenmiş fazlar kullanılmıştır. Güç kaybı tüm seçeneklerde aynı ideal tepe gücüne göre hesaplanmış, desenler kendi tepe değerlerine göre normalize edilmemiştir. Görünür açısal kesitteki en yüksek tepenin yönü, iki gözlem ızgarası ve bağımsız türev hesabıyla kontrol edilmiştir. Bu çalışma için kabul sınırları 1° yönlendirme hatası ve 1 dB hedef kaybı olarak belirlenmiş, sınıra eşit değerler de kabul edilmiştir. İncelenen seçenekler arasında her iki koşulu sağlayan en düşük çözünürlük, 58 hedefte 2 bit, 28°, 32° ve 50° hedeflerinde 3 bittir. Örneklenen bütün hedeflerde iki koşulu sağlayan en düşük sabit çözünürlük 3 bittir. Bu durumda en büyük yön hatası 0,670429°, en büyük güç kaybı 0,241483 dB'dir. Fazör izdüşümünden elde edilen deterministik kayıp üst sınırı, 3 bit için yaklaşık 0,687693 dB'dir. Bu sınır, aynı ideal modelde hedef fazının tanımlandığı tüm hedef açılarında yalnız güç kaybı koşulunu garanti eder; yön hatasını sınırlamaz. 29° ve 31° hedeflerinde 2 bit için ortak faz vektörünün oluşturduğu desenin tepesinin tam 30° olduğu analitik olarak gösterilmiştir. Her iki yön hatası da tam 1° olup kabul sınırına eşittir. Çözünürlük seçimi, örneklenen hedefler ve tanımlanan besleme kuralıyla sınırlıdır. Çalışma fiziksel anten doğrulaması veya yeni bir optimizasyon algoritması içermemektedir.

Anahtar kelimeler: ideal düzgün doğrusal dizi; faz nicemlemesi; hüzme yönlendirme hatası; hedef yöndeki güç kaybı; faz çözünürlüğü.

ABSTRACT

Under phase quantization, acceptable target-direction power loss does not necessarily ensure that pointing error remains within its acceptance limit. This study examines pointing error and target-direction power loss in an ideal uniform linear array of 16 elements with half-wavelength spacing. Excitation amplitudes are equal and the common phase offset is fixed at zero. Continuous-phase excitation is compared with 2-bit, 3-bit, and 4-bit quantization, rounding each element phase to the nearest discrete value. Target angles span 0°–60° in 1° increments. Evaluating four excitation options at 61 targets gives 244 cases, 183 of which use quantized phases. Loss is calculated relative to the same ideal peak power, without normalizing patterns to their own peaks. The highest peak direction in the visible angular cut is checked using two observation grids and an independent derivative calculation. Study-specific limits are 1° pointing error and 1 dB target loss, including equality. Among the resolutions examined, the lowest satisfying both limits is 2 bits at 58 targets and 3 bits at 28°, 32°, and 50°. For a fixed resolution across all sampled targets, 3 bits is the lowest of these options. Its maximum error and loss are 0.670429° and 0.241483 dB. A deterministic loss bound obtained by phasor projection is approximately 0.687693 dB for 3 bits. Within the same ideal model, it guarantees only the loss criterion at all target angles where the phase is defined; it does not bound pointing error. For 2-bit excitation at 29° and 31°, the common phase vector produces an analytically verified peak at exactly 30°. Both errors equal the 1° acceptance limit. Resolution selection is restricted to the sampled targets and specified excitation rule. No physical antenna validation or new optimization algorithm is presented.

Keywords: ideal uniform linear array; phase quantization; beam pointing error; target-direction power loss; phase resolution.

GİRİŞ

Faz kontrollü anten dizilerinde hüzme yönü, elemanlara uygulanan karmaşık uyarımlarla belirlenir. Sürekli faz dağılımı ayrık durumlarla temsil edildiğinde oluşan faz hataları, hedef yöndeki alan toplamını, tepe yönünü ve yan lobları farklı biçimlerde etkileyebilir. Dizi faktörü, eleman konumları ile uyarımların etkisini eleman deseninden ayrı incelemeye olanak verir. Gerçek antenin alan deseni hesaplanırken eleman deseni ve karşılıklı kuplaj da dikkate alınmalıdır [1].

Dijital faz kaydırıcıların dizi deseni üzerindeki etkileri uzun süredir araştırılmaktadır. Goto ve Cheng, nicemlemeden kaynaklanan yan lobları azaltmak için eleman fazlarında düzenlemeler incelemiştir [2]. Smith ve Guo, faz nicemleme hatalarını rastgeleleştirme yöntemlerini karşılaştırmış [3]; Jiang ve diğerleri rastgele fazlama yaklaşımlarını hüzme yönlendirme hatası açısından değerlendirmiştir [4]. Clénet ve Morin ise bit sayısına ve tarama koşullarına bağlı desen değişimlerini dizi faktörü üzerinden incelemiştir [5].

Hüzme yönünün ayrık adımlarla değişmesi ile hedef açıdan sapması farklı ölçütlerdir. Hatcher, hüzme konumundaki bu adımları incelemiş; sürekli fazda eşdeğer olabilen merkez ve kenar faz referanslarının nicemleme sonrasında farklı sonuçlar verebildiğini göstermiştir

[6]. Clénet ve Morin faz referansını dizi merkezinde alırken [5], burada ilk eleman referans alınmıştır. Bu nedenle sayısal sonuçlar karşılaştırılırken faz referansının aynı olup olmadığına dikkat edilmelidir.

Faz durumlarının seçimi de çözünürlük kadar önemlidir. Kamoda ve diğerleri, genlik ağırlıkları ve faz durumuna bağlı kayıpları içeren yansıtıcı dizi modellerinde, nicemleme öncesindeki ortak faz ofsetinin kazanç kaybını etkilediğini göstermiştir [7]. Yi Zhang ve diğerleri, faz uyarımlarını belirlemek için doğrusal programlama kullanmıştır [8]. Periyodik şablon telafisi [9] ile simetrik ve rastgele simetrik faz telafisi [10], nicemlemeden kaynaklanan yönlendirme hatasını azaltmak için geliştirilmiştir. Daha sık eleman yerleşimini uzaysal delta-sigma faz seçimiyle birleştiren mimariler de hatanın görünür bölgedeki dağılımını değiştirebilir [11].

Faz çözünürlüğünün etkisi, kullanılan performans ölçütüne göre de değişir. Li ve diğerleri, yönlü modülasyonda nicemlemenin SINR ve gizlilik hızı üzerindeki etkilerini istatistiksel hata varsayımları altında analiz etmiştir [12]. Pánek ve diğerleri sentez yöntemi, tarama yönü ve nicemleme duyarlılığını birlikte değerlendirmiştir [13]. Shao ve diğerleri, karma çözünürlüklü bir mimaride 16 elemanlı ve yarım dalga boyu aralıklı doğrusal dizinin yönlendirme hatasını ve yan loblarını incelemiştir [14]. Gerekli en düşük uyarım biti sayısı da desen kısıtları altında karma tamsayılı programlamayla araştırılmıştır [15].

Nicemlemeyi sentez sürecine dahil eden çalışmalar, ayrık faz kısıtlarını eleman konumu ve uyarım seçimiyle birlikte ele almaktadır [16, 17]. Kuplajlı dizilerde dijital faz sentezi, tam dalga analiziyle de birleştirilmiştir [18]. Tablo 1, bu incelemeyle ilişkili çalışmaların modellerini ve değerlendirme ölçütlerini özetlemektedir. Önceki algoritmalar aynı veri üzerinde yeniden uygulanmadığından karşılaştırma, yöntemlerin kapsamıyla sınırlıdır.

Tablo 1. İlgili çalışmaların dizi modelleri ve değerlendirme ölçütleri.

Çalışma	Dizi modeli	Faz kontrolü veya karar	Başlıca değerlendirme
Pánek vd. [13]	Düzlemsel dizi	Sentez ve nicemleme duyarlılığı	Desen koşulları ve tarama
Shao vd. [14]	16 elemanlı λ/2 ULA	Karma çözünürlük ve faz seçimi	Yön hatası ve yan loblar
Zhang vd. [15]	Doğrusal ve düzlemsel diziler	Minimum uyarım biti optimizasyonu	Verilen desen kısıtları
Echeveste vd. [18]	Kuplajlı gerçek elemanlar	Tamsayılı dijital faz seçimi	Tam dalga alanları ve desen
Bu çalışma	16 elemanlı λ/2 ideal ULA	Sabit yuvarlama ile 2, 3 ve 4 bit	Yön hatası ve hedef güç kaybı

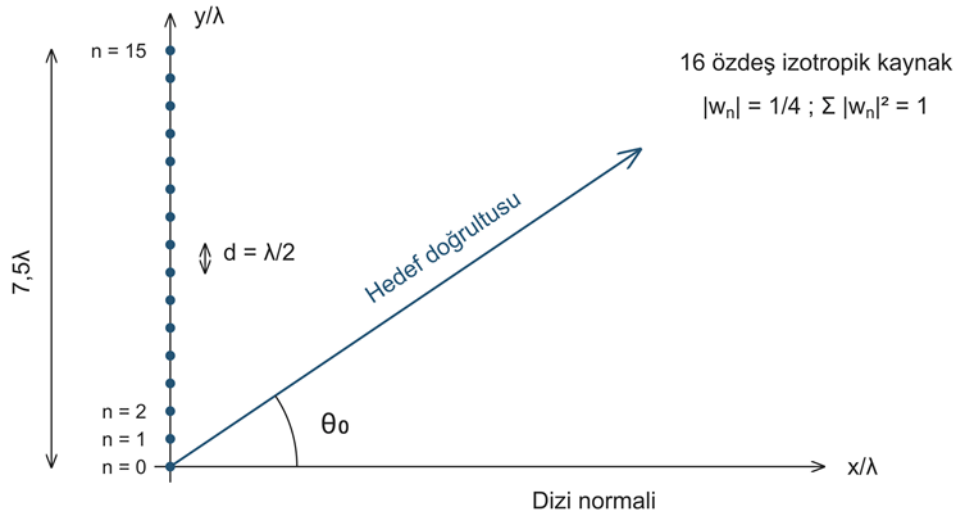
ULA, düzgün doğrusal diziyi ifade eder. Çalışmaların geometri, uyarım ve kabul koşulları farklıdır; tablo bir performans sıralaması değildir.

Bu çalışmada, eşit genlikli ideal bir doğrusal dizide faz nicemlemesinin yönlendirme hatasına ve hedef yöndeki güç kaybına etkisi incelenmiştir. Hedef yöndeki kayıp 1 dB'yi aşmazken yönlendirme hatasının 1° sınırını aşıp aşmadığı araştırılmıştır. Her hedef açı için yeterli çözünürlük ve örneklenen bütün hedeflerde kullanılabilecek sabit çözünürlük ayrı ayrı belirlenmiştir. Güç kaybı analitik bir üst sınırla değerlendirilmiş, kabul sınırında kalan iki yönlendirme hatası da kayıtlı faz dağılımları üzerinden doğrulanmıştır.

YÖNTEM

Dizi geometrisi ve uyarım

Dar bant ve uzak alan varsayımları altında N=16 özdeş izotropik eleman, y ekseni üzerinde d=λ/2 aralıklarla yerleştirilmiştir. Eleman indisi n=0,…,15, konum y_n=nλ/2 ve toplam dizi açıklığı 7,5λ'dır. Gözlem açısı θ ile hedef açısı θ_0, dizi normali olan +x ekseninden +y yönüne doğru ölçülür. İnceleme, xy düzleminde −90° ile 90° arasındaki görünür kesitle sınırlıdır. Bu kesitteki tepe, üç boyutlu uzayda tek bir ışıma doğrultusu olarak yorumlanmaz. Konumlar dalga boyuna göre normalize edildiğinden belirli bir çalışma frekansı veya fiziksel anten boyutu tanımlanmamıştır.



Şekil 1. İdeal eleman konumları ve xy düzlemindeki açı tanımı. Noktalar izotropik kaynakları gösterir; hedef doğrultusu şematiktir.

Sürekli fazlı referans dizide eleman fazı ve ağırlığı Denklem (1) ile tanımlanır. Her elemanın genliği 1/4 seçildiği için ağırlıkların genliklerinin kareleri toplamı bütün modellerde birdir. Bu normalizasyon ideal uyarım vektörünün ölçeğini sabit tutar; gerçek bir besleme ağının güç tüketimini veya toplam yayılan gücü temsil etmez.

$$\varphi_n^{(c)}(\theta_0) = -\pi n \sin\theta_0, \quad w_{c,n}(\theta_0) = \frac{1}{4} e^{j\varphi_n^{(c)}(\theta_0)} \tag{1}$$

İlk elemanın fazı ve nicemleme öncesindeki ortak faz ofseti sıfır alınmıştır. Sürekli fazlı uyarımda ortak ofset yalnızca alanın ortak fazını değiştirir. Ancak nicemlemeden önce uygulandığında seçilen ayrık faz durumlarını da değiştirebilir [7]. Burada genlik dağılımı, eleman konumları ve ortak faz ofseti sabit tutulmuş, bu değişkenler için optimizasyon yapılmamıştır.

Faz nicemlemesi ve dizi faktörü

b bit faz çözünürlüğünde 2^b eşit aralıklı faz durumu kullanılır. $\Delta_b = 2\pi/2^b$ olduğundan 2, 3 ve 4 bit için faz adımları sırasıyla 90°, 45° ve 22,5°'dir. En yakın faz durumuna yuvarlama kuralı Denklem (2)'de verilmiştir. Faz önce mod 2π işlemiyle $[0,2\pi)$ aralığına getirilir, ardından en yakın durum indisine yuvarlanır. İki duruma eşit uzaklıktaysa üst indis seçilir; indis, faz durumlarının sayısına göre mod işlemiyle geçerli aralıkta tutulur.

$$Q_b(\varphi) = \Delta_b \bmod \left(\left\lfloor \frac{\mathrm{mod}(\varphi,2\pi)}{\Delta_b} + \frac{1}{2} \right\rfloor, 2^b\right), \quad \Delta_b = \frac{2\pi}{2^b} \tag{2}$$

Sayısal uygulamada yarım adıma uzaklığı en fazla 10^{-10} derece olan fazlar için de üst indis seçilmiştir. Bu aralık yalnızca yuvarlama kararında kullanılır; kabul sınırlarını değiştirmez. Her elemanın fazı ayrı ayrı nicemlenmiş, elemanlar arasındaki tek bir faz artışı yuvarlanıp dizi boyunca tekrarlanmamıştır. Nicemlenmiş ağırlık $w_{b,n} = 1/4 \exp\left[jQ_b\left(\varphi_n^{(c)}\right)\right]$ olarak tanımlanır. Dizi faktörü, sürekli ve nicemlenmiş uyarımlarda aynı uzaysal faz işareti kullanılarak Denklem (3) ile hesaplanmıştır.

$$F_b(\theta;\theta_0) = \sum_{n=0}^{15} w_{b,n}(\theta_0) e^{j\pi n \sin\theta} \tag{3}$$

İki kabul koşulu ve çözünürlük seçimi

Her hedef açı için $\theta_{p,b}$, dizi faktörü gücünün görünür kesitteki en büyük değerine karşılık gelen açıdır. Bu açıyı belirlemek için kesitteki bütün tepe adayları karşılaştırılmıştır. Ortak güç referansına göre normalize edilmiş en yüksek değerden en fazla 10^{-10} fark gösteren birden çok ayrı tepe varsa tepe yönü belirsiz kabul edilir. Bu güç toleransı, yönlendirme hatasının 1° kabul sınırını değiştirmez. Mutlak yönlendirme hatası Denklem (4) ile tanımlanır.

$$e_b(\theta_0) = |\theta_{p,b} - \theta_0| \tag{4}$$

Hedef yöndeki güç kaybı, sürekli fazlı ideal dizinin aynı hedefteki tepe gücüne göre hesaplanmıştır. $|F_c(\theta_0;\theta_0)|^2 = 16$ ve ortak referansa göre normalize güç $P_{rel,b}(\theta;\theta_0) = |F_b(\theta;\theta_0)|^2/16$ olduğundan kayıp Denklem (5) ile bulunur. Hedefteki güç azalmasını gizlememek için desenler kendi tepe değerlerine göre ayrı ayrı normalize edilmemiştir. Burada hesaplanan kayıp, gerçek bir antenin kazanç kaybı veya faz kaydırıcının ekleme kaybı değildir.

$$L_b(\theta_0) = -10 \log_{10}\left(\frac{|F_b(\theta_0;\theta_0)|^2}{16}\right) \tag{5}$$

İncelenen çözünürlük kümesi B={2,3,4}, hedef açı kümesi T={0°,1°,…,60°} olarak seçilmiştir. Kabul koşulları, bu çalışma için $e_b \le 1°$ ve $L_b \le 1$ dB olarak belirlenmiştir; bu sınırlar genel bir anten standardından alınmamıştır. Her hedefte iki koşulu da sağlayan en düşük bit değeri Denklem (6) ile seçilir. Sınır değerlerine eşit sonuçlar kabul edilir ve seçimden önce sayısal sonuçlar yuvarlanmaz. Koşulları sağlayan aday yoksa seçim tanımsız bırakılır.

$$b_{\min}(\theta_0) = \min\{b \in \{2,3,4\}: e_b(\theta_0) \le 1°, L_b(\theta_0) \le 1 \text{ dB}\} \tag{6}$$

Örneklenen bütün hedeflerde kullanılabilecek en düşük sabit çözünürlük Denklem (7) ile belirlenir. Her bit değeri, bütün hedeflerde her iki koşul açısından ayrı ayrı sınanır. Böylece

yönlendirme hatasının bit sayısıyla her zaman azalacağı varsayılmadan seçim yapılır. Hedefe göre bulunan en düşük değerlerin yalnızca en büyüğünü almakla yetinilmez. Buradaki en düşük çözünürlük, B kümesi ve belirtilen besleme kuralı için tanımlıdır.

$$b_{\text{fix}} = \min\{b \in B : e_b(\theta_0) \leq 1°, L_b(\theta_0) \leq 1 \text{ dB}, \forall \theta_0 \in T\} \quad (7)$$

Hedef yöndeki güç kaybının analitik sınırı

Hedef yönde ideal uyarım fazı ile uzaysal faz birbirini götürür. Bu nedenle normalize alan, elemanların faz hatalarını temsil eden birim fazörlerin ortalamasıdır. Hedefteki normalize güç $R_b(\theta_0) = P_{rel,b}(\theta_0;\theta_0)$ ile gösterilsin. n'inci elemanın faz hatası δ_n, uygulanan nicemlenmiş fazdan ideal fazın çıkarılması ve farkın $[-\pi,\pi)$ aralığındaki eşdeğerine dönüştürülmesiyle tanımlanır. İdeal en yakın durum nicemlemesinde $|\delta_n| \leq \pi/2^b$ sağlanır. Yuvarlama kararında kullanılan sayısal aralığı da kapsamak için $\alpha_b = \pi/2^b + \tau$ alınabilir; burada τ, 10^{-10} derecenin radyan karşılığıdır. İncelenen bit değerleri için $\alpha_b < \pi/2$ olduğundan her fazörün gerçek kısmı en az $\cos(\alpha_b)$'dir. Eşit genlikli model için Denklem (8) buradan elde edilir.

$$R_b(\theta_0) = \left|\frac{1}{N}\sum_{n=0}^{N-1} e^{j\delta_n}\right|^2 \geq \cos^2(\alpha_b) \quad (8)$$

Denklem (5) ve (8) birlikte kullanıldığında hedef yöndeki kayıp için Denklem (9)'daki üst sınır elde edilir. Fazörlerin gerçek eksene izdüşümüne dayanan bu deterministik sınır, faz hatalarının bağımsız veya düzgün dağılımlı olduğu varsayımını gerektirmez. Ortalama kaybı değil, kaybın aşamayacağı değeri verir. Ancak tepenin açısal konumunu sınırlamadığından yönlendirme hatası koşulunun yerine kullanılamaz.

$$L_b(\theta_0) \leq -20 \log_{10}\left[\cos\left(\frac{\pi}{2^b} + \tau\right)\right] \quad (9)$$

Sayısal hesaplama ve tepe konumunun doğrulanması

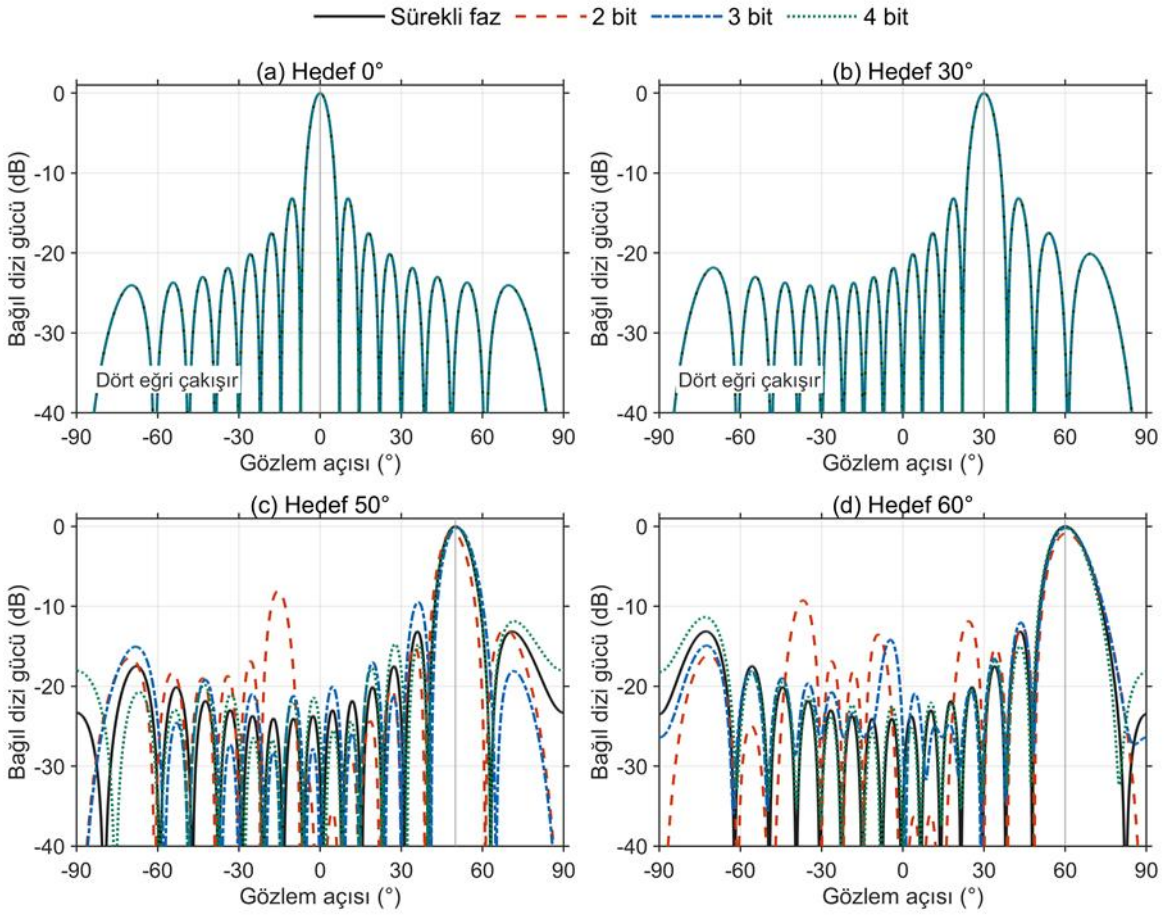
Hesaplar MATLAB R2023a ile yürütülmüştür. 61 hedefin her birinde sürekli fazlı uyarım ve üç nicemleme seçeneği olmak üzere toplam 244 durum değerlendirilmiş; bunların 183'ünde nicemlenmiş uyarım kullanılmıştır. Görünür kesit önce 0,01° aralıkla taranmış, yerel tepe konumları komşu örneklerin arasındaki aralıkta fminbnd ile daha hassas belirlenmiştir. Kesitin iki uç noktası da karşılaştırmaya alınmıştır. Aynı hesap 0,005° gözlem aralığıyla tekrarlanmıştır. Bağımsız kontrol için u=sinθ değişkeninde 0,001 aralıklı türev taraması ve işaret değişimi görülen aralıklarda fzero ile kök arama uygulanmıştır. Izgarada türevin tam sıfır olduğu noktalar ve kesitin uç noktaları da bu kontrolün tepe adaylarına dahil edilmiştir.

İki gözlem ızgarasıyla elde edilen tepe açıları arasındaki en büyük fark $2{,}49\times10^{-7}$°, bağımsız türev yöntemiyle bulunan fark ise $2{,}44\times10^{-7}$°'den küçüktür. Bu uyum sayısal tutarlılığı destekler; sonlu bir türev ızgarası, bütün durağan noktaların bulunduğuna ilişkin matematiksel bir kanıt sağlamaz. İncelenen 244 durumda eşit en yüksek tepelerden kaynaklanan bir yön belirsizliği görülmemiştir. Kabul sınırına çok yakın sonuçlar, Araştırma ve Bulgular bölümünde açıklanan analitik hesapla ayrıca kontrol edilmiştir.

ARAŞTIRMA VE BULGULAR

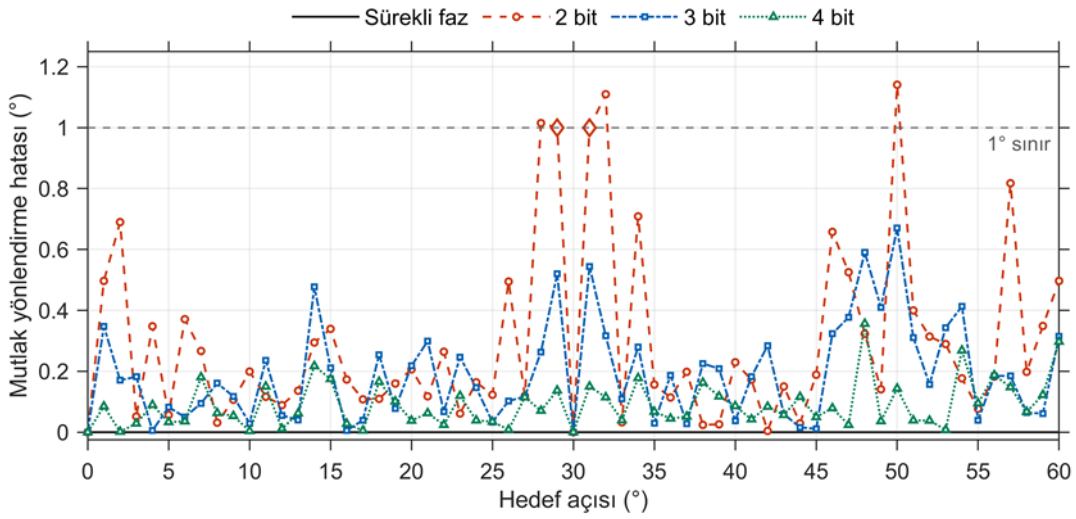
Dizi desenleri ve performans ölçütleri

Şekil 2, 0°, 30°, 50° ve 60° hedeflerindeki dizi faktörü desenlerini göstermektedir. 0° ve 30° hedeflerinde ideal fazlar incelenen bütün faz kümeleriyle tam olarak temsil edildiğinden eğriler çakışır. Diğer hedeflerde nicemleme, hedef yöndeki güç ile tepe konumunu farklı ölçüde değiştirir. Faz adımı ve hüzmenin açısal sapması aynı nicelik değildir; hüzme sapması bütün elemanların fazlarıyla oluşan desene bağlıdır.

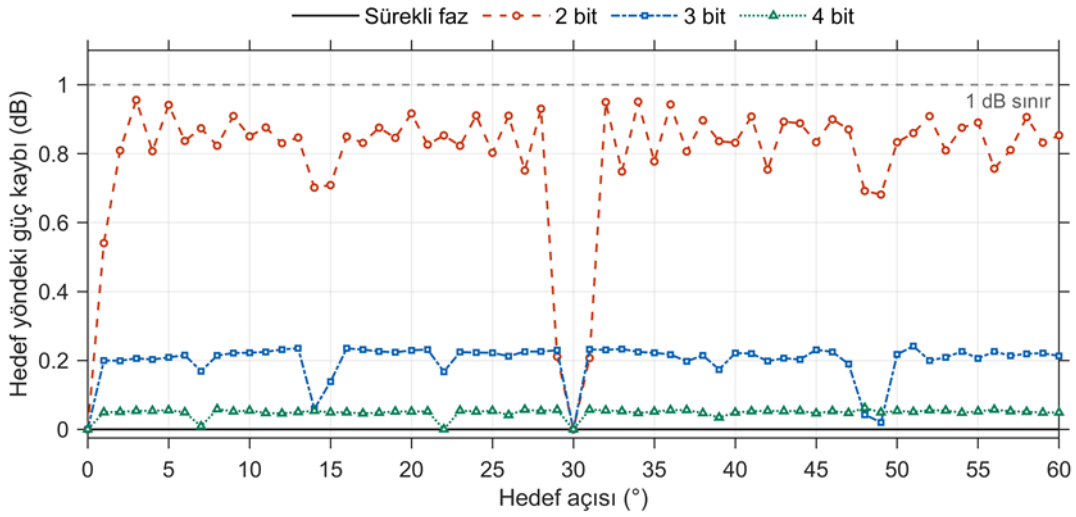


Şekil 2. (a) 0°, (b) 30°, (c) 50° ve (d) 60° hedeflerinde ortak ideal tepeye göre normalize dizi faktörü desenleri. Düşey çizgiler hedef açılardır. 0° ve 30° için dört eğri çakışır. Görsel alt sınır −40 dB'dir.

Mutlak yönlendirme hatasının hedef açıya göre değişimi Şekil 3'te, hedef yöndeki güç kaybı ise Şekil 4'te verilmiştir. 2, 3 ve 4 bit için en büyük yönlendirme hataları sırasıyla 1,140817°, 0,670429° ve 0,356260°'dir. İlk iki değer 50°, son değer 48° hedefinde oluşmuştur. En büyük güç kayıpları sırasıyla 0,955841 dB, 0,241483 dB ve 0,062138 dB olup 3°, 51° ve 48° hedeflerinde görülmüştür. Dolayısıyla en büyük yönlendirme hatası ile en büyük güç kaybı aynı hedefte oluşmayabilir.



Şekil 3. Örneklenmiş 61 hedefte mutlak yönlendirme hatası ve 1° kabul sınırı. Elmaslar, 29° ve 31° hedeflerinde analitik olarak doğrulanan tam 1° hatayı gösterir. Çizgiler yalnız hesaplanan örnekleri birleştirir.



Şekil 4. Örneklenen 61 hedefte ortak ideal referansa göre hedef yöndeki güç kaybı ve 1 dB kabul sınırı. Bütün uyarımlar aynı normalizasyona sahiptir.

Tablo 2, hesaplanan en büyük hata ve kayıpları Denklem (9)'daki analitik üst sınırla birlikte göstermektedir. 3 bit için yaklaşık 0,688 dB olan üst sınır, 1 dB kabul sınırının altındadır. Bu nedenle aynı model ve nicemleme hata sınırı altında güç kaybı koşulu, ideal hedef fazının tanımlandığı bütün yönlerde sağlanır. Yönlendirme hatasına ilişkin değerlendirme ve her iki koşulun birlikte sağlandığı sonucu ise hesaplanan 61 hedefle sınırlıdır. 2 bit için analitik üst sınırın 1 dB'yi aşması, kayıp koşulunun sağlanmadığı anlamına gelmez; incelenen 61 hedefin tamamında hesaplanan kayıp 1 dB'nin altındadır.

Tablo 2. İncelenen faz çözünürlüklerinde sayısal sonuçlar ve güç kaybının analitik üst sınırı.

Bit	Faz adımı (°)	En büyük hata (°)	En büyük kayıp (dB)	İki koşulu sağlayan	Kayıp üst sınırı (dB)
2	90	1,140817	0,955841	58/61	3,010300
3	45	0,670429	0,241483	61/61	0,687693
4	22,5	0,356260	0,062138	61/61	0,168521

Sayısal maksimumlar 61 hedef için hesaplanmıştır. Son sütun Denklem (9)'daki analitik üst sınırdır; hesaplanan en büyük kayıpla çakışması gerekmez ve yönlendirme hatasını kapsamaz. Yuvarlama kararında kullanılan sayısal tolerans hesaba katılmıştır. Değerler altı ondalık basamakla gösterilmiştir.

50° hedefinde iki kabul koşulu farklı sonuç verir. 2 bit için güç kaybı 0,833232 dB ile kabul sınırının altında kalırken yönlendirme hatası 1,140817° ile 1° sınırını aşmıştır. Aynı hedefte 3 bit için hata 0,670429°, kayıp 0,217548 dB'dir. Bu örnekte yalnız güç kaybına bakılması yeterli değildir; çözünürlük seçimini yönlendirme hatası belirler. İncelenen 183 nicemlenmiş uyarımın tamamı kayıp koşulunu sağladığından diğer hedeflerde de seçim yönlendirme hatasına bağlıdır.

Kabul sınırındaki yönlendirme hatalarının analitik kontrolü

29° ve 31° hedeflerinde 2 bit faz dağılımı, [0°,270°,180°,90°] dizisinin dört kez tekrarlanmasıyla oluşur. Her iki hedef için aynı ağırlık vektörü kullanıldığından desenler de aynıdır ve dizi faktörü Denklem (10)'a indirgenir. Böylece hedef açı değişse de nicemlenmiş faz dağılımının aynı kalabildiği görülür.

$$F(\theta) = \frac{1}{4}\sum_{n=0}^{15} \exp\left[j\pi n\left(\sin\theta - \frac{1}{2}\right)\right] \qquad (10)$$

Üçgen eşitsizliğinden $|F(\theta)| \leq 4$ elde edilir. Eşitlik, bütün terimler aynı fazdayken sağlanır; bunun koşulu $\sin\theta = 1/2 + 2k$, $k \in \mathbb{Z}$'dir. Görünür kesitte tek çözüm $\theta = 30°$ olduğundan iki hedefin de mutlak yönlendirme hatası tam 1°'dir. Her iki sonuç, eşitliğe izin veren kabul koşulunu sağlar ancak tam kabul sınırındadır. Sayısal aramada bulunan 30,0000000280793° değeri, 29° hedefinin yalnızca $2{,}8\times10^{-8}$° düzeyindeki sayısal kalıntı nedeniyle başarısız sınıflandırılmasına yol açabilirdi. Bu sınıflandırma, karar eşiği genişletilmeden kayıtlı fazların analitik tepe açısıyla düzeltilmiştir.

Hedefe bağlı ve sabit çözünürlük seçimi

Tablo 3, incelenen çözünürlükler arasında her iki koşulu sağlayan en düşük bit değerini göstermektedir. 61 hedefin 58'inde 2 bit yeterliyken 28°, 32° ve 50° hedeflerinde 3 bit seçilmiştir. Hiçbir hedefte 4 bit seçilmesine gerek kalmamıştır. 2 bit üç hedefte başarısız olurken 3 bit bütün hedeflerde iki koşulu da sağladığından, Denklem (7) ile belirlenen en düşük sabit çözünürlük 3 bittir. Bu çözünürlükte en büyük yönlendirme hatası ile 1° kabul sınırı arasında yaklaşık 0,330° fark vardır. Bu fark yalnız hesaplanan hedefler için geçerlidir; üretim veya donanım toleransını ifade etmez.

Tablo 3. Her hedefte iki koşulu birlikte sağlayan en düşük faz çözünürlüğü.

Hedef açılar (°)	Hedef sayısı	Minimum bit	Faz adımı (°)	En büyük hata (°)	En büyük kayıp (dB)
0-27	28	2	90	0,689788	0,955841
28	1	3	45	0,263471	0,225812
29-31	3	2	90	1,000000	0,211209
32	1	3	45	0,316352	0,230688
33-49	17	2	90	0,708711	0,950903
50	1	3	45	0,670429	0,217548
51-60	10	2	90	0,817478	0,908707

Seçim 2, 3 ve 4 bit seçenekleri arasındadır. Aralıklar yalnız 1° aralıklı tam sayı örneklerini kapsar. Son iki sütun, her grupta seçilen bit değerine ait en büyük hata ve kayıpları verir; bu değerler aynı hedefte oluşmak zorunda değildir. 29° ve 31° için hata analitik olarak tam 1°'dir. Değerler altı ondalık basamakla gösterilmiş, seçimde yuvarlanmamış sonuçlar kullanılmıştır.

TARTIŞMA

Hedef yöndeki güç kaybının küçük olması, desen tepesinin hedef açıda kalmasını garanti etmez. Denklem (9) güç kaybına bir üst sınır getirirken tepe konumunun belirlenmesi görünür kesitin ayrıca incelenmesini gerektirir. Yönlü modülasyonda SINR kaybını sınırlamak için yeterli bulunan bit sayısı [12], buradaki yönlendirme hatası koşulunun da sağlanacağını göstermez. Yan lob düzeyi de literatürde ayrı bir tasarım ölçütü olarak ele alınmaktadır [2, 3].

Faz referansının sabit tutulması hesapların yeniden üretilebilmesini sağlar, ancak sonuçları seçilen besleme kuralına bağlar. Ortak faz ofseti [7], doğrusal programlama [8] veya periyodik ve simetrik telafi yöntemleri [9, 10] kullanıldığında ayrık faz dağılımları ve 2 bitin yetersiz kaldığı hedefler değişebilir. Bu nedenle 28°, 32° ve 50° için 3 bit seçilmesi, olası bütün 2 bit faz dağılımlarının başarısız olacağını göstermez. Karma çözünürlüklü [14] ve delta-sigma [11] mimarilerinin sonuçları da burada kullanılan sabit yuvarlama kuralından ayrı değerlendirilmelidir.

Bit sayısını doğrudan sentez değişkeni olarak kullanan çalışmalarda desen kısıtları ile faz dağılımı birlikte ele alınır [15]. Eleman konumlarını da değiştiren ayrık faz sentezleri [16, 17] daha geniş bir tasarım uzayını araştırır. Burada ise geometri, genlikler, ortak faz ofseti ve yuvarlama kuralı sabittir. Bu sabit modelde elde edilen sonuçlar, farklı faz seçme yöntemlerinin aynı koşullarda karşılaştırılması için bir başlangıç oluşturabilir.

İnceleme tek bir eleman sayısı, eleman aralığı ve genlik dağılımıyla yürütülmüştür; bu değişkenler veya yan lob koşulları için duyarlılık analizi yapılmamıştır. 1 bit çözünürlük de incelenmemiştir. 1° aralıklarla örneklenen hedeflerin arasında kalan ve hesaplanmayan açılarda iki kabul koşulunun birlikte sağlandığı sonucuna varılamaz. Grafiklerdeki çizgiler

yalnız hesaplanan noktaları birleştirir. 4 bitin bu incelemede en düşük çözünürlük olarak seçilmemesi, daha sıkı yönlendirme hatası veya yan lob koşullarında gereksiz olduğu anlamına gelmez.

Gerçek antenlere ilişkin sonuçlar için eleman deseni, karşılıklı kuplaj, sonlu zemin, besleme ağı ve faz kaydırıcının duruma bağlı kayıpları da modellenmelidir. Dizi faktörü sentezinin ayrıntılı alan çözümünden ayrı ele alınması [13] ve kuplajlı dizilerde dijital faz sentezinin tam dalga modeliyle birleştirilmesi [18], bu gereksinimi ortaya koymaktadır. Buradaki sonuçlar ideal dizi faktörü modeliyle sınırlıdır; belirli bir anten geometrisi, S11, gerçek anten kazancı, prototip veya ölçüm sonucu içermez.

SONUÇ

16 elemanlı, yarım dalga boyu aralıklı ve eşit genlikli ideal doğrusal dizide sürekli fazlı uyarım ile eleman bazında 2, 3 ve 4 bit faz nicemlemesi karşılaştırılmıştır. Ortak faz ofseti sıfır tutulduğunda, 1° yönlendirme hatası ve 1 dB güç kaybı sınırlarını birlikte sağlayan en düşük çözünürlük 58 hedefte 2 bit, 28°, 32° ve 50° hedeflerinde 3 bittir. Bu seçim incelenen bit değerleri ve hesaplanan 61 hedef için geçerlidir. Bütün hedeflerde kullanılabilecek en düşük sabit çözünürlük 3 bit olup bu durumda en büyük yönlendirme hatası 0,670429°, en büyük güç kaybı 0,241483 dB'dir.

Fazör izdüşümünden elde edilen analitik sınır, aynı ideal modelde 3 bit için hedef yöndeki güç kaybının bütün tanımlı yönlerde 1 dB'nin altında kaldığını gösterir. Bu sınır yönlendirme hatasını kapsamaz. 29° ve 31° hedeflerindeki tam 1° hatalar, tepeyi 30°'de oluşturan faz dağılımından analitik olarak doğrulanmıştır. Sonuçlar, faz çözünürlüğü seçilirken güç kaybı ve yönlendirme hatasının birlikte değerlendirilmesi gerektiğini göstermektedir. Farklı besleme kuralları veya gerçek anten modelleri için gerekli bit sayısı yeniden belirlenmelidir.

KAYNAKÇA

[1] A. K. Bhattacharyya, Phased Array Antennas: Floquet Analysis, Synthesis, BFNs, and Active Array Systems, John Wiley & Sons, 2006. DOI: 10.1002/0471769126.

[2] N. Goto, D. K. Cheng, "Sidelobe-reduction techniques for phased arrays using digital phase shifters," IEEE Transactions on Antennas and Propagation, c. 18, no. 6, ss. 769–773, 1970. DOI: 10.1109/TAP.1970.1139797.

[3] M. S. Smith, Y. C. Guo, "A comparison of methods for randomizing phase quantization errors in phased arrays," IEEE Transactions on Antennas and Propagation, c. 31, no. 6, ss. 821–828, 1983. DOI: 10.1109/TAP.1983.1143152.

[4] W. Jiang, Y. Guo, T. Liu, W. Shen, W. Cao, "Comparison of random phasing methods for reducing beam pointing errors in phased array," IEEE Transactions on Antennas and Propagation, c. 51, no. 4, ss. 782–787, 2003. DOI: 10.1109/TAP.2003.811105.

[5] M. Clénet, G. A. Morin, "Visualization of radiation-pattern characteristics of phased arrays using digital phase shifters," IEEE Antennas and Propagation Magazine, c. 45, no. 2, ss. 20–35, 2003. DOI: 10.1109/MAP.2003.1203115.

[6] B. R. Hatcher, "Granularity of beam positions in digital phased arrays," Proceedings of the IEEE, c. 56, no. 11, ss. 1795–1800, 1968. DOI: 10.1109/PROC.1968.6753.

[7] H. Kamoda, J. Tsumochi, T. Kuki, F. Suginoshita, "A study on antenna gain degradation due to digital phase shifter in phased array antennas," Microwave and Optical Technology Letters, c. 53, no. 8, ss. 1743–1746, 2011. DOI: 10.1002/mop.26145.

[8] Y. Zhang, G. Zhao, H. Sun, M. He, Q. Chen, "Linear Programming Phase Feeding Method for Phased-Array Scanning," IEICE Transactions on Electronics, c. E99-C, no. 7, ss. 892–894, 2016. DOI: 10.1587/transele.E99.C.892.

[9] R. Zhang, N. Chen, S. Qiu, W. Sheng, "Periodic template compensation phase feeding method for phased array antenna," IET Microwaves, Antennas & Propagation, c. 17, no. 1, ss. 26–42, 2023. DOI: 10.1049/mia2.12311.

[10] S. Qiu, J. Ye, R. Zhang, X. Ma, W. Sheng, "Random symmetric phase feeding compensation method for phased array radar based on equivalent monopulse model," IET Microwaves, Antennas & Propagation, c. 17, no. 9, ss. 731–748, 2023. DOI: 10.1049/mia2.12381.

[11] J. D. Krieger, C.-P. Yeang, G. W. Wornell, "Dense Delta-Sigma Phased Arrays," IEEE Transactions on Antennas and Propagation, c. 61, no. 4, ss. 1825–1837, 2013. DOI: 10.1109/TAP.2013.2241719.

[12] J. Li, L. Xu, P. Lu, T. Liu, Z. Zhuang, J. Hu, F. Shu, J. Wang, "Performance Analysis of Directional Modulation With Finite-Quantized RF Phase Shifters in Analog Beamforming Structure," IEEE Access, c. 7, ss. 97457–97465, 2019. DOI: 10.1109/ACCESS.2019.2929549.

[13] D. Pánek, T. Orosz, P. Karban, D. C. D. Gnawa, H. K. Neghab, "Performance Comparison of Quantized Control Synthesis Methods of Antenna Arrays," Electronics, c. 11, no. 7, makale 994, 2022. DOI: 10.3390/electronics11070994.

[14] F. Shao, H. Wang, C. Huang, G. Li, W. Gong, "A Novel Phased Array Architecture with Mixed-Resolution Phase Shifters," IEICE Transactions on Communications, c. E108-B, no. 6, ss. 733–740, 2025. DOI: 10.23919/transcom.2024EBP3132.

[15] X. Zhang, X. Shi, C. Liu, X. Zhang, "Minimizing Excitation Quantization Bits in Pattern Synthesis via Mixed-Integer Programming," IEEE Transactions on Antennas and Propagation, c. 73, no. 11, ss. 8790–8804, 2025. DOI: 10.1109/TAP.2025.3587538.

[16] D. Xia, X. Zhang, "Synthesis of Sparse Arrays With Discrete Phase Constraints via Mixed-Integer Programming," IEEE Antennas and Wireless Propagation Letters, c. 23, no. 3, ss. 1030–1034, 2024. DOI: 10.1109/LAWP.2023.3342143.

[17] X. Shi, X. Zhang, C. Liu, X. Zhang, "Array geometry optimization with excitation quantization constraints: A mixed-integer programming approach," Digital Signal Processing, c. 170, makale 105795, 2026. DOI: 10.1016/j.dsp.2025.105795.

[18] J. I. Echeveste, M. Á. González de Aza, J. Rubio, J. Zapata, "Synthesis of coupled antenna arrays using digital phase control via integer programming," IET Microwaves, Antennas & Propagation, c. 12, no. 6, ss. 999–1003, 2018. DOI: 10.1049/iet-map.2017.0838.

PASİF UHF RFID SİSTEMLERİNDE ETİKET YÖNELİM DAĞILIMI VE GÜÇ MARJINA GÖRE POLARİZASYON SEÇİMİ

POLARIZATION SELECTION IN PASSIVE UHF RFID SYSTEMS BASED ON TAG ORIENTATION DISTRIBUTION AND POWER MARGIN

Ahmet TURGUT
Ondokuz Mayıs Üniversitesi, Elektrik-Elektronik Mühendisliği Bölümü, Samsun, Türkiye
ORCID: 0000-0001-6729-0266

Muhammet Rıza KARADAVUT
Ondokuz Mayıs Üniversitesi, Elektrik-Elektronik Mühendisliği Bölümü, Samsun, Türkiye
ORCID: 0000-0001-6507-3890

ÖZET

Pasif UHF RFID sistemlerinde polarizasyon uyumsuzluğu, etiket çipine aktarılan RF gücünü ve güç eşiğini sağlayan yönelimleri etkiler. Ancak çevrimde en az bir uygun yayın dilimi bulunması, güç eşiğinin toplam ne kadar süreyle sağlandığını tek başına göstermez. Bu çalışmada sabit doğrusal, ideal dairesel ve ardışık iki dik doğrusal okuyucu polarizasyonu; hedef yönünde aynı aktif EIRP ve aynı toplam gözlem süresi için karşılaştırılmıştır. İdeal doğrusal polarizasyonlu etiketin yayılma yönüne dik düzlemdeki yönelimi çevrim boyunca sabit tutulmuş, ileri bağlantı serbest uzay uzak alan modeliyle hesaplanmıştır. Kapsama olasılığı ve ortalama uygun süre oranı, yönelim destekleri ile güç eşiğini sağlayan açısal aralıkların kesişimlerinden analitik olarak elde edilmiştir. On bir yönelim senaryosu, 290 güç marjı ve beş anahtarlama boşluğu oranı incelenmiştir. Kapsama ve ortalama süre gereksinimlerinin 16 birleşimi için uygun seçenekler ve Pareto kümeleri belirlenmiş; etiket başına süre koşulu ayrı bir politika olarak değerlendirilmiştir. Sabit tohumlu Monte Carlo doğrulamasında, 990 karşılaştırma için en büyük mutlak fark 0,002544 olmuş ve önceden belirlenen 0,007276 kabul sınırını aşmamıştır. Kapsama gereksinimi 0,90 ve ortalama süre gereksinimi 0,40 olan ana profilde, üniform yönelim ve sıfır boşluk için ardışık H/V'nin ilk uygun ızgara marjı 2,4 dB'dir. CP'nin tam eşiği yaklaşık 3,0103 dB, H/V'nin sürekli kapsama geçişi ise yaklaşık 2,3791 dB'dir. Asimetrik yönelimde düşük kapsama gereksinimleri, sabit doğrusal polarizasyonun daha yüksek ortalama uygun süre oranı ile H/V'nin daha yüksek kapsaması arasında ödünleşme oluşturmuştur. Sayısal incelemeye ayrılan 72 sınır kaydı tam kesir hesabıyla çözümlenmiştir. Elde edilen uygun seçenek kümeleri, yönelim dağılımına, güç marjına ve süre politikasına bağlıdır. Bulgular ideal modelin bu koşullarına aittir; fiziksel anten tasarımı, ölçüm, çip çalışma süresi veya gerçek RFID okuma başarısı hakkında sonuç vermez.

Anahtar kelimeler: Pasif UHF RFID, polarizasyon seçimi, yönelim dağılımı, güç marjı, eşik üstü süre

ABSTRACT

Polarization mismatch in passive UHF RFID systems affects the RF power delivered to the tag chip and the orientations that meet its power threshold. The presence of an eligible slot in a cycle and the total eligible time fraction are distinct measures. This study compares fixed linear, ideal circular, and sequential orthogonal linear reader polarizations at the same active EIRP in the target direction and for the same total observation time. The orientation of an ideal linearly polarized tag, confined to the plane perpendicular to propagation, is held fixed within each cycle. A free-space far-field forward link is assumed. Coverage probability and the mean eligible time fraction are calculated analytically from intersections of orientation supports with threshold eligibility intervals. Eleven orientation scenarios, 290 power margins, and five switching gap fractions are examined. Feasible options and Pareto sets are determined for 16 combinations of coverage and mean time requirements; a separate per-tag time policy is evaluated. Fixed-seed Monte Carlo validation gives a maximum absolute discrepancy of 0.002544 across 990 comparisons, below the predefined bound of 0.007276. For the main requirements of 0.90 coverage and a 0.40 mean time fraction, uniform orientation and zero gap give a first feasible grid margin of 2.4 dB for sequential H/V. The exact CP threshold is approximately 3.0103 dB, while the continuous H/V coverage crossing is approximately 2.3791 dB. Asymmetric orientation and lower coverage requirements yield a tradeoff between the higher mean eligible time fraction of fixed linear polarization and the higher coverage of sequential H/V. All 72 boundary records marked for numerical review are resolved using exact rational calculations. The option sets depend on orientation distribution, power margin, and time policy within the stated ideal model; they do not establish measured antenna performance or successful RFID reads.

Keywords: Passive UHF RFID, polarization selection, orientation distribution, power margin, time above threshold

GİRİŞ

Pasif UHF RFID etiketinde çip, okuyucudan gelen RF gücüyle beslenir. Anten ile çip arasındaki empedans uyumuna bağlı güç aktarımı ve okuyucu alanıyla polarizasyon eşleşmesi, ileri bağlantının güç bütçesini etkiler [1, 2, 4]. Etiketin geri saçılım yanıtı ise geri bağlantının ve okuyucu algılama koşullarının da sağlanmasını gerektirir [3, 5]. Bu nedenle çip giriş gücünün eşiği sağlaması, tek başına başarılı bir RFID okumasını göstermez.

Okuyucu polarizasyonunun yazılımla değiştirilmesi ile doğrusal, dairesel ve anahtarlanan doğrusal durumların karşılaştırılması literatürde incelenmiştir. RF-Boost, polarizasyon kontrolünü okuma ve konumlandırma için kullanırken POLAR, kontrollü polarizasyonu etiket keşfi ve konumlandırmayla birleştirir [8, 9]. Bu çalışmalarda güç kalibrasyonu ve tarama süresi de değerlendirilmiştir. Dolayısıyla üç seçeneğin karşılaştırılması veya ortak EIRP kullanımı, burada başlı başına bir yöntem yeniliği olarak ele alınmamıştır.

Okuyucu anteni tasarımlarında yeniden ayarlanabilir polarizasyonlu yama yapıları ve birden fazla doğrusal polarizasyon durumu incelenmiştir [10, 11]. Dairesel polarizasyonlu

elemanlardan oluşan okuyucu dizilerinde ışınım deseninin yeniden yapılandırılması, polarizasyon durumunu değiştirmekten farklı bir yaklaşımdır [12]. Burada kullanılan ideal polarizasyon katsayıları, bu antenlerin kazancı, eksenel oranı veya anahtarlama kaybı hakkında bilgi vermez.

Çoklu RF portları, çift polarizasyonlu metal üstü etiketler ve karakteristik modlarla yönelim duyarlılığının azaltılması, çeşitliliğin etiket tarafında uygulanmasına yönelik çözümlerdir [6, 13, 15]. Yakın yerleşimli etiketlerde de polarizasyon çeşitliliği kullanılmıştır [14]. Dönen etiketin geri saçılım fazından yönelim kestirimi ile birden fazla etiketten alınan geri saçılım sinyallerinin güç istatistikleriyle yönelim algılanması ise çevrim boyunca sabit yönelim varsayan ileri güç hesabından farklı problemlerdir [16, 17].

Yönelim ve paket içeriğini birlikte inceleyen deneysel çalışmalar, yönelim duyarlılığı ile uygulama ortamı arasındaki ilişkiyi gösterir [18]. Çoklu etiket etkileşiminin istatistiksel ileri bağlantı değerlendirmesi ile sönümleme ve girişimin sistem performansına etkisi de ayrı araştırma konularıdır [19, 20]. Bu çalışmadaki dağılımlar ölçülmüş etiket nüfuslarını temsil etmez; serbest uzaydaki tek ideal etikete ilişkin varsayımsal senaryolardır. Bu varsayımlarla polarizasyon ve süre paylaşımı aynı referans altında incelenmiştir.

Bu çalışmada üç strateji, tanımlanan yönelim dağılımı ve güç marjı için kapsama olasılığı ve ortalama uygun süre oranıyla karşılaştırılmıştır. İki gereksinimi birlikte sağlayan seçenekler belirlenmiş, ardından aynı koşullardaki uygun seçeneklerin Pareto kümeleri hesaplanmıştır. Bu kümeler, kapsama ile süre paylaşımı arasındaki ilişkiyi ve birden fazla seçeneğin uygun kaldığı bölgeleri gösterir. Çalışma yeni bir anten veya evrensel olarak üstün bir polarizasyon algoritması önermez; belirtilen model için koşullu seçim sonuçları sunar.

ARAŞTIRMA VE BULGULAR

İleri bağlantı modeli ve ortak güç referansı

Etiket doğrusal polarizasyonlu kabul edilir. θ, yayılma yönüne dik düzlemde etiket ekseni ile sabit H okuyucu ekseni arasındaki açıdır. LP ekseninin π radyan dönmesi güç kuplajını değiştirmediğinden $\theta \in [0,\pi)$ kullanılır. Etiketin konumu ve yönelimi bir gözlem çevrimi boyunca sabittir; anten deseninin düzlem dışı değişimi hesaplanmaz. Aynı uzaklık r için j aktif durumundaki çip giriş RF gücü, serbest uzay uzak alan bağıntısıyla yazılır [2, 4, 7].

$$P_{chip,j}(\theta,r) = E\, G_{\text{tag}}\, \tau \left(\frac{\lambda}{4\pi r}\right)^2 p_j(\theta) \quad (1)$$

Burada E, aktif yayın sırasında hedef yönündeki toplam EIRP'yi; G_{tag}, doğrusal ölçekte etiket anten kazancını; τ, anten ile çip arasındaki empedans güç aktarım katsayısını; λ ise dalga boyunu gösterir. G_{tag} ve τ, polarizasyon kuplajından ayrı tutulur. Besleme veya anahtarlama kaybı EIRP'ye dahil edilmişse aynı kayıp çip gücünden yeniden düşülmez. İdeal CP toplam EIRP'ye göre normalize edildiğinden 1/2 kuplaj katsayısına ek bir 3 dB kayıp uygulanmaz [7].

$$p_H(\theta) = \cos^2\theta,\ \ p_V(\theta) = \sin^2\theta,\ \ p_{CP} = \frac{1}{2} \quad (2)$$

Referans marjı M, tam polarizasyon eşleşmesindeki çip gücü P_{ref} ve çip RF güç eşiği P_{th} ile tanımlanır. Fiziksel EIRP, frekans, mesafe veya çip duyarlılığına sayısal değer atanmaz;

karşılaştırmalar M üzerinden normalize edilir. Güç eşiği $\gamma p_j(\theta)\geq 1$ ile sağlanır ve eşitlik dahildir. Sıfır kuplaj, hiçbir sonlu M için bu eşiği sağlayamaz.

$$M = 10\log_{10}\left(\frac{P_{\text{ref}}}{P_{\text{th}}}\right),\quad \gamma = 10^{\frac{M}{10}} \tag{3}$$

Süre paylaşımı ve olay olasılıkları

Sabit H doğrusal polarizasyonu ve CP, toplam T boyunca aktiftir. Ardışık H/V, ana durumda her biri T/2 süreli iki dik doğrusal yayın dilimi kullanır. Anahtarlama boşluğunun duyarlılık incelemesinde H→V ve V→H geçişleri aynı çevrimde birer kez sayılır. Geçişlerin toplam yayınsız süresinin T'ye oranı d ile gösterilir. Her aktif dilimde E ve M sabit tutulur.

$$w_H = w_V = \frac{1-d}{2},\quad 0 \leq d < 1 \tag{4}$$

Boşluklu karşılaştırmada aynı aktif EIRP ve aynı toplam T korunur. Yayınsız aralıklar nedeniyle d>0 iken H/V'nin yönsel EIRP–zaman integrali, LP ve CP'ninkinden farklıdır. Boşluğu telafi etmek için aktif güç veya toplam gözlem süresi artırılmaz. Seçilen d değerleri, donanımdan ölçülmüş anahtarlama süreleri değildir.

$I_j(\theta)$, $\gamma p_j(\theta)\geq 1$ koşulunun gösterge fonksiyonudur. Her stratejinin uygun süre oranı q_s, pozitif süreli aktif dilimlerin eşik göstergeleri süre paylarıyla ağırlıklandırılarak hesaplanır. H ve V durumlarında aynı θ kullanılır; yönelim, durumlar arasında yeniden örneklenmez.

$$q_s(\theta) = \sum_j w_{sj}\, I_j(\theta) \tag{5}$$

$$C_{any,s} = Pr(q_s > 0),\quad Q_s = \mathbb{E}[q_s] \tag{6}$$

C_{any}, çevrimde en az bir pozitif süreli uygun dilim bulunma olasılığıdır; Q ise yönelim dağılımına göre ortalama uygun süre oranıdır. Q, kesintisiz besleme süresini veya çipin gerçek çalışma süresini göstermez. P_{H} ve P_{V}, H ve V olaylarının; P_{U} ve P_{B}, bu olayların birleşiminin ve kesişiminin; P_{C} ise CP olayının olasılığını gösterir. Denklem (8)'de C_{H}, C_{CP} ve C_{SEQ}, ilgili stratejilerin C_{any} değerleridir.

$$P_U = P_H + P_V - P_B \tag{7}$$

$$(C_H, C_{CP}, C_{SEQ}) = (P_H, P_C, P_U) \tag{8}$$

$$\left(Q_H, Q_{CP}, Q_{SEQ}\right) = \left(P_H, P_C, \frac{1-d}{2}(P_H + P_V)\right) \tag{9}$$

Her iki H/V diliminin süresi pozitif olduğu sürece d, C_{any} değerini değiştirmez; q ve Q, d=0 değerlerinin (1−d) katıdır. Ayrı etiket başına süre politikasında α∈{0,25; 0,50; 0,75} için $C_{\alpha,s}$=Pr($q_s\geq\alpha$) kullanılır. Bu politika $C_{\alpha}\geq 0{,}90$ ile değerlendirilir ve birincil Q≥0,40 koşulunun yerine geçirilmez. Polarizasyon kaybı $-10\log_{10}p$, sabit bir durum için normalize ileri bağlantı eşik menzili ise $\sqrt{p}$ olarak tanımlanabilir [1, 7]. Fiziksel menzil hesabı veya ayrı bir menzil sonucu üretilmemiştir.

Senaryolar ve gereksinime bağlı seçim

İncelenen senaryolar, eksensel üniform dağılım ile θ=mod(μ+V,π), V∼U[−Δ,Δ] biçimindeki sarılmış üniform sektörlerden oluşur. Δ, sektörün yarı genişliğidir; standart sapma değildir. 0° sınırını aşan destekler iki aralığa ayrılır ve kırpılmaz. Sabit H okuyucu ekseni, senaryoya göre yeniden yönlendirilmez.

Tablo 1. İncelenen yönelim dağılımları

Senaryo	Dağılım	Merkez μ	Yarı genişlik Δ
S00	Eksensel üniform	—	—
S01	Sarılmış üniform sektör	0°	5°
S02	Sarılmış üniform sektör	0°	15°
S03	Sarılmış üniform sektör	0°	30°
S04	Sarılmış üniform sektör	45°	5°
S05	Sarılmış üniform sektör	45°	15°
S06	Sarılmış üniform sektör	45°	30°
S07	Sarılmış üniform sektör	90°	5°
S08	Sarılmış üniform sektör	90°	15°
S09	Sarılmış üniform sektör	90°	30°
S10	Sarılmış üniform sektör	30°	30°

S10, H/V eksenlerine göre asimetrik olan [0°,60°] sektörünü temsil eder. M, −3…25 dB aralığında 0,1 dB adımlı 281 düzenli nokta ile önceden tanımlanan 9 ek sınır noktası olmak üzere toplam 290 noktada incelenmiştir. Beş boşluk oranı d∈{0; 0,01; 0,05; 0,10; 0,20} kullanılmıştır. Bu değerler varsayımsal çalışma girdileridir; ölçülmüş yönelim veya donanım parametreleri değildir.

Birincil uygunluk, $C_{any} \geq c_{req}$ ve $Q \geq q_{req}$ koşullarının birlikte sağlanmasıyla belirlenmiştir. Ana profilde c_{req}=0,90 ve q_{req}=0,40 kullanılmıştır. Duyarlılık ailesi, c_{req}∈{0,70; 0,80; 0,90; 0,95} ve q_{req}∈{0,25; 0,40; 0,50; 0,75} değerlerinin 16 birleşiminden oluşur. Bir uygun strateji, diğerine göre iki ölçütte de en az eşit ve en az birinde kesin olarak büyük değer veriyorsa onu baskılar. İki ölçütte de aynı değerleri veren stratejiler birlikte korunur; boş, tekli, eşdeğer ve ödünleşmeli kümeler ayrı raporlanır. Seçim için toplam puan veya sabit strateji önceliği kullanılmamıştır.

Analitik hesap ve sayısal doğrulama

Analitik değerler, uygunluk olaylarının yönelim destekleriyle kesişim uzunluklarının toplam destek genişliğine bölünmesiyle hesaplanmıştır. Hesap olay integrallerine dayandığından sabit açısal örnekleme ağı gerektirmez. CP eşik eşitliği, sıfır kuplaj, sıfır süre ve ortak H/V olay özdeşlikleri ayrıca kontrol edilmiştir. MATLAB R2023a kod doğrulamasındaki 110 kontrolün ve tam taramanın 21 tutarlılık kontrolünün tamamı geçmiştir. Toplam 15.950 tarama noktası, 255.200 birincil karar ve 47.850 ayrı etiket başına süre kararı kaydedilmiştir.

Monte Carlo, yalnız d=0 için analitik sonuçları doğrulamak amacıyla uygulanmıştır. C_{α}, 990 karşılaştırmalı doğrulama ailesine dahil değildir; etiket başına süre çıktıları analitik hesaplanmıştır. Her senaryo için N=100000 yönelim örneği, başlangıç tohumu 20260930 ve twister üreteci kullanılmıştır. Aynı yönelim örnekleri H/V durumları, stratejiler ve seçilmiş 15 marj için korunmuştur. Üç stratejinin C_{any} ve Q çıktıları için K=11×15×3×2=990 karşılaştırma yapılmıştır. [0,1] aralığındaki bağımsız örnekler için Hoeffding eşitsizliğinin iki taraflı biçimi ve birleşim sınırı kullanılarak β=0,05 aile hata olasılığına karşılık gelen kabul sınırı önceden belirlenmiştir [21]. Karşılaştırmaların birbirinden bağımsız olması, bu birleşim sınırı için gerekli değildir.

$$\varepsilon = \sqrt{\frac{\ln\left(\frac{2K}{\beta}\right)}{2N}} \tag{10}$$

C_{any} ve Q için Monte Carlo ile analitik değerler arasındaki en büyük mutlak fark 0,002544375 olup ε=0,007275501 sınırının altında kalmıştır. Bu sınır yalnız seçilmiş 990 kontrol ailesi için geçerlidir; tüm tarama noktalarına veya gerçek donanım performansına ait bir güven aralığı değildir. Uygunluk kararları Monte Carlo kestiriminden üretilmemiş ve kabul sınırı fiziksel güç eşiğine eklenmemiştir. Bağımsız kapalı ifadeler ile analitik olay olasılıkları arasındaki en büyük fark yaklaşık $4{,}61\times10^{-15}$ bulunmuştur.

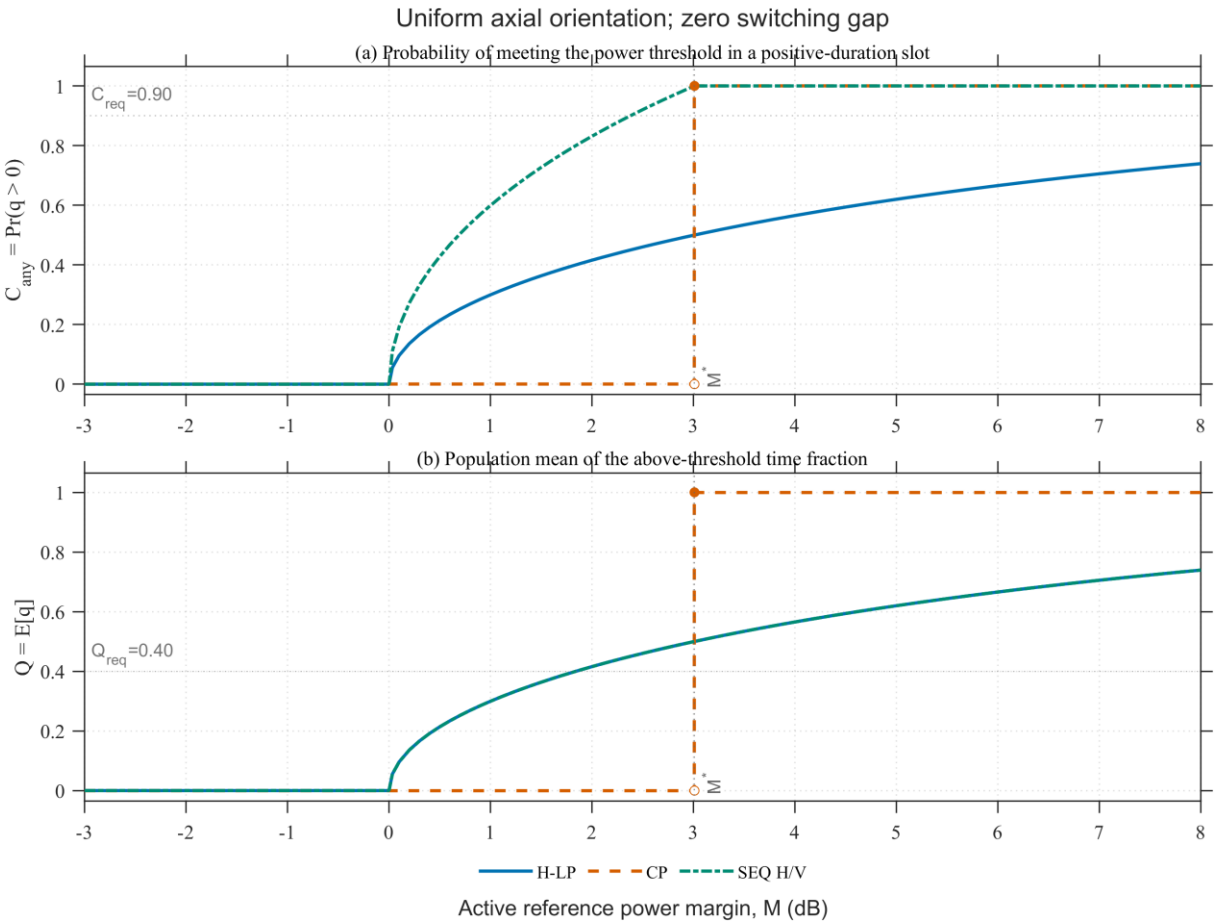
Tam taramada sayısal incelemeye ayrılan 72 birincil kayıt, tam sayı cinsinden açısal uzunluklar ve indirgenmiş kesirlerle yeniden değerlendirilmiştir. Ayrı MATLAB hesabı ile bağımsız tam kesir hesabı, 70 kayıtta uygun seçenek bulunmadığını, 2 kayıtta ise tek uygun seçeneğin ardışık H/V olduğunu doğrulamıştır. İlk hesaplanan uygunluk ve Pareto kümeleri değişmemiş; inceleme bekleyen kayıtların kesin doğrulaması tamamlanmıştır. Sonuç tablolarında bu kesin doğrulamayı içeren güncel kararlar kullanılmıştır.

Ana gereksinim altında polarizasyon seçimi

İdeal CP'de güç eşiği, bütün düzlem içi yönelimler için aynı marjda sağlanır. Bu marjın altında C_{any}=Q=0, eşikte ve üstünde C_{any}=Q=1 olur. Eşik eşitliği aşağıdaki tam ifadeyle belirlenmiştir; yuvarlanmış marj değeri kullanılmamıştır.

$$M_* = 10\log_{10} 2 \tag{11}$$

Şekil 1, üniform yönelim ve d=0 için kapsama olasılığı ile ortalama uygun süre oranını ayrı gösterir. H/V, toplam süreyi iki polarizasyon durumu arasında paylaşarak sabit H'ye göre daha geniş bir yönelim kümesini kapsar. Ana kapsama gereksiniminde H/V'nin ilk uygun ızgara marjı 2,4 dB'dir; CP'nin tam ifadeyle tanımlanan eşiği yaklaşık 3,010299956640 dB'dir. Bu değerler aktif referans güç marjlarıdır; dBm cinsinden mutlak güç veya ölçülmüş anten menzili değildir.



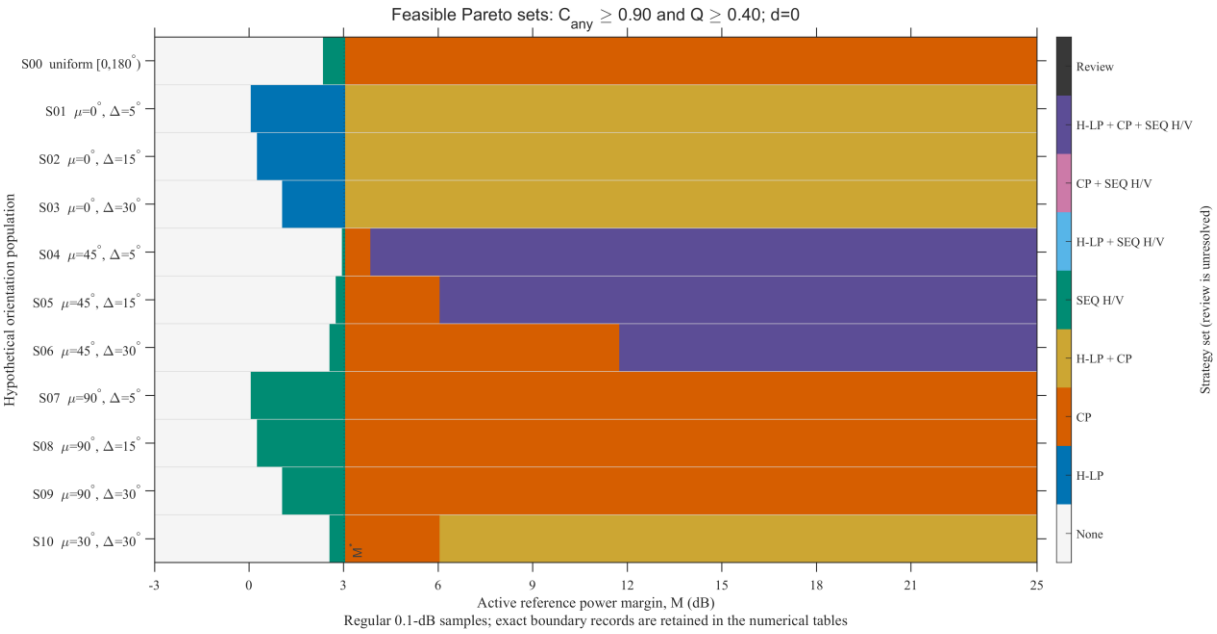
Şekil 1. Eksensel üniform yönelim ve d=0 için C_{any} ve Q eğrileri. Kapsama ve ortalama uygun süre oranı gereksinimleri ayrı çizgilerle gösterilmiştir; CP basamağı tam M_* sınırındadır.

Üniform dağılımda 0≤M<M_* için H'nin uygunluk yarı açısı a=arccos($10^{-M/20}$) radyandır. H/V olayları ayrık olduğundan $C_{any,SEQ}$=4a/π ve Q_{SEQ}=(1−d)2a/π olur. C_{any}=0,90 için sürekli marj sınırı −20log₁₀(cos40,5°)≈2,379089692602 dB'dir. Bu sınır, 2,4 dB ilk uygun ızgara noktasından ayrı raporlanır. Düzlem içi üniform yönelim, üç boyutlu izotropik yönelimden farklı bir varsayımdır.

Tablo 2. Ana profil ve d=0 için ilk doğrulanmış uygun ızgara marjları (dB)

Senaryo	H doğrusal	CP	Ardışık H/V
S00	16,200000	3,010300	2,400000
S01	0,033115	3,010300	0,033115
S02	0,300000	3,010300	0,300000
S03	1,100000	3,010300	1,100000
S04	3,700000	3,010300	3,000000
S05	5,300000	3,010300	2,800000
S06	9,000000	3,010300	2,600000
S07	Izgarada yok	3,010300	0,033115
S08	Izgarada yok	3,010300	0,300000
S09	Izgarada yok	3,010300	1,100000
S10	4,700000	3,010300	2,600000

Tablo 2, taranan −3…25 dB aralığındaki ilk uygun ızgara noktalarını verir. "Izgarada yok", yalnız bu aralıkta uygun nokta bulunmadığı anlamına gelir. Uygun bir seçenek başka bir strateji tarafından baskılanabileceğinden tablo, Pareto tercihini tek başına belirtmez. Şekil 2, aynı ana profil için uygun seçeneklerin Pareto kümelerini gösterir. CP, eşikte ve üstünde (1,1) değerleriyle Pareto kümesinde kalır; aynı değerleri veren diğer seçenekler de eşdeğer kümede korunur.

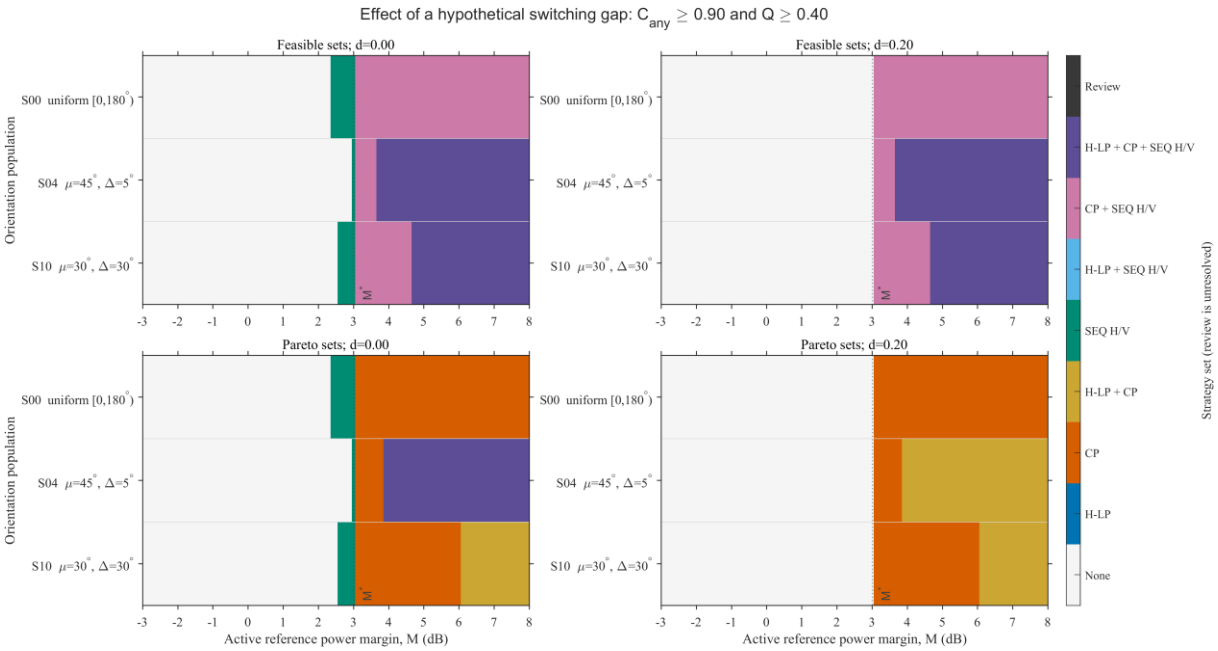


Şekil 2. C_{any}≥0,90 ve Q≥0,40 koşullarında d=0 için senaryoya bağlı Pareto kümeleri. Harita, düzenli 0,1 dB adımlı noktaları gösterir; hücre sınırları sürekli modeldeki kesin geçiş marjları değildir. Ek kritik marjlar, sayısal tarama tablolarında ayrıca değerlendirilmiştir.

H ekseni çevresindeki sektörlerde sabit H ve ardışık H/V aynı yönelimleri kapsadığında, sabit H daha yüksek Q sağlayarak H/V'yi baskılayabilir. V ekseni çevresindeki sektörlerde, sabit H'nin güç eşiğini sağlayamadığı düşük marjlarda H/V uygun olabilir. 45° merkezli sektörlerde ilk uygun H/V marjı, sektör genişliğine göre değişir. Sonuçlar, belirtilen destekler ve sabit H okuyucu ekseni için geçerlidir; okuyucu ekseninin ayrıca optimize edildiği bir tasarıma genelleştirilmez.

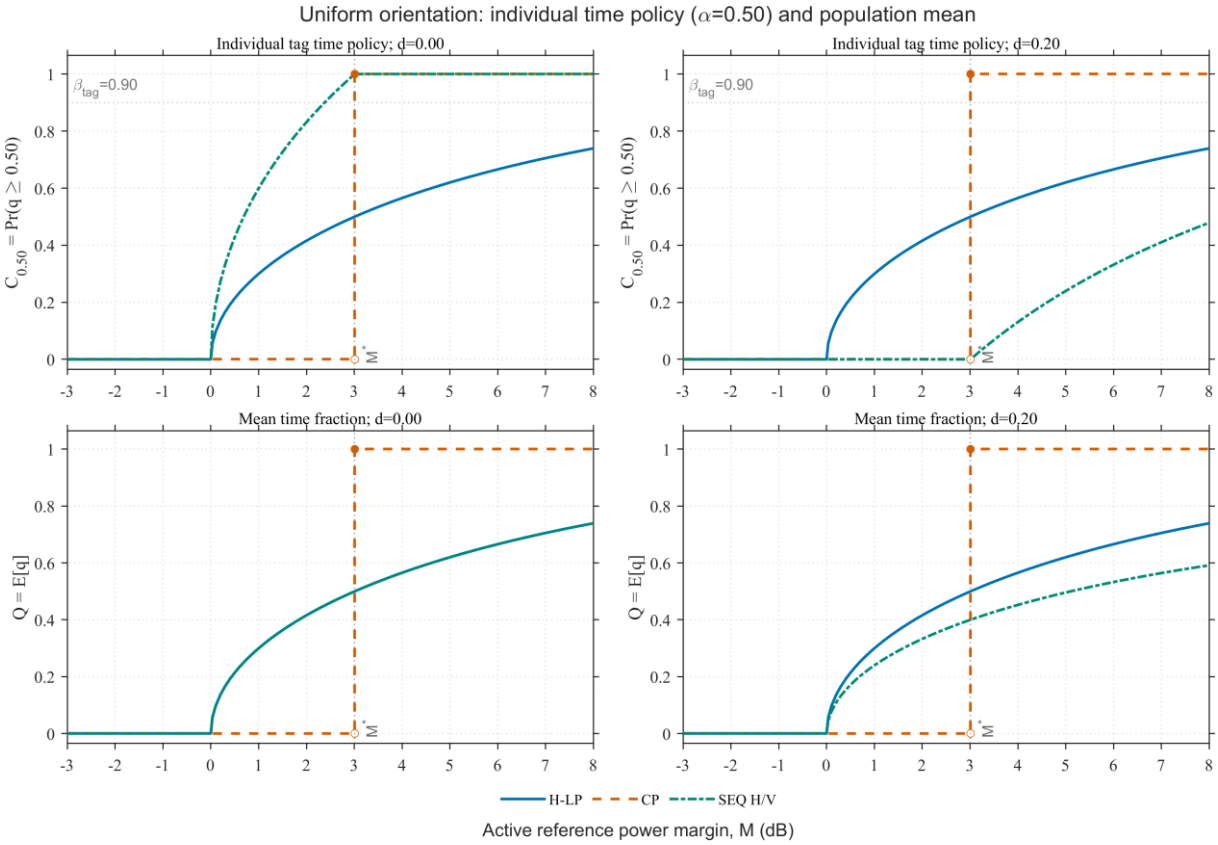
Anahtarlama boşluğu ve etiket başına süre

H/V için Q≥(1−d)C_{any}/2 olduğundan C_{any}≥0,90, d≤1/9 iken Q≥0,40 koşulunu da sağlar. Bu nedenle ana d=0 değerlendirmesinde ortalama süre koşulu ek eleme yapmaz; Q yine bir çıktı ve Pareto ölçütüdür. d=0,20 için kapsama koşulu, süre koşulunu tek başına garantilemez. Bu boşluk oranında CP eşiğinin altındaki ayrık H/V bölgesinde Q=0,40C_{any} olduğundan ana süre koşulu ancak C_{any}=1 ile sağlanır. Üniform yönelimde CP eşiğinin altında tam kapsama sağlanamaz.



Şekil 3. Ana profil için S00, S04 ve S10 senaryolarında d=0 ile d=0,20 karşılaştırması. Uygun kümeler ve Pareto kümeleri ayrı gösterilmiştir; aktif güç marjı sabittir.

Etiket başına uygun süre oranı için α=0,50 seçildiğinde, d=0 için tek uygun H veya V dilimi yeterlidir ve $C_{\alpha,\mathrm{SEQ}}=P_{\mathrm{U}}$ olur. Seçilen pozitif d değerlerinde {0,01; 0,05; 0,10; 0,20}, tek dilimin payı 0,50'nin altında kalır. Her iki dilim de uygunsa toplam uygun süre oranı 0,50 koşulunu sağlar; dolayısıyla $C_{\alpha,\mathrm{SEQ}}=P_{\mathrm{B}}$ olur. Q'nun (1−d) ile ölçeklenmesi ile bu etiket başına süre olayının değişmesi ayrı sonuçlardır. P_{B} açıklaması, burada yalnız incelenen pozitif d değerleri için verilmiştir.



Şekil 4. S00 için α=0,50 etiket başına süre kapsaması ve ortalama uygun süre oranı Q. Gösterilen pozitif d değerlerinde α koşulu, yalnız her iki H/V dilimi de uygun olduğunda sağlanır.

Asimetrik yönelim ve koşullu seçenek kümeleri

Birincil karar tablosunda 45 kayıtta ödünleşmeli Pareto kümeleri bulunmuş; bu kayıtların tamamı S10 senaryosunda oluşmuştur. C_{any}≥0,70 ve Q≥0,25 profilinde beş d değeri için toplam 25; C_{any}≥0,70 ve Q≥0,40 profilinde d≤0,10 olan dört değer için toplam 20 kayıt vardır. Bu kayıtlar düzenli 2,6…3,0 dB noktalarındadır. Ana C_{any}≥0,90 ve Q≥0,40 profilinde ödünleşmeli kayıt yoktur; eşdeğer seçenekler ayrı tutulmuştur.

S10, M=2,8 dB ve d=0 için sabit H'de C_{any}≈0,726301 ve Q≈0,726301; ardışık H/V'de ise C_{any}≈0,952602 ve Q≈0,476301 bulunur. C_{any}≥0,70 ve Q≥0,40 profilinde iki seçenek de uygundur. H daha yüksek ortalama uygun süre oranı, H/V daha yüksek kapsama sağladığından birbirlerini baskılamazlar. Ana 0,90 kapsama gereksiniminde H elenir. Aynı metrik değerleriyle farklı gereksinimlerin farklı uygun ve Pareto kümeleri vermesi, bu örnekte açıkça görülür.

Kesin sınır incelemesindeki iki H/V uygun kaydı, S00 ve d=0,10 için C_{any}≥0,70 ve Q≥0,40 ile C_{any}≥0,80 ve Q≥0,40 profillerine aittir. B07=−10log₁₀(cos²40°) olarak tanımlanan kesin marjda $C_{any,SEQ}$=8/9 ve Q_{SEQ}=2/5 bulunur; süre koşulu eşitlikle sağlanır. Bu iki profilin ilk doğrulanmış uygun H/V ızgara marjı yaklaşık 2,314920668930 dB'dir. Bu noktadaki 8/9 kapsama, ana 0,90 gereksinimini karşılamadığından ana sonuç değişmez.

Modelin uygulama sınırları

Sonuçlar, aynı aktif güç referansı ve tanımlanan yönelim dağılımları altında hangi seçeneklerin iki gereksinimi sağladığını gösterir. Anten geometrisi ve üretim bu çalışmanın kapsamı dışındadır; eksenel oran, yön örüntüsü, çok yollu yayılım, malzeme yüklemesi ve çoklu etiket kuplajı hesaplanmamıştır. Tanımlanan uygun süre oranı, çipte enerji birikmesini veya açılma dinamiğini temsil etmez. Başarılı bir RFID okuması için geri bağlantı ve protokol zamanlaması koşulları da sağlanmalıdır [3, 5]. c_{req}, q_{req} ve α, ölçülmüş ürün koşulları veya bir standarttan alınmış zorunlu değerler değildir; bu çalışmanın politika parametreleridir.

SONUÇ

İncelenen modelde sabit doğrusal, ideal CP ve ardışık H/V seçimi; güç marjına, yönelim dağılımına ve süre gereksinimine bağlıdır. Ana profilde üniform yönelim ve sıfır boşluk için H/V, 2,4 dB ilk uygun ızgara noktasında koşulları sağlar; CP'nin tam eşiği yaklaşık 3,0103 dB'dir. H ekseni çevresindeki dar sektörlerde, aynı kapsamayı sağlayan sabit H'nin ardışık H/V'ye göre daha yüksek uygun süre oranı verebildiği görülmüştür. S10'un asimetrik desteğinde düşük kapsama profilleri, iki ölçüt arasında ödünleşme oluşturmuştur.

Her iki H/V dilimi pozitif süreli olduğu sürece, anahtarlama boşluğu C_{any}'yi değiştirmez ve Q'yu (1−d) ile ölçeklendirir. Etiket başına süre koşulunda ise seçilen pozitif boşluk oranları uygunluk olayını değiştirebilir. Bu koşullardaki uygun ve Pareto kümeleri, belirtilen model ve gereksinimler için seçim sonuçlarını verir. Donanım uygulamasında anten performansı, geri bağlantı ve protokol zamanlaması ayrıca değerlendirilmelidir.

KAYNAKÇA

[1] Pavel V. Nikitin, K. V. S. Rao. “Antennas and Propagation in UHF RFID Systems.” 2008 IEEE International Conference on RFID, ss. 277–288, 2008. DOI: 10.1109/RFID.2008.4519368.

[2] K. V. Seshagiri Rao, Pavel V. Nikitin, Sander F. Lam. “Antenna design for UHF RFID tags: a review and a practical application.” IEEE Transactions on Antennas and Propagation, 53(12), ss. 3870–3876, 2005. DOI: 10.1109/TAP.2005.859919.

[3] Pavel V. Nikitin, K. V. S. Rao. “Theory and measurement of backscattering from RFID tags.” IEEE Antennas and Propagation Magazine, 48(6), ss. 212–218, 2006. DOI: 10.1109/MAP.2006.323323.

[4] Pavel V. Nikitin, K. V. S. Rao. “Performance limitations of passive UHF RFID systems.” 2006 IEEE Antennas and Propagation Society International Symposium, ss. 1011–1014, 2006. DOI: 10.1109/APS.2006.1710704.

[5] Daniel G. Kuester, David R. Novotny, Jeffrey R. Guerrieri. “Forward and reverse link constraints in UHF RFID with passive tags.” 2010 IEEE International Symposium on Electromagnetic Compatibility, ss. 680–685, 2010. DOI: 10.1109/ISEMC.2010.5711359.

[6] Pavel V. Nikitin, K. V. S. Rao. “Performance of RFID tags with multiple RF ports.” 2007 IEEE Antennas and Propagation Society International Symposium, ss. 5459–5462, 2007. DOI: 10.1109/APS.2007.4396783.

[7] Pavel V. Nikitin, K. V. S. Rao. “Reply to "Comments on 'Antenna Design for UHF RFID Tags: A Review and a Practical Application'".” IEEE Transactions on Antennas and Propagation, 54(6), ss. 1906–1907, 2006. DOI: 10.1109/TAP.2006.875934.

[8] Laura Dodds, Nazish Naeem, Aline Eid, Fadel Adib. “Software-Controlled Polarization for Longer-Range RFID Reading and Localization.” 2023 IEEE International Conference on RFID (RFID), ss. 90–95, 2023. DOI: 10.1109/RFID58307.2023.10178674.

[9] Laura Dodds, Isaac Perper, Aline Eid, Fadel Adib. “A Handheld Fine-Grained RFID Localization System with Complex-Controlled Polarization.” Proceedings of the 29th Annual International Conference on Mobile Computing and Networking (ACM MobiCom ’23), makale 7, ss. 1–15, 2023. DOI: 10.1145/3570361.3592504.

[10] Enrico Tolin, Francesca Vipiana, Simona Bruni, Achim Bahr. “Polarization Reconfigurable Patch Antenna for Compact and Low Cost UHF RFID Reader.” 2019 IEEE International Conference on RFID Technology and Applications (RFID-TA), ss. 128–130, 2019. DOI: 10.1109/RFID-TA.2019.8892109.

[11] Trang Hoang-Thu, Hung Pham-Duy, Hung Tran-Huy, Hyun Chang Park. “A Simple Patch Antenna Design with Multiple Linear Polarizations for RFID Readers.” IEEE Latin America Transactions, 24(6), ss. 629–635, 2026. DOI: 10.1109/TLA.2026.11494746.

[12] Md Abu Saleh Tajin, Kapil R. Dandekar. “Pattern Reconfigurable UHF RFID Reader Antenna Array.” IEEE Access, 8, ss. 187365–187372, 2020. DOI: 10.1109/ACCESS.2020.3031296.

[13] E.-S. Yang, H.-W. Son. “Dual-polarised metal-mountable UHF RFID tag antenna for polarisation diversity.” Electronics Letters, 52(7), ss. 496–498, 2016. DOI: 10.1049/el.2016.0076.

[14] Qi Zhang, Michael J. Crisp, Richard V. Penty, Ian H. White. “Reduction of Proximity Effects on UHF Passive RFID Systems by Using Tags With Polarization Diversity.” IEEE Transactions on Antennas and Propagation, 63(5), ss. 2264–2271, 2015. DOI: 10.1109/TAP.2015.2403875.

[15] Abubakar Sharif, Jun Ouyang, Muhammad Ali Imran, Qammer H. Abbasi. “Orientation insensitive UHF RFID Tag Antenna with polarization diversity using Characteristic Mode Analysis.” 2019 IEEE International Symposium on Antennas and Propagation and USNC-URSI Radio Science Meeting, ss. 651–652, 2019. DOI: 10.1109/APUSNCURSINRSM.2019.8888324.

[16] Emidio Di Giampaolo, Francesco Martinelli, Fabrizio Romanelli. "Exploiting Polarization Mismatch to Estimate the Orientation of Rotating UHF RFID Tags." IEEE Journal of Radio Frequency Identification, 7, ss. 284–292, 2023. DOI: 10.1109/JRFID.2023.3263383.

[17] Rasmus Krigslund, Petar Popovski, Gert F. Pedersen. "Orientation Sensing Using Multiple Passive RFID Tags." IEEE Antennas and Wireless Propagation Letters, 11, ss. 176–179, 2012. DOI: 10.1109/LAWP.2012.2185918.

[18] Robert H. Clarke, Diana Twede, Jeffrey R. Tazelaar, Kenneth K. Boyer. "Radio frequency identification (RFID) performance: the effect of tag orientation and package contents." Packaging Technology and Science, 19(1), ss. 45–54, 2006. DOI: 10.1002/pts.714.

[19] Aiman Mughal, Jithin Mudakkarappilli Sudersanan, Shermila Mostarshedi, Benoit Poussot, Jean-Marc Laheurte. "Statistical Evaluation of the Coupling Effects Between Tags in a UHF RFID Forward Link." IEEE Journal of Radio Frequency Identification, 7, ss. 257–266, 2023. DOI: 10.1109/JRFID.2023.3293207.

[20] Abdelmoula Bekkali, Sicheng Zou, Abdullah Kadri, Michael Crisp, Richard V. Penty. "Performance Analysis of Passive UHF RFID Systems Under Cascaded Fading Channels and Interference Effects." IEEE Transactions on Wireless Communications, 14(3), ss. 1421–1433, 2015. DOI: 10.1109/TWC.2014.2366142.

[21] Wassily Hoeffding. "Probability Inequalities for Sums of Bounded Random Variables." Journal of the American Statistical Association, 58(301), ss. 13–30, 1963. DOI: 10.1080/01621459.1963.10500830.

PİEZOELEKTRİK HAPTİK SİNYALLERİN ALGISAL KARAKTERİZASYONU İÇİN TAŞINABİLİR BİR TEST CİHAZI TASARIMI

DESIGN OF A PORTABLE TEST DEVICE FOR PERCEPTUAL CHARACTERIZATION OF PIEZOELECTRIC HAPTIC SIGNALS

Özgür TAMER
Dokuz Eylül Üniversitesi, Elektrik Elektronik Müh. Böl., İzmir

Ömür Öcal
Core Bina Otomasyon Teknolojileri San ve Tic Ltd. Şti., İzmir, Turkey

Mehmet Öztemel
Core Bina Otomasyon Teknolojileri San ve Tic Ltd. Şti., İzmir, Turkey

ÖZET

Bu çalışmada, piezoelektrik haptik sinyallerin kullanıcı tarafından ayırt edilebilirliğinin belirlenmesi için geliştirilen taşınabilir bir test cihazı sunulmaktadır. Sistem; ESP32 tabanlı kontrol, MAX77501 piezo sürücü, 4×3 kapasitif buton dizisi ve mobil tarayıcıdan erişilen web arayüzünü bir araya getirmektedir. Python tabanlı sentez altyapısında on iki sinyal ailesi tanımlanmıştır. Sağlanan referans grafikte yedi dalga formu 32 kHz örnekleme hızında, 12, 30, 60 ve 80 Vpp hedef gerilimlerle gösterilmektedir. Test sırasında seçilen altı sinyal iki buton grubuna rastgele dağıtılmakta, kullanıcı aynı hissettiği uyaranları eşleştirmekte ve sonuçlar raporlanmaktadır. Teknik belgelerde 0,9 µF kapasitanslı, 120 V sınıfı eyleyicilerin sürülmesinde düşük gerilim kilidi olayları ve mekanik yük altında kararsızlık bildirilmiştir. Frekans azaltılması daha yüksek komut seviyelerini mümkün kılmış, ancak kararlı çalışma doğrulanmamıştır. Çalışma; donanım tasarımı, sinyal sentezi, eşleştirme protokolü ve fiziksel doğrulama gereksinimlerini birlikte ele almaktadır.

Anahtar Kelimeler: Piezoelektrik haptik; sinyal sentezi; algısal karakterizasyon; eşleştirme testi; MAX77501; gömülü sistem.

ABSTRACT

This paper presents a portable test device developed to assess the perceptual discriminability of piezoelectric haptic signals. The system combines ESP32-based control, a MAX77501 piezo driver, a 4×3 capacitive button array, and a browser-based mobile interface. Twelve signal families are defined in a Python synthesis framework. The supplied reference plot illustrates seven waveforms at a sampling rate of 32 kHz and target voltage swings of 12, 30, 60, and 80 Vpp. During a test, six selected signals are randomly assigned to two button groups; the participant matches stimuli perceived as identical, and the responses are reported. Technical records describe undervoltage lockout events and mechanical-load-dependent instability when driving 120 V-class actuators with a capacitance of 0.9 µF. Lowering the

frequency enabled higher command settings, but stable operation was not established. The study integrates device architecture, waveform synthesis, the matching protocol, and physical validation requirements.

Keywords: Piezoelectric haptics; waveform synthesis; perceptual characterization; matching test; MAX77501; embedded systems.

INTRODUCTION (GİRİŞ)

Dokunsal geri bildirim, insan–makine etkileşiminde görsel ve işitsel kanalları tamamlayan bir bilgi aktarım yöntemidir. Vibrotaktil ekranlara ilişkin literatür, algısal özelliklerin eyleyici teknolojisi ve uygulama bağlamıyla birlikte değerlendirilmesi gerektiğini göstermektedir [1]. Piezoelektrik sürüşte gerilim profili, mekanik bağlantı ve temas koşulları birlikte hissedilen uyaranı belirlemektedir.

Bu çalışmanın odağı, akıllı ev oda kontrol paneline yönelik daha geniş bir Ar-Ge projesinden türetilen haptik test cihazının sunulmasıdır . Amaç, farklı dalga biçimlerinin yalnızca üretilmesi değil, kullanıcılar açısından ne ölçüde ayrıştığının kayıt altına alınmasıdır. Böylece panelde kullanılacak bildirimler için karıştırılma eğilimi düşük aday sinyallerin seçilmesine yönelik bir altyapı sağlanır.

Araştırma problemi ve kapsam

Dokunma algısındaki dört psikofizik kanalın birlikte yaklaşık 0,4 Hz'den 500 Hz'in üzerine uzanan bir duyarlılık aralığı oluşturduğu bildirilmiştir [2]. Bu bulgu, tek bir "ideal frekans" yerine farklı zamansal profillerin araştırılmasını destekler; cihazın aynı aralıkta kalibre edildiği anlamına gelmez.

El biyomekaniği boyunca yayılan titreşimlerin duyusal bilgiyi dönüştürebildiği gösterilmiştir [3]. Bu nedenle elektriksel referans dalga formu, parmak ucuna iletilen mekanik dalga formuyla özdeş kabul edilmemelidir.

Bildirinin katkısı; prototip mimarisini, on iki sinyal ailesini ve altı çiftli eşleştirme yöntemini ortak bir karakterizasyon çerçevesinde sunmaktır. Ön gözlemler, analitik hesaplamalar ve önerilen doğrulamalar ayrı tutulmuştur.

ARAŞTIRMA VE BULGULAR

1. Cihaz tasarımı ve çalışma prensibi

Donanımın işlevsel yapısı

Çalıpmamız, özel bir üç boyutlu baskı gövde içine yerleştirilen prototipi ve 4×3 kapasitif buton girişini tanımlamaktadır . ESP32 mikrodenetleyicisi, dokunma olaylarının işlenmesi ve Wi-Fi üzerinden test hizmetinin sunulmasında kullanılmaktadır. Üretilen prototipte piezo sürüş için MAX77501 entegresi kullanılmıştır .



Şekil 1. Haptik test cihazı prototipi. Gövde ve buton yüzeylerinin fiziksel düzeni gösterilmektedir .

İşlevsel akış; butona dokunulması, ilgili uyaran kimliğinin belirlenmesi, sürüş komutunun uygulanması, titreşimin hissedilmesi ve kullanıcının eşleştirme yanıtının web arayüzünden kaydedilmesidir. Kontrol zinciri ile sonuç raporlama zinciri ayrıdır; bu ayrım, eşleştirme kararının uyaran üretiminden bağımsız izlenmesini sağlamaktadır.

Piezo sürücü ve gerilim tanımları

Üreticiye göre MAX77501, 2,8–5,5 V giriş beslemesinden 110 Vpk-pk genliğe kadar tek uçlu dalga formu üretebilir; 2 µF'a kadar piezo yükler için optimize edilmiştir. Entegre 12 bit oynatma DAC'ı, RAM oynatma ve gerçek zamanlı akış kipleri, 8k RAM ve 9k FIFO tamponları ile 25 MHz SPI arabirimi içerir [4]. Bunlar sürücü özellikleridir; prototipin her yükte aynı performansı gösterdiğine ilişkin ölçüm değildir.

130 Hz'de yaklaşık %30 düzeyindeki ayarla çalıştırılabilen 120 V sınıfı eyleyicilerin, daha düşük frekansta %100 ayarda tahrik edilebildiği, fakat tutarlı çalışma gözlenmediği raporlanmıştır , . Yüzde ayarlarının fiziksel güç, DAC ölçeği veya gerilim yüzdesine karşılığı belgelenmemiştir. Bu ifadeler "komut seviyesi" olarak kullanılmış; %100 ayar 120 V çıkış ya da tam mekanik kapasite anlamına getirilmemiştir.

Haberleşme ve arayüz

Cihaz yerel Wi-Fi erişim noktası üzerinden "Haptik_Test_Cihazi" ağına bağlanan telefon, tablet veya bilgisayara web hizmeti sunar. Kılavuzda erişim adresi 192.168.4.1 olarak verilmektedir . Buradaki mobil uygulama, ayrı bir yerel uygulama değil tarayıcı tabanlı arayüzdür. Başlangıçta yeşil LED iki saniye yanıp söner; test sırasında sabit yanar ve test sonunda söner.

Kullanıcı fiziksel butonlardan uyaranı alırken operatör sanal ızgaradan yanıtı kaydeder. Bağlanan çiftlerin devre dışı bırakılması, aynı butonun ikinci kez eşleştirilmesini önler. Bu durum yönetimi, test kayıtlarının altı benzersiz çiftten oluşmasını sağlar .

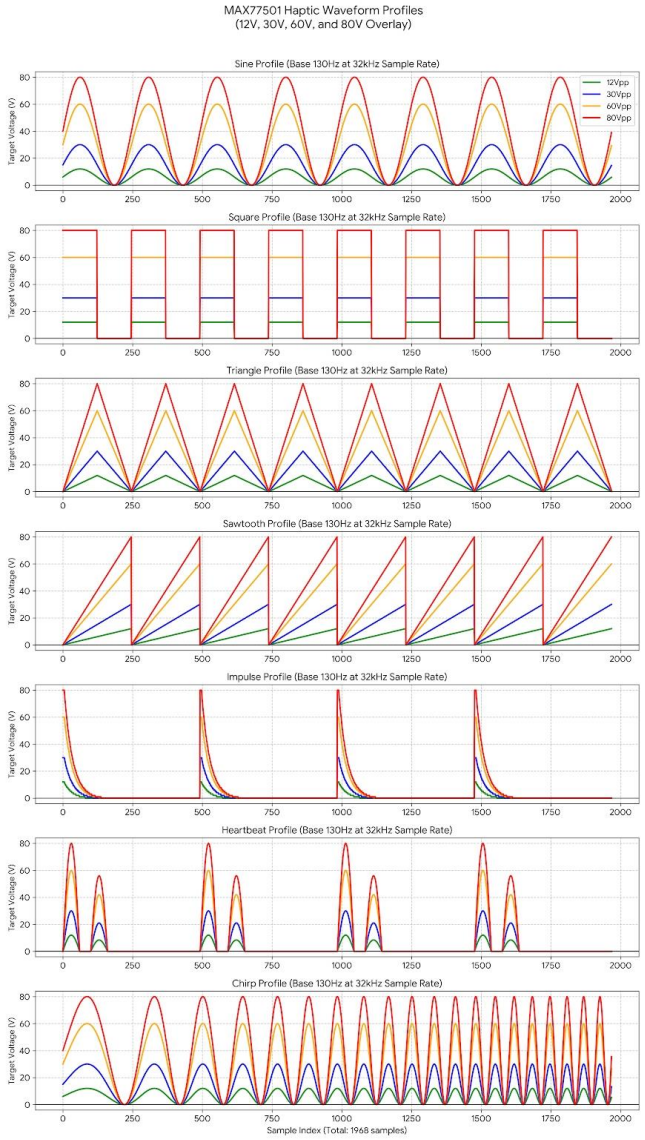
2. Sinyal kütüphanesi ve sentez

On iki sinyal ailesi

Frekans ve genlik parametreleri değiştirilebilen bir Python betiğiyle on iki profil üretilmiştir . Tablo I tam kütüphaneyi verir; Şekil 2 ise bu ailelerden yedisini görselleştirir.

TABLO I. Profil kütüphanesi .

No	**Profil**	**No**	**Profil**
1	Sinüs	7	Ters yönlü darbe
2	Genliği modüle edilmiş sinüs	8	Boşluklu sinüs
3	Üçgen	9	Değişken testere dişi
4	Testere dişi	10	Kalp atışı
5	Kare	11	Chirp
6	Darbe / impulse	12	Artan–azalan chirp



Şekil 2. Sağlanan referans grafik: sinüs, kare, üçgen, testere dişi, üstel sönümlü darbe, çift atımlı kalp atışı ve chirp profilleri. Yeşil, mavi, turuncu ve kırmızı eğriler sırasıyla 12, 30, 60 ve 80 Vpp hedef salınımları temsil eder. Grafik etiketleri 32 kHz örnekleme ve 1968 örnek belirtir. Eğriler hedef gerilimlerdir; ölçülmüş sürücü çıkışı veya ivme kaydı değildir.

Grafikteki sinüs, kare, üçgen ve testere profilleri benzer tekrar aralığına sahiptir. Darbe ve kalp atışı paketleri daha seyrek tekrarlanır; chirp'in anlık frekansı artar. Dolayısıyla "130 Hz taban" etiketi tüm profillerin tek ve sabit bir temel frekansa sahip olduğunu göstermez.

Örnekleme ve süre

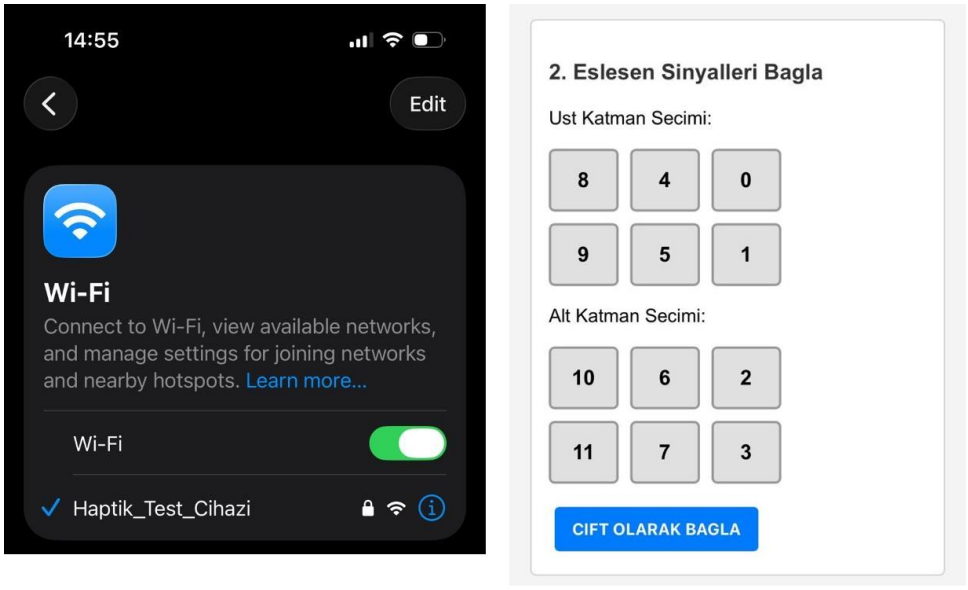
Örnekleme hızı f_s ve örnek sayısı N için oynatma penceresi $T = N/f_s$ olarak hesaplanır. Bu kampsamda 30 Hz profiller için fs = 32 kHz ve N = 8000 verilmiştir; bu değerler T = 250 ms ve 7,5 periyot eder . Referans görselde N = 1968 olduğundan pencere 61,5 ms'dir. 130 Hz için bu pencerede yaklaşık 7,995 periyot bulunur; sayı tam sekiz periyot olarak sunulmamalıdır.

Dalga biçimi parametreleri

Unipolar sinüs için temsilî hedef ifade $v[n] = (V_{pp}/2)\{1 + \sin(2\pi f\, n/f_s + \varphi)\}$ olarak sunulmaktadır. Bu ifade merkez değerin $V_{pp}/2$ olduğunu açıklar; betiğin gerçek kaynak kodu paylaşılmadığından birebir uygulama formülü olarak sunulmamıştır. Darbede sönüm sabiti, kalp atışında iki atım aralığı, chirp'te başlangıç/bitiş frekansları ve modülasyonda zarf frekansı kayıt altına alınmalıdır.

3. Mobil web arayüzü ve test akışı

Kılavuzda bağlantı, grup seçimi, buton eşleştirme, testin sonlandırılması ve yazdırma/PDF olarak kaydetme adımları tanımlanmıştır . Şekil 3-4, kılavuz içine gömülü ekran görsellerinden alınmıştır. Belgede yer alan örnek sonuçlar, bu bildirinin katılımcı veri seti olarak değerlendirilmemiştir.



(a) (b)

Şekil 3(a). Kullanım kılavuzundaki mobil ekran görseli; tarayıcı üzerinden kullanılan test sisteminin işleyişini belgeleyen arayüz örneği . Şekil 3(b). Kullanım kılavuzundaki diğer mobil ekran görseli. Arayüz, fiziksel cihaz üzerinde hissedilen uyaranlara ilişkin test adımlarının yürütülmesini sağlar .

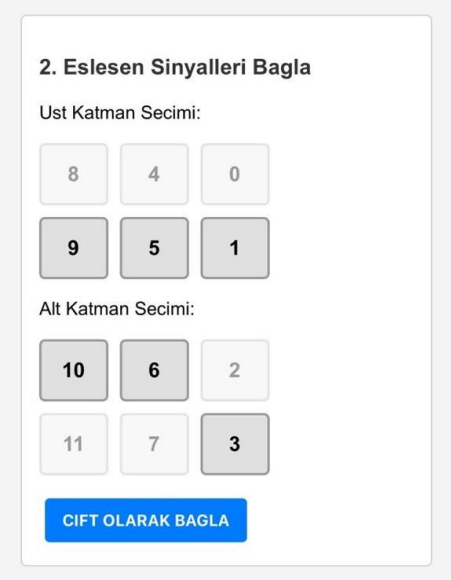
Oturum yönetimi

Yeni test başlatıldığında seçilen altı sinyal iki katmana rastgele yerleştirilir. Kullanıcının aynı hissettiğini bildirdiği bir üst ve bir alt buton seçilir; "çift olarak bağla" işlemiyle her ikisi kilitlenir. Altı çift tamamlandığında sonlandırma komutu, gizli sinyal kimliklerini ve doğru/yanlış durumlarını gösteren sonuç tablosunu açar .

4. Karakterizasyon yöntemi

Gruplar ve kimlik eşlemesi

Kılavuz dört test grubu tanımlar: ilk altı sinyal, ikinci altı sinyal, tek kimlikler (1, 3, 5, 7, 9, 11) ve çift kimlikler (0, 2, 4, 6, 8, 10) . Bu kimlikler sıfır tabanlıdır; Tablo I'deki 1–12 sunum sıra numaralarıyla karıştırılmamalıdır.



(a)



(b)

Şekil 4(a). Kullanım kılavuzundan mobil arayüz görünümü. Eşleştirme ve sonuç yönetimi aynı yerel web hizmeti üzerinden gerçekleştirilir . Şekil 4(b). Raporlama akışını belgeleyen ekran örneği.

Körleme ve kontrol değişkenleri

Kılavuz düzeni "çift kör" olarak adlandırır . Rastgele dağıtım tek başına çift körlüğü kanıtlamaz. Katılımcı ve operatörün test sürerken gizli kimliklere erişememesi, hata geri bildiriminin yalnızca oturum sonunda açılması ve yeniden oynatmaların önceden belirlenen kurala bağlanması doğrulanması planlanmaktadır.

Temas edilen parmak, basma kuvveti, temas süresi ve tutuş biçimi sabitlenmelidir. Eğitim denemeleri deneyden ayrı tutulmalı; grup sırası dengelenmeli ve işitsel ipuçları kontrol edilmelidir. Bunlar tamamlandığı iddia edilen işlemler değil, nicel kullanıcı deneyine geçiş için önerilen protokol şartlarıdır.

Algısal özelliklerin elde edilmesi

Bir oturum için skor S = K/6 olarak tanımlanabilir; K doğru çift sayısıdır. Rastgele bir birebir eşleştirmede beklenen doğru çift sayısı 1, beklenen skor 1/6'dır. Ancak kilitlenme nedeniyle kararlar bağımsız değildir; altı eşleştirmeyi bağımsız Bernoulli denemeleri saymak uygun değildir. Anlamlılık değerlendirmesinde permütasyon yaklaşımı veya katılımcı/oturum düzeyli yöntem tercih edilmelidir.

5. Elektriksel ön bulgular

Kapasitif yük modeli

Yapılan çalışmalarda eyleyici kapasitansı 0,9 µF olarak verilmektedir . Basitleştirilmiş kapasitif modelde $i(t) = C\, dv(t)/dt$ ve sinüs için $I_{pk} = 2\pi f\, C\, V_{pk}$ bağıntıları geçerlidir. 130 Hz ve 80 V_{pp} hedefinde V_{pk} = 40 V olduğundan yaklaşık I_{pk} = 29,4 mA bulunur.

İdeal kapasitörün bir tam periyotta ortalama aktif gücü sıfırdır. Reaktif güç $Q = 2\pi f\, C\, V_{rms}^2$ olup aynı örnek için yaklaşık 0,59 var eder. Gerçek giriş gücü; sürücü verimi, piezo kayıpları, enerji geri kazanımı ve mekanik yükle değişir. Bu nedenle CV^2f ölçeklemesi gerçek tüketimin tam ölçümü olarak kullanılamaz.

Mekanik yük altında davranış

Eyleyiciye mekanik kuvvet uygulandığında tüketim profilinin değiştiği ve UVLO kesmesinin görüldüğü bildirilmiştir . Nedensel mekanizma izole edilmemiştir. Empedans değişimi, besleme düşümü ve mekanik bağlama etkileri olası açıklamalardır; hiçbiri ölçülmüş transfer fonksiyonu olmadan kesin neden olarak ileri sürülmemelidir.

6. Doğrulama ve sınırlılıklar

Elektriksel ve mekanik ölçüm planı

Cihaz, mevcut kapsamıyla kontrollü uyaran sunumu ve yanıt kaydı platformudur. Mekanik sinyal özelliklerinin doğrudan elde edilmesi için ivmeölçer veya lazer vibrometre gibi bağımsız ölçüm altyapısı gerekir. Referans gerilim ile yüzey ivmesi eş zamanlı kaydedildiğinde, frekans cevabı Ha/v(f) = A(f)/V(f) ve zaman alanı ölçütleri değerlendirilebilir.

Kalibrasyonda çıkış Vpp, DC ofset, giriş minimum gerilimi ölçülmeli; yükselme/sönüm zamanı, RMS ivme, tepe ivme ve spektral bileşenler çıkarılmalıdır. Aynı genlikte farklı profiller eşit mekanik şiddet üretmeyebileceği gözlemlenmiştir. Algısal ayrışmanın biçimden mi şiddetten mi kaynaklandığını ayırmak için gerilim eşleme ve mekanik RMS eşleme deneyleri ayrı tasarlanmalıdır.

Kare ve testere profillerindeki keskin geçişler yüksek frekans bileşenleri içerir. Gerçek sürücü, montaj ve piezo yük bu bileşenleri sınırlayabileceğinden, ideal grafikler fiziksel yüzeyde aynen yeniden üretildiği varsayımıyla yorumlanmamalıdır. Kare/darbe uyaranlarında akım talebi yalnızca 130 Hz sinüs hesabıyla değerlendirilmemelidir.

Kullanım alanı ve geliştirme yönü

Platformun öncelikli kullanım alanı, oda kontrol paneli için dokunsal bildirim adaylarını seçmektir. Sonraki aşamada farklı gerilim, paket süresi ve frekans kombinasyonlarının ayırt edilebilirliği ölçülebilir.

SONUÇ

Piezo haptik sinyallerin algısal karakterizasyonu için geliştirilen cihaz; 4×3 kapasitif giriş, ESP32 tabanlı kontrol, MAX77501 sürüş ve yerel mobil web arayüzünü birleştirmektedir. On iki sinyal ailesi ve altı çiftli rastgele eşleştirme düzeni, kullanıcı yanıtlarının sistematik toplanmasına yönelik uygulanabilir bir mimari sunmaktadır. Cihaz fotoğrafı, arayüz görselleri ve referans dalga formları tasarımın farklı katmanlarını belgelemektedir.

Başlıca sonraki adımlar; fiziksel çıkış kalibrasyonu, körleme kontrolü ve ham kullanıcı verileriyle tekrarlı deneylerdir. Çalışmanın mevcut sonucu, doğrulama sınırları açıkça tanımlanmış bir test cihazı tasarımıdır.

Teşekkür

Bu çalışmada kullanılan prototip, 3251355 numaralı “Yapay Zekâ Tabanlı Haptik Geri Bildirimli Akıllı Ev Sistemlerine Entegre Yüksek Teknolojik Bir Oda Kontrol Paneli Geliştirilmesi” projesinin belgelenen faaliyetlerine dayanmaktadır .

REFERENCES (KAYNAKLAR)

[1] S. Choi and K. J. Kuchenbecker, "Vibrotactile display: Perception, technology, and applications," Proceedings of the IEEE, vol. 101, no. 9, pp. 2093–2104, 2013. doi: 10.1109/JPROC.2012.2221071.

[2] S. J. Bolanowski Jr., G. A. Gescheider, R. T. Verrillo, and C. M. Checkosky, "Four channels mediate the mechanical aspects of touch," J. Acoust. Soc. Am., vol. 84, no. 5, pp. 1680–1694, 1988. doi: 10.1121/1.397184.

[3] Y. Shao, V. Hayward, and Y. Visell, "Compression of dynamic tactile information in the human hand," Science Advances, vol. 6, no. 16, Art. no. eaaz1158, 2020. doi: 10.1126/sciadv.aaz1158.

[4] Analog Devices, "MAX77501: 110Vpk-pk High-Efficiency Piezo Haptic Actuator Boost Driver," product information and data sheet, Rev. 0. Online: https://www.analog.com/en/products/max77501.html. Accessed: Oct. 9, 2026. DOI bulunmamaktadır.

ELMA VE ÜZÜM POSALARIYLA ZENGİNLEŞTİRİLMİŞ ATIŞTIRMALIK PROTEİN BARLARIN FİZİKSEL, TEKSTÜREL VE DUYUSAL ÖZELLİKLERİNİN DEĞERLENDİRİLMESİ

EVALUATION OF THE PHYSICAL, TEXTURAL AND SENSORY PROPERTIES OF SNACK PROTEIN BARS ENRICHED WITH APPLE AND GRAPE POMACE

Beliz HÜNKAR
Ege Üniversitesi, Fen Bilimleri Enstitüsü, Sürdürülebilir Tarım ve Gıda Sistemleri Anabilim Dalı
Ege University, Graduate School of Natural and Applied Sciences, Department of Sustainable Agriculture and Food Systems
ORCID ID: 0009-0006-7071-9637

Ahsen RAYMAN ERGÜN
Doç. Dr. Ege Üniversitesi, Mühendislik Fakültesi, Gıda Mühendisliği Anabilim Dalı
Assoc. Prof. Dr., Ege University, Faculty of Engineering, Department of Food Engineering
ORCID ID: 0000-0003-0943-1950

Neslihan ÇOLAK
Dr. Öğr. Üyesi, Ege Üniversitesi, Güneş Enerjisi Enstitüsü, Enerji Anabilim Dalı
Assist. Prof. Dr., Ege University, Solar Energy Institute, Department of Energy
ORCID ID: 0000-0002-0868-0448

ÖZET

Bu çalışmanın amacı, kontrollü ön işlem uygulanmış elma ve üzüm posasının protein bar üretiminde kullanılabilirliğini araştırmak ve posa ilavesinin ürünlerin fiziksel, tekstürel ve duyusal özellikleri üzerindeki etkilerini incelemektir. Meyve suyu endüstrisinde açığa çıkan elma ve üzüm posaları, içerdikleri değerli bileşenler sayesinde fonksiyonel gıda üretiminde kullanılabilecek önemli yan ürünlerdir. Hurma, kakao, Hindistan cevizi yağı ve bezelye proteini kullanılarak posa içermeyen kontrol formülasyonu (F0) hazırlanmıştır. Aynı temel bileşenlere ek olarak %10 ve %20 oranlarında elma ve üzüm posası karışımı içeren iki farklı protein bar formülasyonu (sırasıyla F1 ve F2) geliştirilmiştir. Örneklerin nem, su aktivitesi, pH ve CIE L*ab** renk değerleri belirlenmiştir. Tekstür profil analiziyle sertlik, yapışkanlık, esneklik, koheziflik, sakızımsılık ve çiğnenebilirlik incelenmiştir. Duyusal değerlendirme, 15 panelist tarafından dokuz puanlı hedonik ölçekle yapılmıştır. Posa içeren örneklerde nem ve su aktivitesi değerleri yükselmiştir. F0, F1 ve F2 formülasyonlarının nem içerikleri sırasıyla %14,80, %17,44 ve %19,64 olarak belirlenmiştir. Su aktivitesi değerleri aynı sırayla 0,657, 0,688 ve 0,748; pH değerleri ise 6,29, 6,41 ve 6,55 olarak bulunmuştur. Renk analizinde F2 formülasyonunun kırmızılık (a*) ve sarılık (b*) değerleri diğer örneklerden daha yüksek, parlaklık (L*) değeri ise daha düşük bulunmuştur. En yüksek sertlik, sakızımsılık ve çiğnenebilirlik ortalamaları F1 formülasyonunda belirlenmiştir. F2 formülasyonunda ise bu değerlerin azaldığı görülmüştür. Duyusal değerlendirmede genel beğeni ortalamaları 7,40–8,00 arasında değişmiştir. En yüksek puan F2 (8,00) formülasyonunda elde edilmiştir. Sonuç

olarak, elma ve üzüm posasının protein bar formülasyonunda kullanılması ürünlerin renk ve tekstür özelliklerinde değişikliklere neden olmuştur. Geliştirilen formülasyonlar duyusal değerlendirmede yüksek beğeni puanları alarak kabul görmüştür. Posa oranının artmasıyla nem ve su aktivitesi değerleri de yükselmiştir. Çalışma, meyve işleme yan ürünlerinin katma değerli atıştırmalıklara dönüştürülmesi açısından sürdürülebilir bir alternatif sunmaktadır. İleriki çalışmalarda özellikle yüksek posa içeren ürünlerin saklama koşullarının ve raf ömrünün daha ayrıntılı incelenmesi gerekmektedir.
Anahtar Kelimeler: Elma posası, üzüm posası, protein bar, tekstür, duyusal değerlendirme, yan ürünlerin değerlendirilmesi, sürdürülebilirlik.

ABSTRACT

This paper aims to investigate the potential use of pretreated apple and grape pomace in protein bar production and to examine the effects of pomace addition on the physical, textural, and sensory properties of the products. Apple and grape pomace generated by the fruit juice industry are valuable by-products with potential applications in functional food production. A pomace-free control formulation (F0) was prepared using dates, cocoa, coconut oil, and pea protein. Two additional protein bar formulations (F1 and F2) were developed using the same basic ingredients with 10% and 20% apple and grape pomace mixture, respectively. Moisture content, water activity, pH, and CIE L*a*b* color parameters were measured. Texture profile analysis included hardness, adhesiveness, springiness, cohesiveness, gumminess, and chewiness. Sensory evaluation was conducted by 15 panelists using a nine-point hedonic scale. Moisture content and water activity increased in the pomace-containing samples. Moisture contents of F0, F1, and F2 were 14.80%, 17.44%, and 19.64%, respectively. Corresponding water activity values were 0.657, 0.688, and 0.748, while pH values were 6.29, 6.41, and 6.55. F2 showed higher redness (a*) and yellowness (b*) values but lower lightness (L*) than the other formulations. The highest mean hardness, gumminess, and chewiness values were observed in F1, while these values decreased in F2. Mean overall liking scores ranged from 7.40 to 8.00, with F2 receiving the highest score (8.00). In conclusion, incorporating apple and grape pomace into protein bars resulted in changes in their color and textural properties. The developed formulations received high sensory liking scores and were well accepted. Moisture content and water activity also increased with increasing pomace levels. This study offers a sustainable alternative for converting fruit processing by-products into value-added snacks. Future studies should further investigate storage conditions and shelf life, particularly for products containing higher pomace levels.
Keywords: Apple pomace, grape pomace, protein bar, texture, sensory evaluation, by-product valorization, sustainability.

GİRİŞ

Gıda endüstrisinde üretim ve işleme faaliyetleri sırasında önemli miktarda organik yan ürün açığa çıkmaktadır. Bu yan ürünlerin yeterince değerlendirilememesi, ekonomik kayıpların

yanı sıra atık yönetimi ve çevresel sürdürülebilirlik açısından çeşitli sorunlara yol açmaktadır (Zhu vd., 2023). Son yıllarda sürdürülebilir gıda üretimi, döngüsel ekonomi ve kaynak verimliliği yaklaşımlarının önem kazanmasıyla birlikte, gıda işleme yan ürünlerinin yeniden değerlendirilmesine yönelik çalışmalar artmıştır (Kumaraguruparaswami vd., 2025; Zhu vd., 2023). Özellikle meyve ve sebze işleme endüstrisinde açığa çıkan kabuk, çekirdek ve posa gibi yan ürünler, diyet lifi, fenolik bileşikler ve çeşitli biyoaktif bileşenler içermeleri nedeniyle katma değerli gıda bileşenleri olarak değerlendirilebilmektedir (Raczkowska & Serek, 2024). Bu yan ürünlerin gıda formülasyonlarında kullanılması, kaynakların daha etkin değerlendirilmesi ve sürdürülebilir üretim yaklaşımlarının desteklenmesi açısından önem taşımaktadır (Kumaraguruparaswami vd., 2025; Zhu vd., 2023).

Meyve suyu endüstrisinin önemli yan ürünleri arasında yer alan elma ve üzüm posaları, besinsel bileşimleri ve teknolojik özellikleri bakımından dikkat çekmektedir(Asif vd., 2023; Kurćubić vd., 2024). Meyvelerin preslenmesi sonucunda elde edilen posa, işlenen meyvenin türüne ve uygulanan üretim yöntemine bağlı olarak kabuk, meyve eti, çekirdek ve lifli dokuların farklı oranlarda bulunduğu heterojen bir yapıya sahiptir (Raczkowska & Serek, 2024). Elma posası, çözünür ve çözünmez diyet lifleri, pektin, doğal şekerler ve fenolik bileşikler içermesi nedeniyle gıda formülasyonlarında kullanılabilecek alternatif bir hammadde olarak değerlendirilmektedir (Asif vd., 2023). Üzüm posası ise özellikle kabuk ve çekirdek fraksiyonlarında bulunan fenolik asitler, flavonoidler, antosiyaninler ve tanenler bakımından önem taşımaktadır (Kurćubić vd., 2024). Bununla birlikte, meyve posalarının kimyasal bileşimi ve fonksiyonel özellikleri; meyve çeşidi, olgunluk düzeyi, işleme koşulları ve uygulanan ön işlemler gibi faktörlere bağlı olarak değişebilmektedir (Asif vd., 2023; Kurćubić vd., 2024).

Meyve posalarının gıda formülasyonlarına dahil edilmesi, ürünlerin besinsel özelliklerinin yanı sıra fiziksel ve tekstürel yapılarında da değişikliklere neden olabilmektedir (Blicharz-Kania vd., 2023; Raczkowska & Serek, 2024). Özellikle posa yapısındaki diyet liflerinin su bağlama ve su tutma özellikleri, ürünün nem dağılımını, yapısal bütünlüğünü ve mekanik davranışını etkileyebilmektedir (Asif vd., 2023). Ayrıca meyve posalarında bulunan doğal pigmentler ve posa partiküllerinin özellikleri, ürünlerin renk ve görünümünde farklılıklar oluşturabilmektedir. Bu nedenle posa ilavesinin ürün kalitesi üzerindeki etkilerinin değerlendirilmesinde fiziksel, tekstürel ve duyusal özelliklerin birlikte ele alınması önem taşımaktadır (Blicharz-Kania vd., 2023).

Pratik tüketim olanağı sunan atıştırmalık barlar, farklı hammaddelerin bir arada kullanılabildiği ve alternatif gıda bileşenlerinin değerlendirilmesine uygun ürün grupları arasında yer almaktadır. Protein içeren bar formülasyonlarında bitkisel protein kaynakları, meyve türevleri, yağlı bileşenler ve tatlandırıcılar bir arada kullanılabilmektedir. Ancak kullanılan bileşenlerin özellikleri ve formülasyondaki oranları, barların sertlik, çiğnenebilirlik, yapışkanlık ve duyusal kabul edilebilirlik gibi kalite özelliklerini etkileyebilmektedir (Blicharz-Kania vd., 2023). Bu durum, alternatif hammaddelerle geliştirilen bar formülasyonlarında uygun bileşen oranlarının belirlenmesini önemli hale getirmektedir.

Blicharz-Kania ve ark. (2023), elma ve üzüm posası ilavesinin şekersiz tahıl barlarının besinsel, fiziksel ve duyusal özellikleri üzerindeki etkilerini araştırmıştır. Çalışmada, kontrol formülasyonunda bulunan kuru üzümün belirli miktarlarda elma veya üzüm posasıyla ikame edilmesi sonucunda ürünlerin nem içeriğinin ve çözünür diyet lifi miktarının arttığı belirlenmiştir. Posa ilavesinin barların mekanik dayanımında artışa ve renk özelliklerinde değişikliklere neden olduğu da bildirilmiştir. Duyusal değerlendirme sonuçlarında ise ürünlerin tat bakımından kabul edilebilirliğinin korunduğu, ancak özellikle elma posası içeren örneklerde aroma ve tekstür açısından daha düşük değerlendirmeler elde edildiği görülmüştür. Araştırmacılar, posa türü ve ilave miktarının ürünün fiziksel ve duyusal özellikleri üzerinde farklı etkiler oluşturabileceğini ortaya koymuştur. Bu bulgular, meyve posalarının atıştırmalık bar üretiminde kullanılabilirliğini desteklemekle birlikte, farklı formülasyonlarda uygun posa oranlarının belirlenmesinin önemini göstermektedir (Blicharz-Kania vd., 2023).

Meyve posası içeren atıştırmalık ürünlerde fiziksel ve tekstürel özelliklerin yanı sıra nem içeriği ve su aktivitesinin de değerlendirilmesi gerekmektedir. Su aktivitesi, gıdalarda mikroorganizmaların gelişme potansiyelinin ve çeşitli kimyasal ve biyokimyasal değişimlerin değerlendirilmesinde kullanılan önemli bir parametredir (Peker & Şengün, 2025). Özellikle nem içeriği yüksek bileşenlerin kullanıldığı ürünlerde su aktivitesinin belirlenmesi, depolama stabilitesinin değerlendirilmesi açısından önem taşımaktadır. Bununla birlikte, pH ve renk özelliklerinin tekstür parametreleriyle birlikte incelenmesi, farklı formülasyonların kalite özelliklerinin daha kapsamlı biçimde karşılaştırılmasına olanak sağlamaktadır (Blicharz-Kania vd., 2023).

Literatürde elma ve üzüm posalarının çeşitli gıda ürünlerinde değerlendirilmesine yönelik çalışmalar bulunmakla birlikte, mevcut araştırmalarda kullanılan hammaddeler, posa işleme koşulları ve ürün formülasyonları farklılık göstermektedir (Asif vd., 2023; Kurćubić vd., 2024). Özellikle (Blicharz-Kania vd., 2023) tarafından gerçekleştirilen çalışmada elma ve üzüm posaları tahıl bazlı bar formülasyonlarında ayrı ayrı değerlendirilmiştir. Buna karşılık, kontrollü nem düzeyine kadar ön işlem uygulanmış elma ve üzüm posalarının birlikte kullanıldığı, hurma ve bezelye proteini esaslı atıştırmalık bar formülasyonlarında posa ilave oranının fiziksel, tekstürel ve duyusal özelliklerle ilişkisinin incelenmesi, araştırılmaya değer bir konudur. Bu kapsamda farklı posa oranlarının ürünlerin yapısal özellikleri ve tüketici kabulü üzerindeki etkilerinin birlikte değerlendirilmesi, söz konusu yan ürünlerin alternatif protein bar formülasyonlarında kullanım potansiyelinin anlaşılmasına katkı sağlayabilir.

Bu çalışmanın amacı, kontrollü ön işlem uygulanmış elma ve üzüm posalarının atıştırmalık protein bar üretiminde kullanılabilirliğini araştırmak ve farklı posa ilave oranlarının ürünlerin fiziksel, tekstürel ve duyusal özellikleri üzerindeki etkilerini belirlemektir. Bu kapsamda hurma, kakao, Hindistan cevizi yağı ve bezelye proteini kullanılarak posa içermeyen kontrol formülasyonu (F0) ile %10 (F1) ve %20 (F2) oranlarında elma ve üzüm posası karışımı içeren protein bar formülasyonları geliştirilmiştir. Ürünlerin nem içeriği, su aktivitesi, pH ve renk özellikleri ile tekstür profili ve duyusal kabul edilebilirlikleri değerlendirilmiştir. Elde edilen bulgular doğrultusunda, meyve işleme endüstrisi yan ürünlerinin katma değerli atıştırmalık

ürünlere dönüştürülme potansiyelinin ortaya konulması ve sürdürülebilir ürün geliştirme çalışmalarına katkı sağlanması hedeflenmiştir.

MATERYAL VE YÖNTEM

Bu çalışmada atıştırmalık protein bar üretiminde elma ve üzüm posaları, hurma, kakao, Hindistan cevizi yağı ve bezelye proteini kullanılmıştır. Üretimde kullanılan hammaddeler yerel manav, market ve aktarlardan temin edilmiştir. Elma ve üzüm posaları, meyvelerin işlenmesi sonucunda elde edilerek protein bar formülasyonlarında değerlendirilmiştir.

Elma ve Üzüm Posalarının Hazırlanması

Elma ve üzüm posaları, meyvelerin katı meyve sıkacağında sıkılmasıyla elde edilmiştir. İşlem sonrasında elma posasının başlangıç nem içeriği %77, üzüm posasının başlangıç nem içeriği ise %68 olarak belirlenmiştir. Elde edilen posalar, etüv tepsilerine yaklaşık 3 mm kalınlığında olacak şekilde yayılmıştır. Ardından 65 °C sıcaklıkta, nem içerikleri yaklaşık %60 düzeyine ulaşıncaya kadar kontrollü kurutma işlemine tabi tutulmuştur.

Kurutma işlemi sonrasında posalar tamamen kuru veya toz forma dönüştürülmeden, ulaşılan nem düzeyinde protein bar formülasyonlarına dahil edilmiştir.

Protein Bar Formülasyonlarının Hazırlanması

Protein bar üretiminde öncelikle hurmaların çekirdekleri çıkarılmış ve püre haline getirilmiştir. Hazırlanan hurma püresine bezelye proteini, kakao ve Hindistan cevizi yağı ilave edilerek temel bar karışımı oluşturulmuştur. Bu karışım, posa içermeyen kontrol formülasyonu (F0) olarak belirlenmiştir.

Kontrol formülasyonu esas alınarak, farklı oranlarda elma ve üzüm posası içeren iki formülasyon daha hazırlanmıştır. F1 formülasyonuna toplam %10, F2 formülasyonuna ise toplam %20 oranında elma ve üzüm posası ilave edilmiştir. Her iki formülasyonda da elma ve üzüm posaları eşit miktarlarda kullanılmıştır. Posa ilavesi, hurma püresi miktarı azaltılarak gerçekleştirilmiş; bezelye proteini, kakao ve Hindistan cevizi yağı miktarları bütün formülasyonlarda sabit tutulmuştur.

Tablo 1. Protein bar formülasyonlarında kullanılan hammaddelerin miktarları (g/17 g ürün formülasyonu)

Hammadde	**F0 (Kontrol)**	**F1 (%10 posa)**	**F2 (%20 posa)**
Hurma püresi	12,75	11,05	9,35
Bezelye proteini	1,70	1,70	1,70
Kakao	0,85	0,85	0,85
Hindistan cevizi yağı	1,70	1,70	1,70
Elma posası	–	0,85	1,70
Üzüm posası	–	0,85	1,70
Toplam (g)	**17,00**	**17,00**	**17,00**

Formülasyonlarda yer alan tüm bileşenler homojen bir karışım elde edilinceye kadar karıştırılmış ve hazırlanan karışımlar bar kalıbına koyularak şekillendirilmiştir. Şekillendirilen örnekler 85 °C sıcaklıktaki etüvde 1,5 saat süreyle pişirilmiştir. Böylece kontrol grubu (F0) ile farklı oranlarda elma ve üzüm posası içeren F1 ve F2 protein bar örnekleri elde edilmiştir.

Fizikokimyasal Analizler

Protein bar örneklerinin fizikokimyasal özelliklerini belirlemek amacıyla nem içeriği, su aktivitesi (a_w), pH ve renk analizleri gerçekleştirilmiştir.

Nem İçeriği Analizi

Protein bar örneklerinin nem içerikleri, halojen ısıtma prensibiyle çalışan infrared nem tayin cihazı (Shimadzu MOC63u, Japonya) kullanılarak termogravimetrik yöntemle belirlenmiştir (Janas & Kowalska, 2023). Her formülasyon için üç tekrarlı ölçüm gerçekleştirilmiş ve sonuçlar yüzde (%) nem içeriği olarak ifade edilmiştir.

Su Aktivitesi Analizi

Protein bar örneklerinin su aktivitesi (a_w) değerleri, ISO 18787:2017 standardı esas alınıp su aktivitesi ölçüm cihazı kullanılarak belirlenmiştir. Her formülasyon için beş tekrarlı ölçüm gerçekleştirilmiş ve sonuçlar a_w değeri olarak ifade edilmiştir (International Organization for Standardization, 2017).

pH Analizi

Protein bar örneklerinin pH değerleri, (Cemeroğlu, 2018) tarafından belirtilen yöntem temel alınarak dijital pH metre (Thermo Scientific, Orion 3 Star, ABD) kullanılarak belirlenmiştir. Her formülasyon için üç tekrarlı ölçüm gerçekleştirilmiş ve elde edilen sonuçlar ortalama pH değeri olarak ifade edilmiştir.

Renk Analizi

Protein bar örneklerinin renk özellikleri, (Rayman Ergün vd., 2020) tarafından kullanılan yöntem doğrultusunda CIE L*a*b* renk sistemi ile değerlendirilmiştir. Bu sistemde L* değeri açıklık-koyuluk düzeyini, a* değeri kırmızı-yeşil renk eksenini ve b* değeri sarı-mavi renk eksenini temsil etmektedir. Her formülasyon için beş tekrarlı ölçüm gerçekleştirilmiş ve elde edilen L*, a* ve b* değerleri karşılaştırılmıştır.

Tekstür Profil Analizi

Protein bar örneklerinin tekstürel özellikleri, (Bourne vd., 1978) tarafından açıklanan çift sıkıştırma prensibine dayalı tekstür profil analizi (Texture Profile Analysis, TPA) yöntemi esas alınarak değerlendirilmiştir. Analizlerde 36 mm çapında düz silindirik prob (P/36R) kullanılmıştır. Ölçüm öncesi, test ve test sonrası hızları 1 mm/sn, tetikleme kuvveti ise 0,1 N olarak belirlenmiştir. İki sıkıştırma döngüsü arasında 5 saniyelik bekleme süresi uygulanmıştır. Her formülasyon için 10 tekrarlı ölçüm gerçekleştirilmiş ve elde edilen kuvvet-zaman eğrilerinden sertlik (hardness), yapışkanlık (adhesiveness), esneklik (springiness), koheziflik (cohesiveness), sakızımsılık (gumminess) ve çiğnenebilirlik (chewiness) parametreleri değerlendirilmiştir.

Duyusal Değerlendirme Analizi

Protein bar örneklerinin duyusal özellikleri, (Altuğ, 1993) tarafından belirtilen duyusal değerlendirme yöntemi referans alınarak, 15 panelist tarafından dokuz puanlı hedonik ölçek kullanılarak değerlendirilmiştir. Panelistler örnekleri görünüş, renk, koku, tat, tekstür ve genel kabul edilebilirlik özellikleri bakımından puanlamıştır.

Değerlendirme sırasında örnekler üç basamaklı kodlarla tanımlanmış; F0, F1 ve F2 formülasyonları sırasıyla 123, 532 ve 286 kodlarıyla panelistlere sunulmuştur. Dokuz puanlı hedonik ölçekte yüksek puanlar daha yüksek beğeni düzeyini temsil etmiştir.

Her bir duyusal özellik için panelistlerden elde edilen puanlar değerlendirilerek formülasyonların duyusal kabul edilebilirlikleri karşılaştırılmıştır.

İstatistiksel Analiz

Araştırma kapsamında elde edilen veriler ortalama ve standart sapma değerleriyle ifade edilmiştir. Fizikokimyasal ve renk parametrelerinde formülasyonlar arasındaki farklılıkların değerlendirilmesinde tek yönlü varyans analizi (ANOVA), anlamlı farklılıkların bulunduğu durumlarda grupların karşılaştırılması için Tukey HSD testi kullanılmıştır. Aynı panelistler tarafından değerlendirilen duyusal özelliklerin karşılaştırılmasında Friedman testi uygulanmıştır. İstatistiksel anlamlılık düzeyi $p < 0,05$ olarak kabul edilmiştir.

BULGULAR VE TARTIŞMA

Nem İçeriği ve Su Aktivitesi Analizi Sonuçları

Farklı oranlarda elma ve üzüm posası içeren protein bar örneklerinin nem içeriği ve su aktivitesi değerleri Tablo 2'de verilmiştir.

Tablo 2. Protein bar örneklerinin nem içeriği ve su aktivitesi değerleri

Parametre	**F0 (Kontrol)**	**F1 (%10 posa)**	**F2 (%20 posa)**
Nem içeriği (%)	14,80 ± 0,60	17,44 ± 1,16	19,64 ± 1,46
Su aktivitesi (a_w)	0,657 ± 0,012	0,688 ± 0,002	0,748 ± 0,005

Değerler ortalama ± standart sapma olarak verilmiştir. Nem içeriği için n = 3, su aktivitesi için n = 5.

Tablo 2'de sunulan sonuçlara göre, protein bar örneklerinin nem içeriği ve su aktivitesi değerlerinin posa ilave oranındaki artışa bağlı olarak yükseldiği belirlenmiştir. Kontrol örneğinde (F0) %14,80 olan nem içeriği, F1 ve F2 formülasyonlarında sırasıyla %17,44 ve %19,64'e yükselmiştir. Benzer şekilde su aktivitesi değerleri F0, F1 ve F2 örneklerinde sırasıyla 0,657, 0,688 ve 0,748 olarak belirlenmiştir.

Bu artışın, yaklaşık %60 nem içeriğine sahip posaların formülasyona dahil edilmesi ve posa bileşenlerinin su tutma özellikleriyle ilişkili olabileceği düşünülmektedir. Meyve posalarında bulunan diyet liflerinin ürünlerin nem tutma davranışını etkileyebildiği bildirilmiştir (Asif vd., 2023; Raczkowska & Serek, 2024). Benzer şekilde (Blicharz-Kania vd., 2023), elma ve üzüm posası ilavesinin tahıl barlarının nem içeriğini artırabildiğini belirtmiştir. Elde edilen sonuçlar, posa ilavesinin protein barların nem içeriği ve su aktivitesi üzerinde etkili olabileceğini göstermektedir. Bununla birlikte, özellikle F2 formülasyonunda belirlenen yüksek su aktivitesi değeri, ürünün depolama stabilitesi açısından ayrıca değerlendirilmelidir.

pH Analizi Sonuçları

Protein bar örneklerinin pH analizine ilişkin sonuçlar Tablo 3'te sunulmuştur.

Tablo 3. Protein bar örneklerinin pH analiz sonuçları

Formülasyon	pH (Ortalama ± SS)
F0	6,29 ± 0,04^{c}
F1	6,41 ± 0,03^{b}
F2	6,55 ± 0,02^{a}

Farklı üst simge harfler, Tukey HSD testine göre formülasyonlar arasında istatistiksel olarak anlamlı farklılık bulunduğunu göstermektedir ($p < 0,05$). n = 3.

Tablo 3'te sunulan sonuçlara göre, protein bar örneklerinin pH değerlerinin posa ilave oranınd aki artışa bağlı olarak yükseldiği ve formülasyonlar arasındaki farklılıkların istatistiksel olarak anlamlı olduğu belirlenmiştir ($p < 0,001$). Kontrol örneğinde (F0) 6,29 ± 0,04 olan pH değeri, F1 formülasyonunda 6,41 ± 0,03'e, F2 formülasyonunda ise 6,55 ± 0,02'ye yükselmiştir. Tukey çoklu karşılaştırma testi sonucunda üç formülasyonun da birbirinden anlamlı düzeyde farklı olduğu belirlenmiştir ($p < 0,05$). Gözlenen artışın, posa ilavesiyle birlikte hurma püresi oranının azalması ve formülasyon bileşiminin değişmesiyle ilişkili olabileceği düşünülmektedir. Bununla birlikte, hammaddelerin asitlik özellikleri ayrı ayrı belirlenmediğinden, pH değişiminin kesin nedeni ortaya konulamamıştır.

Renk Analizi Sonuçları

Tablo 4. Protein bar örneklerinin renk özellikleri ve istatistiksel analiz sonuçları

Parametre	F0 (Kontrol)	F1 (%10 posa)	F2 (%20 posa)	p değeri
L*	11,52 ± 0,45^{a}	11,52 ± 1,09^{a}	10,59 ± 0,32^{a}	0,096
a*	3,43 ± 0,36^{b}	3,16 ± 0,33^{b}	4,69 ± 0,33^{a}	<0,001
b*	2,90 ± 0,17^{b}	2,85 ± 0,49^{b}	4,40 ± 0,43^{a}	<0,001

Değerler ortalama ± standart sapma olarak verilmiştir (n = 5). p değerleri tek yönlü ANOVA ile hesaplanmıştır. Aynı satırda farklı üst simge harfler, Tukey HSD testine göre istatistiksel olarak anlamlı farklılıkları göstermektedir ($p < 0,05$).

Tablo 4'te sunulan protein bar örneklerinin renk özellikleri incelendiğinde, posa ilavesinin a* ve b* değerleri üzerinde istatistiksel olarak anlamlı etkisi olduğu belirlenirken ($p < 0,001$), L* değerlerindeki farklılık anlamlı bulunmamıştır ($p > 0,05$). En düşük L* değeri 10,59 ile F2 formülasyonunda elde edilmiş ve yüksek posa ilavesiyle ürün renginde koyulaşma eğilimi gözlenmiştir. F2 formülasyonunun a* (4,69) ve b* (4,40) değerleri, F0 ve F1 örneklerinden anlamlı düzeyde yüksek bulunmuştur ($p < 0,05$). Bu değişimlerin, meyve posalarının doğal pigmentleri ve fenolik bileşenleriyle ilişkili olabileceği düşünülmektedir (Kurćubić vd., 2024; Raczkowska & Serek, 2024). Benzer şekilde (Blicharz-Kania vd., 2023), elma ve üzüm posası ilavesinin tahıl barlarının renk özelliklerini etkilediğini bildirmiştir.

Tekstür Profil Analizi Sonuçları

Tablo 5. Protein bar örneklerinin tekstür analiz sonuçları

Parametre	F0	F1	F2
Sertlik (gf)	6646,75 ± 1107,96	7121,60 ± 1276,20	5776,62 ± 909,19
Yapışkanlık (gf·sn)	−354,48 ± 92,27	−418,70 ± 172,44	−310,80 ± 138,53
Esneklik	0,122 ± 0,014	0,128 ± 0,020	0,127 ± 0,012
Koheziflik	0,081 ± 0,009	0,084 ± 0,015	0,076 ± 0,006
Sakızımsılık (gf)	534,65 ± 101,65	590,14 ± 91,89	437,48 ± 67,85
Çiğnenebilirlik	65,09 ± 14,93	75,85 ± 19,30	55,70 ± 11,50

Değerler ortalama ± standart sapma olarak verilmiştir.

Protein bar örneklerinin tekstürel özellikleri incelendiğinde, %10 posa içeren F1 formülasyon unun Tablo 5'te görüldüğü üzere en yüksek sertlik, sakızımsılık ve çiğnenebilirlik ortalamalar ına sahip olduğu belirlenmiştir. Bu parametrelerin en düşük değerleri ise %20 posa içeren F2 formülasyonunda elde edilmiştir. Bulgular, posa ilave oranının ürünün mekanik özelliklerini doğrusal olmayan bir şekilde etkileyebileceğini göstermektedir. Buna karşılık esneklik ve koheziflik değerleri formülasyonlar arasında birbirine yakın bulunmuştur. Gözlenen farklılıkların, posa bileşenlerinin su tutma özellikleri ve formülasyonun yapısal bileşimindeki değişimlerle ilişkili olabileceği düşünülmektedir.

Duyusal Analiz Sonuçları

Tablo 6. Protein bar örneklerinin duyusal değerlendirme sonuçları

Parametre	F0	F1	F2
Görünüş	7,33 ± 1,88	7,53 ± 1,30	7,67 ± 0,98
Renk	7,40 ± 1,72	7,67 ± 0,98	7,93 ± 0,80
Koku	7,27 ± 1,03	7,47 ± 1,19	7,27 ± 1,44
Tat	7,27 ± 1,71	7,20 ± 1,52	8,07 ± 1,10
Tekstür	7,40 ± 1,30	6,80 ± 2,01	7,13 ± 1,41
Genel kabul edilebilirlik	7,53 ± 1,25	7,40 ± 1,30	8,00 ± 0,85

Değerler ortalama ± standart sapma olarak verilmiştir (n = 15). Duyusal değerlendirme dokuz puanlı hedonik ölçekle gerçekleştirilmiştir. Hiçbir parametrede anlamlı farklılık belirlenmemiştir (p > 0,05).

Protein bar örneklerinin duyusal analiz sonuçları incelendiğinde, %20 elma ve üzüm posası iç eren F2 formülasyonunun Tablo 6'da görüldüğü üzere 8,00 puanla en yüksek genel kabul edil ebilirlik ortalamasına ulaştığı belirlenmiştir. Kontrol örneğinde 7,53 olan genel kabul edilebilirlik puanının F2 formülasyonunda 8,00'e yükselmesi, yüksek posa ilavesiyle tüketici beğenisinde artış eğilimi olduğunu göstermiştir. F2 formülasyonu tat (8,07), renk (7,93) ve görünüş (7,67) açısından da en yüksek ortalama puanları almıştır. Bununla birlikte, formülasyonlar arasındaki duyusal farklılıklar istatistiksel olarak anlamlı bulunmamıştır (p > 0,05). Bu bulgular, %20 oranında elma ve üzüm posası ilavesinin duyusal açıdan olumlu bir

eğilim oluşturduğunu ve F2 formülasyonunun incelenen örnekler arasında en yüksek genel beğeni ortalamasına sahip olduğunu ortaya koymaktadır.

SONUÇ VE ÖNERİLER

Bu çalışmada, kontrollü ön işlem uygulanmış elma ve üzüm posalarının atıştırmalık protein bar formülasyonlarında değerlendirilme potansiyeli fiziksel, tekstürel ve duyusal özellikler açısından incelenmiştir. Elde edilen bulgular, posa ilave oranının ürün özellikleri üzerinde farklı etkiler oluşturduğunu göstermiştir.

Posa oranının artmasıyla birlikte ürünlerin nem içeriği, su aktivitesi ve pH değerlerinde yükselme gözlenmiştir. Renk analizinde %20 posa içeren F2 formülasyonunun kırmızılık (a*) ve sarılık (b*) değerleri anlamlı düzeyde artarken, açıklık (L*) değerindeki farklılık istatistiksel olarak anlamlı bulunmamıştır. Tekstürel açıdan %10 posa içeren F1 formülasyonu en yüksek sertlik, sakızımsılık ve çiğnenebilirlik değerlerini gösterirken, %20 posa ilavesinde bu parametreler azalmıştır.

Duyusal değerlendirmede ise F2 formülasyonu, 8,00/9 genel kabul edilebilirlik puanıyla en yüksek ortalamaya ulaşmış; tat, renk ve görünüş bakımından da öne çıkmıştır. Formülasyonlar arasındaki duyusal farklılıklar istatistiksel olarak anlamlı olmamakla birlikte, bu sonuç %20 oranında posa ilavesinin tüketici beğenisi açısından olumlu bir eğilim oluşturduğunu göstermektedir.

Genel olarak bulgular, elma ve üzüm posalarının protein bar üretiminde değerlendirilmesinin, meyve işleme yan ürünlerinin katma değerli gıda bileşenlerine dönüştürülmesi açısından uygulanabilir bir yaklaşım olduğunu ortaya koymaktadır. Bununla birlikte, özellikle yüksek posa oranında artan su aktivitesi dikkate alınarak sonraki çalışmalarda mikrobiyolojik stabilite ve raf ömrünün farklı depolama koşullarında incelenmesi önerilmektedir. Ayrıca posa oranı ve ön işlem koşullarının optimize edilmesi, ürünlerin besinsel bileşiminin ve diyet lifi içeriğinin belirlenmesi, teknolojik ve duyusal özelliklerin birlikte geliştirilmesine katkı sağlayacaktır.

KAYNAKÇA

Altuğ Tomris. (1993). *Duyusal Test Teknikleri* (1. bs.). Ege Üniversitesi Mühendislik Fakültesi Yayınları.

Asif, M., Javaid, T., Razzaq, Z. U., Khan, M. K. I., Maan, A. A., Yousaf, S., Usman, A., & Shahid, S. (2023). Sustainable utilization of apple pomace and its emerging potential for development of functional foods. *Environmental Science and Pollution Research, 31*(12), 17932-17950. https://doi.org/10.1007/s11356-023-28479-9

Blicharz-Kania, A., Vasiukov, K., Sagan, A., Andrejko, D., Fifowska, W., & Domin, M. (2023). Nutritional Value, Physical Properties, and Sensory Quality of Sugar-Free Cereal Bars Fortified with Grape and Apple Pomace. *Applied Sciences, 13*(18), 10531. https://doi.org/10.3390/app131810531

Bourne, M. C., Kenny, J. F., & Barnard, J. (1978). COMPUTER-ASSISTED READOUT OF DATA FROM TEXTURE PROFILE ANALYSIS CURVES1. *Journal of Texture Studies*, *9*(4), 481-494. https://doi.org/10.1111/j.1745-4603.1978.tb01219.x

Cemeroğlu, Bekir Sıtkı. (2018). *Gıda Analizleri* (4. bs.).

International Organization for Standardization. (2017). *Foodstuffs—Determination of water activity* (ISO 18787:2017). https://www.iso.org/standard/63379.html

Janas, S., & Kowalska, M. (2023). Accuracy of drying selected products using a moisture analyzer method based on infrared radiation. *Metrology and Measurement Systems*, 305-321. https://doi.org/10.24425/mms.2023.144873

Kumaraguruparaswami, M., Subramani, D., & S R, P. (2025). Food Wastes and By-Products as Valuable Ingredients for Processed Foods. *Journal of Food Process Engineering*, *48*(8), e70199. https://doi.org/10.1111/jfpe.70199

Kurćubić, V. S., Stanišić, N., Stajić, S. B., Živković, S., Kurćubić, L. V., Živković, V., Jakovljević, V., Mašković, P. Z., & Mašković, J. (2024). Valorizing Grape Pomace: A Review of Applications, Nutritional Benefits, and Potential in Functional Food Development. *Foods*, *13*(24), 4169. https://doi.org/10.3390/foods13244169

Peker, A. K., & Şengün, İ. (2025). *Potential use of food wastes in functional foods: A review of microbial safety studies*.

Raczkowska, E., & Serek, P. (2024). Health-Promoting Properties and the Use of Fruit Pomace in the Food Industry—A Review. *Nutrients*, *16*(16), 2757. https://doi.org/10.3390/nu16162757

Rayman Ergün, A., Kutlu, B., Ayriç, F., & Baysal, T. (2020). Ilımlı Elektrik Alan ve Ultrases Ön İşlemlerinin Mikrodalga ve Derin Yağda Kızartma Teknikleriyle Üretilen Havuç Cipslerinin Renk ve Nem İçeriği Üzerine Etkisi. *Akademik Gıda*, *18*(4), 382-389. https://doi.org/10.24323/akademik-gida.850902

Zhu, Y., Luan, Y., Zhao, Y., Liu, J., Duan, Z., & Ruan, R. (2023). Current Technologies and Uses for Fruit and Vegetable Wastes in a Sustainable System: A Review. *Foods*, *12*(10), 1949. https://doi.org/10.3390/foods12101949

NUMERICAL INVESTIGATION OF NUCLEATE FLOW BOILING OF R744 UNDER CONSTANT HEAT FLUX

Ekin Emek DİLBAZ
Res. Assist., Istanbul Technical University, Faculty of Mechanical Engineering, Department of Mechanical Engineering, 34437, Istanbul/TURKIYE.
ORCID: 0009-0009-0016-5554

Ersin SAYAR
Assoc. Prof. Dr., Istanbul Technical University, Faculty of Mechanical Engineering, Department of Mechanical Engineering, 34437, Istanbul/TURKIYE.
ORCID: 0000-0001-7764-9332

ABSTRACT

With the ban on the employment of high-GWP refrigerants, the utilization of low-GWP refrigerants has become widespread. R744, also known as carbon dioxide, is a refrigerant with a GWP value of 1, which serves as the reference value. R744 is also an A1 safety class refrigerant listed in the ASHRAE 34-2024 standard; it is non-flammable and non-toxic at low and medium concentrations. In this study, the flow boiling of R744 was numerically investigated using the commercial CFD code FLUENT. The problem domain consists of a stainless steel tube with an internal diameter of 6 mm and an external diameter of 8 mm. Three different meshes were examined as part of the mesh independence study. As a result of the mesh independence study, it was decided to use a mesh with 576,000 elements. In the numerical method, the coupled solver was employed for pressure-velocity coupling, and the Eulerian-Eulerian approach was adopted as the multiphase model. The k-ω SST turbulence model was utilized for turbulence modeling. Non-equilibrium wall boiling model was used to predict the mass transfer. The boundary conditions of the study are a heat flux of 10 kW/m² from the outer wall of the pipe, a no-slip condition at the inner wall, a saturation temperature of -7.8°C, and mass fluxes of 300 and 350 kg/m²s. Although the margin of error is high at vapor qualities below 10%, maximum relative error of 3% has been observed beyond this point. In conclusion, the flow boiling characteristics of R744 in the nucleate boiling region have been numerically investigated and validated through experimental studies. The results obtained can serve as a basis for future research.

Keywords: R744, Flow Boiling, CFD, Heat Transfer Coefficient.

FARKLI UÇUŞ SENARYOLARINDA METASEZGİSEL OPTİMİZASYON TABANLI PID KONTROLCÜLERİN QUADROTOR İHA ÜZERİNDEKİ PERFORMANSLARININ KARŞILAŞTIRILMASI

COMPARISON OF THE PERFORMANCE OF METAHEURISTIC OPTIMIZATION-BASED PID CONTROLLERS FOR A QUADROTOR UAV UNDER DIFFERENT FLIGHT SCENARIOS

Melike YAPAR
Yüksek Lisans Öğrencisi, Erciyes Üniversitesi, Fen Bilimleri Enstitüsü, Mekatronik Mühendisliği Anabilim Dalı
M.Sc. Student, Erciyes University, Graduate School of Natural and Applied Sciences, Department of Mechatronics Engineering
ORCID ID: 0009-0002-0328-6596

İkbal ESKİ
Prof. Dr., Erciyes Üniversitesi, Mühendislik Fakültesi, Mekatronik Mühendisliği Anabilim Dalı
Prof. Dr., Erciyes University, Faculty of Engineering, Department of Mechatronics Engineering
ORCID ID: 0000-0002-5222-313X

ÖZET

Bu çalışmada, quadrotor insansız hava aracının (İHA) konum ve yönelim kontrolünde kullanılan klasik PID kontrolcü ile Parçacık Sürü Optimizasyonu (PSO), Genetik Algoritma (GA) ve Yapay Arı Kolonisi (ABC) algoritmaları kullanılarak optimize edilen PID kontrolcülerin performansları karşılaştırılmıştır. Quadrotorun altı serbestlik dereceli doğrusal olmayan dinamik modeli MATLAB/Simulink ortamında oluşturulmuş ve konum ile yönelim kontrolü için kaskat PID kontrol yapısı kullanılmıştır. Klasik PID kazançları MATLAB PID Tuner ile belirlenirken, optimize edilmiş PID kazançları PSO, GA ve ABC algoritmaları kullanılarak elde edilmiştir. Optimizasyon sürecinde zaman ağırlıklı mutlak hata integrali (ITAE) ile aşım değerini birlikte dikkate alan bir amaç fonksiyonu kullanılmıştır. Kontrolcülerin farklı çalışma koşullarındaki performanslarını incelemek amacıyla nominal uçuş, %20 kütle artışı, çoklu referans takibi ve rüzgâr bozucusu senaryoları uygulanmıştır. Kontrol performansı temel olarak ITAE ve kök ortalama kare hata (RMSE) ölçütleri üzerinden değerlendirilmiş; ilgili senaryolarda aşım, yerleşme zamanı ve rüzgâr sırasında oluşan tepe hata değerleri de dikkate alınmıştır. Elde edilen sonuçlar, meta-sezgisel optimizasyon tabanlı PID kontrolcülerin birçok konum ve yönelim kontrol durumunda klasik PID kontrolcüye göre daha düşük hata değerleri sağlayabildiğini göstermiştir. Bununla birlikte, PSO, GA ve ABC algoritmalarının göreli performanslarının kontrol eksenine ve uygulanan uçuş senaryosuna bağlı olarak değiştiği ve tüm koşullarda mutlak üstünlük sağlayan tek bir optimizasyon yönteminin bulunmadığı belirlenmiştir.

Anahtar Kelimeler: Quadrotor İHA, PID Kontrol, Metasezgisel Optimizasyon, Uçuş Kontrolü, MATLAB/Simulink

ABSTRACT

This study compares the performance of a conventional PID controller with PID controllers optimized using Particle Swarm Optimization (PSO), Genetic Algorithm (GA), and Artificial Bee Colony (ABC) algorithms for the position and attitude control of a quadrotor unmanned aerial vehicle (UAV). A six-degree-of-freedom nonlinear dynamic model of the quadrotor was developed in MATLAB/Simulink, and a cascaded PID control structure was employed for position and attitude control. The conventional PID gains were determined using MATLAB PID Tuner, whereas the optimized PID gains were obtained using the PSO, GA, and ABC algorithms. During the optimization process, an objective function incorporating both the Integral of Time-weighted Absolute Error (ITAE) and overshoot was employed. To evaluate the controllers under different operating conditions, nominal flight, 20% mass increase, multi-reference tracking, and wind disturbance scenarios were considered. Control performance was evaluated primarily using ITAE and root mean square error (RMSE), while overshoot, settling time, and peak error during wind disturbance were also considered where appropriate. The results showed that the metaheuristic optimization-based PID controllers achieved lower error values than the conventional PID controller in many position and attitude control cases. However, the relative performance of PSO, GA, and ABC varied depending on the control axis and flight scenario, indicating that no single optimization method provided absolute superiority under all evaluated conditions.

Keywords: Quadrotor UAV, PID Control, Metaheuristic Optimization, Flight Control, MATLAB/Simulink

ÜÇLÜ PERİYODİK MİNİMAL YÜZEYLER İÇİN GELİŞTİRİLEN NUSSELT SAYISI KORELASYONLARI ÜZERİNE KISA BİR DERLEME

A BRIEF REVIEW OF NUSSELT NUMBER CORRELATIONS DEVELOPED FOR TRIPLY PERIODIC MINIMAL SURFACES

Ali CELEN
Gümüşhane Üniversitesi, Mühendislik ve Doğa Bilimleri Fakültesi, Makine Mühendisliği Bölümü
Gümüşhane University, Faculty of Engineering and Natural Sciences, Department of Mechanical Engineering
ORCID ID: 0000-0003-3593-5183

ÖZET

Son yıllarda eklemeli imalat teknolojisindeki gelişmeler üçlü periyodik minimal yüzeyler kullanılarak geleneksel ısı değiştiricilerine kıyasla daha karmaşık yüzeye sahip kompakt ısı değiştiriciler üretmeyi mümkün kılmıştır. Kompakt ısı değiştiricilerin üretimine ek olarak ısı değiştiricilerin tek parça halinde üretilebilmesi diğer bir avantaj olarak karşımıza çıkmaktadır. Üçlü periyodik minimal yüzeylerde ısıl sınır tabakadaki değişimler ve ikincil akışların oluşması daha yüksek ısıl performansın elde edilmesini de sağlamaktadır. Bu çalışmada, üçlü periyodik minimal yüzeylerde Nusselt sayısının deneysel ve sayısal olarak araştırıldığı son yıllardaki çalışmalar değerlendirilmiştir. İlk olarak, üçlü periyodik minimal yüzeyler için Nusselt korelasyonu geliştirilen araştırmalardaki geometri türleri, hücre boyutları, malzeme ve gözeneklilik değerleri tablolaştırılmıştır. İkinci olarak, bu çalışmalardaki çalışma şartları verilmiş olup birim hücre boyutlarının 2,54–32,76 mm, porozite değerlerinin 0,20–0,95 ve Reynolds sayılarının yaklaşık 10–50.000 arasında değiştiği görülmüştür. Bu çalışmalarda, Gyroid ve Primitive tipi yüzeylerde ısı transferi diğer geometri tiplerine kıyasla daha fazla incelenmiş ve Gyroid tipi yüzeyler yüksek ısı transferi performansı ile ön plana çıkmıştır. Nusselt sayısının tahmini için geliştirilen denklemler ve geçerli olduğu aralıklar verilmiş her geometri tipi için uygun Nusselt sayısının seçimine vurgu yapılmıştır. Sonuç olarak, göz önüne alınan çalışma şartları dikkate alınarak kullanılabilecek Nusselt sayısı korelasyonları sunulmuş olup üçlü periyodik minimal yüzeyler için tüm geometrileri ve çalışma koşullarını kapsayan genel geçer tek bir Nusselt sayısı korelasyonunun henüz ortaya konulamadığı belirlenmiştir.

Anahtar Kelimeler: Üçlü Periyodik Minimal yüzeyler, Isı Transferi, Nusselt Sayısı, Eklemeli İmalat

ABSTRACT

In recent years, advancements in additive manufacturing technology have made it possible to produce compact heat exchangers with more complex surfaces compared to traditional heat exchangers by using triply periodic minimal surfaces. In addition to the production of compact heat exchangers, the ability to manufacture heat exchangers as a single part presents another advantage. The changes in the thermal boundary layer and the formation of secondary

flows in triply periodic minimal surfaces also contribute to achieving higher thermal performance. In this study, the recent works investigating the Nusselt number experimentally and numerically on triply periodic minimal surfaces have been evaluated. First, the types of geometries, cell sizes, materials, and porosity values in the studies that developed the Nusselt number correlations for triply periodic minimal surfaces were tabulated. Secondly, the working conditions in these studies have been provided, showing that the unit cell sizes range from 2.54 to 32.76 mm, the porosity values range from 0.20 to 0.95, and the Reynolds numbers range from approximately 10 to 50,000. In these studies, heat transfer on Gyroid and Primitive type surfaces has been examined more extensively compared to other geometry types, and Gyroid type surfaces have stood out with their high heat transfer performance. The equations developed for the estimation of the Nusselt number and their valid ranges have been provided, emphasizing the selection of appropriate Nusselt numbers for each geometry type. In conclusion, Nusselt number correlations that can be used considering the working conditions have been presented, and it has been determined that a single universal Nusselt number correlation covering all geometries and working conditions for triply periodic minimal surfaces has not yet been established.

Keywords: Triply Periodic Minimal Surfaces, Heat Transfer, Nusselt Number, Additive Manufacturing

REF: Akademik Teşvik

Tarih: 30.10.2026

İlgili Makama;

"XIII-INTERNATIONAL AEGEAN CONFERENCES on Innovation Technologies & Engineering 26-27 Ekim 2026 tarihleri arasında İzmir/Türkiye'de Türkiye (48) ve diğer ülkelerden (57) – *India: 6, Kazakhstan: 3, Nigeria: 13, Slovenia: 2, Pakistan: 3, Botswana: 6, Morocco: 11, Algeria: 1, Lithuania: 1, Azerbaijan: 1, Kosovo: 1, China: 1, QATAR: 1, Romania: 7*– akademisyen/araştırmacılarının katılımıyla gerçekleşmiştir. Kongre 16 Ocak 2020 Akademik Teşvik Ödeneği Yönetmeliğine getirilen "Tebliğlerin sunulduğu yurt içinde veya yurt dışındaki etkinliğin uluslararası olarak nitelendirilebilmesi için Türkiye dışında en az beş farklı ülkeden sözlü tebliğ sunan konuşmacının katılım sağlaması ve tebliğlerin yarıdan fazlasının Türkiye dışından katılımcılar tarafından sunulması esastır." değişikliğine uygun düzenlenmiştir.

Assoc. Prof. Dr. Mehmet Emin KALGI
Head of Organizing Committee

T.C.
ARDAHAN ÜNİVERSİTESİ REKTÖRLÜĞÜ
İlahiyat Fakültesi

Sayı : E-56430641-900-2600043777 19.10.2026
Konu : Akademik Temsilci (Doç. Dr. Mehmet Emin KALGI)

DAĞITIM YERLERİNE

İlgi : İslam Felsefesi Ana Bilim Dalı Başkanlığının 16.10.2026 tarihli ve E-66604117-900-2600043681 sayılı yazısı.

Fakültemiz öğretim üyelerinden Doç. Dr. Mehmet Emin KALGI'nın, 26-27 Ekim 2026 tarihleri arasında İzmir/Türkiye'de düzenlenecek olan "13. Uluslararası Ege Kongreleri" kapsamında gerçekleştirilecek Sosyal ve Beşeri Bilimler Kongresi, Sağlık ve Fen Bilimleri Kongresi ile İnovasyon ve Mühendislik Bilimleri Kongrelerinin düzenleme komitesinde akademik temsilci olarak yolluksuz ve yevmiyesiz katılım sağlaması hususunun;

Gereğini olurlarınıza arz ederim.

Güven KARAKOYUN
İlahiyat Fakültesi Fakülte Sekreteri

OLUR
Prof. Dr. Mustafa YILDIZ
İlahiyat Fakültesi Dekanı

DAĞITIM LİSTESİ
Sayın Doç. Dr. Mehmet Emin KALGI
Felsefe ve Din Bilimleri Bölümü
Personel Daire Başkanlığı

Bu belge, güvenli elektronik imza ile imzalanmıştır.
Belge Doğrulama Kodu: 9FMCCAH Belge Takip Adresi: https://www.turkiye.gov.tr/ardahan-universitesi-ebys

Adres: Ardahan Üniversitesi Kampüsü, Çamlıçatak Mevkii, 75002, Merkez/ARDAHAN
Telefon No: (0 478) 2117563 Faks No: (0 478) 2117565
e-Posta: if@ardahan.edu.tr İnternet Adresi: www.ardahan.edu.tr
Kep Adresi: ardahanuni@hs01.kep.tr
Bilgi için : Abdullah Bingöl
İlahiyat Fakültesi Tekniker
Telefon No: (0 478) 2117563
Direkt Hat: